

UNIVERSITÀ
DELLA CALABRIA



DIPARTIMENTO DI
CHIMICA E TECNOLOGIE
CHIMICHE
CTC

DIPARTIMENTO DI
FARMACIA E SCIENZE
DELLA SALUTE E
DELLA NUTRIZIONE
DFSSN

Thesis

Submitted for the degree of

DOCTOR OF PHILOSOPHY OF THE UNIVERSITY OF CALABRIA

Ph.D. Program in TRANSLATIONAL MEDICINE

Cycle XXXV

**Small molecules from cycloaddition reactions: synthesis,
theoretical perspectives, and biological evaluation**

SSD CHIM/06

Matteo Antonio Tallarida

Supervised by Professor Loredana Maiuolo

Reviewed by

Prof. Martin Breugst

Prof. Floris P. J. T. Rutjes

Coordinator of the Ph.D. Program

Prof. Stefania Catalano

Abstract

Italiano

Il presente lavoro di ricerca è relativo al corso di dottorato in Medicina Traslazionale del Dipartimento di Farmacia e Scienze della Salute e della Nutrizione dell'Università della Calabria. Il progetto è stato svolto presso il Dipartimento di Chimica e Tecnologie Chimiche della stessa istituzione sotto la supervisione della Prof.ssa Loredana Maiuolo nel Laboratorio di Sintesi Organica e Preparazioni Chimiche (LabOrSy) diretto dal Prof. Antonio De Nino. L'oggetto principale di questa ricerca riguarda l'utilizzo di reazioni di cicloadizione per la sintesi di *small molecules* con potenziale attività biologica. Accanto alla parte sintetica, sono stati condotti una serie di studi computazionali per chiarire il meccanismo di alcune delle reazioni riportate. Inoltre, sono stati eseguiti studi di docking molecolare per proporre potenziali bersagli per alcuni dei substrati sintetizzati.

Il lavoro è suddiviso in quattro parti principali. Il primo capitolo è dedicato alla sintesi di 1,2,3-triazoli 1,5-disostituiti, a una serie di studi di docking molecolare e alla loro valutazione biologica come inibitori dell'apertura del poro di transizione di permeabilità mitocondriale. La seconda parte è dedicata alla sintesi assistita da microonde di bisfosfonati isossazolidinici come potenziali inibitori della farnesil pirofosfato sintasi (hFPPS). Il terzo capitolo si concentra sull'uso di ilidi al piridinio come reagenti per la sintesi multicomponente di indolizine e ciclopropil spiroossindoli. Questi ultimi sono stati al centro di un approfondito studio computazionale DFT-QM. Il quarto capitolo riguarda la sintesi e lo studio meccanicistico della reazione di espansione radicalica di derivati norbornanici. Anche in questo caso viene riportato uno studio computazionale del meccanismo. Gli studi computazionali riportati nei capitoli 1, 3 e 4 sono stati condotti nell'ambito di un periodo di ricerca estero presso il Computational Chemistry Group diretto dal Dott. Gonzalo Jiménez Osés del Center for Cooperative Research in Biosciences (CIC bioGUNE) di Derio (Spagna).

Abstract

English

The research work is related to a Ph.D. course in Translational Medicine of the Department of Pharmacy, Health, and Nutritional Sciences, University of Calabria. The project was carried out at the Department of Chemistry and Chemical Technologies of the same institution under the supervision of Prof. Loredana Maiuolo in the Laboratory of Organic Synthesis and Chemical Preparations (LabOrSy) headed by Prof. Antonio De Nino. The main subject of this research regards the use of cycloaddition reactions for the synthesis of small molecules with potential biological activity in diverse contexts. Alongside the prominent synthetic part, a series of QM computational studies were conducted to clarify some reaction mechanisms. In addition, molecular docking studies were performed to propose potential targets for some of the prepared compounds. The work is subdivided into four main parts. The first chapter is dedicated to the synthesis of 1,5-disubstituted 1,2,3-triazoles, to a series of molecular docking simulations, and to the biological evaluation of two compounds as inhibitors of the permeability transition pore opening event. The second part is about the microwave-assisted synthesis of isoxazolidine bisphosphonates as potential farnesyl pyrophosphate synthase (hFPPS) inhibitors. The third chapter focuses on the use of pyridinium ylides as building blocks for the multicomponent synthesis of indolizines and spirocyclopropyl oxindoles. The reaction mechanism regarding these latter was computationally investigated. The fourth – and last – chapter regards the synthesis and the radical expansion reaction of norbornane derivatives. A computational assessment of the mechanism is reported also in this case. All the computational studies reported in chapters 1, 3, and 4 were conducted in the frame of an abroad research stay spent in the Computational Chemistry Group headed by Dr. Gonzalo Jiménez Osés of the Center for Cooperative Research in Biosciences (CIC bioGUNE).

Acknowledgments

I thought that the hardest part would have been writing the rest of the thesis, but when I started to think about the best possible acknowledgments, I suddenly realized it would have been a tough task. These last three years have been a mess: if Ph.D. is a hard journey *per se*, all the struggles, the stress, and the anxiety that the pandemic brought into our lives certainly made it even harder. But I do not regret every single day I've been through not only for the science I've had the honor to learn, but firstly (and foremost) for the extraordinary people that have been part of all of it. Here I'll try to thank them all.

I'd like to thank my mentor, supervisor, educator, teacher, and guide: Professor Loredana Maiuolo. She has been a real catalyst for my education, giving me the possibility to "graze" in the lab and, most importantly, allowing me to be wrong. An authentic safety net. I could not have hoped for better, and I feel extremely grateful for all the teachings and esteem.

Thank you to Professor Antonio De Nino, the head of my lab. When I needed an explanation, he has always been capable of converting every meeting into an authentic class of organic chemistry. He thought me to ask the right questions, and that's one of the most precious skills I'll always carry with me.

A huge thank you to Dr. Gonzalo Jiménez Osés, who hosted me for eight months in his research group at the CIC bioGUNE of Derio (Spain). There are no sufficient words to express how grateful I am. An amazing person and scientist, always available and interested in my scientific education, not only in my results. His curiosity has been inspiring.

The members of both groups contributed immensely to my professional and personal time. I'd like to thank Dr. Claudio D. Navo, Dr. Francesca Peccati, Ángel Torres Mozas,

Reyes Nuñez Franco, and Sara Alunno Rufini from the Computational Chemistry Group of CIC bioGUNE. Thank you also to Dr. Antonio Franconetti García for his kindness and company. Their scientific and human contribution to this thesis is invaluable. Thank you to my labmates: Dr. Vincenzo Algieri, Dr. Fabrizio Olivito, Antonio Jiritano. A huge thank you to Professor Paola Costanzo for the help inside and outside this thesis. Many thanks to Carmelina Bartucca, Veronica Cozzolino, Vincenzo Spinoso, and Concetta Bartucca who spent some time in our lab as undergraduate students. Without them, I probably wouldn't have had the time to deliver such a huge work.

Several groups also collaborated on this thesis. I thank Professor Salvatore Nesci and his group at the University of Bologna for their work on the biological evaluation of some of our compounds. Thank you also to Professor Pedro Merino and his group at the University of Zaragoza and to Dr. Ignacio Delso of the University of East Anglia for their work on bisphosphonates. Thanks to Professor Antonio José Moreno Vargas and his group at the University of Sevilla for giving me the chance to be part of their project about norbornane radicals.

And now it is time to get more personal and *Italian* for a bit.

La persona che più di tutto merita la mia ammirazione e riconoscenza è mia madre. Questa tesi di dottorato è solo l'ultimo di tutti i risultati che grazie al suo supporto sono stato in grado di raggiungere. Ha sempre riposto fiducia in me e nelle mie scelte, lavorando duramente per far sì che potessi dedicarmi interamente ai miei studi. Ciò che sono lo devo a lei e, per questo, questa tesi le è interamente dedicata.

A big thank you goes to Fabiola. She has been remarkable in these three years in helping me to find motivation, inspiration, and patience. I'm extremely grateful to this fantastic woman whose talent and intelligence inspire me to give my best every day.

And now some friends: some closer, some others spread all over the continent, but always in my thoughts. Thank you to Marco, Leonardo, Antonio C., Michael, Marzio, Mattia, Federico, Thierry, Andrei, Fabio, David, Mario, Maria Eugenia, Andrea (*aka* Fottemberg), Nico, Antonio F., Luana, Erika, Stefano, Emilio, Mariagrazia, Carlo, Sergio, Tommaso, Jesse, Manuel (*aka* Donto), Francesco (*aka* Yoshi), Gioacchino, and Lorenzo.

Matteo Antonio Tallarida
University of Calabria
November 2022

Contents

Chapter 1	8
Introduction	8
1. 1,3-dipolar cycloaddition: a non-aging tool in heterocycles synthesis	9
2. Recent advances in 1,2,3-triazole synthesis	15
2.1 Catalytic synthesis of 1,4 DTs	16
2.2 Catalytic synthesis of 1,5 DTs	28
2.3 Catalytic synthesis of 4,5 DTs	39
Results and Discussion	44
<i>Research line 1a</i> - Pyrimidine nucleobase-containing 1,5-disubstituted 1,2,3-triazoles: synthesis and molecular docking studies	44
<i>Research line 1b</i> - 1,5-DTs as mitochondrial Ca ²⁺ -activated F ₁ F ₀ -ATP(hydrol)ase: synthesis and <i>in vitro</i> studies	51
Chapter 2	62
Introduction	62
1. Bisphosphonates: a 50-years-lasting successful story	63
1.1 BPs metabolism and biological targets	65
1.2 Structure activity relationship	68
1.3 BPs in medicine	72
1.4 Synthetic strategies	74
2. Microwave-assisted 1,3-DPCA: two compatible strategies	79

Results and Discussion	97
<i>Research line 2 – New class of isoxazolidine bisphosphonates as potential human farnesyl pyrophosphate synthase (hFPPS) inhibitors.....</i>	<i>97</i>
Chapter 3	101
Introduction	101
1. Recent developments in <i>N</i> -heterocycles synthesis using pyridinium ylides.....	102
1.1 Synthesis of pyrrole derivatives.....	102
1.2 Reactions with acetylene and alkene derivatives.....	105
1.3 Metal-catalyzed reactions.....	126
2. Indolizines: an overview on their biological activities.....	130
2.1 Anti-inflammatory activity.....	131
2.2 Anti-tuberculosis and anti-microbial activity.....	131
2.3 Antioxidant activity.....	132
2.4 Phosphatase inhibitors.....	132
2.5 Anti-HIV activity.....	133
2.6 Hypoglycemic activity.....	133
2.7 Antitumoral activity.....	134
Results and Discussion	136
<i>Research line 3a – DDQ-mediated multicomponent access to polysubstituted indolizines</i>	<i>136</i>
3. Spirocyclopropyl oxindoles: recent advances and biological activities.....	144
3.1 <i>Path a</i> – from 3-alkylidene oxindoles.....	145
3.2 <i>Path b</i> – from oxindoles.....	153
3.3 <i>Path c</i> – from 3-chlorooxindoles.....	155
3.4 <i>Path d</i> – from diazooxindoles.....	161
3.5 Biological activities.....	164
Results and Discussion	166

<i>Research line 3b</i> – Highly diastereoselective multicomponent synthesis of spirocyclopropyl oxindoles enabled by rare-earth metal salts	166
Chapter 4	175
Studies on the regioselective rearrangement of azanorbornanic aminyl radicals into 2,8-diazabicyclo[3.2.1]oct-2-ene systems.....	175
Results and discussion	178
<i>Experimental studies</i>	178
<i>Computational studies</i>	183
Conclusions.....	185
Conclusions	186
List of References	188
Experimental Section	208
Annex I	249
Annex II	252

Chapter 1

1,2,3-triazoles: synthesis, biological activity, and docking studies

Introduction

Triazoles are a large family of nitrogen-containing compounds that raised a huge interest in organic chemistry in the last years, mainly due to their biological value and their facile accessibility. Such compounds can be found in two isomeric forms: 1,2,3-triazoles and 1,2,4-triazoles. In this chapter we will focus on the firsts, describing the synthesis of a series of pyrimidine nucleobase-containing 1,2,3-triazoles and a preliminary docking study over a set of hot topic targets (*research line 1a*). In addition, a thorough study of the synthesis and the biological evaluation of two substrates will be presented (*research line 1b*), wherein the potential pharmacological activity of our compounds in the frame of the mitochondrial permeability regulation was assessed.

Before going into the details of the research lines of this first chapter, we will give the reader an overview of the theory of cycloaddition reactions. This elucidation will be useful for the second and the third chapter of this thesis too. Then, we will thoroughly describe the principal novelties regarding the synthesis of 1,4-, 1,5- and 4,5-disubstituted 1,2,3-triazole (1,4-DTs, 1,5-DTs, and 4,5-DTs, respectively) from 2015, which will help to understand the context of the presented research pipelines.

1. 1,3-dipolar cycloaddition: a non-aging tool in heterocycles synthesis

Since their first appearance in scientific literature by the pioneering work of Rolf Huisgen and co-workers,¹ 1,3-dipolar cycloadditions (1,3-DPCAs) rapidly became a hallmark in heterocyclic chemistry. As part of the class of cycloaddition reactions, 1,3-DPCAs are part of the huge category of pericyclic reactions for the typical cyclic geometry of the transition states, together with electrocyclic reactions, sigmatropic reactions, and others. The reaction proceeds by means of the interaction of two partners: a 1,3-dipole and a dipolarophile. Both classes of compounds have been thoroughly investigated: as for 1,3-dipoles, these consist of a zwitterion with four π electrons delocalized over three heteroatoms, generally from the 14th, 15th, and 16th groups of Periodic Table. Such a system is commonly depicted using a Lewis structure wherein there is a positive charge localized on the central atom and a negative charge hosted by one of the peripheral atoms (**Figure 1**). In this regard, Huisgen defined two classes of 1,3-dipoles: the allyl and the propargyl-allene 1,3-dipoles. Allyl-type 1,3-dipoles are canonically represented by a bent structure, while the propargyl-allene-type are linear. In this thesis, our interest will span three different systems: azides (object of this chapter), nitrones (**Chapter 2**), and azomethine ylides (**Chapter 3**).

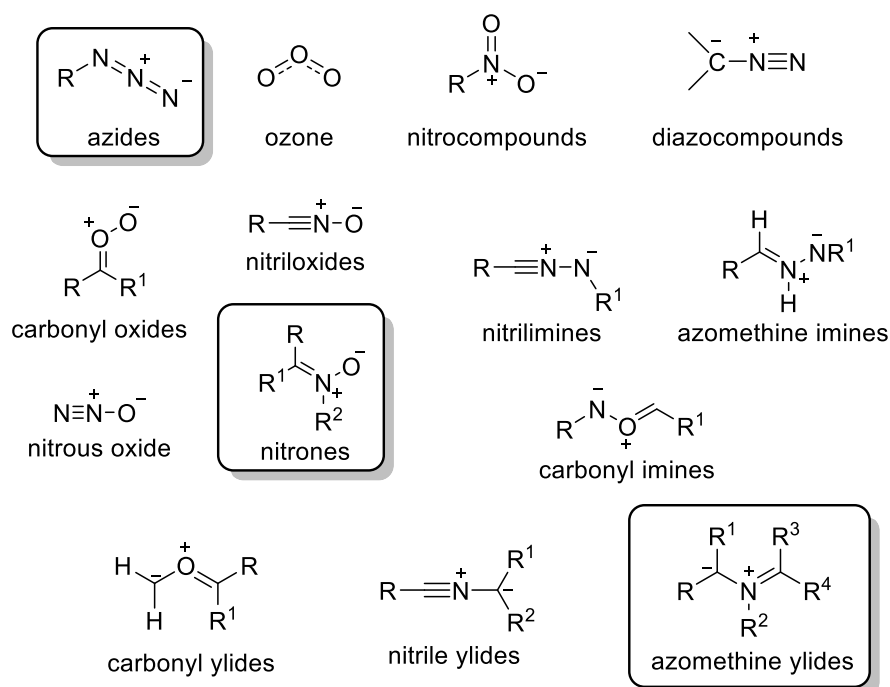


Figure 1. Main 1,3-dipoles. The species employed in this thesis are highlighted.

As for dipolarophiles, diversity is much bigger. A suitable dipolarophile can be indeed a compound containing a π system, being an olefin or a propargyl derivative. For instance, we can find unsaturated carbonylic compounds, alcohols, amines, halo compounds, and hydrocarbons just to name a few. Such versatility allowed the investigation of an enormous quantity of substrates and procedures in the last years, giving rise to one of the most prolific research fields in organic chemistry.

One of the most debated aspects regarding 1,3-DPCAs has been the mechanism. Even though modern experimental and computational organic chemistry helped a lot in this sense,² it could be instructive to briefly survey the main theories proposed to explain the unique features of 1,3-DPCAs. The main theories involved zwitterionic, radical, and four-center-concerted mechanisms. In particular, Firestone has been one of the most important supporters of the radical theory,³ which has been disputed shortly after by Huisgen based on some evidence. First, being 1,3-DPCAs known for their stereospecificity, a radical mechanism would not be acceptable because it would lead to the formation of both stereoisomers. Second, the general energetics of the reaction is way lower than the typical energetics of a radical reaction. Lastly, the kinetics is only moderately influenced by the polarity of the solvent: a radical process, on the other hand, would strongly be dependent on it. In addition, two works published in 1977 by Geittner⁴ and Sustmann⁵ about the kinetics and the perturbational analysis of a model reaction with diazomethane furtherly supported Huisgen's thesis. In such a process, 1,3-dipole and dipolarophile come closer from two parallel planes going through a suprafacial interaction that brings to the formation of two new σ bonds. Invoking the frontiers molecular orbitals (FMO) theory,⁶ as for the vast majority of orbital interactions, as closest in energy the two interacting orbitals are, the easiest the resulting overlap – hence the formation of the new bonds – will be.

In this frame, the Hückel model was used for defining the mathematical shape of the wavefunctions representing the FMO involved in the interaction. As for a general dipolarophile, the number of molecular orbitals (MO) obtainable will be equal to the number of atomic orbitals (AO) combined, according to the following mathematical equation:

$$\Psi_k = c_1^k p_{z,1} + c_2^k p_{z,2}$$

Where c_s^k represents the superposition coefficient, reflecting the weight of each AO in the linear combination, and being mathematically proportional to: $c_s^k \propto \sin\left(\frac{\pi ks}{n+1}\right)$, where s is AO considered and n is the number of the considered atoms. In this regard, the lowest MO in energy will be the HOMO (Highest Occupied Molecular Orbital) of the system, and the successive one will be defined as the LUMO (Lowest Unoccupied Molecular Orbital).⁷ A graphical depiction (**Figure 2**) allows us to notice how the energetics of each wavefunction is inversely proportional to the number of points in which the function changes of sign. In this case, we assumed that each superposition coefficient was equal because the dimension of the lobes of the two considered p_z orbitals is the same.

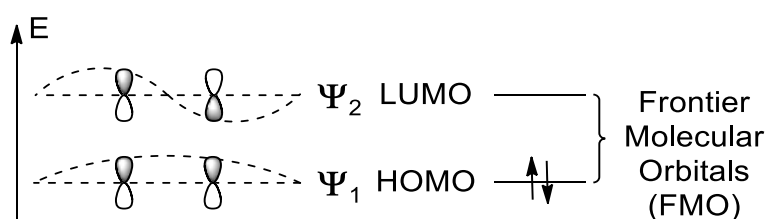


Figure 2. Graphical depiction of the FMO obtained by combination of two p_z orbitals of a general dipolarophile with the Hückel method.

The same can be done for a general 1,3-dipole: in such case, it is possible to use as a reference the system of allyl anion, wherein four π electrons are delocalized over three atoms. In doing so, we will have a linear combination of three p -type AO, hence three MO of shape:

$$\Psi_k = c_1^k p_{z,1} + c_2^k p_{z,2} + c_3^k p_{z,3}$$

As can be seen from the graphical representation of this system (**Figure 3**), the lowest energy MO and the LUMO are characterized by a variation in the superposition coefficients because the size of the lobes of two p AO is lower than the central atom.

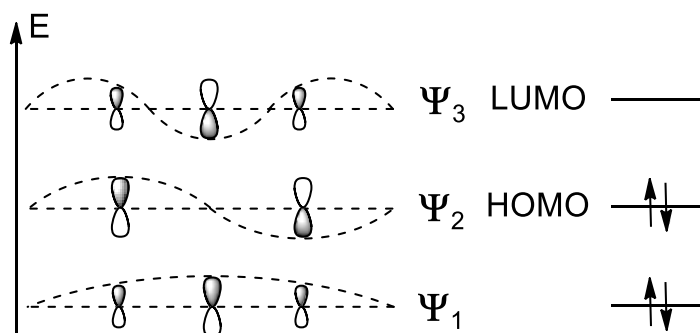


Figure 3. Graphical depiction of the FMO obtained by combination of three p_z orbitals of a general allyl-anion-type 1,3-dipole with the Hückel method.

Such an approach results particularly useful if the effect of different substituents on the reaction partners needs to be considered. The presence of electron-releasing groups (ERGs) and/or electron-withdrawing groups (EWGs) will increase or decrease the LUMO/HOMO energies, determining an FMO-driven control of the reaction. There are three possible conditions (**Figure 4**): HOMO-controlled reaction, where the HOMO of the 1,3-dipole reacts with the LUMO of the dipolarophile. LUMO-controlled reaction, in which the LUMO of the 1,3-dipole reacts with the HOMO of the dipolarophile. Lastly, Sustmann studied a series of cases where the difference in energy between the HOMO and the LUMO of each reaction partner is so close that is not possible to define a clear HOMO- or LUMO-driven approach.

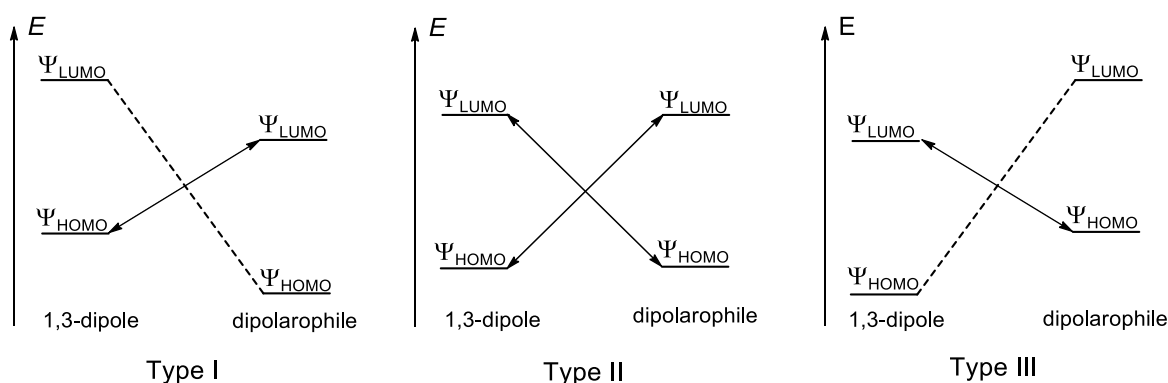


Figure 4. Sustmann's classification of 1,3-DPCA reactions.

Sustmann's classification resulted to be particularly useful in the rationalization of regioselectivity in most 1,3-DPCA. Without considering any catalyst and/or external factors that could influence regiochemistry, FMO theory can be used to foresee with good approximation whereas the presence of an ERG or an EWG substituent drives a regioisomer to prevail. In this context, Houk *et al.*⁸ pioneered the computational studies aimed to understand the regio- and periselectivity of 1,3-DPCA using qualitative perturbation molecular orbital theory. According to them, substituents that increase the energy of the HOMO of the 1,3-dipole or that decrease the energy of the LUMO of the dipolarophile will direct the reaction towards a HOMO-controlled profile. Conversely, substituents that decrease the energy of the LUMO of the 1,3-dipole or that increase the energy of the HOMO of the dipolarophile, will determine a LUMO-controlled reaction course.

Among the most peculiar factors that made 1,3-DPCAs so versatile and widespread, their stereochemistry can certainly be mentioned. Stereochemistry in 1,3-DPCA is driven by a great variety of factors, first and foremost the above-cited typical

mechanism wherein the two reaction partners come close from two parallel planes. In addition, it is possible to find studies on the stereochemistry of 1,3-DPCAs based on the presence of secondary orbital interactions, steric hindrance, hydrogen bonds, and dipole-dipole electrostatic interactions.⁹⁻¹¹ Two transition states are possible during such interaction and we can picture them considering two examples from the synthesis of triazoles and isoxazolidine. The *exo*- and *endo*-like approaches generate a pair of diastereoisomers (**3** and **4**), each one in a racemic mixture. Considering a mechanism in which a nitrene or an azide **1a-1b** and a dipolarophile **2a-2b** are reacting, the *endo*-like approach will be the one wherein the nitrogen of the nitrene **1a** is on the same side of the two substituents (R²- and R³-) of the olefin **2a**. Conversely, in the *exo*-like approach, the nitrogen will be opposite to the olefin substituents. As for the case of triazoles, the *endo*-like approach will be the one in which the phenyl group of the azide **1b** is on the same side as the X substituent of the dipolarophile **2b**. Although this kind of approach could appear unfavorable, one should consider the above-mentioned secondary orbital interactions: in this case, due to the presence of a phenyl group, a carbonyl, or another aromatic group on the dipolarophile, could help in stabilizing the energy of the transition state (TS) (**Figure 5**). Lastly, the *exo*-like approach is characterized by the presence of the -X substituent on the dipolarophile **2b** opposite to the phenyl substituent on the 1,3-dipole **2a**.

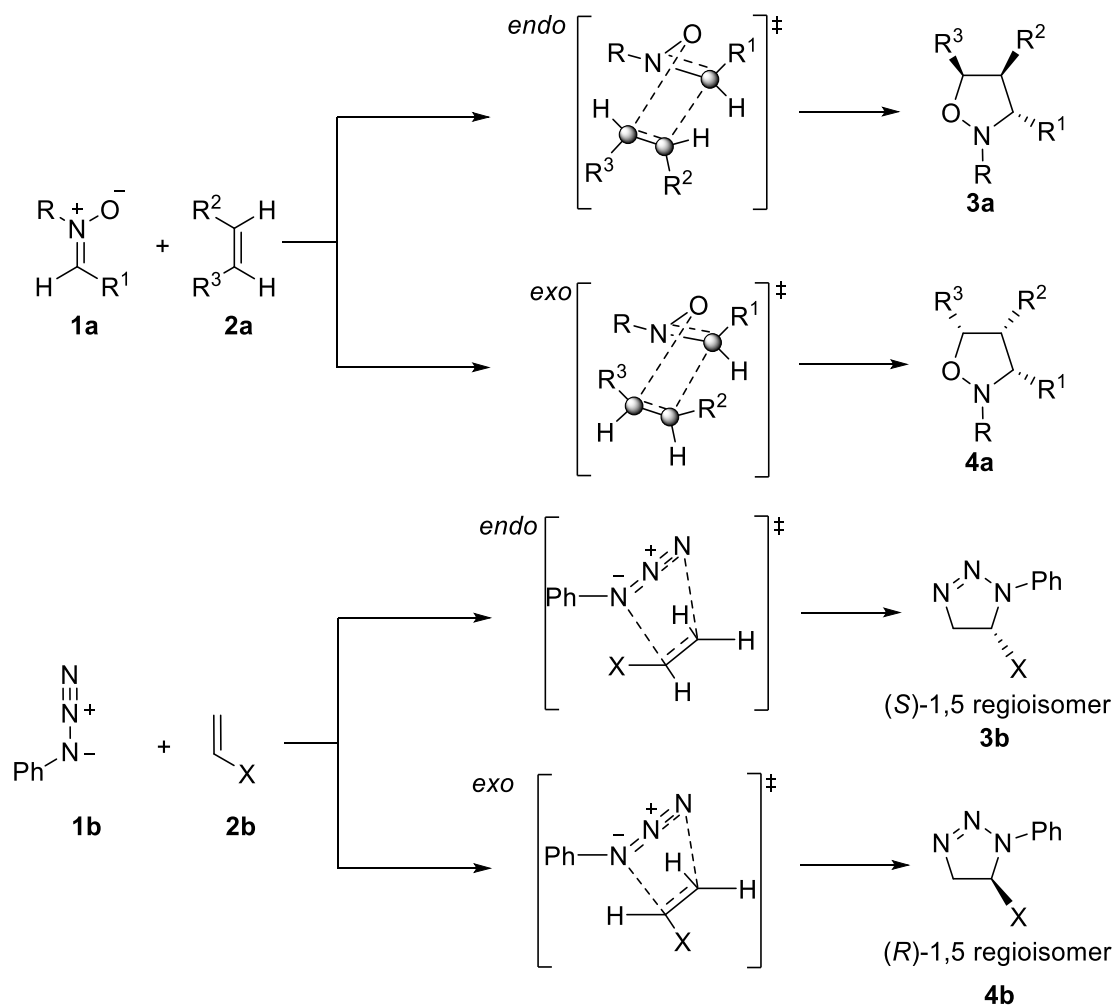
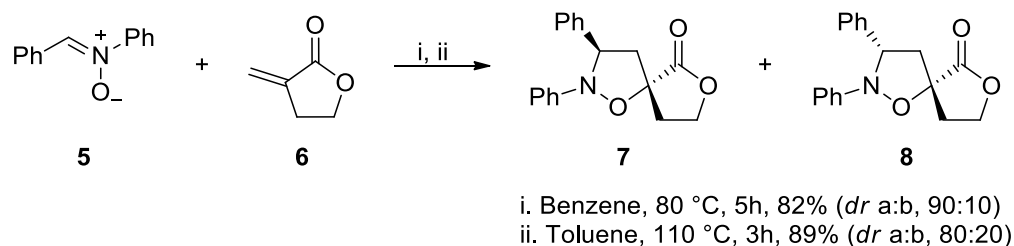


Figure 5. *endo*- and *exo*-approach in 1,3-DPCA. Regiochemistry was not considered.

An instructive example of the interactions that direct the stereochemistry in 1,3-DPCAs can be recovered from the work of Cacciarini *et al.*¹² (**Scheme 1**). In this regard, a notable diastereoisomeric excess has been obtained when an isoxazolidine (**7** and **8**) was obtained from the reaction between *C,N*-diphenyl nitron **5** and methylene- γ -butyrolactone **6**. The reason for such selectivity can be attributed to the analysis of the *exo* and the *endo* modes of interaction of the two partners (**Figure 6**): in the *exo*-approach, there will be a predominant steric repulsion due to the two *sp*³ hydrogens in β to the carbonyl group of the lactone. Conversely, the *endo*-mode will not face such a steric hindrance and will be even more lowered in energy by secondary orbital interaction between the π electrons of the aromatic system of the 1,3-dipole and the π electrons of the carbonyl group of the dipolarophile.



Scheme 1. 1,3-DPCA between *C,N*-diphenyl nitronium ion and methylene- γ -butyrolactone.

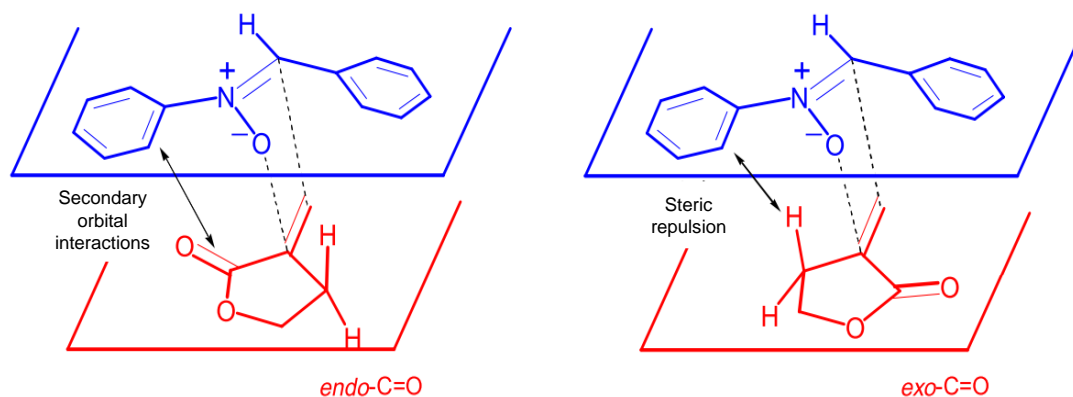


Figure 6. *endo* and *exo* transition states of the reaction reported in **Scheme 1**.

2. Recent advances in 1,2,3-triazole synthesis

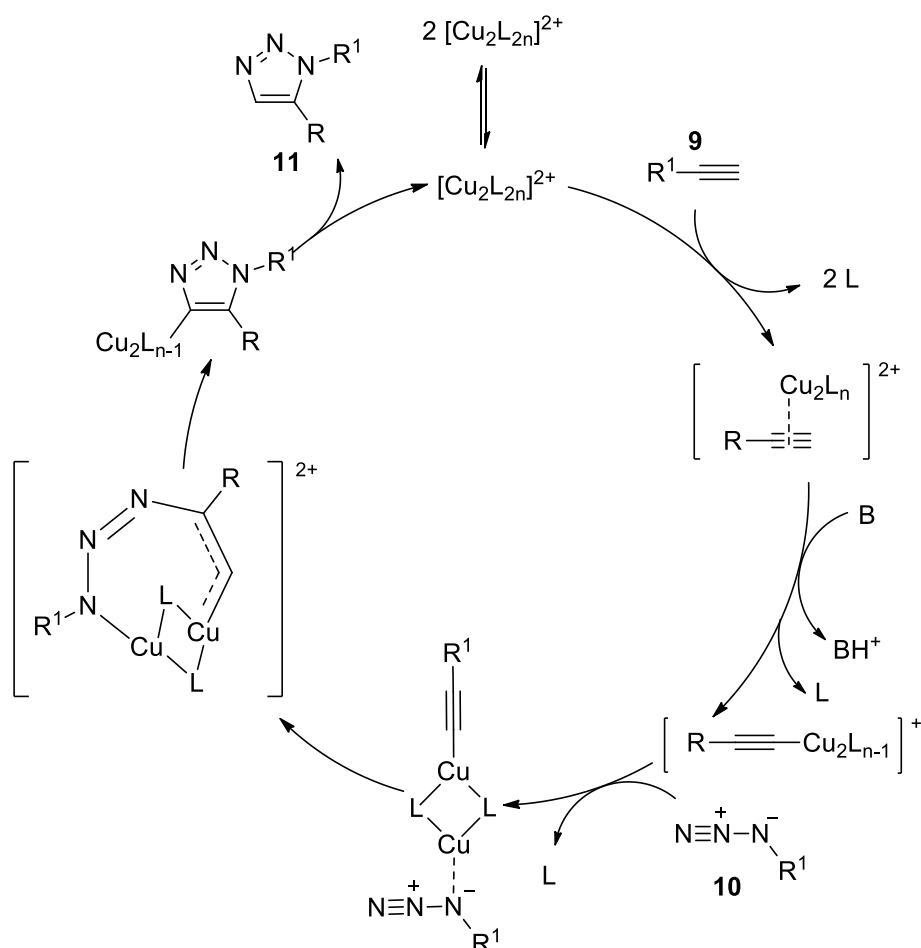
1,2,3-triazoles can be obtained in different ways based on the desired degree of substitution. Of these, 1,4- and 1,5-DTs were at the center of thorough studies in the last forty years. In this regard, two groundbreaking papers by Rostovstev from the Sharpless group¹³ and by Tornøe from the Meldal group¹⁴ appeared in 2002 reporting the so-famous copper-assisted cycloaddition reaction (CuAAC) for the highly regioselective synthesis of 1,4-DTs and shaping the concept of click chemistry. Ru (II)-based catalysts **9**, conversely, allowed to obtain 1,5-DTs **15** in a very regioselective fashion, following the Ru-catalyzed azide-alkyne cycloaddition (RuAAC).¹⁵ Such advancements were recognized with the Nobel Prize 2022, awarded to K. Barry Sharpless, Morten Meldal, and Carolyn R. Bertozzi for “the development of click chemistry and bioorthogonal chemistry”.

In this paragraph, the main advancement in the field of 1,4-, 1,5-, and 4,5-DTs synthesis will be reported, focusing on the catalytic methods proposed since 2015 according to a much broader review paper published in 2021 as part of this Ph.D. thesis.¹⁶ Interested readers will find other general dissections of the literature at the following references.¹⁷⁻²⁰ As happened for the vast majority of synthetic protocols in fine chemistry, synthesis of 1,2,3-triazoles benefited from increased attention towards

more eco-sustainable approaches in preparing such highly valued scaffolds. These advances were devoted to the implementation of new Lewis catalysts, non-conventional solvents, and eco-compatible materials and technologies.^{21,22} Moreover, microwave-assisted organic synthesis (MAOS) has been thoroughly deepened. In this regard, in **Chapter 2** we will survey such technology for its use in the preparation of our target compounds.

2.1 Catalytic synthesis of 1,4 DTs

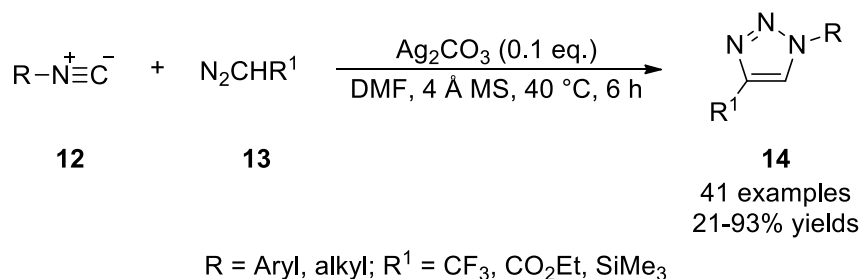
Despite the great attention towards Cu (I)-catalyzed protocols for accessing 1,4-DTs (**Scheme 2**), important advancements with other metals and in metal-free conditions were reported in the last years.^{23,24}



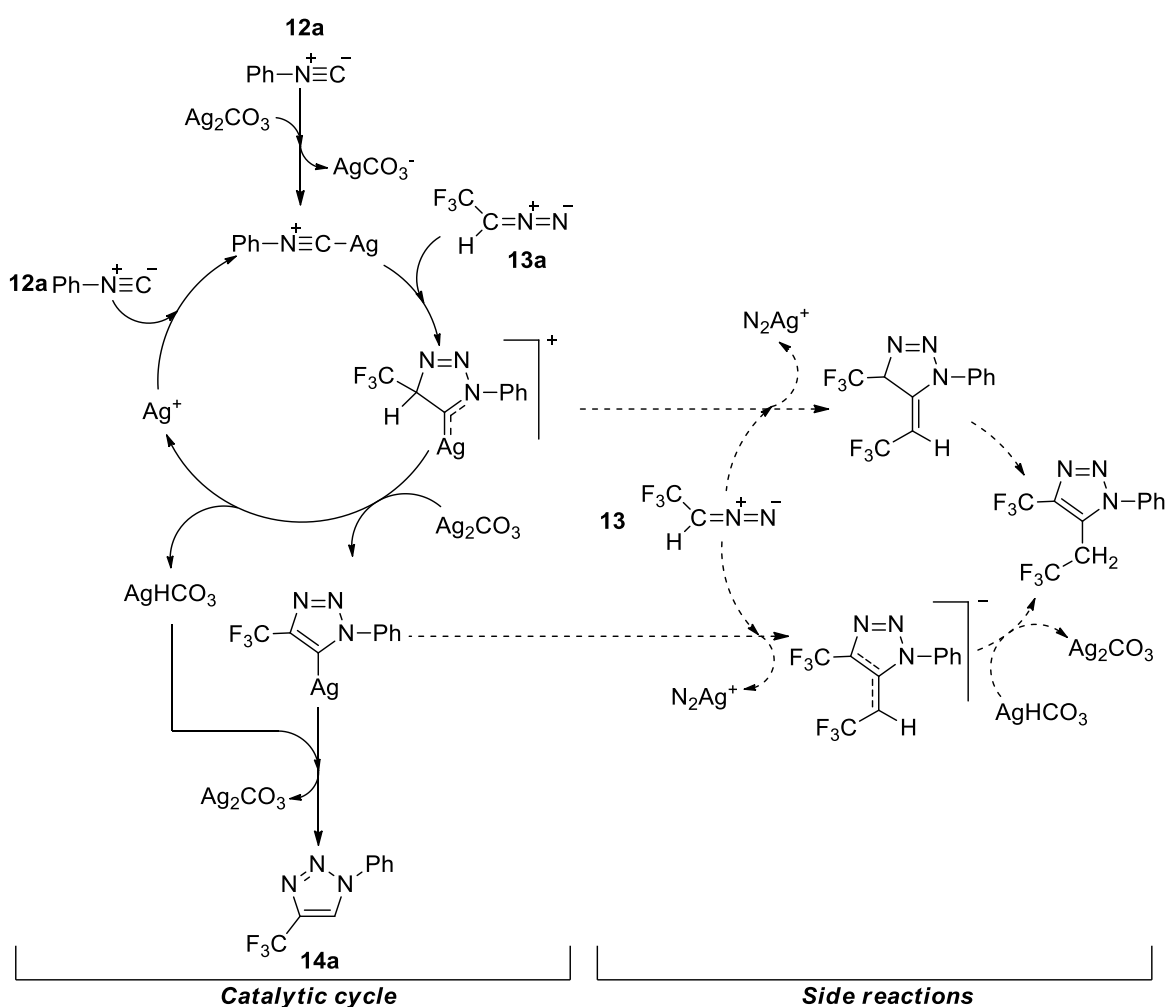
Scheme 2. Catalytic cycle for a CuAAC reaction.

One of the most suitable alternatives to Cu (I) appeared to be Ag (I). In this frame, Wang and co-workers²⁵ proposed an Ag (I)-catalyzed approach for the synthesis of 1,4-DTs (**Scheme 3**). Although the complete role exerted by such metal was not fully understood, Ag (I) was thought to be involved not only in the cycloadditive step but

also in the subsequent deprotonation and protonation steps. With the help of DFT,²⁶ it has been hypothesized that Ag (I) could play a role in increasing the electrophilicity of the isocyanide reaction partner, making the cycloaddition step energetically more favorable (**Scheme 4**).



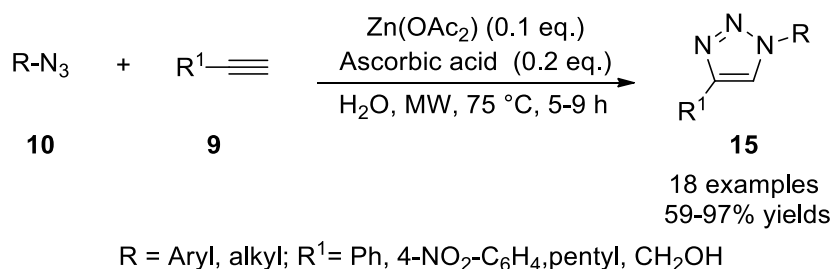
Scheme 3. Ag-catalyzed cycloaddition isocyanides and diazo compounds.



Scheme 4. Proposed reaction mechanism for the Ag-catalyzed synthesis of 1,4-DTs.

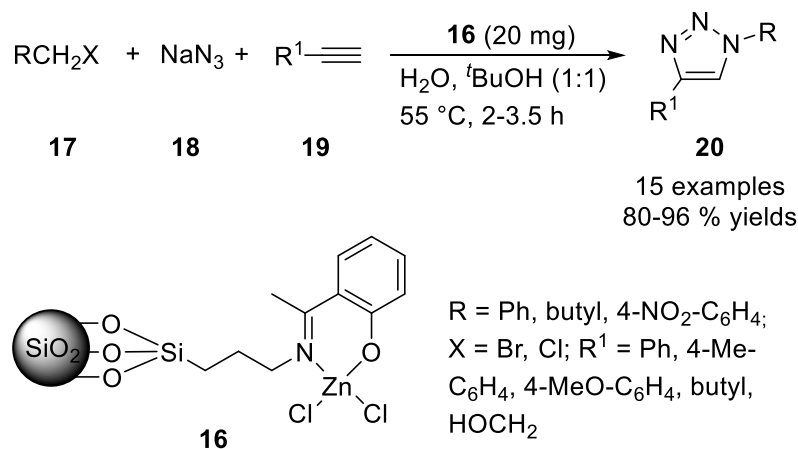
Following an approach regarding the use of zinc on charcoal,²⁷ new procedures have been recently introduced for the azide-alkyne cycloaddition. For instance, it has been possible to access 1,4-DTs using $\text{Zn}(\text{OAc})_2$, according to a work proposed by Morozova *et al.*²⁸ in 2017. In this case, the catalyst was tested over alkyl and aryl azides **10** in

combination with internal and terminal alkynes **9**, giving the desired products **15** with good to excellent yields (**Scheme 5**).



Scheme 5. 1,4-DTs from zinc azide-alkyne cycloaddition (ZnAAC).

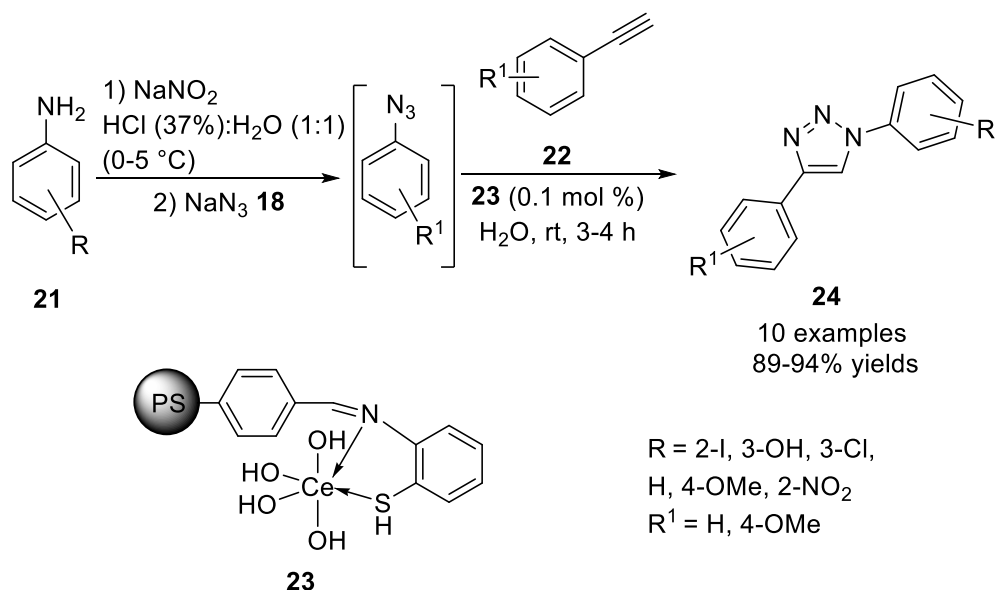
Sharma and co-workers proposed a reusable silica-supported organic-inorganic hybrid zinc catalyst.²⁹ The catalyst was obtained by covalent immobilization of 2-hydroxy-acetophenone on aminopropyl functionalized silica and subsequent metalation with ZnCl₂ (**16**, SiO₂@APTES@2HAP-Zn). **16** was tested in a click chemistry reaction between diverse halides **17** and terminal alkynes **19** in the presence of sodium azide **18** using a mixture of water and *t*-BuOH as a solvent, giving excellent yields (**Scheme 6**).



Scheme 6. One-pot synthesis of 1,4-DTs catalyzed by the SiO₂@APTES@2HAP-Zn catalyst.

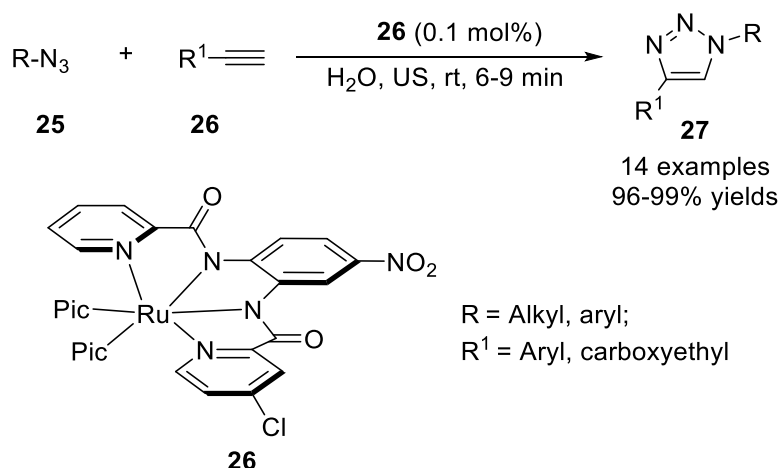
Mondal and collaborators proposed a strategy to prepare a heterogeneous catalyst based on Ce (III) for the one-pot synthesis of 1,4-DTs starting from arylamines.³⁰ In doing so, Ce (III) was immobilized on a polystyrene support previously functionalized with 2-aminothiophenol. The polystyrene-Ce-aminothiophenol catalyst (**23**, PS-Ce-amtp) was tested on the reaction between aryl azides, deriving from the corresponding anilines **21** and aryl alkynes **22** in aqueous medium at room temperature. The resulting 1,4-DTs **24** were obtained in excellent yields after 4 h (**Scheme 7**). As for the proposed

mechanism, the key intermediate was proposed to be a cerium-containing six-membered species. Recycling tests were also performed, resulting in good yields.



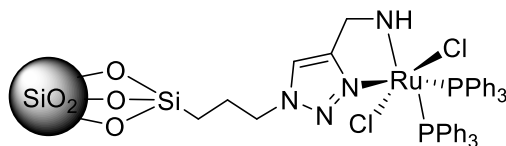
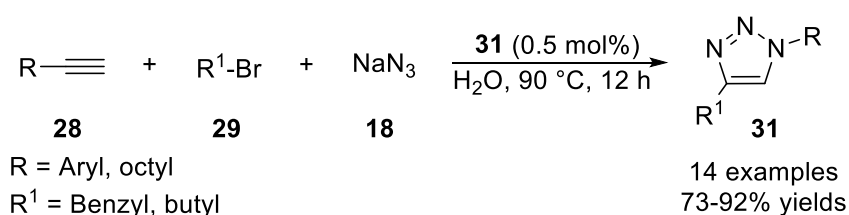
Scheme 7. PS-Ce-amtp **23** catalyzed click reaction of aryl amines and aryl alkynes.

Other important advances were reported using Ru and Ir-based catalysts. In this regard, Arafa and collaborators³¹ developed a regioselective protocol in which the Ru catalyst **26** was used for a series of azide-alkyne cycloadditions in water assisted by ultrasonic irradiation (**Scheme 8**). This procedure overcame the primary limitations associated with the use of ruthenium for azide-alkyne cycloaddition processes, such as the general lengthy reaction times, limited applicability, and thermal activation, by exploiting ultrasonic irradiation as an energy source. A sonosynthetic technique was also used to obtain the catalyst starting from diamide ligands, which were produced by combining picolinic acids and *o*-phenylene diamines in the presence of triphenyl phosphite as the coupling agent. Finally, the diamide ligands first reacted with [Ru (DMSO)₄]Cl₂ and subsequently with 4-picoline to give **26**. Even though all the prepared catalysts gave access to the desired product in quantitative yields in about 7 minutes, **26** was chosen as the most active one in amounts of 0.1 mol%. Then, using various benzyl, phenyl, and cyclohexyl azides **25** with aromatic and heteroaromatic alkynes **26**, the scope of the reaction was broadened. The yields were quantitative (96-99%) in all cases. By evaluating the activity of **26** in the one-pot synthesis of new coumarin/1,4-DTs hybrids, the generality, and the scope of this approach were successfully assessed.



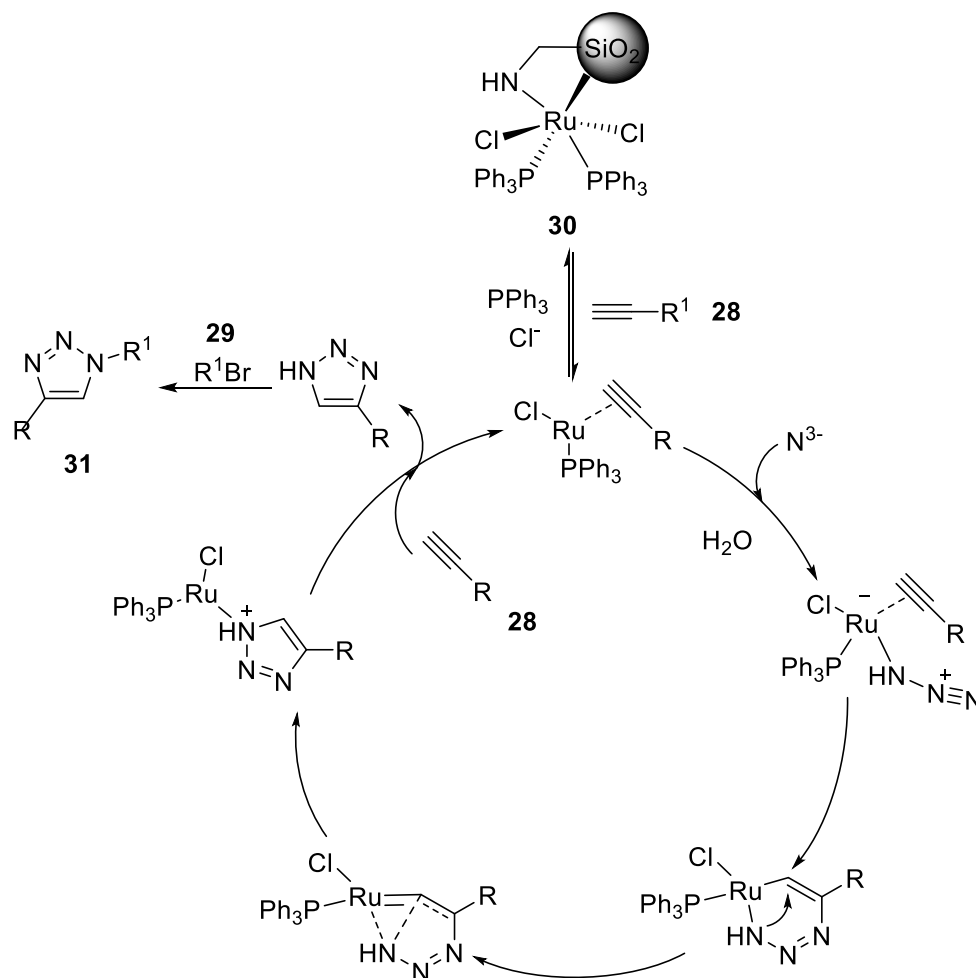
Scheme 8. Ru-complex catalysis under US irradiation of 1,3-dipolar cycloaddition towards 1,4-DTs.

Sharma *et al.*³² developed a heterogeneous ruthenium catalyst in 2017 *via* click chemistry. A 1,2,3-triazole moiety was anchored to a mesoporous SBA-15 zeolite, then [RuCl₂(PPh₃)₃] was immobilized on such modified zeolite, and the resulting catalyst SBA-15-Tz-Ru (II) TPP **30** was tested for the one-pot preparation of 1,4-DTs in water (**Scheme 9**). In this way, benzyl bromides **29** was reacted with various aryl alkynes **28** in the presence of sodium azide **18** in 12 hours at 90 °C giving the desired 1,4-DTs in optimal yields. The authors also hypothesized a plausible reaction mechanism (**Scheme 10**), wherein Ru catalyzed the azide-alkyne reaction to form 4-substituted-1*H*-1,2,3-triazole, which underwent an *in situ* substitution reaction with benzyl bromide **29** to give the *N*-benzylated-product **31**.



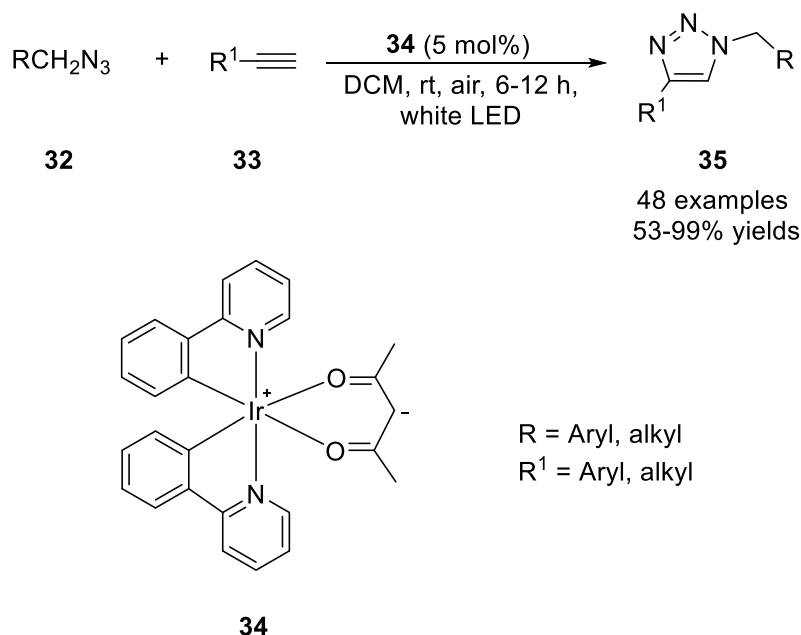
30

Scheme 9. Azide-alkyne cycloaddition catalyzed by the SBA-15-Tz-Ru(II)TPP (**30**).



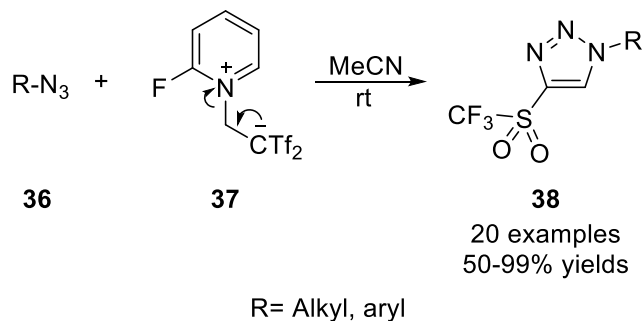
Scheme 10. Plausible mechanism for the click reaction catalyzed by SBA-15-Tz-Ru(II)TPP .

In recent years increasing efforts have been placed on the use of visible light as an environmentally friendly source of energy. Wu and colleagues looked at such an approach as a new route for the synthesis of 1,4-DTs in 2020,³³ wherein several catalysts were employed to quickly and efficiently synthesize triazoles from aliphatic and aromatic azides **32** in the presence of alkynes **33**. The authors explored various common photocatalysts, such as Eosin Y, [Ru(bpy)₃Cl₂] \cdot 6H₂O, [Ir(ppy)₃], [(piq)₂Ir(acac)] **34** and others, in different solvents, and under various wavelengths. Using [(piq)₂Ir(acac)] **34** as a catalyst in DCM as a solvent for 6 hours and white LED light, the optimal reaction conditions were assessed (**Scheme 11**). Good results were obtained under modest reaction conditions, with no need for heat or an inert environment. The investigation of the scope of the reaction led to good functional group tolerance and moderate to optimal yields. The catalyst was also recycled four times with just a small loss in the reaction yield.



Scheme 11. Photocatalyzed azide-alkyne cycloaddition (Pc-AAC) by an iridium complex **34**.

As for the metal-free synthesis of 1,4-DTs, Alcaide *et al.* proposed a regioselective procedure for the preparation of *C*-trifluoromethanesulfonyl triazoles in 2015, by using 2-(2-fluoropyridinium-1-yl)-1,1-bis[(trifluoromethyl)sulfonyl]ethane-1-ide **37** in the presence of several azides (**Scheme 12**).³⁴



Scheme 12. Metal-free synthesis of 1-alkyl- or 1-aryl-4-triflyl-1,2,3-triazoles at room temperature.

The aromatic azides needed longer reaction times (3-48 h) when compared to the aliphatic ones, which reacted with **37** almost instantly. The chemoselectivity was also investigated. For sugar **38a** and lactam-linked triazoles **38b**, good yields were obtained with no loss of chirality (**Figure 7**).

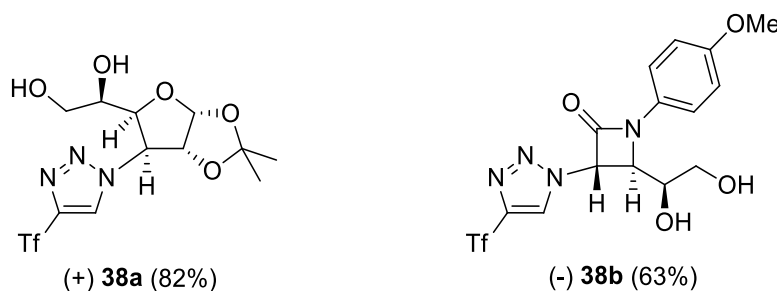
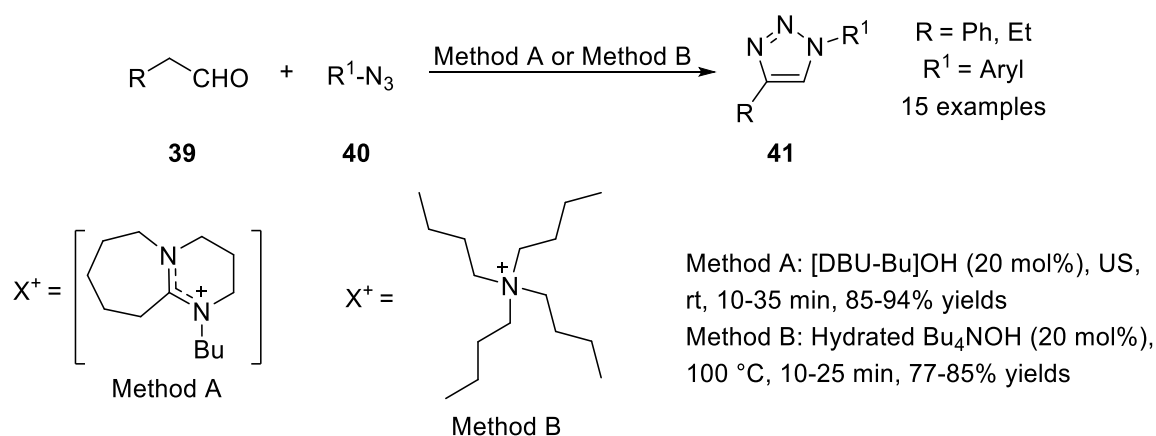


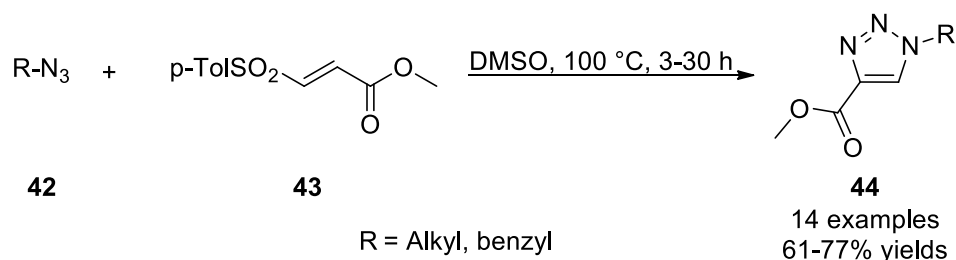
Figure 7. Alcaide synthesis of sugar and lactam-containing 1,4-DTs with retention of configuration.

Enolizable aldehydes were employed in alkaline conditions with aryl azides to explore more sustainable methods by using an alternate energy source and ILs as solvents. In a procedure described by Singh *et al.*,³⁵ the authors used 1,8-diazabicyclo[5.4.0]undec-7-ene (DBU) coupled in IL, which in this form is easier to extract from the reaction mixture. To expand the use of ILs under conventional heating, the use of hydrated Bu_4NOH was investigated too (**Scheme 13**). Triazole compounds were formed in both cases with good yields and short reaction times.



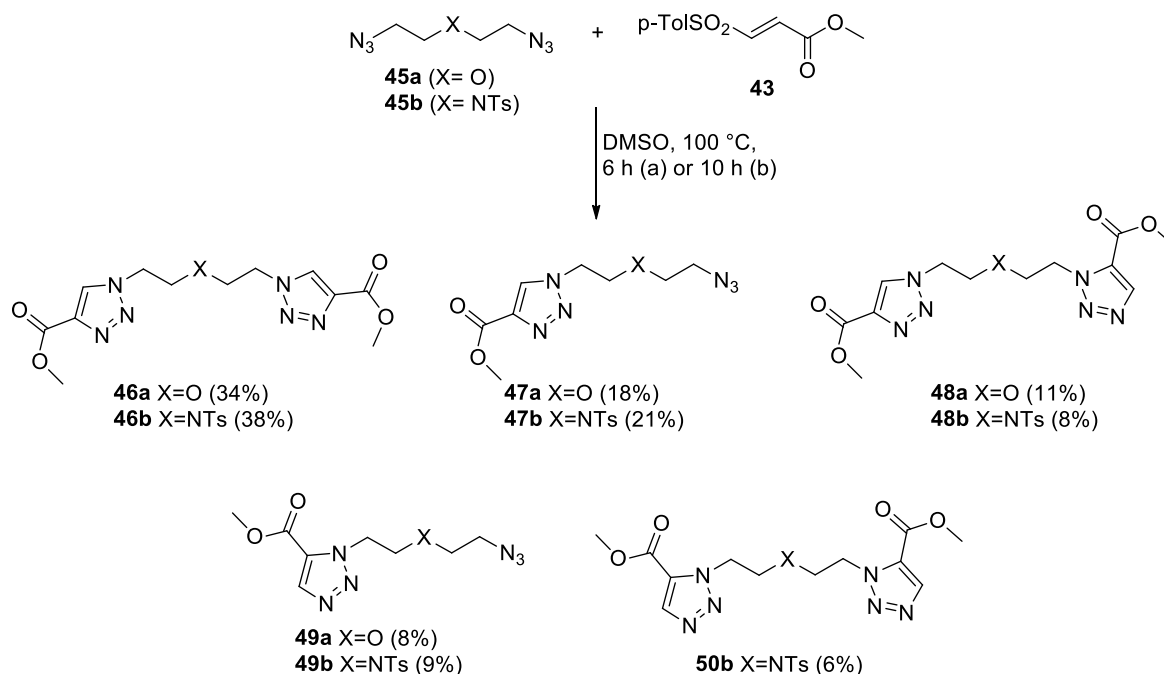
Scheme 13. Synthesis of 1,4-DTs in ILs.

(*E*)-methyl 3-tosyl acrylate **43** was investigated by Das *et al.*³⁶ for the synthesis of methylcarboxylated esters-functionalized 1,4-DTs **44** through a [3+2] cycloaddition reaction. Azide **42** was combined with a wide range of alkyl azides **42** to afford compound **44** in good yields (**Scheme 14**).



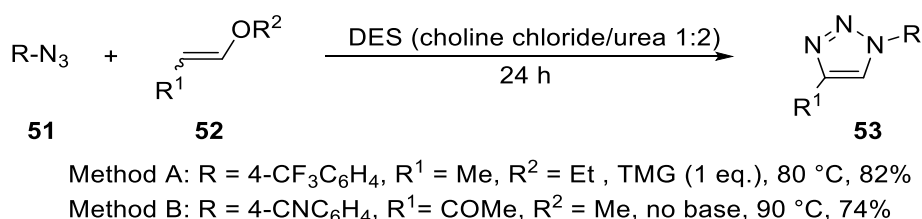
Scheme 14. Synthesis of 4-carboxylated 1,4-DTs **44**.

Using the same protocol, the authors also tested **43** with various diazides **45a-45b**. In this case, unsymmetrical bis-triazoles were obtained, bearing bis-1,4-DTs, 1,4-DTs, 1,5-DTs and bis-1,5-DTs residues, although this latter was the minor product (**Scheme 15**).



Scheme 15. Reaction of **43** with diazides **45a** or **45b**.

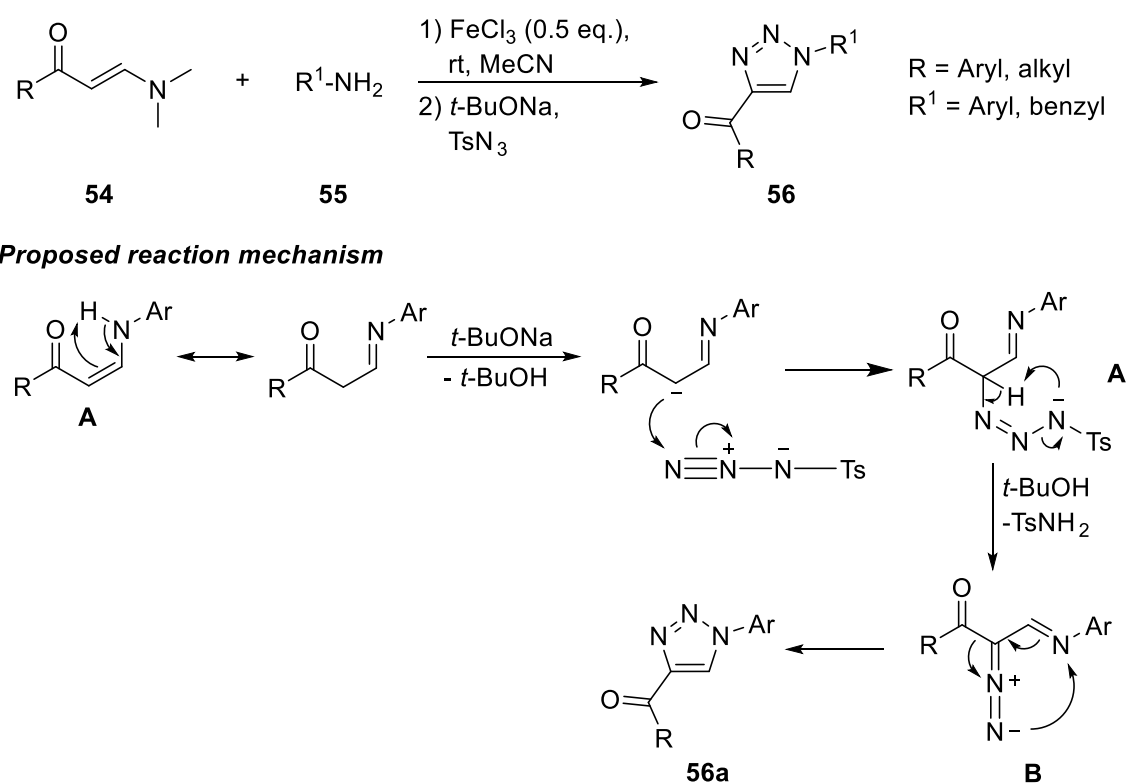
Sebest and collaborators³⁷ used a deep eutectic solvent (DES) made up of choline chloride and urea (1:2) for obtaining 1,4-DTs from azides and internal olefins. Such an approach, wherein eco-compatible DESs are used as reaction media for 1,3-DPCA, has been thoroughly reviewed by De Nino and co-workers in 2021.²¹ In this work, the authors searched for the best reaction conditions to afford 1,2,3-triazoles in a one-pot fashion. Using 1,1,3,3-tetramethyl-guanidine (TMG), 1,5-DTs were prepared in DES after 24 h at rt (method A), while, for the 1,4-DTs species, it was necessary to heat the reaction mixture (method B). Although the limited tolerance of this approach, the 1,4-DTs **53** were obtained in a very eco-friendly manner (**Scheme 16**).



Scheme 16. Synthesis of 1,2,3-triazoles in the presence of DES.

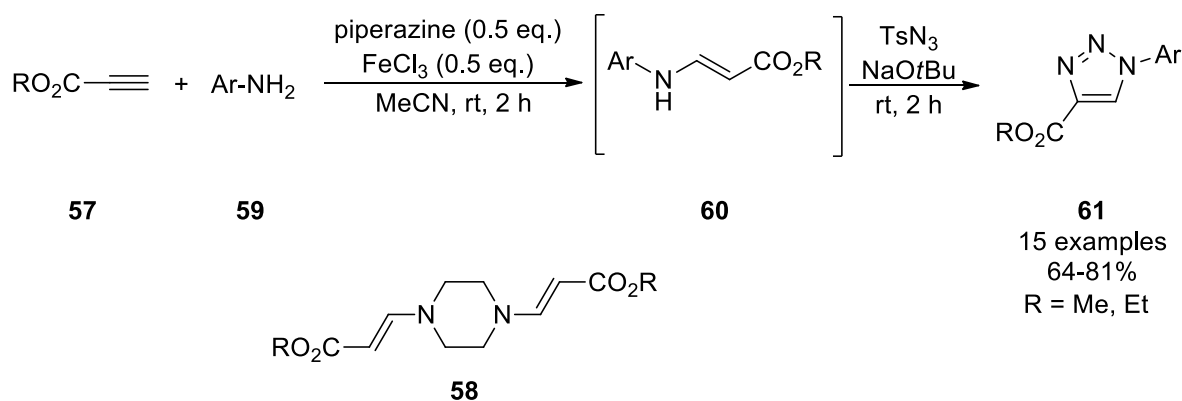
Wan *et al.* used tosyl azide as a nitrogen source in a cycloaddition procedure in the presence of enaminones.³⁸ In this study, the authors sought the cycloaddition of the

enaminones **54** by using *t*-BuONa as a base catalyst in MeCN at room temperature. In the first stage, the transamination reaction between **53** and amines **54** needed to be catalyzed by a Lewis acid, such as FeCl₃. The newly obtained enaminone reacted with tosylazide to form **56**, whilst the base was only added in the second step. A typical Regitz diazo transfer reaction was proposed in the suggested reaction mechanism to form the diazo intermediate A, which rearranged to form the cycloadduct **56a** (**Scheme 17**).



Scheme 17. Domino reaction and the plausible mechanism for the synthesis of 1,4-DTs from enaminones.

The same research group used alkyl propiolates in a domino reaction to access an active enamine as an intermediate, allowing the switchable synthesis of 1,5- and 1,4-DTs.³⁹ 1,5-DTs were obtained without the use of azides, while for the 1,4-isomers tosylazide was necessary as a nitrogen source (**Scheme 18**). In this case, it was proved that the intermediate **58** is formed by an *aza*-Michael addition of alkyl propiolate **57** in the presence of piperazine. The final 1,4-DTs **61** was accessed in the subsequent step by combining **58** with the proper aniline **59** to form the intermediate **60**. A Lewis acid (FeCl₃) was required in the first step to catalyze the transamination between the aniline and the *in situ* obtained tertiary amine, whereas *t*-BuONa was required in the second step as a base additive in a Regitz diazo transfer reaction.



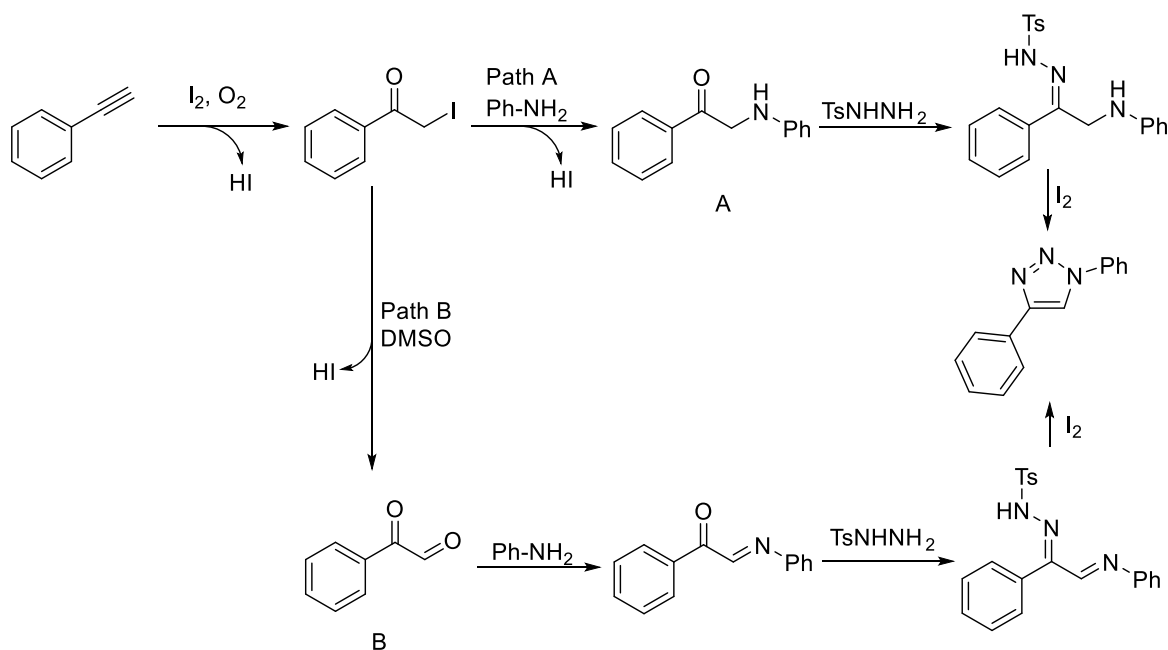
Scheme 18. Preparation of 1,4-DTs through the enamine activation.

New synthetic protocols helped to bypass the use of azides. In this frame, two distinct strategies can be distinguished: the first calls for the use of oxidants (I_2 or O_2) to promote the cycloaddition of *N*-tosylhydrazones and anilines, while the second relies on base conditions or the presence of strong leaving groups. The Wang research group investigated the first approach,⁴⁰ while a good example of the second one can be recovered from the work proposed by Mani *et al.*⁴¹ (**Scheme 18**). It involved the direct transformation of aryl alkynes **63** using I_2 in a O_2 atmosphere: in this case, the use of *N*-tosylhydrazone **64** and aniline **62** allowed the introduction of the needed nitrogen atoms without using azide derivatives. Two plausible mechanisms were proposed (**Scheme 19**). The first one (path A) brought to the product through the α -iodoacetophenone intermediate A. The second one (path B) needed the conversion of α -iodoacetophenone to a phenylglyoxal **B** through a Kornblum oxidation mechanism.



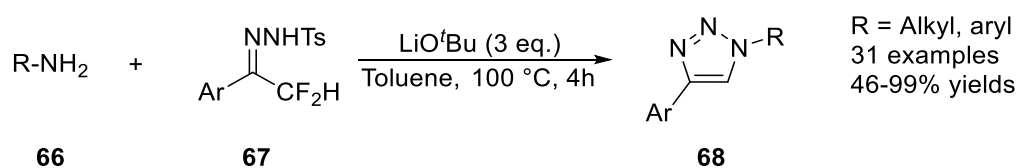
R = Aryl, benzyl

Scheme 18. Metal-free synthesis of 1,4-DTs in oxidative conditions.



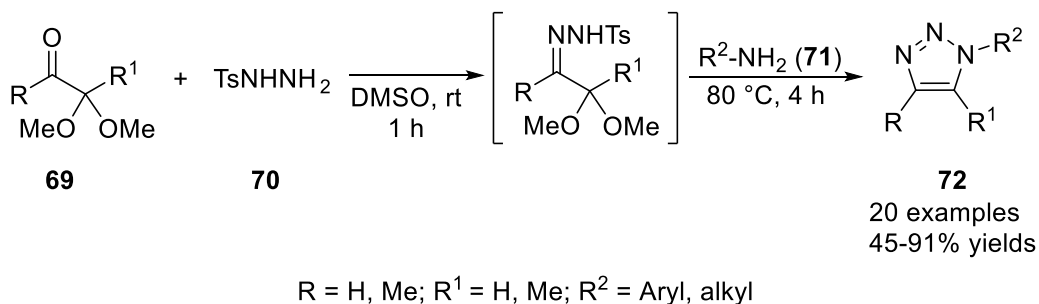
Scheme 19. Proposed mechanism of 1,4-DTs synthesis in oxidative conditions.

As for the cycloaddition of tosylhydrazones bearing a good leaving group at the α -position, several works have recently been described. In this frame, Zhou *et al.* in 2019 used α,α -difluoro-*N*-tosylhydrazones **67** to perform the synthesis of 1,2,3-triazoles by cleaving C-F bonds (**Scheme 20**).⁴² As a result, it was possible to use aryl substrates in this reaction as well, in the presence of LiOtBu. The reaction conditions and scope were investigated, observing a good functional tolerance for the R-group, optimal yields and, more importantly, bypassing the use of metals, oxidants, and azides.



Scheme 20. α,α -difluoro-*N*-tosylhydrazone **67** as a starting substrate for the synthesis of 1,4-DTs.

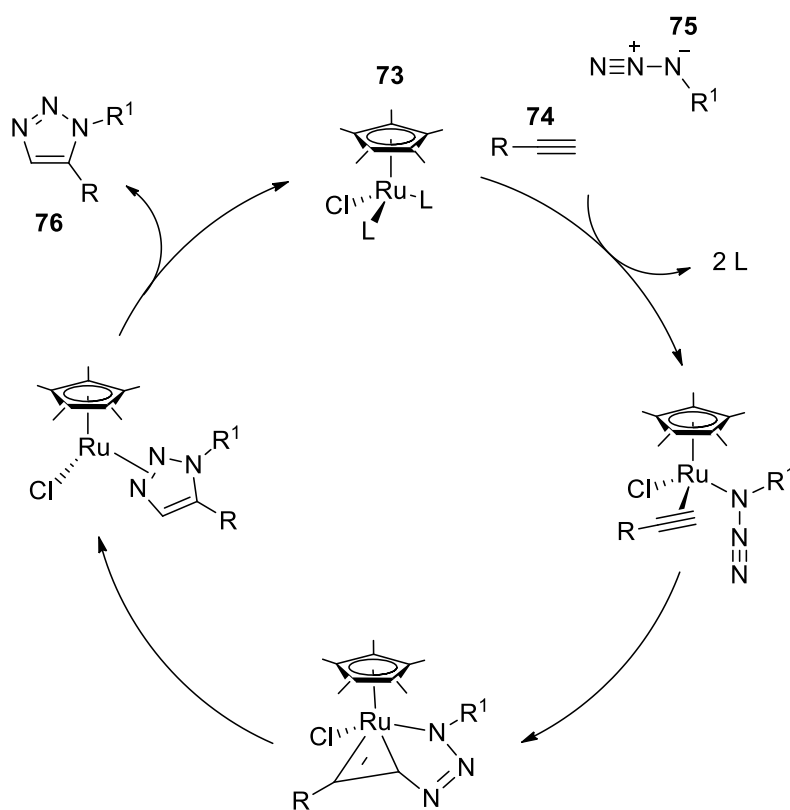
α,α -dichloro-*N*-tosylhydrazones were easily prepared from α,α -dichloroketones and tosyl hydrazine **70**. Zhender and colleagues⁴³ pioneered the use of the α,α -dimethoxy acetal functional groups in place of the α,α -halo functional group due to its low stability and the undesired formation of by-products. The *N*-tosylhydrazones **70** were obtained from α -ketoacetals **69** and were converted in the desired 1,4-DTs **72** by simply heating in the presence of the desired primary amine **71** with an 87% of yield. The scope of such a method was explored with global good yields both for the 1,4- and the trisubstituted species (**Scheme 21**).



Scheme 21. Synthesis of 1,4-DTs from α, α -dimethoxy ketones **69** and primary amines **71**.

2.2 Catalytic synthesis of 1,5-DTs

The major advances in the metal-catalyzed synthesis of 1,5-DTs mostly continue the trend before 2015 and consists of Ru (II)-catalyzed reactions for the preparation of bioactive triazolyl cores *via* the RuAAC (**Scheme 22**).



Scheme 22. RuAAC catalytic cycle, according to Boren *et al.*¹⁵

1,5-DTs are particularly useful in medicinal chemistry, not only for their biological activity *per se* but also for their role as peptido-⁴⁴ and glycomimetics.⁴⁵ Of note, one particular Ru complex, Cp*RuCl(COD) (**Figure 8**), was successfully employed to access a series of peptide bond isosteres (**78** and **79**)^{46,47} and minigastrin analogs **80**.⁴⁸

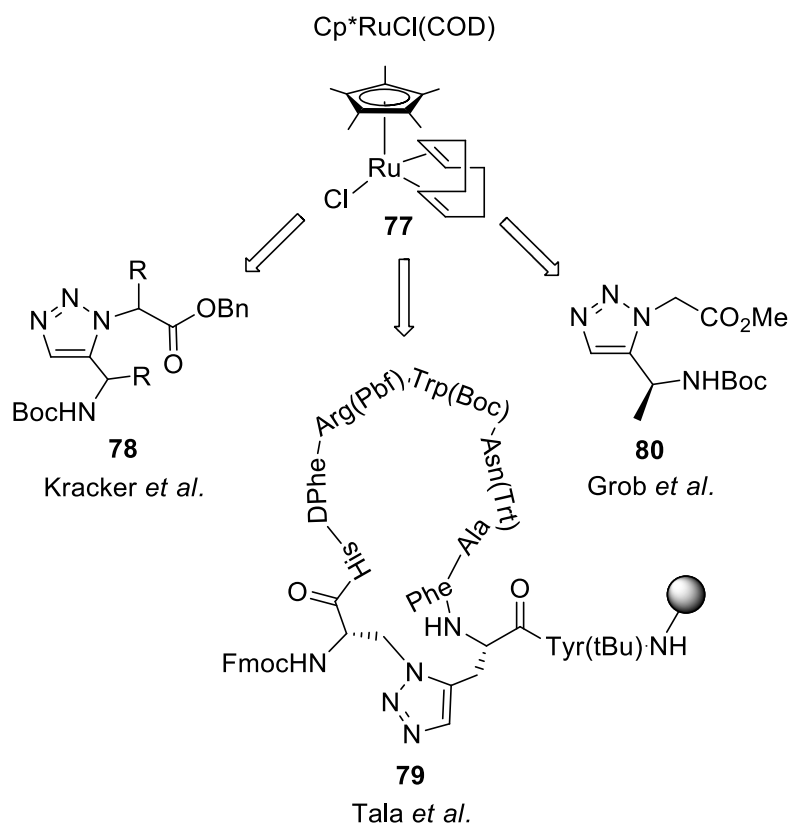
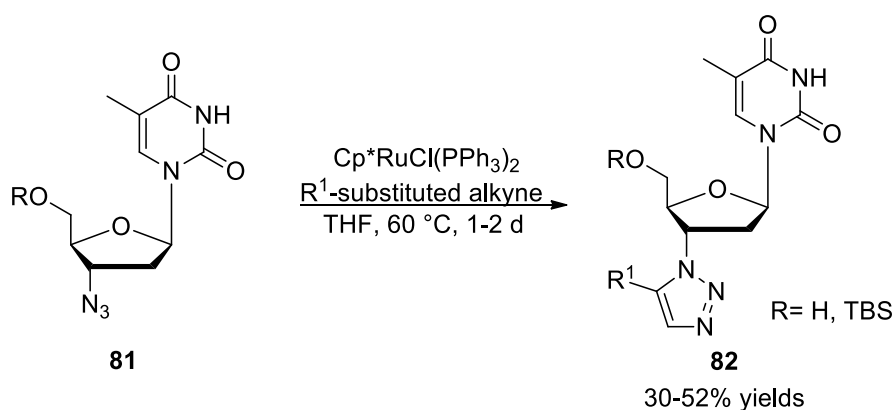


Figure 8. Some selected applications of the use of Cp* $\text{Ru}(\text{Cl})\text{COD}$ for the synthesis of 1,5-DTs derivatives.

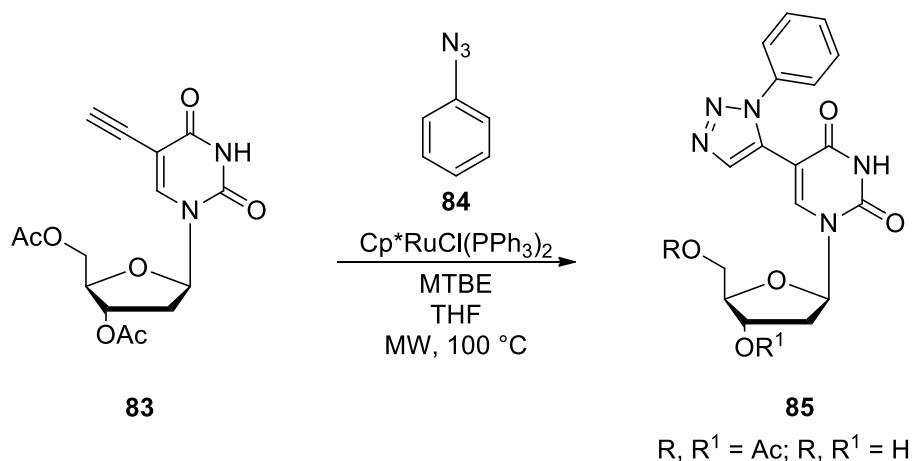
In 2015, Vernekar and collaborators⁴⁹ developed a new series of antiviral triazoles **82** active against West Nile (WNV) and Dengue virus (DENV). Such compounds were 5'-silylated nucleoside scaffolds derived from 3'-azidothymidine (AZT) **81**, synthesized *via* a classic RuAAC with Cp* $\text{Ru}(\text{Cl})(\text{PPh}_3)_2$ in THF as a solvent (**Scheme 23**).



Scheme 23. Vernekar synthesis of nucleoside-functionalized 1,5-DTs.

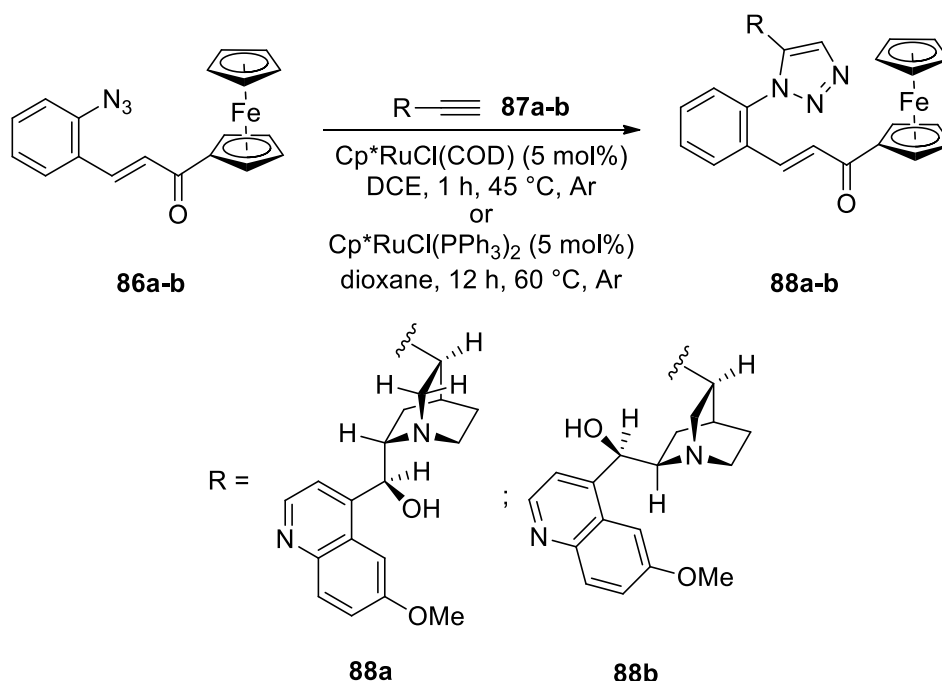
The development of new nucleobase-inspired motifs linked to triazole rings has been furtherly deepened by Pettersson and co-workers⁵⁰. A RuAAC route for the preparation of 8-triazolylpurines as inhibitors of the MDM2/p53 interaction was proposed, using an MW-assisted Cp* $\text{RuCl}(\text{PPh}_3)_2$ -catalyzed procedure in DMF at 120 °C. One year later,

Hornum and co-workers⁵¹ proposed an approach for the insertion of 1,2,3-triazolyl moieties directly on a pyrimidine ring (**Scheme 24**). Such an approach might be seen as a reversal of the Vernekar method (**Scheme 23**): in this case, the nucleoside scaffold **83** serves as the dipolarophile while the phenyl azide **84** plays as a 1,3-dipole.



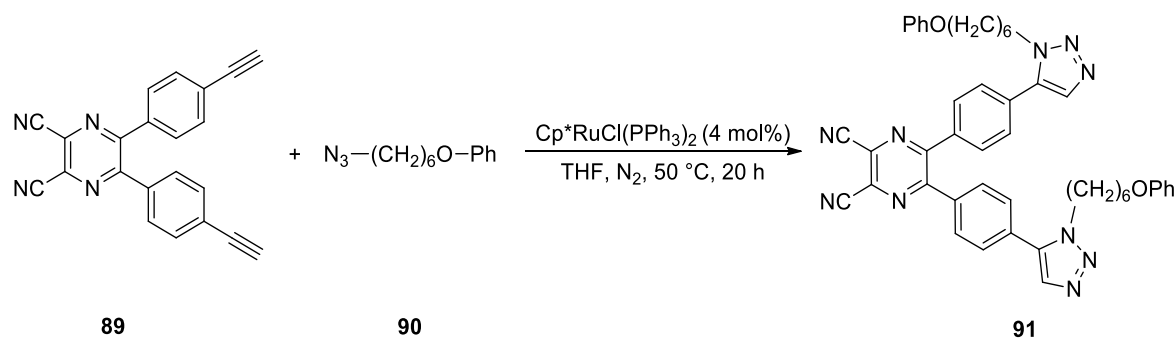
Scheme 24. Hornum synthesis of 1,5-disubstituted 1,2,3-triazoles linked to a pyrimidine ring **85**.

To form 1,5-functionalized 1,2,3-triazoles, Kocsis and co-workers⁵² proposed a synthetic approach for the Ru-catalyzed synthesis of cinchona-chalcone hybrids. From a 2-azidochalcone derivative **86a-b** and a propargyl derivative **87a-b**, a chalcone moiety has been directly linked to a ferrocene **88a-b** using the triazole ring as a linker (**Scheme 25**). The complexes were *in vitro* tested against HepG-2 and HT-29 cells showing significant cytostatic activity.

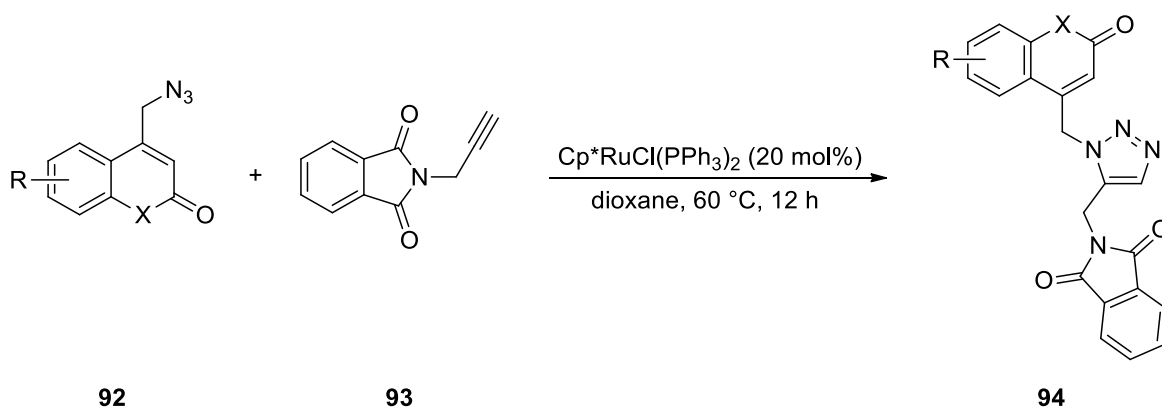


Scheme 25. 1,5-disubstituted 1,2,3-triazoles-containing ferrocene-cinchona hybrids.

A method for the synthesis of the 1,5-disubstituted 1,2,3-ditriazole **91** was proposed in 2015,⁵³ a compound that showed significant aggregation-enhanced emission properties and formed red-emissive charge transfer complexes. The 1,5-disubstituted product was formed through the RuAAC method and Cp^{*}RuCl(PPh₃)₂ as a catalyst (**Scheme 26**). A click chemistry-based approach for the regioselective synthesis of 1,5-coumarinyl 1,2,3-triazoles **94** was also published by Anand *et al.* (**Scheme 27**).⁵⁴



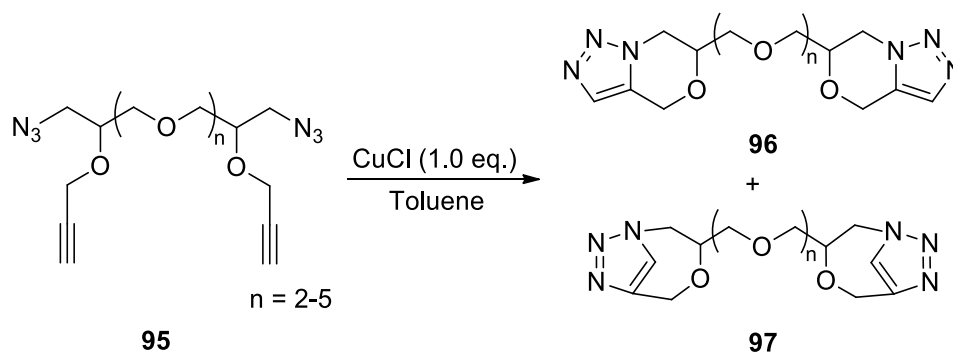
Scheme 26. 1,5-DTs with aggregation-enhanced emission characteristics developed by the Chen group.



X = O, NH; R = 6-Cl, 8-CH₃, 6-CH₃, 7,8-di-CH₃, 7-CH₃, 5,7-di-CH₃, benzof[quinoline], 7-OCH₃, 7-Cl

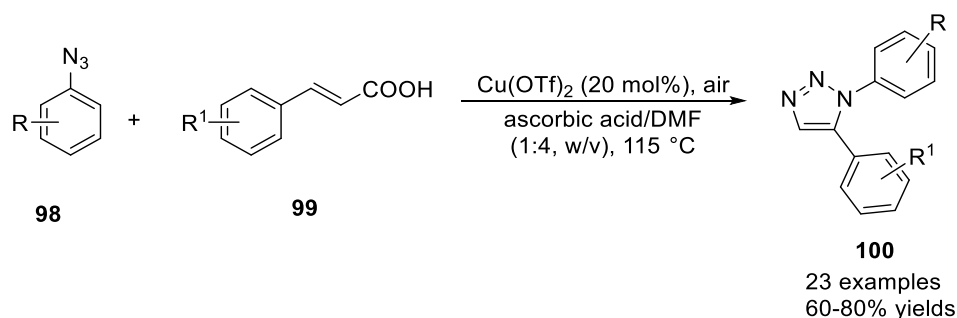
Scheme 27. 1,5-DTs as photosensitizer developed by the Anand group.

As for the new alternatives to Ru catalysts, innovative Cu-, Ni-, and Er-based protocols will be here briefly described. Two notable developments were proposed by Mekni⁵⁵ and Kumar *et al.*⁵⁶ In the first report, the authors attempted an intramolecular 1,3-DPCA of polyoxyethylene diazidoalkynes **95** catalyzed by a Cu (I) salt (**Scheme 28**). As the result, it has been obtained a mixture of polyoxyethylene 1,5-disubstituted fused-di(1,2,3-triazole)-1,4-oxazines **96** and 1,4-disubstituted mono(1,2,3-triazole)azidoalkyne crown ethers **97**.



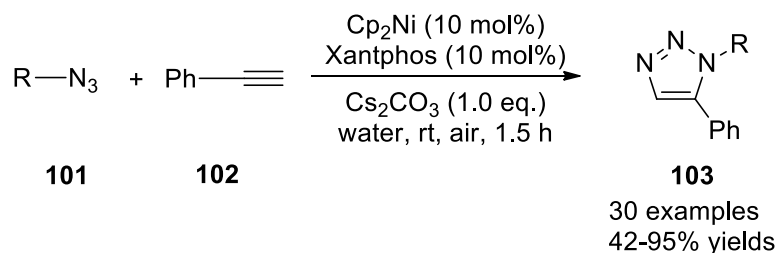
Scheme 28. Preparation of polyoxoethylene 1,5-disubstituted fused-di(1,2,3-triazole)-1,4-oxazines **96** via a Cu (I)-catalyzed intramolecular 1,3-dipolar cycloaddition.

As for the second report, the authors proposed the first use of Cu (I) for the synthesis of 1,5-disubstituted 1,2,3-triazoles **100** through the coupling of phenyl azide derivatives **98** and styryl carboxylic acid derivatives **99** with optimal yields (60-80%) (**Scheme 29**). In this case, Cu (I) has been generated *in situ* from $\text{Cu}(\text{OTf})_2$ using ascorbic acid (25% w/v) in DMF. The main advantage of such a method consisted of the use of carboxylic acids as reactants, which are not compatible with the classical RuAAC protocol. A reasonable interpretation of the mechanistic course of the reaction included an initial 1,3-DPCA followed by two decarboxylation and aromatization steps with the formation of the desired products **100**.

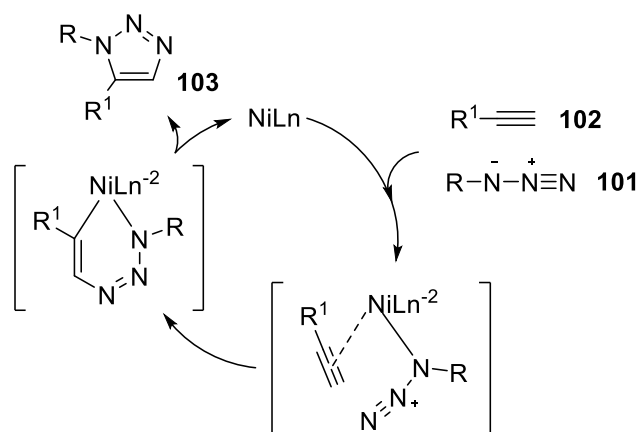


Scheme 29. Kumar Cu(I)-catalyzed synthesis of 1,5-DTs.

Nickel displayed a very high catalytic activity in combination with green and mild conditions in a very interesting paper by Kim *et al.*⁵⁷ In this case, the authors proposed a convenient procedure in which the regioselective synthesis of 1,5-DTs **103** was achieved using Cp_2Ni and Xantphos at 10 mol% in water at room temperature (**Scheme 30**).

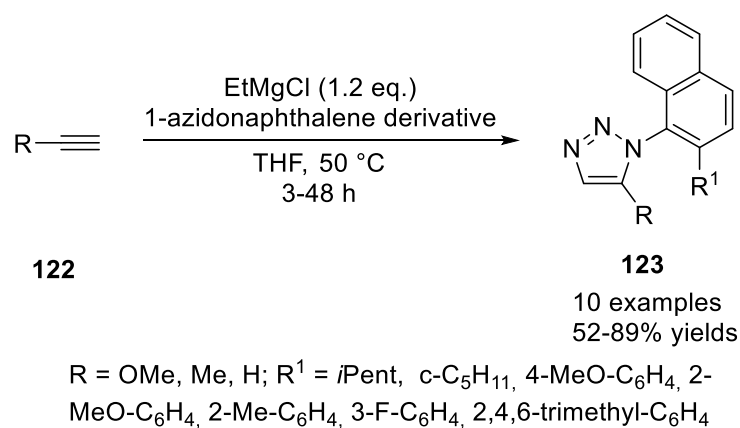


Scheme 30. NiAAC synthesis of 1,5-disubstituted 1,2,3-triazoles.



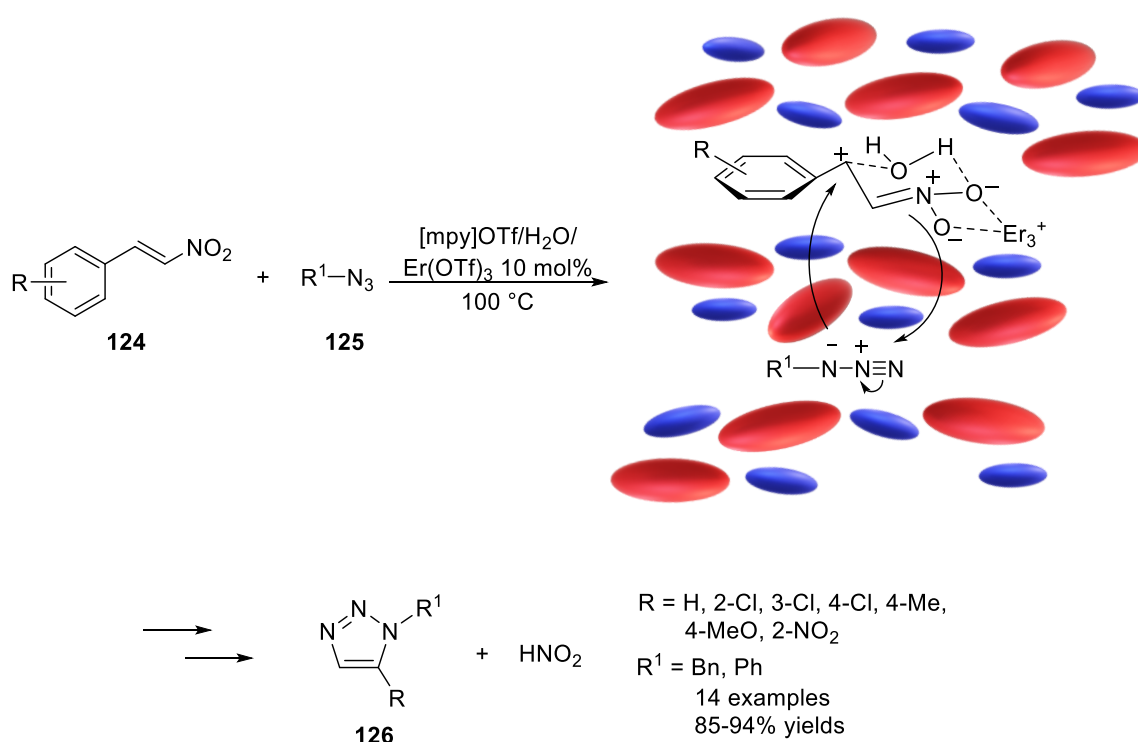
Scheme 31. Nickel-catalyzed synthesis of 1,5-DTs.

Recently, other interesting strategies expanded the role of metals in the synthesis of 1,5-DTs. By immobilizing AlCl_3 on $\gamma\text{-Al}_2\text{O}_3$, the Nanjundaswamy group developed a regioselective method for accessing to 1,5-disubstituted compounds.⁵⁸ Moreover, the Mahadari group focused on the *in situ* synthesis of chloromagnesium acetylides to form sterically hindered compounds. In particular, starting from 1-azidonaphthalene derivatives, 1,2,3-triazoles bearing a 1-(2-methoxy-1-naphthyl)-5 group **123** were prepared (**Scheme 32**).⁵⁹ On the other hand, one can argue that the *in situ* formation of acetylides through EtMgCl would be poorly compatible with carbonyl-containing substrates.



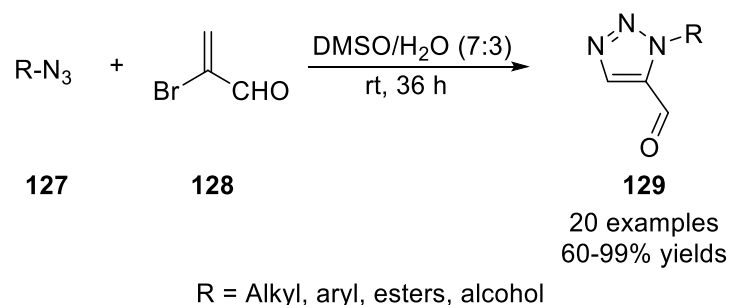
Scheme 32. Naphthyl-functionalized 1,5-DTs from chloromagnesium acetylides.

Lastly, notable improvements came from the introduction of new Lewis acid catalysts in combination with IL media.^{60,61} In both cases, an IL made up of pyridine and methyl trifluoromethanesulfonate ([mPy]OTf)⁶² was combined with FeCl₃ or Er(OTf)₃ giving the desired products in high yields and allowing the reusability of the catalytic system. A brief description of the method and the plausible mechanism of the Fe (III)-catalyzed reaction will be given in the next paragraph given that it has been used to prepare the 1,5-DTs of the *research line 1b* of this chapter. As for the role of Er(OTf)₃, a plausible mechanism was proposed (**Scheme 33**) invoking the ionic self-assembly (ISA)⁶³ which forces the reactants to assume a stacked conformation.



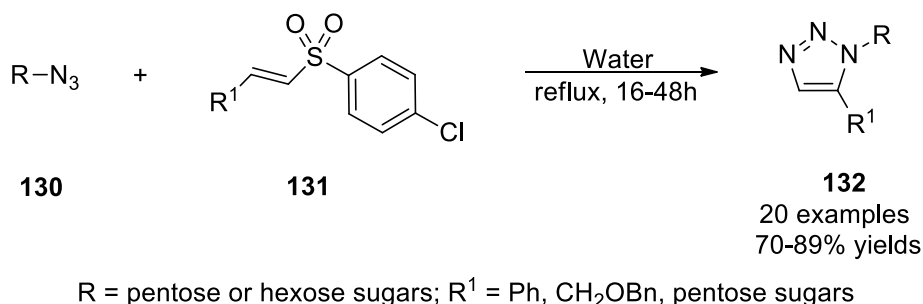
Scheme 33. Plausible mechanism of Er(OTf)₃-synthesis of 1,5-DTs in IL.

As for the metal-free synthesis of 1,5-DTs, the methodology developed by Zhang and co-workers in 2019 resulted interesting.⁶⁴ In this case, α -bromoacrolein (**128**) was chosen to give the desired cycloaddition product in the presence of various aryl and alkyl azides **127** in a mixture made up of DMSO and H₂O at room temperature (**Scheme 34**).



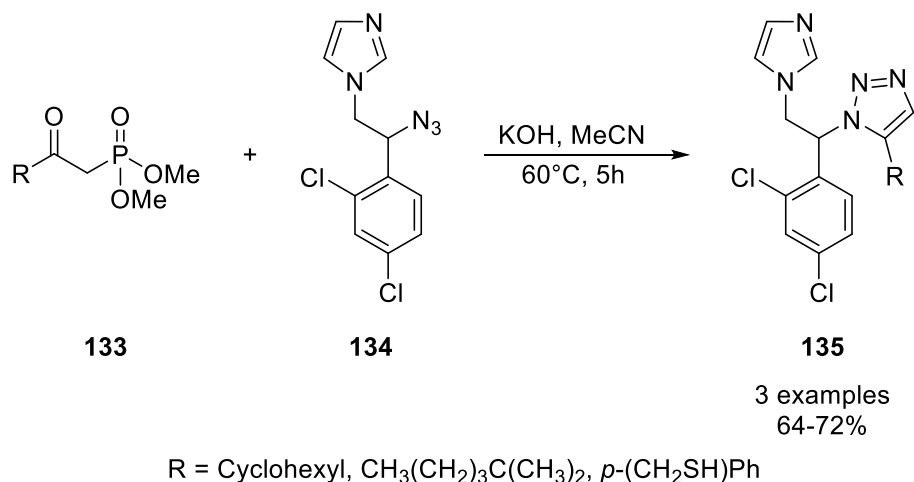
Scheme 34. α -bromoacrolein as dienophile for cycloaddition with azides.

In 2015, Kayet *et al.*⁶⁵ prepared 1,5-disubstituted 1,2,3-triazolylated monofuranosides and difuranosides in aqueous media. The reaction consisted of a 1,3-DPCA between vinyl sulfone derivatives (**131**) with four different azidofuranosides (**130**) (**Scheme 35**). The desired products were obtained in high yields (70-89%) by simply refluxing the reactants in aqueous media.



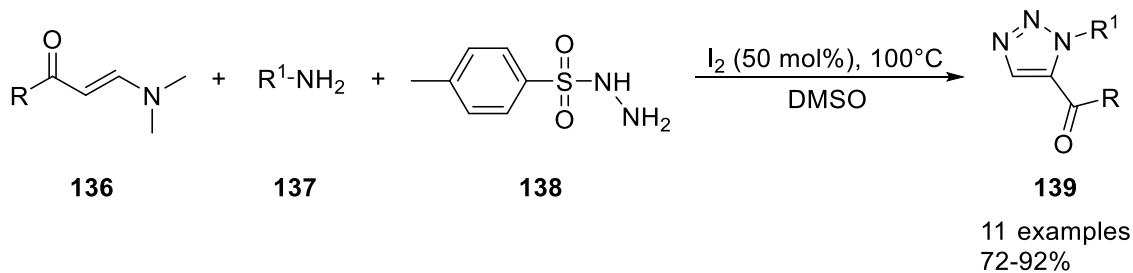
Scheme 35. Synthesis of 1,5-disubstituted 1,2,3-triazolylated monofuranosides and difuranosides **132**.

Successively, the same authors synthesized other 1,5-DTs derivatives bearing a disaccharide scaffold which were evaluated as inhibitors of the ribonuclease A.⁶⁶ Of note, by adding two carboxyl groups on the substrates the best inhibition degree was achieved, with an inhibition constant (K_i) of $65 \pm 3 \mu\text{M}$. González-Calderón *et al.*⁶⁷ proposed the metal-free synthesis of novel 1,5-DTs-containing miconazole analogs **135** as promising antifungal agents, obtained from the azide-enolate 1,3-DPCA (**Scheme 36**). The reaction can be considered as a base-assisted 1,3-DPCA performed in presence of potassium hydroxide and acetonitrile as a solvent. In this case, the base was needed to deprotonate the β -ketophosphonate **133** and generating *in situ* the dipolarophile.



Scheme 36. Synthesis of 1,5-DTs **135** as miconazole analogs.

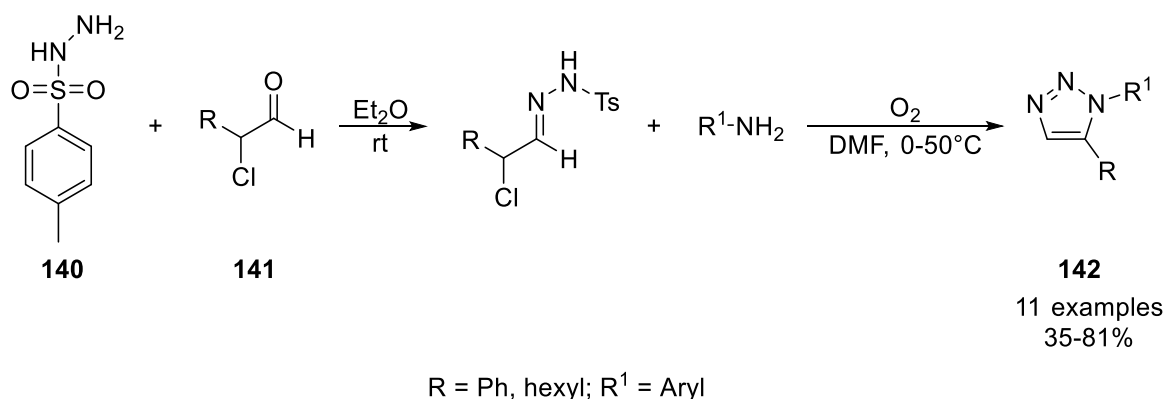
Wan and co-authors⁶⁸ proposed a metal- and azide-free regioselective reaction for the synthesis of 1,5-DT derivatives *via* a I_2 -assisted three-component reaction involving enamines **136**, tosylhydrazine **138** and primary amines **137** (**Scheme 37**).



R = Bn, 4-MeO-C₆H₄, 4-NO₂-C₆H₄, 4-Cl-C₆H₄, alkyl; R¹ = Ph, 2-furyl, 2-thienyl, 1-naphthyl, pyrazolyl

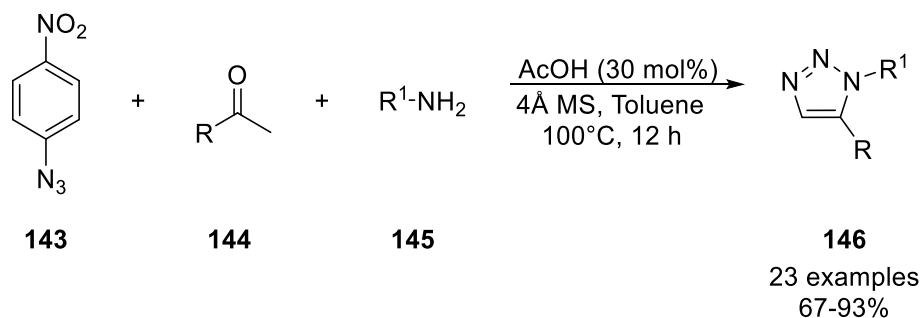
Scheme 37. Synthesis of 1,5-DTs **139** in metal- and azide-free conditions.

1,5-DTs **142** were also synthesized by Bai *et al.*⁶⁹, wherein an aerobic oxidative cycloaddition between α -chlorotosylhydrazones **141** and arylamines **140** was proposed (**Scheme 38**). Even in this case, it was possible to avoid the use of metals and azides, and the reaction outcome was unaffected by the chemical nature of the substituent groups.



Scheme 38. Regioselective synthesis of 1,5-DTs **142** via oxidative cycloaddition.

In 2016, Thomas and co-workers, starting from widely available reagents such as primary amines **145**, enolizable ketones **144**, and 4-nitrophenyl azide **143**, proposed a convenient procedure to access 1,5-DTs **146** in a multicomponent fashion.⁷⁰ The reaction resulted to be regioselective and was conducted in the presence of acetic acid as a catalyst (**Scheme 39**). All the products were obtained with good to high yields (67-93%).

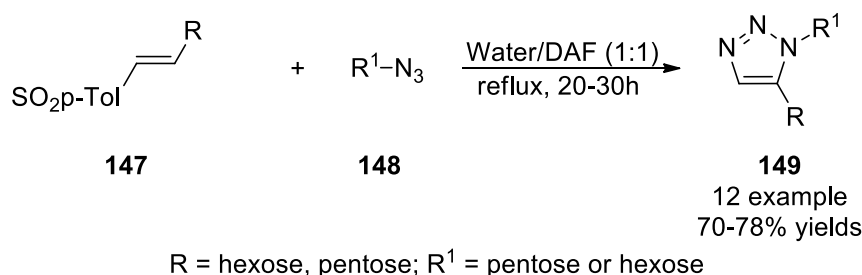


R = Aryl, heterocycles; R¹ = Aryl, allyl, alkyl

Scheme 39. Multicomponent reaction for synthesis of 1,5-DTs **146**.

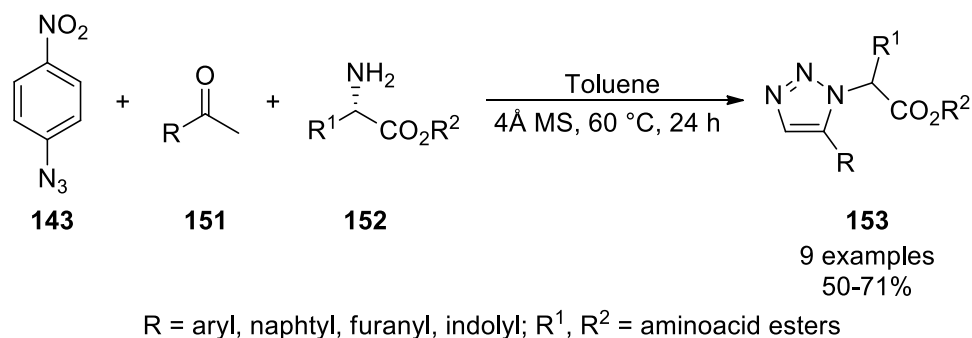
Kayet and Pathak⁷¹ synthesized a series of 1,5-disubstituted 1,2,3-triazolylmethylene-linked disaccharides (1,5-DTM) **149** in a biodegradable hydroxylammonium-based aqueous IL without the use of catalysts (**Scheme 40**). The products were obtained through a 1,3-DPCA between a series of vinyl sulfonylmethylene-modified pyranoses or furanoses **147** and a series of sugar azides **148**. The same authors used the so-reported procedure to synthesize a 1,5-DTM-linked disaccharide which displayed a potential inhibitory activity towards the ribonuclease A.⁶⁶ In this case, the additional methylene bridge between the 1,5-DT ring and the sugar moiety may play a role in increasing the conformational flexibility of the final product. *N,N*-dimethylethanolammoniumformate (DAF) and water were used to conduct the reaction at reflux. In comparison to the same reaction carried out in traditional

solvents, the mixture of IL and water significantly decreased the reaction time and improved the purity of the crude.



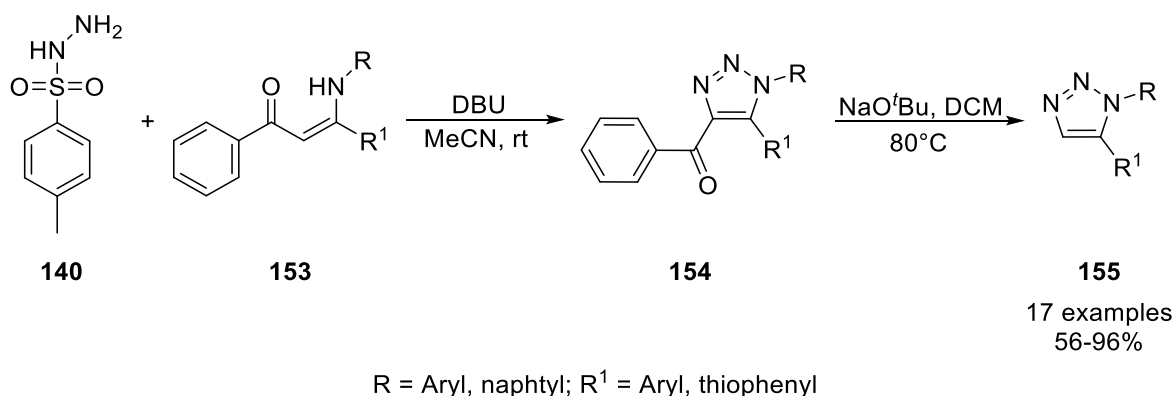
Scheme 40. Synthesis of 1,5-DTM-linked disaccharides **149**.

In 2018, the synthesis of 1,5-DTs **153** was proposed by Silveir-Dorta and colleagues.⁷² Such a synthesis involved amino esters **152** and commercially available enolizable ketones **151** in presence of **143** (**Scheme 41**). The experimental outcome showed that the reaction is not influenced by whether the ketones were electron-rich or electron-deficient. The products were produced in all cases with the retention of the chiral center and with high yields.



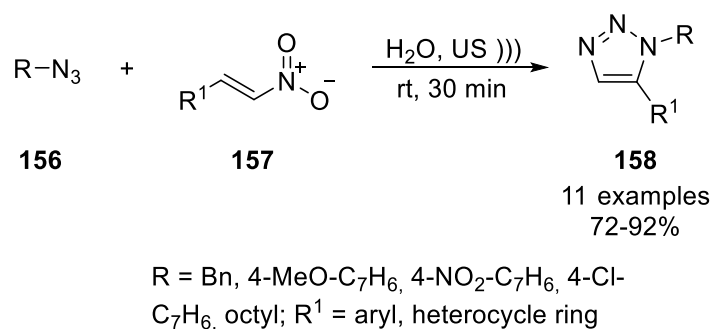
Scheme 41. Metal-free enantioselective synthesis of 1,5-DTs **153**.

Zhang *et al.*⁷³ proposed a regioselective, base-promoted synthesis using trisubstituted 1,2,3-triazoles **154** as the starting point for a C-C bond cleavage reaction. More thoroughly, under alkaline conditions from DBU, enaminones **153** reacted with tosyl azide **140** to produce trisubstituted 1,2,3-triazoles **154** that, if treated with NaOtBu, gave the desired compound (**Scheme 42**).



Scheme 42. Regiospecific synthesis of 1,5-DTs **155** through a C-C bond cleavage on 1,4,5-trisubstituted 1,2,3-triazoles **154**.

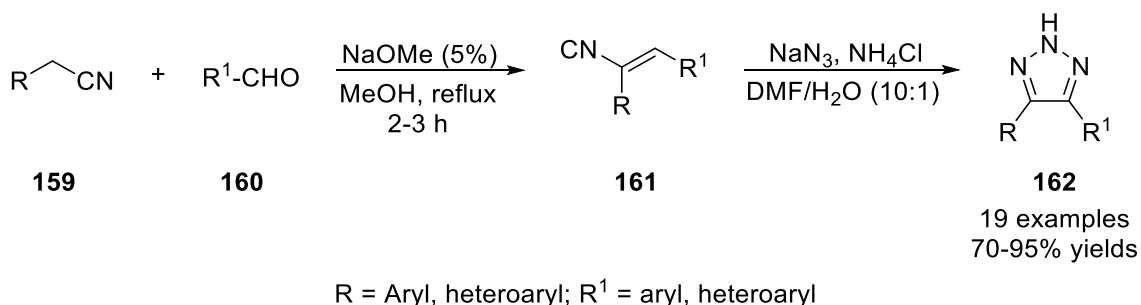
More recently, Kiranmye and co-workers⁷⁴ published the synthesis of 1,5-DTs **158** in an aqueous medium under ultrasound-assisted conditions. The synthetic route was simple and consisted of the eliminative 1,3-DPCA of azides **156** with nitroolefins **157** (**Scheme 43**). Such an approach exhibited high substrate versatility, short reaction times, simple work-up procedures, high regioselectivity, and good scalability.



Scheme 43. Synthesis of 1,5-DTs **158** via catalyst-free eliminative 1,3-DPCA.

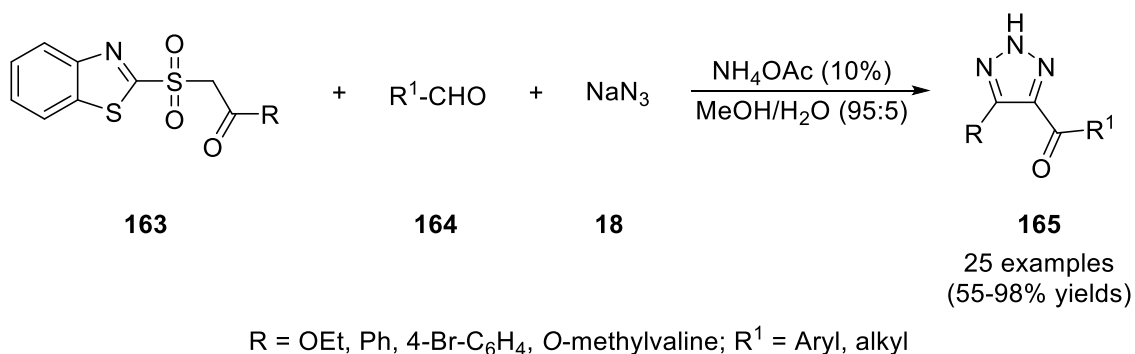
2.3 Catalytic synthesis of 4,5 DTs

4,5-DTs can be considered the direct precursors of 2-substituted 1,2,3-triazoles, an interesting scaffold from a biological perspective. For instance, 1,2,3-triazole moieties disubstituted at the C-4 and C-5 positions recently demonstrated to behave as analogous to combretastatin A-4, an anti-mitotic agent **162**.⁷⁵ In this case, the key intermediate was a (*Z*)-2,3-diarylacrylonitrile derivative **159** which, in the presence of NaN₃, gave the targeted 4,5-DTs **162** (**Scheme 44**). Among the prepared compounds, the ones structurally like combretastatin A-4 showed better anticancer activity after being tested on different human cell lines.



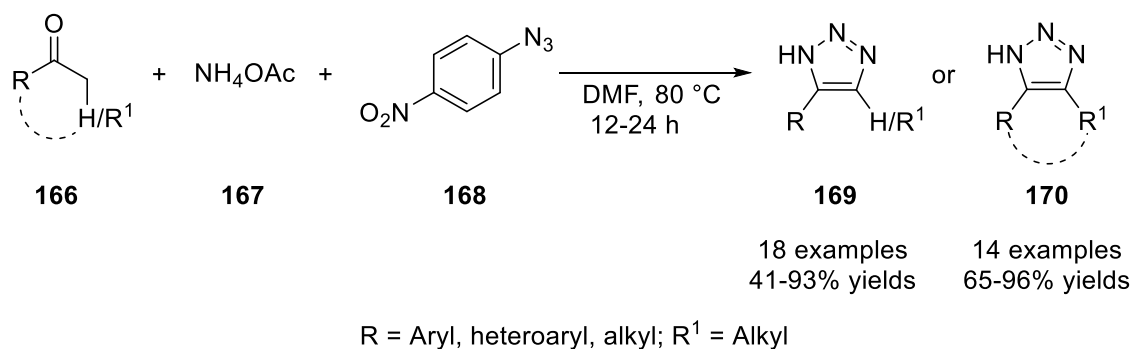
Scheme 44. Synthesis of 4,5-DTs analogs of combretastatin A-4.

Chai and collaborators suggested an alternative process in which ammonium salts were used as catalysts. In this case, benzothiazol-2-yl sulfones (Julia reagents) were proposed as precursors for vinyl sulfones **163** in a three-component reaction with aldehydes **164** and sodium azide **18**, under mild reaction conditions. Such an approach showed a wide applicability, working well with aryl or alkyl aldehydes as well as esters, ketones, and amides.⁷⁶



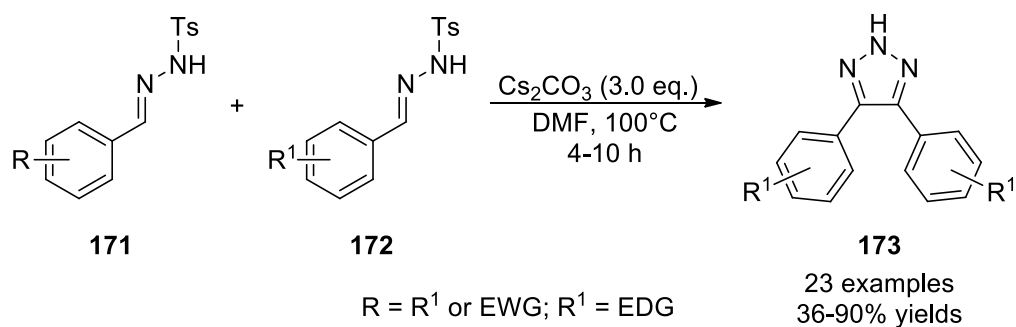
Scheme 45. Synthesis of 4,5-DTs using Julia reagents.

Thomas *et al.*⁷⁷ used enolizable cyclic ketones in a one-pot manner to form 4,5-fused *NH*-triazoles **169** and **170** (**Scheme 46**). In doing so, it resulted easy to access 4,5-fused, mono- and disubstituted *NH*-triazoles with potential biological activity by employing readily available commercial ketones. Even in this case, high functional group tolerance and regioselectivity was observed.



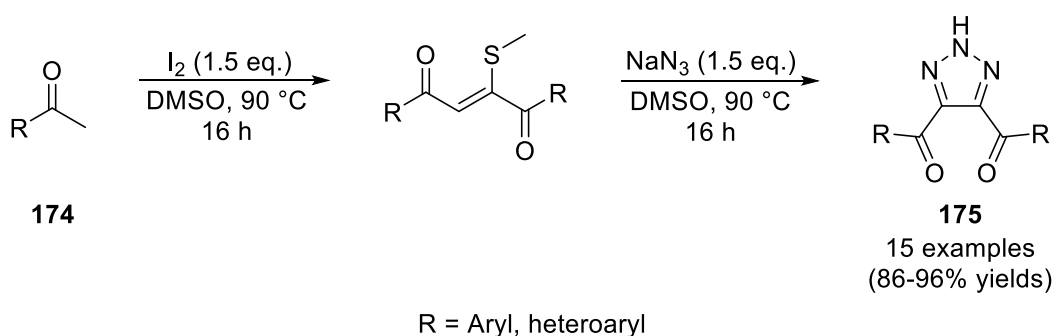
Scheme 46. Synthesis of *NH*-triazoles.

As for the azide-free synthesis of 4,5-DTs, to the best of our knowledge only one example is reported in the literature. In this case, Panda and co-workers exploited the amphiphilic nature of *N*-tosylhydrazones **171** and **172** to perform, in mild alkaline conditions, a regioselective [3+2] cyclization (**Scheme 47**). It is worth noting that higher reaction times and lower yields were obtained with electron-rich aryl hydrazones.⁷⁸



Scheme 47. Synthesis of 4,5-DTs in the presence of *N*-tosylhydrazones.

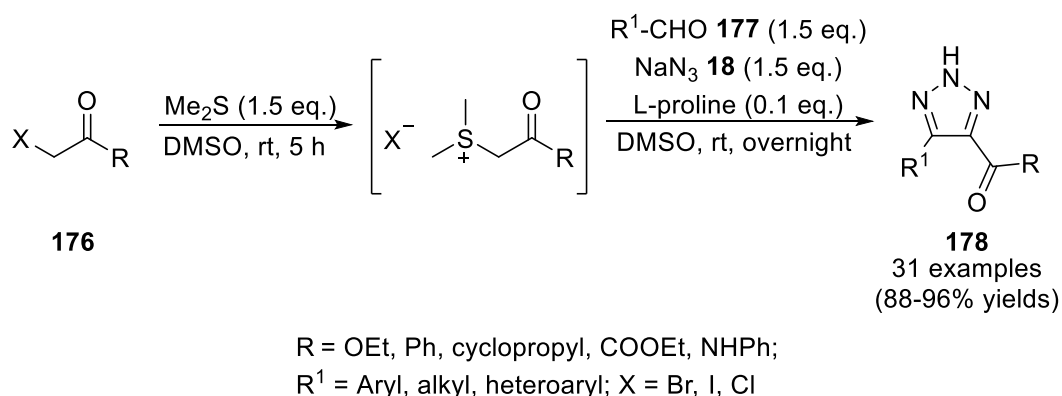
As seen so far, various starting materials were used along with ammonium salts as catalysts to obtain *N*-unsubstituted 1,2,3-triazoles. More recently, Swarup and collaborators⁷⁹ investigated a different strategy by forming 2-methylthio 1,4-enediones from ketones **174** at 90 °C, in the presence of I₂ and DMSO as the source of the thio-functionality (**Scheme 47**). By using this approach, symmetrical 4,5-DTs **175** were obtained in good yields.



Scheme 48. Preparation of *N*-unsubstituted 1,2,3-triazoles **175** from 2-methylthio 1,4-enediones **174**.

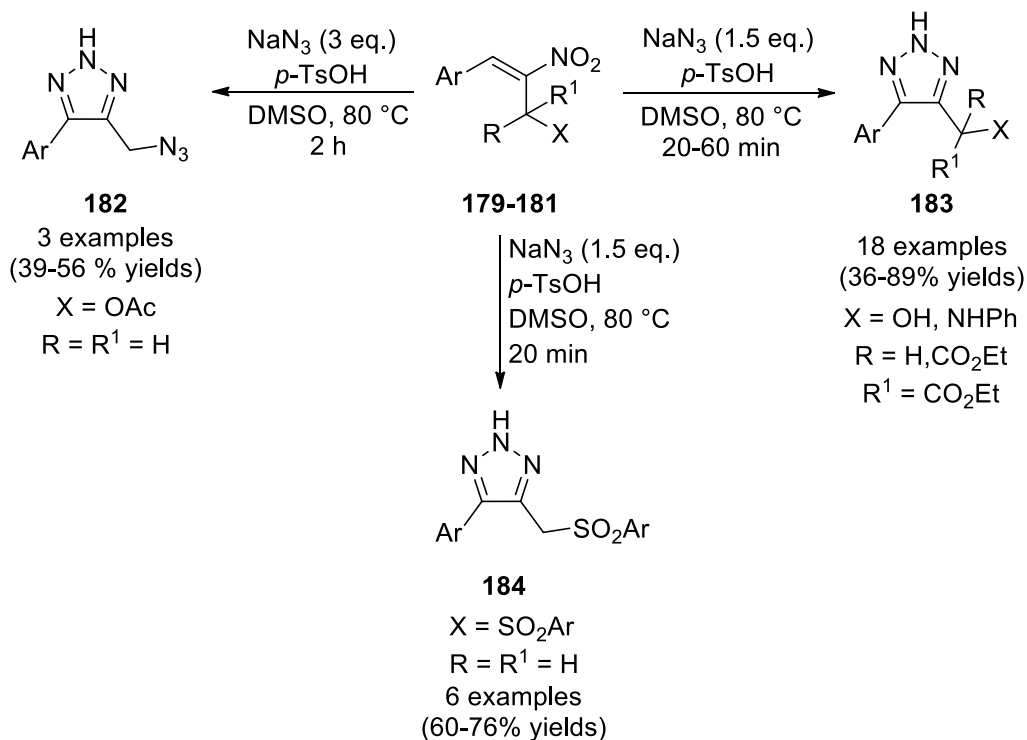
Wu G.-L. exploited the presence of an electron-deficient double bond in olefinic sulfur salts to synthesize 4,5-DTs with a [3+2] cycloadditive approach in 2017 (**Scheme 49**).⁸⁰ In this study, α -haloacetate **176** was transformed in the appropriate sulfur salt and then reacted with benzaldehyde **177** in the presence of L-proline to give the desired products **178** in high yields (95%). In the same conditions, additional small organic compounds such as morpholine (91%), piperidine (93%), and various amino

acids were investigated. This process showed also good tolerance for different organohalides, in addition to aldehyde as starting reagents.



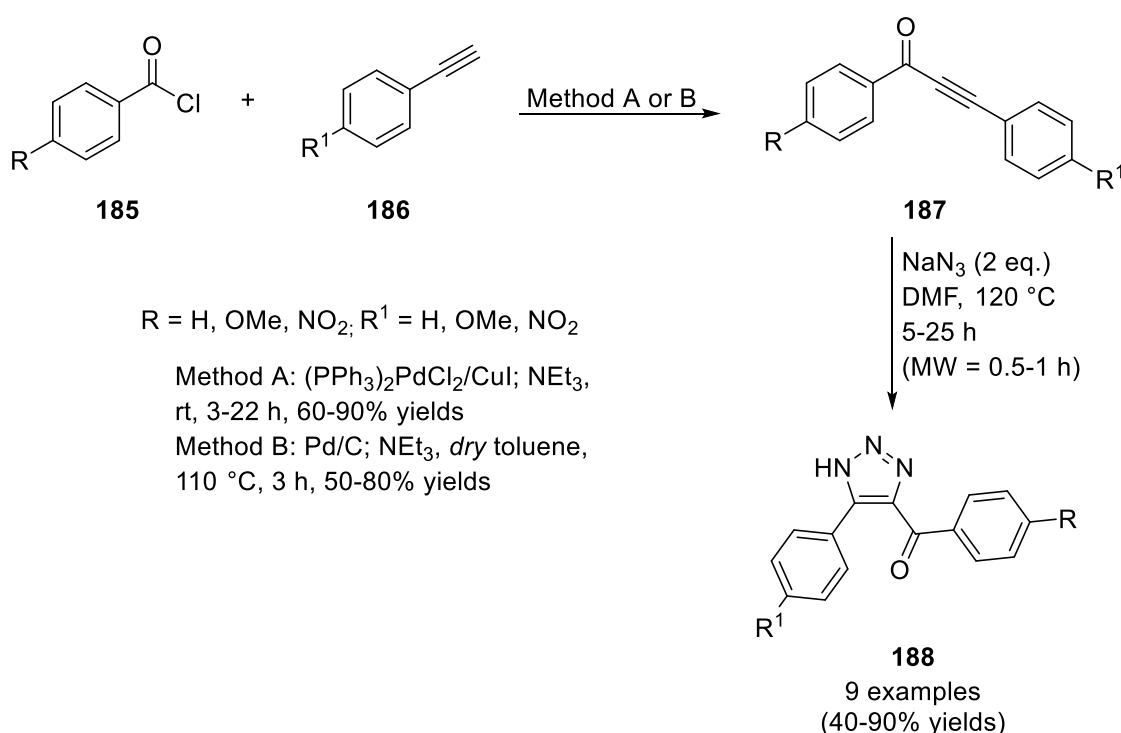
Scheme 49. Synthesis of 4,5-DTs using sulfur salts as intermediates.

The use of nitroalkenes was widely investigated for the preparation of *NH*-1,2,3-triazoles.^{81,82} Reddy *et al.* focused on readily available α -functionalized nitroolefins for the acid-assisted synthesis of 4,5-DTs. To form 4,5-DTs **182**, **183**, and **184**, respectively, the optimal reaction conditions were established by using *p*-toluenesulfonic acid in stoichiometric amounts with nitroallylic acetates **179** or nitroallylic alcohols **180** and nitroallylic sulfones **181** in the presence of sodium azide **18** (**Scheme 50**). The authors proposed also a mechanism in which the additional acid activated the nitro group *via* an *H*-bond, facilitating the leaving of HNO₂.⁸³



Scheme 50. Acid-assisted synthesis of 4,5-DTs.

Lastly, Rocha *et al.*⁷⁹ reported the preparation of 4,5-DTs in DMF at 110 °C, starting from 1,3-diarylprop-2-yn-1-ones **187**, previously obtained by a Sonogashira cross-coupling reaction of aryl chlorides **185** with aryl acetylenes **186** (**Scheme 51**). Nine different alkynes **187** were obtained working both in homogenous phase using [(PPh₃)₂PdCl₂/CuI] as the catalyst at room temperature or in heterogeneous phase with (Pd/C) at 110 °C. Finally, the 1,3-diarylprop-2-yn-1-ones **187** reacted with sodium azide **18** to give *NH*-1,2,3-triazoles **188** under conventional heating. In some cases, microwave assistance improved the outcomes allowing shorter reaction times and better yields.



Scheme 51. Two-step procedure for the synthesis of 4,5-DTs.

Results and Discussion

Research line 1a - Pyrimidine nucleobase-containing 1,5-disubstituted 1,2,3-triazoles: synthesis and molecular docking studies

As for the topic of this Chapter, we decided to follow an already existent research line of the laboratory that hosted this Ph.D. project for the synthesis of 1,5-DTs with an eye to their use in biological contexts. The principal objective of this research topic was to propose a rapid, clickable procedure to synthesize 1,5-DTs bearing a pyrimidine nucleobase moiety. The results herein reported were published in *Molecules* in 2022 (see **Annex II** for the details). At the root of this choice, there was the notable biological activity displayed by natural and modified nucleosides, both as therapeutics^{84,85} or as diagnostic probes.⁸⁶ Such compounds can be considered to be part of the class of “nucleoside analogs”: in our case, the triazole group replaced the sugar moiety of a natural nucleoside, but other examples in which the triazole scaffold replaces the nucleobase⁸⁷ or acts as linker⁸⁸ are common (**Figure 9**).

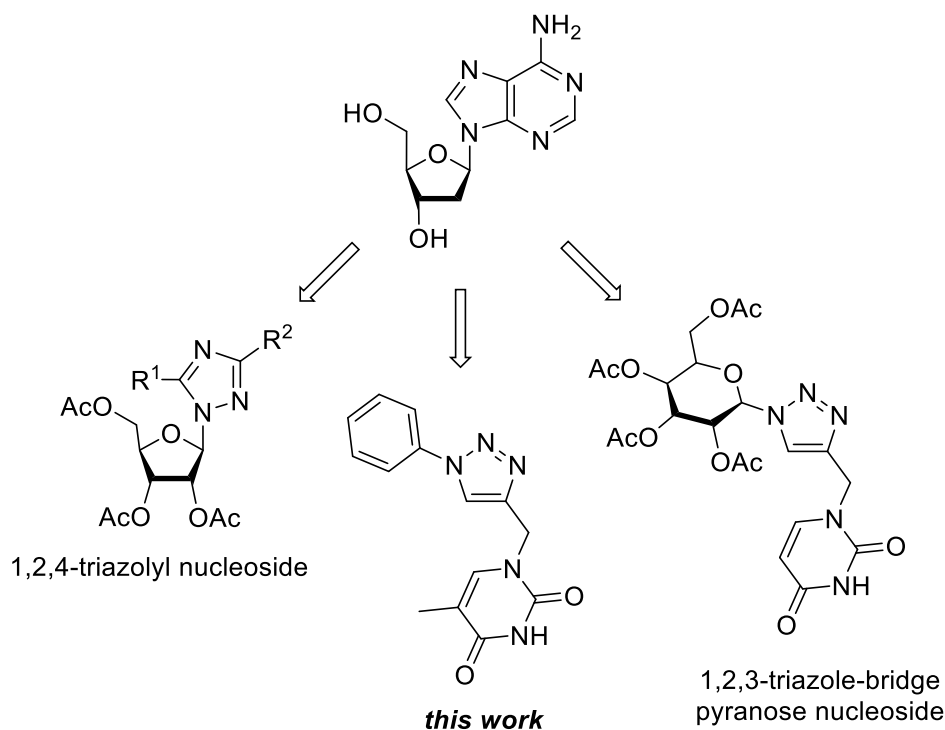
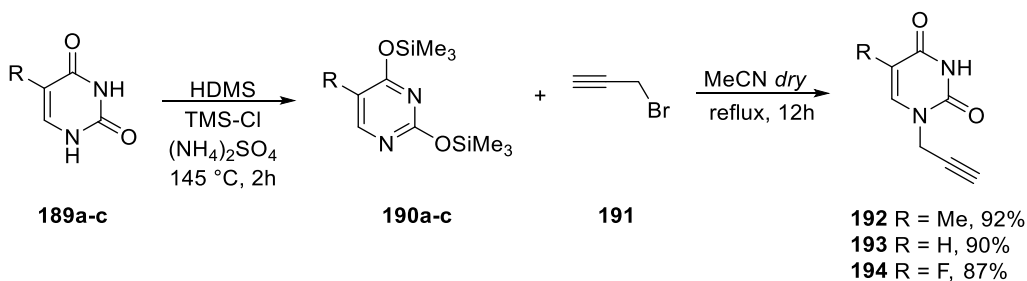


Figure 9. Some representative examples where a triazole scaffold was employed in place of a nucleobase, of a sugar (this work), or as the linker in constructing new nucleoside derivatives.

To date, the use of a 1,2,3-triazole core in place of the sugar moiety has been mainly deepened towards the synthesis of 1,4-DTs. In this regard, the most representative

examples were proposed by the Santillan group in 2013, where a series of purine and pyrimidine-containing 1,2,3-triazoles has been synthesized and successfully evaluated against steel acid corrosion.^{89,90} Nonetheless, Elayadi *et al.*⁹¹ developed a synthetic protocol aimed to obtain novel uracil-containing 1,4-DTs nucleoside analogs that showed promising antiviral activity against the H3N2 subtype of influenza A. On the other hand, we noticed a lack of synthetic efforts in proposing new routes to access nucleobase-containing 1,5-DTs derivatives. Hence, in this project, we exploited the experience of the hosting lab in triazole synthesis^{60,61,92} to perform the synthesis of the target compounds through the 1,3-DPCA reaction between propargyl pyrimidine derivatives and phenyl azide. To obtain the desired dipolarophiles, we commenced our study by finding the best procedure to obtain *N*1-propargyl nucleobases with high selectivity. In the literature were available a one-step reaction protocol⁹³ or a procedure in which a bis(trimethylsilyl)pyrimidine nucleobase intermediate was formed using *N,O*-bis(trimethylsilyl)-acetamide (BSA).⁹⁴ None of the referenced procedures were suitable for our scopes given that the first yielded the products with low selectivity, while the second gave a non-neglectable decrease in yield. Hence, inspired by a two-reaction step protocol optimized in the hosting lab,⁹⁵ we decided to use an *O*-protection with a transient group (**Scheme 52**). In this frame, the starting nucleobase **189a-c** was treated under N₂ with hexamethyldisilazane (HDMS), trimethylsilyl chloride (TMS-Cl), and (NH₄)₂SO₄ yielding the silylated intermediates **190**. Then, without any further purification, the crude was evaporated and used for the subsequent *in situ* propargylation with propargyl bromide **191**, giving the desired products **192-194** in very high yields and excellent selectivity.

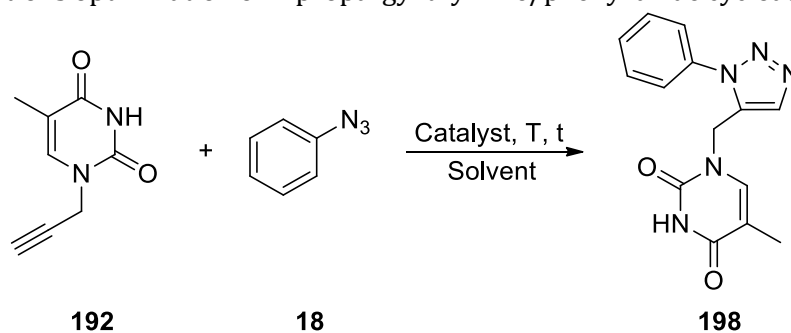


Scheme 52. Synthesis of *N*1-propargyl pyrimidine nucleobases.

Hence, the 1,3-DPCA reaction between the so-far obtained propargyl derivatives **192-194** and phenyl azide **18** was optimized. 1-propargyl thymine **192** was selected to optimize the reaction conditions, in the presence of a series of Lewis acid catalysts chosen from our experience. As reported in **Table 1**, the first attempts (entries 1 and

2) were performed using $\text{Er}(\text{OTf})_3$ 20 mol%, the propargyl nucleobase and phenyl azide in a 1:2 ratio in CH_2Cl_2 or THF as solvents at 60 °C. Even after 24 h, no product was observed. By increasing the temperature to 100 °C, it was possible to isolate the desired products with a 15% yield (entry 3). For this reason, MeCN and MeNO₂ were tested at 100 °C and 120 °C, respectively, obtaining yields comprised between 30% and 50% (entry 4-6) after 24 h. The use of DMF and $\text{Er}(\text{OTf})_3$ was determinant to improve the reaction conditions so far obtained, providing the desired product with 75% yield and drastically reducing the reaction time from 24 to 8 h (entry 7). Then, a series of Lewis acids were screened in combination with DMF (entry 8-11), obtaining further improvements with FeCl_3 , giving the desired triazole in 8 h and 88% yield in a regioselective fashion. We also tested the same reaction conditions without any Lewis acid, obtaining a mixture of 1,5 and 1,4 regioisomers after 24 h (70:30 ratio, respectively): such evidence proved not only the catalytic efficacy of FeCl_3 but also its role in the regioselectivity of the reaction. A similar result was obtained when toluene was evaluated as the reaction media (entry 13), obtaining a slight improving in terms of yield but not in regioselectivity in the presence of FeCl_3 20 mol% (entry 14). Finally, [mPy](OTf)/IL was screened as a solvent, aiming at the recyclability of the whole catalytic and reaction media. However, such conditions were incompatible with 1-propargyl thymine due to its particularly high solubility in the IL solvent, which made impossible the recover by liquid-liquid extraction.

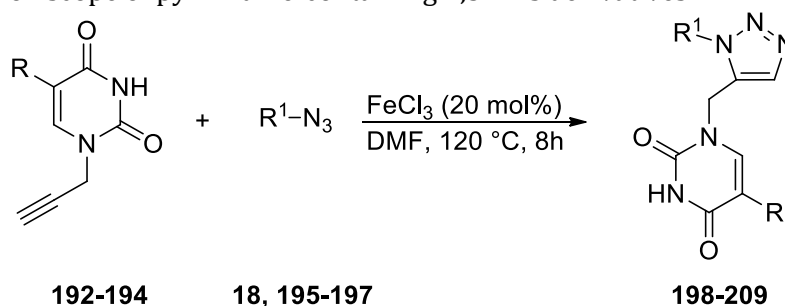
Once found the proper reaction conditions, the scope was tested over various azides **18** and **195-197** and propargyl nucleobases **192-194** (Table 2). As reported, all the *N*1-propargyl nucleobases **192-194** showed high reactivity in Fe (III)-catalyzed conditions, affording high yields in good times. On the other hand, the reactivity of azides **195-197** was influenced by the nature of the substituent group: this is the case of benzyl azide (entries 4-6), which gave lower yields if compared with phenyl azide **18** (entries 1-3). Similarly, the presence of an EWG as the nitro group reduced the nucleophilicity of the dipole (entries 7-9), whilst an EDG as the methoxy group in the same position resulted to be more prone to react (entries 10-12). Nonetheless, in all cases the reaction yields and the regioselectivity towards the 1,5-disubstituted product were excellent.

Table 1. Conditions optimization of 1-propargyl thymine/phenyl azide cycloaddition reaction.

Entry ^a	Solvent	Catalyst	T (°C)	Time (h)	Yield (%) ^b
1	CH ₂ Cl ₂	Er(OTf) ₃	60	24	-
2	THF	Er(OTf) ₃	60	24	-
3	THF	Er(OTf) ₃	100	24	15
4	CH ₃ CN	Er(OTf) ₃	100	24	30
5	CH ₃ CN	Er(OTf) ₃	120	24	53
6	CH ₃ NO ₂	Er(OTf) ₃	120	24	50
7	DMF	Er(OTf) ₃	120	8	75
8	DMF	Yb(OTf) ₃	120	24	70
9	DMF	ZnCl ₂	120	24	71
10	DMF	CeCl ₃	120	24	72
11	DMF	FeCl ₃	120	8	88
12	DMF	-	120	24	56
13	Toluene	-	120	24	40
14	Toluene	FeCl ₃	120	24	48
15	[mPy](OTf)	FeCl ₃	120	24	-

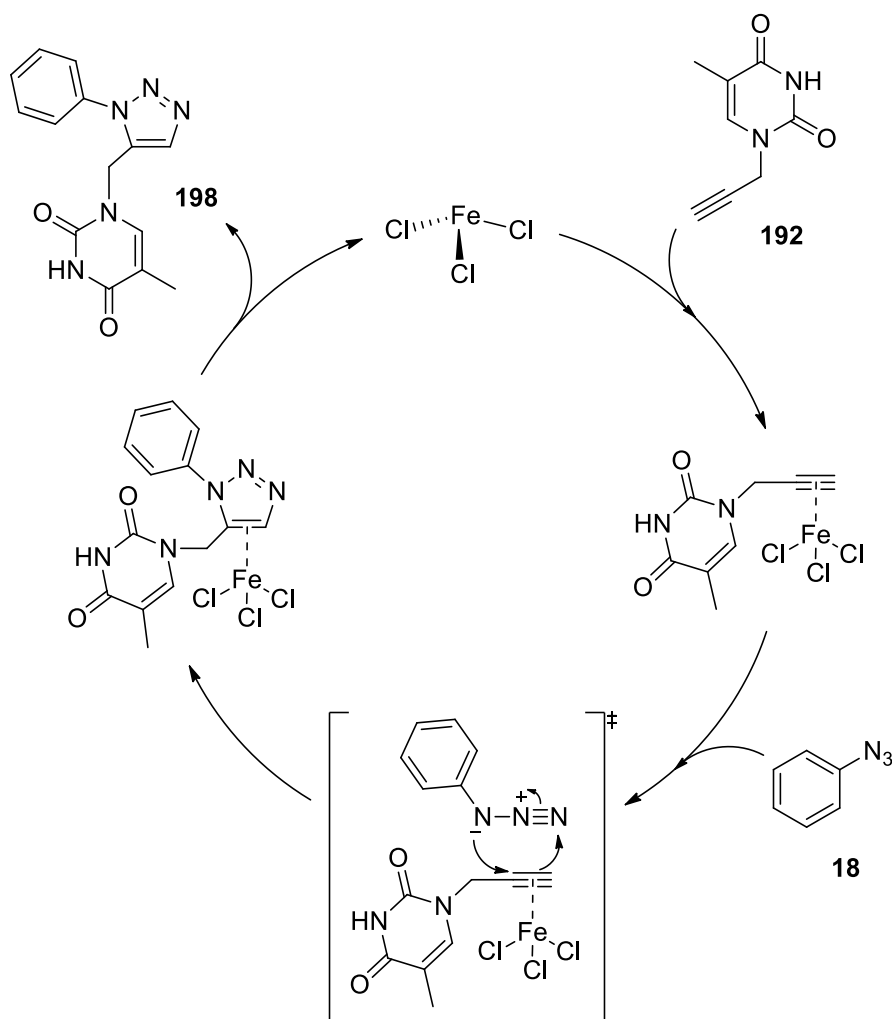
^aReaction conditions: 1-propargyl thymine (1 eq.), catalyst (0.2 eq.), phenyl azide (2 eq.), in DMF for appropriate time. ^bIsolated yield.

As for the plausible mechanism, in **Scheme 53** we reported the role exerted by the catalyst in activating the dipolarophile. In this regard, Fe (III) salt directs the coordination towards the propargyl group of nucleobase derivative. Then, the so-formed complex gives the 1,3-DPCA reaction with the azide reactant. Then, the obtained intermediate evolves to the final product regenerating the catalyst.

Table 2. Reaction scope of pyrimidine-containing 1,5-DTs derivatives.

Entry ^a	R	Nucleobase	R ¹	Azide	Product	Yield (%) ^b
1	CH ₃	192	Ph	18	198	88
2	H	193	Ph	18	199	90
3	F	194	Ph	18	200	88
4	CH ₃	192	Bn	195	201	85
5	H	193	Bn	195	202	87
6	F	194	Bn	195	203	84
7	CH ₃	192	(4-NO ₂)Ph	196	204	83
8	H	193	(4-NO ₂)Ph	196	205	86
9	F	194	(4-NO ₂)Ph	196	206	82
10	CH ₃	192	(4-CH ₃ O)Ph	197	207	90
11	H	193	(4-CH ₃ O)Ph	197	208	92
12	F	194	(4-CH ₃ O)Ph	197	209	89

^aReaction conditions: N1-nucleobase **49-51** (1 eq.), FeCl₃ (0.2 eq.), azide **52-55** (2 eq.), in DMF for appropriate time. ^bIsolated yield.



Scheme 53. Plausible catalytic mechanism.

Lastly, a preliminary investigation on the potential biological activity of our products was performed for the full set of the above-reported compounds over 16 targets using GOLD (CCDC Discovery) and the ChemScore scoring function to perform a molecular docking study. The work was carried out in the Computational Chemistry Group (CompChem) of the CIC bioGUNE (Derio, Spain) headed by Dr. Gonzalo Jiménez Osés as part of the abroad research stay of this Ph.D. thesis. The targets were chosen for being at the center of great attention in the last years due to their implication in different pathologies. Human norovirus is one of the major causes of nonbacterial gastroenteritis in humans and targets the protruding P domain dimer (P-dimer) of a GII. Norovirus strain (**Figure 11, A**) could be a successful strategy in drug discovery. Eosinophil-derived neurotoxin (EDN) (**Figure 11, B**) is a member of the Ribonuclease A (RNase A) superfamily involved in inflammatory disorders and in the immune response system. Metallo β -lactamase (**Figure 11, C**) is a family of enzymes employed by bacteria to hydrolyze β -lactam drugs as carbapenems, determining the resistance

to antibiotics. Hence, the discovery of new inhibitors capable of blocking such receptors could be of interest in combating bacterial infective diseases. As for the target reported in **Figure 11, D**, SARS-CoV-2 NSP13 helicase are potential targets for new antivirals due to its essential role in viral replication and its high sequence conservation. Compounds **204** and **205** resulted to be the best-ranked ones, matching, or exceeding in some cases, the score of the co-crystallized ligand in the original structure, suggesting that these compounds might be able to bind the selected targets. Binding interactions mostly involve hydrogen bonds with charged residues, or with the protein backbone.

Receptor	Best scores												
	Ligand	198	199	200	201	202	203	204	205	206	207	208	209
SET Domain Bifurcated Protein 1	31.0	28.6	28.5	28.3	28.3	27.9	28.5	25.4	25.4	24.9	28.8	26.9	27.5
Human Norovirus Capsid Protein	21.3	20.3	19.3	19.4	19.6	21.0	18.3	21.6	21.7	20.5	20.6	20.3	20.0
Eosinophil-derived Neurotoxin	16.7	23.7	22.2	21.5	23.7	23.1	22.8	26.8	26.1	25.4	24.1	22.4	22.3
p38 Mitogen-Activated Protein Kinase	28.6	28.5	26.2	27.0	24.7	24.5	22.5	24.7	23.6	23.1	24.7	23.9	23.2
Metallo- β -lactamase	34.5	35.3	34.3	32.6	34.8	34.0	32.8	36.6	36.7	35.2	33.9	35.3	34.0
Human Protein Kinase CK2	26.4	23.0	20.6	19.8	23.4	20.8	19.4	21.0	23.1	21.5	22.2	22.1	20.8
SARS-CoV-2 NSP13 Helicase	22.1	21.7	21.2	18.9	18.3	18.4	18.1	21.3	22.3	21.1	19.6	21.7	18.1

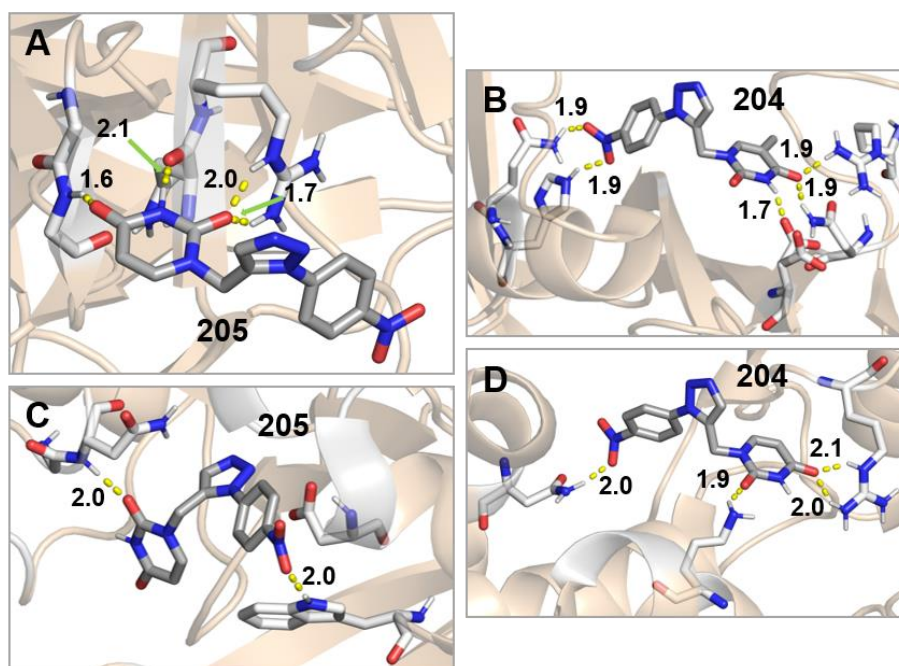
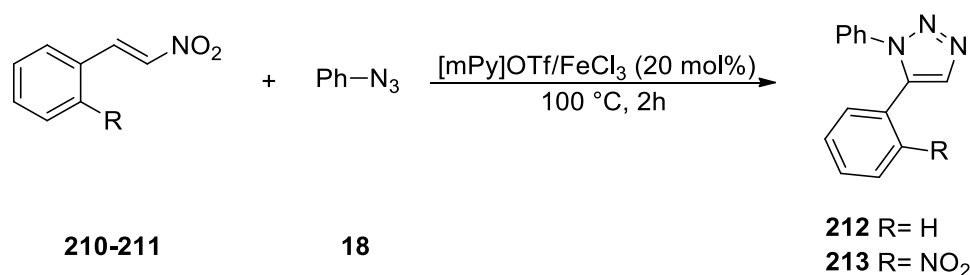


Figure 10. Docking score and docking poses (A-D) of the synthesized compounds. Only the analysis with a RMSD values minor than 1.5 Å for the natural ligand docking pose simulation were reported.

Research line 1b – 1,5-DTs as mitochondrial Ca^{2+} -activated F_1F_0 -ATP(hydrol)ase: synthesis and *in vitro* studies.

The present research has been developed following a previous pipeline in which a series of 1,5-DTs were obtained implementing an IL/Fe (III)-based synthetic protocol. In this regard, an introduction to this methodology will be done, followed by a description of the biological targets and the experimental results obtained. The results herein reported were published in *Annals of the New York Academy of Sciences* in 2021 and in *Pharmacological Research* in 2023 (see **Annex II** for the details).

Two compounds (**212** and **213**) were at the center of a series of biochemical and cellular studies to regulate the activity of the mitochondrial Ca^{2+} -activated F_1F_0 -ATP(hydrol)ase. Such compounds were obtained following an optimized protocol (**Scheme 54**) developed by the hosting laboratory in collaboration with the University of Zaragoza in 2018 (see **Experimental Section**).⁶⁰



Scheme 54. Synthesis of 1,5-DTs as mitochondrial Ca^{2+} -activated F_1F_0 -ATP synthase inhibitors.

The role of Fe (III) salt and the regioselectivity were thoroughly deepened with the help of DFT (**Figure 10**): as expected, the catalyst acted as the Lewis acid, coordinating the oxygen atom of the nitro group of an ω -nitrostyrene. Such an interaction stabilized the reacting dipolarophile, contributing to lowering the upcoming rate-determining step (cycloaddition step) by 5.7 kcal/mol.

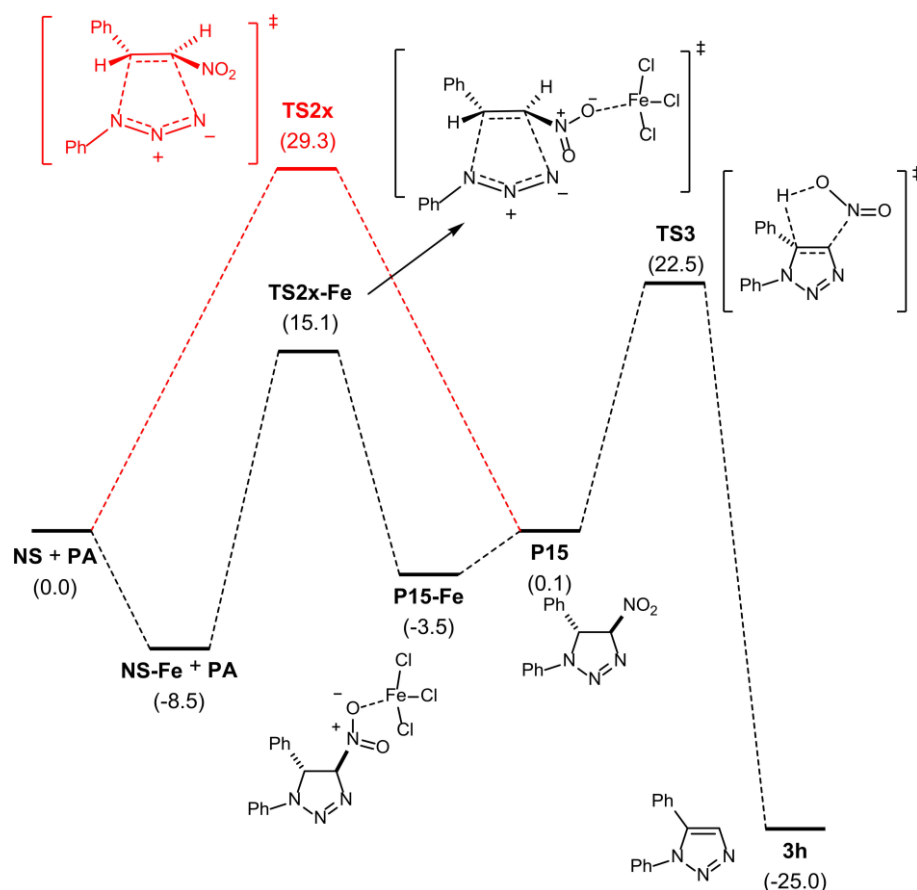


Figure 10. Reaction pathway for the iron (III)-catalyzed synthesis of 1,5-DTs calculated with PCM/B3LYP-D3BJ/Def2SVP. Adapted from De Nino *et al.*⁶⁰

Compounds **212** and **213** were evaluated over the above-cited biological target to control the mitochondrial permeability transition pore (mPTP) opening. Such a biological event is a hot topic in biochemistry for a series of reasons. mPTP is an alteration of the inner membrane of mitochondria (IMM), whose formation is a consequence of several physiopathological conditions associated with brain injury, stroke, cancer, etc. As firstly described in 1979,⁹⁶ once mPTP is formed, IMM permeability is dramatically reduced, leading to the rapid loss of the mitochondrial membrane potential ($\Delta\Psi_{mt}$) and of adenosine triphosphate (ATP). The consequential osmotic shock brings the rupture of the outer mitochondrial membrane (OMM), resulting in necrosis.⁹⁷ The study of such phenomenon became of interest for its pharmacological relevance, particularly since 1990 when it has been shown its strategic importance as a cell death regulator.⁹⁸ In this regard, interested readers can refer to these review papers, in which the state-of-the-art of knowledge about mPTP formation is contextualized in the frame of brain damage,⁹⁹ heart diseases,¹⁰⁰ and cancer.¹⁰¹ Noteworthy, important evidence related the mPTP formation to the fate of the membrane enzyme F_1F_0 -ATP synthase. Although this exact mechanism is under

investigation, the discovery of new small molecules capable of regulating such biological events is of high interest. On the other hand, it is possible to argue that a modest number of compounds have been proposed in the last years, and even fewer studies on the mechanism of regulation were conducted.¹⁰² To date, the most potent compounds towards this target were identified thanks to high-throughput screening (HTS) studies. Such an approach allowed researchers to identify some cinnamic anilides derivatives as potent mPTP regulators.¹⁰³

In the frame of this Ph.D. thesis, inspired by the growing number of studies proving the biological relationship between mPTP opening and F_1F_0 -ATP synthase, we collaborated with the Nesci group from the University of Bologna to biochemically evaluate some of our substrates. As previously said, compounds **212** and **213** resulted to be active in counteracting the opening of mPTP. Such activity was deepened through a preliminary study published in 2020 by the *Annals of the New York Academy of Sciences*.¹⁰⁴ In this work, we proved that our 1,5-DTs were capable of inhibiting only the Ca^{2+} -activated enzyme but not the Mg^{2+} -containing isoform, a factor of particular importance given that the inhibition of the latter would block the hydrolysis of ATP, hence the cellular metabolism. In our study, the inhibition resulted to be mutually exclusive and uncompetitive for the ATP natural ligand because the inhibition took place only when the complex Ca^{2+} -ATPase-ATP was formed. The mutual exclusion, on the other hand, was attributed to a shared enzyme site. The study was subdivided into three main sections: evaluation of the mitochondrial bioenergetics, preliminary studies on the mechanisms of inhibition, and mPTP sensitivity in presence of both inhibitors. As for the mitochondrial bioenergetics, the objective of these experiments was to assess the effect exerted by **212** and **213** on the mitochondrial respiration in NADH- and succinate-energized mitochondria with the titration method on both enzyme isoforms. As anticipated, both compounds did not affect the respiratory chain activity for the Mg^{2+} -activated enzyme but only for the Ca^{2+} -containing enzyme (**Figure 11**).

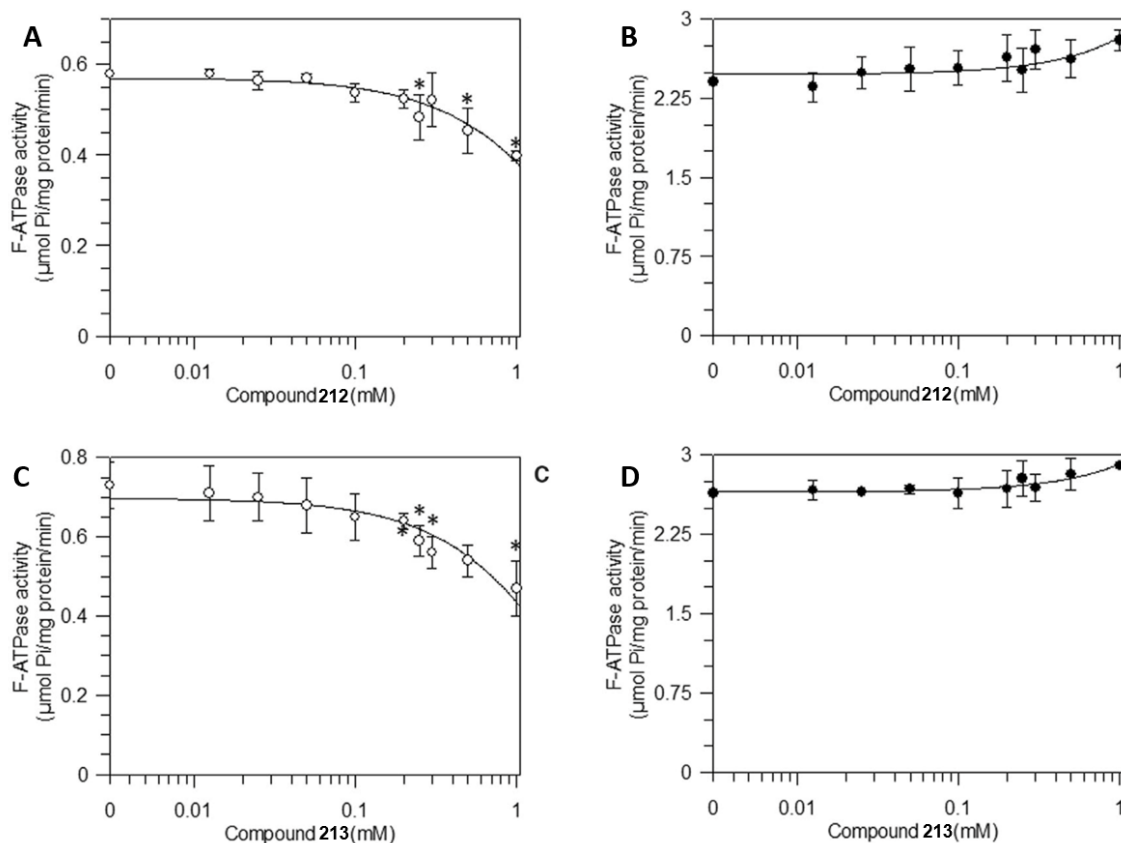


Figure 11. Effect of 1,5-DTs derivatives **212** and **213** on mitochondrial Ca²⁺ and Mg²⁺-activated F₁F₀-ATPase activity. Ca²⁺-activated F₁F₀-ATPase (○) and Mg²⁺-activated F₁F₀-ATPase activities (●) in the presence of increasing concentrations of compound **212** (A and B) and **213** (C and D).

The second part of the work was devoted to investigating the mechanism of inhibition of the ligands with a series of kinetic experiments towards the Ca²⁺-activated enzyme and our substrates in the presence and in the absence of ATP. The experimental evidence showed that both **212** and **213** exert an uncompetitive inhibition and bind only to the enzyme-ATP complex. Considering that the bonding was not affected by increasing ATP concentration, it was possible to conclude that both compounds were not targeting the ATP binding site. Their interaction with the enzyme site might induce a conformational change, hence interfering with the catalytic hydrolysis of the enzyme's natural substrate. The inhibition kinetic parameters are reported in **Table 3**. It is noteworthy that the dissociation constant of the enzyme-substrate complex (K'_i) is 1.09 ± 0.04 and 1.07 ± 0.05 mM for compounds **212** and **213**, respectively. Such an outcome indicates the enzyme-substrate complex formation is independent of the triazole structure. Furthermore, due to the value of the inactivation constant (k_{inact}) of compound **212** ($1.93 \times 10^{-3} \pm 0.26 \times 10^{-3}$) and of compound **213** ($0.86 \times 10^{-3} \pm 0.14 \times 10^{-3}$), it is possible to conclude that **212** is more rapid in exerting its inhibitory activity than

213, suggesting a different mechanism of action even if the site of action might be the same. Finally, the value related to the potency of mechanism-based inhibitor (k_{inact}/K'_i) gave us a clue about the inhibitor efficiency. Considering also that **212** shows a k_{inact}/K'_i value 2.2 order of magnitude higher than **213**, the first is markedly more potent than the latter.

Table 3. Inhibition kinetic parameters of Ca^{2+} -activated enzyme activity in presence of compounds **212** and **213**. Data are the mean values obtained from three sets of experiments carried out on distinct mitochondrial preparations.

	Compound 212	Compound 213
K'_i (mM)	1.09 ± 0.04	1.07 ± 0.05
k_{inact} (s^{-1})	$1.93 \times 10^{-3} \pm 0.26 \times 10^{-3}$	$0.86 \times 10^{-3} \pm 0.14 \times 10^{-3}$
k_{inact}/K'_i ($\text{mM}^{-1} \text{s}^{-1}$)	1.77×10^{-3}	0.80×10^{-3}

Finally, we focused on the mPTP sensitivity to compounds **212** and **213**. In doing so, mPTP has been evaluated *via* spectrofluorometrical analysis as a function of the calcium retention capacity (CRC), a measure of the capability of mitochondria to retain Ca^{2+} in the mitochondrial matrix, which decreases when mPTP opens. Based on such an experimental design, Ca^{2+} ions are released from mitochondria as a consequence of mPTP opening: the variation of Ca^{2+} , in this case, can be calculated as the fluorescence intensity ratio of (Fura-FF high Ca^{2+})/(Fura-FF low Ca^{2+}), where Fura-FF is a cell-permeable calcium indicator. When we treated our mitochondria samples with **212** and **213**, mPTP opening was inhibited as can be observed in **Figure 12**. Such inhibition was the consequence of an increase in CRC upon subsequent 10 μM Ca^{2+} additions at fixed time intervals, which corresponded to a rise in the (Fura-FF high Ca^{2+})/(Fura-FF low Ca^{2+}) ratio: in the presence of our compounds, it indicates that mitochondria attain a higher threshold value of Ca^{2+} concentration to trigger mPTP formation. Hence, a higher concentration of Ca^{2+} is needed to allow mPTP opening. Nonetheless, **212** and **213** resulted to behave differently. **212** attains a lower CRC value than **213**: in this regard, we speculated that the different effects on the mPTP of the two compounds were due to a different kind of molecular interaction for each ligand. Such a difference might affect the mPTP size, meaning that a lower CRC value might be a consequence of a larger mPTP size.¹⁰⁵

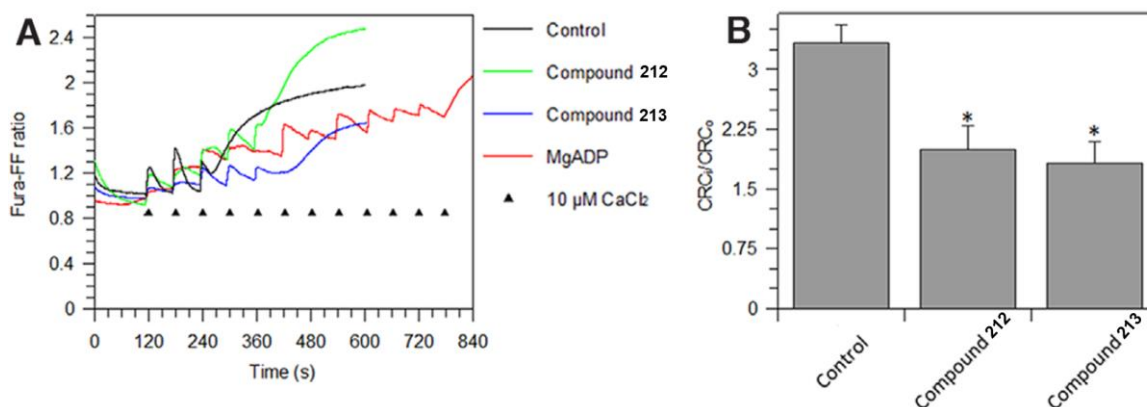


Figure 12. Evaluation of mPTP opening. Curves (A) represent the CRC expressed as the Fura-FF ratio (see text), evaluated in response to 10 μM CaCl_2 pulses (black triangles). Quantitation of the mPTP (B) expressed as the ratio of the number of 10 μM CaCl_2 pulses required to induce mPTP formation in Mg-ADP-inhibited (CRC_i) and untreated (CRC₀) mitochondria.

Our preliminary study convinced us to deepen the extraordinary and innovative activity displayed by compounds **212** and **213**. The results of this additional study furtherly endorsed the protective effect of our 1,5-DTs, adding more thorough studies on the mPTP event showing that blocking the mPTP opening counteracts the post-ischemic reperfusion injury and the hypertension-related vascular damage, two factors that might pave the way to a pharmacological application of our substrates. In this case, the research was divided into three sections: first, it has been evaluated how **212** and **213** counteract the mPTP formation by acting on the F₁ domain of the Ca²⁺-activated enzyme. Then, a cell viability study was performed, evaluating the metabolism protective effect of our substrates on ischemia-reperfusion in vascular endothelial cell models. Lastly, a study on the activity of compounds **212** and **213** towards cerebral endothelial cells (ECs) isolated from stroke-prone spontaneously hypertensive rat (SHRSP) was conducted, with the aim of evaluating the activity of our inhibitors in counteracting hypertension-related stroke damages.

The knowledge about mitochondrial dysfunction in cardiovascular diseases (CVDs) is still in its infancy but it is possible to recover important data from the literature. In CVDs, damaged mitochondria are certainly related to serious consequences (i.e. cell death) due to the essential role of such organelles in eukaryotic cells such as ATP synthesis, calcium homeostasis, oxidative stress response, and regulated cell death.¹⁰⁶ As anticipated at the beginning of this paragraph, mitochondrial homeostasis is strongly dependent on mPTP opening.¹⁰⁷ Two channels are recognized as the basis of the mPTP event: adenine nucleotide translocator (ANT)-related mPTP opening can be triggered by cyclophilin D (CyPD) as a consequence of mitochondrial Ca²⁺ levels in

matrix¹⁰⁸ or by the replacement of natural mitochondrial F₁F₀-ATP synthase cofactor (Mg²⁺) by Ca²⁺.^{109,110} This last hypothesis was strongly supported by the cryo-EM study of the entire mammalian F-type ATP synthase of the Sazanov group in 2020¹¹¹, who also proposed a model for the mPTP opening: first, the Ca²⁺ replaces Mg²⁺ in the catalytic sites of the enzyme, inducing a conformational change in F₁ domain that are transmitted through the peripheral stalk to F₀ domain. Then, the lipid plugs from the hole of the c-ring is pulled out, leading to the c-ring lumen expansion, hence to the mPTP opening.

As for the investigation of the mechanism of inhibition, we focused on the F₁ portion because we detected that the ATP hydrolysis process was sensitive to the presence our compounds. Hence, we determined the concentration in which our inhibitors exerted the best activity on mPTP opening (1 μM and 0.5 μM for **212** and **213**, respectively). Then, we selected 75 μM NBD-Cl (**214**), 0.8 μM resveratrol (**215**), and 0.2 mM piceatannol (**216**) compounds (**Figure 13**), known for interacting with the F₁ domain.^{112,113} Our aim was to perform mutual exclusion studies with binary mixtures of **212** and **213** in presence of the selected inhibitors. In this frame, two scenarios were possible: a ternary complex, made up of one of our inhibitors, the known inhibitor and F₁ domain, or a binary complex, made up of one of the evaluated inhibitors (triazoles or the others) and F₁ domain. This last outcome would point out that one inhibitor prevents the binding of the other(s) on the enzyme, competing for the binding site.

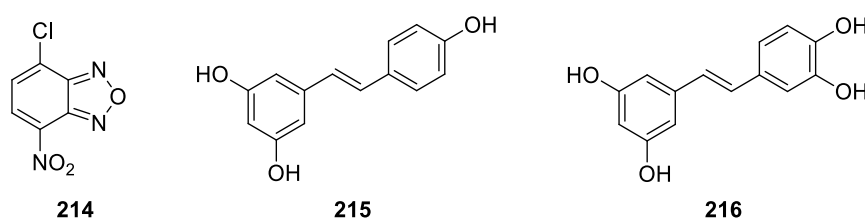


Figure 13. Structures of F₁ domain inhibitors and corresponding interacting sites (*follows in the next page*).

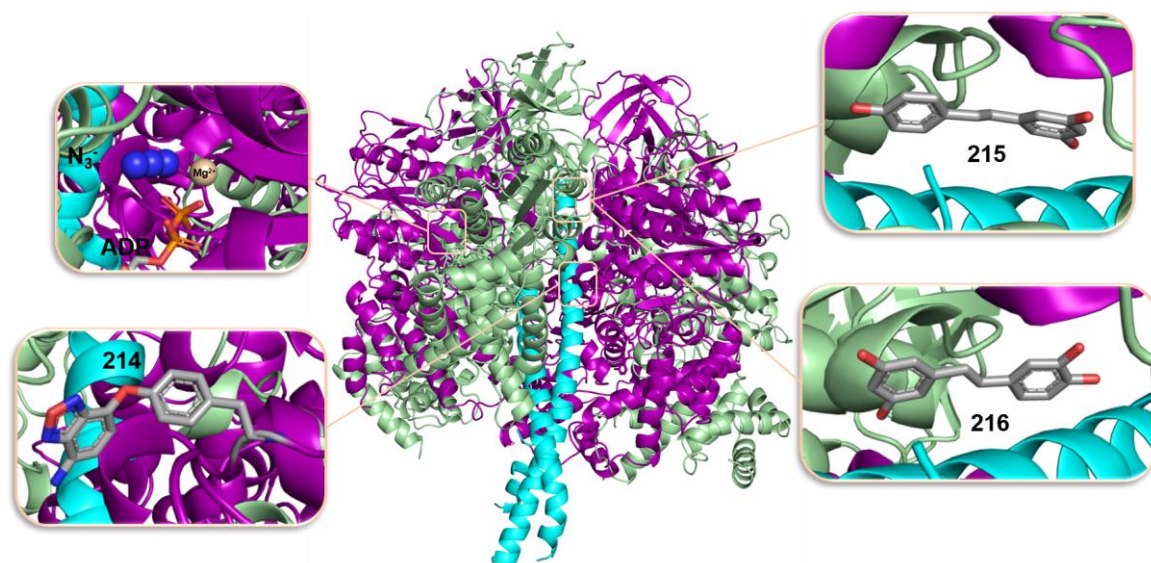


Figure 13. Structures of known F1 domain inhibitors and their interacting sites.

Azide anion is known for inhibiting the F₁ domain of mitochondrial ATP synthase by interacting with the Mg²⁺ ion of the active site when complexed with ADP.¹¹⁴ In our case, binary mixtures of **212** and azide gave a plot with parallel straight lines suggesting a mutual exclusion (**Figure 14, A**). As for the activity of NBD-Cl **214**, in **Figure 14, B** it is possible to observe the results from the competition experiments between **214**, **212**, and **213**. The intercept of the straight lines represents the values of $\alpha K'_i$, where α is the interaction constant and K'_i is the dissociation constant of the ternary complex. The interaction constant, on the other hand, gave us a clue on how the binding of a known simultaneous inhibitor (i.e., NBD-Cl, resveratrol, piceatannol, etc.) affected ($\alpha \neq 1$) or did not affect ($\alpha = 1$) the binding of one of our inhibitors to the target. According to Orris *et al.*,¹¹² NBD-Cl takes part in a covalent inhibition binding to a residue of Tyr-311 of the β subunit (**Figure 13**, in pale green) in empty conformation. In our case, **212** took part in a simultaneous interaction in the presence of **214** ($\alpha \neq 1$), forming a ternary complex. On the other hand, **213** resulted to compete with **214**, as can be seen from **Figure 14, B** wherein parallel straight lines were reported and in which the slopes were independent by the presence of **213**. Based on such evidence, we hypothesized that the residue of Tyr-311 of the β subunit might be the molecular target of our inhibitor. Hence, we performed an additional experiment using tetranitromethane (TNM), a compound known for its ability to induce the nitration of tyrosine residues or the formation of dityrosine.¹¹⁵ TNM and **213** resulted to be mutually exclusive (**Figure 14, C**), hence we thought that the latter might chemically behave similarly to TNM. Analyzing *via* UV/vis spectroscopy the content of

nitrotyrosine and dityrosine in mitochondria incubated with increasing concentrations of **213**, we noticed a significant formation of dityrosines (over 1.7 nmol **213**/μg mitochondrial protein), whilst the level of nitrotyrosine was not detectable.

Resveratrol **215** and piceatannol **216** are two phytopolyphenols that interact with the hydrophobic pocket of the F₁ domain, at the interface between the γ subunit (**Figure 13**, in cyan) and the β_{TP} subunit (**Figure 13**, in pale green). Resveratrol **215**, when evaluated in the presence of our **212** and **213**, gave a simultaneous interaction with the enzyme, hence forming the above-referred ternary complex. In **Figure 16, D** it is possible to observe the activity of the enzyme in the presence and in the absence of fixed concentrations of **215** as a function of increasing concentrations of **212** and **213**. In this case, α resulted to be lower than 1 and we concluded that a synergistic effect between **215** and **212** or **213** is present, hence our inhibitors might favor the binding of **215**.

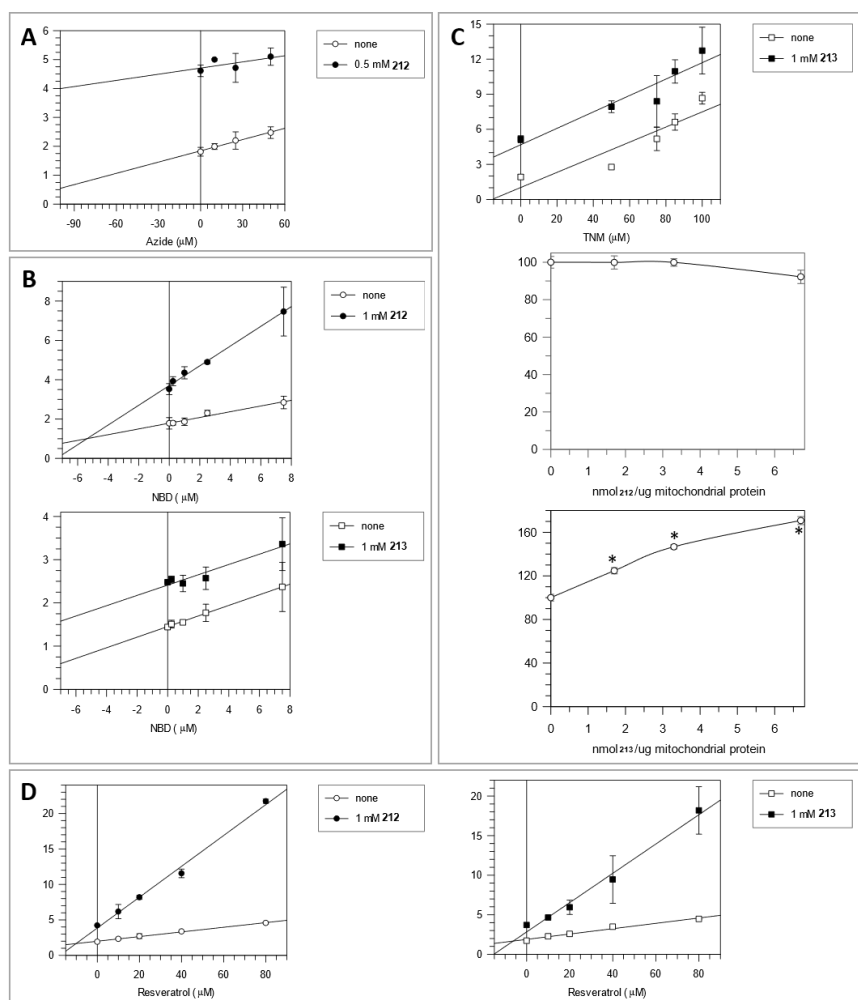


Figure 14. Exclusion plots of **212** and **213** versus various known F₁-ATP synthase known inhibitors.

Cell viability and metabolism protective evaluation of our compounds allowed us to assess the protective role of our triazoles from ischemia-reperfusion-related damages in vascular endothelial cells.

In collaboration with Dr. Chiara Bernardini from the University of Bologna, mitochondrial oxidative phosphorylation system (OXPHOS) and glycolysis production in presence of our compounds were evaluated under basal metabolic conditions measuring the oxygen consumption rate (OCR), and the extracellular acidification rate (ECAR) on a Seahorse XFp extracellular flux analyzer. These two parameters are critical indicators of normal cellular metabolic function because the first allows us to keep track of the factors that trigger the switch from healthy oxidative phosphorylation to aerobic glycolysis. The second gives us a clue on the rate of conversion of pyruvate to lactic acid. In this case, our compounds did not affect the metabolic function of a porcine aortic endothelial cell (pAECs) model because OCR values of functional metabolic profile in the presence and in the absence of **212** and **213** at different concentrations did not differ from the control tests. Furthermore, our substrates resulted to be capable of preserving basal and maximal respiration, the proton leak, and the ATP turnover: such evidence might confirm that mitochondria are the molecular targets of our inhibitors in the pAECs model. pAEC is also a good model to study the endothelial dysfunction related to impaired mitochondrial physiology during cardiovascular diseases (CVDs). Endothelial cells contain fewer mitochondria than cardiomyocytes, and several physiopathological alterations during I/R injury involve mitochondria. The *in vitro* evaluation of the I/R effect on cell viability was assessed by measuring the mitochondrial bioenergetics metabolism in terms of reduction of OCR values, using an I/R free cellular model as control. In this case, all the key parameters of mitochondrial activities, except the spare respiratory capacity, were decreased with I/R if compared with the control. An increase in basal respiration, proton leak, maximal respiration, and ATP turnover in presence of 1 μM **212** and 0.5 μM **213** has been detected. Both triazoles did not allow the I/R cells to reach the OCR values.

The third part of the study regarded the evaluation of the inhibitors in cerebral endothelial cells (ECs) isolated from SHRSP and was performed by the Rubattu group at the Sapienza University of Rome. SHRSP is a well-characterized model for studying human hypertensive disease and related vascular damage.¹¹⁶ Primary cerebral ECs

obtained from SHRSP pups were exposed to saline load to mimic the *in vivo* conditions. As consequence, the activity of mitochondrial complex I (C-I) was dramatically reduced, as expected, due to the decrease in the NAD⁺:NADH ratio. To our delight, **212** and **213** (1 μM and 0.5 μM, respectively) were able to recover C-I activity in ECs exposed to high saline concentrations. As for ECs viability, **212** and **213** were capable to recover cell viability and displayed a beneficial effect towards angiogenesis. Both compounds rescued the endothelial capability to form a vessel-like tube on a Matrigel substrate. Moreover, our 1,5-DTs were evaluated in restoring the vascular function in vessels isolated from SHRSP exposed to a four-week treatment with a high-salt Japanese-style diet, a dietary regimen able to accelerate stroke occurrence by promoting vascular dysfunction.¹¹⁷ In this case, both compounds were able to rescue the vascular function.

With the results from *research lines 1a* and *1b* in hand, we can conclude this chapter highlighting the notable biological potential of our 1,5-DTs, which shade new light on the applicability of this class of molecules. Nonetheless, in *research line 1a* we established a new, simple, and clickable protocol for attaining high regioselectivity by using FeCl₃, a cheap, commercial, and stable catalyst. Further studies will be performed, towards the biological evaluation of the pyrimidine-containing 1,5-DTs, whilst *in vivo* studies on compounds **212** and **213** have been already planned for the near future.

Chapter 2

Isoxazolidine bisphosphonates as potential farnesyl pyrophosphate synthase inhibitors

Introduction

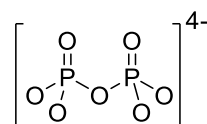
Within the most successful categories of small molecules currently available, bisphosphonates (BPs) occupy a relevant position in terms of medical interest and business, being at the center of a market of millions of dollars every year. Discovered by the end of the 19th century, the first successful BPs were developed and optimized in Davos (Switzerland) at the end of '60. Since then, the research on BPs never stopped with more than 25.000 scientific papers, 6.000 of which published in the last 10 years according to Scopus[®]. The roots of such success can be found in their unique biological activities and for drug repurposing reasons. As the reader will see in this chapter, BPs display notable biological properties exerted in orthopedics and, ultimately, in oncology. Moreover, the pharmaceutical industry is strongly interested in discovering new compounds due to the expiry of the patents on the first discovered molecules. In the present chapter, we will present a synthetic protocol for the preparation of a novel class of isoxazolidine bisphosphonates, obtained through the implementation of 1,3-DPCA techniques combined with a solvent-free microwave-assisted approach. In doing so, we aimed to combine the biological properties of the typical BPs scaffold with

the isoxazolidine ring, a heterocycle contained in a huge number of bioactive compounds.¹¹⁸ Molecular dynamics and docking simulations are ongoing to elucidate the potential of our BPs as inhibitors of the human farnesyl pyrophosphate synthase (*hFPPS*) in collaboration with Dr. Ignacio Delso from the University of East Anglia and Prof. Pedro Merino from the University of Zaragoza,

Before deepening the details of research proposed in this chapter, a review of the literature regarding the discovery and the principal BPs, alongside the survey of their biological activity, will be done. Then, a brief overview of the use of microwaves in organic synthesis for the synthesis of heterocyclic cores will be presented, with a focus on the preparation of isoxazolidine cores.

1. Bisphosphonates: a 50-years-lasting successful story

The first evidence regarding the discovery of BPs can be recovered from two works dated 1969 by Herbert Fleisch from Davos, Switzerland. In the first work, Fleisch and co-workers¹¹⁹ assessed the inhibition of the hydroxyapatite dissolution *in vitro* and of the bone resorption *in vitro* and *in vivo*. Hydroxyapatite is a mineral form of calcium apatite that composes 50% of the volume and 70% of the weight of human bones. At the time, to find a compound (or a series of) capable of inhibiting the dissolution of such a mineral was of great interest given that it would have paved the way to new strategies for regulating bone remodeling and the pathologies related to its imbalance. In this regard, the Francis group started from very simple evidence: pyrophosphate **1** (PPi) (**Figure 1**), an anion naturally present in blood plasma, inhibits the precipitation of hydroxyapatite crystals *in vitro* even at low concentrations. However, pyrophosphate derivatives are not active when given orally to the presence of pyrophosphatases in the intestine and kidney which hydrolyze the P-O-P bond.



1

Figure 1. Structure of the inorganic pyrophosphate (PPi).

Hence, they managed to find chemical analogs to PPi which were not sensitive to rapid hydrolysis. In this frame, two compounds met this requirement: sodium ethane-1-hydroxy-1,1-diphosphonate **2** and sodium methylene diphosphonate **3**, also known as medronic acid in its acid form. Both compounds possess an important structural

property: the P-C-P bond in place of the P-O-P bond, one structural motif that would have been the core of all BPs developed in the last forty years.

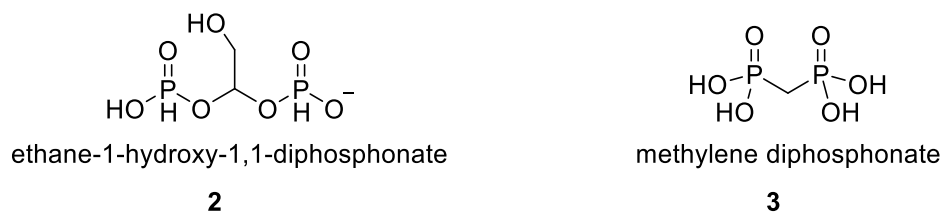


Figure 2. Structure of ethane-1-hydroxy-1,1-diphosphonate **2** and methylene diphosphonate **3**.

Once tested the activity of these compounds towards the precipitation and the crystallization of hydroxyapatite *in vitro* and on the calcification of rat aortas *in vivo*, in their second work the authors described the activity of two BPs, namely dichloromethylenediphosphonate and methylenediphosphonate. In this case, the authors ran their tests on the dissolution of apatite crystals *in vitro* and on bone resorption in tissue culture and living rats. These two studies nowadays are considered a milestone in BPs biochemistry studies.

Before elucidating the main strategies for the synthesis of BPs, it could be instructive to understand the mechanisms at the basis of their action, their structural classification, and the structure-activity relationships responsible for their pharmacological role. Although BPs are a blockbuster in pharmaceuticals, their exact mechanism of action in a biological context was understood only in the last 20 years. BPs lower bone remodeling (or bone turnover) *via* two distinct mechanisms: a physicochemical and a cellular one. The physicochemical activity is related to the role exerted by the PPI, hence influencing the time of aggregation and dissolution of the crystals of hydroxyapatite. The second one is much more complex and decisive. Bone remodeling is a highly complex phenomenon exerted by two types of cells: osteoclasts and osteoblasts. Osteoclasts lead the replacement phase of the bone tissue, whilst osteoblasts form and deposit the new one. In particular, the phenomenon of bone resorption guided by osteoclasts is composed of three steps: 1) adhesion of the osteoclast to the bone matrix, 2) localized lowering of the pH, and 3) enzymatic digestion of the bone matrix. BPs act specifically on step number two: an acid pH makes possible their dissolution, being then interiorized by osteoclasts as a calcium complex.¹²⁰ Such a particular uptake play also a role in the high specificity of BPs towards bone cells: considering that only osteoclasts are capable of such a pH lowering,

only such cells can absorb BPs *in vivo*. For the same reasons, the diffusion of BPs within cytosol is regulated by pH variations, allowing their localization into the peroxisomes.

1.1 BPs metabolism and biological targets

A convenient classification of BPs is based on the presence of nitrogen in R, R¹, or in both positions (**Figure 3**). Hence, we can have non-nitrogenous BPs (or, simply, BPs) and nitrogenous BPs (*N*-BPs). Although it could seem a simple, chemical classification, BPs and *N*-BPs differentiate by great variability in terms of their metabolic fate, hence their possible targets and, ultimately, their medical applications.

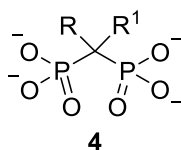


Figure 3. General structure of a BP.

Non-nitrogenous BPs are the first class of BPs developed. The most famous BPs of this family are etidronate **5** (Didronel®), clodronate (Benfos®, Loron®) **6**, and tiludronate **7** (Skelid®) (**Figure 4**).

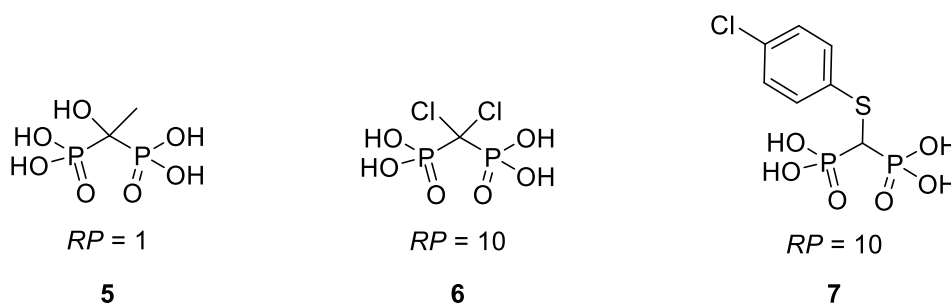


Figure 4. Structure of the most important non-nitrogenous BPs in their acid forms. “RP” stands for relative potency versus etidronate **5**, which possess an RP value of 1.

The metabolism of such a class of BPs involves the formation of a metabolic analog of the ATP, in which the molecule of BPs replaces the phosphate group in β,γ position **7** (**Figure 5**). These metabolites are formed by the activity of aminoacyl-tRNA synthetase (aaRS or ARS), also called tRNA-ligase, which is also the natural target of PPI. Once formed, these metabolites are highly resistant to hydrolysis: hence, they accumulate within the cytosol interfering with other metabolic pathways and leading to osteoclast apoptosis.¹²¹ As said, being the uptake of the BPs, extremely specific, such an apoptotic event is mainly related to osteoclasts and only in a very reduced number of osteoblasts.¹²²

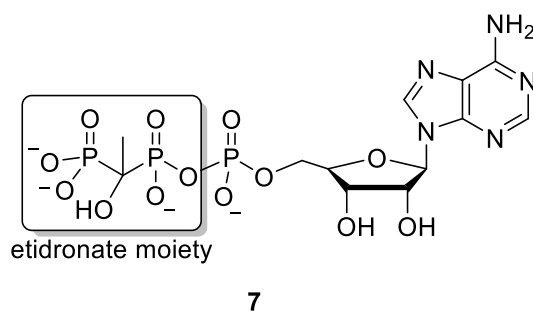


Figure 5. Structure of etidronate metabolite ATP analog 7.

N-BPs are characterized by a biological impact up to 10.000 times superior to non-nitrogenous BPs. The presence of an atom of nitrogen also confers a great chemical and structural versatility, being the component of functional groups such as amines, enamines, imines, isoxazolidines, etc., that can be present in the R¹ and/or the R² position. The principal *N*-BPs are reported in **Figure 6** and are pamidronate (APD, Aredia®) **8**, neridronate (Nerixiav®) **9**, alendronate (Fosamax®) **10**, ibandronate (Boniva® in the US, Bonviva® in Asia) **11**, risedronate (Actonel®) **12**, and zoledronate (Zometa®, Aclasta®) **13**.

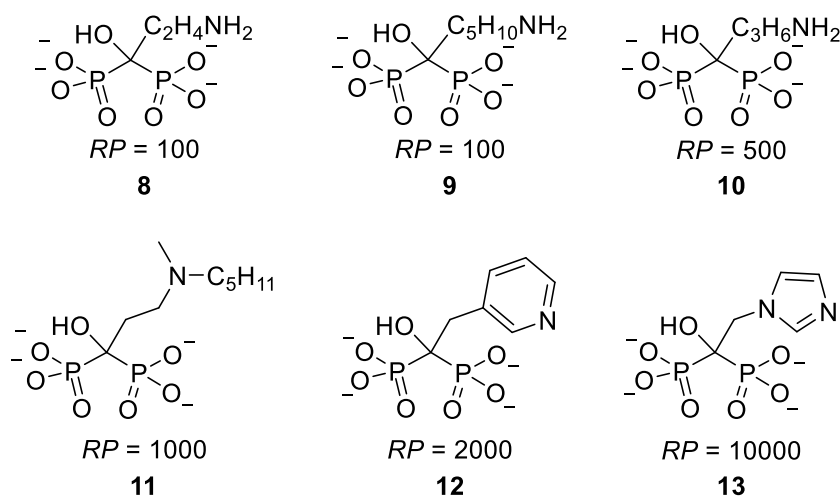
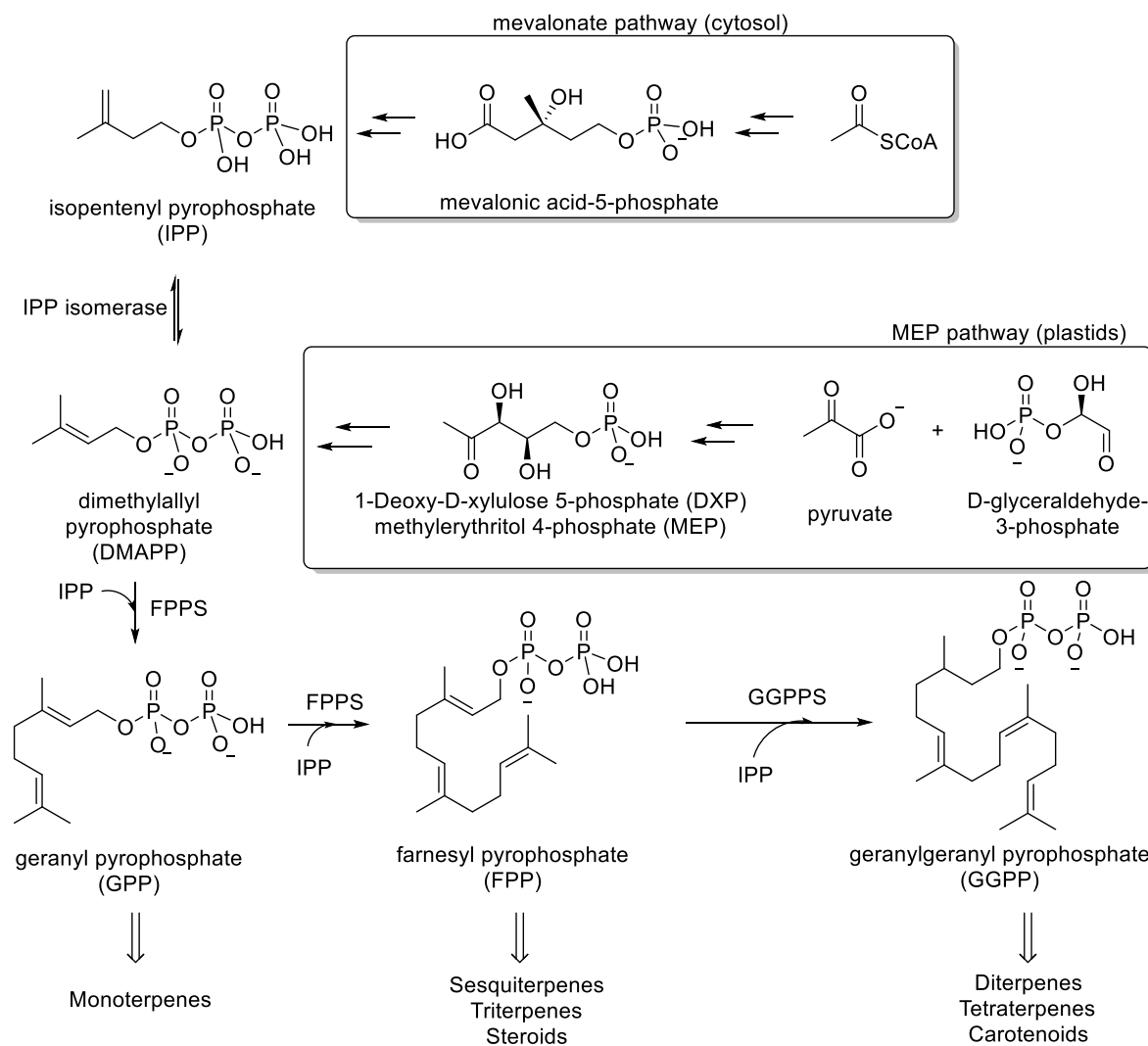


Figure 6. Structures of the principal *N*-BPs available on the market.

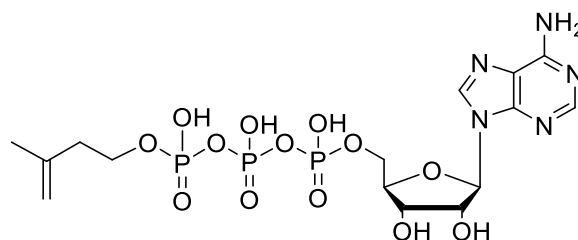
N-BPs biochemical activity is exerted at the level of the mevalonate pathway,¹²³ a fundamental process in which isoprenoids are biosynthesized ubiquitously in eubacteria, archaebacteria, and eukaryotes, by the consecutive condensation of the five-carbon monomer isopentyl diphosphate (IPP) to its isomer dimethylallyl pyrophosphate (DMAPP) (**Scheme 7**).¹²⁴ Given the importance of such a biochemical pathway, it is easy to imagine how its key enzymes can be valuable drug targets, especially for anticancer purposes.¹²⁵



Scheme 7. Biosynthesis of isoprenoids in the mevalonate pathway. Farnesyl pyrophosphate synthase (FPPS) and geranylgeranyl pyrophosphate synthase (GGPPS) are key enzymes.

The inhibition of the mevalonate pathway blocks, in particular, one subsequent cellular process known as protein prenylation. Prenylation consists of a series of post-translational modifications where isoprenoid chains composed of 15-20 atoms are transferred to some proteins,¹²⁶ conferring to them the capability to anchor on the cell membranes and to interact within their biological context. Once a “farnesylated” or a “geranylgeranylated” protein is obtained, it becomes part of the cell prenylome, comprising up to 2% of all proteins in mammals. The main biological targets of the *N*-BPs are FPPS, GGPPS, and adenine nucleotide translocator (ANT), also known as ADP/ATP translocase. As FPPS, ANT is an indirect target of the action of *N*-BPs on the mevalonate pathway: by inhibiting this biochemical pathway, an ATP analog **14** (ApppI, **Figure 8**) is formed by the action of aminoacyl-tRNA synthetase leading to the apoptosis of the osteoclasts.¹²⁷ Such metabolite is also responsible for the release of

inflammatory cytokines, thereby contributing to the acute-phase symptoms after the assumption of *N*-BPs.^{128,129}



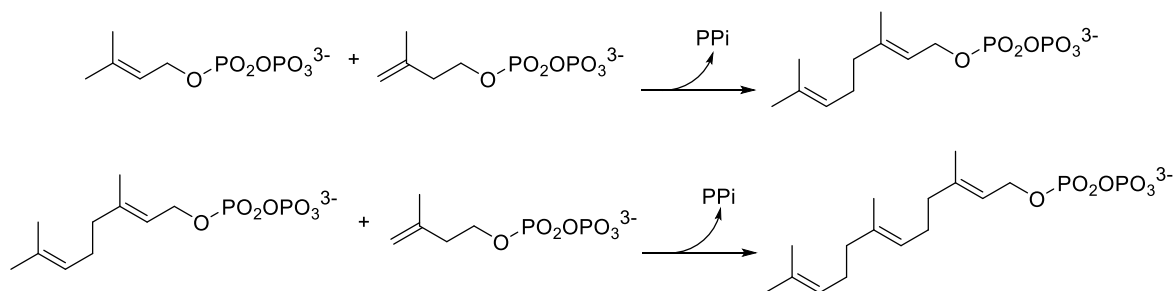
14

Figure 8. Structure of the Apppl metabolite **14**.

As for GGPPS, Agabiti *et al.*¹³⁰ elucidated how the apoptotic event might be induced by a series of alterations in the expression of some key proteins. By comparing the effects of a farnesyl diphosphate synthase inhibitor (zoledronate **13**) and a geranylgeranyl diphosphate synthase (GGDPS) inhibitor (digeranyl bisphosphonate) on lymphocytic leukemia cell proliferation and apoptosis, it was assessed the augmented expression of RhoA and Rap1 proteins, whilst the expression of Rac proteins resulted inhibited. The roles exerted by these proteins are multiple: Rho proteins, for instance, regulate the morphology and the motility of cells.¹³¹ Rap1 proteins are related to the ability of cells to migrate to other tissues, playing a key role in metastasis formation.¹³² Lastly, Rac are involved in tissue adhesion, migration, and cell lifecycle progression.¹³³ These are only some of the growing pieces of evidence regarding the possible targets of *N*-BPs, not only in orthopedics but also in oncology: a field that is still in its infancy.

1.2 Structure activity relationship

BPs interaction with their targets has been thoroughly deepened. The great availability of crystallographic structures in the Protein Data Bank (PDB) helped in elucidating not only the molecular interactions but also in designing new substrates. With the aim of clarifying the key molecular processes, it could be instructive to understand the composition of the active site of the biological targets involved, particularly for FPPS which will be the final target of the BPs presented in this chapter. FPPS catalyzes the condensation reaction between dimethylallyl pyrophosphate (DMAPP) with two molecules of 3-isopentyl pyrophosphate in a two-step process, according to **Scheme 1**.



Scheme 1. Synthesis of farnesyl pyrophosphate catalyzed by FPPS.

Structural information and structure-activity relationship (SAR) data directed the discovery of new *N*-BPs and the understanding of the mechanism of the known ones.^{123,134-137} An instructive example can be recovered from the crystallographic structure of risedronate **12** in complex with FPPS:¹³⁶ the phosphonate group on the inhibitor mimics the ones possessed by the natural substrate, hence blocking the interaction of the cofactors (Mg^{2+}) and IPP (**Figure 10, A**) in an aspartate-rich region of the enzyme. Moreover, the nitrogen in the R^2 sidechain of the inhibitor is also involved in another type of interaction, being oriented for a hydrogen bond with the hydroxyl group of a Thr201 residue and the oxygen of a carbonyl group in a Lys200 residue (**Figure 10, B**). When FPPS catalyzes its natural condensation reaction, these residues stabilize a carbocation intermediate. Hence, the sidechain of **12** might act as a transition state analog.¹³⁸

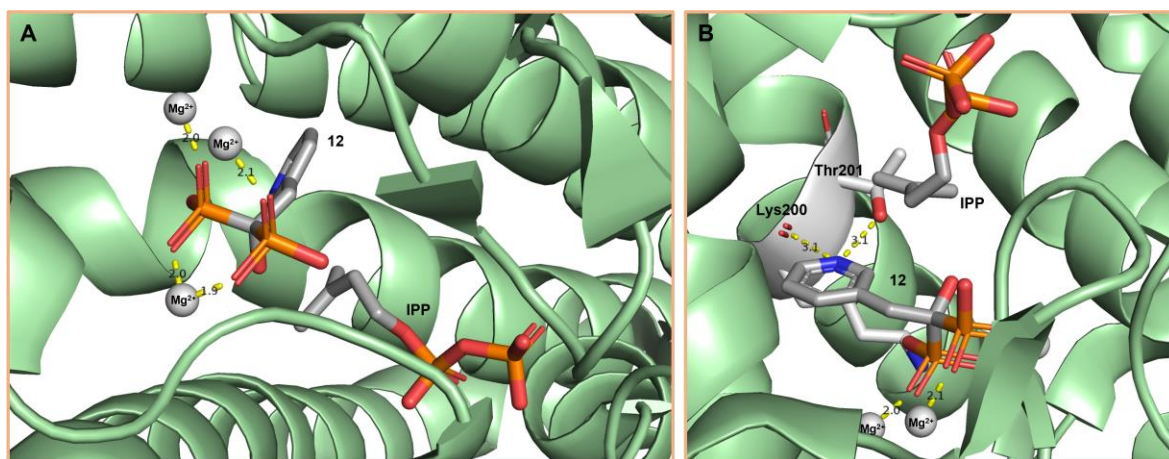


Figure 10. Active site of FPPS in complex with risedronate **224**.

A thorough SAR study on the inhibition of FPPS was published in 2008 by Dunford *et al.*¹³⁹ Due to the time-dependent isomerization mechanism of FPPS inhibition in the presence of *N*-BPs, in this work the initial and the final K_{is} and the isomerization constant K_{isom} for a set of *N*-BPs were calculated. As reported in **Figure 3**, the structural peculiarities of BPs are the phosphonate-carbon-phosphonate (O-P-C-P-O) backbone,

the phosphonate groups, the hydroxyl moiety (R), and the nitrogen-containing moiety (R¹). In this case, the rational modification of these sidechains was of great help in understanding the SAR between the inhibitors and the enzyme.

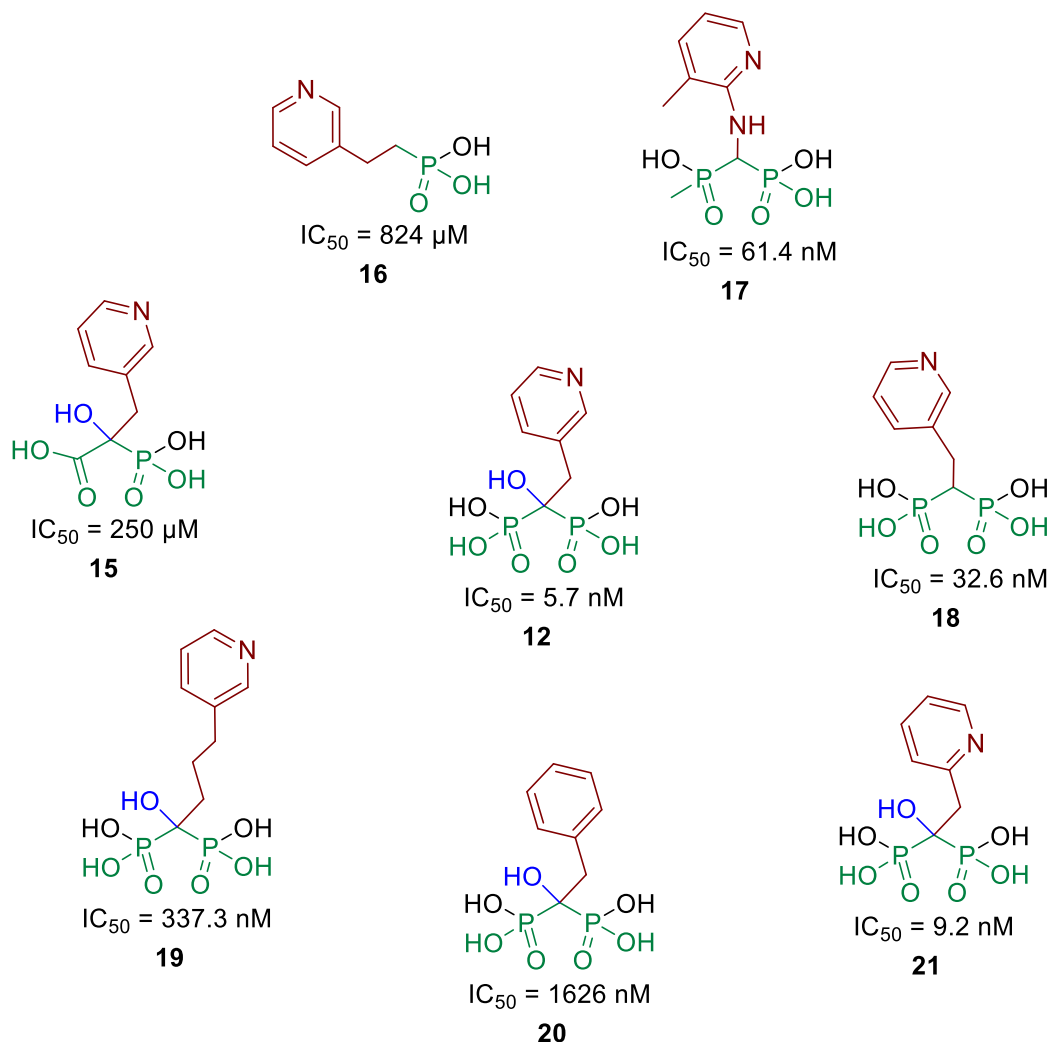


Figure 11. Structure of some BPs used for SAR studies.

The O-P-C-P-O backbone is certainly the most important: as illustrated in **Figure 11**, the complete removal of a phosphonate group (green group) from risedronate **12**, resulted in almost complete loss of inhibition (compound **16**), with a final IC₅₀ of 824 μM. Furthermore, the replacement of one of the phosphonate groups with a carboxyl moiety (compound **15**) resulted in a 44000-fold loss in potency if compared to **12**. As for such substrates, the inhibition was worse than that achieved by PPI. Substitution of a hydroxyl group (compound **17**) with a methyl group resulted in the worst inhibitory activity, but not as much as happened for the other compounds. It is possible to conclude that the magnesium-dependent aspartate-phosphonate interaction is a vital component in the inhibitor binding. As for the role of hydroxyl moiety, it has been

shown that it forms a water-mediated interaction with Gln240, also near Asp242 that coordinates one atom of magnesium. Removing the hydroxyl group (compound **18**) led to a reduction of the inhibitory activity ($IC_{50} = 32.6$ nM). In this case, the absence of the hydroxyl group suggested that it may play a role in mediating the stabilization of the isomerized state. Lastly, as for the nitrogen-containing moiety (R^1 , in brown), we know from the crystal structure reported in **Figure 10** that risedronate exploits the interaction of its *N*-containing moiety with Thr201 and Lys200. A modification introduced at this position (compound **21**) revealed a loss in the ability to inhibit FPPS but not as dramatic as happened for the bisphosphonate backbone. Of note, the phenyl analog **20** highlighted the contribution of such moiety in leading the time-dependent inhibition and not only the potency of the substrate. Two factors might be pivotal in this sense: the protonation state and the symmetry of the sidechain. Risedronate **12** holds an acceptor of a hydrogen bond at the nitrogen position which can be helpful in mediating a rapid interaction with the active site. In addition, the phenyl analog **20** is symmetric, whilst a nitrogen atom could double the ability of risedronate to interact with the residues of the binding pocket.

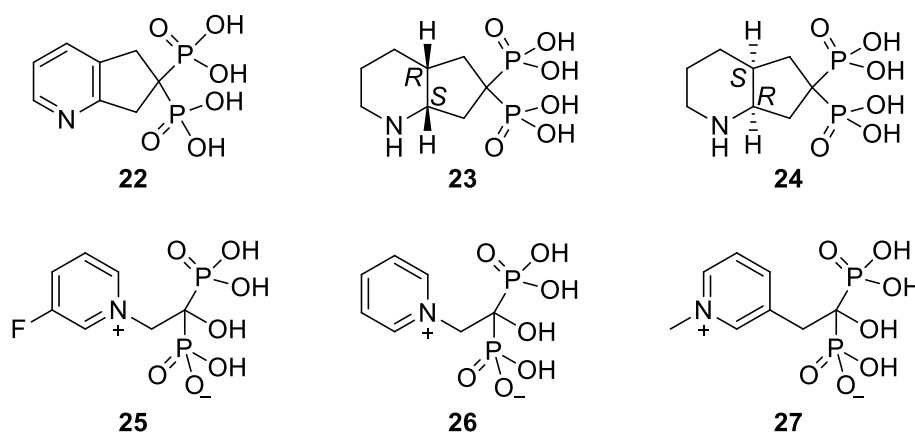


Figure 12. Structure of some representatives *N*-BPs. The R^2 moiety is designed to contain a spiro ring (upper row) and a positively charged group (lower row).

As for other SAR instructive modifications of risedronate, compound **22** (known as NE58086)¹⁴⁰ possess a lower IC_{50} to risedronate (2588 nM). In this case, the lower potency was attributed to the lack of conformational changes of the *N*-containing sidechain. In addition, the nitrogen atom resulted moved 1.8 Å away from the interacting residue. The introduction of a stereochemical variability in R^2 helped to elucidate other properties. In our case, compound **24**, which possesses a (1*R*,6*S*) configuration, resulted to be about 20 times more potent than its enantiomer **23** (1*S*,6*R*). As for positively charged *N*-BPs, the risedronate *N*-methyl analog **25** is not able

to take part in interactions with the Thr residue but its potency was not so dramatically influenced (19.6 nM), suggesting that might be present a C-H-O type interaction with the methyl group that stabilizes the complex.¹⁴¹ The same happened for compounds **26** and **27**, in which the rare formation of a C-H-N type bridge led to good activity.

Finally, a brief mention of the effect of lipophilicity on *N*-BPs potency. The last twenty years assisted in the extensive growth of works regarding lipophilic BPs as potential dual inhibitors of FPPS and GGPPS. Such perspective stimulated the works of the Oldfield group, which discovered potent BPs inhibitors active against protists,¹⁴² as $\gamma\delta$ T cells stimulators,¹⁴³ as substrates capable of targeting bacteria cell walls, and quinone biosynthesis.¹⁴⁴ In most cases, the increased activity of such substrates should not be attributed to a different mechanism of action but only to higher bioavailability. In this way, it has been possible to synthesize BPs without the geminal hydroxyl group (R¹) maintaining a good inhibitory activity according to a QSAR study published in 2003.¹⁴⁵

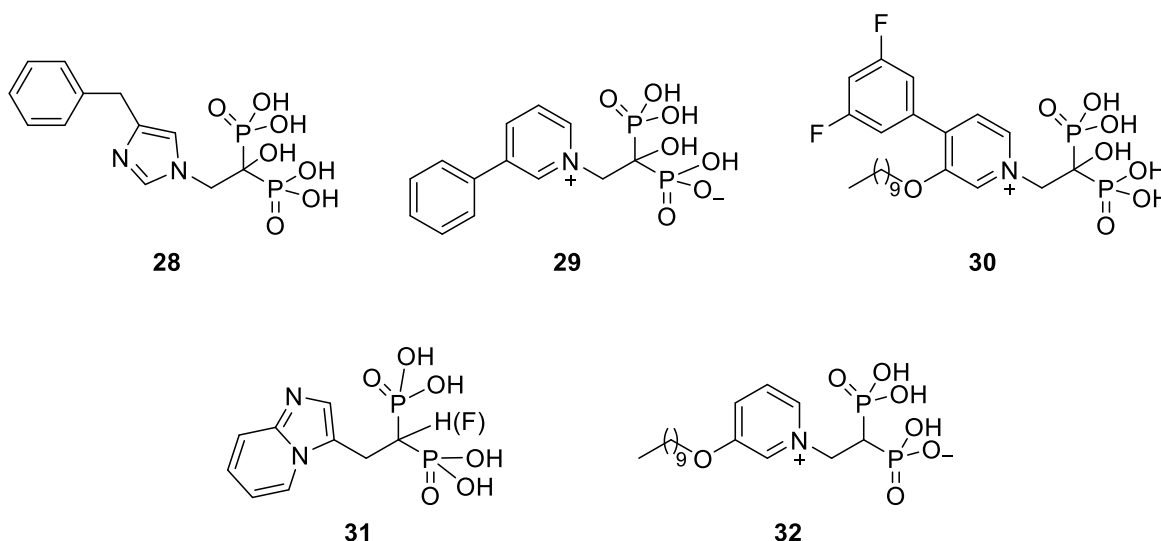
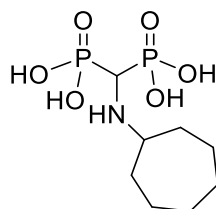


Figure 13. Some representative structures of lipophilic *N*-BPs.

1.3 BPs in medicine

Orthopedics benefited the most from the approval of BPs in the pharmaceutical market. BPs are largely employed for the treatment of osteonecrosis¹⁴⁶ and to stimulate bone tissue healing.¹⁴⁷ Different studies showed that the use of alendronate **10** reduces the need to resort to surgery and the levels of *N*-terminal telopeptide, a urinary biomarker for bone resorption.¹⁴⁸ The use of BPs is being extended also to orthopedic surgery for the post-operative treatments of arthroplasties.¹⁴⁹ In this sense, BPs stimulate tissue healing, minimizing the negative effects related to bone remodeling. The main BPs currently used at this scope are pamidronate **8**, zoledronate **13**, and incadronate **33**,¹⁵⁰

which display an interesting R¹ lipophilic motif and no geminal hydroxyl group at the R position (**Figure 14**). Lastly, post-surgery treatment inhibited bone resorption, favoring the connection of the bone tissue with the prosthesis. In this case, along with N-BPs, also the clodronate is being used.



33

Figure 14. Structure of incadronate **33** (depicted as incadronic acid).

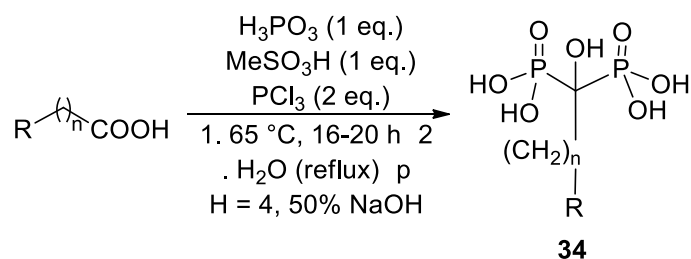
In addition to orthopedics, oncology is a medical field that might benefit too from the research on BPs. Different studies showed the ability of BPs to reduce the diffusion of bone metastasis¹⁵¹ and, in some cases, to act also on other tumoral cells. More detailed mechanisms of action are still underway, but it is possible to recognize four main factors that raise interest in BPs applicability in oncology.¹²⁹ BPs reduce the proliferation of cancer cells in bone marrow, inhibiting the release of metabolites responsible for cancer diffusion. In addition, BPs can prevent the formation of pre-metastatic niches and angiogenesis and might be used in combination with already-approved chemotherapeutic drugs. Finally, BPs improve the ability of the immune system to identify and eliminate tumors (immune surveillance).

Lastly, BPs are fundamental drugs in the Paget disease treatment.¹⁵² Paget disease can be classified as a metabolic disorder of the skeleton in which an unbalance between bone resorption and bone formation takes place. The results of such an alteration consist of an increased risk of osteolysis and the augmented risk of fractures and deformities. In this sense, the advantage of using BPs is double: BPs not only help in balancing bone turnover but are also useful in diagnostics in combination with ^{99m}Tc,¹⁵³ a nuclear metastable isomer of ⁹⁹Tc. The main BPs used in this field are alendronate **10**, risedronate **12**, and zoledronate **13**.¹⁵⁴ The latter, administrated as a single-dose intravenous administration, induced a high response in 96% of patients after 2 years, and in 87% of cases after 5-6 years. Specifically, the use of N-BPs not only helps in the normalization of bone metabolism but also in improving the global quality of life of patients.

1.4 Synthetic strategies

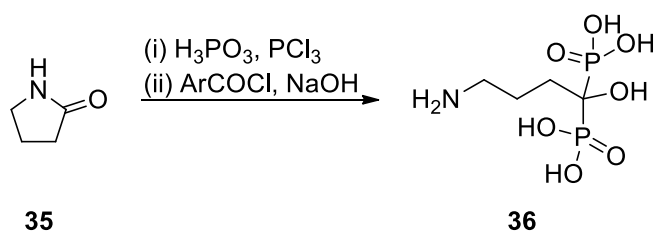
Being BPs a hot topic in medicinal chemistry for almost fifty years, a huge number of chemical procedures have been proposed for their preparation. In general, four main approaches are known in the literature, and in this paragraph, we will report some examples of each one.

An important class of reactions consists of the use of carboxylic acids with phosphoric reactants. One of the first examples in this sense was proposed in 1995¹⁵⁵ and consisted of the *in situ* conversion of the carboxylic acid reactant in acyl chloride which was then converted to the desired bisphosphonic acid **34** in the presence of phosphoric acid (**Scheme 2**).

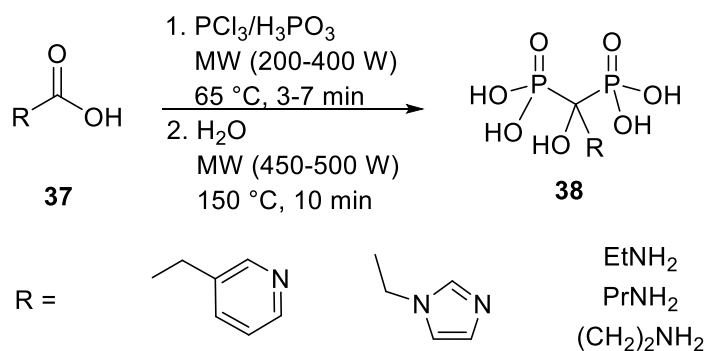


Scheme 2. Kieczkowski-Jobson synthesis of bisphosphonic acids **34**.

More recently, this methodology allowed to use of ammonium reactants for the synthesis of pamidronate **8** and alendronate **10**.¹⁵⁶ The latter was also obtained from pyrrolidone **34** from the hydrolysis in water and methanesulfonic acid, followed by treatment with PCl_3 (**Scheme 3**).¹⁵⁷



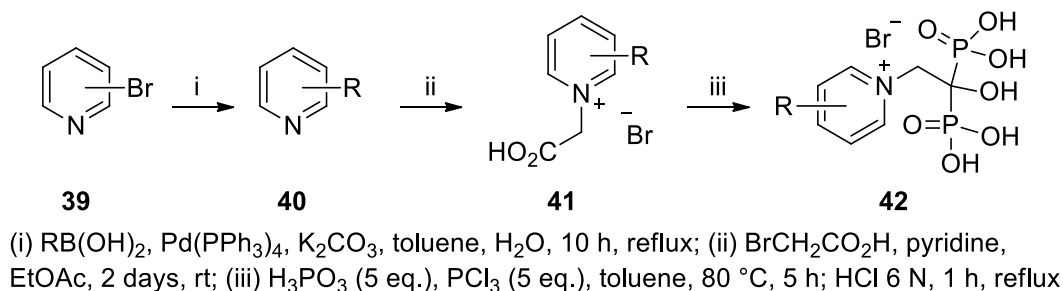
Scheme 3. Synthesis of alendronate **10** from pyrrolidone.



Scheme 4. MW-assisted synthesis of *N*-BPs.

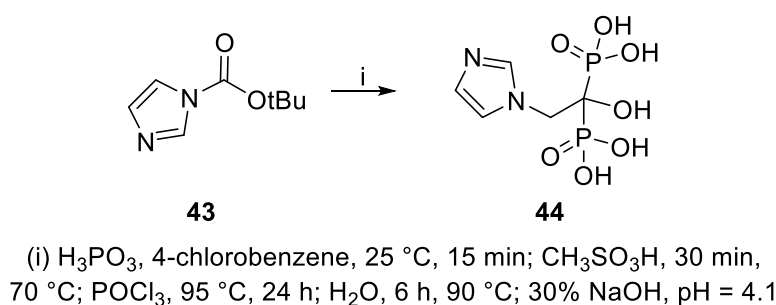
As for the synthesis of heterocycles-containing BPs on the R¹ moiety as risedronate and zoledronate **13**, an interesting protocol was proposed by Mustafa *et al.*¹⁵⁸ where the target products **38** were obtained in microwave-assisted fashion with reduced times and high yields (**Scheme 4**).

As we observed in Paragraph 1.2, pyridinium *N*-BPs present an important advantage in terms of interaction with two key residues of the FPPS pocket. Hence, the development of synthetic strategies for such substrates was an important research field in the past. In this regard, the Oldfield group developed a systematic approach to achieving such compounds (**Scheme 5**) starting from bromo-substituted pyridines **39** coupled with the desired alkyl group through a Suzuki Pd (II)-catalyzed reaction. The product was then converted to a pyridinium salt *via* a nucleophilic substitution reaction driven by the pyridine nitrogen towards a bromo-substituted carboxylic acid **41**. Then, the so-obtained product was treated following the Kieczkowski-Jobson synthesis reported in **Scheme 5**, in which the conversion to bisphosphonic acids **42** passed from an acyl chloride intermediate.



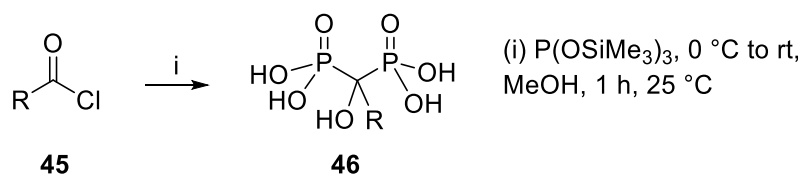
Scheme 5. Synthesis of pyridinium-containing *N*-BPs.

As for the synthesis of etidronate **5**, alendronate **10**, pamidronate **8**, ibandronate **11**, risedronate **12** and zoledronate **13**, Keglevich and co-workers¹⁵⁹ proposed a procedure in which phosphorus (V) oxychloride (POCl₃) was used in a one-pot multigram reaction (**Scheme 6**).



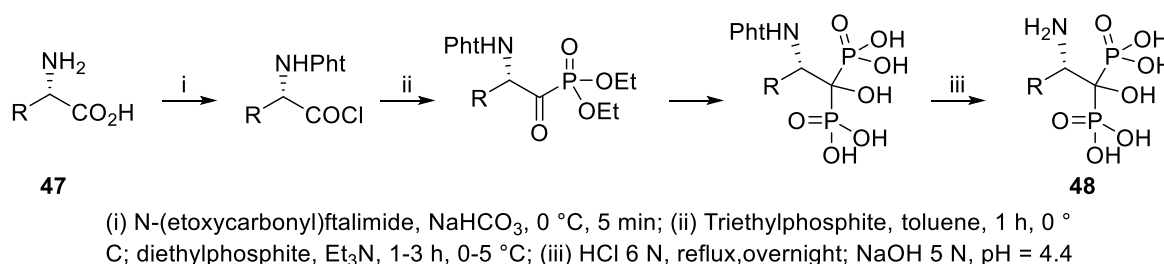
Scheme 6. One-pot synthesis of *N*-BPs in the presence of POCl₃.

On the other hand, it has been observed that the use of sterically bulky carboxylic acids was affected by low yields. Hence, another approach consisted of using a reaction between acylphosphonates and dialkyl phosphites with acyl chlorides **45** and trialkyl phosphites (**Scheme 7**). In this case, the obtained acylphosphonate reacted with another equivalent of trialkyl phosphite affording the product **46**. Such an approach was used by Lecouvey *et al.*¹⁶⁰, in which tris(trimethylsilyl) phosphite was used as a phosphorylating agent.



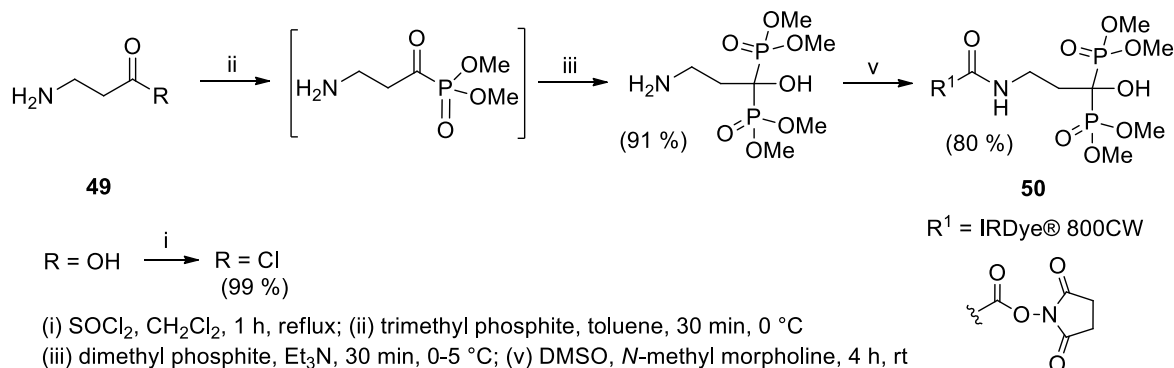
Scheme 7. Lecouvey synthesis of BPs *via* tris(trimethylsilyl) phosphite.

It has been reported also the use of trialkyl phosphite as a phosphorylating agent. In this case, the reaction was conducted with the aim to obtain α -amino acid BPs **48** from the amino acid reactant **47** (**Scheme 8**).¹⁶¹

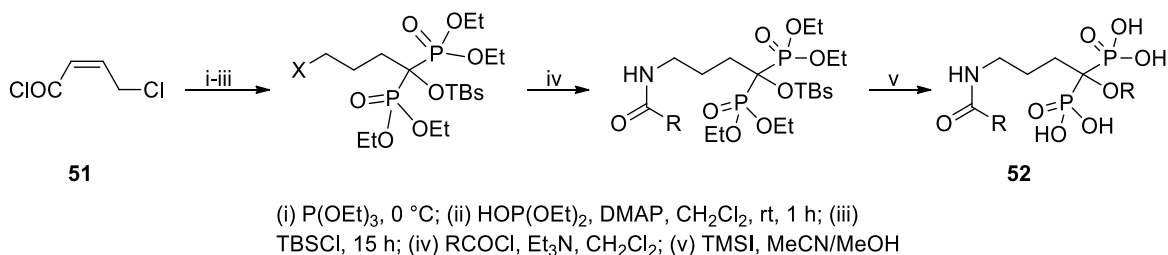


Scheme 8. Mizrahi method for the synthesis of α -amino acid BPs.

The use of such methodology allowed to access fluorophores BPs **50** to be used as contrast agents.¹⁶² In this case, amino acid **49** substrates were previously converted in acyl chloride using SOCl_2 (**Scheme 9**).



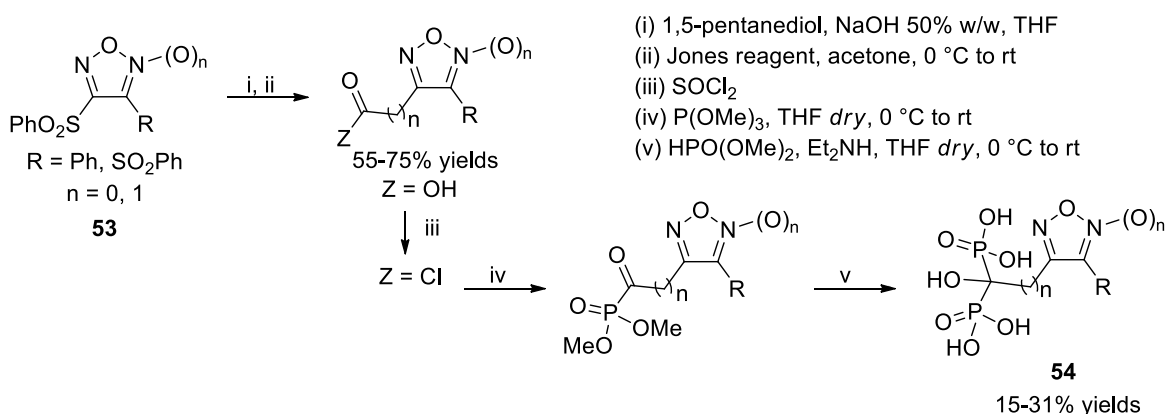
Scheme 9. Synthetic protocol for the synthesis of *N*-BPs as fluorophores.



Scheme 10. Synthesis of alendronate analogs.

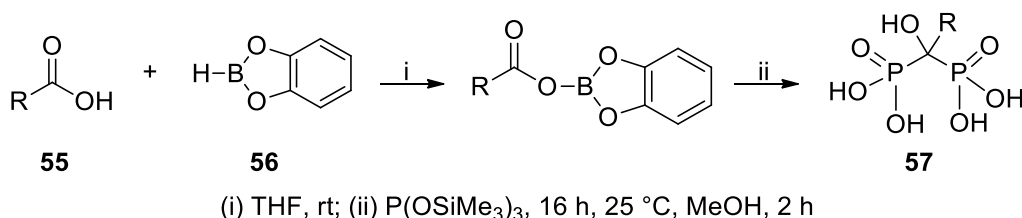
As for the preparation of alendronate analogs, it is possible to use the trialkyl phosphite method to access alendronate derivatives **52** *via* a three-step one-pot procedure. In this frame, it has been necessary to protect the geminal hydroxyl group to prevent side reactions during the acylation step (**Scheme 10**).¹⁶³

Of note, an interesting procedure reported by Lolli and colleagues¹⁶⁴ (**Scheme 11**) was used to synthesize *N*-BPs containing a furazane (1,2,5-oxadiazole) ring in the side chain (R^1 position) **54**.



Scheme 11. Synthesis of furazane-containing *N*-BPs.

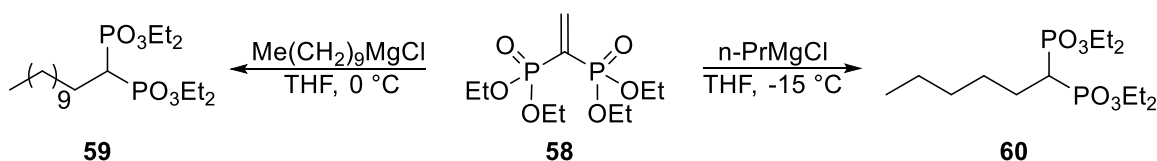
Lastly, the approach reported by Egorov *et al.*¹⁶⁵ is worth to be mentioned. In this last example, the synthesis of the desired BPs **57** was achieved using dioxaborolane **56** as an alternative to the acyl chlorides (**Scheme 12**). In doing so, no dry conditions were needed, and the formation of acids due to the use of acyl chlorides was avoided.



Scheme 12. Synthesis of BPs using dioxaborolane as reagent.

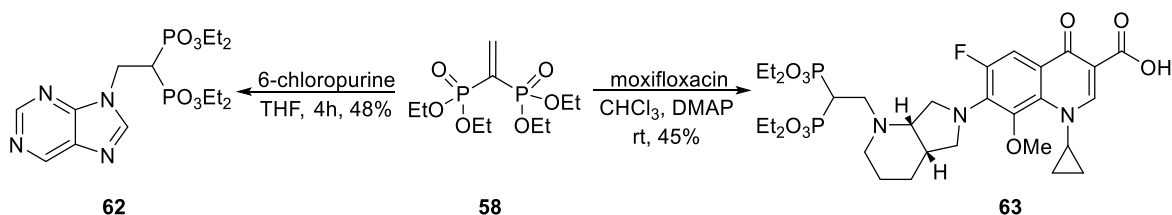
The third approach to the synthesis of functionalized BPs exploits the use of tetraethyl ethenylidenebisphosphonate **58**. Such reagents allowed great synthetic versatility in

the last years: their reactivity is typical of the electron-deficient alkenes; hence they can take part in conjugate addition reactions with various nucleophiles. In addition, it can be used as a dipolarophile (see **Chapter 1**) or dienophile in different 1,3-DPCAs or Diels-Alder reactions, allowing to access products wherein the bisphosphonic moiety is in co-presence with five or six-membered cycles and heterocycles. As can be easily imagined, such a reagent is also a good Michael acceptor and reacts with Grignard reagents. Such an approach allowed to access lipophilic BPs **59** and **60**,¹⁶⁶ as reported in **Scheme 13**.

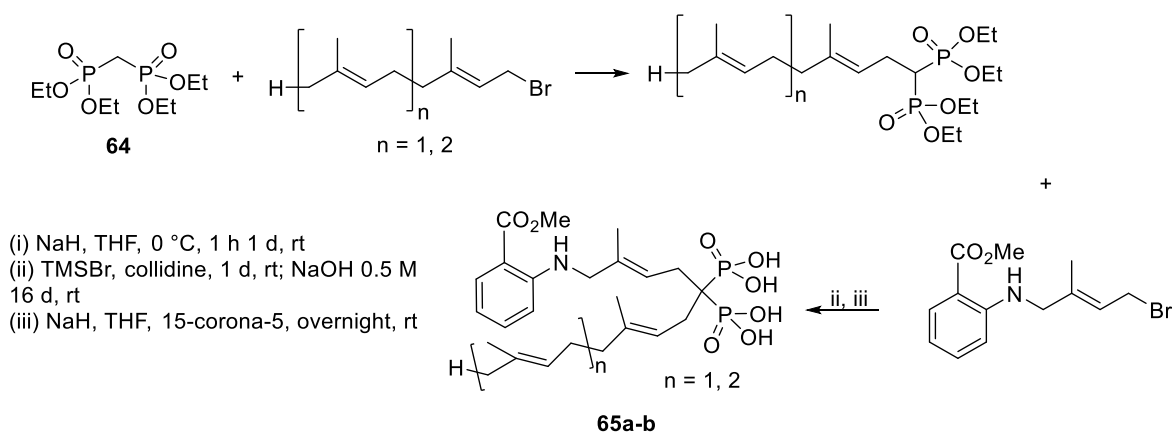


Scheme 13. Synthesis of lipophilic BPs using tetraethyl ethenylidenebisphosphonate **254**.

58 not only resulted active with strong nucleophiles, but also in combination with mercaptans and amines. In this regard, it was possible to obtain the desired BPs bearing a fluoroquinolone function¹⁶⁷ **63** as antibacterial, or nucleobase-functionalized BPs¹⁶⁸ **62** using triazabicyclodecene (TBD) as a catalyst (**Scheme 14**).



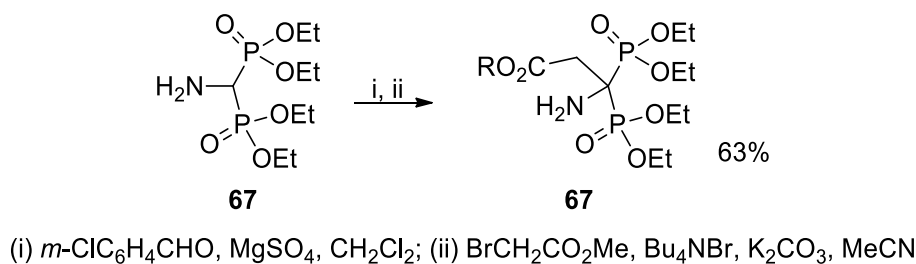
Scheme 14. Synthesis of fluoroquinolone **255** and purine-containing **256** N-BPs.



Scheme 15. Synthesis of farnesyl and geranyl BPs derivatives **65a-b** from tetraalkylmethyl bisphosphonates **64**.

Finally, the fourth important approach used in the BPs synthesis consists of the alkylation reaction of tetraalkylmethyl bisphosphonates **64** (**Scheme 15**). Such an

approach resulted to be useful in accessing BPs without the hydroxyl group in the geminal position. Of note, an instructive example can be recovered from the work of Valentijn and co-workers,¹⁶⁹ wherein the authors reported the alkylation reaction using farnesyl or geranyl bromide affording the corresponding BP **65** after hydrolysis. Similarly, it was possible to achieve the alkylation of an amino BP **67**.¹⁷⁰ In this case, it was necessary to protect first the reactant using methyl-2-bromoacetate (**Scheme 16**).



Scheme 16. Alkylation of amino BPs.

2. Microwave-assisted 1,3-DPCA: two compatible strategies

Microwave-assisted organic synthesis (MAOS) is known from its first application dated 1986 when Giguere¹⁷¹ and Gedye¹⁷² showed the great potential of microwaves as a source of heat to carry out cycloaddition, hydrolysis, oxidation, and esterification reactions. In this paragraph, we will report the main advances in microwave-assisted 1,3-DPCA, with a specific focus on the use of nitrones as 1,3-dipoles, being the major topic of this chapter. One important benefit introduced by MAOS is the chance to reach a very rapid, homogeneous, and localized heat. In this way, numerous protocols benefited from it both in terms of yields and kinetics,¹⁷³ and now it can be considered a mature technology scalable to an industrial level.¹⁷⁴ The response to MW irradiation strongly depends on the nature of the reagents used given that only polar compounds are influenced by the electromagnetic field applied. Nonetheless, heating can be transmitted to the other non-responsive compounds by convection. A peculiar characteristic of the MAOS approach resides in the homogeneity of the temperatures reached in the sample, as said. In a conventional way, the heat is spread by convection and conduction phenomena and is directed from the external source of heat to the core of the sample. MW, on the contrary, induces heating based on the molecular interaction with the radiation, resulting in a homogenous and much more rapid process (**Figure 15**).

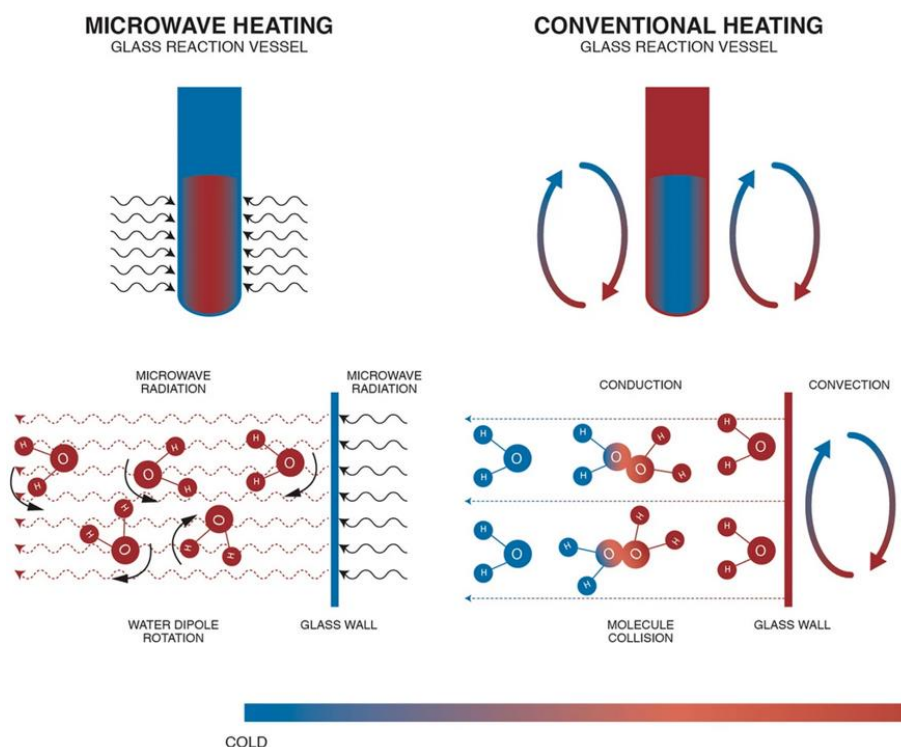
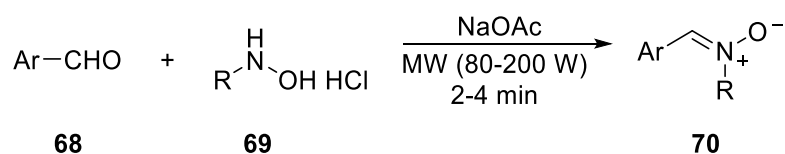


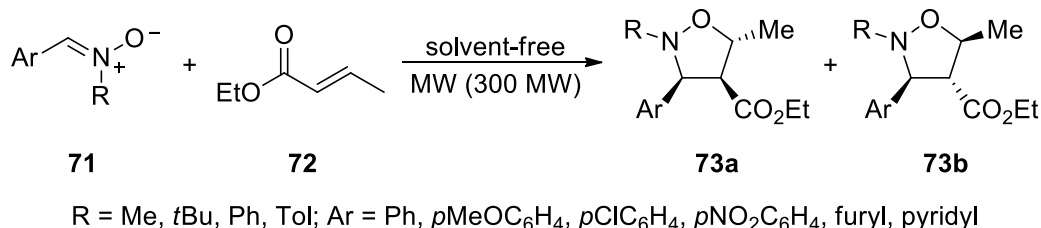
Figure 15. Comparison of microwave heating versus conventional heating. Image adapted from Sweygers *et al.*¹⁷⁵ under the terms of the Creative Commons CC BY license.

An interesting work of 2010 by Haque and co-workers¹⁷⁶ pointed out that the kinetics for nucleation and crystal growth of a metal-organic framework (MOF) material (MIL-53(Fe)) were influenced. In this case, it was confirmed that the rate of both events was markedly higher than the conventional heating, and it was related to physical effects such as the formation of hot spots.

As for the subject of this chapter, the MAOS technique has been successfully applied to the synthesis of heterocycles,¹⁷⁷ particularly to five-membered rings.^{178,179} In addition, the precursors used in the synthesis of these scaffolds benefited too from the use of MW. It is the case of nitrones, which were accessed in high yields and reduced times by Andrade *et al.*¹⁸⁰ in 2008 (**Scheme 17**). In this case, the synthesis of *N*-alkyl-*C*-arylnitrones **70** was accessed, also reducing the amount of hydroxylamines **69** classically needed.



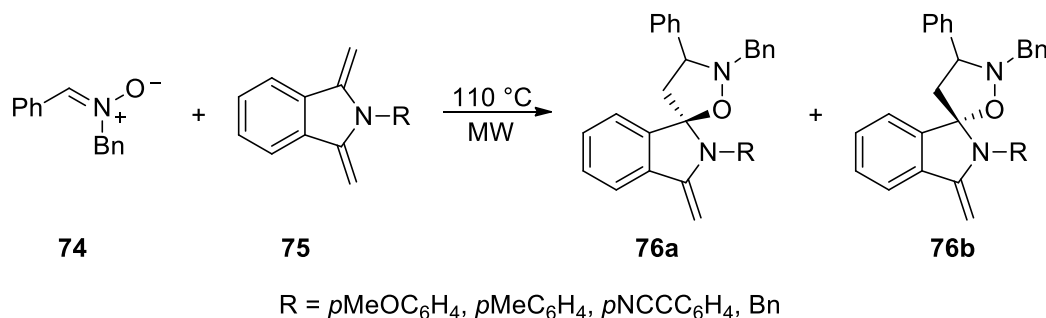
Scheme 17. MAOS of *N*-alkyl-*C*-arylnitrones **260**.



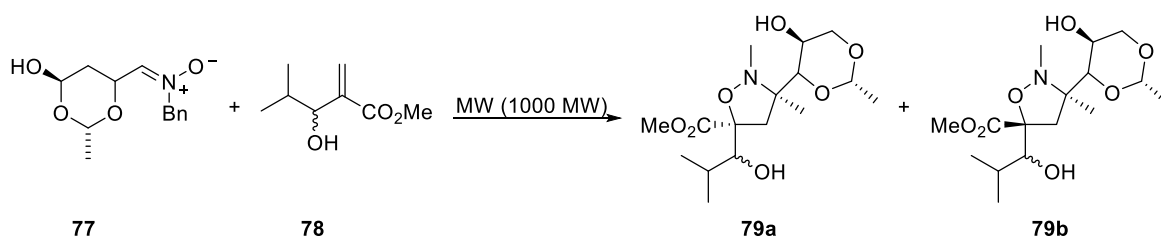
Scheme 18. MW-assisted synthesis of isoxazolidines.

The so-obtained products were then used as 1,3-dipoles in 1,3-DPCA reactions to obtain isoxazolidines **73** (**Scheme 18**). In this regard, the dipolarophile was ethyl *trans*-crotonate **72** in solvent-free conditions. The regioselectivity was variable because the nitrones were bearing bulky or methyl groups at the R position: in the first case, the dipole was mainly in its *Z* configuration (*endo* approach favored), whilst was present as a mixture of *E/Z* isomers when bearing the methyl group. The reaction resulted to be also stereoselective because only 3,4-*trans* and 4,5-*trans* products were obtained.

Regioselectivity over isoxazolidine ring formation was achieved by Dugovič and co-workers too¹⁸¹ by combining 3-methylene-*N*-substituted isoindolones **75** and the nitron **74** (**Scheme 19**). In this report, it has been clearly pointed out the advantage of such technology because the yields were doubled with respect to the classical heating approach.



Scheme 19. Dugovic MAOS of spiroisoxazolidines.

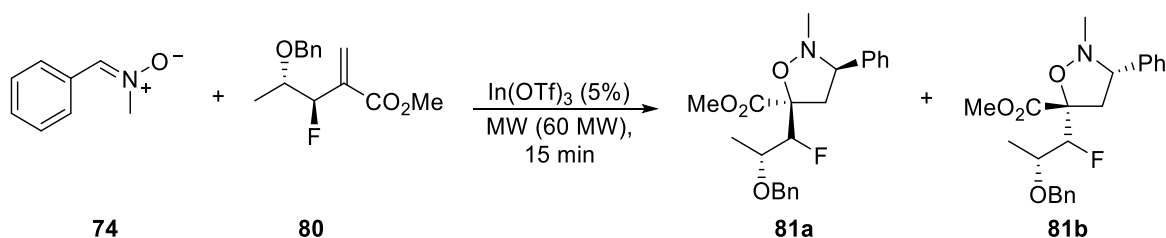


Scheme 20. 1,3-DPCA reaction of nitrones **77** on Baylis-Hillman adducts **78**.

In another report by the same research group, the reactivity of nitrones in MW conditions towards the Baylis-Hillman adduct **78** was investigated. In this case, the

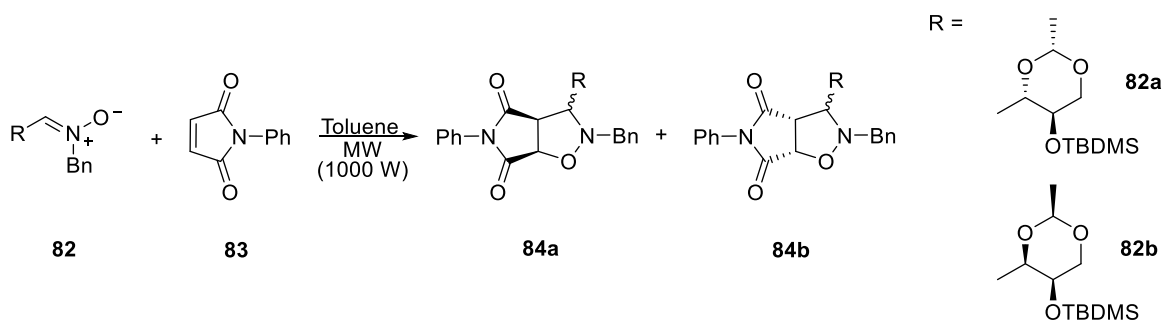
reaction proceeded with high regioselectivity affording the desired 5-substituted compounds **79a** and **79b** in 1 hour (**Scheme 20**). As for stereochemistry, the less sterically hindered side of the nitron **77** guided the attack on the dipolarophile giving *C-3/C-5 cis* heterocycles.

The use of Baylis-Hillman-inspired adducts was also useful in the synthesis of fluorine-containing compounds. By replacing the hydroxyl group with a fluorine atom, it was possible to obtain reactant **80** which easily underwent 1,3-DPCA in the presence of MW, affording the spiroisoxazolidines **81a** and **81b** reported in **Scheme 21**. In this frame, the reaction was carried out in solvent-free conditions in the presence of $\text{In}(\text{OTf})_3$ as a catalyst with 61% yield and a **81a:81b** diastereomeric ratio (*dr*) of 90:10.

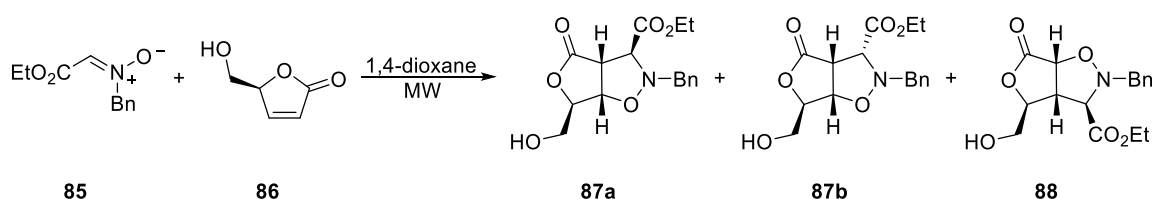


Scheme 21. Diastereoselective synthesis of fluorine-containing isoxazolidine derivatives.

D-erythrose and D-threose-containing nitrones **82** were used in combination with N-phenylmaleimide **83** in the regioselective synthesis of bicyclic isoxazolidine in diastereomeric mixture (**84a** and **84b**) (**Scheme 22**).¹⁸²



Scheme 22. 1,3-DPCA of exose-containing nitrones.

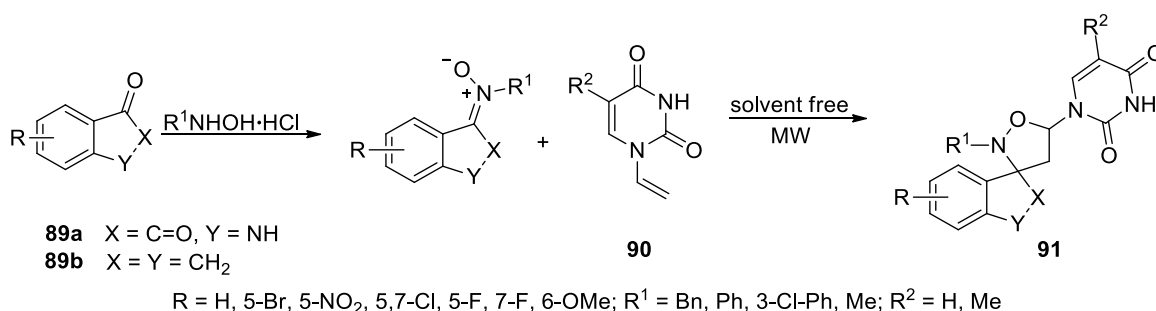


Scheme 23. 1,3-DPCA between nitron **85** and lactone **86**.

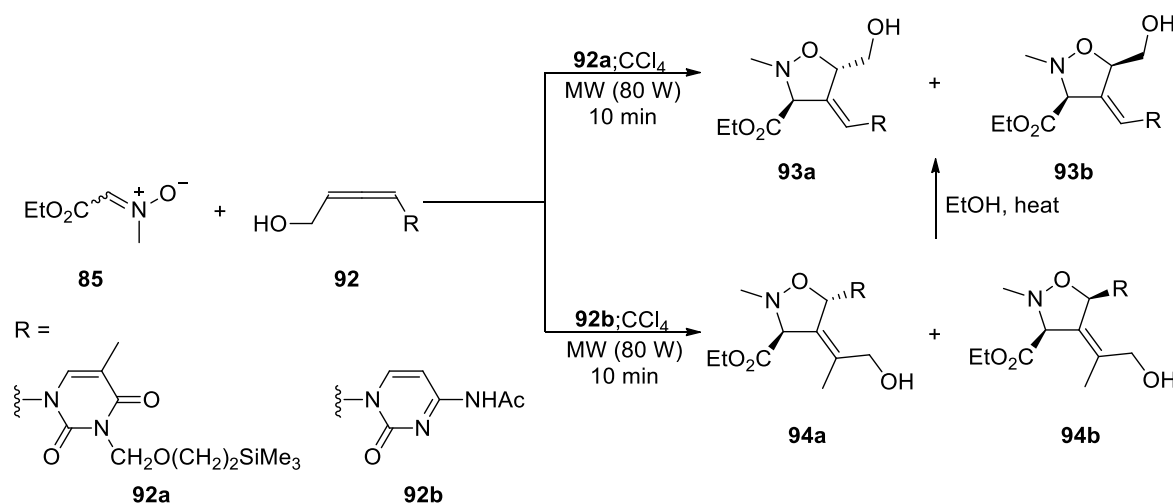
Lactones **86** were also shown to be good dipolarophiles when reacted with nitron **85** in 1,4-dioxane assisted by MW (**Scheme 23**). In this case, two diastereoisomers **87a**

and **87b** were obtained in the presence of another regioisomer **88**, with ratios of 64:23:10, respectively.¹⁸³

MAOS protocols were useful in also preparing nucleoside analogs. The replacement of the native ribose unit with a different heterocyclic moiety, such as an isoxazolidine analog, is one of the methods used in drug design to enhance the biological features of naturally occurring and synthetic *C*-nucleosides. Two instructive examples can be recovered from the literature. In 2017, Maiuolo *et al.*¹⁸⁴ proposed the use of MW to access spiroisoxazolidine-containing nucleobases **91** using indanone and isatin derivatives **89** as starting compounds for the preparation of the dipoles (**Scheme 24**). The indane derivatives were evaluated as inhibitors of the MDM2-p53 interaction, revealing a discrete activity in the antiproliferative screening against A549 human lung adenocarcinoma cells and human SH-SY5Y neuroblastoma cells.¹⁸⁵



Scheme 24. Synthesis of nucleobase-containing spiroisoxazolidines **91** as potential MDM2-p53 interaction inhibitors.

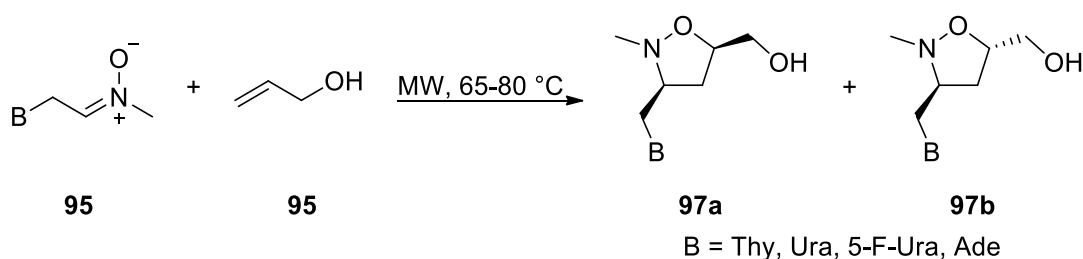


Scheme 25. Synthesis of nucleobase-containing isoxazolidines from allenes **92**.

Chiacchio *et al.*¹⁸⁶ obtained nucleobase-functionalized methyleneisoxazolidine **93** and **94** starting from allenes **92** as dipolarophiles (**Scheme 25**). In this case, the cycloaddition between *C*-ethoxycarbonyl-*N*-methylnitrone **85** and **92a** was studied, using MW-assisted conditions in CCl₄ as a solvent. As result, a 1:1 diastereomeric

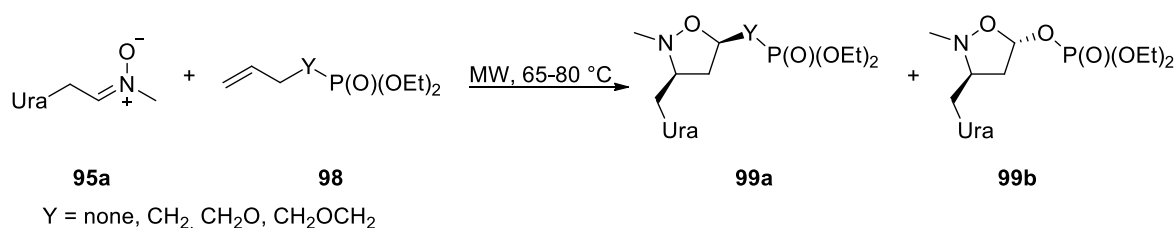
mixture of products was obtained in 50% yield after 45 minutes. When conventional heating was used, reaction times were prolonged to 480 minutes with a poor yield (20%) and the same *dr*. In the presence of *N*-acetylcytallene **92b**, the reaction outcome was different because the addition of the nitron took place over the internal C=C double bond of the allene, with formation of the compounds **94a** and **94b** in 10 minutes instead of 45 minutes as previously observed. Of note, it was possible to convert the so-obtained compounds in the products formed with the first dipolarophile (**93a** and **93b**) when a prolonged heating in ethanol was applied to the reaction vessel.

Another example of the replacement of the furanose ring with an isoxazolidine moiety can be recovered from the work published by Gotkowska and co-workers (**Scheme 26**).¹⁸⁷ In this frame, a methylene bond was introduced between the sugar mimetic ring and the nucleobase, accessed by the use of allyl alcohol **95**. According to 2D NMR data, there was excellent regioselectivity towards the 5-substituted isoxazolidines and moderate to good diastereofacial selectivity in favor of the *cis* isomer **97a**. The results showed a notable reduction in reaction time when compared to those achieved under classic conditions (from 15 h to 2.5 h).



Scheme 26. MW-assisted synthesis of homonucleosides.

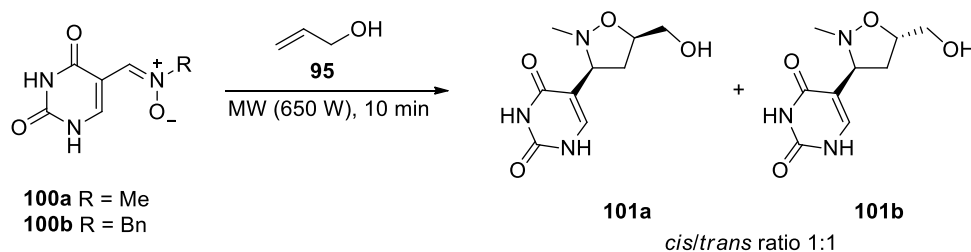
Additionally, vinyl-, allyl-, vinyloxymethyl-, and allyloxymethylphosphonates **98** reacted with uracil-derived nitron **95a** to form a mixture of two diastereoisomers of 5-phosphonated homonucleosides **99a** and **99b**, with the *cis* isomer (**99a**) being more abundant than the *trans* isomer (**99b**) (**Scheme 27**).



Scheme 27. Synthesis of 5-phosphonated homonucleosides **99a** and **99b**.

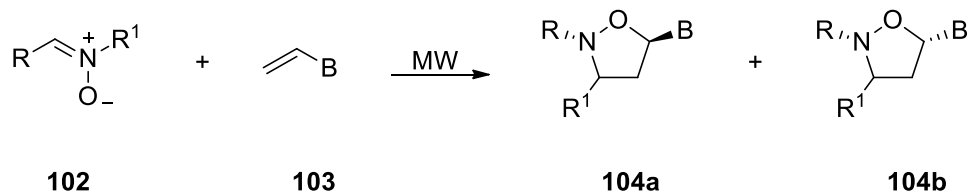
An interesting approach gave nucleoside-isoxazolidine derivatives using the nucleobases **100a-b** working as 1,3-dipoles and not as dipolarophile as previously

described (**Scheme 28**).¹⁸⁸ In this case, *trans* and *cis* isoxazolidinyl pseudouridines **101a** and **101b** were synthesized by cycloaddition reaction between the *N*-benzyl- and (*Z*)-*N*-methyl-*C*-(5-uracil)nitrones (**100a** and **100b**) and allylic alcohol **95**. The compounds were produced in yields of 80-85% after being microwave-irradiated for 10 min without the use of a solvent or catalysts.



Scheme 28. Synthesis of nucleoside-isoxazolidine analogs **101a-b** using a nucleobase-functionalized nitronium as a 1,3-dipole **100a-b**.

In another study, Bortolini and co-workers¹⁸⁹ accessed 3'-substituted-4'-*aza*-2',3'-dideoxynucleosides **104a** and **104b**, hence achieving the functionalization of the *N*-position of the isoxazolidine ring with a nucleobase scaffold. The synthetic protocol was carried out in the absence of any solvents and/or catalysts (**Scheme 29**).



B = Thy, Ura, Cyt, 5-F-Ura, Ade; R = Me, Bn, *t*-butyl; R¹ = Ph, 2-furyl, 2-Cl-C₆H₄, 2-OH-C₆H₄, 4-OH-C₆H₄, 4-NO₂-C₆H₄

Scheme 29. Synthesis of *N,O*-nucleosides *via* cycloaddition of nitrones **102** and vinyl nucleobases **103**.

The formation of the cycloadducts occurred in good yield and with great *cis-trans* selectivity (up to 99:1 in some cases) (*de* 98%). The stereoselectivity of the reaction can be explained by considering the possible way of approaching of the two species, invoking either an *exo*-approach of the alkene to the (*Z*)-nitronium or an *endo*-approach for the (*E*)-nitronium isomer. As for the *trans*-cycloadducts **104b**, the approach was predominantly of (*Z*)-*exo* type, because *N*-*tert*-butyl and *N*-aryl nitrones exist almost exclusively as *Z* isomers. On the other hand, with *N*-methyl, *N*-phenyl, and *N*-benzyl nitrones, the formation of small amounts of *E* isomers by potential *E/Z* interconversion was observed, giving a clue on the reduced formation of the *trans* isomer. NMR experiments performed at variable temperatures showed the presence of the sole (*Z*)-isomer of nitronium, even after MW irradiation for 10 minutes, excluding the possibility

of *E/Z* isomerization. Hence, the minor amounts of the *trans*-cycloadduct were explained with the (*Z*)-*endo*-approach, which is unfavored in the presence of bulky *N*-substituents (**Figure 16, TS1**).

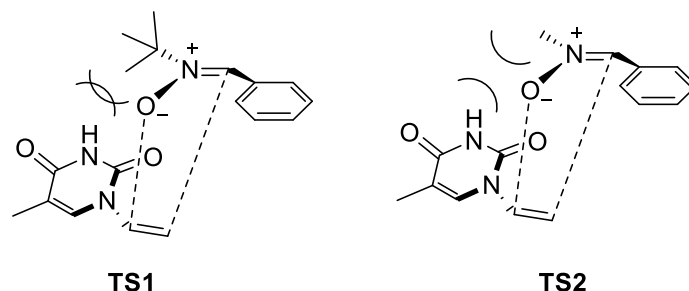
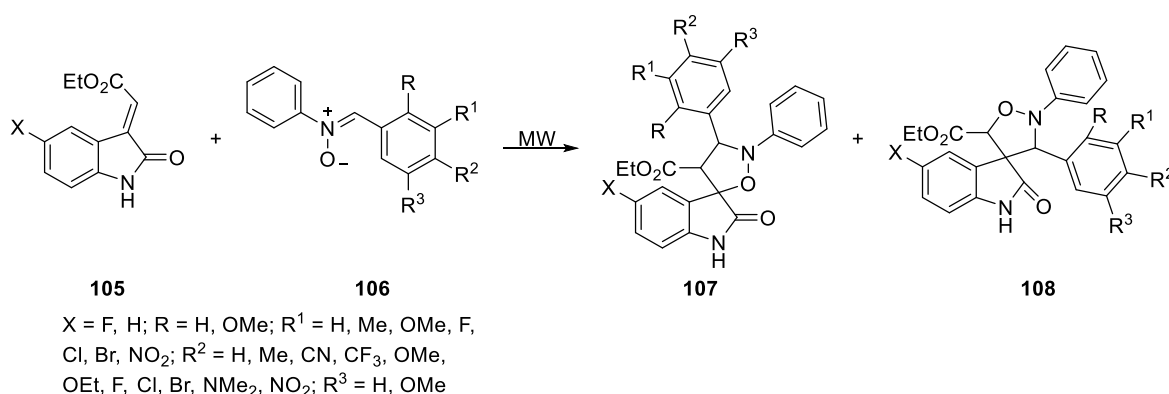


Figure 16. Model transition states for the diene-dienophile approach.

By means of *in vitro* assays, the majority of *N,O*-nucleoside derivatives obtained with this method were tested towards the inhibition of the growth of Ji-Joye cells, Jurkat cells, human lymphoblastoid cell lines (LCL), and human lymphoblastoid cell lines (LCL), showing good bioactivity at a relatively low concentration.

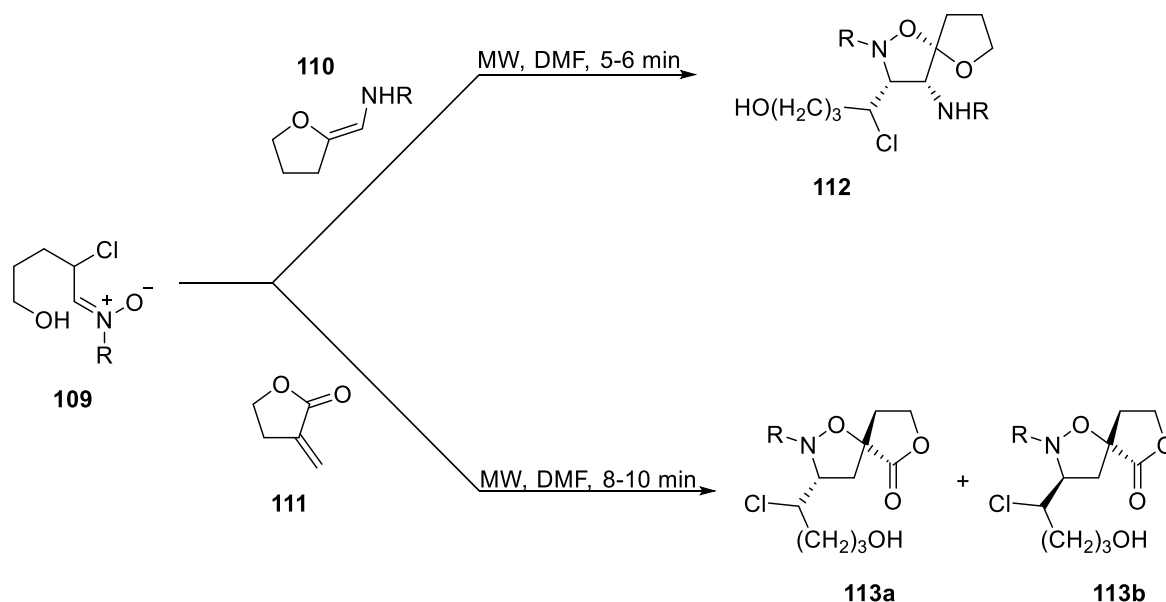


Scheme 30. MW-assisted synthesis of spiro-indoline-isoxazolidines.

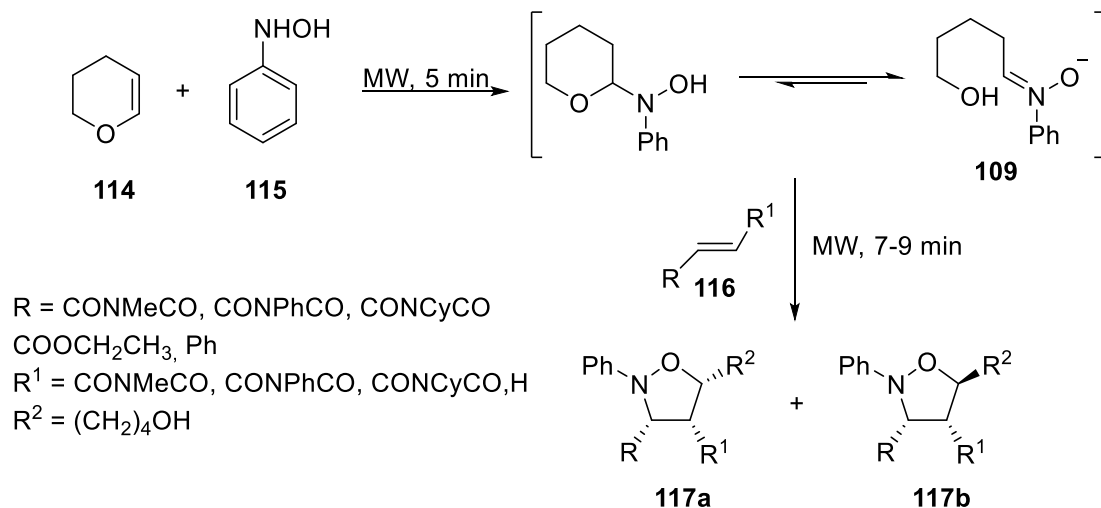
Notable advancements were proposed by Malhotra *et al.* in 2012 in the field of MW-assisted spirocompounds synthesis.¹⁹⁰ In this case, the cycloaddition between **105** and substituted *N*-diphenylnitron **106** afforded spiro-indoline-isoxazolidines **107** and **108** (**Scheme 30**). Due to a possible exocyclic double bond shifting, the regioselectivity of the reaction was completely reversed for substrates **105** containing fluorine at the *C*-5 position of the isatin ring. In this frame, it is probable that the high electronegativity of such a substituent reduces the electronic density of the aromatic ring, promoting the conjugation of the oxindole nitrogen lone pair. NMR studies allowed to assign the relative configuration of the three newly developed stereocenter, being (*R*) *C*3', (*R*) *C*5', and (*S*) *C*4' for atoms 3 and 4, and (*R*) *C*3', (*R*) *C*5', and (*R*) *C*4' for atoms 5 and 6. The so-prepared substrates were *in vitro* evaluated towards human umbilical vein

endothelial cells (HUVECs) to test their potency as anti-inflammatory agents, detecting a considerable activity.

In the same year,¹⁹⁰ using α -chloronitrones (**109**) as a dipole and α -*N*-methyl/phenyl furan derivatives (**110**) or α -methylene- γ -butyrolactone (**111**) as dipolarophiles, the synthesis of 5-spiro isoxazolidines **112**, **113a**, and **113b** was carried out under microwave radiation in a domestic oven (5-10 minutes) (**Scheme 31**). In this regard, good diastereoselectivity was obtained in the reaction with α -methylene- γ -butyrolactone, where a mixture of diastereoisomers in the ratio 75:25 in favor of *exo*-cycloadducts was detected. As for α -*N*-methyl/phenyl furan derivatives, excellent regio- and diastereoselectivity towards the 5-isomer *via* an *exo*-approach was observed.

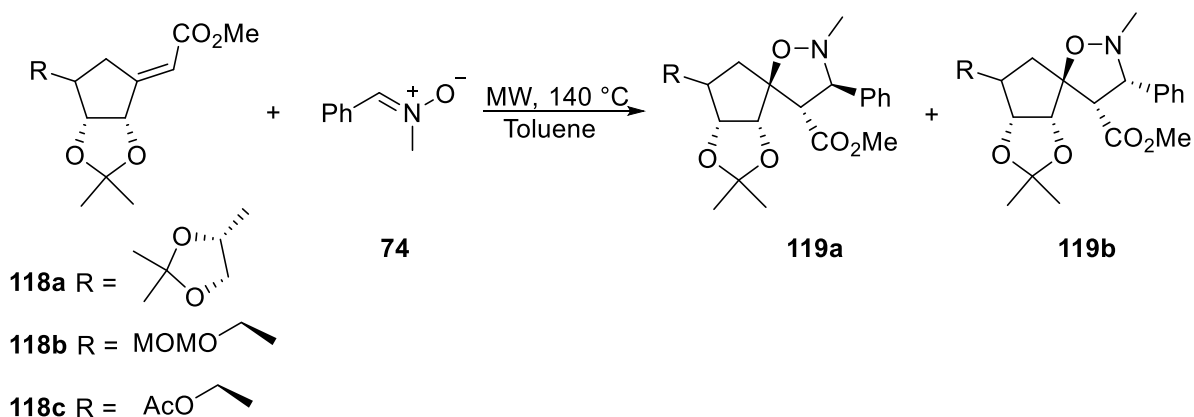


Scheme 31. MW-assisted spiroisoxazolidines preparation accessed by different dipolarophiles.



Scheme 32. Chakraborty synthesis of isoxazolidine derivatives **117** from an *in situ* generated nitron **109**.

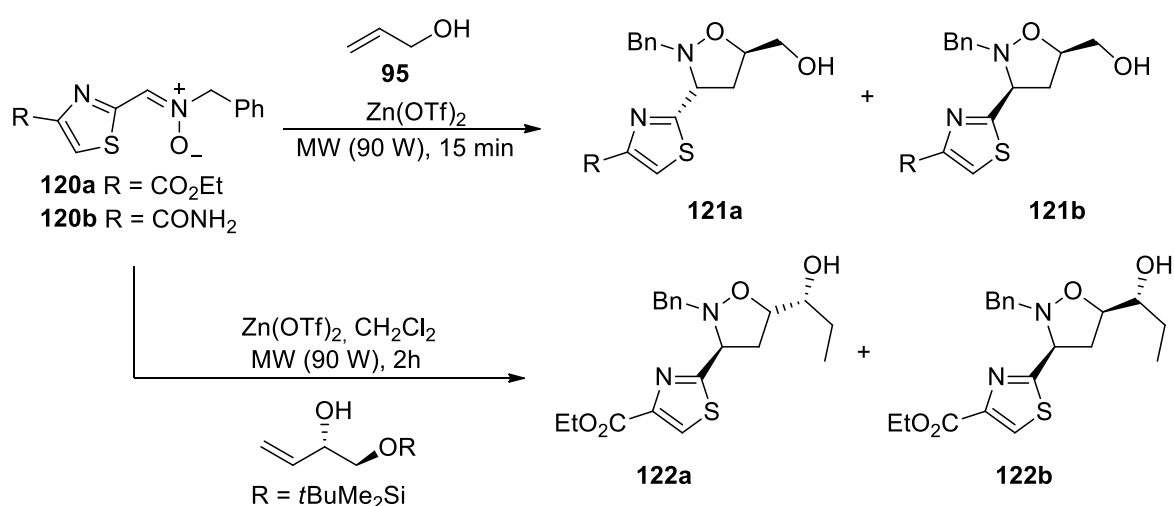
The same compound **109** was an intermediate in the reaction protocol proposed by Chakraborty *et al.* in 2012 (**Scheme 32**).¹⁹¹ In this work, the green synthesis of heterocyclic adducts from an *in situ*-prepared dihydropyran nitron-derivative was achieved. Thanks to this feature, a set of cyclic and acyclic alkenes reacted with non-isolable nitrones in the absence of solvents, obtaining bicyclic *cis*-isoxazolidines **117a** with high yields and moderate diastereofacial control. The isoxazolidine ring adopts an envelope shape with the nitrogen atom oriented out of the envelope (minor conformation) or within the envelope (major conformation), supporting the hypothesis of an *exo*-approach of *Z*-nitron for the formation of the major product. The configuration of *H*-3, *H*-4, and *H*-5 is *cis* in all diastereomers as well as in the two examples of cycloaddition with acyclic nitrones.



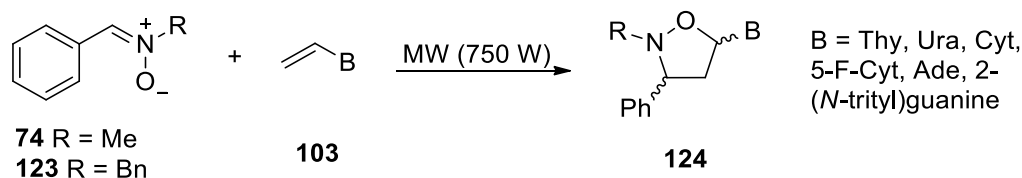
Scheme 33. MW-assisted synthesis of spiro sugar-isoxazolidines.

Other spirocompounds were obtained by Richard and co-workers in 2016¹⁹², when *gulo* and *ribo* furano-*exo*-glycans **118a-c** in combination with nitron **74** gave spiro-

sugar-isoxazolidines **119a-b** (Scheme 33). As for the *E*-configured *gulo* derivative **118a-E**, cycloaddition with **74** in toluene under microwave irradiation for 2 hours gave a mixture of *C*-3 isomers. *Exo*-glycal **118b-Z** containing a methoxymethyl protecting group was also selected, and following cycloaddition with nitrone **74**, two cycloadducts were formed in 94% yield. However, attempts to selectively deprotect the methoxymethyl group were ineffective. Hence, the reaction was carried out on the *exo* glycal **118c-Z** using acetate protection. The reaction with nitrone **74** gave a set of two separate cycloadducts **119a-b**, with an overall yield of 87%. Spiro sugar-isoxazolidines were successfully functionalized at two sites, namely *C*-4 and *C*-7, with arginine, arginine mimetics, and guanidine-containing moieties for peptidomimetics design. Additionally, 1,3-DPCA reaction between nitrones **120** and allylic alcohol **95** was used to prepare Tiazofurin analogs (Scheme 34),¹⁹³ a *C*-nucleoside with significant anticancer action against numerous human malignancies. The nitrones reacted with allylic alcohol **95** (10 eq.) to produce the isoxazolidines **121a-b** in 60-80% yields when subjected to microwave radiation and solvent-free conditions. According to the authors, in such conditions, reaction times that would have taken 15-20 days under traditional heating were drastically shortened to 1-3 hours. The synthesis of the *cis* isoxazolidine derivative **121a** as the main product only took 15 minutes thanks to the use of a Lewis acid, Zn(OTf)₂. In the presence of a such catalyst and dichloromethane as a solvent, the nitrones reacted also with chiral dipolarophiles with high *cis* selectivity.



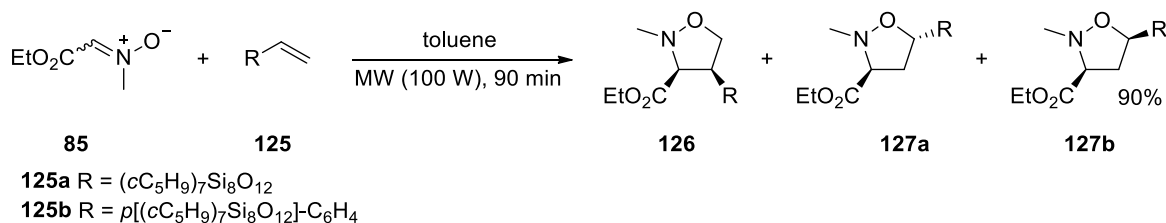
Scheme 34. MW-assisted synthesis of Tiazofurin analogs.



Scheme 35. 1,3-DPCA solvent-free reaction between *C*-phenyl nitrones and unprotected vinyl nucleobases.

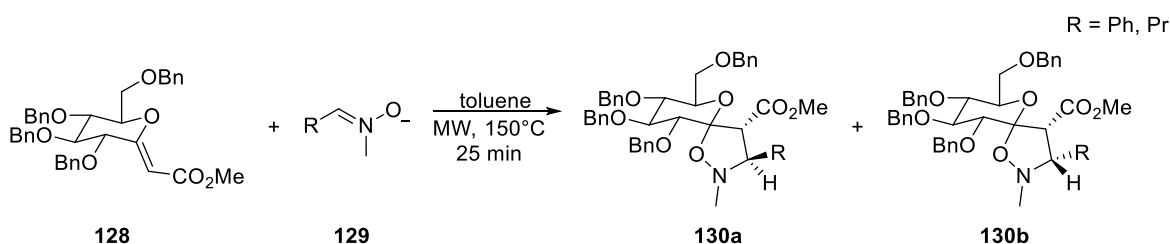
The MW-assisted solvent-free 1,3-DPCA with *N*-methyl-*C*-phenylnitrone **74** or *N*-benzyl-*C*-phenylnitrone **123** and unprotected vinyl nucleobases **103** (**Scheme 35**) gave the 4-*aza*-2,3-dideoxynucleoside **124** in good time and yields.¹⁹⁴ In this case, before the reaction, the two reagents were mixed in a mortar and then blended in a vortex. The 1-substituted isoxazolidines were obtained in regioselective fashion with *endo/exo* 70:30 *dr*.

A useful route to access functionalized vinyl-polyhedral oligomeric silsesquioxanes (POSSs) and styryl-POSSs was proposed in 2005 (**Scheme 36**).¹⁹⁵ Even in this case, the 1,3-DPCA resulted to be regio- and stereoselective, affording the *trans* isomer **127a** as the major product. Moreover, when **125b** was used as a dipolarophile it was noted the complete inversion of the diastereoselectivity, obtaining **127b** as the major product.



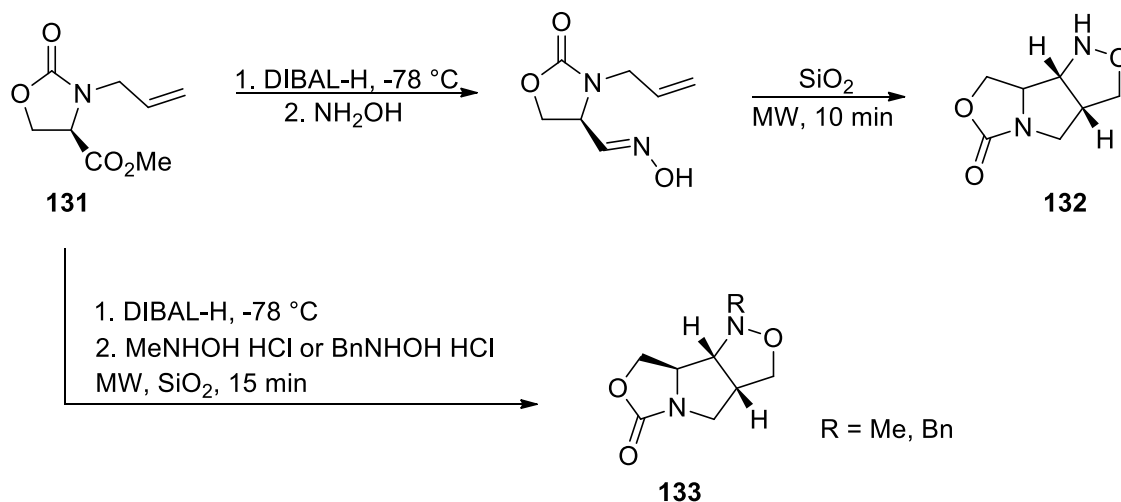
Scheme 36. Synthesis of vinyl-POSSs and styryl-POSSs through MW-assisted 1,3-DPCA.

MW-assisted 1,3-DPCA involving *exo*-glycals **128** and *N*-methylnitrones **129** gave spiroisoxazolidines **130a-b** in a regioselective and stereoselective way (**Scheme 37**). In contrast to the lack of reaction products under normal thermal conditions, high yields were achieved after only 25 min.¹⁹⁶



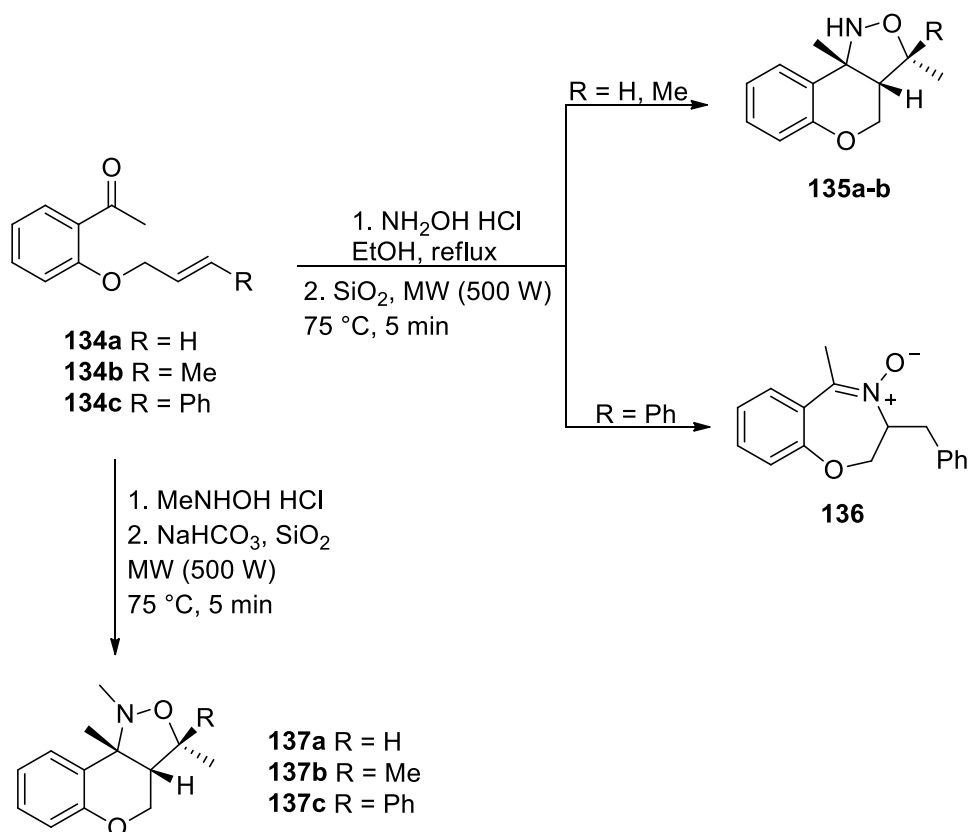
Scheme 37. *exo*-glycal-based spiroisoxazolidines synthesis.

In a similar way, chiral tricyclic isoxazolidines **132** and **133** were obtained in 80% of yields by the intramolecular cycloaddition reaction of oximes and nitrones generated from L-serine methyl ester on the surface of silica gel (**Scheme 38**).¹⁹⁷



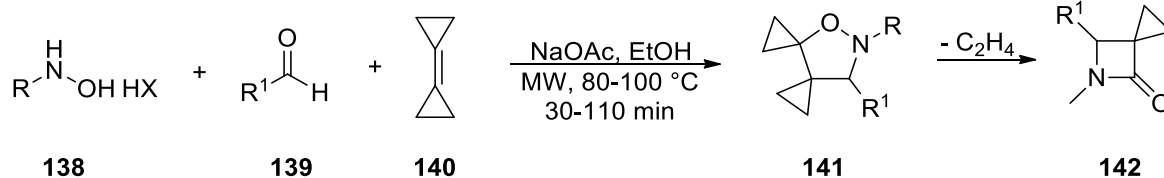
Scheme 38. MW-assisted synthesis of chiral tricyclic isoxazolidines.

N-unsubstituted nitrones and *N*-methylnitrones gave intramolecular 1,3-DPCA reaction as reported in **Scheme 39**.¹⁹⁸ The *N*-methylnitrone derivatives gave fused isoxazolidines **135** in up to 97% of yields.



Scheme 39. MW-assisted 1,3-DPCA of fused isoxazolidine.

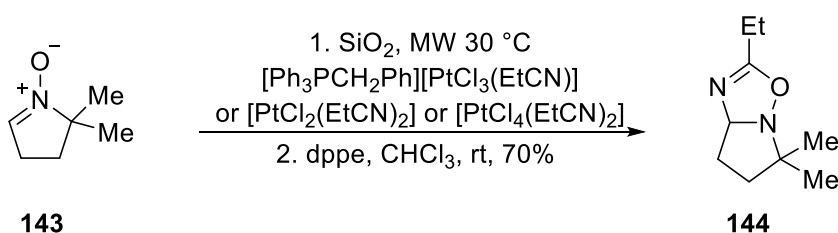
Methylenecyclopropane **140** (Scheme 40) gave a cycloaddition reaction in the presence of *in situ*-formed nitrones from oximes **138** and aldehydes **139**, to yield spiroisoxazolidines **141**.¹⁹⁹ Such a spirocyclopropanated intermediate underwent rearrangement with loss of ethylene, affording the β -lactam **142** in 78% of yields after 30 to 120 min.



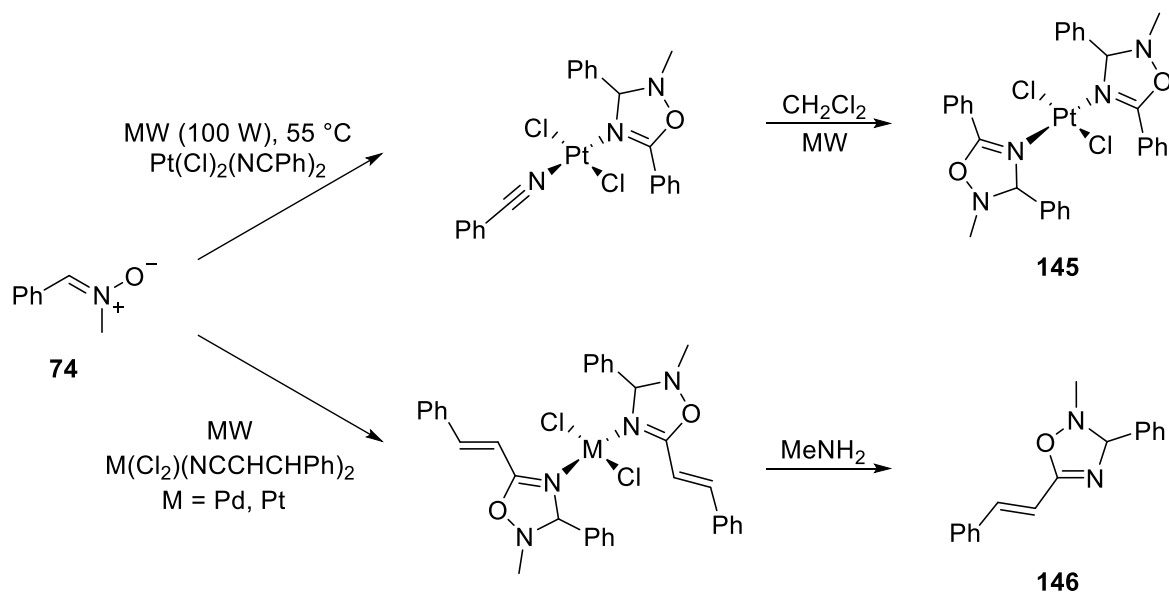
R = Bn, $\text{CH}_2\text{C}_6\text{H}_4\text{OCH}_3$, CHPh_2 , *t*Bu, Me; HX = HCl or $(\text{COOH})_2$; $\text{R}^1 = \text{H}, \text{CO}_2\text{Et}, \text{CO}_2\text{Me}$

Scheme 40. MW-assisted synthesis of β -lactams from *in situ* generated nitrones.

Other heterocycles such as 2,3-dihydro-1,2,4-oxadiazoles were obtained by 1,3-dipolar cycloadditions of nitrones to nitriles, according to the literature.²⁰⁰ It is an interesting example because nitriles are not as reactive as alkenes in cycloadditions, resulting in a few examples in the literature regarding the synthesis of 2,3-dihydro-1,2,4-oxadiazoles. However, it has been demonstrated that the 1,3-DPCA reaction outcome can be enhanced by coordinating the nitrile group to a metal, often Pd (II) or Pt (II).²⁰¹ A study also demonstrated how *C,N*-diphenylnitronone **143** reacted in the presence of microwave irradiation to give the correspondent oxadiazole **144** in 39% yield (Scheme 41).²⁰² Only a 4% yield of the identical compound could be produced under standard heating conditions.

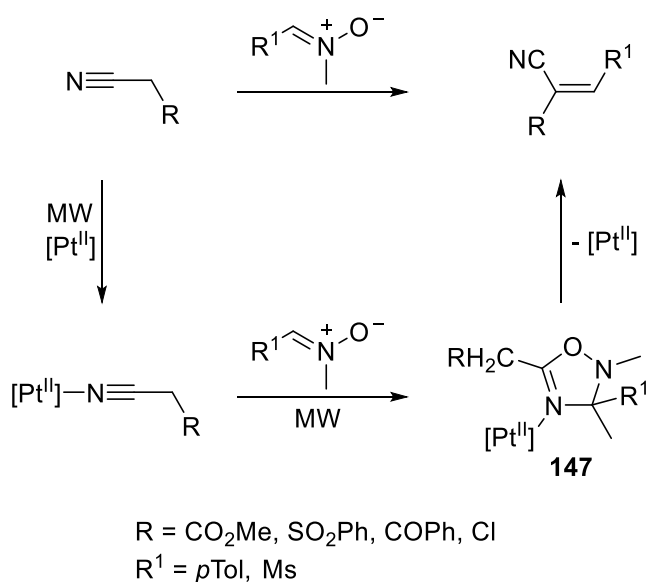


Scheme 41. Pt-assisted synthesis of 2,3-dihydro-1,2,4-oxadiazoles **327**.



Scheme 42. MW-assisted cycloaddition between *N*-methyl-*C*-phenylnitrone **74** and Pd and Pt complexes.

The use of Pd and Pt (II)-coordinated benzonitrile complexes as dipolarophiles enhanced the reaction rate of 25 times in comparison with the typical thermal process (**Scheme 42**), leading to products **146** with 50% yields after 3 minutes of reaction.²⁰³ In this case, after 65 minutes of MW irradiation, it was possible to detect a 50% yield of the bis-adduct **145**.

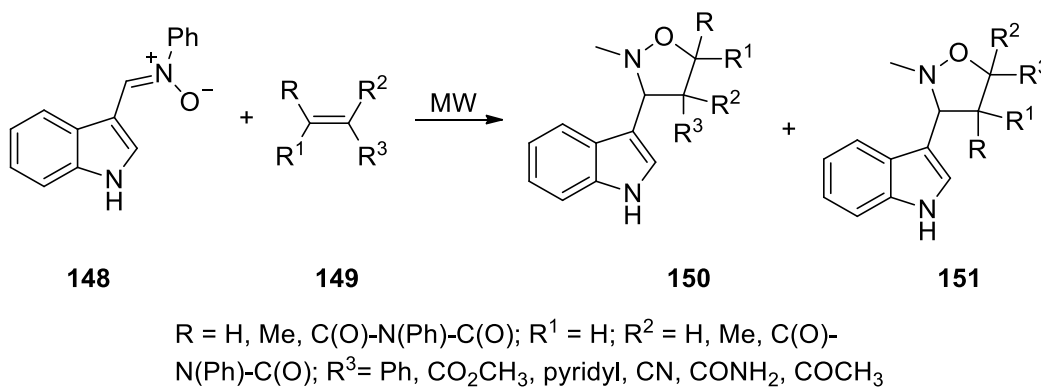


Scheme 43. Solid phase 1,3-DPCA reaction between Pt (II)-coordinated organonitriles and acyclic nitrones.

In addition, acyclic nitrones and organonitriles reacted with acidic methylenic groups to access polysubstituted (*E*)-alkenes (**Scheme 43**). In this case, oxadiazoline species **147** were formed when the organonitriles underwent [3+2] cycloaddition with the

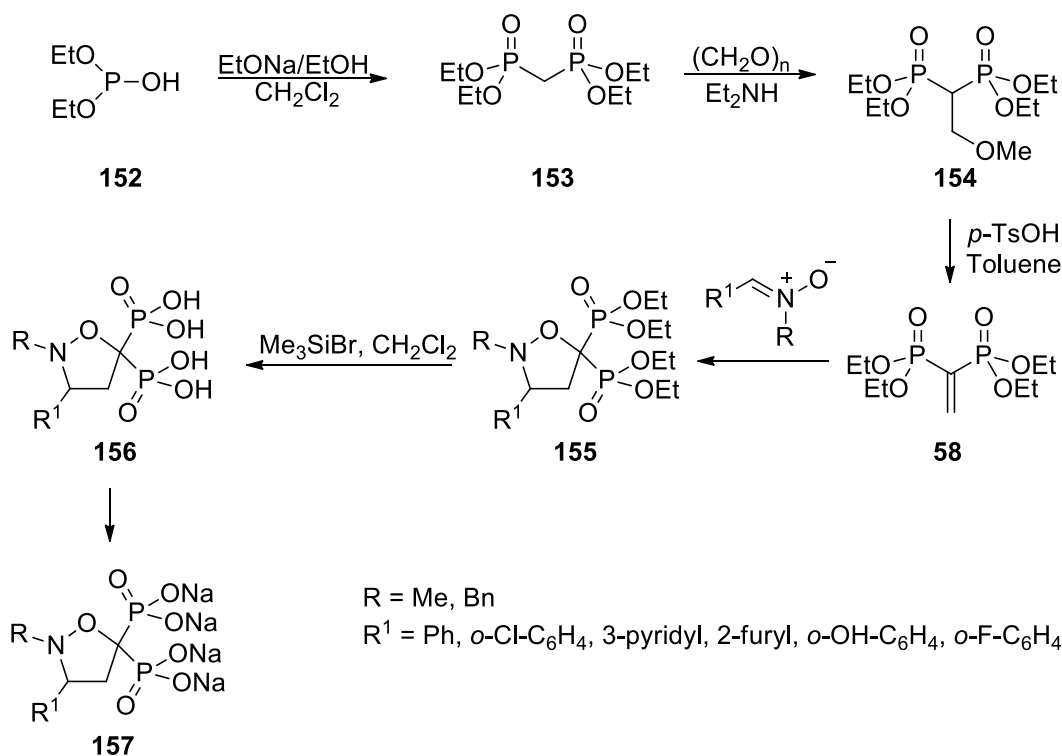
acyclic nitrones after being coordinated to Pt (II). Cyano-alkenes and MeHNOH were formed *via* the release and retrocycloaddition of the oxadiazoline complexes **147**. In this frame, MWs helped to speed up the process, especially in co-presence of SiO₂, with up to 80% yields.

Pyridinyl isoxazolidines were obtained too by means of MWs. In this regard, a work by 2012 by Sharma and collaborators²⁰⁴ aimed to obtain such compounds bearing a pyridyl group at the C-3 position (**Scheme 44**). In doing so, the MW-assisted solvent-free reaction between C-(3-indolyl)-N-phenylnitron **148** and mono-substituted, disubstituted, and cyclic dipolarophiles **149** at 150 W and 100 °C gave the desired products in good yields and times. Moreover, good regioselectivity towards **150** was assessed and the substrates were evaluated in human cancer cell lines.



Scheme 44. Synthesis of substituted 3-indolyl-isoxazolidines.

Finally, we would like to report some examples to give some context for the research work (*research line 2*) of this chapter.

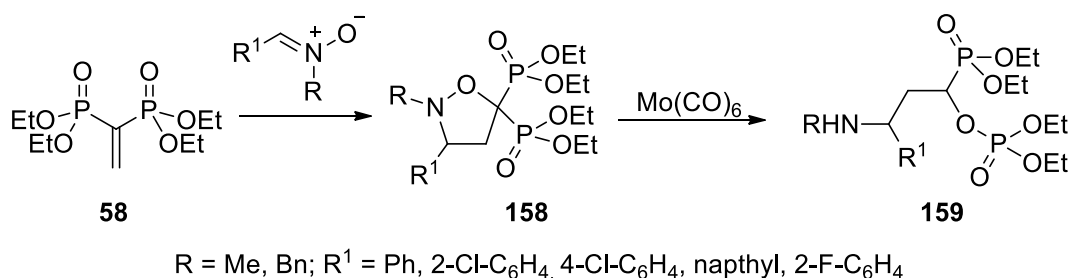


Scheme 45. Synthesis of isoxazolidine bisphosphonate through the MW-assisted cycloaddition of tetraethylvinylidene-1,1-bisphosphonate **157** with nitrones.

One of the first MW-assisted syntheses of isoxazolidine bisphosphonates was proposed by Bortolini *et al.*²⁰⁵ in 2011 (**Scheme 45**). In this protocol, the preparation of the dipolarophile **58** was achieved in high yields and a three-step reaction from diethyl phosphite **152** in the presence of sodium ethoxide. After several attempts to optimize the reaction protocol, free-solvent MW irradiation conditions were preferred to conventional conditions. To complete the cycloaddition and isolate the bisphosphonate isoxazolidines **155** in high yields, a 200 W potency and a small excess of dipole were tested. By using decoupling ^1H NMR experiments, the regiochemistry was also investigated, assessing that the 5-bisphosphonate isomer was the sole regioisomer. As for the mechanism, it was possible to confirm that the *N*-oxygen atom of the nitrone partner attacks the geminal carbon of the vinylidene group. Given that bisphosphonates are mainly administrated as a sodium salt, the synthesis was continued by hydrolyzing the bisphosphonate esters **155**. The resultant acids **156** were converted into the corresponding disodium salts **157** by reaction with aqueous sodium hydroxide.

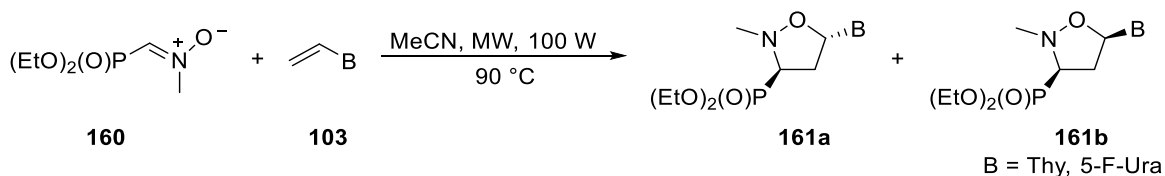
Another notable application of such technology in the synthesis of isoxazolidine bisphosphonates was proposed in 2014.²⁰⁶ Using solvent-free conditions, a set of bisphosphonates **158** with an isoxazolidine ring at the geminal position was prepared.

Hence, by successively cleaving the N-O bond, the isoxazolidine ring was expanded, resulting in the formation of *gem*-phosphonate-phosphates **159**. (**Scheme 46**).



Scheme 46. Synthesis and ring-opening of isoxazolidine bisphosphonates **158**.

Truncated phosphonated carbocyclic 2'-oxa-3'-*aza* nucleosides (TPCOANs) are a family of N,O-nucleosides that mimic the first monophosphate group of natural nucleosides by having a phosphonate group that is directly attached to the C4'-position of the isoxazolidine moiety. A single-step method for obtaining TPCOANs was proposed (**Scheme 47**),²⁰⁷ wherein the 1,3-DPCA between vinylnucleobases **103** and phosphonate nitrones **160** was implemented. By selecting the solvent and reaction conditions (acetonitrile, 100 W, 90 °C), it was finally possible to isolate phosphonated cycloadducts **161a** and **161b** with good yields and high *dr*.



Scheme 47. Synthesis of truncated phosphonated carbocyclic 2'-oxa-3'-*aza* nucleosides.

Results and Discussion

Research line 2 – New class of isoxazolidine bisphosphonates as potential human farnesyl pyrophosphate synthase (hFPPS) inhibitors

The research presented in this paragraph will be focused on the results obtained for the synthesis of novel isoxazolidine bisphosphonates through MW-assisted 1,3-DPCA. Molecular dynamics, docking simulations, and STD NMR studies are underway to simulate the interaction of our compounds with the human farnesyl pyrophosphate synthase (*hFPPS*) in collaboration with Dr. Ignacio Delso from the University of East Anglia and Prof. Pedro Merino from the University of Zaragoza. With the results reported in other papers^{189,194,206} in hand, we designed and synthesized a new type of nitrogen-containing BPs, in which the O-P-C-P-O moiety, as well as the *gem*-hydroxyl group, were preserved on the final products (**Figure 16**).

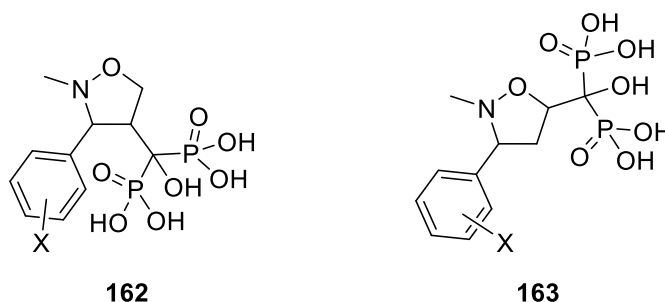
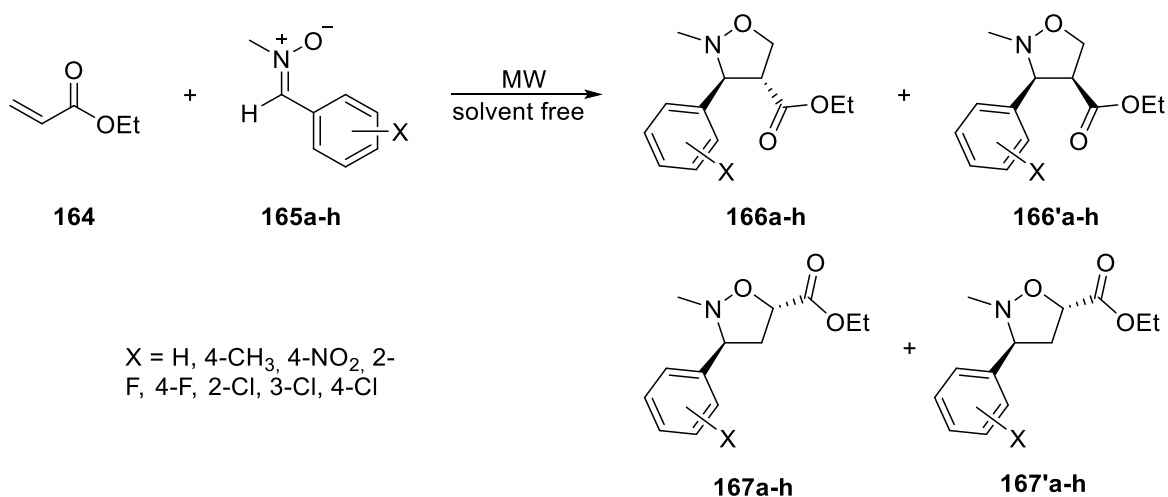


Figure 16. Structure of synthesized *gem*-hydroxyl isoxazolidine bisphosphonic acids **162** and **163**.

The first step in the synthesis of isoxazolidine-bisphosphonates **162** and **163** required a solvent-free 1,3-DPCA between ethyl acrylate **164** and nitrones **165a-h** (**Scheme 48**).



Scheme 48. Synthetic procedure followed to prepare the isoxazolidine BP derivatives.

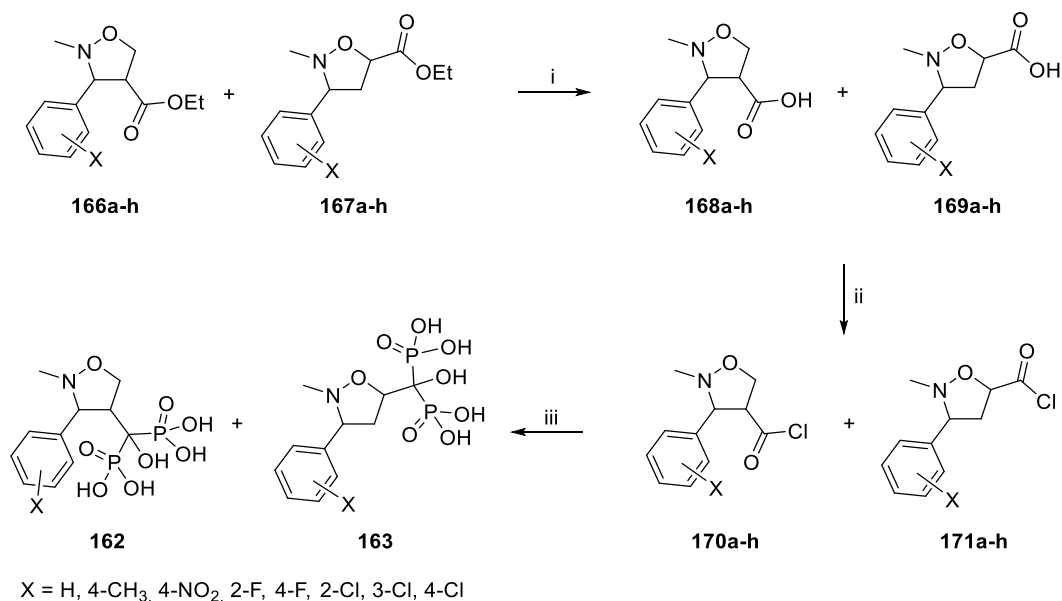
The process is very straightforward and is about mixing the two components together in a vessel inside a microwave oven set to 750 W for times ranging from 6 to 10 minutes. The cycloaddition reaction between ethyl acrylate **164** and nitron **165a** was used as the model reaction. The optimal reaction conditions were assessed to be 750 W of power, 138 °C of temperature, and a 1:2 ratio of nitron:vinyl ester. As reported in **Table 1**, the cycloadducts were obtained as a mixture of two regioisomers **166** and **167** (*C4*- and *C5*-substituted isomers, respectively) and two couple of diastereoisomers (**166a-h:166'a-h** and **167a-h:167'a-h** *endo:exo* isomers, respectively) with a major *endo* stereoselectivity of the most abundant *C5*-substituted isomer (**167a-h**), in coherence to literature data.²⁰⁸

Table 1. Results obtained by 1,3-dipolar cycloaddition reaction between nitrones and ethyl acrylate.

Entry	Nitron	X	Cycloadducts	Yield (%)	Ratio of adducts ^a 166:166':167:167'
1	165a	H	166a; 166'a; 167a; 167'a	98	8:17:74.5:0.5
2	165b	<i>p</i> -CH ₃	166b; 166'b; 167b; 167'b	95	10.5:17:72:0.5
3	165c	<i>p</i> -NO ₂	166c; 166'c; 167c; 167'c	97	9.5:18.5:71:1
4	165d	<i>o</i> -F	166d; 166'd; 167d; 167'd	99	7:17:70:6
5	165e	<i>p</i> -F	166e; 166'e; 167e; 167'e	97	8:20:71.5:0.5
6	165f	<i>o</i> -Cl	166f; 166'f; 167f; 167'f	98	3.5:22:74:0.5
7	165g	<i>m</i> -Cl	166g; 166'g; 167g; 167'g	96	9:15:75:1
8	165h	<i>p</i> -Cl	166h; 166'h; 167h; 167'h	99	9.5:18:72:0.5

^aDiastereoisomer ratio determined by ¹H NMR

The presence of an aromatic moiety deriving from nitrones **165a-h** may also add secondary interactions (π - π stacking) between compounds **162-163** and the biological target, as demonstrated for isoxazolidines with similar substituents.¹⁸⁹ As for reactivity, yields and stereoselectivity do not appear to be dependent to the tested substituents. Hence, by means of a multistep process (**Scheme 49**), the obtained cycloadducts **166a-h** and **167a-h** were converted into the desired bisphosphonates **162a-h** and **163a-h**.



Scheme 49. Reaction conditions: i) NaOH, EtOH, rt, 24h; ii) (COCl)₂, CH₂Cl₂ *dry*, rt, 4h; iii) 1. P(OSiMe₃)₃, THF *dry*, rt, 24h; 2. MeOH, rt, 3h.

Initially, the ester group was hydrolyzed in the corresponding acid derivative, without isolating the species **168a-h** and **169a-h**. Hence, the reaction crude was treated to convert the so-obtained compounds into the corresponding acid chloride derivatives (**170a-h** and **170a-h**). The direct treatment of acyl chloride substrates **170a-h** and **170a-h** with tris(trimethylsilyl) phosphite at room temperature and subsequent addition of methanol, afforded the expected *gem*-hydroxyl isoxazolidine bisphosphonic acids **162a-h** and **163a-h** in a single step and excellent yields (**Table 2**).

Table 2. Synthesized *gem*-hydroxyl isoxazolidine bisphosphonic acids **162a-1h** and **163a-h**.

Entry	Ester derivative	Bisphosphonate	Yield (%)	Ratio of adducts BP1:BP1':BP2:BP2'
1	166a and 167a	162a; 162'a; 163a; 163'a	98	9:18.5:72:0.5
2	166b and 167b	162b; 162'b; 163b; 163'b	99	10:18:71.5:0.5
3	166c and 167c	162c; 162'c; 163c; 163'c	96	10:18.5:70:1.5
4	166d and 167d	162d; 162'd; 163d; 163'd	98	7.5:17:70:6.5
5	166e and 167e	162e; 162'e; 163e; 163'e	98	8.5:20:70.5:1
6	166f and 167f	162f; 162'f; 163f; 163'f	97	4.5:22:72.5:1
7	166g and 167g	162g; 162'g; 163g; 163'g	99	9:18:71.5:1.5
8	166h and 167h	162h; 162'h; 163h; 163'h	99	10:20:68:2

In conclusion, in this *research line*, we successfully implemented a green protocol for the MW-assisted synthesis of *N*-BPs and related precursors. Computational studies (molecular dynamics and docking) and STD NMR experiments are ongoing to assess the interaction mode of our compounds with *h*FFPS, a modern target that could expand the frontiers of these drugs 50 years after their debut.

Chapter 3

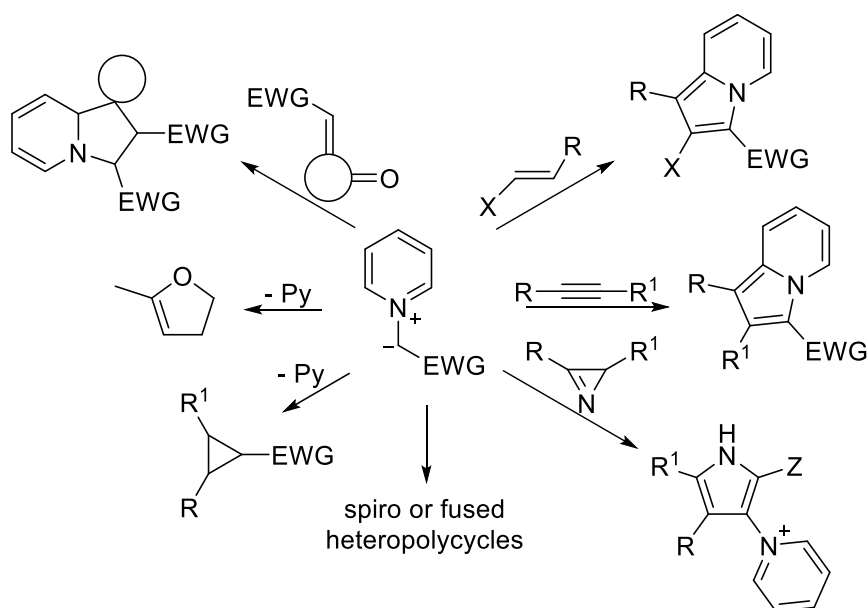
Pyridinium ylides: useful tools in multicomponent synthesis

Introduction

In this chapter we will focus on pyridinium ylides, versatile reagents largely used in small molecule synthesis. In particular, we will focus on their use in 1,3-DPCA and cyclopropanation reaction for accessing indolizines and spirocyclopropyl oxindoles, respectively. In both cases, pyridinium ylides resulted particularly suitable for the implementation of multicomponent protocols, with save of time and solvents. Hence, in the first paragraph, we will survey the use of such species for constructing *N*-heterocycles. In doing so, we will highlight the main strategies for the synthesis of indolizines and a brief overview about their extended biological activities will be reported. The third paragraph will be devoted to reporting the use of pyridinium ylides for the multicomponent synthesis of our polysubstituted indolizines (*research line 3a*). In the fourth paragraph, the general strategies for preparing spirocyclopropyl oxindoles and their principal biological activity will be described. Then, in the last paragraph our research regarding the use of pyridinium ylides as Michael donators in a cyclopropanation reaction will be presented (*research line 3b*). This last part will be enriched by a series of QM calculations devoted to elucidating the reaction mechanism and to deepening the observed diastereoselectivity of the reaction.

1. Recent developments in *N*-heterocycles synthesis using pyridinium ylides

Pyridinium ylides are one of the most versatile building blocks in heterocyclic chemistry. Such type of organic synthesis greatly benefited from the development of protocols based on the reactivity of pyridinium ylides, capable of behaving as nucleophiles, 1,3-dipoles, and in some cases, as electrophiles (**Scheme 1**). The story of these tools begins in 1935 when the Krohnke synthesis of a stable pyridinium ylide was published.²⁰⁹ If interested, the reader can refer to other recent thorough reviews regarding the use of pyridinium ylides up to the beginning of 2012.^{210,211}

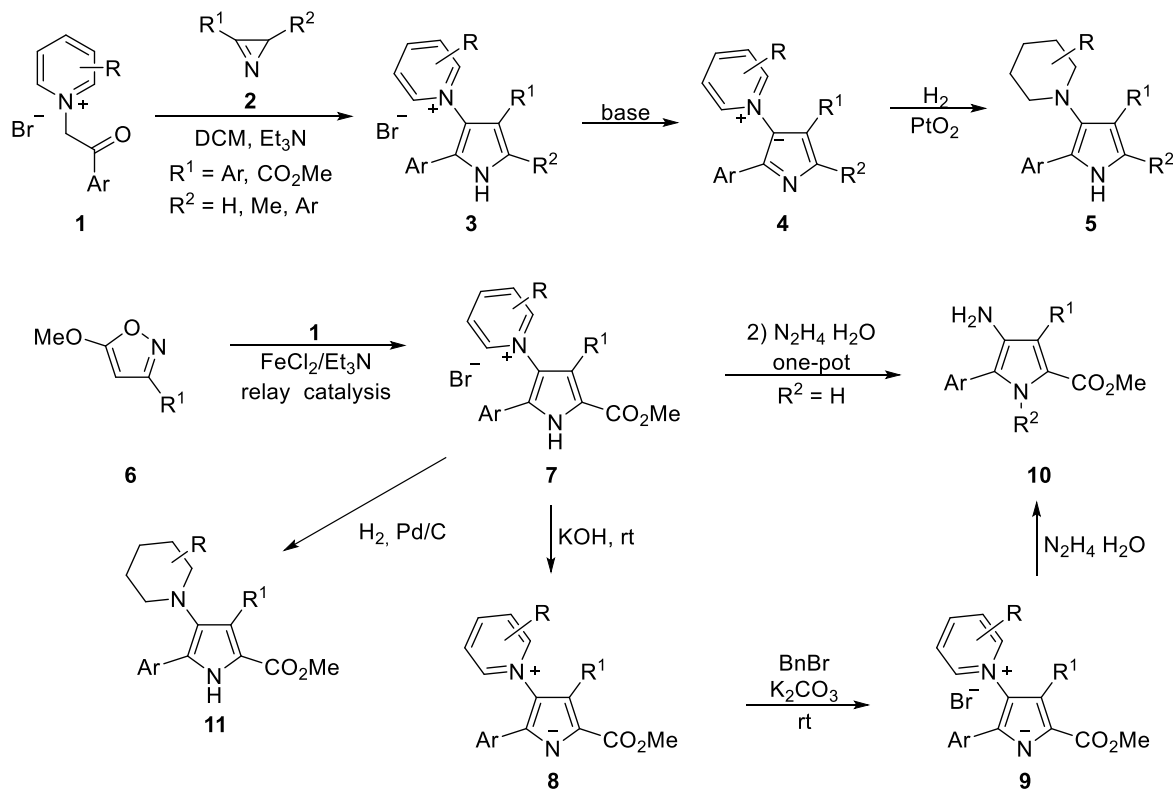


Scheme 1. Synthetic applications of pyridinium ylides.

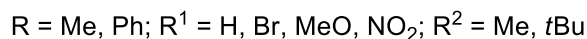
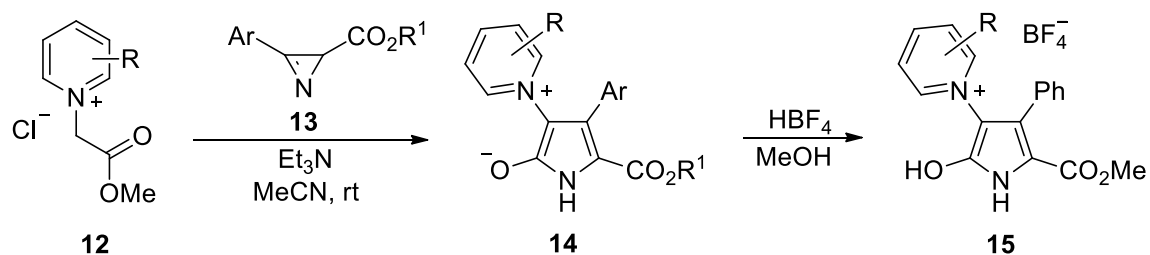
1.1 Synthesis of pyrrole derivatives

One of the most important applications of pyridinium ylides regards the pyrrole synthesis, which recently benefited from some updates (**Scheme 2**). A generic approach for the reaction of pyridinium salts **1** with 2*H*-azirines **2** to produce 1-(pyrrol-3-yl) pyridinium salts **3**, ylides **4**, and aminopyrroles **5** has recently been proposed.²¹² By treating salts **3** with a base, a new class of stable 3-(pyridinium-1-yl)pyrrolides **4** were produced in high yields. In the presence of the Adams catalyst, hydrogenation of ylides **4** produced 1-(pyrrol-3-yl)piperidines **5** in good yields. By reaction of 5-methoxyisoxazoles with pyridinium ylides in the presence of a FeCl₂/Et₃N binary catalytic system, pyridinium salts **7** were obtained. Subsequently, **7** was treated with hydrazine, obtaining methyl 4-aminopyrrole-2-carboxylate **11**.²¹³ The reaction passed by the alkyl azirine-2-carboxylate intermediate, wherein Fe(II) was the catalyst.

By exploiting the nucleophilic reaction to form pyrrolypyridinium ylides **8** from salts **7**, this method enabled the addition of a substituent at the pyrrole nitrogen. Lastly, methyl 4-piperidinopyrrole-2-carboxylates **11** were also obtained by the catalytic reduction of pyrrolypyridinium salts **7**.



Scheme 2. Synthesis of 1-(pyrrol-3-yl)pyridinium salts **3**, ylides **4**, and aminopyrroles **5, 10, 11**.

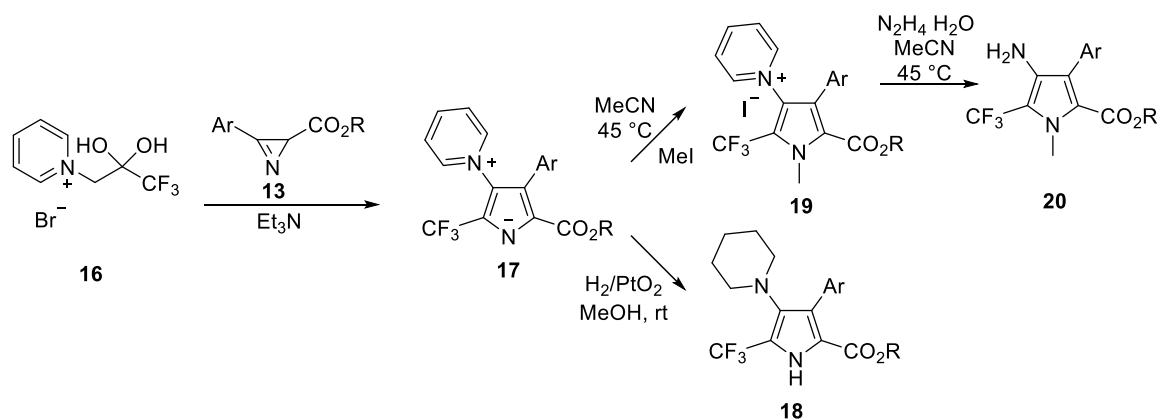


Scheme 3. Synthesis of heterocyclic betaines **14**.

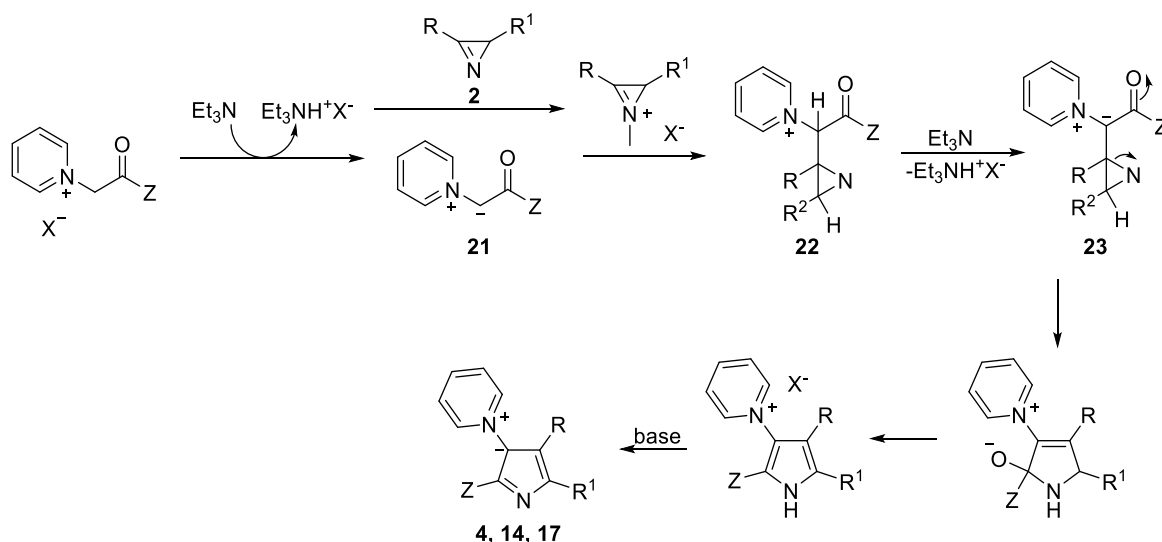
By reacting azirinecarboxylates **13** with methoxycarbonylmethylpyridinium ylides **12**, new betaine-containing pyridinium pyrrolides **14** were obtained in good yields (**Scheme 3**).²¹⁴ Both in solution and the solid state, betaines can be found as their *NH*-tautomers. The main peculiarity of such compounds resides in the intramolecular charge transfer between the positively charged pyridinium group and the negatively charged pyrrole unit, which leads to their typical longwave absorption band. In addition, the formation of α -hydroxypyrrole **15** with a 3-pyridinium group was made

possible by the acidification of betaine **14**. However, the experimental outcome showed some limitations. For instance, it was impossible to isolate betaine derivatives bearing *N,N*-dimethylaminopyridine, quinoline, or isoquinoline moieties. Additionally, attempts to replace the pyridine heterocycle with an imidazole group also failed.

Based on the azirine ring expansion method, trifluoromethyl-substituted aminopyrroles were prepared using pyridinium bromide **16** as a building block (**Scheme 4**).²¹⁵ The first products, piperidinylsubstituted pyrroles **17**, were hydrogenated with H_2/PtO_2 to give pyridinium pyrrolides **19**, which were converted by a methylation/hydrazinolysis reaction into α -trifluoromethyl- β -aminopyrroles **20**. The low thermal stability of the ylide **17** was determined by its reduced thermal stability.



Scheme 4. Synthesis of trifluoromethyl-substituted aminopyrroles.



Scheme 5. Plausible mechanism of the formation of pyrrolylpyridinium salts and ylides.

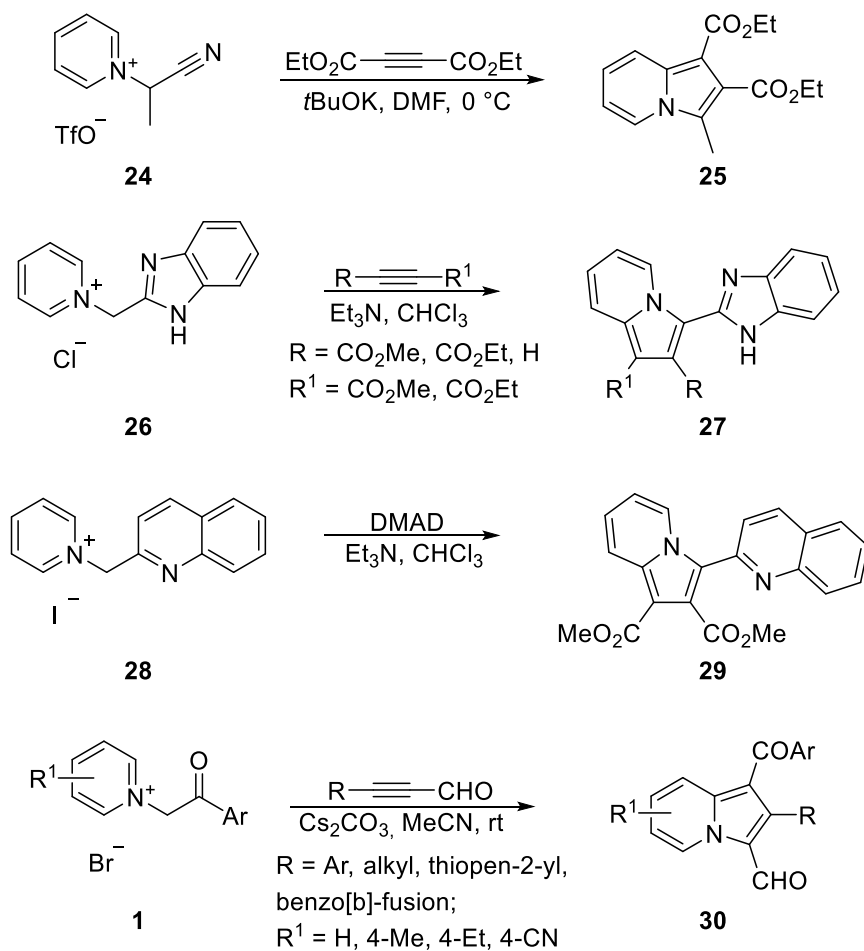
A plausible reaction mechanism for the formation of 3-(pyridinium-1-yl)pyrrolides **4**, **14**, **17** was proposed to pass by the nucleophilic attack of the pyridinium ylide **21** on

the C=N bond of the protonated azirine, forming the aziridine intermediate **22** (**Scheme 5**). Dehydrohalogenation of the latter to aziridinyl-substituted pyridinium ylide **23**, followed by rearrangement and aromatization, gave the final product. A variety of azolium ylides was used in such process to prepare various pyrrole derivatives.^{216,217}

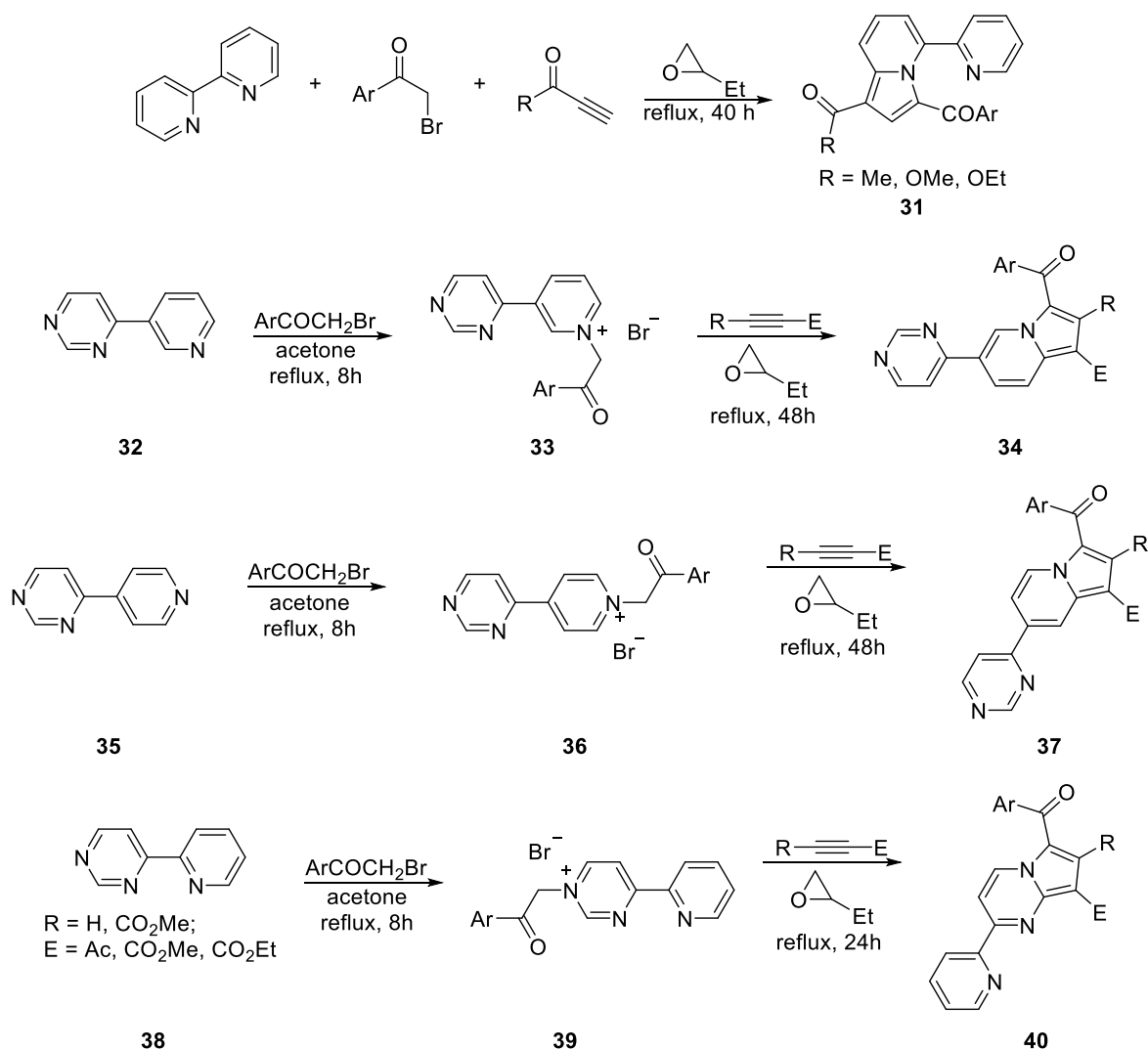
1.2 Reactions with acetylene and alkene derivatives

Pyridinium ylide reactivity towards acetylenes and alkenes can be considered a pillar for indolizine synthesis. There are several different synthetic methods for obtaining indolizine moieties, but the [3+2]-cycloaddition of pyridinium ylides, made from α -halocarbonyl or diazo compounds, with electron-deficient olefins or alkynes is the most used approach by far. 1,3-DPCA followed by oxidation procedures are typically used in the reaction of pyridinium ylides with olefins, whilst the use of alkynes as dipolarophile do not require the use of oxidants.

Acetylenes are one of the most important reaction partners for pyridinium ylides, as said (**Scheme 6**). Under alkaline conditions, 1,3-DPCA/HCN elimination was used to form indolizine **25** from the reaction of the cyano-substituted pyridinium triflate **24** with dimethyl acetylenedicarboxylate (DMAD).²¹⁸ The formation of indolizines was not obtained when pyridinium ylide reacted with other alkynes, such as phenylacetylene, propyne, pentyne, or hexyne.²¹⁹ Indolizine derivatives **27** were obtained from the cycloaddition of salt **26** and electron-deficient alkynes in the presence of a base. Similarly, when quinolinyl-substituted salts **28** reacted with DMAD, quinolinylindolizine **29** was produced in a modest yield.²¹⁹ By reaction of aryl-substituted pyridinium ylides deriving from salt **1** to aryl-, heteroaryl-, and alkyl-substituted propiolaldehydes, indolizine-1-carbaldehydes **30** were also accessed. Such an approach provided highly-functionalized derivatives with a broad substrate scope and mild reaction conditions.²²⁰



Scheme 6. Synthesis of indolizines by cycloaddition of pyridinium ylides to alkynes.

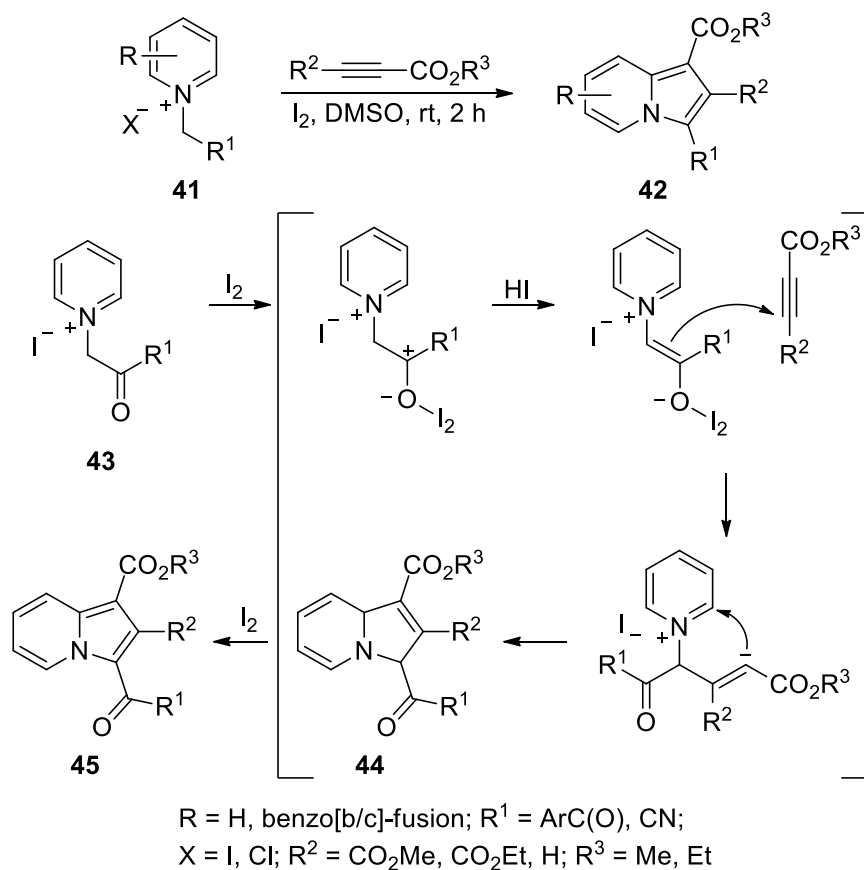


Scheme 7. Synthesis of indolizines and pyrrolo[1,2-*c*]pyrimidines from diazines.

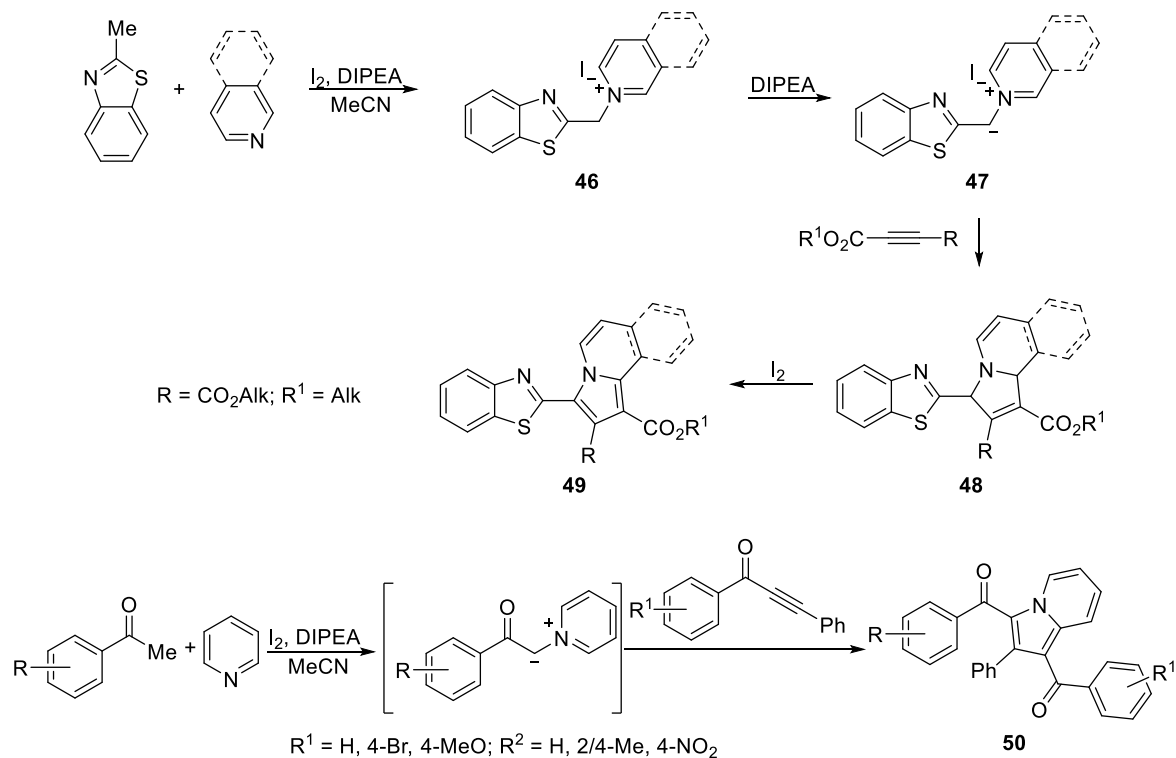
Georgescu *et al.*²²¹ described a one-pot, three-component method for synthesizing pyridyl-substituted indolizines **31** using readily available reactants such as 2-2'-dipyridyl-substituted bromoacetophenones, and nonsymmetrical electron-poor alkynes (**Scheme 7**). To generate the pyridinium ylide, the reaction was conducted in 1,2-epoxybutane, which functioned as a solvent and acid scavenger. It was also discovered that the structure of pyridylpyrimidines had an impact on the outcome of an analogous process. By using the *in situ* formed *N*-ylides from the appropriate cycloimmonium bromides, the 1,3-DPCA reaction over 4-(pyridyl)pyrimidine structural isomers was employed for the annulation of the pyrrole ring. As expected, phenacyl bromide quaternized 3-pyridylpyrimidine **32** and 4-pyridylpyrimidine **35** at the pyridine nitrogen to produce pyridinium bromides **33** and **36**. The indolizine derivatives **34** and **37** were obtained by the subsequent reaction of pyridinium *N*-ylides with different alkynes. However, the steric hindrance in pyrrolo[1,2-

c]pyrimidines **40** caused by the bromoketone reaction with the pyridine nitrogen in pyridylpyrimidine **38** oriented the reaction towards pyrimidinium *N*-ylides **39**.

By means of the 1,3-DPCA/aromatization protocol reported by Liu *et al.* (Scheme 8),²²² the iodine-promoted synthesis of acylindolizinecarboxylates **42** from pyridinium isoquinolinium and quinolinium salts **41** and acetylenecarboxylates was achieved. Of note, moderate to good yields were obtained when ylides with both electron-deficient and electron-rich substituents in the aroyl group reacted. The authors also proposed a mechanism wherein an I₂-induced dehydroiodation of pyridinium salt **43** took place, followed by a Michael-type addition to the alkyne to give dihydroindolizine **44**, and then by a final oxidation with I₂ to give the expected indolizine **45**.

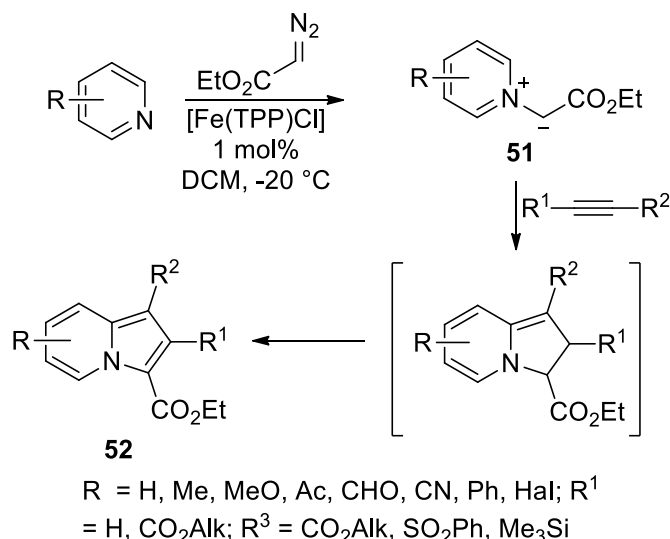


Scheme 8. I₂-induced indolizine synthesis and the proposed reaction mechanism.



Scheme 9. I_2/DIPEA -promoted synthesis of benzothiazolyl- and 1,3-diaroyl-substituted indolizine derivatives.

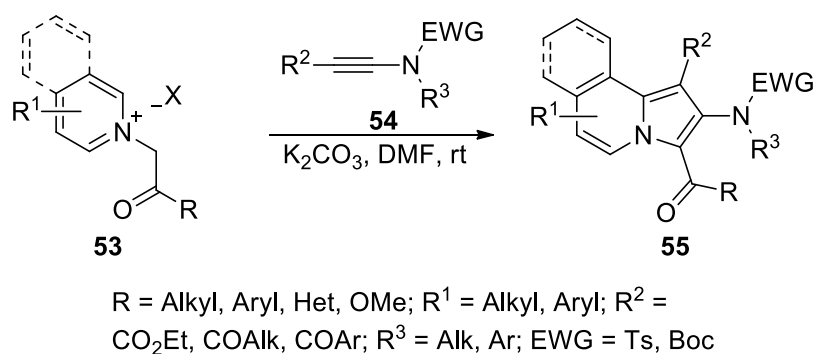
By using 2-methylbenzothiazole, pyridine or isoquinoline, and acetylenecarboxylates, Yavari and co-workers²²³ recently reported a method to form benzothiazolyl-substituted indolizines **49** in the presence of I_2 and DIPEA (**Scheme 9**). Cycloaddition of pyridinium and isoquinolinium ylides was suggested to react with the propargyl derivative to give compound **48**, which was oxidized to final product **49**. By using a similar procedure, 1,3-diaroyl-substituted indolizines **50** were synthesized in good yields using a molecular I_2 -mediated three-component reaction involving acetophenone, pyridine, and arylacetylene.



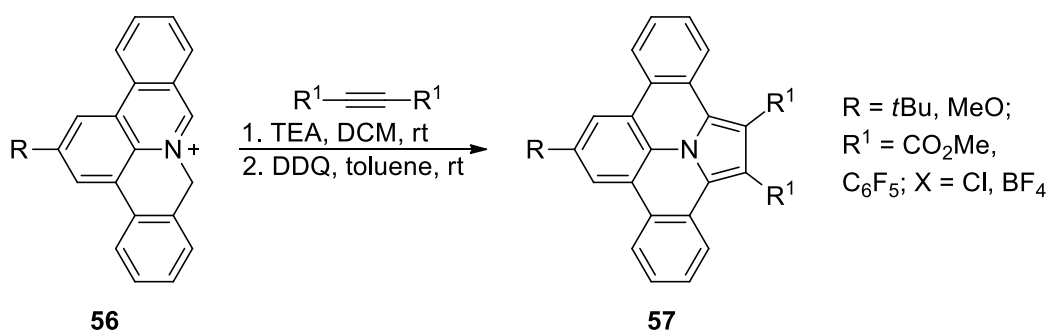
Scheme 10. Iron-catalyzed indolizine synthesis.

The multicomponent reaction combining commercially available alkyne, pyridine, and ethyl diazo acetate to give indolizine-3-carboxylates **52** was successfully developed by Douglas, Pordea, and Dowden (**Scheme 10**).²²⁴ In such a procedure, pyridines and diazo compounds were involved in a Fe[(THPP)Cl]-catalyzed reaction that gave ylides **51**. Indolizines **52** were then obtained *via* the cycloaddition/oxidation reaction of ylides **51** with various internal alkynes, resulting in moderate to good yields. The formation of mixtures of isomers was probably due to the low regioselectivity of the cycloaddition step. To access indolizines in good yields, electron-deficient alkynes were needed.

Stabilized pyridinium ylides formed by the deprotonation of salts **53** were successfully cycloadditioned to *N*-ethynylamides **54** (**Scheme 11**). Ylide formed from the isoquinolinium salt was revealed to be also a good reaction partner for the cycloaddition with ynamide, giving an easy access to substituted 2-aminoindolizines **55**.²²⁵



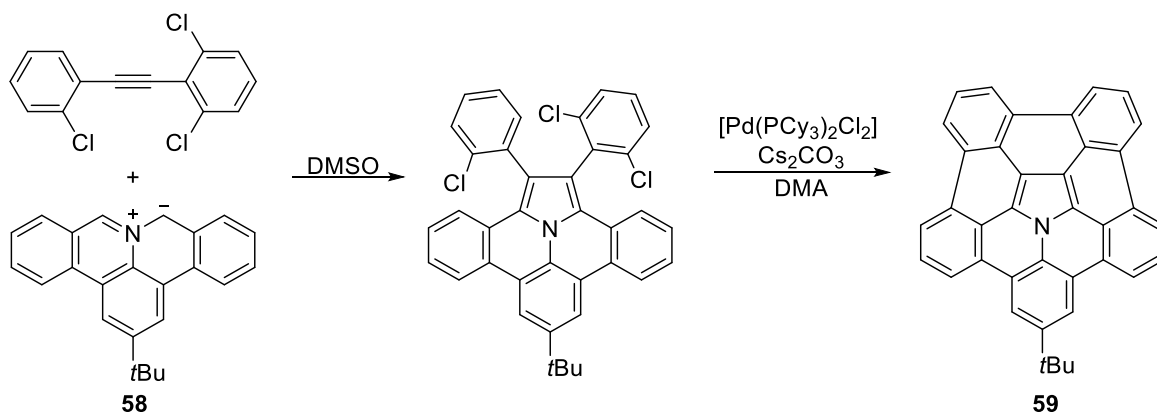
Scheme 11. Synthesis of 2-aminoindolizines **55**.



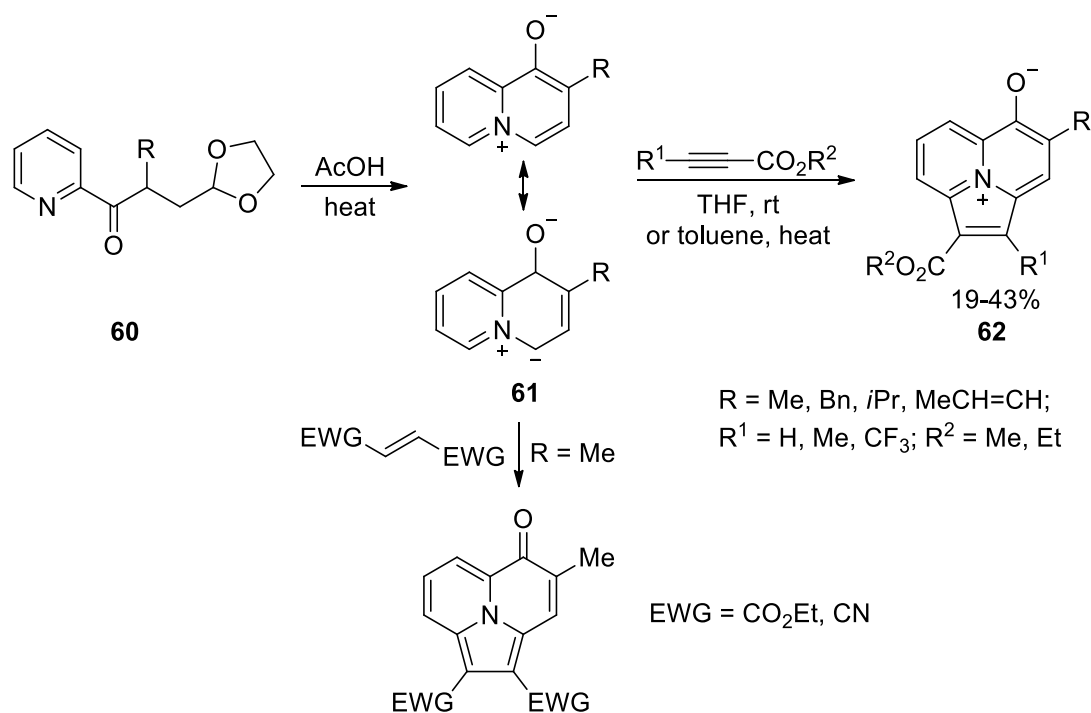
Scheme 12. Synthesis of benzo[7,8]indolizino[6,5,4,3-def]phenanthridines **57**.

Isoquinolinophenanthridinium-containing polycyclic aromatic azomethine ylides **56** were used in the synthesis of novel nitrogen *ortho*- and *peri*-fused aromatic polycycles (**Scheme 12**).²²⁶ One-pot DDQ oxidation of the cycloadducts gave the aromatic derivatives **57**, all of which displayed good optoelectronic properties, high extinction coefficients and optimal fluorescence quantum yields.

The synthesis of nitrogen-doped corannulene derivatives by means of the 1,3-DPCA of a polycyclic aromatic azomethine ylide **58** to diaryl acetylene was also reported (**Scheme 13**). Compared to the original corannulene, this molecule resulted to be the first example of a corannulene derivative with an internal heteroatom and distinctive structural and physical properties.



Scheme 13. Synthesis of *aza*-corannulene **59**.

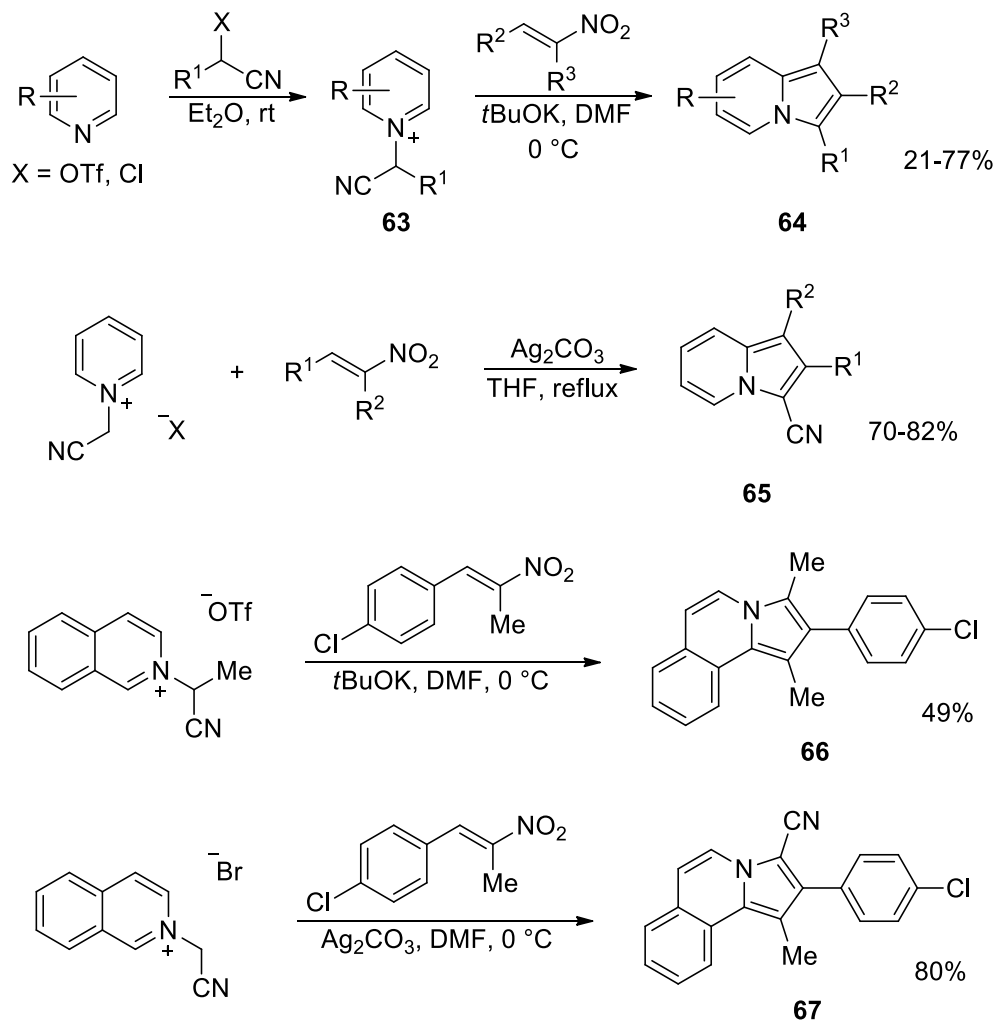


Scheme 14. Synthesis of pyrrolo[2,1,5-*de*]quinolizine derivatives **62**.

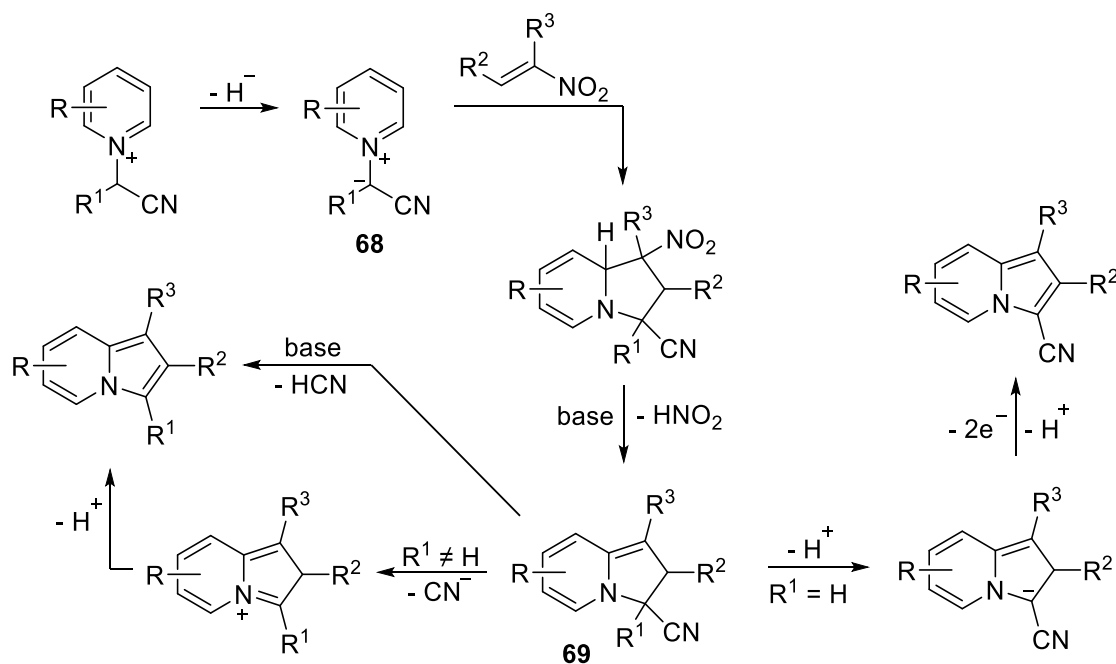
Mesoionic heterobetaines, like the quinolizinium derivatives **61**, were obtained in good yields by the cyclization of ketones **60** (Scheme 14). Such compounds underwent regioselective [3+2]-cycloaddition with electron-poor acetylene derivatives to form the pyrrolo[2,1,5-*de*]quinolizine compounds **62**. Ylides **61** resulted to be reactive only in the presence of alkynes, whilst no reaction was observed with other dipolarophiles, such as electron-poor olefins or thioketones. Hence, ylides **61** reacted with fumaronitrile and ethyl fumarate in the presence of Pd/C as a dehydrating agent, leading to the corresponding products **62**, albeit in low yields.

Alkenes are important reaction partners for the synthesis of indolizines and other polycyclic-fused systems. Electron-deficient alkenes are more widely accessible than electron-deficient alkynes. As a result, the scope of the reactions with pyridinium ylides can be greatly expanded, and the cost of syntheses reduced. When electrophilic alkenes have good leaving groups, the corresponding indolizines can be synthesized from tetrahydro adducts intermediates either by dehydrogenation with an excess of oxidant or *via* aromatization by elimination reactions. This happens, for instance, when [3+2]-cycloaddition reactions are used. Interesting examples reported the use of *N*-alkylated pyridines with cyanohydrin triflates or α -halonitriles to give pyridinium salts **63**, which in alkaline conditions reacted with nitroolefins to give polysubstituted indolizines **64** (Scheme 15).²¹⁸ Overall, pyridine, aldehydes, and nitroalkenes can be

used to form the indolizine core. Instead, indolizine-3-carbonitriles **65** were obtained from compound **64** when bromoacetonitrile was employed for the *N*-alkylation of pyridine. Other azines may be used to replace the pyridine moiety, accessing the corresponding heterocyclic systems **66** and **67**.



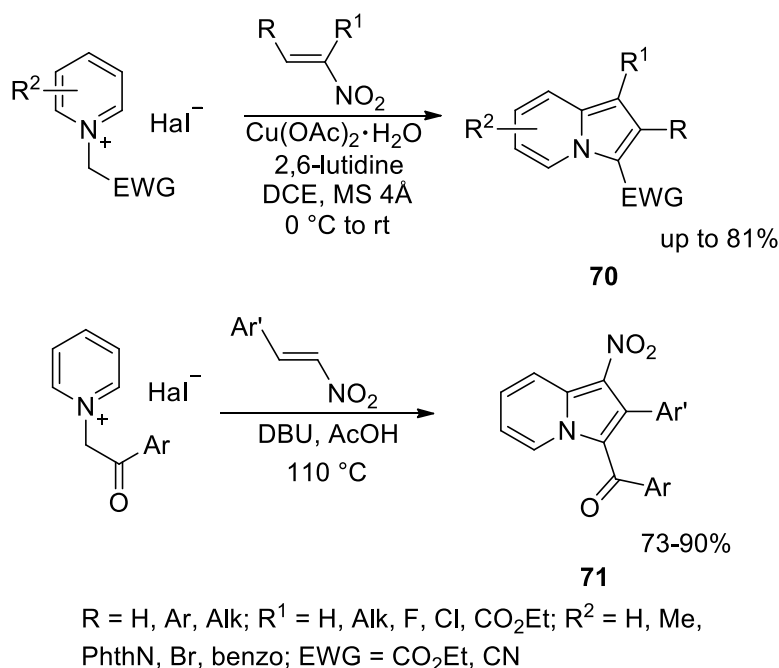
Scheme 15. Indolizine synthesis *via* cyano-substituted pyridinium ylides.



Scheme 16. Substituent effect on the aromatization step of intermediate cycloadduct **69** in indolizine synthesis.

In **Scheme 16** it is possible to observe an interesting example on the use of nitroalkene derivatives. In this case, the CH-acidity of the intermediate **69** was at the basis of the different reaction outcome by using α -substituted and α -unsubstituted 1-(cyanomethyl)pyridinium salts **68**. In this case, intermediate **69** bearing an α -substituent gave dehydrocyanation reaction, whilst deprotonation followed by oxidation took place for the unsubstituted ones.

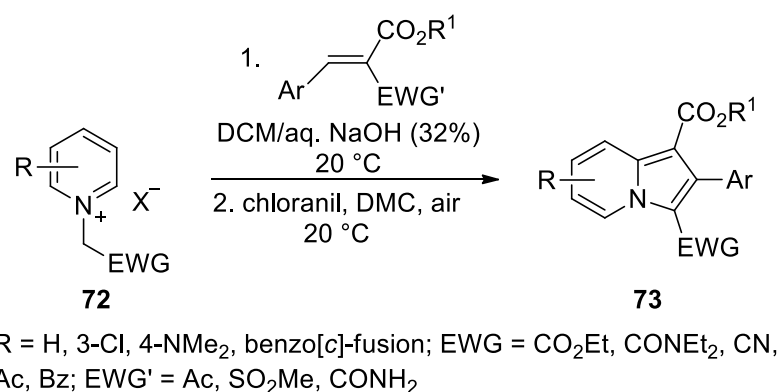
Recently, a generic protocol for the synthesis of indolizines **70** from nitroalkenes, including α -fluoronitroalkenes, was described (**Scheme 17**).²²⁷ In this example, Cu (II) acetate induced the oxidative annulation of *in situ*-formed pyridinium ylides. As said, α -fluoronitroalkenes were also successfully used in the reaction, allowing an easy access to several 1-fluoroindolizines in up to 81% yield. In contrast to reactions with electron-neutral substrates, such as sterically hindered *ortho*-bromo-substituted compounds and electron-rich *para*-methoxy-substituted substrates, reactions with β -fluoro- β -nitrostyrenes bearing electron-withdrawing substituents at the *para*-positions progressed much faster.



Scheme 17. Synthesis of indolizines by cycloaddition of pyridinium ylides with nitroalkenes.

By employing acetic acid as a solvent and a DBU-mediated [3+2]-annulation of pyridinium salts with β -nitrostyrenes, substituted 1-nitroindolizines **71** were also obtained (**Scheme 17**).²²⁸ In comparison to β -nitrostyrenes with carbocyclic aromatic rings, heterocyclic analogs of β -nitrostyrenes gave significantly lower yields (73-75%) and longer times.

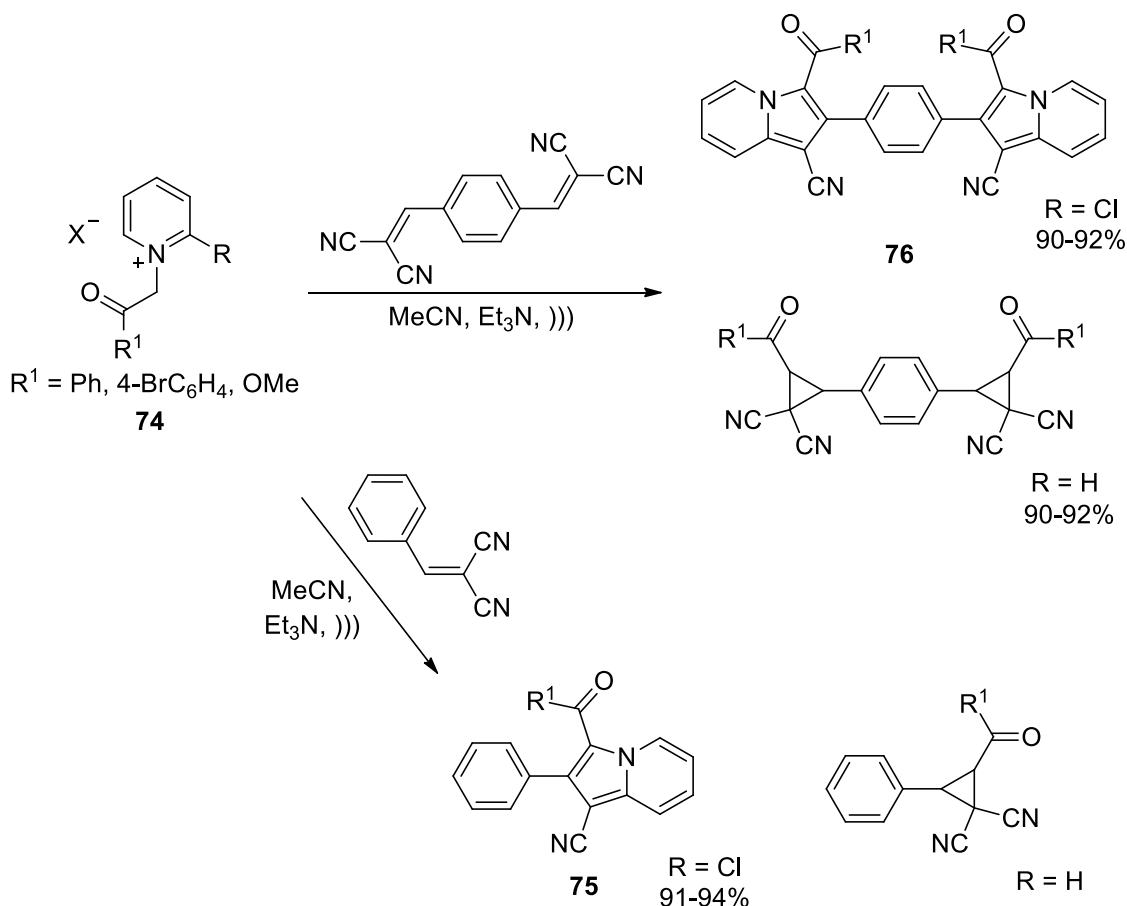
Allgäuer and Mayr²²⁹ used stepwise [3+2]-cycloaddition reaction to synthesize tetrahydroindolizine cycloadducts from pyridinium ylides, obtained *in situ* from pyridinium salts **72** in alkaline conditions (**Scheme 18**).



Scheme 18. Indolizine **73** synthesis from arylidene malonates and related Michael acceptors.

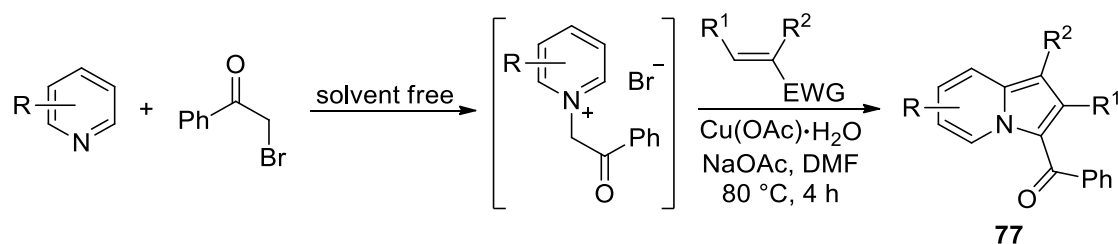
Moreover, by dehydrogenating and removing the acceptor group, the treatment of the crude reaction mixtures with chloranil in the presence of sodium hydroxide gave 1-(ethoxycarbonyl)indolizines. When the [3+2]-cycloadducts were oxidatively aromatized to form indolizines, the yield of the final products approximately followed

the leaving group behavior tendency of the substituents being $\text{CN} < \text{CO}_2\text{Me} \approx \text{CO}_2\text{Et} < \text{COMe}, \text{SO}_2\text{Me}, \text{and } \text{CONH}_2$. The reaction also worked well with alkylidene malonates and was not limited only to Michael acceptors with aryl substituents.



Scheme 19. Ultrasound-promoted synthesis of indolizines **75** and bis-indolizines **76**.

Starting from salts **74** ($\text{R} = \text{Cl}$), Abaszadeh and Seifi²³⁰ developed an ultrasound-assisted procedure to induce the [3+2]-cycloaddition/elimination reaction of arylidenemalononitriles with 2-chloropyridinium ylides, forming indolizines **75** and bisindolizines **76** in high yields (**Scheme 19**). Under the same conditions, the 2-chloro-unsubstituted pyridinium ylides gave the corresponding cyclopropane derivatives. Following a one-pot approach, Hu *et al.*²³¹ reported the use of a $\text{NaOAc}/\text{Cu}(\text{OAc})_2$ -based system to synthesize polysubstituted indolizines **77** from α -bromoacetophenone, pyridines, and electron-deficient alkenes (**Scheme 20**).

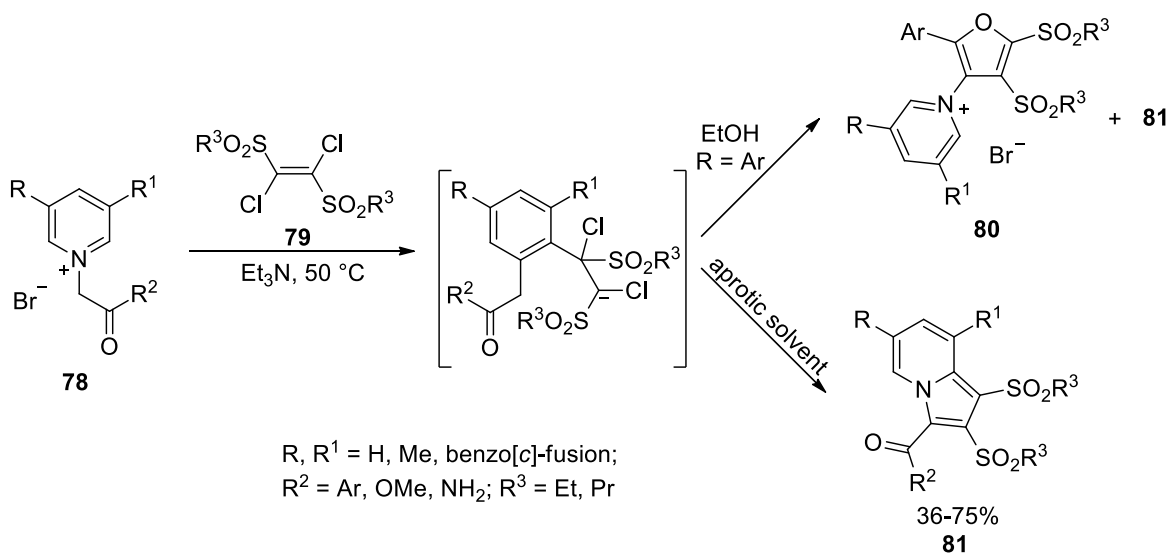


R = H, Me, CN, CO₂Me, NMe₂, Cl, benzo[*b*]-fusion; R¹ = H, Alk, Ar, CO₂R; R² = H, Me

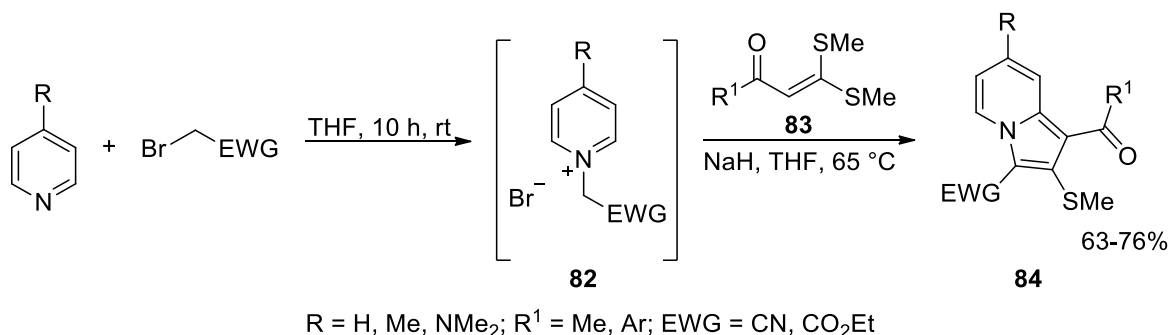
Scheme 20. NaOAc/Cu(OAc)₂-induced one-pot indolizine **77** synthesis.

Of note, numerous functional groups, including the formyl moiety, did not influence the overall yield. On the other hand, 4-vinylpyridine did not give the desired product due to a concurrent polymerization reaction.

An interesting way to obtain sulfur-containing indolizines at the 1- or 2-positions exploited the reaction between pyridinium salt **78** and (*E*)-1,2-di(alkylsulfonyl)-1,2-dichloroethenes **79** in the presence of Et₃N. Such reaction, reported by Dontsova *et al.*²³², allowed the facile synthesis of 1,2-di(alkylsulfonyl)indolizine derivatives **81** (**Scheme 21**). In the presence of aroylmethyl, methoxycarbonylmethyl, and carbamoylmethyl pyridinium salts as well as isoquinolinium salts, the procedure gave good yields, and it was also discovered that carrying out the reaction in aprotic solvents only indolizines **81** were formed. In addition to indolizine **81**, the reaction in ethanol gave the furan derivative **80**.



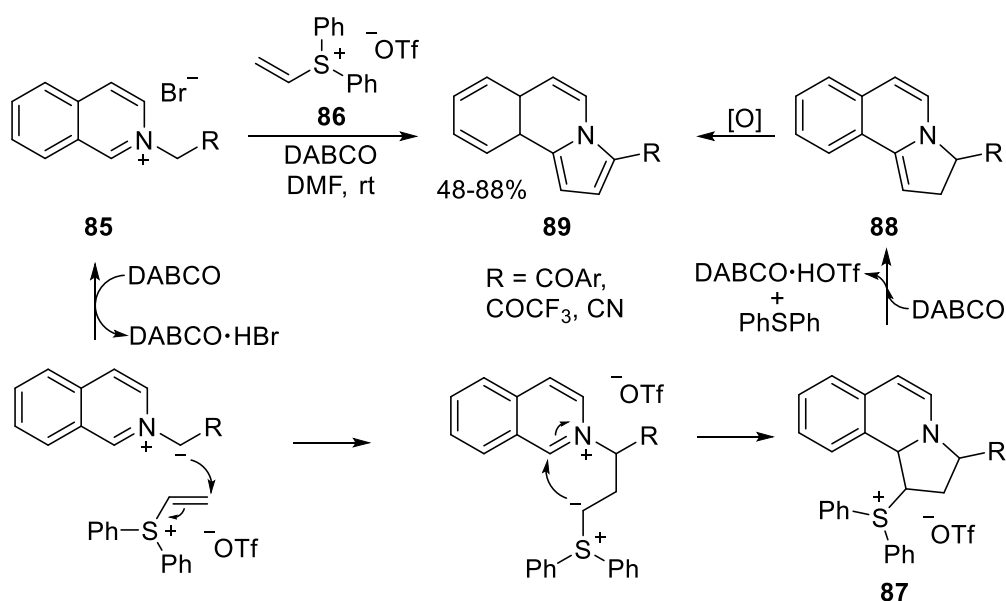
Scheme 21. Synthesis of 1,2-di(alkylsulfonyl)-substituted indolizines **81**.



Scheme 22. One-pot synthesis of methylsulfonyl-substituted indolizines **84**.

The recent synthesis of indolizines with a methylsulfonyl group in the 2-position was reported by Shanmugam and co-authors.²³³ By combining *in situ*-obtained pyridinium ylides **82** with α -oxoketene dithioacetals **83** in a one-pot, three-component reaction in the presence of NaH, the authors were able to access indolizines **84** (**Scheme 22**). *Ortho*-CF₃- and *ortho*-Me-substituted pyridines produced mixtures of the corresponding two regioisomers.

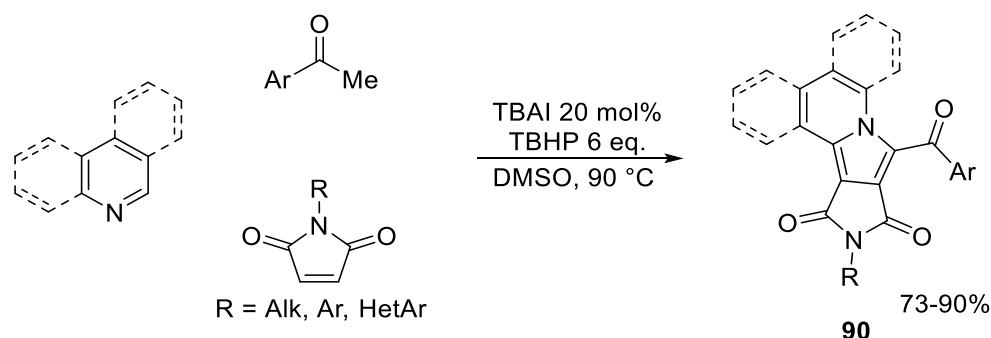
Highly functionalized indolizines and their benzo-fused derivatives were synthesized using the sulfur-containing dipolarophiles **79** and **83** (**Scheme 23**).²³⁴ In the presence of *in situ*-formed isoquinolinium ylides, vinyl sulfonium salts **86** gave the synthesis of 2,3-unsubstituted pyrrolo[2,1-*a*]isoquinolines **89**. The reaction took place in mild conditions and often had good product yields. Pyrroloisoquinoline **89** was then formed by the final oxidation step from intermediate **88**.



Scheme 23. Synthesis of 2,3-unsubstituted pyrrolo[2,1-*a*]isoquinolines **89**.

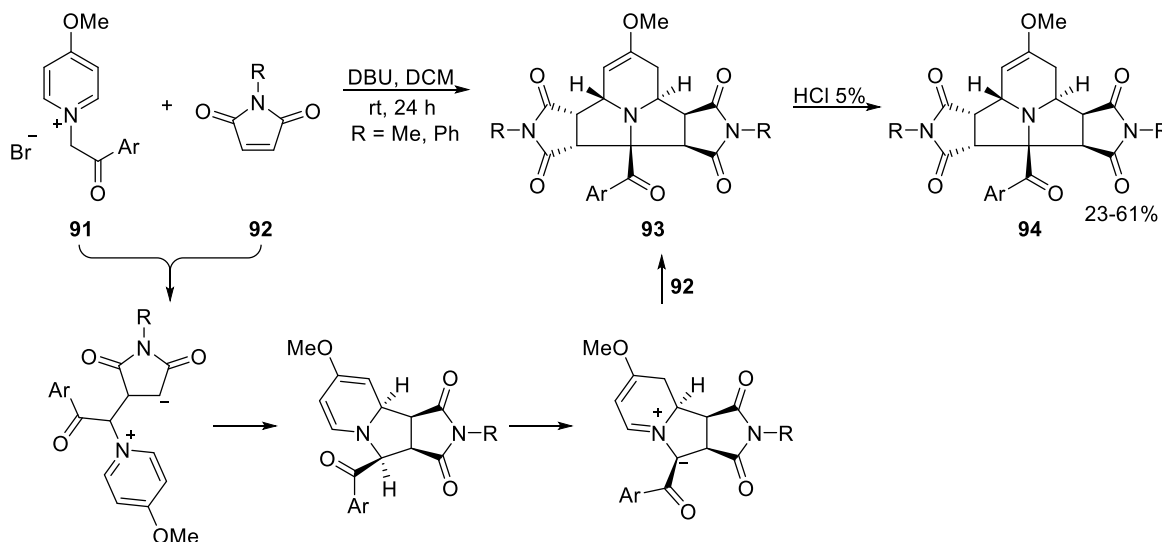
In the presence of a TBAI (N-tetrabutylammonium iodide)/TBHP (tert-butylhydroperoxide) system, pyridines, acetophenones, and maleimides, pyrrolo[3,4-

a]indolizine-1,3(2H)-diones **90** were obtained in a three-component protocol, passing by the formation of pyridinium ylides as intermediate (**Scheme 24**).²³⁵



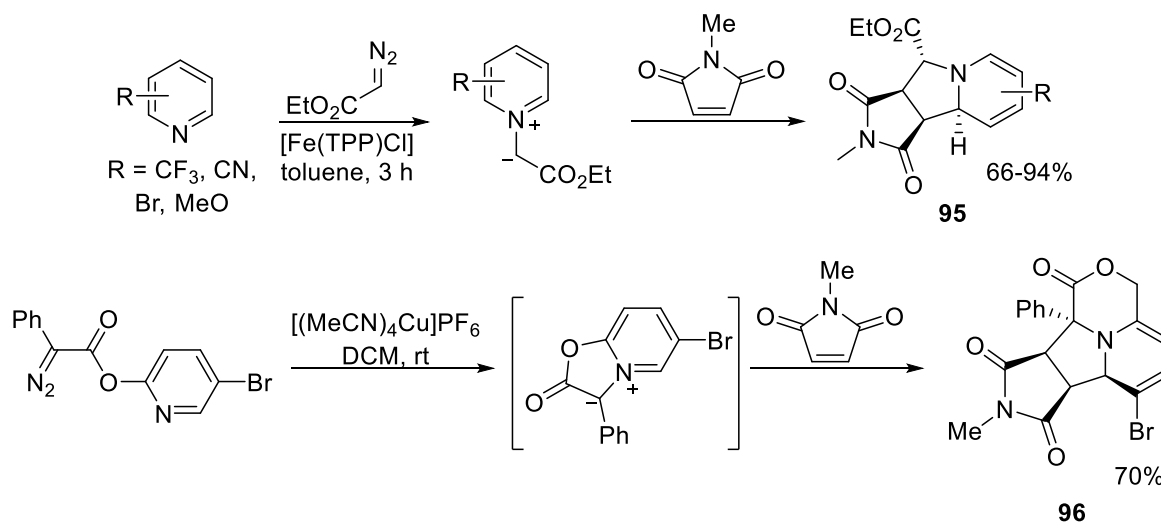
Scheme 24. Synthesis of pyrrolo[3,4-*a*]indolizine-1,3(2H)-diones **90**.

Furthermore, the double [3+2]-cycloaddition of 4-methoxy-substituted pyridinium ylide **91** to maleimides **92** was reported by Liu and co-authors.²³⁶ The tricyclic skeleton of the alkaloid 261C (**Scheme 25**) was obtained by such a reaction, which was carried out with a high diastereoselectivity. Of note, during the purification step, cycloadduct **93** partly hydrolyzed on silica gel. By acid hydrolysis of polycycles **93**, discrete yields of deprotected pyrrolo[2,1,5-*cd*]indolizines **94** were detected.



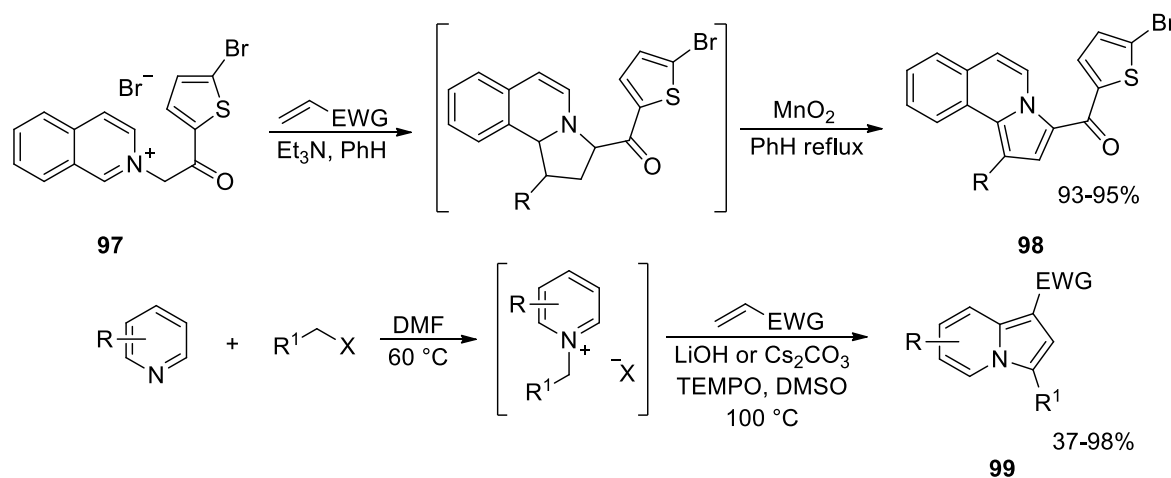
Scheme 25. Double [3+2]-cycloaddition of pyridinium ylides to maleimides.

To achieve the *ortho*-fused tetrahydroindolizidines **95** and **96** from pyridines, diazo esters, and *N*-methylmaleimide (**Scheme 26**), Dowden and co-authors²³⁷ proposed an Fe (III) or a Cu (I)-catalytic method. The production of pyridinium ylides as an intermediate allowed the reaction to take place under mild conditions and resulted in good product yields with great diastereoselectivity.

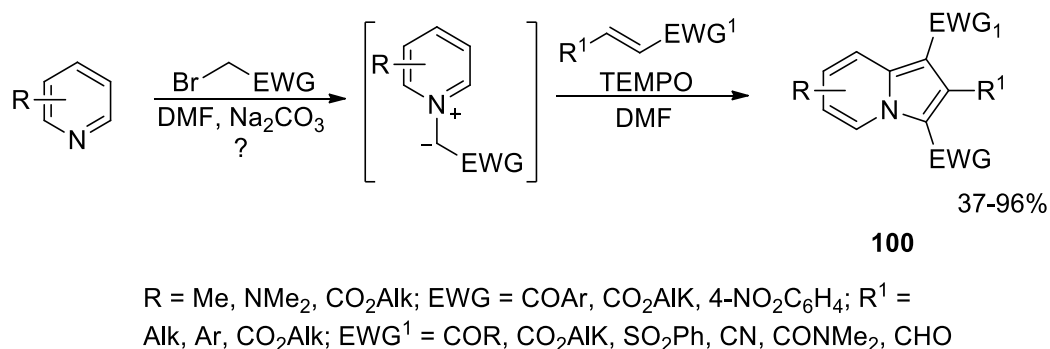


Scheme 26. Cycloadditions of diazo-derived pyridinium ylides to *N*-methylmaleimide.

In the presence of oxidizing agents like MnO_2 and 2,2,6,6-tetramethylpiperidine-*N*-oxyl (TEMPO), acrylic acid derivatives resulted to be suitable dipolarophiles for the preparation of 1,3-disubstituted indolizines from pyridinium and isoquinolinium ylides. To access pyrroloisoquinolines **98** in high yields, the thienoylmethyl-substituted isoquinolinium salt **97** reacted with acrylonitrile and ethyl acrylate in the presence of Et_3N and MnO_2 (**Scheme 27**).²³⁸ Using LiOH or Cs_2CO_3 as a base and TEMPO as an oxidant, indolizines **99** were obtained through a one-pot reaction from pyridines, primary halogenated hydrocarbons, and acrylic acid derivatives or acrolein.²³⁹ However, the alkaline hydrolysis with lithium hydroxide made less effective the reaction with methyl 6-bromohexanoate, which has a more easily hydrolysable ester group.

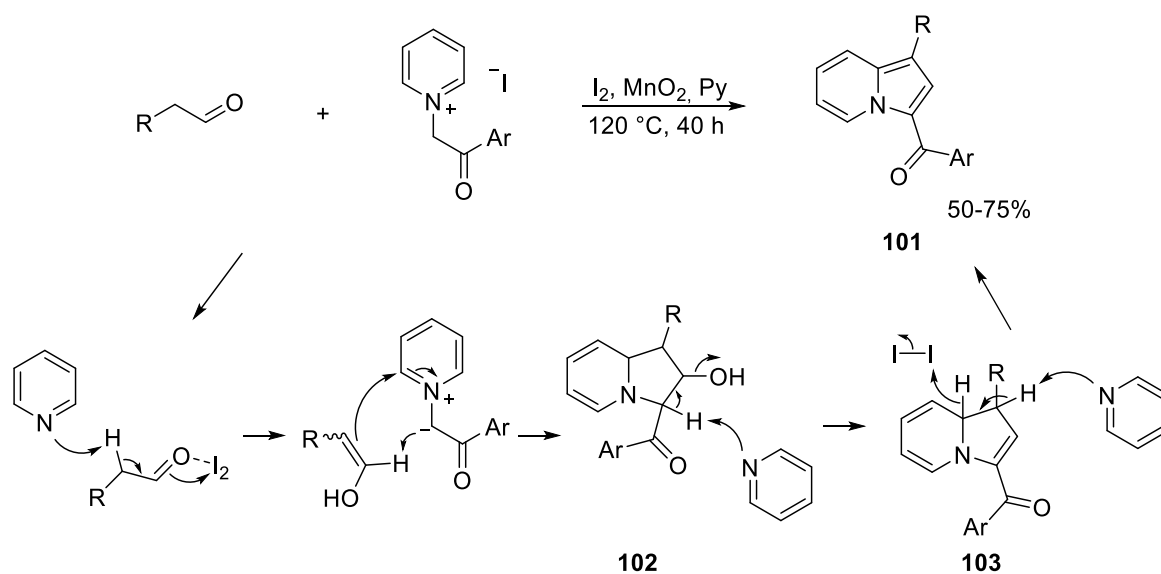


Scheme 27. Synthesis of 1,3-disubstituted indolizines from acrylic acid derivatives.



Scheme 28. One-pot synthesis of 1,2,3-trisubstituted indolizines.

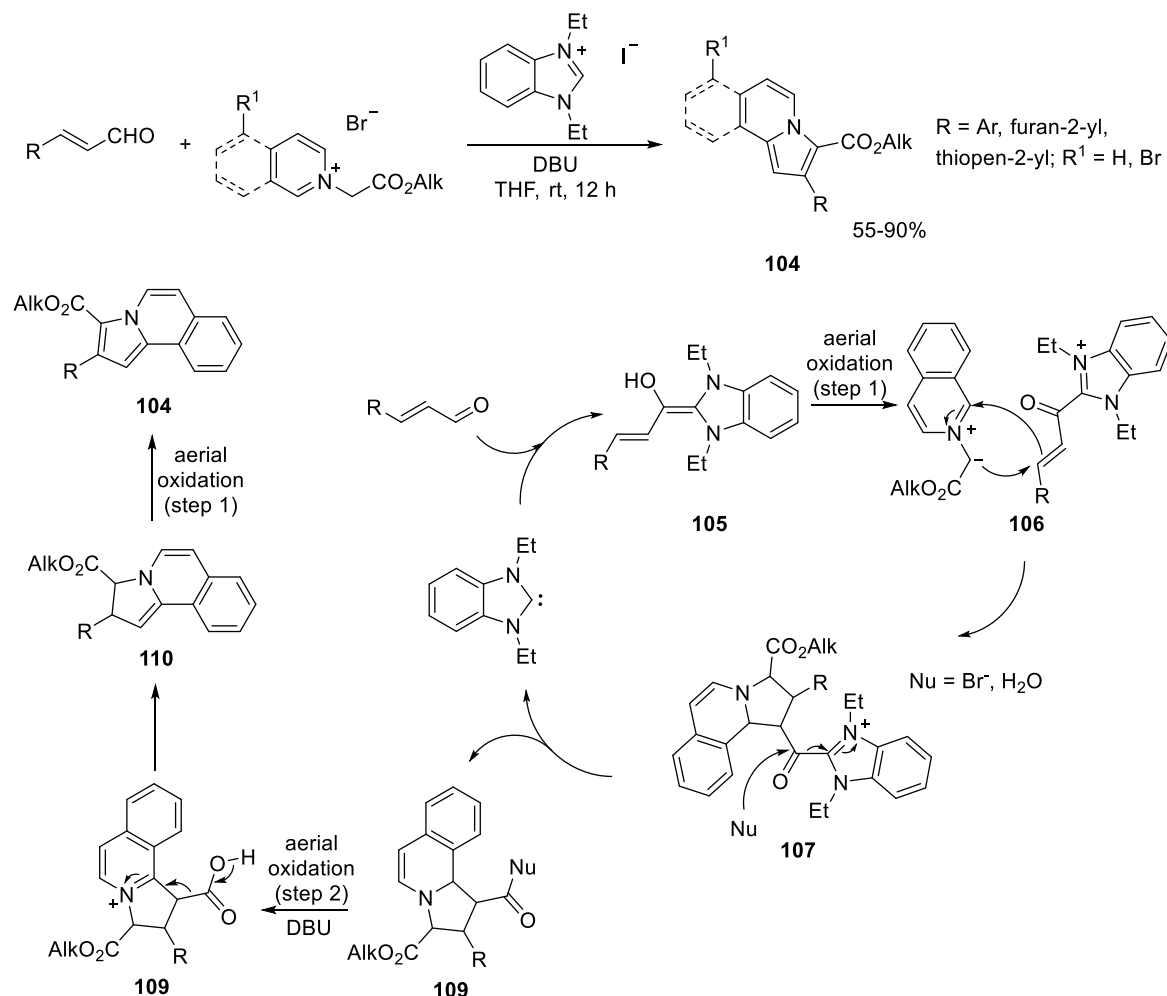
Another approach for the preparation of 1,2,3-substituted indolizines exploited pyridine, an alkylating agent, and an electron-deficient alkene. As result, indolizines **100** were formed in a one-pot manner by using a Na₂CO₃/TEMPO system for the (**Scheme 28**).²⁴⁰ In general, most of the electron-deficient alkenes readily reacted with the *in situ*-formed dipole. On the contrary, only a very little amount of the expected product was detected using coumarin.



Scheme 29. Synthesis of 1-alkylindolizines **101** and plausible mechanism for their formation.

Pyridinium salts and aliphatic aldehydes were the starting materials in another method for obtaining 1,3-disubstituted indolizines (**Scheme 29**).²⁴¹ A I₂/MnO₂/pyridine system was employed, giving [3+2]-cycloaddition reaction, followed by dehydration, and oxidative aromatization of the resultant dihydroindolizine. Pyridine was employed as both as a base and solvent, whilst molecular iodine functioned as a catalyst and as a dehydroaromatization reagent. A plausible mechanism was proposed wherein the deprotonation of the pyridinium salt with pyridine took place and the ylide subsequently cycloadditioned to the enol produced

by the I₂-induced enolization of the aldehyde. Then, cycloadduct **102** underwent dehydration to dihydroindolizine **103** followed by oxidation.

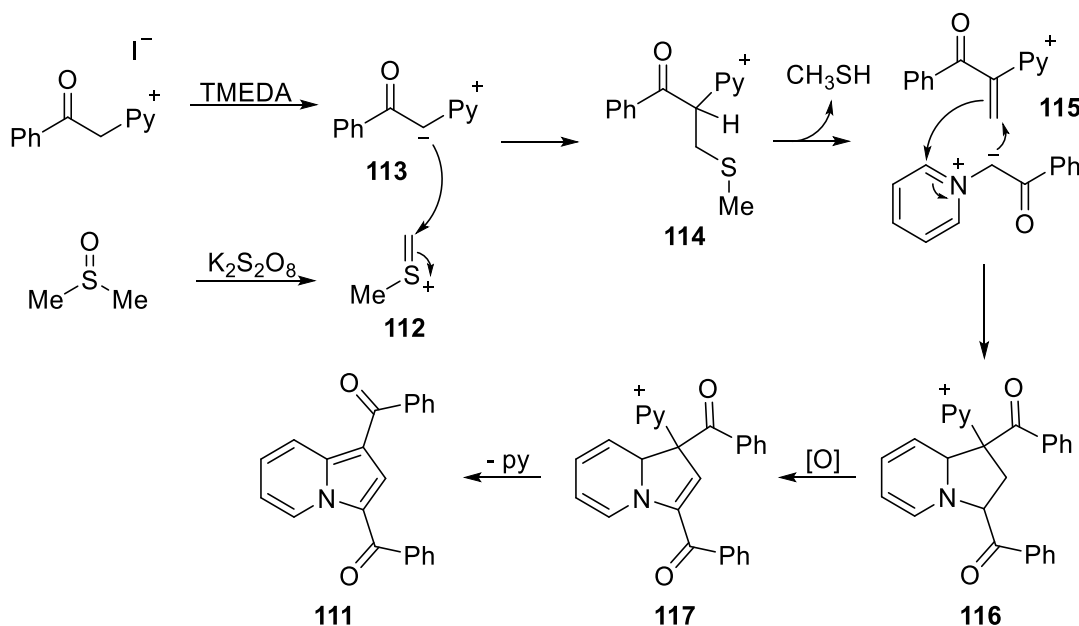


Scheme 30. NHC-mediated synthesis of indolizine and pyrrolo[2,1-*a*]isoquinolines **104** and plausible mechanism for their formation.

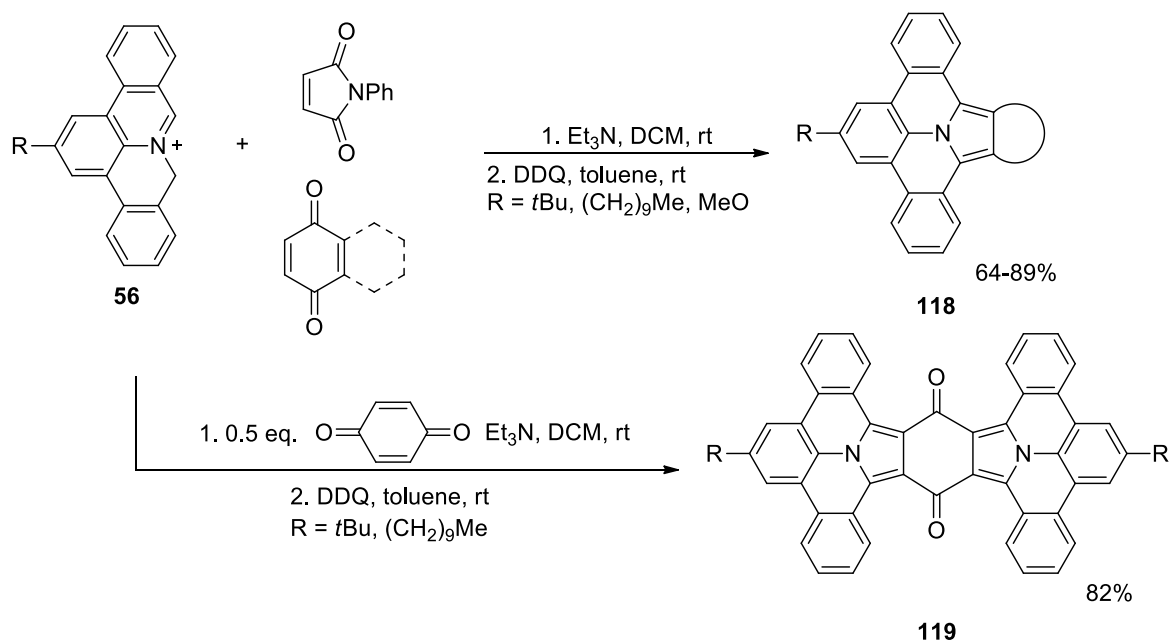
By using the NHC to combine aryl- and heteroaryl-substituted acroleins with pyridinium or isoquinolinium ylides, Nair and co-authors²⁴² reported the synthesis of indolizine and pyrrolo[2,1-*a*]isoquinolines **104** (**Scheme 30**). The synthesis of homoenolate **105** by the reaction of enal with the NHC-catalyst, which underwent oxidation to generate acylazolium intermediate **106**, was one possible reaction pathway. Tetrahydropyrrololisoquinoline **107** was the product of a Michael-type reaction with isoquinolinium ylide. The carbonyl derivative of tetrahydropyrrololisoquinoline **108** was accessed by the subsequent nucleophilic addition to the carbonyl group of **107** passing by two successive aerial oxidations, yielding pyrroloisoquinoline **104**.

Trimethylethylenediamine (TMEDA) and K₂S₂O₈ were used in a trifluoroacetic acid-mediated cascade oxidation/1,3-DPCA reaction with pyridinium salts to obtain

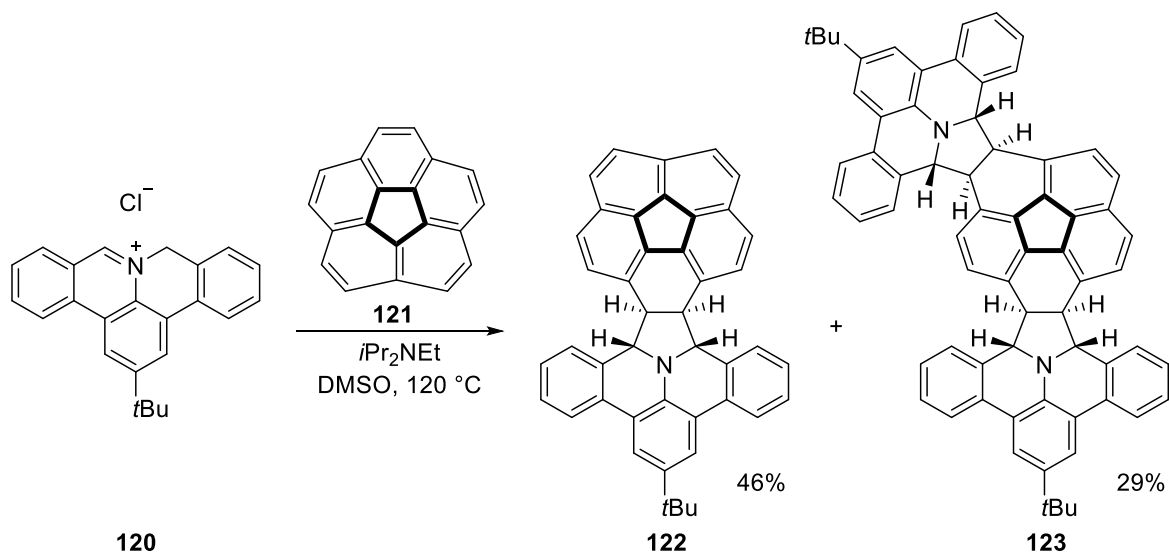
indolizines **111** (Scheme 31).²⁴³ The reaction was only slightly influenced by the electronic nature of the substituents on the aromatic ring system. The conversion of pyridinium iodides bearing different electron-neutral, electron-donating, and halogen substituents took place smoothly and with a 65-92% yield. Indolizines **111** were obtained by 2-furyl- and 2-thienylsubstituted precursors in 75% and 82% yields, respectively. The use of pyridinium salts bearing 3,5-dimethyl, 4-CO₂Me, and 4-CN substituents on the pyridinium ring gave 58-71% yields, but no reaction took place when 4-OMe or 4-I-functionalized salts were used. Of note, DMSO, which served as a one-carbon donor and as a solvent in this reaction, resulted essential. The activation of DMSO by K₂S₂O₈ to produce the thionium ion **112** was hypothesized to be the starting point of the reaction. Then, pyridinium ylide **113** attacked **112** to give intermediate **114**. Hence, intermediate **114** quickly eliminated methanethiol to produce methylene pyridinium salt **115**. To form the expected product **111**, the oxidation of intermediate **116** into dihydroindolizine **117** was needed.



Scheme 31. DMSO-mediated synthesis of 1,3-disubstituted indolizines and plausible mechanism for their formation.



Scheme 32. Cycloaddition of polycyclic azomethine ylides to activated alkene dipolarophiles. The synthesis of *ortho*-fused hepta- and octacyclic compounds **118** (Scheme 32)²²⁶ was achieved by means of a 1,3-DPCA of polycyclic aromatic azomethine ylides to cyclic maleimide and benzoquinone dipolarophiles in the presence of DDQ as an oxidant. As result, extended conjugated *N*-polycyclic aromatic systems **119** were obtained in excellent yields by using benzoquinone, which acted as a double dipolarophile.



Scheme 33. Synthesis of pyrrole-fused corannulenes.

Lastly, it is worth to mention the 1,3-DPCA reaction between polycyclic aromatic azomethine ylide **120** and corannulene **121** (Scheme 33), reported by Tokimaru, Ito, and Nozaki.²⁴⁴ In this frame, a 2:1 cycloadduct **123** was discovered in addition to the expected cycloaddition product **122**. The single-crystal X-ray diffraction analysis of

both products showed that the cycloadditions only took place at the rim bond of corannulene **121** in an *exo* way from the convex side. Then, cycloadducts **122** and **123** were rapidly transformed in the corresponding pyrrole-fused corannulenes **124** and **125** (**Figure 1**), respectively.

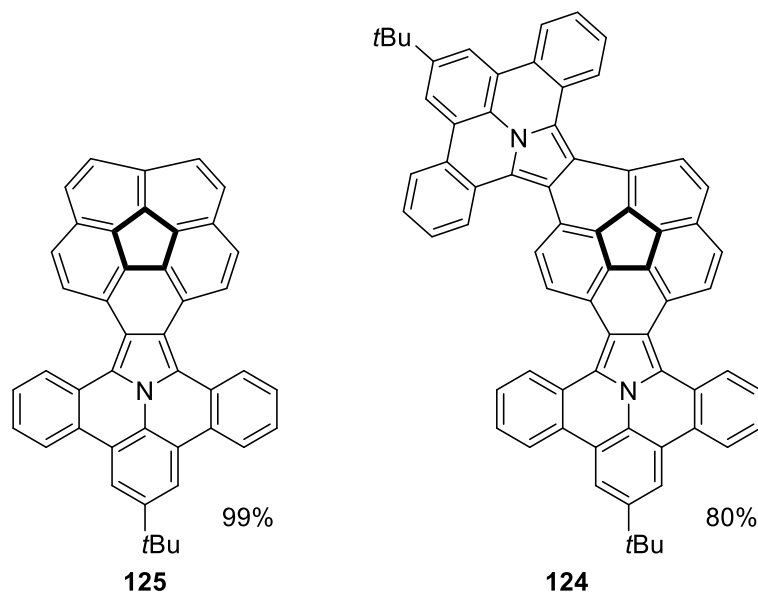
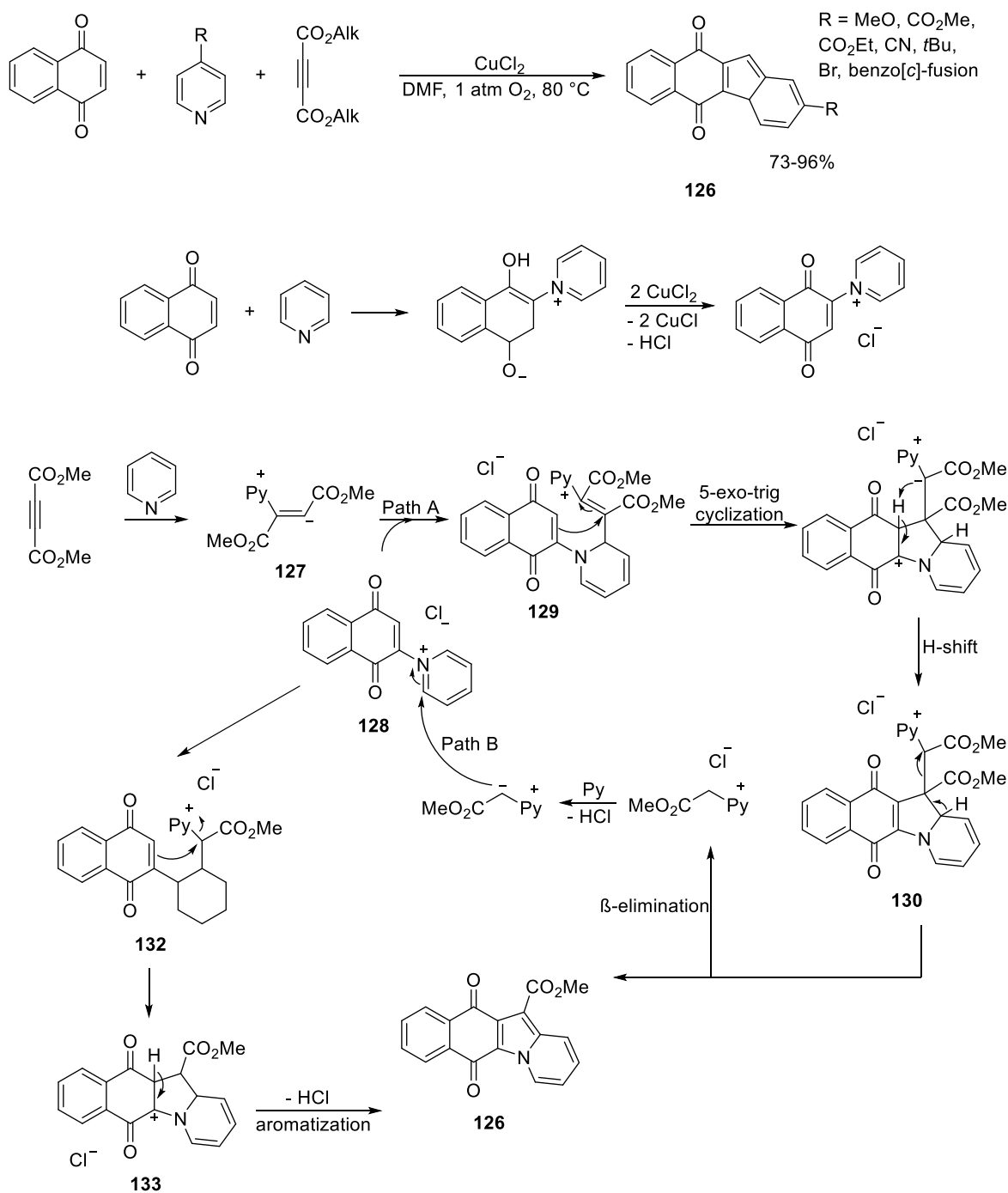


Figure 1. Synthesis of pyrrole-fused corannulenes.

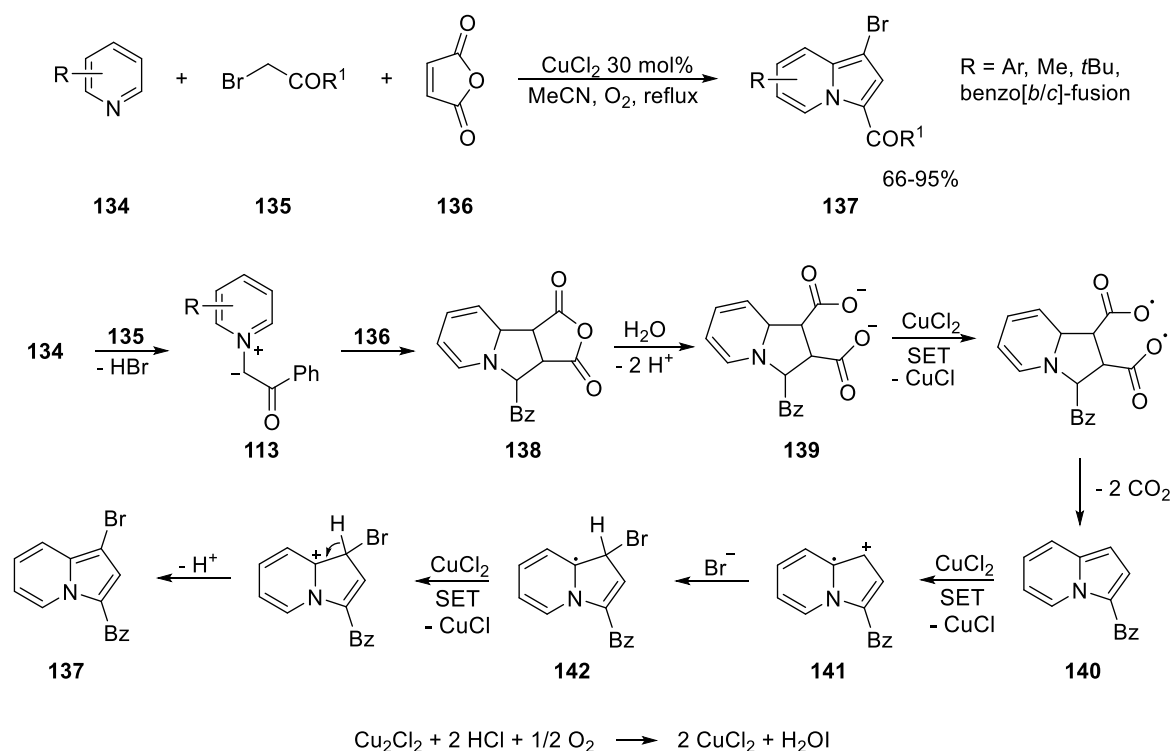
1.3 Metal-catalyzed reactions



Scheme 34. Synthesis of benzopyridoindoles **126** and plausible mechanism for their formation.

The latest advancement we would like to discuss before introducing the biological activities of indolizines regards the metal-catalyzed reactions involving pyridinium ylides. Liu and co-authors reported an innovative one-pot, three-component, Cu (II)-catalyzed method for synthesizing benzo[*f*]pyrido[1,2-*a*]indoles **126** using pyridines, naphthoquinone, and dialkyl acetylene dicarboxylates (**Scheme 34**).²⁴⁵ By using 3-bromopyridine, the 1- and 3-bromo regiomers of methylbenzo[*f*]pyrido[1,2-*a*]indole-

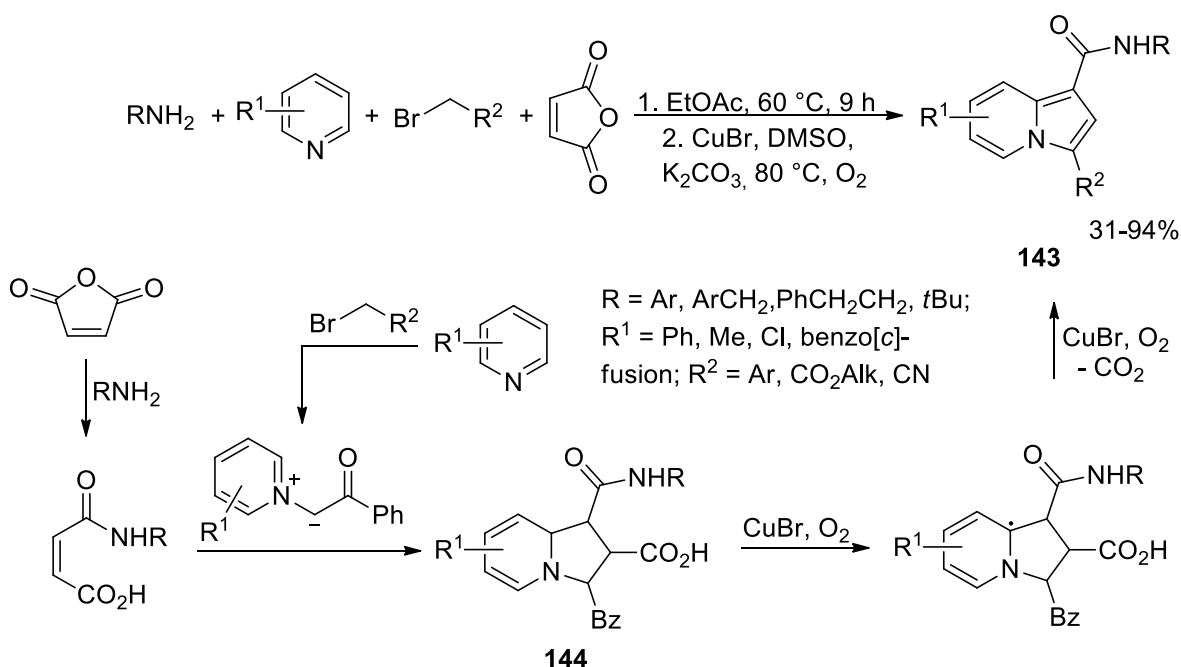
6,11-dione were obtained in yields of 47 and 33%, respectively, whereas the expected product using 2-bromopyridine was not detected, most likely due to the steric effects. Two pathways were proposed in this context: in the first, pyridine behaved as a nucleophile attacking the alkyne with the formation of the zwitterion **127**, which then reacted with intermediate **128** to form **129**. The subsequent proton transfer in **129**, followed with the 5-*exo*-trig cyclization, produced **130**. From intermediate **130**, product **126** was formed *via* β -elimination of the pyridinium salt (Path A). Pyridinium ylide **131** reacted with the intermediate **128** to give **126** through path b. Oxygen-mediated oxidation regenerated the Cu^{2+} catalyst.



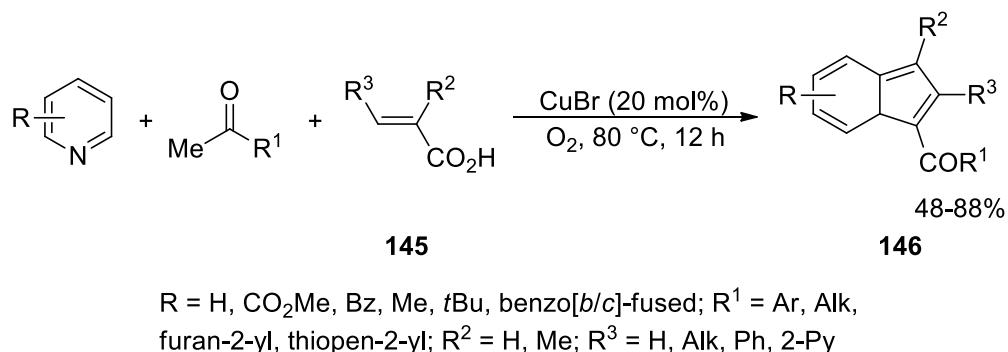
Scheme 35. Synthesis of 1-bromoindolizines **137**.

By combining pyridines **134**, α -acylmethyl bromides **135**, and maleic anhydride **136** in a three-component cascade reaction (**Scheme 35**), 1-bromoindolizines **137** were produced in high quantities.²⁴⁶ The same conditions were applied when 2-bromopyridine was used as a substrate, but no expected product was formed, even in this case most likely because of steric hindrance. As usual, oxygen functioned as the terminal oxidant (TO), regenerating the Cu (II) oxidant once ended the catalytic cycle. Such a reaction can be considered the first example of direct dehydrogenative bromination of indolizine at the *C*-1 site catalyzed by a transition metal. The reaction mechanism likely involved the formation of pyridinium ylide **113**, which then underwent 1,3-DPCA with maleic anhydride, hydrolysis, oxidative decarboxylation,

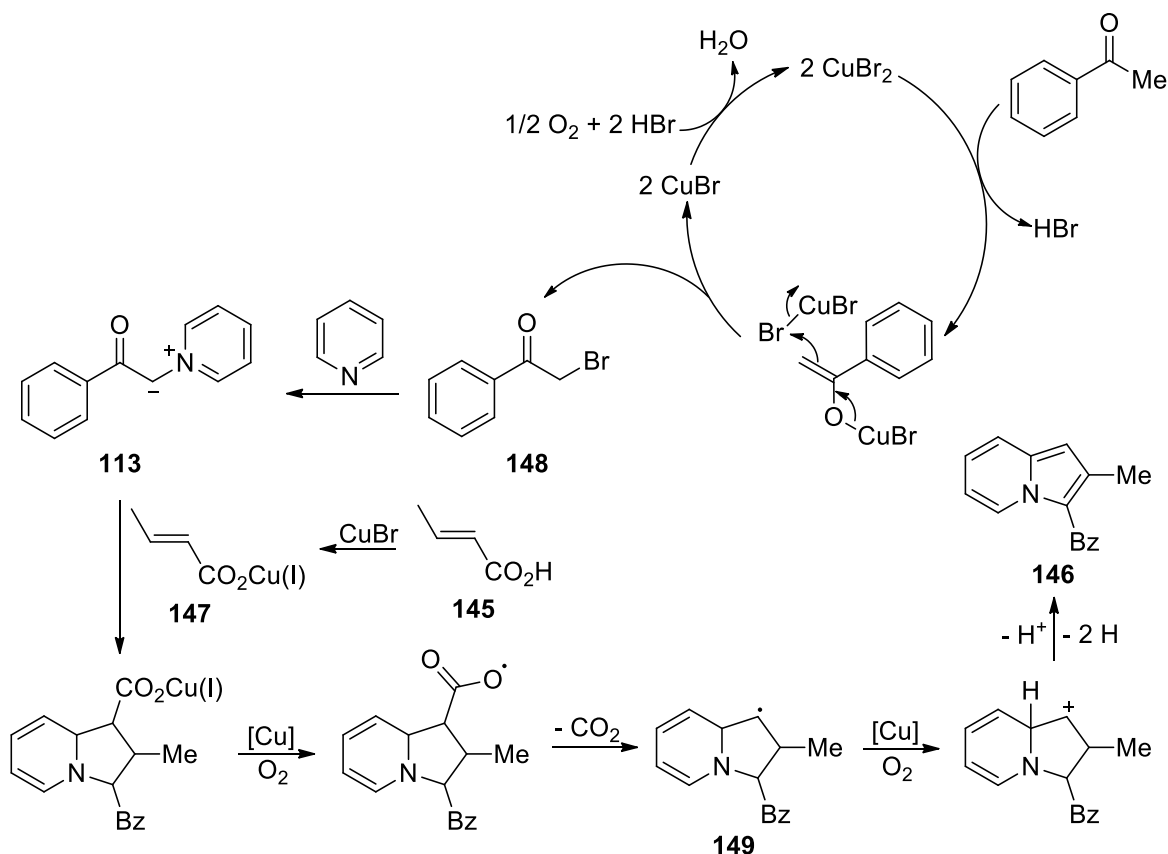
and aromatization to form 3-benzoylindolizine **140**. The radical cation **141** was produced when 3-acylindolizine **140** reacted with CuCl_2 in a single electron transfer (SET) reaction. The latter was captured by the bromide ion to form the radical intermediate **142**, which passing by SET and deprotonation steps gave indolizine **137**. Indolizines **143** were accessed by using pyridines, α -halide carbonyl compounds, primary amines, and maleic anhydride (**Scheme 36**).²⁴⁷ High reaction times and low yields for the desired products were obtained using secondary amines. The crucial process in the reaction pathway resulted to be the aromatization of the tetrahydroindolizine intermediate **144** triggered by copper-catalyzed aerobic oxidative process.



Scheme 36. Synthesis of indolizines **143** under copper-catalyzed aerobic oxidative conditions.



Scheme 37. CuBr-catalyzed synthesis of indolizines **146** from alkenoic acids (*follows in the next page*)

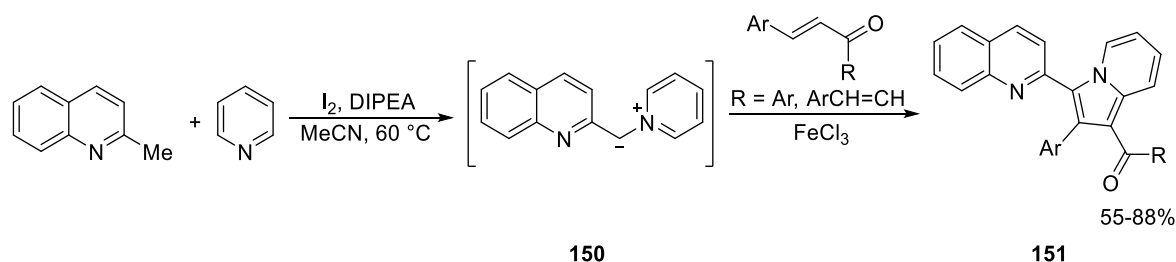


Scheme 37. CuBr-catalyzed synthesis of indolizines **146** from alkenoic acids.

Pyridines, methyl ketones, and alkenoic acids **145** were used as starting materials in another CuBr-catalyzed approach to form indolizine derivatives **146** in an oxygen atmosphere and in solvent-free conditions (**Scheme 37**). The bromination of methyl ketone was the first step in such a copper-catalyzed cascade reaction, which then underwent oxidative decarboxylation, dehydrogenative aromatization, and 1,3-DPCA of the *in situ*-formed pyridinium ylide to an alkenoic acid. This method gave good to optimal yields when tested over the synthesis of a variety of indolizines **146**.²⁴⁸ The most plausible mechanism was also discussed: alkenoic acid **145** and CuBr combined to form salt **147**, which then underwent a Cu (I)-to-Cu (II) conversion in the presence of oxygen. The next step involved the formation of bromide **148** from acetophenone and CuBr₂ which reacted with pyridine to produce ylide **113**. Then, the so-formed product gave cycloaddition to salt **147** and, after an oxidative decarboxylation reaction, the radical intermediate **149**. Through additional oxidation and deprotonation processes, indolizine **146** was finally obtained.

One last example comes from the work of Yavari *et al.*²⁴⁹ In this frame, the synthesis of 1-(isoquinoline-2-yl)indolizines **151** (**Scheme 38**) was accessed by a FeCl₃-catalyzed 1,3-DPCA of pyridinium ylides. The procedure relied on a cascade reaction in which 2-

methylquinoline and pyridine were combined in the presence of DIPEA to generate pyridinium ylides **150**, which was then followed by 1,3-DPCA to chalcones or dibenzylideneacetones.



Scheme 38. Synthesis of 1-(isoquinoline-2-yl)indolizines **151**.

2. Indolizines: an overview on their biological activities

In this paragraph, we will give the reader a brief introduction to the biological activities displayed by indolizines. Such potential joined to the possibility to design simple synthetic protocols, sparked our interest (see *research line 3a*). In this frame, indolizines were described as potential anti-inflammatory and analgesic agents, as well as useful in tuberculosis treatment and as antimicrobics. Nonetheless, many compounds showed antioxidant properties, hypoglycemic activities, and inhibitory activity toward human phosphatase (**Figure 2**). Finally, indolizines were evaluated as antitumoral. The interested reader can refer to the following reviews for a detailed overview of the mentioned properties.²⁵⁰⁻²⁵²

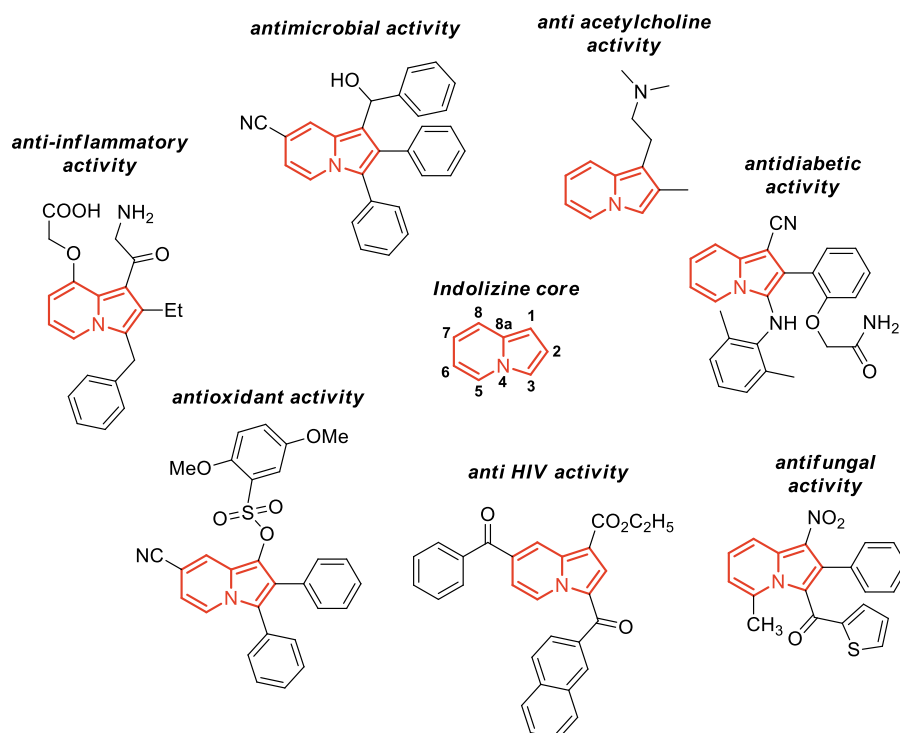


Figure 2. Selected examples of the biological activity of indolizines.

2.1 Anti-inflammatory activity

In 2017, Shrivastava and co-workers²⁵³ proposed a series of indolizines with a promising anti-inflammatory activity. The driving force in this study was the structural similarity of the prepared compounds with indomethacin, a well-known anti-inflammatory drug (**Figure 3**).

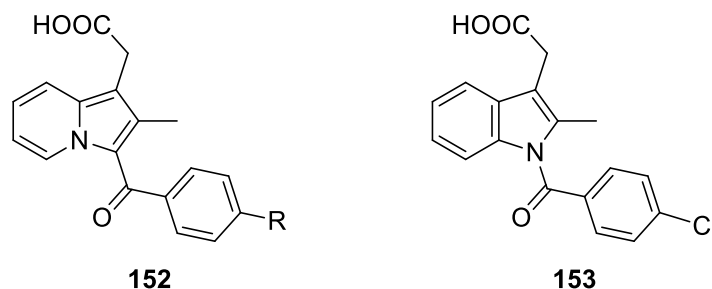
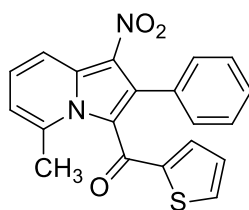


Figure 3. General structures of the some indolizines developed by Shrivastava **152** in comparison with indomethacin **153**.

In vitro studies showed that the anti-inflammatory activity was exerted at the level of three key enzymes involved in the inflammatory response: COX-1 (cyclooxygenase 1), COX-2 (cyclooxygenase 2), and LOX (lipoxygenases). *In silico* studies demonstrated that the indolizine core played a pivotal role in the global biological activity of the substrates. In particular, the aromatic nature of the scaffold favored the interaction with the hydrophobic channel of COX-2 made up of Leu352, Trp387, Phe518, and Met522 residues. In addition, the interaction was furtherly strengthened by the hydrogen bonds with Tyr355 and His90 residues. SAR studies showed also that the presence of electronegative groups (i.e. -CF₃) decreased the biological activity, which is conversely boosted by the presence of a phenyl group at the position 2.

2.2 Anti-tuberculosis and anti-microbial activity

Researching new anti-microbial drugs is a hot topic in the pharma business due to the growing antibiotic resistance displayed by many bacteria. In this regard, some indolizine scaffolds showed antibacterial activities against *E.coli*, *B.subtilis*, *V.cholera*, *Kpneumoniae*, *S.aureus*, *P.aeruginosa*.²⁵² In particular, an indolizine derivative prepared by Darwish *et al.* in 2008 proved its activity towards lanosterol 14 α -demethylase (CYP51A1) (**Figure 4**).²⁵⁴ The selective inhibition of such a target led to the depletion of ergosterol and to the accumulation of lanosterol and related derivatives, hence inhibiting the fungal cell growth.²⁵⁵

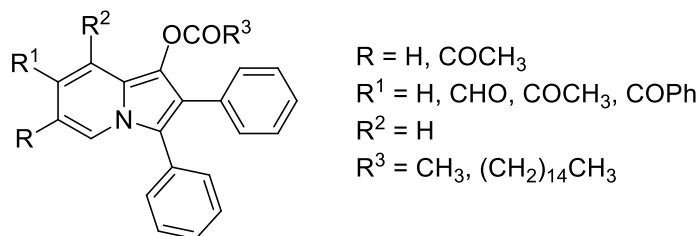


154

Figure 4. Indolizine inhibitor of lanosterol 14 α -demethylase.

2.3 Antioxidant activity

In a work by Nasir *et al.*,²⁵⁶ indolizines displayed a notable antioxidant activity due to their easy oxidation and formation of stable radicals (**Figure 5**). Such compounds exhibited a broad inhibition of lipid peroxidation *in vitro* following several possible mechanisms. According to the authors, one possibility might be the hydrolysis of the esters into indolizinols, which acted as hydrogen atom donors to the radicals produced in the test media, generating neutral indolizinyl radicals as a by-product. Alternately, the lipid peroxidation radical chain events may be stopped by oxidizing the esters to stable cation radicals. With the help of methyl ether, acetate, and α -tocopherol, radical cations might be produced. Another possibility is that the indolizines combine with Fe^{2+} to form complexes, which prevent the start of lipid peroxidation.



155

R = H, COCH_3
 R¹ = H, CHO, COCH_3 , CPh
 R² = H
 R³ = CH_3 , $(\text{CH}_2)_{14}\text{CH}_3$

Figure 5. Indolizine derivatives as antioxidants.

2.4 Phosphatase inhibitors

Phosphatases are a class of hydrolases in charge of the biochemical dephosphorylation in innumerable cellular processes. Hence, it is not hard to imagine how aberrancies in such protein expression or mutations can be involved in numerous pathologies such as cancer and diabetes. In this context, it is possible to recover from the literature how some 3-substituted 1-cyanitrile indolizines were capable of inhibiting these enzymes, as reported by the Kessler group in 2006 (**Figure 6**).²⁵⁷ One of the most interesting aspects of such compounds lies in the polypeptide skeleton at position C7 in compounds **156** and **157**: in particular, it has been cleared that the inhibitory action can be related to the hydrophobic interactions at the active site of the enzyme.

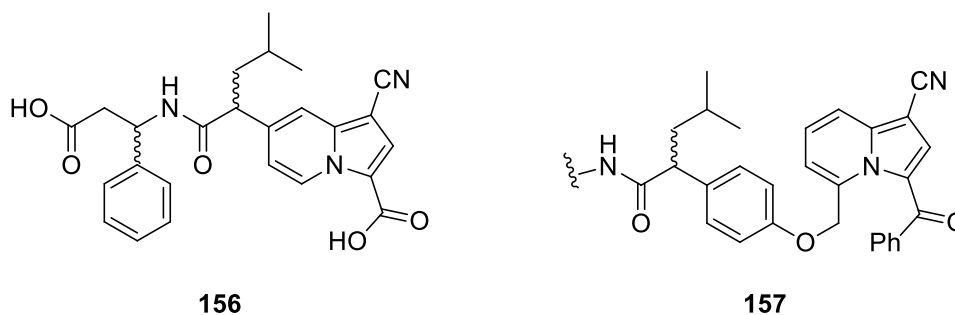


Figure 6. Indolizine derivatives as phosphatase inhibitors.

2.5 Anti-HIV activity

An interesting report by the Zhang group proposed a protocol for the synthesis of some indolizine derivatives capable of disrupting the VIF-ElonginC interaction,²⁵⁸ recognized as one of the key factors in HIV/AIDS etiopathogenesis.²⁵⁹ The prepared 1,3,7-trisubstituted substrates (**Figure 7**) were obtained by optimizing the substituent at the C7 position and evaluating the SAR activity by replacing the phenyl group with other heteroaromatic fragments. Nonetheless, it has been tested also the possible role of various substituents at the *ortho*, *meta*, and *para* positions. Of note, the presence of hydrophilic groups such as OH and NH₂ decreased the biological activity, whilst the replacement of the aromatic group with an aliphatic one dramatically decreased the bioactivity of the substrate. In addition, the naphthyl group at the C3 position revealed its primary importance in leading the interaction with the target too because its replacement with a substituted benzoyl group decreased the activity.

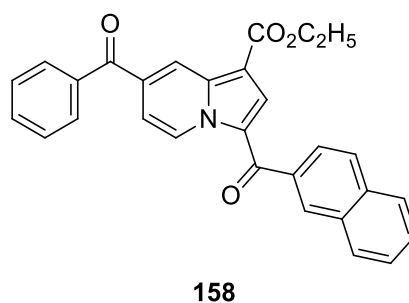


Figure 7. Indolizine derivative as HIV-1 VIF-ElonginC interaction inhibitor.

2.6 Hypoglycemic activity

Indolizine derivatives can also be promising antidiabetics, according to Zhou *et al.*²⁶⁰ In this report, several benzisothiazole and indolizine- β -D-glucopyranosides were able to inhibit the human sodium/glucose co-transporter 2 protein (SGLT2), one of the principal transporters involved in glucose reabsorption in the kidney. The R substituent herein reported (**Figure 8**), was varied to assess the SAR studies for this position, showing that the presence of a Me or a CF₃ improved the inhibitory activity of

the substrate. On the other hand, the presence of OMe, Cl, and F groups was detrimental.

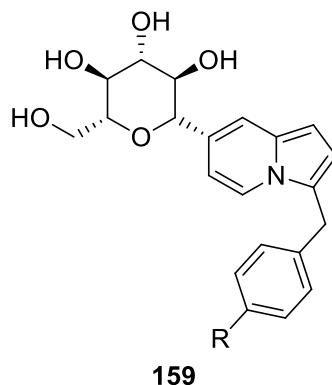


Figure 8. Indolizine- β -D-glucopyranoside derivative as human sodium/glucose cotransporter 2 protein (SGLT2) inhibitor.

2.7 Antitumoral activity

Indolizines proved to be also promising as antiproliferative agents for different human cancer cell lines. In particular, compound **160** (Figure 9) reported by Kim *et al.*²⁶¹ has proved its activity towards the inhibition of the tubulin polymerization process, determining an anti-mitotic activity in HL-60 cell lines. Molecular modeling and SAR studies were also conducted to assess the structural basis of such a mode of action, revealing that the presence of the CN group at the C5 position was pivotal in favoring the interaction with the residues Val181 and Lys352 of the target. Moreover, the presence of a carbonyl group at the C3 position allowed a better interaction with the amidic moiety of an Asp251 residue. It is also worth noting a report of 2016 by Moon and co-workers,²⁶² where indolizine derivatives **161**, **162**, and **163** (Figure 9) were evaluated as inhibitors of the β -catenin. Such target is a key protein involved in the Wnt signaling pathway, whose aberrant activation has been recognized as the basis of poor prognosis in triple-negative breast cancer (TNBC).²⁶³ In particular, compound **163** turned out to be particularly active as a β -catenin inhibitor, allowing the activation of p53 in A549 cancer cell lines.

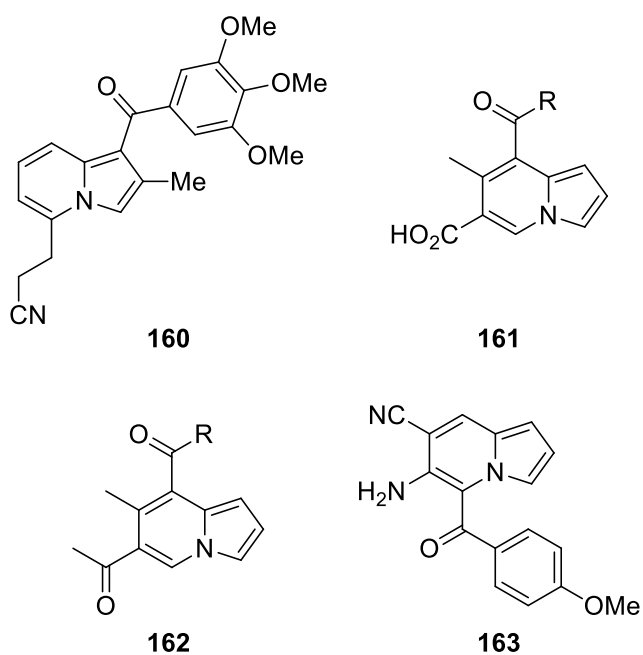
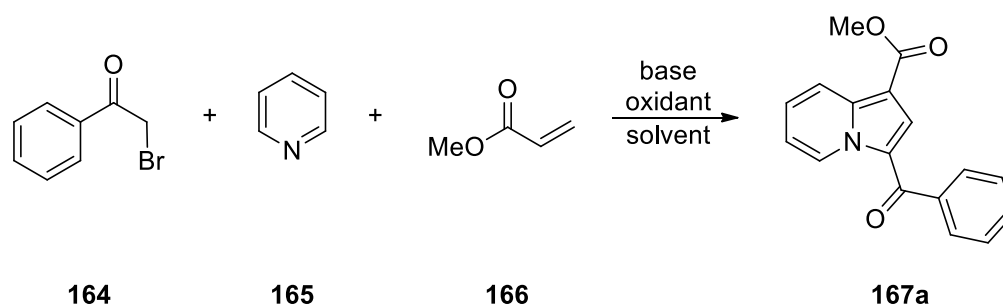


Figure 9. Indolizines as inhibitors of the tubulin polymerization (**160**) and as β -catenin inhibitors (**161-163**).

Results and Discussion

Research line 3a - DDQ-mediated multicomponent access to polysubstituted indolizines

With the state-of-the-art about indolizine synthesis and their biological potential in hand, in this paragraph, we will report the results obtained for *research line 3a* of this Ph.D. thesis about the synthesis of polysubstituted indolizines. The aim of this work was to implement a multicomponent protocol to prompt the development of new compounds of interest. In this regard, several di- and tri-substituted substrates were obtained using a cycloadditive strategy by varying the dipolarophile partner. According to the literature,^{231,254,264,265} the use of a 1,3-DPCA reaction between pyridinium salts and alkenes in the presence of an oxidant and a base was undoubtedly the best-performing method. We commenced our study following the model reaction reported in **Table 1**, wherein 2-bromoacetophenone **164**, pyridine **165**, and methyl acrylate **166**, in the presence of different bases and inorganic oxidants, reacted in a multicomponent fashion to give the desired product. The choice of such polar solvents was mainly due to the presence of scarcely soluble inorganic salts to avoid the formation of biphasic systems.

**Table 1.** Optimization of reaction conditions by varying base and oxidant.

Entry	Molar ratio ^a		Base	Oxidant	Solvent	T (°C)	t (h)	Yield (%) ^b
	166 :	base:oxidant						
1	2:3:1		Et ₃ N	KMnO ₄	DMF	80	24	43
2	3:4:3		NaOAc	Cu(OAc) ₂	ACN	reflux	6	51
3	3:4:3		NaOAc	H ₂ O ₂ 30%	DMF	120	6	32
4	3:4:3		NaOAc	H ₂ O ₂ 30%	ACN	reflux	6	33
5	2:4:2.5		NaOAc	KHSO ₄	DMF	100	1	51
6	2:2:1		NaOAc	KMnO ₄	DMF	120	3	traces
7	3:4:3		NaOAc	CuSO ₄	ACN	reflux	3	43
8	3:4:4		NaOAc	CuSO ₄	DMF	80	24	52
9	3:4:3		NaOAc	I ₂	DMF	80	6	11
10	2:4:4		NaOAc	K ₂ Cr ₂ O ₇	DMF	100	12	64
11	3:4:3		K ₂ CO ₃	Cu(OAc) ₂	ACN	reflux	6	62
12	2:2.5:3		K ₂ CO ₃	Cu(OAc) ₂	H ₂ O	80	24	5
13	2:5:2		K ₂ CO ₃	K ₂ Cr ₂ O ₇	DMF <i>dry</i>	100	12	57
14	3:4:3		K ₂ CO ₃	CuSO ₄	ACN	reflux	5	65
15	2:2:1		K ₂ CO ₃	KHSO ₄	DMF	80	5	22
16	2:5:2		K ₂ CO ₃	KMnO ₄	DMF <i>dry</i>	80	10	61
17	2:5:2		K ₂ CO ₃	KMnO ₄	DMF <i>dry</i>	100	8	73
18	2:5:3		K ₂ CO ₃	Cu(OAc) ₂	DMF <i>dry</i>	100	8	71
19	2:5:3		K ₂ CO ₃	Cu(OAc) ₂	DMF <i>dry</i>	120	8	71
20	3:5:3		K ₂ CO ₃	Cu(OAc) ₂	DMF <i>dry</i>	100	8	72

^a**164** and **165** were used in 1:1 ratio. ^bIsolated products

The results demonstrated that the use of K₂CO₃ gave generally better results than NaOAc or triethylamine (TEA). It was also observed that the same base should be used in strong excess conditions to allow the improvement of reaction yields. The use of Cu(OAc)₂ (entries 2, 11, 12, 18-20) gave good yields but led to an increase in by-product

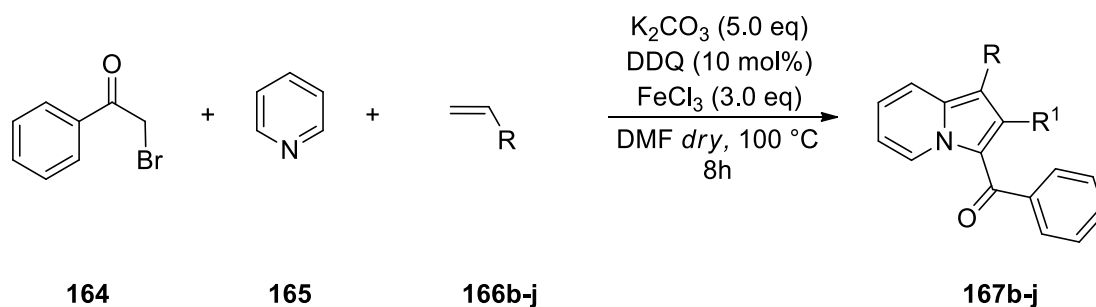
formation. The same can be observed in the presence of CuSO_4 and KHSO_4 (entries 5, 7, 8, 14, 15). Based on this evidence, the conditions reported in entry 17 gave the best results. Then, we wondered how the yield could be improved and if the heterogeneity of the reaction media might play some role in it, given that even the use of DMF and high temperatures did not perfectly dissolve the inorganic load of the mixture. Hence, we hypothesized that the use of an organic oxidant might help in this sense. Our attention was captured on 2,3-dichloro-5,6-dicyano-1,4-benzoquinone (DDQ), very recently employed in the regioselective synthesis of 1-cyano-3-arylindolizines.²⁶⁶ DDQ was tested in stoichiometric amounts (**Table 2**), improving the yields (entries 1-2). Even though the use of DDQ was satisfactory, we wondered if it was possible to reduce the amount of DDQ employed due to the presence of its oxidized form (DDQH_2) which made the purification steps quite difficult. Based on some evidence from the literature,²⁶⁷⁻²⁶⁹ we tested a protocol in which a terminal oxidant was used in stoichiometric amounts in the presence of catalytic DDQ (10-20 mol%) (entries 3-6). To our delight, both MnO_2 and FeCl_3 gave excellent results, giving high yields and better reaction crudes. Of note, the use of FeCl_3 (entries 5 and 6) gave higher yields than MnO_2 (entries 3 and 4): this may be related to the dual action exerted by FeCl_3 , as it can act as a Lewis acid towards the dipolarophile. One test in the absence of DDQ (entry 7) confirmed that FeCl_3 can act as an oxidant *per se*. Given the equivalence in terms of yields, the reaction conditions in which DDQ was at 10 mol% were chosen (entry 5).

Table 2. Optimization of reaction conditions by varying DDQ and terminal oxidant ratio.^a

Entry	Terminal oxidant (TO)	molar ratio		Yield (%) ^b
		DDQ	TO	
1	-	1	0	83
2	-	1	0	85
3	MnO ₂	0.1	3	98
4	MnO ₂	0.2	3	98
5	FeCl ₃	0.1	3	98
6	FeCl ₃	0.2	3	98
7	FeCl ₃	0	3	79

^aReaction conditions: **164** (1 eq.), **165** (1 eq.), **166** (2 eq.), K₂CO₃ (5 eq.), DMF *dry*, 100 °C, 8 h, N₂ atmosphere. ^bIsolated yields.

With these conditions in hand (**Scheme 39**), the synthesis was extended to other dipolarophiles to evaluate the reaction scope (**Figure 10**). The product obtained using ethyl acrylate as a dipolarophile (**167b**) was formed in 96% yields, like those obtained in the model reaction. The use of crotonaldehyde as a dipolarophile led to product **167c** and gave minor yields, presumably due to the aldehyde system which makes the α -carbon less nucleophilic. In this case, prolonging the reaction times did not improve the yields. As for the use of methyl 2-octynoate for the synthesis of the product **167d**, it gave good yields, confirming that the proposed synthetic protocol is suitable for internal alkynes.



Scheme 39. Reaction scope and optimized conditions. 1 eq. of dipolarophiles **166e-j** was used.

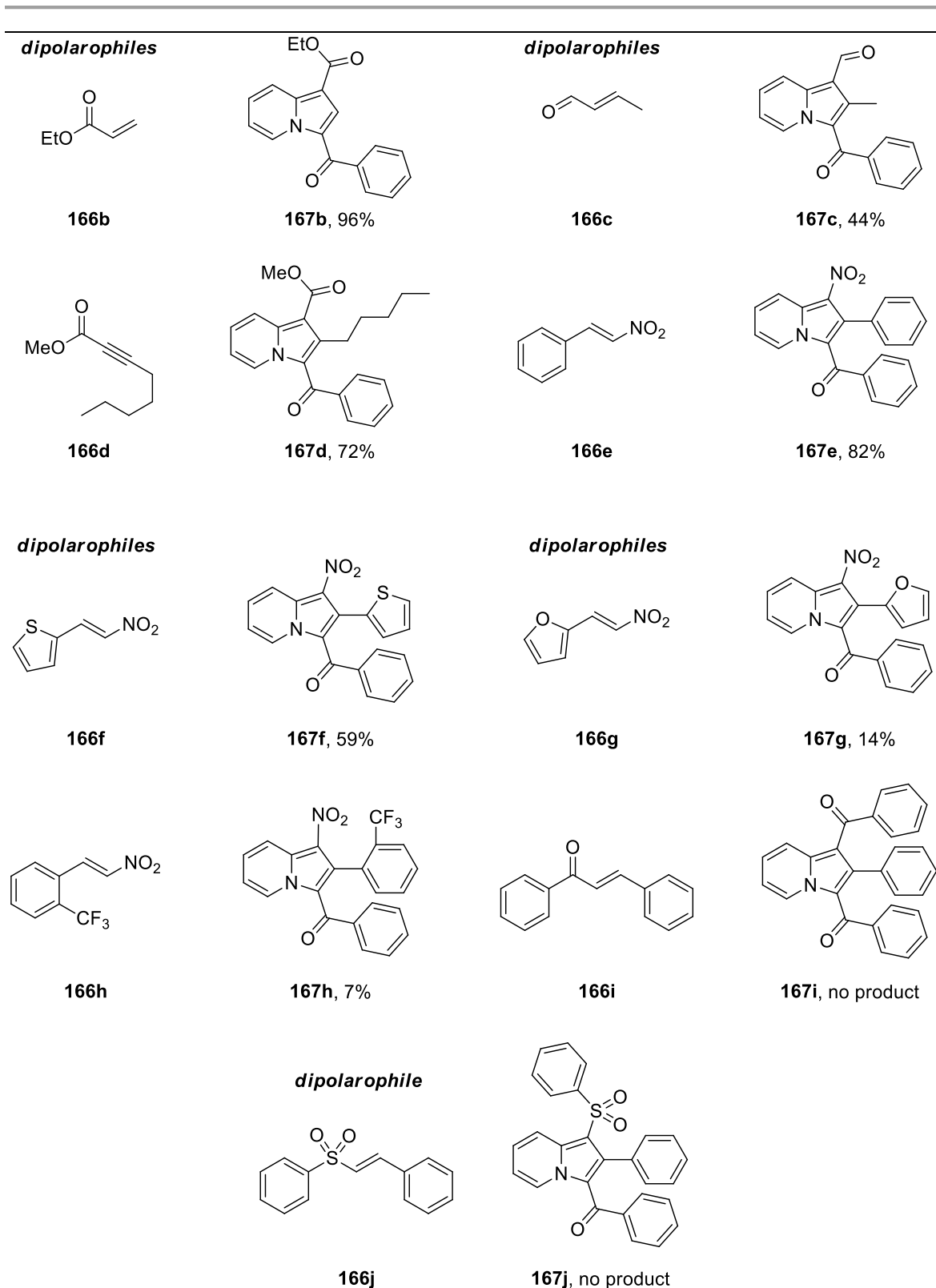
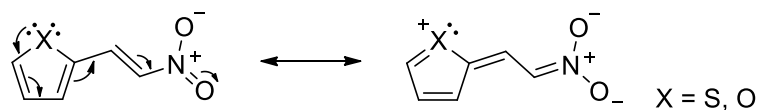


Figure 10. Reaction scope with various dipolarophiles. 1 eq. of dipolarophiles **166e-j** was used.

The product **167a-h** were obtained using the corresponding ω -nitrostyrenes and nitrovinyl derivatives. In this case, a general decrease in the yields was observed,

particularly for the heteroaromatic nitro derivatives presumably due to the electro-inductive effects of the heteroatom (**Scheme 40**).



Scheme 40. Electro-inductive effect of the heteroatoms is responsible for the worst electrophilicity of the α -carbon with respect to the nitro group.

As for the product **167h**, the CF_3 group in the *ortho* position with respect to the vinyl system likely exerted a similar effect giving a 7% yield. Of note, for compounds **167e-167h**, the formation of small to consistent amounts of the products without the NO_2 group at the $C1$ position was observed (**Figure 11**). This is related to the competition between the DDQ-driven oxidation and the elimination of HNO_2 by the newly formed cycloadducts. In this regard, the nature of the aromatic substituent present on the dipolarophile appeared to be decisive, as the ratio of the products with and without the nitro group was 1:1 for compound **167g**.

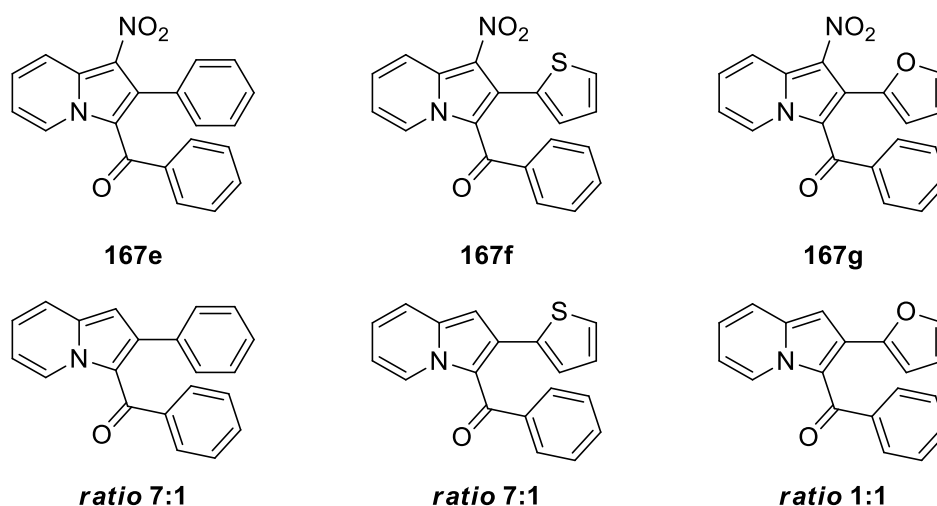
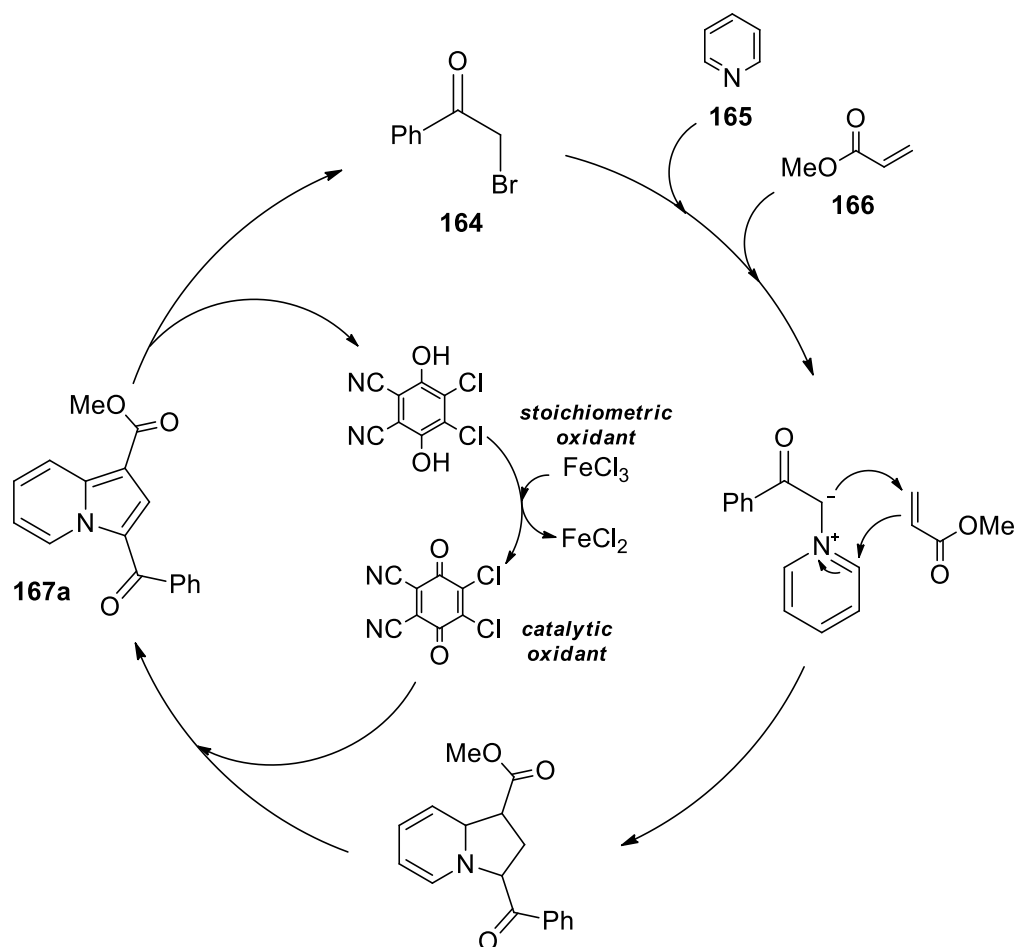


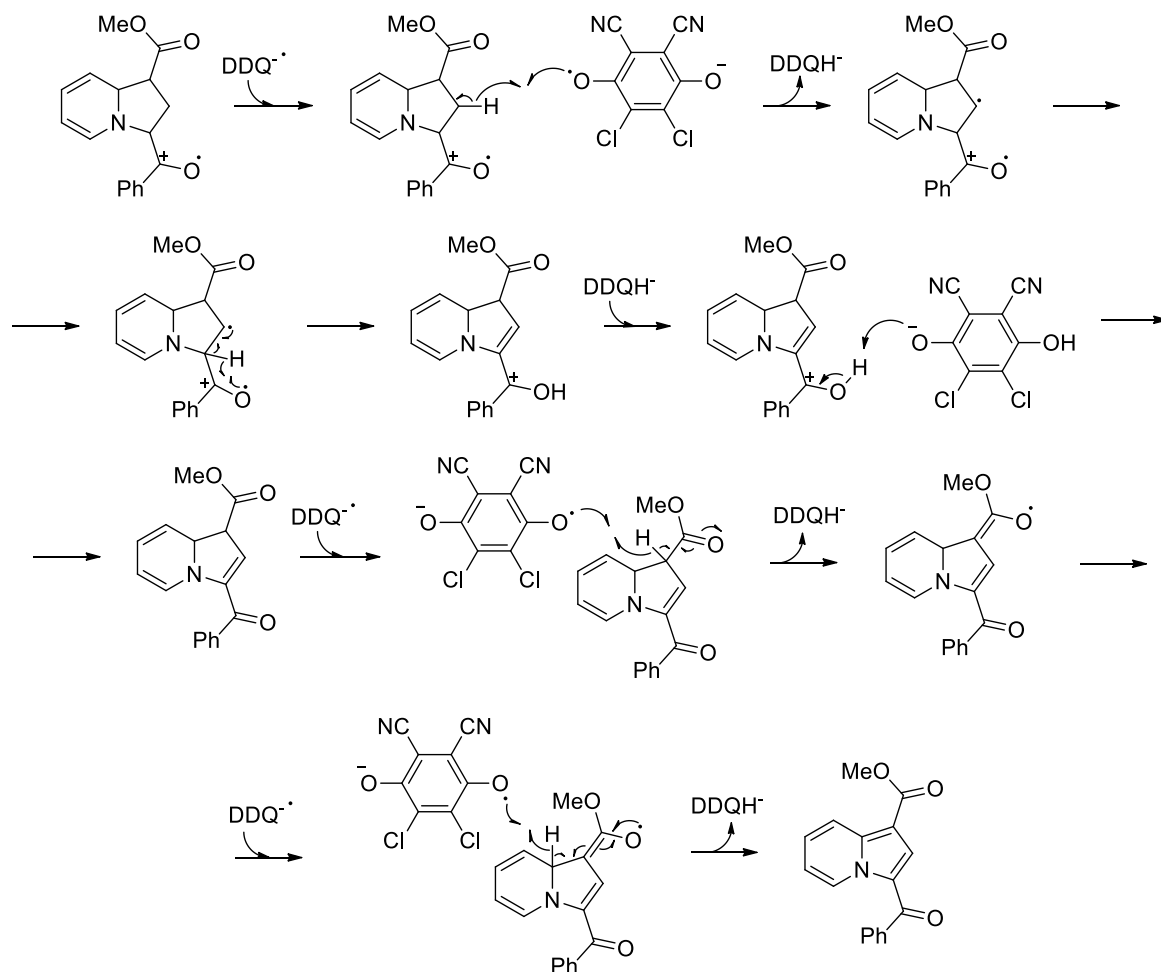
Figure 11. Main product *versus* by-product ratios.

As for the use of other dipolarophiles as chalcone and phenyl *trans*-styryl sulfone (**167i** and **167e**), no product was detected probably due to the particularly low electrophilicity of the β -carbon of the electrophiles.



Scheme 41. Plausible mechanism for the iron (III)-mediated regeneration of the DDQ.

The plausible mechanism is reported in **Scheme 41**. In this case, we hypothesized that a mechanism similar to the one proposed by Liu and Floreancig took place,²⁶⁸ wherein the catalytic DDQ was re-oxidized by the Fe (III) salt. Intrigued by the mechanism of the DDQ-driven oxidation step, we also elaborated a plausible mechanism based on the work of Beak *et al.*²⁷⁰, wherein a single-electron transfer (SET) mechanism was described (**Scheme 42**).



Scheme 42. DDQ-mediated pathway of indolizine formation by single-electron transfer mechanism (SET).

In conclusion, the original research proposed in this paragraph was devoted to implementing a multicomponent approach for the synthesis of di- and tri-substituted indolizines. The use of catalytic amounts of DDQ in combination with stoichiometric quantities of a terminal oxidant (FeCl_3), gave access to a robust method wherein different dipolarophiles turned out to be suitable for the desired reaction. Further studies are ongoing to computationally validate the proposed mechanism.

3. Spirocyclopropyl oxindoles: recent advances and biological activities

In this paragraph, the advances in the synthesis of spirocyclopropyl oxindoles and their importance as potential drugs will be reviewed to give the reader a solid background for the next, and last, paragraph of this chapter. Spirocyclopropyl oxindoles are an interesting scaffold in synthetic organic chemistry given that they bear three structural functions making them unique: a cyclopropyl moiety, a spirocarbon, and an oxindole scaffold (**Figure 12**).

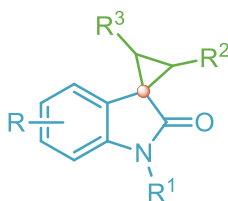
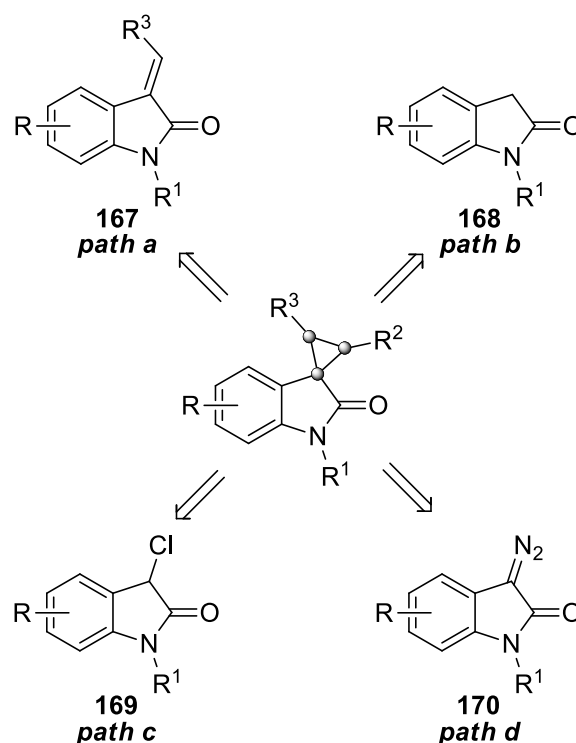


Figure 12. General structure of spirocyclopropyl oxindoles. Oxindole moiety in blue, propyl moiety in green, and spirocarbon is represented by the orange dot.

The development of protocols for accessing spirocyclopropyl derivatives is highly desired in organic chemistry, mainly due to the intrinsic challenge posed by the formation of such a high ring-constrained structure (ca. 27 kcal/mol). With an eye to medicinal chemistry, cyclopropyl moieties can be also in drug development, given that such frameworks play a role in (i) reducing off-target effects, (ii) improving potency, (iii) raising brain permeability, (iv) improving metabolic stability, (v) reducing plasma clearance, (vi) modifying drug pKa, (vii) assisting in an entropically more favorable binding to the target.²⁷¹

Spirocarbon is a hallmark in the modern era of drug design. In the laboratory wherein this project was developed, we've been interested in deepening the synthesis of these structural functions using isatin and indanone spiroisoxazolidine derivatives.^{184,185} Introducing a spirocarbon in an organic compound has been defined as a "way to escape from flatland",²⁷² because having two perpendicular rings can maximize the possible interactions within the biological target. Nonetheless, the introduction of such functionality can be useful for the modulation of solubility, lipophilicity, and log D of the compounds of interest.²⁷³ As for the oxindole scaffold, it is a remarkable nature-inspired moiety known for its synthetic versatility. It presents important intercalating properties alongside its capacity to behave as π - and *H*-bond acceptors.²⁷⁴ With this evidence in hand, in *research line 3b* we exploited the reactivity possessed by pyridinium ylides to access spirocyclopropyl oxindoles through a multicomponent

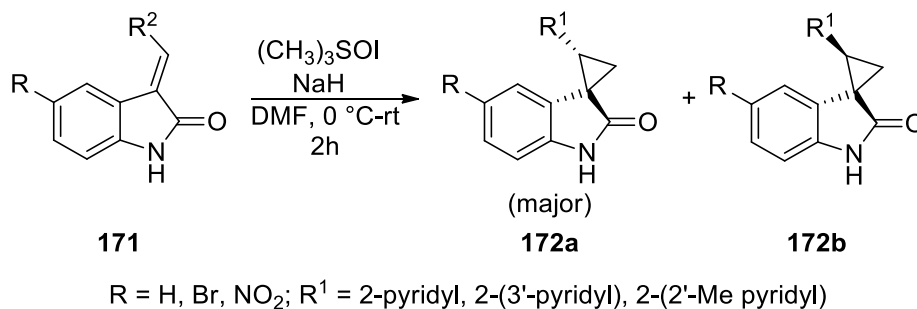
approach. The use of rare-earth metal triflates was fundamental, determining also unexpectedly high diastereoselectivity which was computationally deepened. Before describing such results, it could be instructive to review the latest advancements in their synthesis. The main strategies were reviewed by Cao and Zhou in 2015²⁷⁵ and contemplate four paths: a) from 3-alkylideneoxindoles, b), from oxindoles, c) from 3-chlorooxindoles, d) from diazooxindoles (**Scheme 43**).



Scheme 43. Main starting reagents for the synthesis of spirocyclopropyl oxindoles. Adapted from Cao and Zhou.²⁷⁵

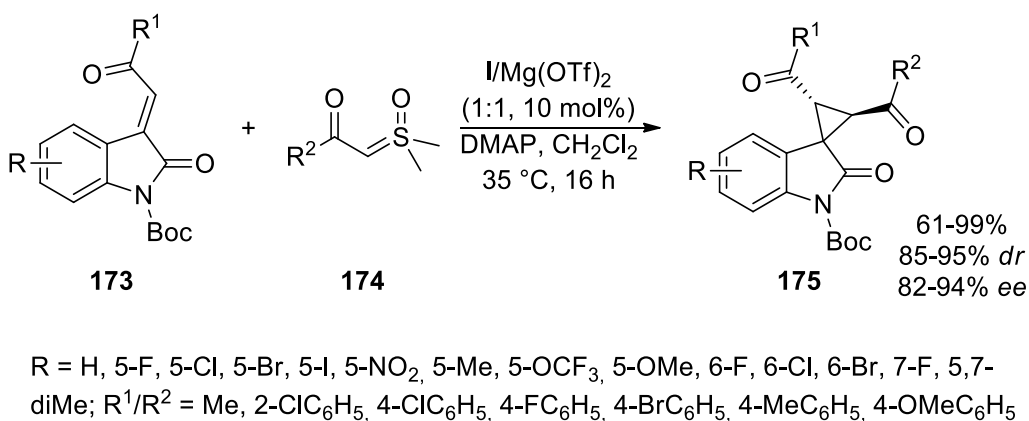
3.1 Path a – from 3-alkylidene oxindoles

One of the most popular ways to form spirocyclopropyl oxindoles is through the cyclopropanation of 3-alkenyloxindoles **167**. The synthesis of the cyclopropane ring is accessed *via* cycloaddition reactions or Michael addition using the appropriate nucleophile. Sulfur ylides, MBH (Morita-Baylis-Hillman) carbonates, diazo compounds, and carbenoids are the most often used reagents in this context. Sulfur ylides were used by Moldavai and co-workers to obtain the target compound *via* a Corey-Chaykovsky reaction wherein the nucleophile was formed *in situ* from TMSOI and NaH (**Scheme 44**).²⁷⁶



Scheme 44. Preparation of spirocyclopropyl oxindoles through a modified Corey-Chaykovsky reaction.

Sulfoxonium ylides were used also by Feng and colleagues²⁷⁷ to catalyze the asymmetric synthesis of spirocyclopropyl oxindoles **175** by means of the N,N' -dioxide **I**/ $\text{Mg}(\text{OTf})_2$ system (**Scheme 45**). Better diastereoselectivity was ensured with the usage of DMAP. On the other hand, enantioselectivity was lost when other metal triflates (Ni , Zn , etc.) were used.



Scheme 45. Enantioselective synthesis of spirocyclopropyl oxindoles **175**.

The stereoselectivity of the reaction was also influenced by the nature of the substituents on the chiral catalyst **I** (**Figure 13**). Diversely substituted N -Boc-protected 3-alkenyloxindoles reacted well with sulfoxonium ylides under the reported optimized conditions. Due to its low electrophilicity, oxindole with free $-NH$ and N -benzyl substitution gave racemic compounds with poor yield.

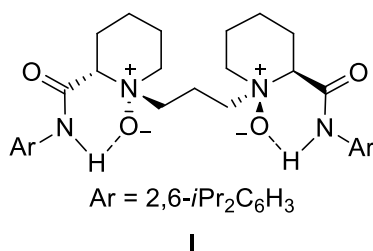
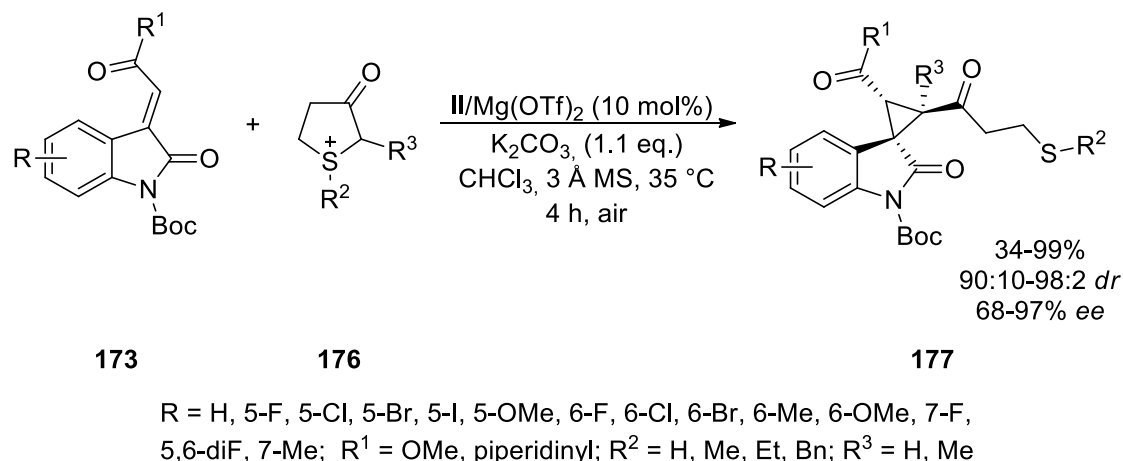


Figure 13. Feng chiral ligand for the enantioselective synthesis of **175**.

The stereoselective cyclopropanation of 3-alkenyl oxindole was later carried out by the same research group using cyclic sulfur ylides **176**.²⁷⁸ The chiral sulfur-containing spirocyclopropanes **177** produced by this common ring-opening/cyclopropanation mechanism resulted in a good atom economy (**Scheme 46**).



Scheme 46. Enantioselective synthesis of sulfur-containing spirocyclopropyl oxindoles **177**.

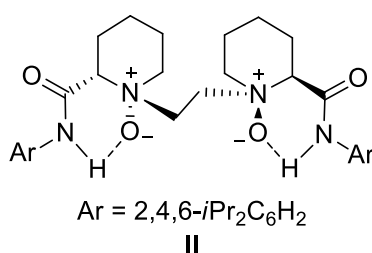
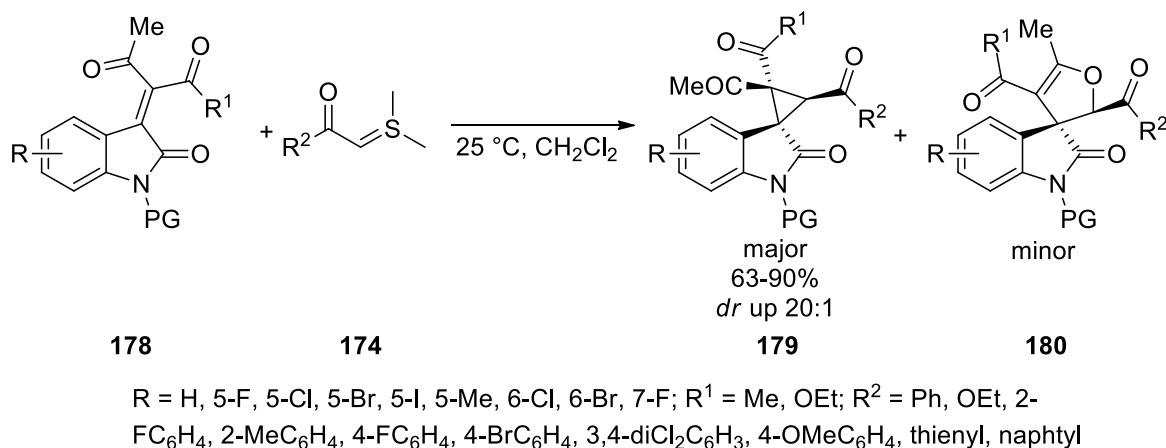


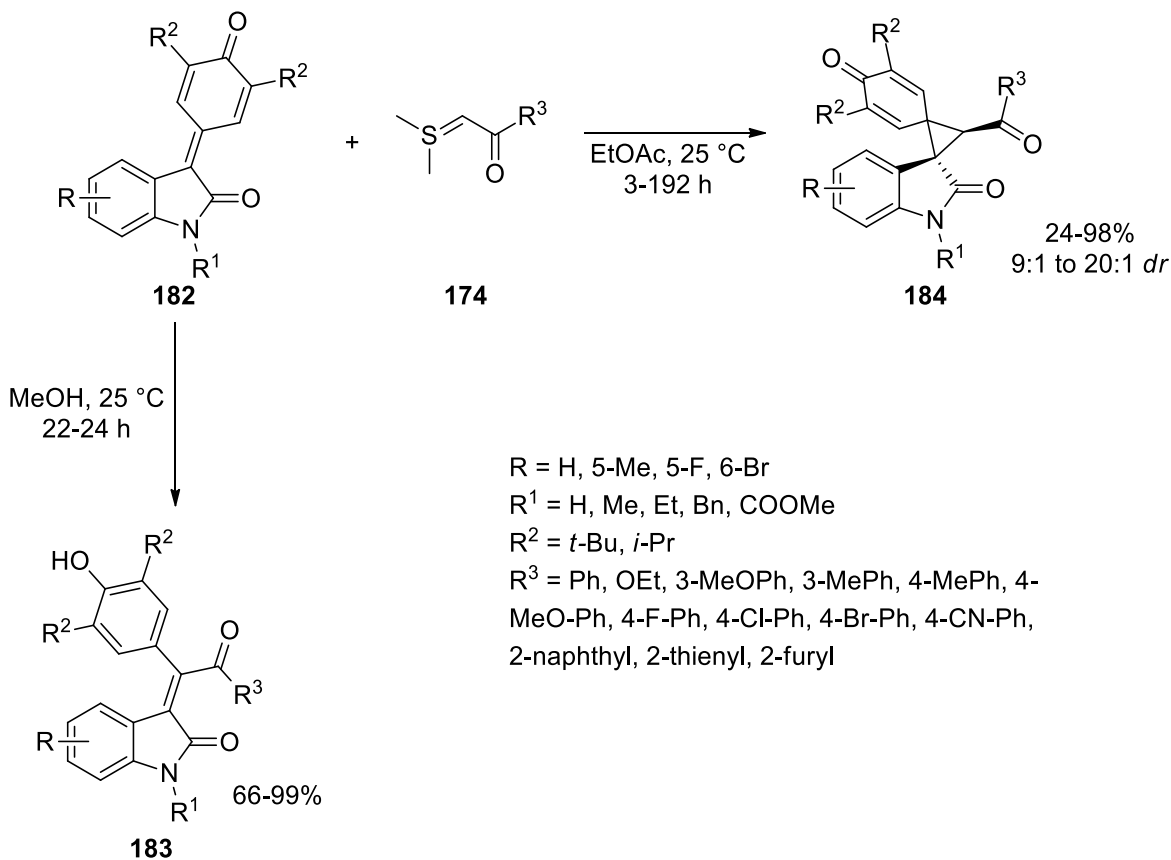
Figure 14. Feng chiral ligand for the enantioselective synthesis of **177**.

3-alkenyl oxindoles with different functionalities showed a high cyclopropanation reactivity towards sulfoxonium ylides. Typically, these reactions take place without the aid of a catalyst *via* [2+1] cycloaddition. One such cycloaddition of tetrasubstituted olefins **178** with sulfur ylides **174** to form spirocyclopropanes **179** was described by Han *et al.*²⁷⁹ (**Scheme 47**). Through the [4+1] pathway, the reaction also gave access to dihydrofuran-fused spirooxindole **180** as a minor product. The same compound, however, was obtained as the major product when the reaction was conducted at a higher temperature.



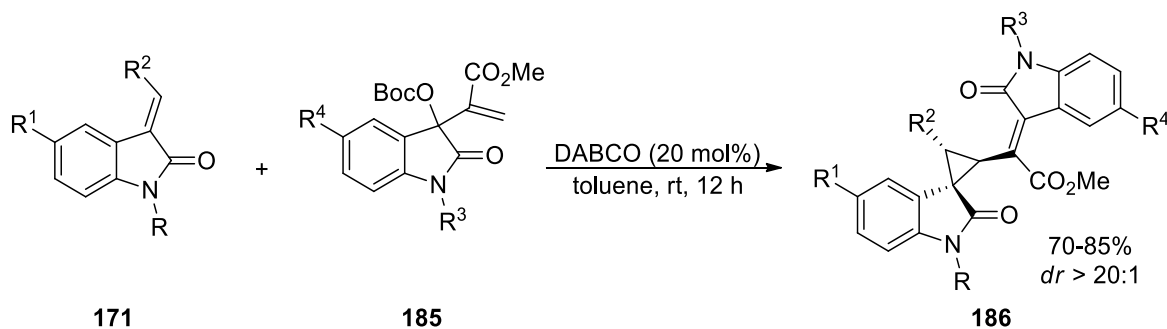
Scheme 47. Synthesis of spirocyclopropyl derivatives *via* sulfur ylides.

Yuan and colleagues²⁸⁰ showed that para-quinone methides **182**, generated from isatin, can give cyclopropanation reaction with sulfur ylides **174** (**Scheme 48**). Using ethyl acetate as a solvent, the process gave product **184**. However, in the presence of methanol, the formation of 3-alkenyloxindoles **183** took place with the formation of SMe₂ as a by-product. From a mechanistic point of view, the formation of **184** was prompted by the ring-opening step in the presence of SMe₂, followed by an intramolecular *H*-shift, and SMe₂ elimination.



Scheme 48. Chemodivergent synthesis of tetrasubstituted olefins **183** and spirocyclopropyl oxindoles **184**.

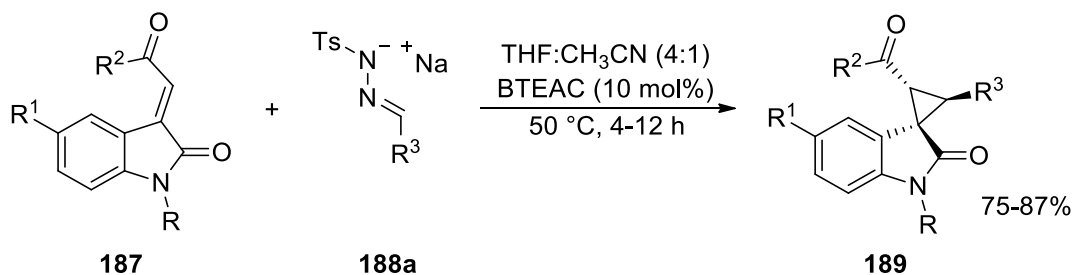
Another approach consisted in using MBH carbonates as Michael acceptors. In this way, the Bhat group prepared the target compounds from the corresponding 3-alkenyloxindoles performing an [2+1] annulation reaction in the presence of DABCO, obtaining a bis-oxindole derivative bearing a spirocyclopropyl scaffold **186** (Scheme 49).²⁸¹



R = Me; R¹ = H, Br, Cl; R² = COC₆H₄, CO₄-ClC₆H₄, CO₄-MeC₆H₄; R³ = Me, Bn, allyl; R⁴ = H, Br

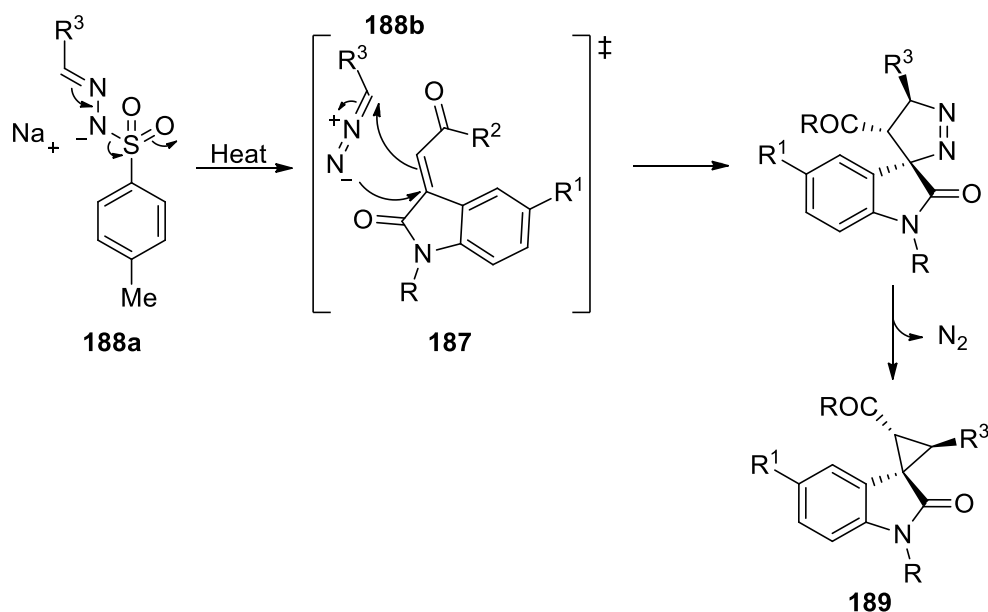
Scheme 49. Synthesis of bis-oxindole derivatives from MBH carbonates.

Diazo compounds are also good synthons for [3+2]-annulation reactions using various olefin reagents. In this approach, N₂ is eliminated, resulting in the formation of a three-membered cyclic structure. However, the direct usage of diazo compounds in the process is very limited due to the instability of such substrates. As a more safe substitute for diazo-compounds, Maurya *et al.*²⁸² reported the diastereoselective cyclopropanation of 3-alkenyloxindoles using the sodium salt of tosyl hydrazones **188a** as the source of nitrogen (Scheme 50). BTEAC (benzyl triethyl ammonium chloride) was employed to increase the solubility of the reagents maintaining an optimal yield. In this frame, aryl diazomethane **188b** was formed *in situ* from the thermal degradation of the tosylhydrazone salt **188a**. Hence, **188b** gave [3+2]-DPCA reaction with **187**, and the subsequent N₂ elimination gave the desired product **189** in a diastereoselective way.

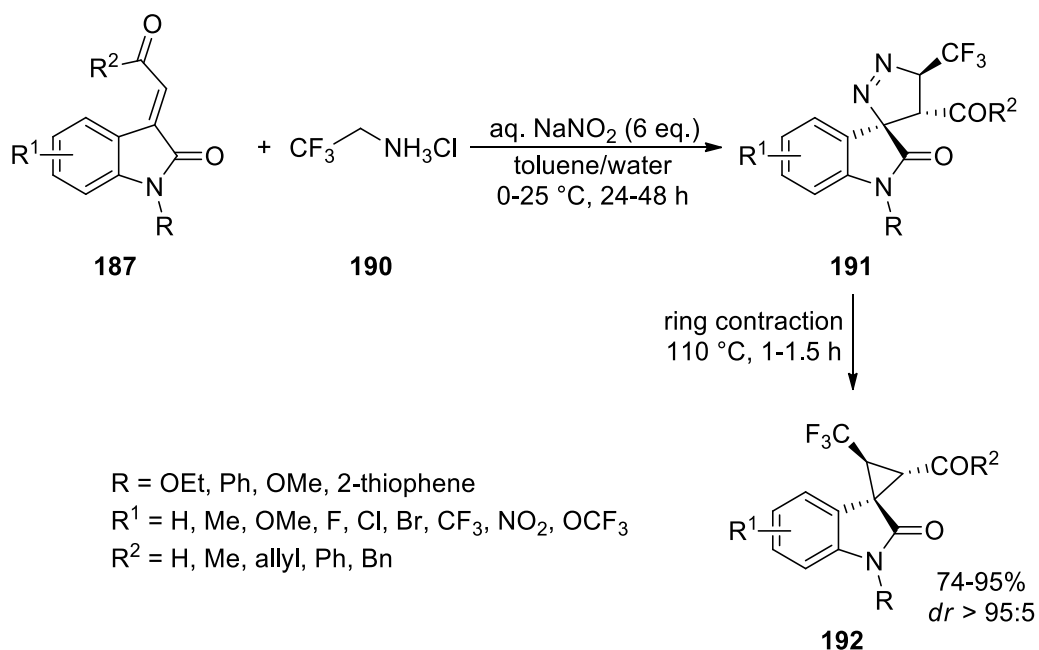


$R = \text{H, Me}$; $R^1 = \text{H, F, Br, Cl, NO}_2$; $R^2 = \text{OEt, Ph, 4-MeC}_6\text{H}_4, \text{4-OMe-C}_6\text{H}_4, \text{4-Cl-C}_6\text{H}_4, \text{4-Br-C}_6\text{H}_4, \text{4-NO}_2\text{-C}_6\text{H}_4, \text{2-naphthyl}$; $R^3 = \text{Ph, 4-OMe-C}_6\text{H}_4, \text{4-CN-C}_6\text{H}_4, \text{4-NO}_2\text{-C}_6\text{H}_4$

proposed mechanism



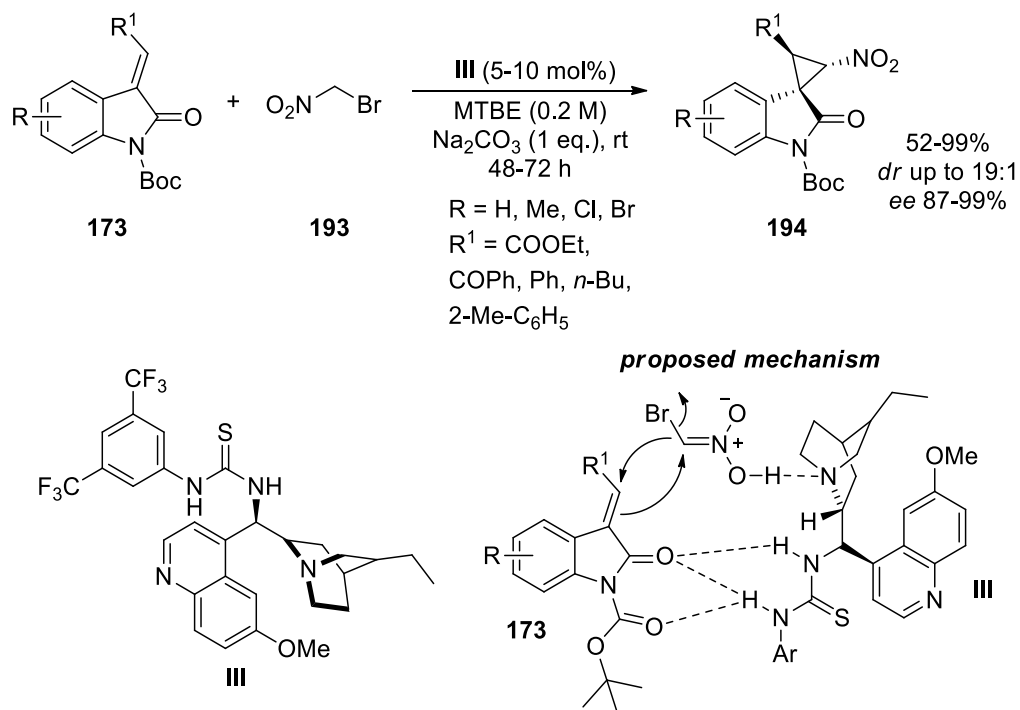
Scheme 50. Cyclopropanation reaction with tosylhydrazone salts **188a** as source of nitrogen.



Scheme 51. Preparation of CF_3 -containing spirocyclopropyl oxindole derivatives **192**.

In a similar way, Li *et al.*²⁸³ proposed an approach to *in situ* generate CF_3CHN_2 from $\text{CF}_3\text{CH}_2\text{NH}_2$ hydrochloride to access sequential [3+2]-cycloaddition/ring contraction of 3-alkenyloxindoles **191** (**Scheme 51**). Such trifluoromethyl-containing products resulted also relevant from a biological point of view. As for the mechanism, cycloadduct **191** was formed by the initial [3+2]-DPCA between **187** and CF_3CHN_2 . At 110 °C, the intermediate passed through a ring-contraction step to form **192**.

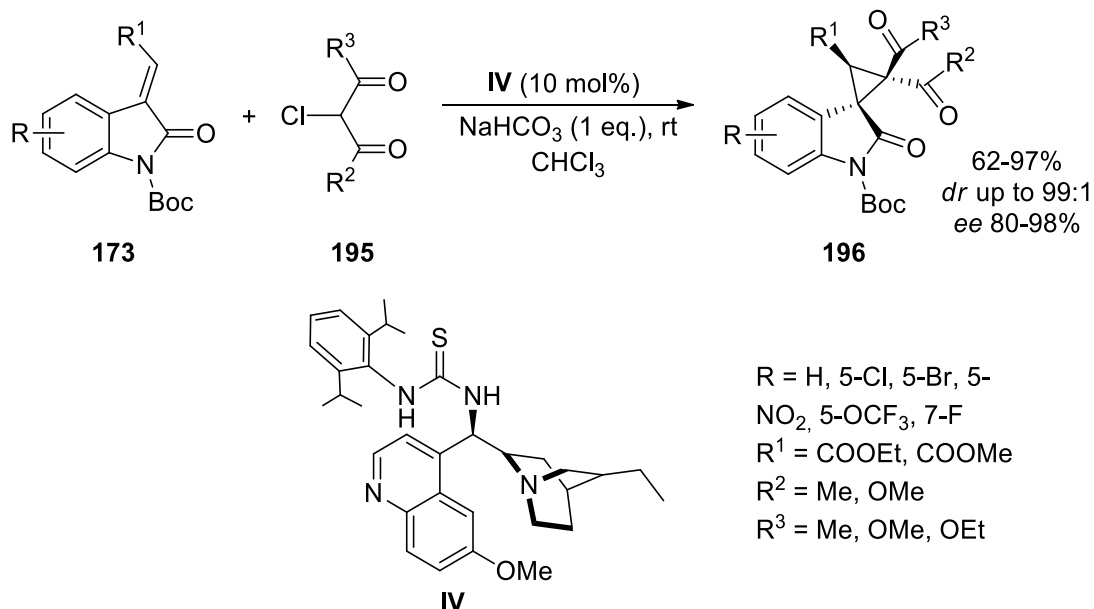
Another approach to accessing such valuable products exploited the reactivity of carbenoids. Carbenoids are C1 synthons suitable to form spirocyclopropyl oxindoles in a diastereo- and enantioselective manner. As an example of their reactivity, it can be considered the reaction of 3-alkenyloxindoles **173** with bromonitromethane **193** which allowed to access the asymmetric Michael-alkylation cascade cyclopropanation reaction (**Scheme 52**).²⁸⁴ In this case, polar solvents were shown to speed up the reaction, whereas strong bases and the type of substitutions on the chiral catalysts employed impacted the stereoselectivity. From a mechanistic perspective, if the cyclopropanation reaction from the *Si*-face of the double bond is considered, catalyst **III** could activate both the olefin and the Michael donor bromonitromethane *via* H-bond interactions.



Scheme 52. Quinine-derivative catalyzed cyclopropanation reaction.

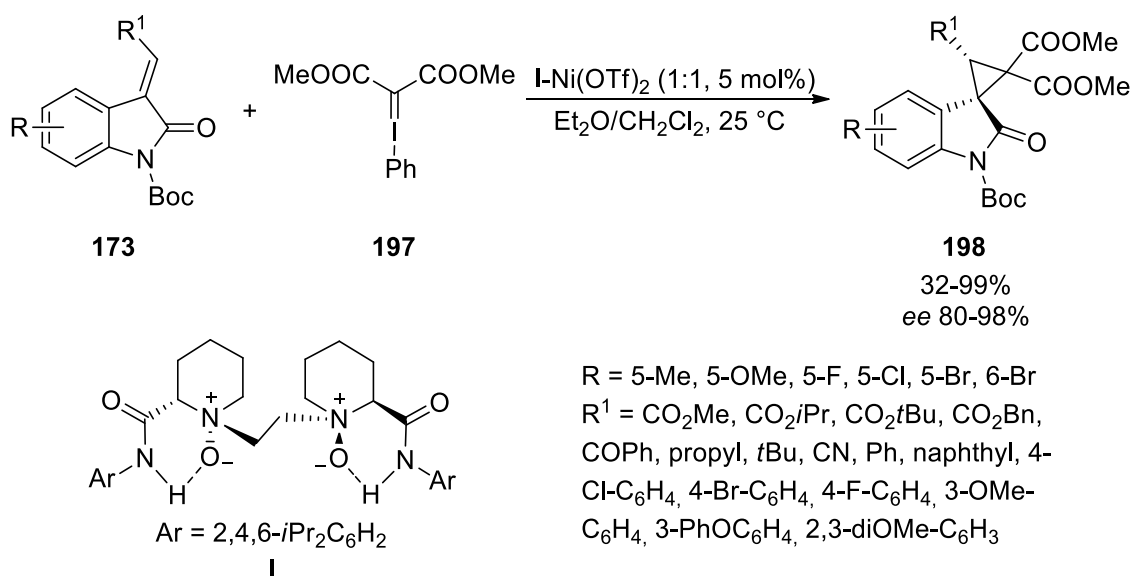
An interesting example described the use of chiral thiourea for catalyzing the Michael addition of α -halo-dicarbonyl compounds **195** as carbenoid (**Scheme 53**). As expected, the reaction resulted to be enantioselective. Thiourea catalyst **IV** induced *Si*-facial

selectivity for the principal diastereoisomer. Functionalizing the chiral catalyst **IV** with a 2',5'-diisopropyl substitution on the aromatic ring helped to improve the final diastereoselectivity, presumably by limiting the rotation of the C-N bond. In the presence of a large excess of α -halo-dicarbonyl compounds **195**, the yield was improved.



Scheme 53. α -halo- β -dicarbonyl compounds **195** addition to 3-alkylidene oxindoles **173**.

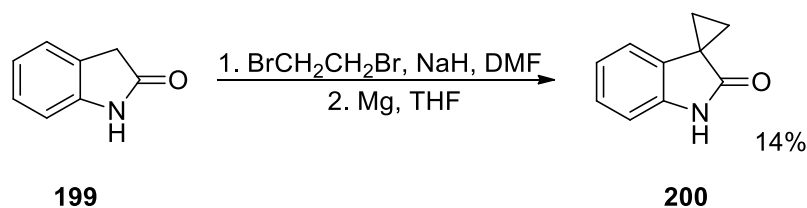
Lastly, it was possible to synthesize similar products by using a chiral N,N' -dioxide **I**-Ni(OTf)₃ catalytic system (**Scheme 54**). Such a system exploited phenyliodonium ylide **197** as a carbenoid source for the enantioselective cyclopropanation of 3-alkenyl oxindoles **173**.



Scheme 54. Enantioselective cyclopropanation reaction with phenyliodonium ylide **197**.

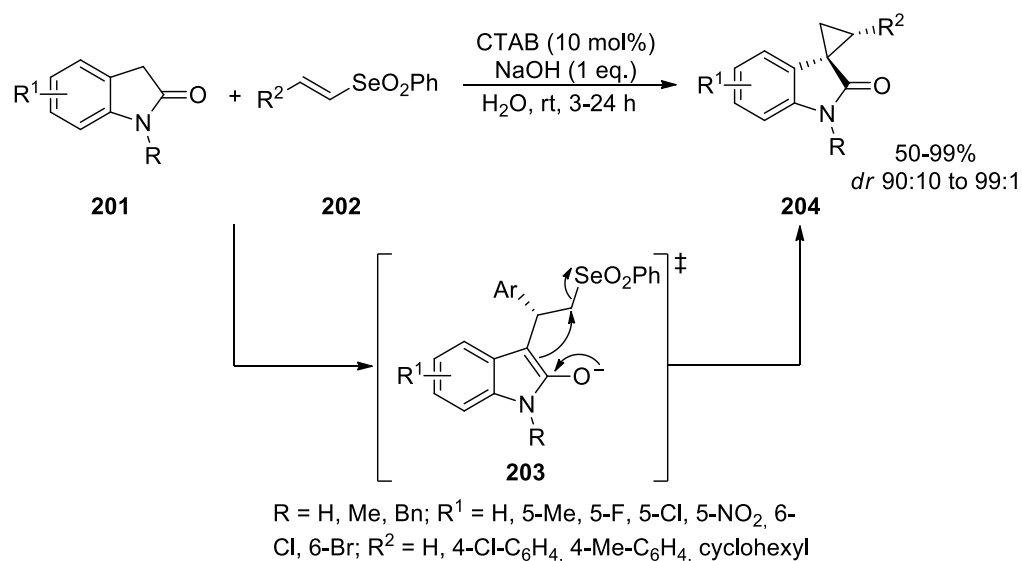
3.2 Path b – from oxindoles

Oxindoles are useful reagents for the preparation of spirocyclopropyl oxindole derivatives. One of the first examples in this context was proposed in 1987 by Robertson and co-workers (**Scheme 55**),²⁸⁵ who prepared the target product **200** from oxindole **199** in the presence of dihaloethane and a strong base (NaH). Due to the acidity of the NH group of the oxindole, protection was needed to avoid the alkylation of the group.



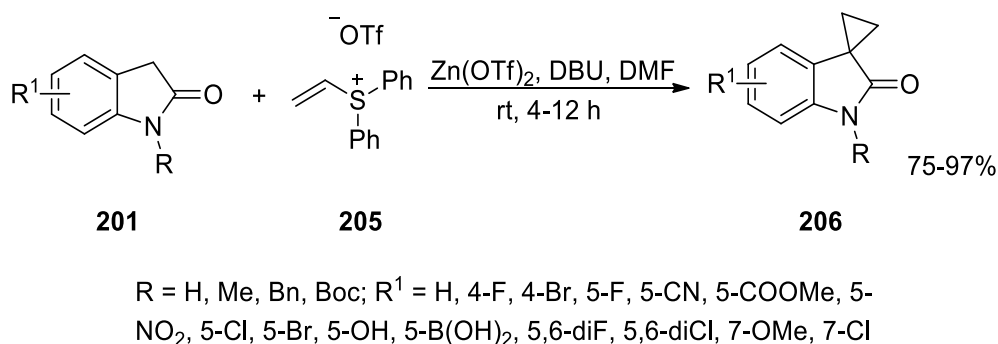
Scheme 55. Synthesis of spirocyclopropyl oxindole **200** from oxindole **199**.

To achieve cyclopropanation of oxindoles **201** in alkaline conditions, Marini *et al.*²⁸⁶ employed vinyl selenones **202** (**Scheme 54**). In this case, the authors managed to improve the reaction rate and diastereoselectivity by using cetyltrimethylammonium bromide (CTAB) as a surfactant, inducing the formation of micellar aggregates and aiding the dispersion of the reagents. As a result, the Michael addition step was accelerated and, as for the mechanism, an intramolecular nucleophilic substitution/domino Michael route was proposed. Moreover, the authors postulated that the high diastereoselectivity observed was due to the stabilization of the Michael adduct **203** by stacking interactions between the oxindole ring and the neighboring aromatic ring in the transition state.



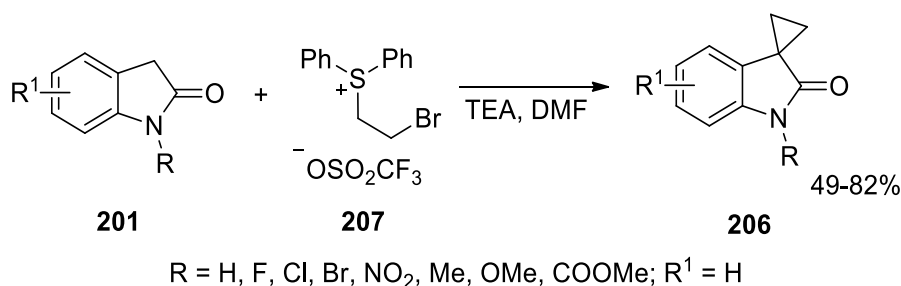
Scheme 54. Cyclopropanation reaction from oxindole derivatives **201** with vinyl selenones **202**.

In a similar work, the Qian group described a vinyl diphenylsulfonium triflate salt **205**-mediated cyclopropanation of oxindoles **201** (**Scheme 55**).²⁸⁷ The main advantages of such an approach consisted in using easily accessible salts and the possibility to apply the protocol with no need for *N*-protection of oxindoles. In this frame, the oxindole nitrogen complexed the metal increasing the acidity of the C3-methylenic proton, allowing the use of DBU to generate the desired nucleophile. In agreement with this hypothesis, the cyclopropanation of *N*-protected oxindoles did not require the addition of Zn(OTf)₂. The applicability of the protocol was tested towards the late-stage functionalization of ropinirole (dopamine agonist), ziprasidone (antipsychotic), and PF562271 (FAK inhibitor).



Scheme 55. Cyclopropanation of oxindoles **201** with diphenyl sulfonium triflate salts **205**.

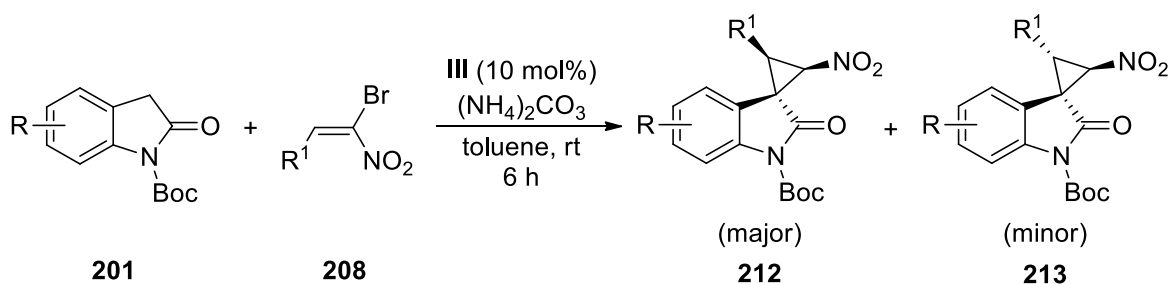
The synthesis of cyclopropyl derivatives **206** from oxindoles **201** was also achieved using bromoethylsulfonium salts **207** in the presence of TEA, as shown by Qin *et al* (**Scheme 56**).²⁸⁸ Even in this case, the use of *N*-protected substrates was needed because high amounts of *N*-alkylated by-products were obtained when the equivalents of bromoethylsulfonium salt were increased.



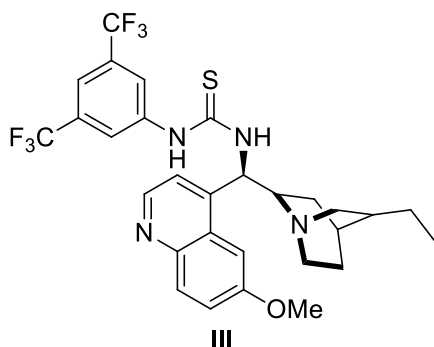
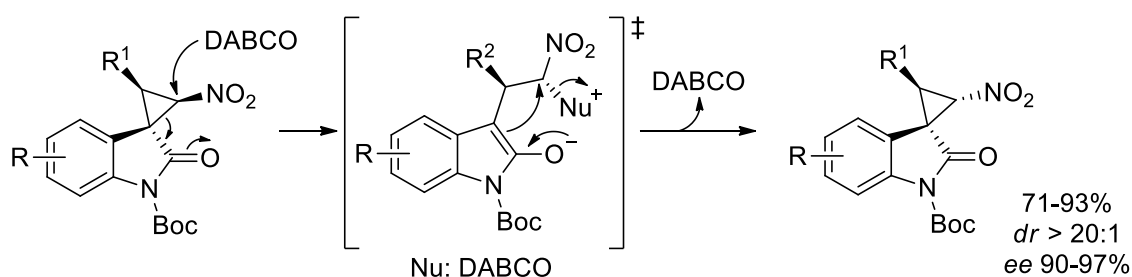
Scheme 56. Synthesis of spirocyclopropyl derivatives using bromoethylsulfonium salts **207**.

To obtain spirocyclopropyl oxindoles asymmetrically, Lu and colleagues²⁸⁹ used nitroolefins **208** and oxindole **201** (**Scheme 57**), adding ammonium carbonate to buffer the HBr formed during the process. Two diastereoisomers, **209** and **210**, were obtained in the first step of the reaction because of the action of the chiral thiourea

catalyst **III**. By treating both diastereoisomers with DABCO, only **209** was susceptible to the presence of such nucleophile, giving rise to a ring opening-closing diastereoselective process.



proposed mechanism



R = H, 5-Cl, 6-Cl
 R¹ = Ph, 2-Br-C₆H₄, 3-Br-C₆H₄, 4-Br-C₆H₄, 2-Cl-C₆H₄, 4-Cl-C₆H₄, 2-F-C₆H₄, 4-F-C₆H₄, 2-Me-C₆H₄, 4-Me-C₆H₄, 2,4-diCl-C₆H₄, isobutyl, phenethyl, 1-naphthyl, 2-naphthyl

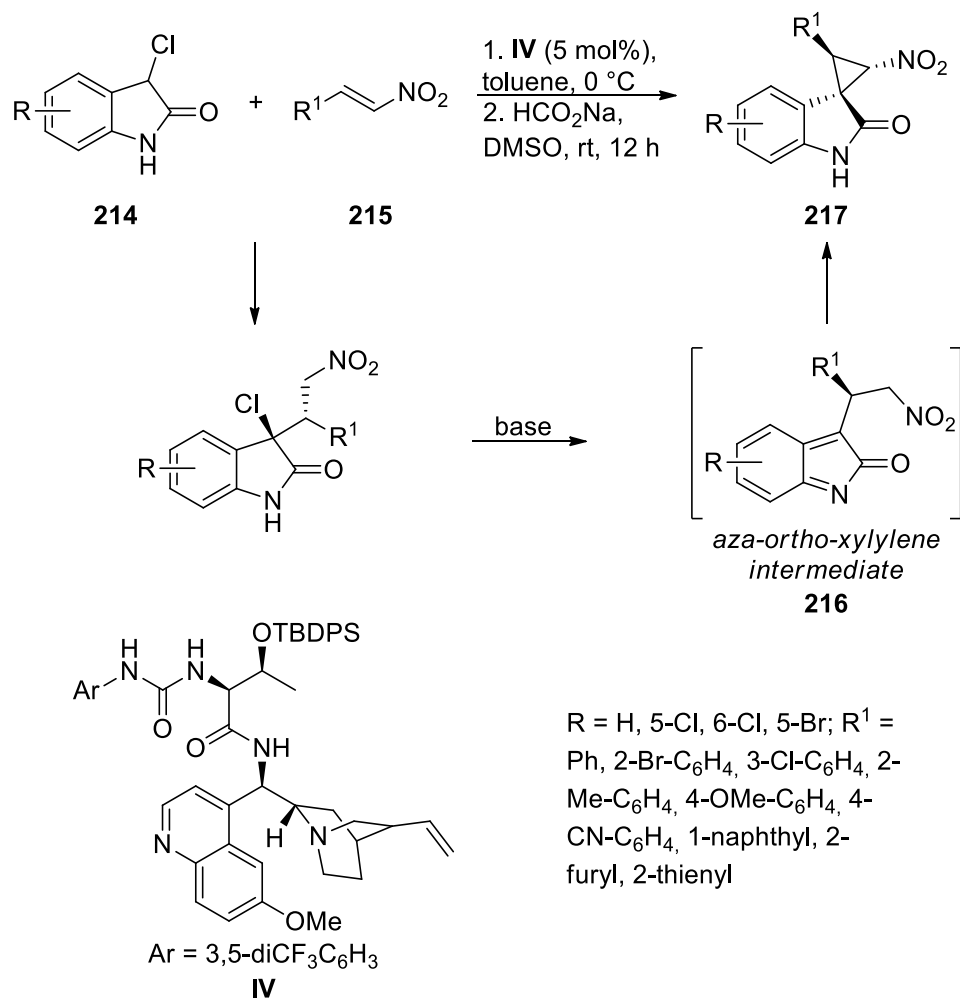
Scheme 57. Asymmetric cyclopropanation of oxindole **201** with olefins **208** and plausible reaction mechanism.

3.3 Path c – from 3-chlorooxindoles

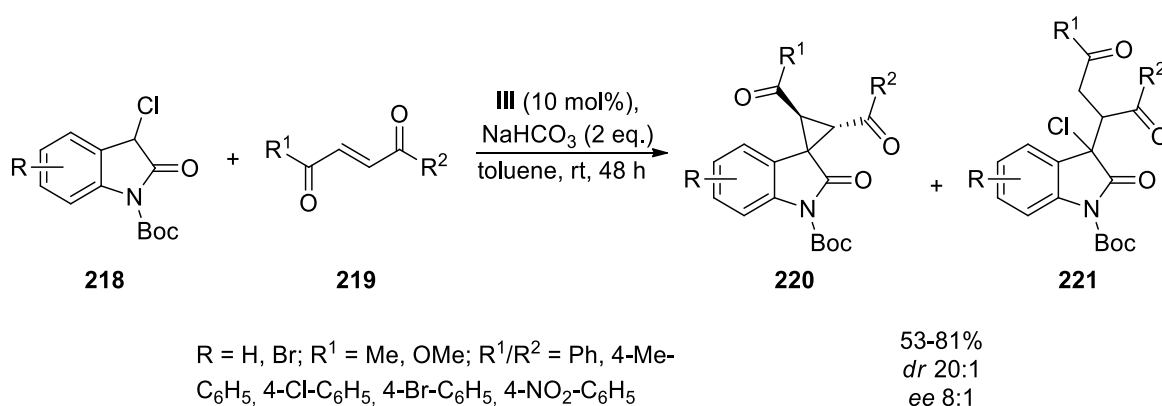
Spirocyclopropyl oxindoles can also be made using 3-halooxindoles, species presenting a double nature since can behave as nucleophiles and electrophiles. Mechanistically speaking, when the formation of a spirocyclopropyl moiety is desired, these substrates often undergo a Michael addition step followed by the typical intramolecular nucleophilic substitution with the elimination of the halide.

An interesting work reported that the use of 3-chlorooxindoles **214** and nitroolefins **215** gave access to spiro-fused nitrocyclopropanes **217** (**Scheme 58**).²⁹⁰ The reaction proceeded well in alkaline conditions in an asymmetric fashion due to the presence of catalyst **IV**, wherein a Michael addition of **214** to nitroolefins produced the *aza-ortho*-

xylylene **216** intermediate, which was then intramolecularly trapped to give the desired product **217**.



Scheme 58. Synthesis of spirocyclopropyl derivatives from 3-chlorooxindoles.

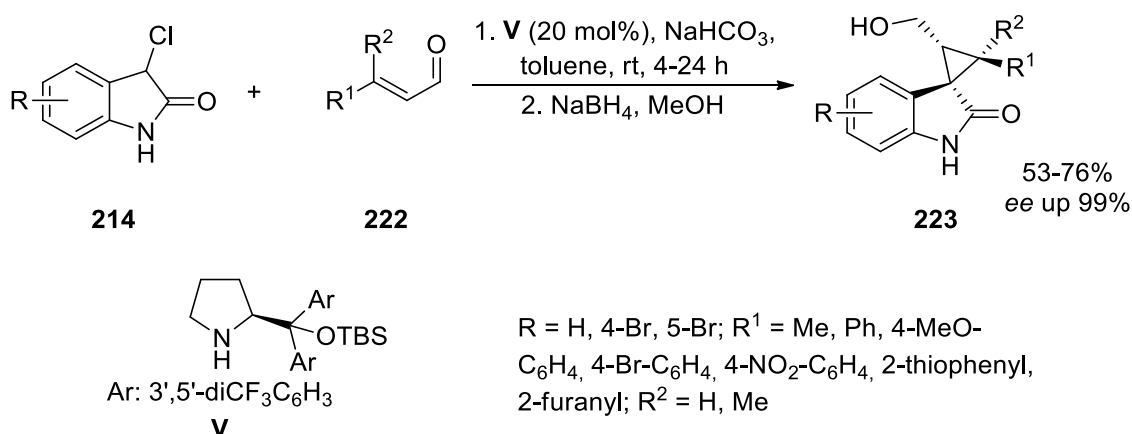


Scheme 59. Enantioselective synthesis of **220** from **218** and asymmetric enones **219**.

Aromatic 1,4-diketone **219** can be also suitable reaction partners with Boc-protected 3-chlorooxindoles **218** (Scheme 59).²⁹¹ The protection was needed due to the reduced acidity of the geminal proton which required a stronger base. The use of such a base would primarily deprotonate the NH group of the oxindole ring, leading to undesired

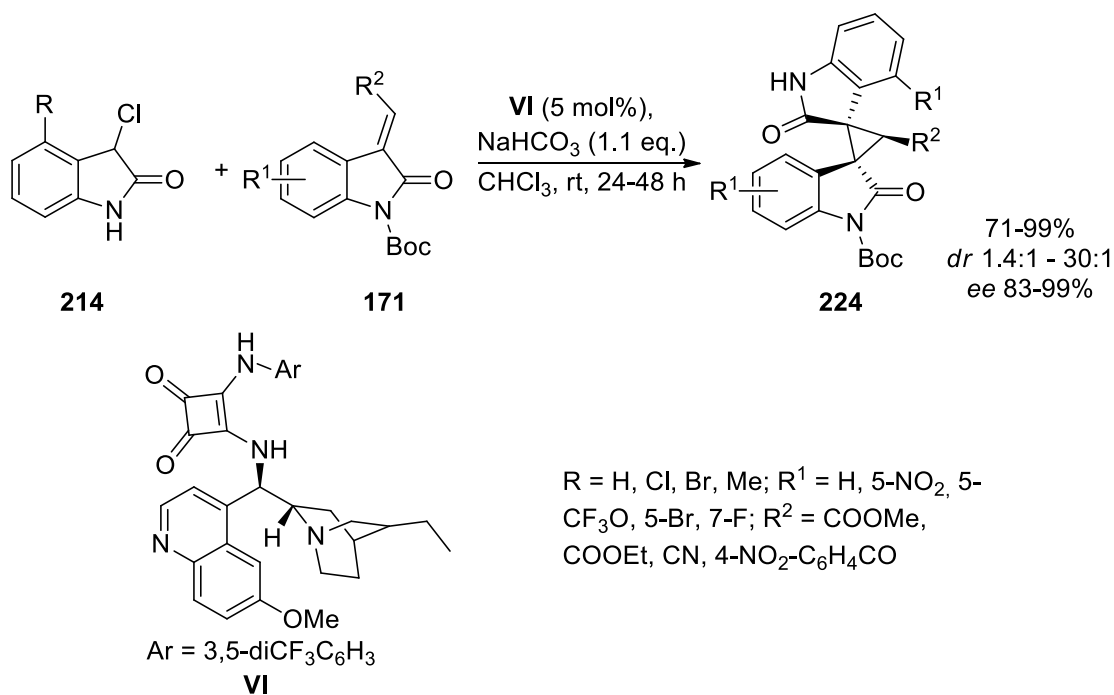
side reactions. Notably, only one stereoisomer was obtained after the Michael addition of non-symmetric enones bearing two reactive electrophilic centers **219**. However, a little amount of uncyclized Michael adduct **221** was detected.

The same group proposed a protocol to prepare highly-substituted spirocyclopropanes **223** by reaction of **214** with alkenes **222** using a proline-derived amino catalyst **V** to control the stereochemistry (**Scheme 60**).²⁹² In this case, to counteract the instability of aldehydes **222**, sodium borohydride was employed to *in situ* reduce such reagents to alcohols.

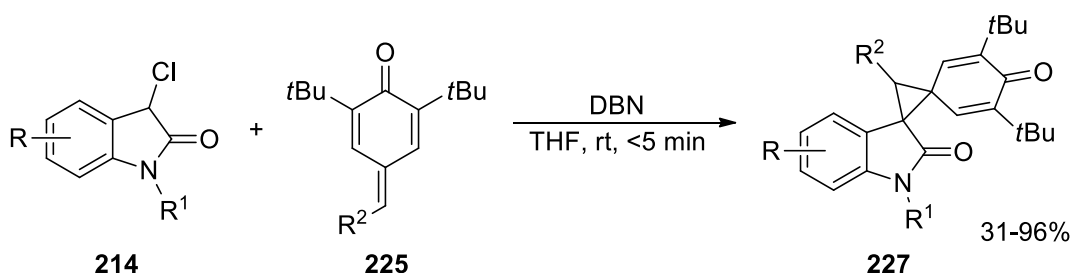


Scheme 60. Proline-derivative organocatalyzed synthesis **223**.

The procedure reported in **Scheme 61** allowed the incorporation of nucleophilic and electrophilic functionalities on 3-chlorooxindoles **214** by using a 3-alkylideneoxindole reagent **171**. In this regard, the use of the 3-halooxindole derivative combined with the presence of the chiral catalyst **VI** allowed good diastereo- and enantiocontrol over the reaction product **224**.

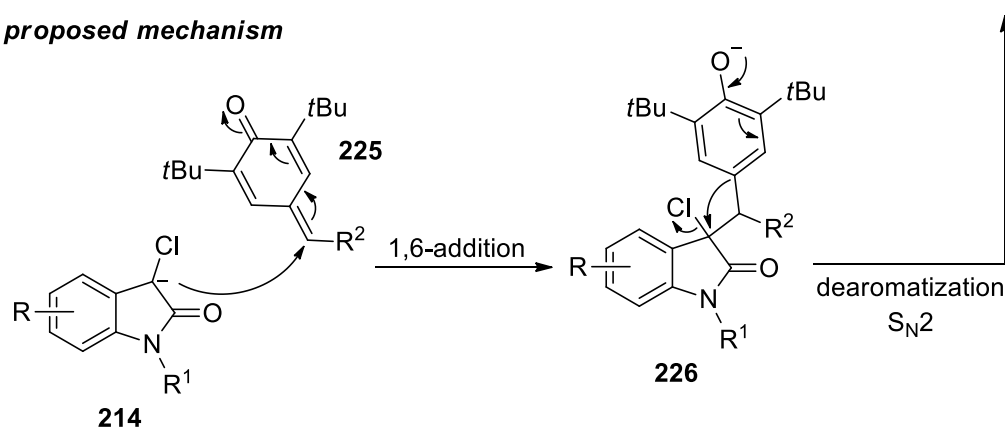


Scheme 61. Enantioselective synthesis of bis-spirooxindoles **224** from 3-chlorooxindole derivatives.



R = H, 5-Cl, 6-Cl, 5-Me, 7-Me; R¹ = H, Me, Bn; R² = 2-Me-C₆H₄, 3-Me-C₆H₄, 4-OMe-C₆H₄, 4-Me-SC₆H₄, 4-Br-C₆H₄, 3,4-Cl₂C₆H₃, 4-CF₃-C₆H₄, 2-AcO-C₆H₄, 2-OH-C₆H₄, 2-thienyl, Me, Ph

proposed mechanism

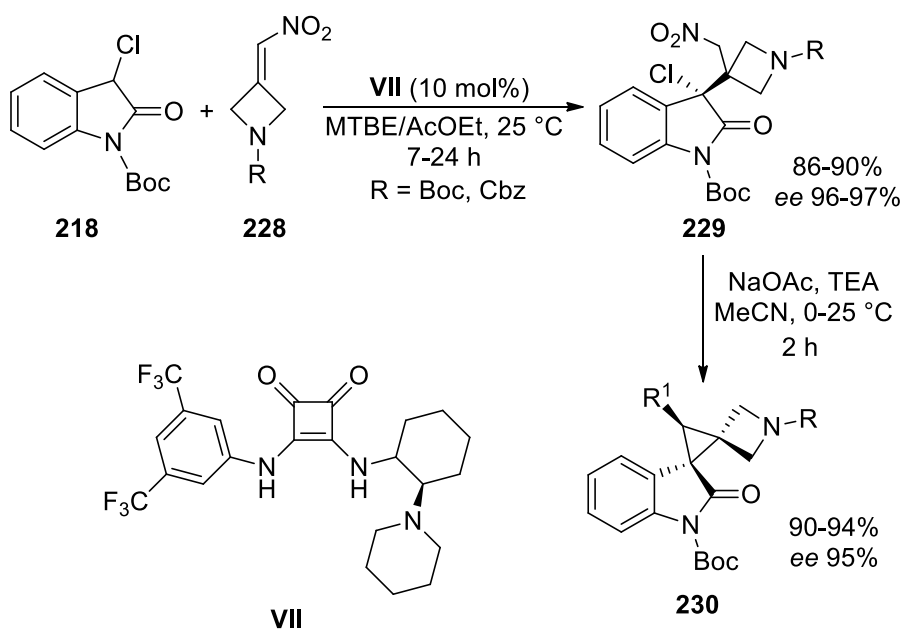


Scheme 62. Cyclopropanation of 3-chlorooxindoles **214** with *p*-quinone methides **225**.

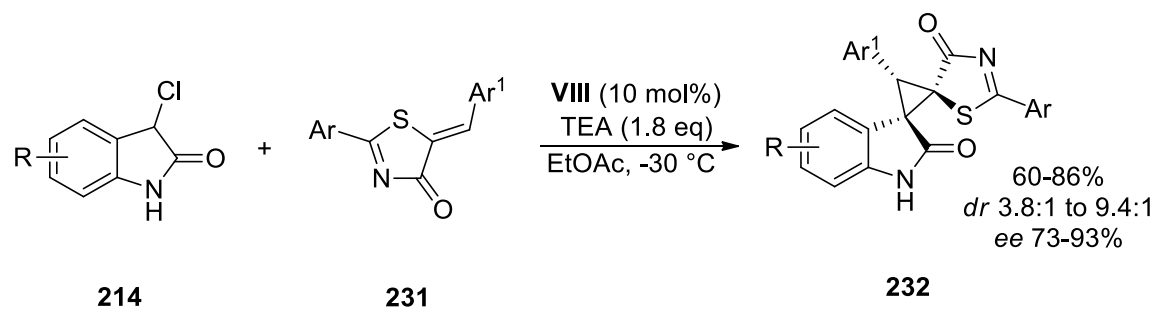
Another useful precursor for cyclopropanation from 1,6-conjugate addition resulted to be *p*-quinone methide (*p*-QMs) **225** (Scheme 62). By reacting **214** with *p*-QMs **225**, Zhao *et al.*²⁹³ developed a DBN-catalyzed approach to form cyclohexadienone-fused

spirocyclopropyl oxindoles **227**. According to the mechanism, DBN started the reaction by deprotonating **214** and forming the carbanion intermediate. The second 3,3-disubstituted oxindole intermediate **226** was formed by the 1,6-conjugate addition of the oxindole to the *p*-QM **225**, which then underwent an intramolecular nucleophilic substitution to yield the target product **227**.

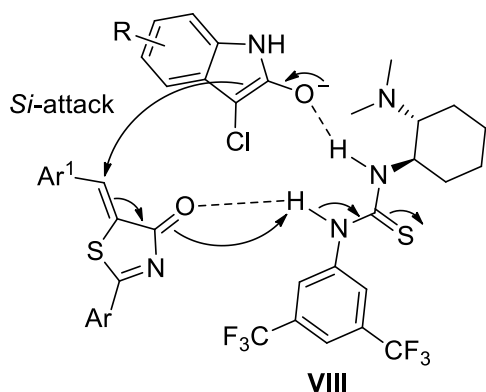
Ding and Wolf²⁹⁴ proposed the enantioselective synthesis of azetidines-functionalized spirocyclopropyl derivatives **230** catalyzed by **VII**. In this case, the halooxindole **218** reacted with azetidines **228** (**Scheme 63**) to form the desired product passing by the 3,3-disubstituted oxindole intermediate **229**.



Scheme 63. Synthesis of azetidines-functionalized spirocyclopropyl oxindoles.



proposed role of the catalyst

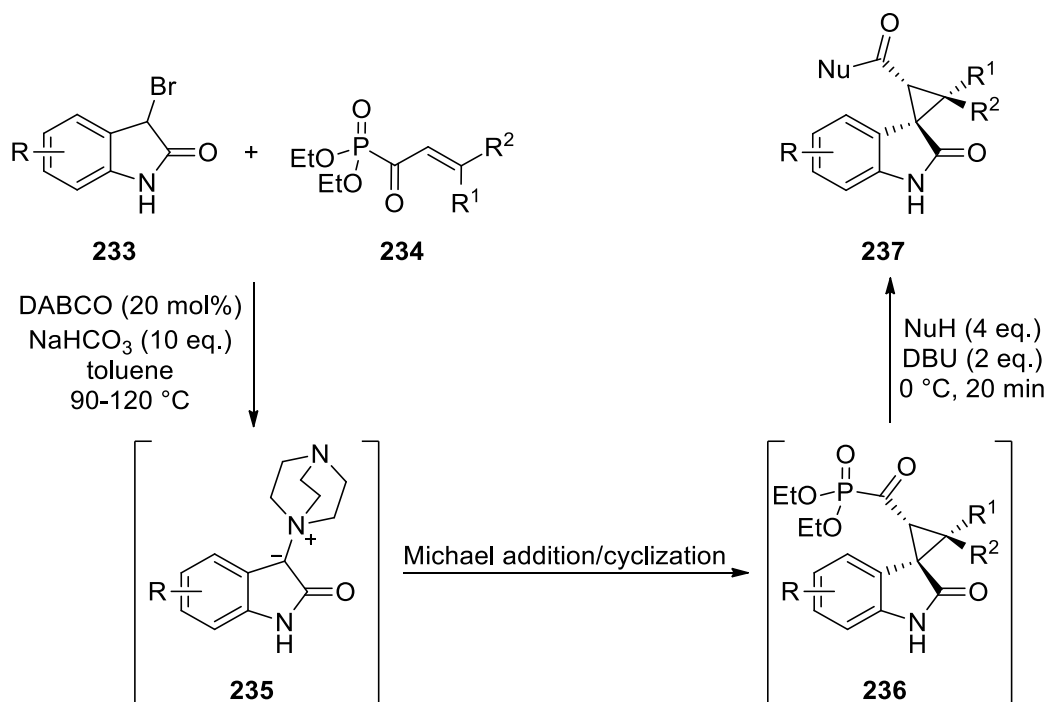


R = H, 4-F, 4-Cl, 5-F, 5-Cl,
 6-Me, 6-Cl, 6-Br; Ar = Ph,
 2-Me-C₆H₄, 4-Me-C₆H₄, 2-
 Cl/F/Br-C₆H₄, 4-MeO-
 C₆H₄; Ar¹ = Ph, 4-Me-
 C₆H₄, 4-Cl-C₆H₄

Scheme 64. Enantioselective synthesis of spiro-thiazolone cyclopropane oxindoles.

In another notable example, the Sheng group²⁹⁴ published a protocol in which spirothiazolone cyclopropane derivatives **232** were synthesized by a [2+1] Michael-alkylation reaction (**Scheme 64**). Of note, the reagents were activated by the presence of a thiourea-based catalyst (**VIII**) through a series of *H*-bond interactions.

One last example was very recently reported by Chen and co-workers (**Scheme 65**).²⁹⁵ In this example, the authors reported a Michael/alkylation cascade reaction using α,β -unsaturated acyl phosphonates **234**, and 3-bromooxindoles **233** with no need for *N*-protecting groups. In the presence of DABCO (20 mol%), the formation of intermediate **235** took place, which then reacted with **234** to give the phosphonate intermediate **236**. Hence, after the treatment with different nucleophiles (MeOH, EtOH, *i*PrOH, and BnOH), the final product was obtained. Of note, with the use of stronger nucleophiles such as benzylamine and morpholine no product was detected.

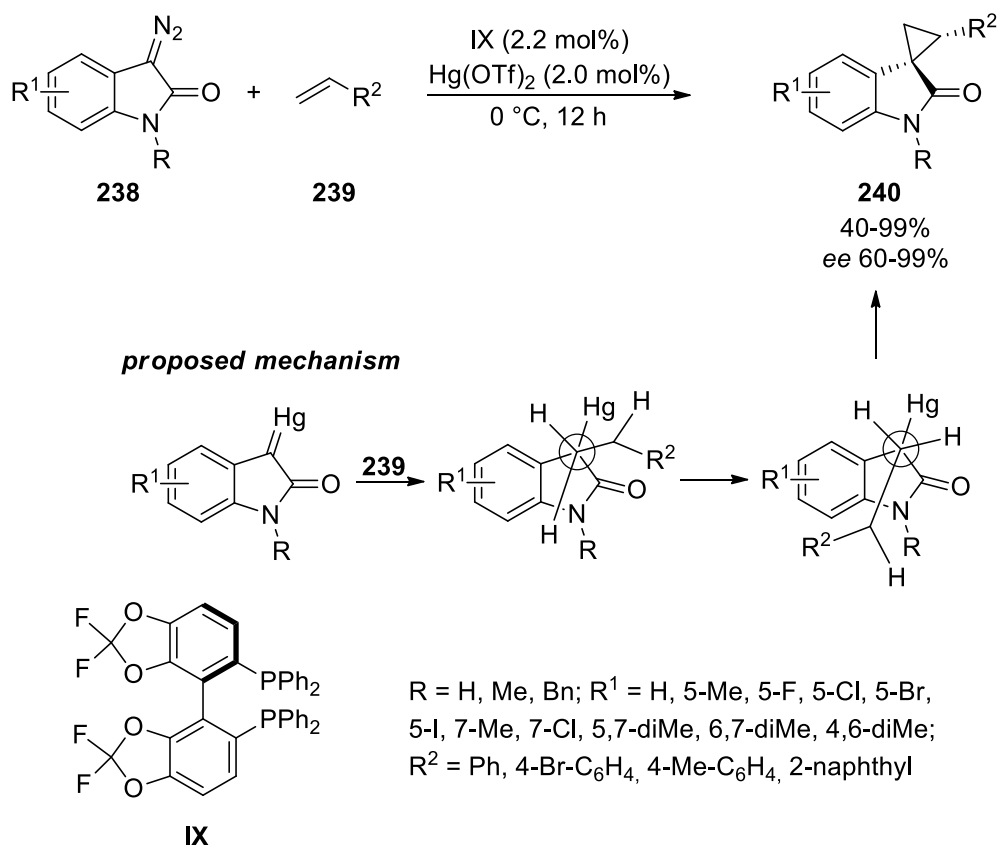


R = H, 5-F, 5-Cl, 5-Me, 5-OMe, 6-Br, 6-Cl, 6-CF₃, 6-COOMe, 7-Me, 7-F; R¹ = H, Me; R² = Me, *n*Pr, 4-CH₃-C₆H₄, 4-Br-C₆H₄, 3-OMe-C₆H₄, 2-thiophenyl; Nu = MeOH, EtOH, *i*PrOH, BnOH

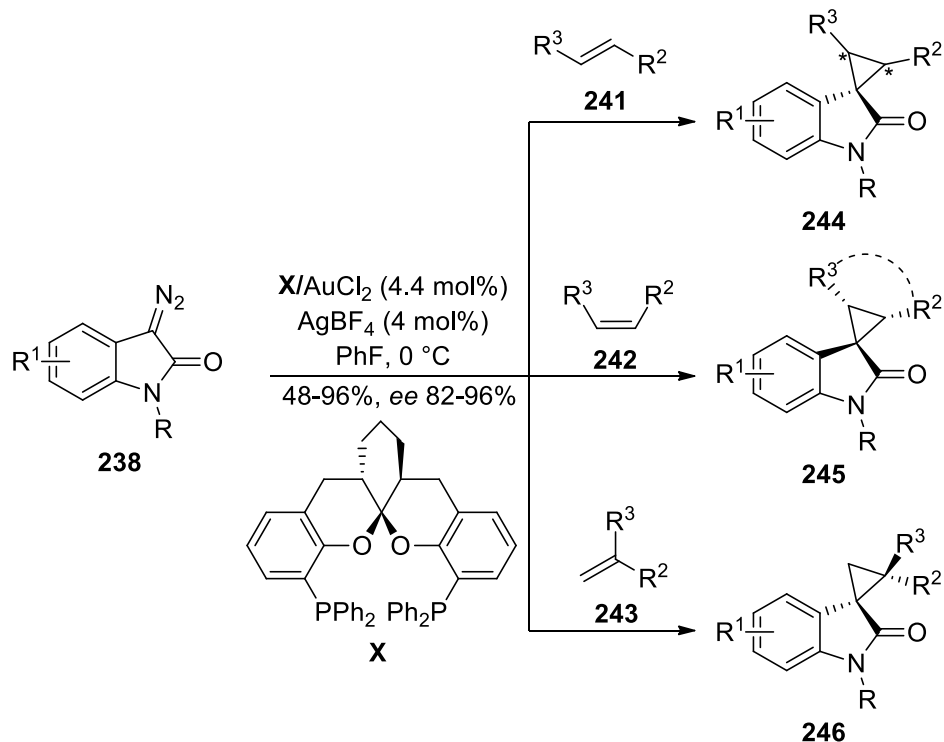
Scheme 65. Synthesis of spirocyclopropyl derivatives **237** from 3-bromooxindole **233**.

3.4 Path d – from diazooxindoles

It is also possible to form spirocyclopropyl oxindoles starting from diazooxindoles using metal-catalyzed and metal-free reactions with electron-rich or electron-poor olefins. Particularly for this latter, the use of appropriate Lewis acids is essential for the cyclopropanation step. In this context, Cao *et al.* proposed two alternative routes catalyzed by Hg(OTf)₂²⁹⁶ and PPh₃AuOTf²⁹⁷ for the stereoselective synthesis of cyclopropyl derivatives. In the first case, the reaction was performed in the presence of the catalytic system made up of (*R*)-difluorophos **IX**/Hg (II), which induced a ligand acceleration effect since in the presence of ligand **IX** the reaction rate markedly increased. On the contrary, when the reaction was carried out without **IX**, less than 7% of the product was isolated. As for the mechanism, alkene **239** approaches the Hg-activated carbenoid. In this way, the production of *trans* as the main product was obtained, due to the R² group of the alkene which favored an orientation pushed away from the metal center (**Scheme 66**).



Scheme 66. Hg-catalyzed cyclopropanation of diazooxindoles **238**.

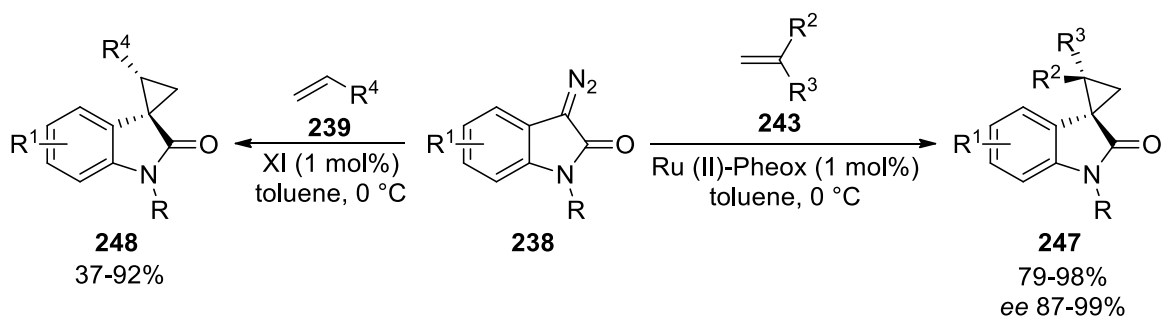


Scheme 67. Au-catalyzed cyclopropanation of diazooxindoles **238**.

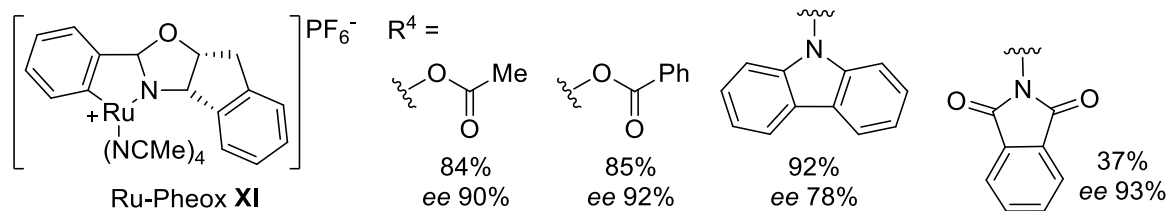
As for the other approach (**Scheme 67**), the cyclopropanation of the alkenes **241-243** was stereoselectively achieved using a spiroketal bisphosphine **X** (SKP)/Au (I)

catalytic system. Of note, *N*-protected diazo derivatives did not give any cyclopropanation reaction and the introduction of other functions on the organic moiety of the catalyst was detrimental to the stereoselectivity.

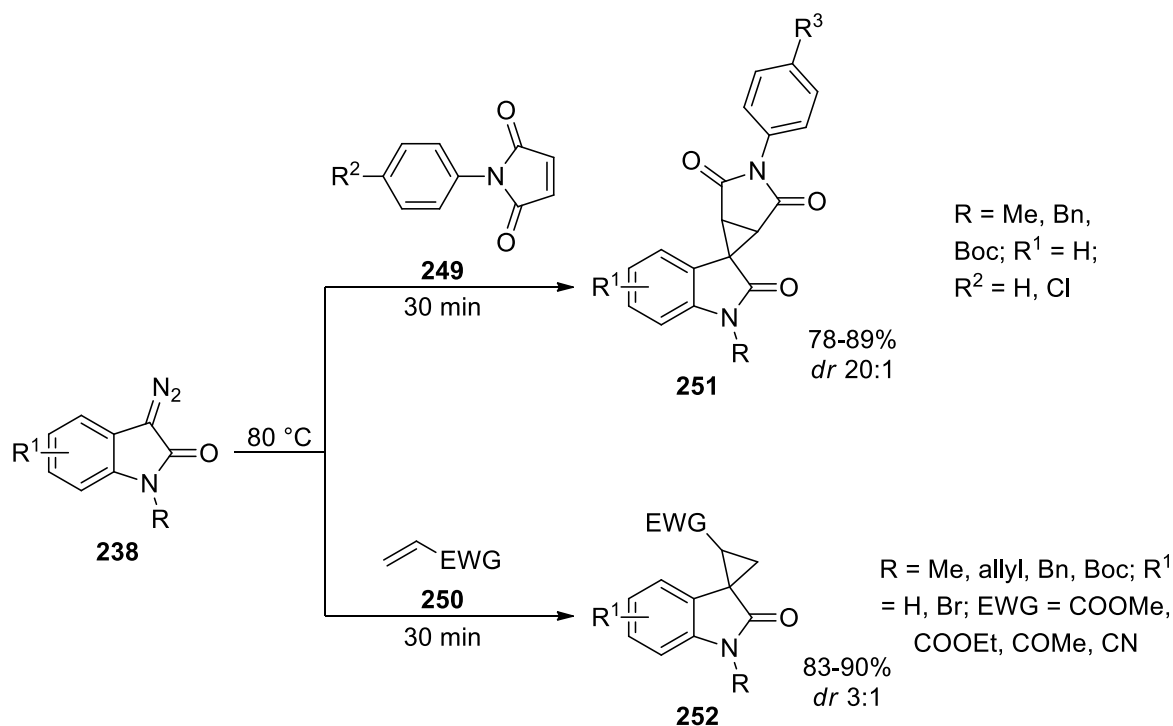
Diazooxindoles **238** were recently shown to give asymmetric spirocyclopropanation reaction with alkenes (**239**, **243**) using a Ru (II)-Pheox **XI** system (**Scheme 68**).²⁹⁸ As for the high enantioselective outcome, it is plausible to hypothesize a mechanism in which the oxindole and ligand **XI** indane ring are forced apart, hence bringing to only one side of the olefin to approach, which results in the formation of one main enantiomer.



R = H, Me, Et, *i*Pr, Bn; R¹ = H, Br, Cl, OMe; R² = H, Me; R³ = 4-Me-C₆H₄, 4-OMe-C₆H₄, 4-Cl-C₆H₄, 4-Br-C₆H₄, 4-NO₂-C₆H₄, 4-NMe₂-C₆H₄



Scheme 68. Ru (II)-Pheox-catalyzed cyclopropanation of diazooxindoles **238**.



Scheme 69. Metal-free cyclopropanation of diazooxindoles **238**.

As for the metal-free preparation of spirocyclopropyl oxindoles from diazooxindoles, Reddy *et al.*²⁹⁹ proposed a practical method for the use of electron-deficient olefins **249-250** (**Scheme 69**). The reaction proceeded *via* a [3+2]-DPCA followed by the ring contraction driven by the elimination of N_2 .

3.5 Biological activities

It is possible to recover from the literature evidence regarding the biological activity of spirocyclopropyl oxindole derivatives (**Figure 15**).

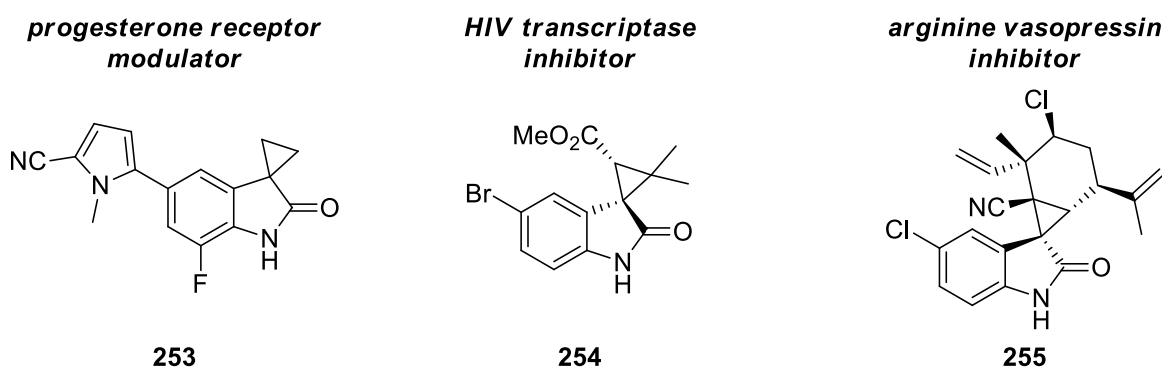


Figure 15. Biologically active spirocyclopropyl oxindole derivatives (*follows in the next page*).

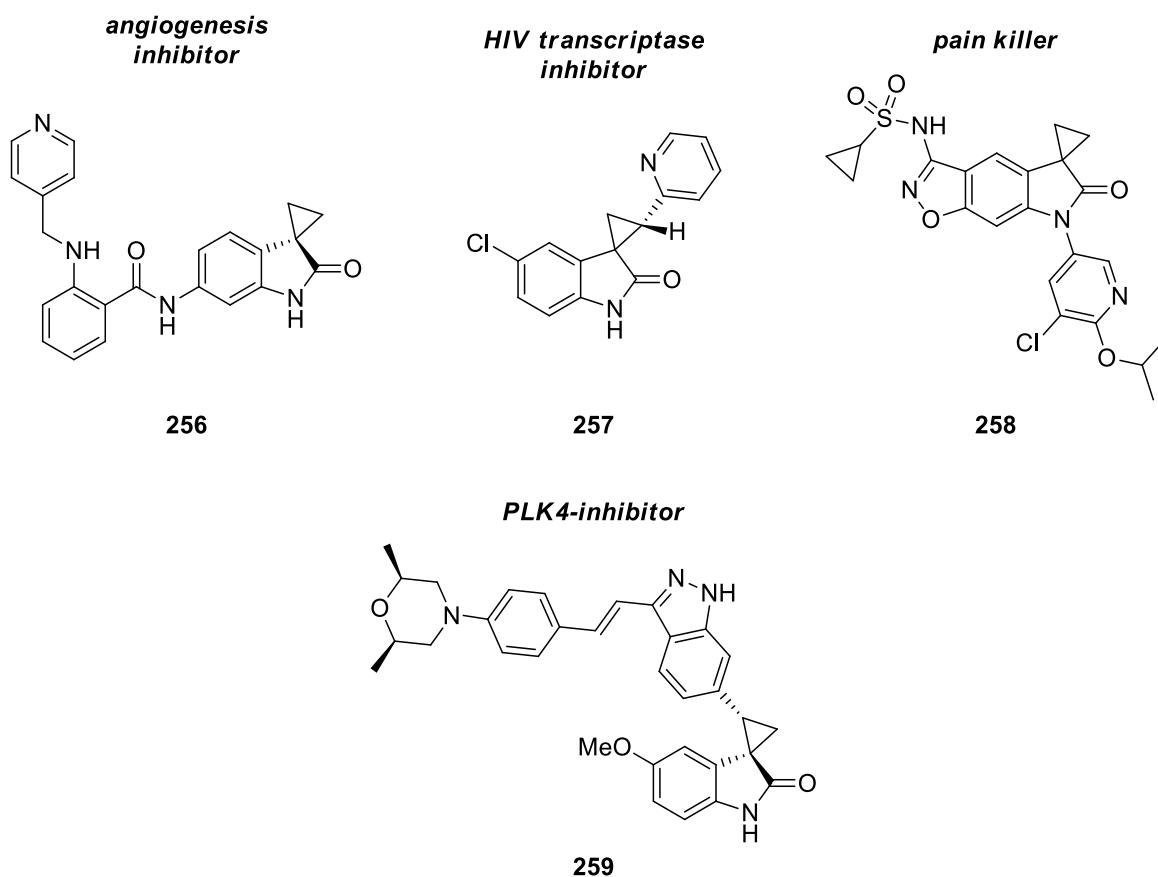


Figure 15. Biologically active spirocyclopropyl oxindole derivatives.

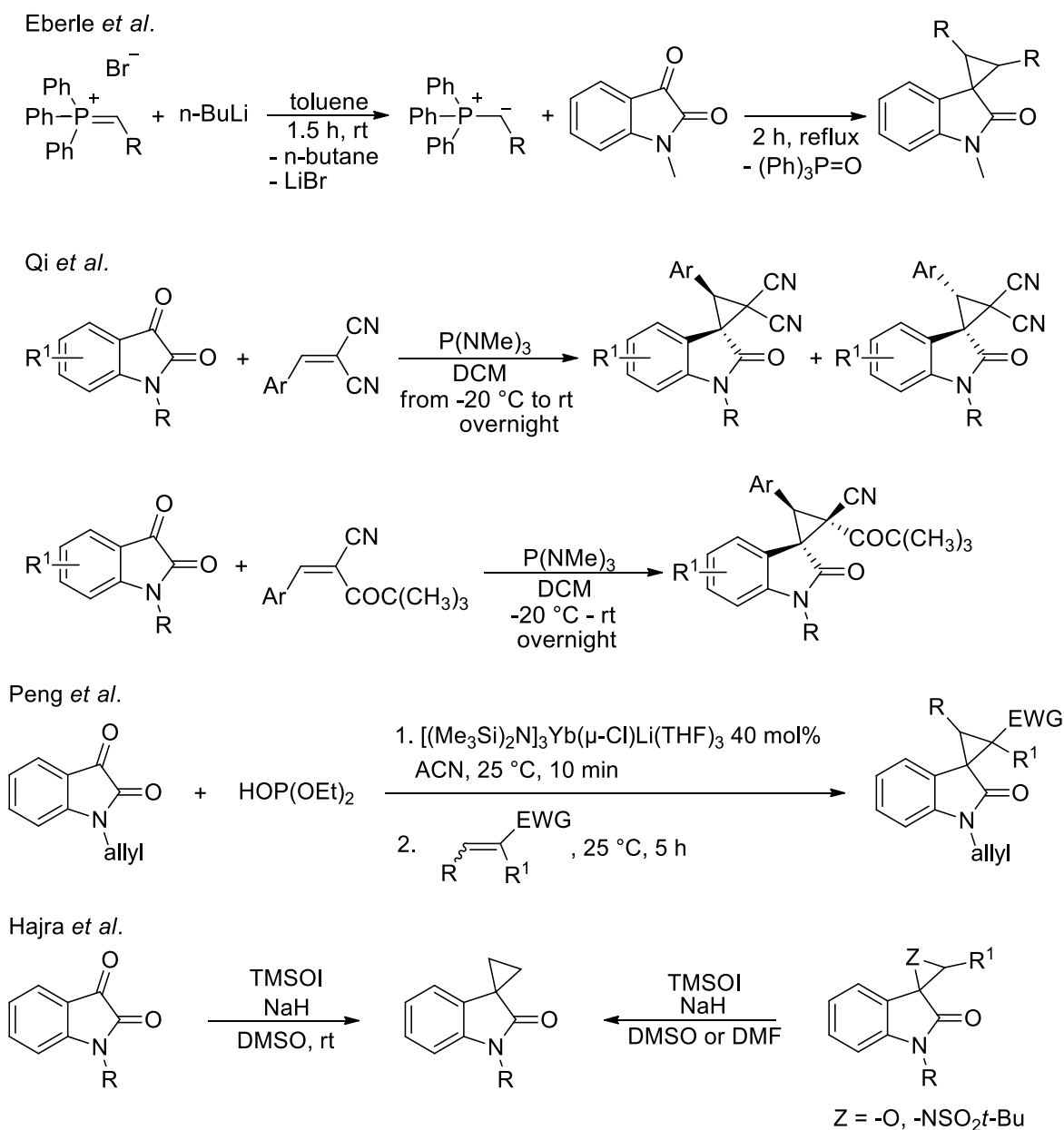
In 2006, two papers by the He group paved the way for the development of spirocyclopropyl derivatives as HIV-1 non-nucleoside reverse transcriptase (NNRT) inhibitors.^{300,301} In the first paper, *via* high-throughput screening (HTS) studies it was possible to introduce systematic structural modifications over the spirocyclopropyl skeleton, assessing the SAR for each compound synthesized. Compound **254** displayed a nanomolar potency ($EC_{50} = 15$ nM). As for the other work, similar compounds were prepared following the same approach, obtaining compound **257** which displayed an EC_{50} of 8 nM. Compound **259** was at the center of a thorough drug-design study published in 2015 by Sampson *et al.*³⁰² In this work, the authors developed a polo-like kinase 4 inhibitor, interesting for being a potential target for cancer therapy. The compound was highly effective in inhibiting its target, displaying an IC_{50} of 2.8 ± 1.4 nM.

Results and Discussion

Research line 3b - Highly diastereoselective multicomponent synthesis of spirocyclopropyl oxindoles enabled by rare-earth metal salts

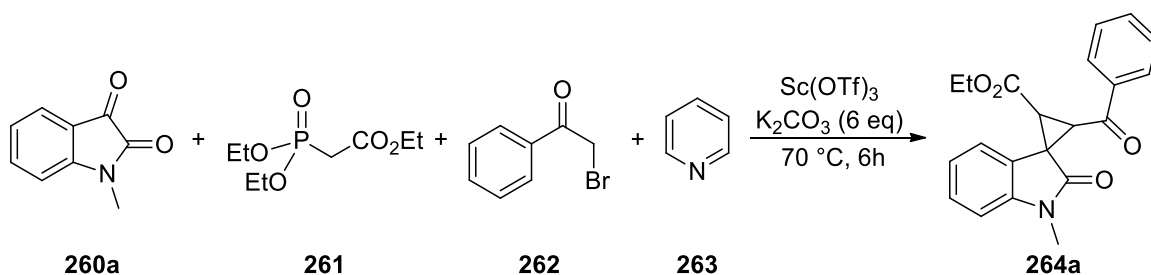
The original research work herein reported has been focused on implementing an innovative multicomponent method for the synthesis of spirocyclopropyl derivatives by using rare-earth metal (REM) triflates as Lewis acids. In this research, the use of REMs, in particular Sc(OTf)₃, gave access to the target compounds with high diastereoselectivity (up to 94:6:0:0). Such feature has been thoroughly deepened by DFT calculations during the abroad research activity of this Ph.D. thesis, in collaboration with Dr. Gonzalo Jiménez Osés of CIC bioGUNE.

We decided to follow a different path for the preparation of the target compounds with respect to those reported in the previous paragraph, starting directly from *N*-methyl isatin derivatives. In this regard, only a few examples were reported in the literature (**Scheme 70**).³⁰³⁻³⁰⁶ Another aspect regards the use of REM salts: such Lewis acid beavering species are known in the literature for their low toxicity³⁰⁷ and versatility,^{308,309} allowing their use in several recent chemical transformations.³¹⁰



Scheme 70. Known synthesis of spirocyclopropyl oxindoles from *N*-alkyl isatin derivatives.

We commenced our study by exploring the four-component reaction between *N*-methylisatin **260a**, triethylphosphonoacetate **261**, 2-bromoacetophenone **262**, and pyridine (Py) **263** in the presence of potassium carbonate (**Table 3**). The *N*-methyl protection of isatin was chosen to avoid the formation of undesired by-products under alkaline conditions.

**Table 3.** Optimization of the reaction conditions in various solvents.^a

Entry	Solvent	T (°C)	Yield (%) ^b
1	DMF	50	-
2	DMF	70	-
3	DMF <i>dry</i>	50	47
4	DMF <i>dry</i>	70	94
5	EtOH	70	-
6	EtOH <i>dry</i>	70	-
7	DCE <i>dry</i>	70	73
8	ACN	50	-
9	ACN <i>dry</i>	70	86
10	Py	70	-
11	Py <i>dry</i>	70	95

^aReaction conditions: **260** (0.1 mmol), **261** (0.1 mmol), **262** (0.25 mmol), **263** (0.35 mmol), Sc(OTf)₃ (20 mol%), solvent (2 mL), N₂ atmosphere if in dry conditions.; ^bIsolated yield.

The choice of solvents for this task was based on the polarity needed for dissolving (or partially dissolving) the inorganic load of the reaction crude. Two factors are worth noting from this screening: the use of ethanol did not lead to the formation of any product and the necessity of working under dry conditions. We hypothesized that these two clues are both related to the great oxophilicity of scandium,³¹¹ which could bring water or ethanol to saturate the metal coordinating sphere, blocking its Lewis acid capability. In fact, preliminary tests in the presence of water did not lead to any product. Polarity seemed to be a key factor in the reaction course because all the highly polar solvents gave good yields, except for ethanol as said. Similarly, temperatures lower than 70 °C dramatically reduced the yield at the same time. DMF and Py, both dry, gave the best conditions, so we decided to use the latter to simplify the experimental procedure and work-up. During the screening of the solvents, we were delighted to realize that the product was obtained with high diastereoselectivity: such

an unexpected outcome prompted us to test other REM salts (**Table 4**), maintaining the triflate as a counterion for their tendency to maintain the ion pair in organic solvents such as pyridine, preserving their non-dissociated nature.³¹²

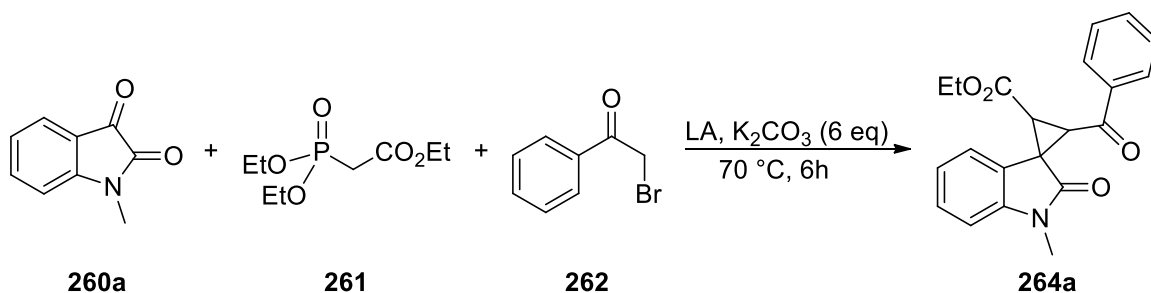


Table 4. Optimization of the reaction conditions with others REM triflates.

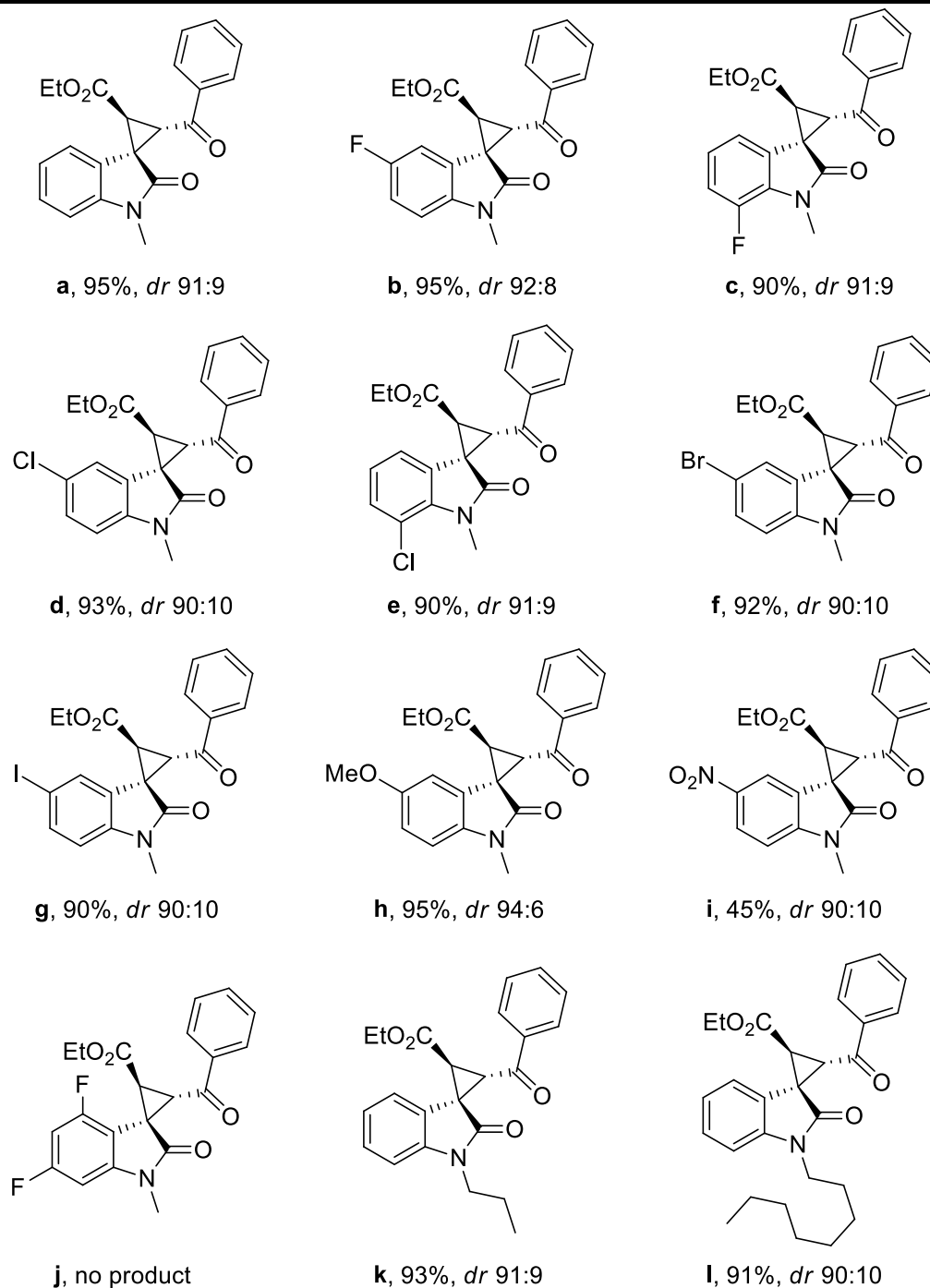
Entry	Lewis acid (LA)	<i>dr</i> ^c	Yield (%)
1 ^a	-	-	-
2 ^b	Sc(OTf) ₃	92:8:0:0	63
3	Sc(OTf) ₃	92:8:0:0	95
4	Er(OTf) ₃	89:11:0:0	88
5	Yb(OTf) ₃	90:10:0:0	90
6	Ho(OTf) ₃	88:12:0:0	81
7	Ce(OTf) ₃	90:10:0:0	79
8	La(OTf) ₃	91:9:0:0	75

^aReaction performed in the absence of a Lewis acid and under prolonged heating; ^b10 mol% Lewis acid was used; ^c*dr* was calculated by GC/MS.

As can be seen, in the absence of a Lewis acid (entry 1) no product was obtained after 24 h. The use of Sc(OTf)₃ at 10 mol% (entry 2) also was detrimental to the formation of the product in 6 h, whilst the diastereoselectivity remained excellent. Hence, doubling the amount of Lewis acid gave optimal yield and *dr*. Fittingly, other REM triflates led to similar or slightly lower yields and selectivity (entries 4-8). In all cases, the reaction is highly diastereoselective towards one isomer (*dr* = 92:8:0:0, **Table 4**, entry 3). We tentatively attributed the observed diastereoselectivity to the special coordinating capabilities of REMs in the presence of the three O-donor carbonyls present in the substrates (see computational study below).³¹³ The structural and stereochemical assignment of the obtained isomers was performed by NOESY NMR experiments. As expected, a *trans* disposition of the ester and aryl ketone substituents at the cyclopropane ring was observed for the major diastereomer in all cases. Using the optimized conditions (Sc(OTf)₃ 20%), the protocol was extended to substrates

264b-1 (Table 5), starting from commercially available isatins previously *N*-alkylated.³¹⁴

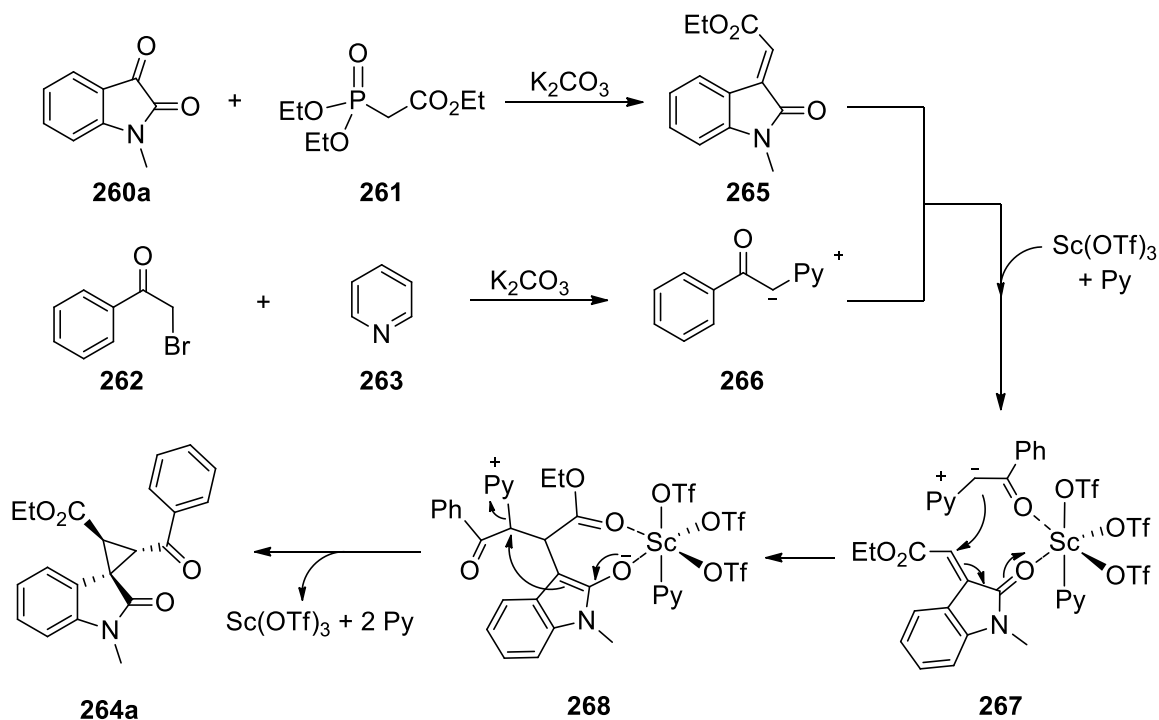
Table 5. Scope of the reaction.^{a-c}



^aReaction conditions: **260** (0.1 mmol), **261** (0.1 mmol), **262** (0.25 mmol), Sc(OTf)₃ (20 mol%), *dry* Py (2 mL), 70 °C, N₂ atmosphere. Yield refers to isolated products, and *dr* values were determined by ¹H NMR analysis of the crude reaction mixture. ^bOnly one arbitrary enantiomer of the major diastereoisomer is shown. ^cStereochemistry was determined by NOESY NMR experiments.

The influence of electron-withdrawing and electron-donating substituents at different positions of the isatin ring was investigated. As can be seen from the results summarized in **Table 5**, no significant variations in yield and stereoselectivity were observed for compounds **264b-l**; for derivative **264i** the presence of a nitro group drastically reduced the reaction yield, whilst the two fluorine atoms prevented the formation of product **264j**. Consequently, the reaction tolerates electron-donating and moderately electron-withdrawing groups at the isatin core, while highly deactivated systems are poorly or not reactive. Lastly, we synthesized compounds with *N*-alkyl chains of different lengths with the aim of tuning the lipophilicity of the final product for possible biological applications, and we were able to isolate **264k** and **264l** in similarly high yields and diastereoselectivity.

Based on the pioneering work done by Bencivenni and Bartoli on Michael-addition-initiated annulations,²⁸⁴ a plausible mechanism for the multicomponent reaction herein was proposed (**Scheme 71**). The such mechanism involves the contemporary formation of 3-alkylidene oxindole **265** through a Horner-Wadsworth-Emmons reaction between *N*-methylisatin **260a** and phosphonate **261**, and of pyridinium ylide **266** from bromoacetophenone **262** and pyridine **263** in the presence of K₂CO₃.³¹⁴ ¹H NMR experiments confirmed the formation of only the (*E*)-isomer of **265**, as expected. In agreement with the recent findings of Boyle *et al.*,³¹⁵ we hypothesized the formation of an octahedral Sc(OTf)₃Py₃ complex after the addition of Sc(OTf)₃ to the reaction mixture. Then, the intermediates **265** and **266** coordinate with the metal through their carbonyl groups by displacing two pyridine molecules and forming complex **267**, which undergoes intramolecular Michael addition. Finally, enolate **268** intramolecularly displaces the pyridinium moiety to form the cyclopropane ring in product **264a**.



Scheme 71. Proposed reaction mechanism

DFT calculations were performed to validate the proposed mechanism and shed light on the origins of the observed stereoselectivity. To this aim, the minimum energy pathways for three diastereomeric spirocyclopropyl oxindoles (**264a**: 1*R*,2*S*,3*S*; **264a**^I: 1*R*,2*R*,3*R*, and **264a**^{II}: 1*R*,2*R*,3*S*) were calculated (**Figure 16** and Experimental Section). All pathways start from the octahedral scandium complex formed by three bromides, one pyridine molecule, and intermediates **265** and **266** coordinated through their carbonyls (initial complex – **IC**). Bromide anions were used to mimic the coordinating behavior of the triflate anions at an affordable computational cost. The first calculated step was the stereoselective Michael addition of the coordinated ylide to the oxindolinylidene with relatively low activation barriers (**TS1_{RR}** and **TS1_{RS}**, $\Delta G^\ddagger = 18.1$ and 23.6 kcal mol⁻¹, respectively) leading to thermoneutral enolates (**Int1b** and **Int1c**, $\Delta G \sim 0$ kcal mol⁻¹). A slightly more stable intermediate is generated from **Int1b** by decooordination of the ketone (in green) and coordination of the ester (in purple) groups (**Int1a**, $\Delta G = -4.5$ kcal mol⁻¹).

The subsequent diastereoselective ring-closing step takes place from enolates **Int1a-c**, where atom *C1* undergoes a nucleophilic attack to atom *C3* with the simultaneous displacement of pyridine (**TS2a-c**). Importantly, for this reaction to take place the pyridinium leaving group and the nucleophilic enolate must be in antiperiplanar conformation. These two reacting groups are in the right orientation in intermediates

Int1a and **Int1b**, thus being able to undergo substitution directly with affordable intrinsic activation barriers (**TS2a** and **TS2b**, $\Delta G^\ddagger = 28.9$ and 24.4 kcal mol⁻¹, respectively) to give *trans*-cyclopropane complexes **Int2a** and **Int2b**. Decoordination from scandium leads to the thermodynamically stable and experimentally observed products **264a** (*1R,2S,3S*) and **264a^I** (*1R,2R,3R*), respectively. On the contrary, **Int1c** cannot undergo the substitution directly, and a carbonyl group exchange implying a very unfavorable decoordination of the enolate (in blue) (**Int1c'**, $\Delta G \sim 30$ kcal mol⁻¹) must take place before nucleophilic substitution, which as a consequence has a prohibitively high activation barrier (**TS2c**, $\Delta G^\ddagger \sim 45$ kcal mol⁻¹) to give the *cis*-cyclopropane complex **Int2c**; this very unfavorable calculated pathway explains why product **264a^{II}** (*1R,2R,3S*), which is also less thermodynamically stable than both *trans* isomers, is not experimentally obtained. No reaction pathway towards stereoisomer **264a^{III}** (*1R,2S,3R*) – also experimentally unobserved – was calculated. The formation of this stereoisomer would require the simultaneous coordination of the three carbonyl groups (i.e., isatin enolate, aryl ketone, and ester) to the metal center, which in turn would require olefin to have (*Z*) configuration. Considering that olefin **265** is formed exclusively as an (*E*) isomer under our reaction conditions, the formation of compound **264a^{III}** was excluded from our calculations.

The lower activation energy of **TS2b**, which is rate-determining and ultimately responsible for the high diastereoselectivity experimentally observed under kinetic conditions, can be attributed to the higher electrophilicity of C3 upon coordination of the phenyl ketone. Hence, the metal center exerts a templating effect by coordinating the reacting fragments in a productive and energetically favored orientation, increasing both reactivity and stereoselectivity in the key ring-closing step.

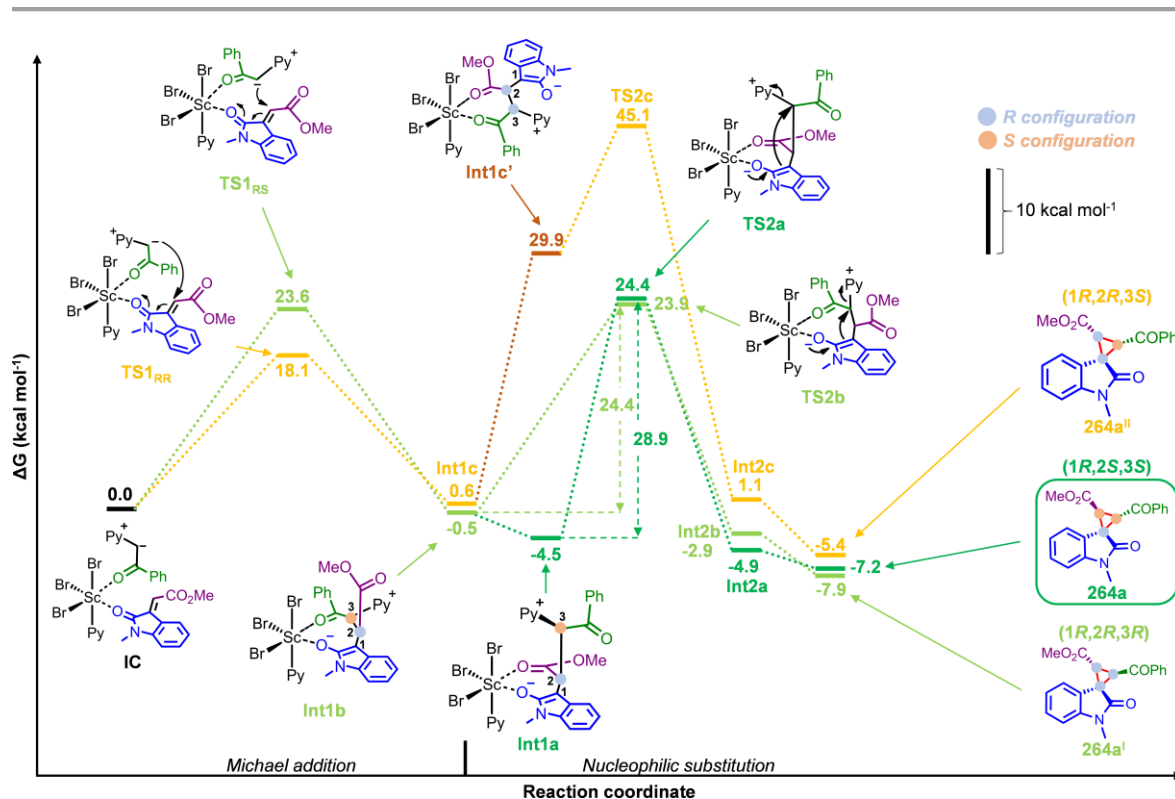


Figure 16. Minimum energy reaction pathway calculated with PCMPyridine/ ω B97X-D/6-31G(d,p) and LanL2DZ effective core potential for Sc and Br atoms. The chemical structure of relevant stationary points is depicted.

In summary, REM triflate salts, particularly scandium triflate, allowed the development of a new, simple route for the multicomponent synthesis of disubstituted spirocyclopropyl oxindole derivatives from isatins in excellent yields and very high diastereoselectivity. DFT calculations support the proposed reaction mechanism and provide an explanation for such selectivity. Of note, the presence of an ester group at the cyclopropyl moiety can be useful for further late-stage transformations. This newly developed protocol is proposed as a valuable entry to diastereopure spirooxindolic compounds with biological potential.

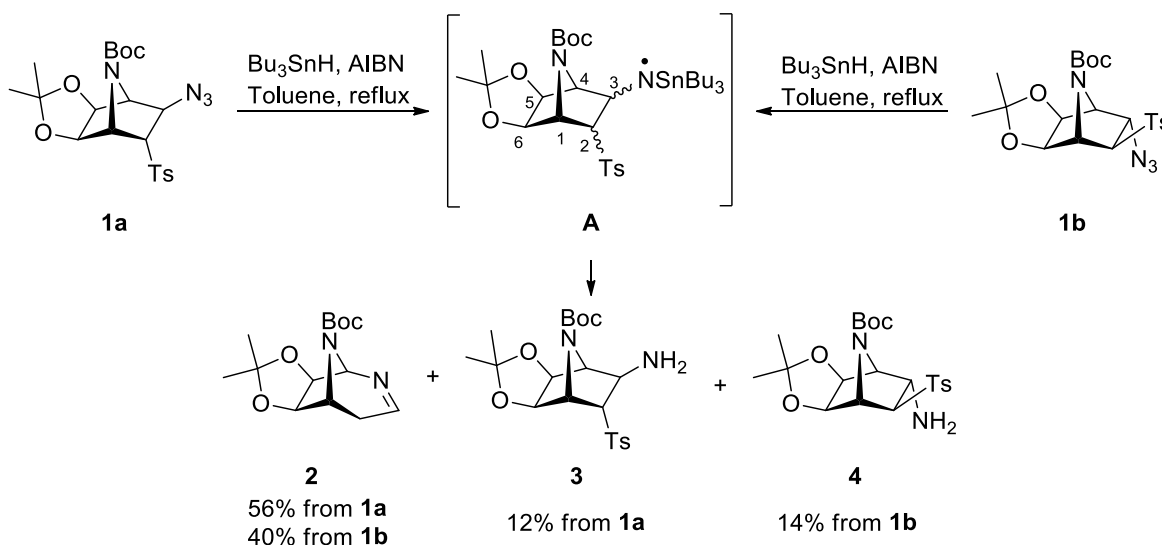
Chapter 4

Quantum mechanical studies on expansion reactions of norbornane derivatives

Studies on the regioselective rearrangement of azanorbornanic aminyl radicals into 2,8-diazabicyclo[3.2.1]oct-2-ene systems

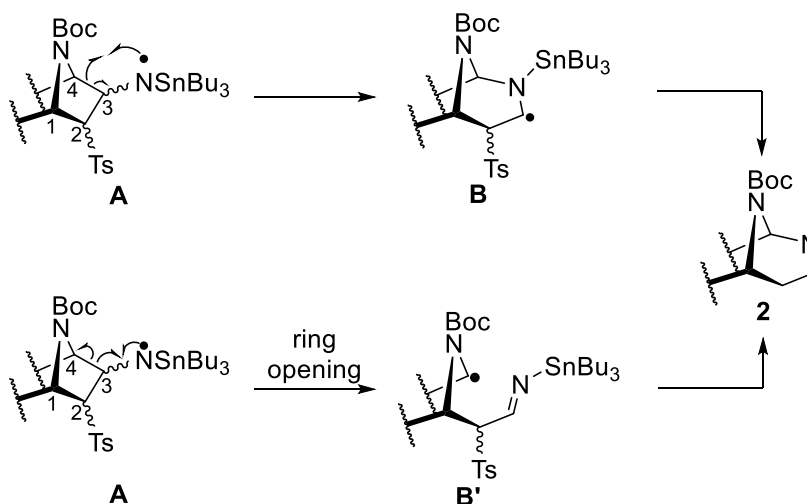
Due to their high reactivity, amino radicals are nitrogen-centered radicals of high interest for synthetic methods involving the formation of C-N bonds. In the presence of catalytic azobisisobutyronitrile (AIBN), an organic azide reacts with tributyltin hydride (Bu_3SnH) to produce the desired intermediate radicals. In this chapter, we describe how azanorbornanic ([2.2.1]azabicyclic) aminyl radicals can be regioselectively rearranged to form 2,8-diazabicyclo[3.2.1]oct-2-ene systems. In particular, we investigated how different bridgehead atoms in the [2.2.1]bicyclic system and the presence of an alkyl substituent at C4 affect the structural requirements for this ring expansion. To assess the impact of the bicyclic skeleton on the rearrangement attempts to conduct this ring expansion on a monocyclic analog were also investigated. The experimental investigation of this chapter was performed by the Moreno-Vargas group at the University of Sevilla, whilst the computational investigation was conducted in the group of Dr. Gonzalo Jiménez Osés at the CIC bioGUNE of Bilbao. This chapter was published in the Journal of Organic Chemistry in 2022 (see **Annex II** for the details).

Natural and synthetic organic substances relevant to biology frequently contain nitrogen.³¹⁶⁻³¹⁸ Therefore, a very active area of research is the development of novel synthetic techniques and approaches for C-N bond synthesis. Due to their high reactivity, aminyl nitrogen-centered radicals that can be produced from organic azides are considered useful intermediates to produce C-N bonds.^{319,320} However, aminyl radicals received way less attention than the commonly employed carbon-centered radicals. Kim and co-workers showed that the homolytic addition of stannyl radicals to aromatic/aliphatic azides with simultaneous loss of N₂ is an excellent method for producing aminyl radicals.³²¹ In this case, tributyltin hydride (Bu₃SnH) and catalytic azobisisobutyronitrile (AIBN) in refluxing benzene were used as reagents. In a previous paper, the Moreno-Vargas group reported that when trying to desulfonylate [2.2.1]azabicyclic-azido sulfones (3-azidoazanorbornanes) **1a** and **1b** in a radical fashion, the expansion of the ring bicyclic system **2** was predominant (**Scheme 1**).³²² This formation of the 2,8-diazabicyclo[3.2.1]oct-2-ene system was hypothesized to take place *via* the intermediate azanorbornan-3-aminyl radical radical **A**. Primary amines **3** or **4**, by-products of the radical reduction of the azide group, were also obtained in reduced amounts together with major compound **2**. It is also known that in the presence of Bu₃SnH/AIBN the competitive radical reduction of aliphatic azides to amines proceeds *via* an intermediate aminyl radical, which is further reduced in the presence of an excess of Bu₃SnH.³²³⁻³²⁶ Even though 3-*endo*-azido **1a** was significantly more prone than **1b** to undergo the radical expansion (56% from **1a** vs 40% from **1b**), both stereoisomers **1a** and **1b** behaved equally in these cases.



Scheme 1. Aminyl radical-initiated ring expansion of [2.2.1]azabicyclic-azido sulfones.

The initially proposed mechanism regarded a regioselective 1,2-shift of the bicyclic aminyl radical **A**'s (C3-C4) bond to generate the expanded radical intermediate **B**, which evolves in the final compound **2** (**Scheme 2**).³²² Spagnolo and collaborators suggested that a ring-opening/ring-closure sequence through intermediate **B'** should be more likely implicated because radical 1,2-shifts of alkyl carbons were essentially unknown.³²⁰ A thorough mechanistic has not been reported yet.



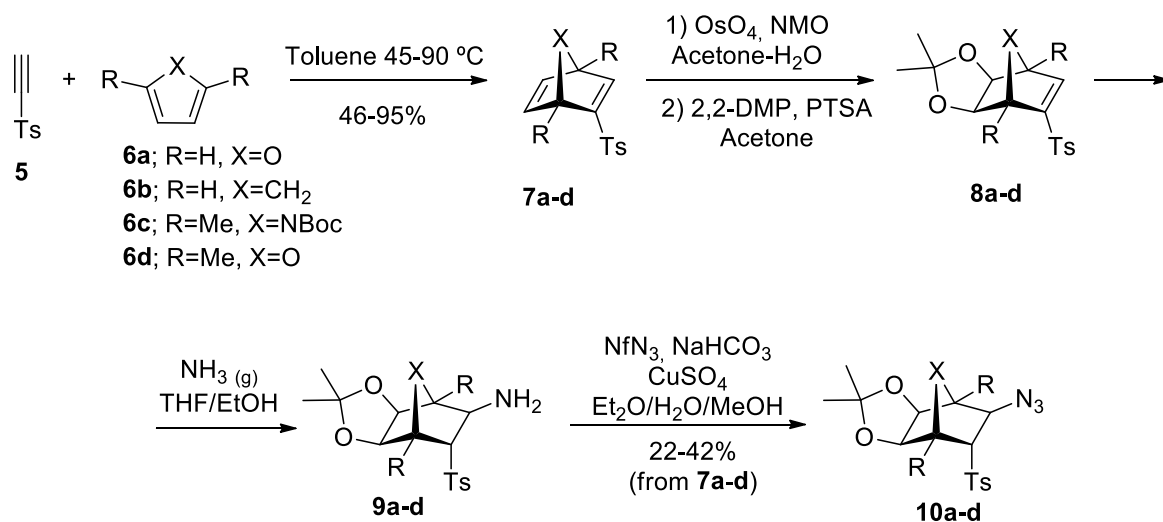
Scheme 2. Proposed radical intermediate structures **B** and **B'**.

The synthesis of 2,8-diheterobicyclo[3.2.1]octanes from readily accessible heteronorborene systems as starting materials could be easily accessed by such a radical ring expansion. 2,8-diheterobicyclo[3.2.1]octanes are interesting building blocks in the synthesis of organic compounds and can be found in the skeleton of a large variety of biologically active natural products,³²⁷ which justifies our interest in finding new strategies of radical expansion. In this case, our purpose was to assess the role of different bridgehead groups and how the presence of an alkyl substituent at C4 conditioned the ring expansion reaction. Moreover, the radical reaction on a monocyclic counterpart was also investigated and a thorough computationally supported reaction mechanism has been proposed.

Results and discussion

Experimental studies

In this work, we synthesized several 3-azido(hetero)norbornane analogs of 3-*endo*-azidoazanorbornane **1a** (compounds **10a-d**) through a more efficient strategy than the one already reported in the literature (**Scheme 3**).³²⁸ Such a new approach only produces *exo*-azido derivatives, which are slightly more susceptible to aminyl radical rearrangement than their *endo*-analog counterparts. Thus, at various temperatures (25-90 °C), Diels-Alder reactions between ethynyl sulfone **5** and readily obtainable or commercially accessible cyclic dienes **6a-d** were carried out. Due to the poor dienic character of pyrrole, the reaction of **5** with pyrrole derivative **6c** was carried out at higher temperatures than those with furan derivatives (**6a** and **6d**) and cyclopentadiene **6b**. All the bicyclic systems (compounds **7a-d**) were isolated as racemic mixtures with a moderate-to-good yield. Similarly to other [2.2.1]heterobicyclic systems,³²⁹⁻³³¹ the selective dihydroxylation of the electron-rich double bond of the bicyclic adducts **7a-d** gave the corresponding diols with total *exo*-face stereoselectivity. Instead of isolating the resultant diols, 2,2-dimethoxypropane (DMP) was added directly to the crudes in the presence of a catalytic amount of acid to form the protected diol derivatives **8a-d**. Of note, attempts to add the azide anion to the vinyl sulfone system (NaN₃ in DMF or TMSN₃ in THF) failed. As a result, we addressed the inclusion of the azide function using a non-direct approach that necessitated the formation of an intermediary amino derivative. The related [2.2.1]bicyclic-amino sulfones **9a-d** were produced by the efficient and *exo*-stereoselective conjugate addition of ammonia to vinyl sulfones **8a-d**. Under mild conditions, these compounds were directly employed in a diazo transfer reaction with nonaflyl azide (NfN₃)³³² to give [2.2.1]bicyclic-azido sulfones **10a-d** with an overall yield comprised between 22% and 42%. (from **7a-d**, 4 steps).



Scheme 3. Synthesis of new [2.2.1]bicyclic β -azido sulfones.

Then, we conducted the radical reaction in the presence of $\text{Bu}_3\text{SnH/AIBN}$ using the so-prepared substrates, in the identical reaction conditions as for **1a**. **Table 1** provides a summary of the optimization process. Only the non-expanded amino derivatives **9a** and **9b** were produced when NBoc in **1a** was substituted by O or CH_2 (compounds **10a** and **10b**) due to the negative impact over the ring expansion step. According to these findings, it is possible to state that O or CH_2 at the bridgehead position of the bicyclic system, unlike NBoc, does not stabilize the adjacent radical on C4 of the corresponding **B'** intermediate (**Scheme 2**). The strength of such stabilization is inversely proportional to the electronegativity of the heteroatom,³³³ however, atoms with available lone pairs can form stabilizing interactions with radical centers (two-center three-electron interaction). This may help to explain why the radical rearrangement does not occur in the norbornane derivative **10a** and the oxanorbornane derivative **10b**, which both have strongly electronegative oxygen at the bridgehead location. The NBoc stabilizing influence on the adjacent radical can explain the observed chemoselectivity.

The yield of the resulting 2,8-diazabicyclo[3.2.1]oct-2-ene system was higher after the radical reaction on azabicyclo **10c**, which has an extra methyl group at C4 compared to azabicyclo **1a** (82% **11c** vs. 56% **2**) that clearly favored the radical ring expansion. The radical rearrangement significantly benefited from a CH_3 substituent at C4 of **10c** because the new C4 turns into a tertiary radical on the equivalent intermediate **B'**. In the case of the oxa-analog **10d**, where the radical rearrangement did not occur and only amine **9d** was produced, this further stabilization revealed insufficient. It is worth

noting that the desulfonylation process did not occur in the reduced [2.2.1]bicyclic amines (compounds **2** and **11c**) but only in the extended [3.2.1]bicyclic systems (**3**, **9a**, **9b**, and **9d**). In this case, an NMR signal corresponding to imine-type proton H3, appeared at 7.66 ppm in the ^1H NMR spectrum, confirming the structure of ring-expanded compound **11c**. Additionally, the ^{13}C NMR spectra showed signals at 162.3 ppm (C3) and 39.3 ppm (C4, linked to two nearby protons in DEPT).

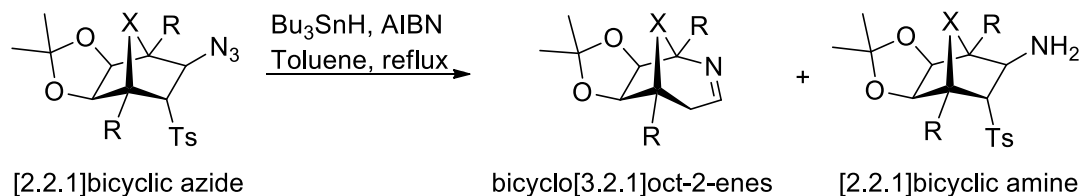
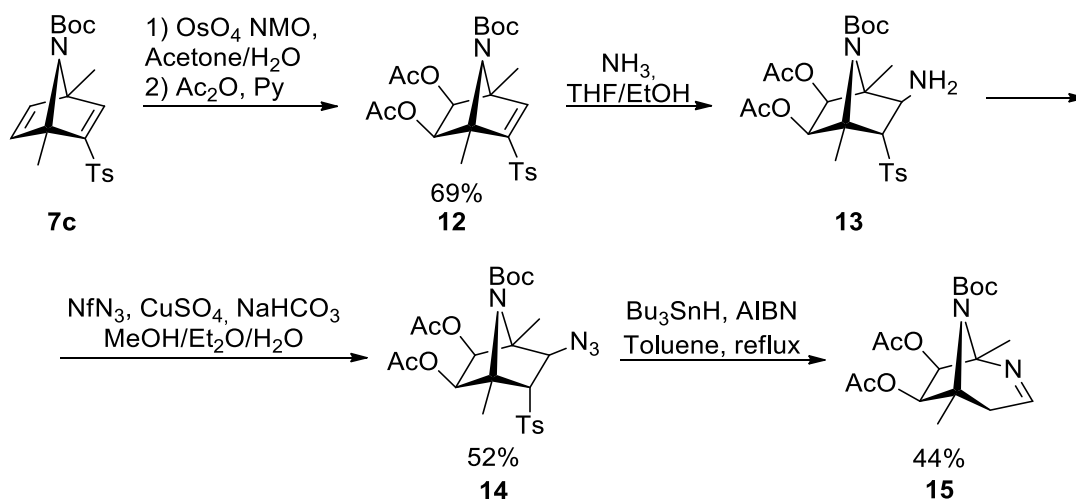


Table 1. Results of the radical ring expansion assays.

Entry	[2.2.1]bicyclic azide	Bicyclo[3.2.1]oct-2-ene ^a	[2.2.1]bicyclic amine ^a
1 ^b	1a (R = H, X = NBoc)	2 , 56%	3 , 12%
2 ^b	10a (R = H, X = O)	-	9a , 90%
3	10b (R = H, X = CH ₂)	-	9b , 74%
4	10c (R = Me, X = NBoc)	11c , 82%	-
5	1a (R = H, X = NBoc)	-	9d , 64%

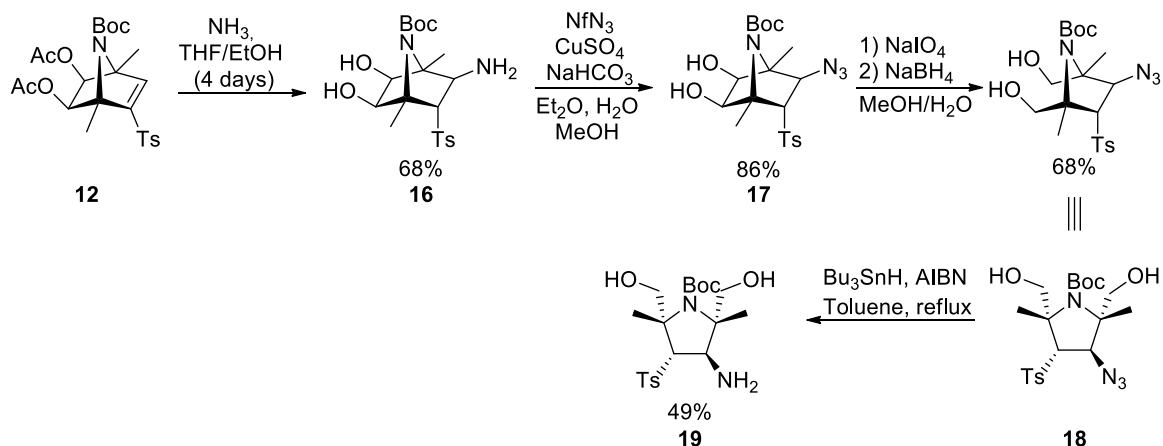
^aYield (%) of the isolated compounds; ^bData from ref. 321; "-" stands for not detected.

Hence, we chose to test the reaction on the diacetylated derivative **14** to better understand how the dioxolane fused cycle affects the radical expansion of the azabicyclic derivatives **1** and **10c** (Scheme 4). Hence, **7c** was dehydroxylated, and the resulting diol was acetylated to form **12**. Following the diazo transfer process and conjugate addition of ammonia, azide **14** was obtained with an acceptable yield. Under standard conditions, treatment of **14** with Bu₃SnH/AIBN gave a mixture of compounds, of which the expanded product 2,8-diazabicyclo[3.2.1]oct-2-ene **15** was separated in 44% yield. This finding suggested that 3-azidoazanorborene **14**, which is less strained, is less susceptible to radical ring expansion than acetonide derivative **10c**. This result may be explained by the additional strain that the acetonide group adds to the azabicyclic system as well as a steric hindrance between NBoc and the isopropylidene group.



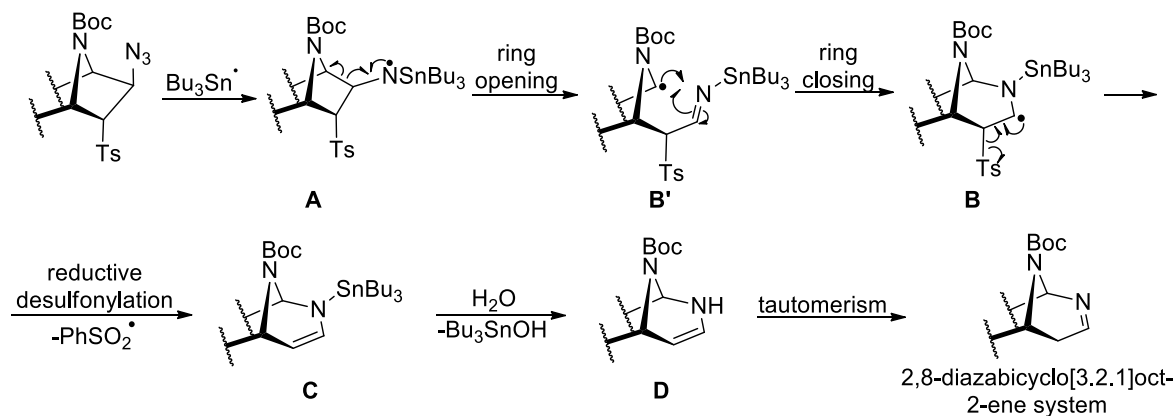
Scheme 4. Synthesis and radical ring expansion of 3-azidoazanorborene **14**.

To completely suppress the influence of the bicyclic skeleton on the reaction, we chose to attempt the radical expansion in pyrrolidine derivative **18** (Scheme 5), a monocyclic analog of the bicyclic compound **14**. As a result, when **12** was treated for 4 days with an excess of ammonia in THF/EtOH, the conjugate addition of NH_3 and concurrent ethanolysis of the ester groups was obtained. Under standard conditions, the resultant bicyclic amino-diol **16** was converted into the azido derivative **17**. The *N*-Boc pyrrolidine derivative **18** was formed in good yield by the oxidative cleavage of diol **17** with NaIO_4 and the subsequent reduction of the resultant aldehydes with NaBH_4 . As a consequence of a $\text{Bu}_3\text{SnH}/\text{AIBN}$ treatment, this compound gave a complex mixture in which no product of the ring radical expansion could be observed. Instead, the main product of the radical reduction of the azide function, amine **19**, was separated with a 49% yield. This finding showed that the *C3-C4* bond cleavage on the corresponding aminyl radical intermediate **A** (Scheme 2) is clearly favored by the rigid [2.2.1]azabicyclic skeleton, whilst the radical reduction of the azide function is the only reaction obtainable for azides embedded in the more conformationally flexible pyrrolidine skeleton (compound **18**).



Scheme 5. Attempt to expand the 3-azidopyrrolidine ring system **18**.

On the basis of this evidence, we propose a mechanism for the ring expansion/desulfonylation sequence leading to 2,8-diazabicyclo[3.2.1]oct-2-ene compounds (**Scheme 6**). The intermediate aminyl radical **A** might undergo a regioselective ring opening that would produce the expanded system **B** once the ring was closed on the carbon-centered radical **B'**. Stannyl enamine **C** might be produced through a desulfonylation reaction, comparable to that reported for allylic sulfones under $\text{Bu}_3\text{SnH/AIBN}$ conditions, which would lead to the formation of the 2,8-diazabicyclo[3.2.1]oct-2-ene system following hydrolysis and tautomerism.



Scheme 6. Mechanism proposed for the radical ring expansion/desulfonylation of [2.2.1]azabicyclic β -azido sulfones.

Computational studies

The mechanism of the ring expansion for the formation of [3.2.1]bicyclic systems (**2**, **11a-d**) was computationally examined. The calculated mechanism starts from norbornan-3-aminy radical intermediates (**Int1**) and analyzes a plausible competition between a stepwise ring expansion, to afford compounds **2** and **11a-d**, and a radical reduction, i. e. hydrogen atom transfer (HAT),³³⁴ to give amines **3** and **9a-d** (**Figure 1a** and Experimental Section **D1-D4**). Abbreviated models were used in all cases by replacing the tosyl and tri-*n*-butylstannane groups with mesyl and trimethylstannane groups, respectively. Methoxycarbamate (Moc) was also employed instead of the Boc group as a simpler model for the protecting group of azanorbornanes **1a** and **10c**. Starting from *N*-centered norbornan-3-aminy radical intermediates (**Int1**) formed upon reaction with Bu₃SnH/AIBN, the first step for the ring expansion reaction is the ring-opening by homolytic cleavage of the C3-C4 bond (**TS1**, see **Scheme 2** for atom labeling) with activation barriers (ΔG^\ddagger) ranging from 12 to 19 kcal mol⁻¹. The subsequent ring-closing step takes place from the carbon-centered radical (**Int2**) to form a bond between C3 and the exocyclic nitrogen (**TS2**). This step was calculated to be rate-limiting for all considered substrates with activation energies (ΔG^\ddagger) ranging from 17 and 22 kcal mol⁻¹. Of note, the formation of bicyclic carbon-centered radical **Int3** upon ring expansion is significantly exergonic with free energies (ΔG) between -12 and -15 kcal mol⁻¹. A final desulfonylation step through a radical elimination reaction from **Int3** was calculated to have very low activation barriers ($\Delta G^\ddagger \approx 2-5$ kcal mol⁻¹) as a result of the stability of the leaving sulfonyl radical.

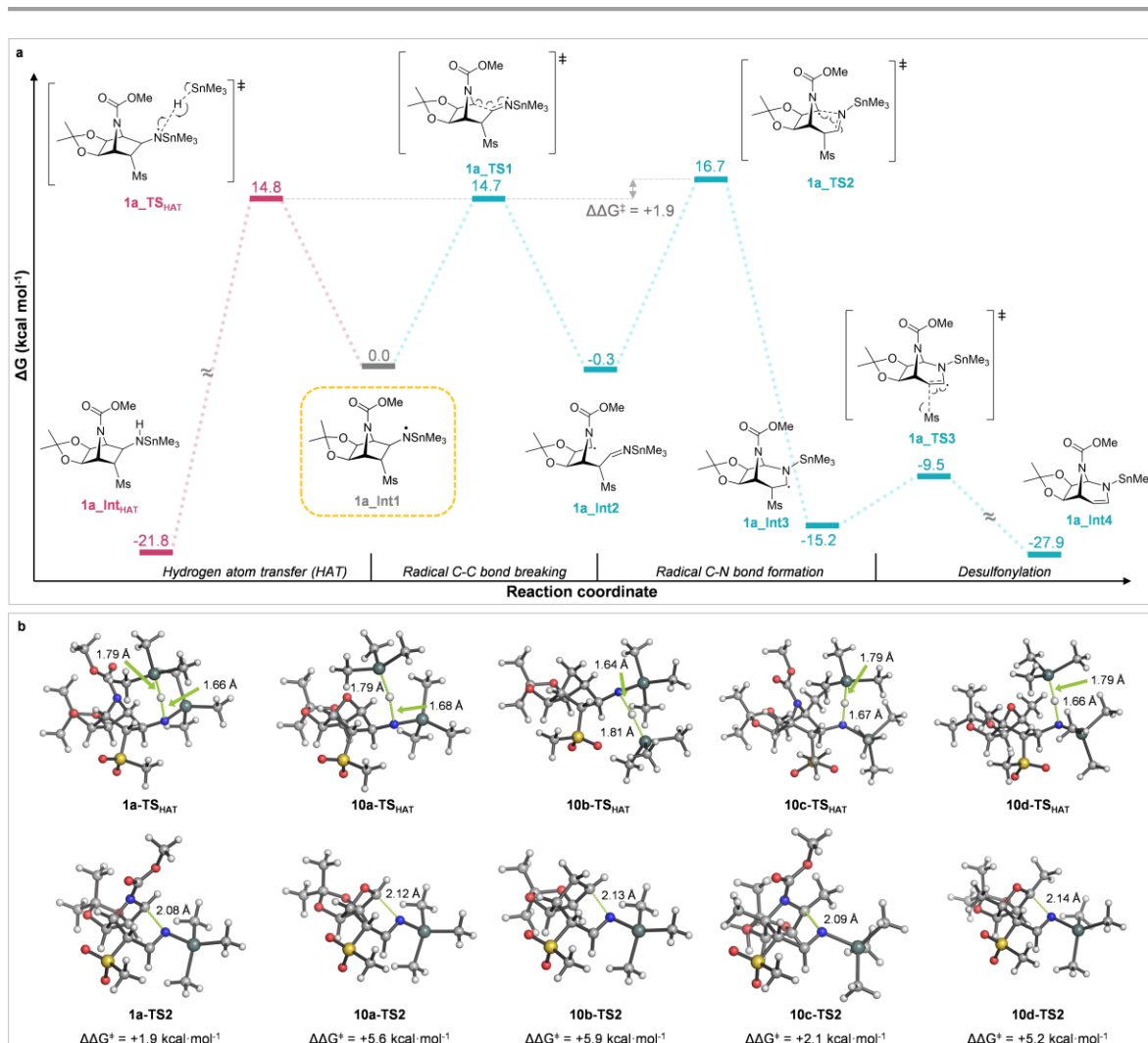


Figure 1. a) Minimum energy reaction pathway for the model of azanorbornane derivative **1a** calculated with PCM(toluene)/M06-2X/6-31G(d,p)+LanL2DZ(Sn). b) Transition structures (TS) and relative activation energies for the competing HAT and ring-expansion reactions ($\Delta\Delta G^\ddagger_{\text{TS2-TSHAT}}$) for all calculated models of bicycles **1a** and **10a-d**.

On the other hand, the competing HAT reactions from a trimethylstannane hydride molecule to radical intermediates **Int1** through transition states **TS_{HAT}**, leading to reduced intermediates (**Int_{HAT}**), have similar activation barriers ($\Delta G^\ddagger \approx 14\text{--}16 \text{ kcal mol}^{-1}$) to those calculated for the ring-expansion process, although different trends were obtained (**Figure 1b**). Norbornane (**10b**) and oxonorbornane (**10a** and **10d**) derivatives showed a preference for the HAT reaction as judged by the difference in the energies of the transition structures for both competing pathways ($\Delta\Delta G^\ddagger_{\text{TS2-TSHAT}} \approx 5\text{--}6 \text{ kcal mol}^{-1}$), in line with the experimental observations. However, these differences in energies were minimal for azanorbornane derivatives **1a** and **10c** ($\Delta\Delta G^\ddagger_{\text{TS2-TSHAT}} \approx 2 \text{ kcal mol}^{-1}$), suggesting that both reactions are energetically feasible and, therefore, competitive.

These computed trends can be attributed to the relative stability of the *N*- and *C*-centered radicals (**Int1** and **Int2**, respectively) for each substrate. The *C*-centered radicals are thermoneutral with respect to the *N*-centered radicals for azanorbornane compounds (**1a** and **10c**), while being quite more unstable for oxanorbornane and norbornane. The *C*-centered radical **Int2** for norbornane **10b** is unstable due to the lack of an adjacent heteroatom with lone pairs at the bridgehead position, whereas the same *C*-centered radicals for azanorbornanes **1a** and **10c** are stabilized by delocalization of the spin density along the adjacent carbamate group (**Figure D5**). Consequently, and according to Hammond's postulate, the activation barrier for the ring-closing transition state (**TS2**) for oxanorbornanes **10a** and **10d** and, more significantly, for norbornane **10b**, are higher than those for the competitive **TS_{HAT}**, thus exhibiting a preference for the HAT reaction (**Figures D1, D2, and D4**). In contrast, azanorbornanes **1a** (**Figure 1a**) and **10c** (**Figure D3**) display lower activation energies for the ring expansion, which becomes competitive with HAT. The homolytic cleavage of the *C2-C3* bond on **Int1** leads to a transition state ca. 4 kcal mol⁻¹ higher in energy than that calculated for the homolytic cleavage of the *C3-C4* bond, which explains the exceptional regioselectivity experimentally observed in the ring expansion.

Conclusions

We have demonstrated that 3-azidoazanorbornanes are excellent substrates for the preparation of 2,3-diazabicyclo[3.2.1]oct-2-ene systems through a regioselective rearrangement of azanorbornanic aminyl radicals. These systems are unknown and can be considered precursors of the 2,8-diheterobicyclo[3.2.1]octane skeleton, which is present in natural products. Experimental and computational studies allowed us to establish the scope of the reaction and provide a mechanistic proposal for this unusual radical rearrangement. The scope of this reaction is limited to the *aza*-analogs where the intermediate radicals are adequately stabilized. Moreover, the rigidity of the azabicyclic skeleton showed to be crucial for the rearrangement to proceed efficiently. With the discovery of this new radical rearrangement, new synthetic strategies involving compounds containing a rigid azido-functionalized azacyclic core could be explored.

Conclusions

With the results presented in this thesis in hand, we can draw some conclusions and future perspectives. In **Chapters 1, 2, and 3**, we've been interested in deepening the use of three types of dipoles, namely azides, nitrones, and pyridinium ylides, to implement a series of procedures for the preparation of biologically interesting compounds through cycloaddition reactions. Preliminary evidence in this sense was reported for the triazoles obtained in **Chapter 1, line 1b**, which will be considered for future *in vivo* evaluations. Within the same chapter, the results reported for the synthesis of triazolyl nucleoside derivatives (*line 1a*) clearly showed that it is possible to prepare such scaffolds in a regioselective way using Fe (III) chloride, an interesting – and way lesser studied – catalyst for click reactions. In addition, a reverse docking study over a large selection of potential targets was performed on the obtained substrates. As for **Chapter 2**, the microwave-assisted synthesis of isoxazolidine-containing BPs was achieved, furtherly endorsing the use of such technology for the preparation of compounds of high interest in medicinal chemistry. The biological potential of our BPs will be thoroughly assessed by molecular dynamics and docking simulations, in combination with STD NMR towards *hFPPS*, a target in oncology. In **Chapter 3**, we exploited the *in situ* preparation of pyridinium ylides, dipoles used for implementing two multicomponent strategies to obtain indolizines and spirocyclopropyl oxindoles. These two classes of molecules are highly appreciated in drug design, being versatile scaffolds capable of interacting very well with numerous biological environments. Of note, the reaction mechanism regarding the synthesis of the spiroderivatives was examined by means of a series of DFT calculations, allowing

us to validate our mechanistic proposal. Finally, in **Chapter 4** the use of another type of cycloaddition reaction, the Diels-Alder reaction, was used to prepare norbornane derivatives which underwent a radical expansion reaction. Such ring systems are widely present in naturally occurring compounds; hence, finding new approaches for their synthesis and, more importantly, for the functionalization (i.e., expansion) of the ring systems could be of interest to the discovery of new biomimetics. As did for the previous chapter, even the proposed radical mechanism of expansion of the ring was thoroughly studied by means of DFT calculations, assessing the role played by the heteroatoms and the degree of substitution of the norbornane ring.

List of References

- (1) Breugst, M.; Reissig, H. U. The Huisgen Reaction: Milestones of the 1,3-Dipolar Cycloaddition. *Angew. Chemie - Int. Ed.* **2020**, *59* (30), 12293–12307. <https://doi.org/10.1002/anie.202003115>.
- (2) Gracia-Vitoria, J.; Osante, I.; Cativiela, C.; Tejero, T.; Merino, P. Experimental and Computational Studies on the 1,3-Dipolar Cycloaddition between Enantiomerically Pure 2,3-Dihydrothiazoles and Nitrones. *European J. Org. Chem.* **2019**, *2019* (27), 4426–4435. <https://doi.org/10.1002/ejoc.201900667>.
- (3) Firestone, R. A. 1,3-Dipolar Cycloadditions. *J. Org. Chem.* **1968**, *1591* (6), 2285–2290.
- (4) Geittner, J.; Huisgen, R.; Sustmann, R. Kinetics of 1,3-Dipolar Cycloaddition Reactions of Diazomethane; A Correlation with Homo-Lumo Energies. *Tetrahedron Lett.* **1977**, *18* (10), 881–884. [https://doi.org/10.1016/S0040-4039\(01\)92781-9](https://doi.org/10.1016/S0040-4039(01)92781-9).
- (5) Sustmann, R.; Wenning, E. Perturbational Analysis of 1,3-Dipolar Cycloaddition Reactions of Diazomethane. *Tetrahedron Lett.* **1977**, No. 10, 877–880.
- (6) Fleming, I. Thermal Pericyclic Reactions. In *Molecular Orbitals and Organic Chemical Reactions*; 2010; pp 253–368. <https://doi.org/10.1002/9780470689493.ch6>.
- (7) Fukui, K. Recognition of Stereochemical Paths by Orbital Interaction. *Acc. Chem. Res.* **1971**, *4* (2), 57–64. <https://doi.org/10.1021/ar50038a003>.
- (8) Houk, K. N.; Sims, J.; Watts, C. R.; Luskus, L. J. The Origin of Reactivity, Regioselectivity, and Periselectivity in 1,3-Dipolar Cycloadditions. *J. Am. Chem. Soc.* **1973**, *95*, 7301–7315.
- (9) Cohen, H.; Benezra, C. Steric and Electronic Factors in 1,3-Dipolar Cycloadditions. The Stereochemical Course of the Addition of Dimethyl Aryl- and Alkyldiazomethylphosphonates to Norbornadiene. *Can. J. Chem.* **1974**, *52* (1), 66–79. <https://doi.org/10.1139/v74-010>.
- (10) Clayden, J.; Greeves, N.; Warren, S. How Important Are Secondary Orbital Interactions in Favoring the Endo Mode in 1,3-Dipolar Cycloadditions of Nitrones? *J. Org. Chem.* **1990**, *55*, 3429–3431.
- (11) Chiacchio, U.; Casuscelli, F.; Corsaro, A.; Rescifina, A.; Romeo, G.; Uccella, N. Stereoselective Control in 1,3-Dipolar Cycloaddition of Nitrones to Substituted Styrenes. *Tetrahedron* **1994**, *50* (22), 6671–6680. [https://doi.org/10.1016/S0040-4020\(01\)89695-2](https://doi.org/10.1016/S0040-4020(01)89695-2).
- (12) Cacciarini, M.; Cordero, F. M.; Faggi, C.; Goti, A. Cycloaddition Reactions of C,N-Diphenylnitrone to Methylene- γ -Butyrolactones. *Molecules* **2000**, *5* (4), 637–647. <https://doi.org/10.3390/50400637>.
- (13) Rostovtsev, V. V.; Green, L. G.; Fokin, V. V.; Sharpless, K. B. A Stepwise Huisgen Cycloaddition Process: Copper(I)-Catalyzed Regioselective “Ligation” of Azides and Terminal Alkynes. *Angew. Chemie - Int. Ed.* **2002**, *41* (14), 2596–2599. [https://doi.org/10.1002/1521-3773\(20020715\)41:14<2596::AID-ANIE2596>3.0.CO;2-4](https://doi.org/10.1002/1521-3773(20020715)41:14<2596::AID-ANIE2596>3.0.CO;2-4).
- (14) Tornøe, C. W.; Christensen, C.; Meldal, M. Peptidotriazoles on Solid Phase: [1,2,3]-Triazoles by Regiospecific Copper(I)-Catalyzed 1,3-Dipolar Cycloadditions of Terminal Alkynes to Azides. *J. Org. Chem.* **2002**, *67* (9), 3057–3064. <https://doi.org/10.1021/jo011148j>.
- (15) Johansson, J. R.; Beke-Somfai, T.; Said Stålsmeden, A.; Kann, N. Ruthenium-Catalyzed Azide Alkyne Cycloaddition Reaction: Scope, Mechanism, and Applications. *Chem. Rev.* **2016**, *116* (23), 14726–14768. <https://doi.org/10.1021/acs.chemrev.6b00466>.
- (16) De Nino, A.; Maiuolo, L.; Costanzo, P.; Algieri, V.; Jiritano, A.; Olivito, F.; Tallarida, M. A. Recent Progress in Catalytic Synthesis of 1,2,3-Triazoles. *Catalysts* **2021**, *11* (9), 1–48. <https://doi.org/10.3390/catal11091120>.
- (17) Agalave, S. G.; Maujan, S. R.; Pore, V. S. Click Chemistry: 1,2,3-Triazoles as Pharmacophores. *Chem. - An Asian J.* **2011**, *6* (10), 2696–2718. <https://doi.org/10.1002/asia.201100432>.
- (18) Schulze, B.; Schubert, U. S. Beyond Click Chemistry-Supramolecular Interactions of 1,2,3-

- Triazoles. *Chem. Soc. Rev.* **2014**, *43* (8), 2522–2571. <https://doi.org/10.1039/c3cs60386e>.
- (19) Lauria, A.; Delisi, R.; Mingoia, F.; Terenzi, A.; Martorana, A.; Barone, G.; Almerico, A. M. 1,2,3-Triazole in Heterocyclic Compounds, Endowed With Biological Activity, Through 1,3-Dipolar Cycloadditions. *European J. Org. Chem.* **2014**, *2014* (16), 3289–3306. <https://doi.org/10.1002/ejoc.201301695>.
- (20) Singh, M. S.; Chowdhury, S.; Koley, S. Advances of Azide-Alkyne Cycloaddition-Click Chemistry over the Recent Decade. *Tetrahedron* **2016**, *72* (35), 5257–5283. <https://doi.org/10.1016/j.tet.2016.07.044>.
- (21) Maiuolo, L.; Algieri, V.; Olivito, F.; De Nino, A. Recent Developments on 1,3-Dipolar Cycloaddition Reactions by Catalysis in Green Solvents. *Catalysts* **2020**, *10* (1). <https://doi.org/10.3390/catal10010065>.
- (22) Martina, K.; Tagliapietra, S.; Veselov, V. V.; Cravotto, G. Green Protocols in Heterocycle Syntheses via 1,3-Dipolar Cycloadditions. *Front. Chem.* **2019**, *7* (FEB), 1–21. <https://doi.org/10.3389/fchem.2019.00095>.
- (23) Neto, J. S. S.; Zeni, G. A Decade of Advances in the Reaction of Nitrogen Sources and Alkynes for the Synthesis of Triazoles. *Coord. Chem. Rev.* **2020**, *409*, 213217. <https://doi.org/10.1016/j.ccr.2020.213217>.
- (24) Saini, P.; Sonika; Singh, G.; Kaur, G.; Singh, J.; Singh, H. Robust and Versatile Cu(I) Metal Frameworks as Potential Catalysts for Azide-Alkyne Cycloaddition Reactions: Review. *Mol. Catal.* **2021**, *504* (January), 111432. <https://doi.org/10.1016/j.mcat.2021.111432>.
- (25) Wang, S.; Yang, L. J.; Zeng, J. L.; Zheng, Y.; Ma, J. A. Silver-Catalyzed [3 + 2] Cycloaddition of Isocyanides with Diazo Compounds: New Regioselective Access to 1,4-Disubstituted-1,2,3-Triazoles. *Org. Chem. Front.* **2015**, *2* (11), 1468–1474. <https://doi.org/10.1039/c5qo00219b>.
- (26) Jia, F.; Zhang, B. Mechanistic Insight into the Silver-Catalyzed Cycloaddition Synthesis of 1,4-Disubstituted-1,2,3-Triazoles: The Key Role of Silver. *New J. Chem.* **2019**, *43* (22), 8634–8643. <https://doi.org/10.1039/c9nj01700c>.
- (27) Meng, X.; Xu, X.; Gao, T.; Chen, B. Zn/C-Catalyzed Cycloaddition of Azides and Aryl Alkynes. *European J. Org. Chem.* **2010**, No. 28, 5409–5414. <https://doi.org/10.1002/ejoc.201000610>.
- (28) Morozova, M. A.; Yusubov, M. S.; Kratochvil, B.; Eigner, V.; Bondarev, A. A.; Yoshimura, A.; Saito, A.; Zhdankin, V. V.; Trusova, M. E.; Postnikov, P. S. Regioselective Zn(OAc)₂-Catalyzed Azide-Alkyne Cycloaddition in Water: The Green Click-Chemistry. *Org. Chem. Front.* **2017**, *4* (6), 978–985. <https://doi.org/10.1039/c6qo00787b>.
- (29) Sharma, R. K.; Mishra, M.; Sharma, S.; Dutta, S. Zinc(II) Complex Immobilized on Amine Functionalized Silica Gel: A Novel, Highly Efficient and Recyclable Catalyst for Multicomponent Click Synthesis of 1,4-Disubstituted 1,2,3-Triazoles. *J. Coord. Chem.* **2016**, *69* (7), 1152–1165. <https://doi.org/10.1080/00958972.2016.1165807>.
- (30) Mondal, P.; Ghosh, S.; Das, S. kanti; Bhaumik, A.; Das, D.; Islam, S. M. Use of an Efficient Polystyrene-Supported Cerium Catalyst for One-Pot Multicomponent Synthesis of Spiro-Piperidine Derivatives and Click Reactions in Green Solvent. *Appl. Organomet. Chem.* **2018**, *32* (4), 1–15. <https://doi.org/10.1002/aoc.4227>.
- (31) Arafa, W. A. A.; Nayl, A. E. A. A. Water as a Solvent for Ru-Catalyzed Click Reaction: Highly Efficient Recyclable Catalytic System for Triazolocoumarins Synthesis. *Appl. Organomet. Chem.* **2019**, *33* (10), 1–12. <https://doi.org/10.1002/aoc.5156>.
- (32) Sharma, P.; Rathod, J.; Singh, A. P.; Kumar, P.; Sasson, Y. Synthesis of Heterogeneous Ru(Ii)-1,2,3-Triazole Catalyst Supported over SBA-15: Application to the Hydrogen Transfer Reaction and Unusual Highly Selective 1,4-Disubstituted Triazole Formation: Via Multicomponent Click Reaction. *Catal. Sci. Technol.* **2018**, *8* (13), 3246–3259. <https://doi.org/10.1039/c7cy02619f>.
- (33) Wu, Z. G.; Liao, X. J.; Yuan, L.; Wang, Y.; Zheng, Y. X.; Zuo, J. L.; Pan, Y. Visible-Light-Mediated Click Chemistry for Highly Regioselective Azide-Alkyne Cycloaddition by a Photoredox Electron-Transfer Strategy. *Chem. - A Eur. J.* **2020**, *26* (25), 5694–5700. <https://doi.org/10.1002/chem.202000252>.
- (34) Alcaide, B.; Almendros, P.; Lázaro-Milla, C. Metal-Free [3+2] Cycloaddition of Azides with Tf₂CCH₂ for the Regioselective Preparation of Elusive 4-(Trifluoromethylsulfonyl)-1,2,3-Triazoles. *Chem. Commun.* **2015**, *51* (32), 6992–6995. <https://doi.org/10.1039/c5cc01223f>.
- (35) Singh, H.; Khanna, G.; Nand, B.; Khurana, J. M. Metal-Free Synthesis of 1,2,3-Triazoles by Azide-Aldehyde Cycloaddition under Ultrasonic Irradiation in TSIL [DBU-Bu]OH and in Hydrated IL Bu₄NOH under Heating. *Monatshefte fur Chemie* **2016**, *147* (7), 1215–1219. <https://doi.org/10.1007/s00706-015-1623-4>.
- (36) Das, J.; Dey, S.; Pathak, T. Metal-Free Route to Carboxylated 1,4-Disubstituted 1,2,3-Triazoles from Methoxycarbonyl-Modified Vinyl Sulfone. *J. Org. Chem.* **2019**. <https://doi.org/10.1021/acs.joc.9b02443>.

- (37) Sebest, F.; Haselgrove, S.; White, A. J. P.; Díez-González, S. Metal-Free 1,2,3-Triazole Synthesis in Deep Eutectic Solvents. *Synlett* **2020**, *31* (6), 605–609. <https://doi.org/10.1055/s-0039-1690736>.
- (38) Wan, J. P.; Cao, S.; Liu, Y. Base-Promoted Synthesis of N-Substituted 1,2,3-Triazoles via Enaminone-Azide Cycloaddition Involving Regitz Diazo Transfer. *Org. Lett.* **2016**, *18* (23), 6034–6037. <https://doi.org/10.1021/acs.orglett.6b02975>.
- (39) Cao, S.; Liu, Y.; Hu, C.; Wen, C.; Wan, J. P. Alkyl Propiolates Participated [3+2] Annulation for the Switchable Synthesis of 1,5- and 1,4-Disubstituted 1,2,3-Triazoles Containing Ester Side Chain. *ChemCatChem* **2018**, *10* (21), 5021–5025. <https://doi.org/10.1002/cctc.201801366>.
- (40) Cai, Z.-J.; Lu, X.-M.; Zi, Y.; Yang, C.; Shen, L.-J.; Li, J.; Wang, S.-Y.; Ji, S.-J. I₂/TBPB Mediated Oxidative Reaction of N-Tosylhydrazones with Anilines: Practical Construction of 1,4-Disubstituted 1,2,3-Triazoles under Metal-Free and Azide-Free Conditions. *Org. Lett.* **2014**, *16*, 5108–5111.
- (41) Mani, G. S.; Donthiboina, K.; Shaik, S. P.; Shankaraiah, N.; Kamal, A. Iodine-Mediated C-N and N-N Bond Formation: A Facile One-Pot Synthetic Approach to 1,2,3-Triazoles under Metal-Free and Azide-Free Conditions. *RSC Adv.* **2019**, *9* (46), 27021–27031. <https://doi.org/10.1039/c9ra06005g>.
- (42) Zhou, Q.; Fu, Z.; Yu, L.; Wang, J. Transition-Metal-Free [4+1] Cycloaddition for the Synthesis of 1,2,3-Triazole from α,α -Difluoro-N-Tosylhydrazone and Amine through C-F Bond Cleavage. *Asian J. Org. Chem.* **2019**, *8* (5), 646–649. <https://doi.org/10.1002/ajoc.201800514>.
- (43) Zehnder, L. R.; Hawkins, J. M.; Sutton, S. C. One-Pot, Metal- And Azide-Free Synthesis of 1,2,3-Triazoles from α -Ketoacetals and Amines. *Synlett* **2020**, *31* (2), 175–178. <https://doi.org/10.1055/s-0039-1691526>.
- (44) Pedersen, D. S.; Abell, A. 1,2,3-Triazoles in Peptidomimetic Chemistry. *European J. Org. Chem.* **2011**, No. 13, 2399–2411. <https://doi.org/10.1002/ejoc.201100157>.
- (45) Crich, D.; Yang, F. Phenylthiomethyl Glycosides: Convenient Synthons for the Formation of Azidomethyl and Glycosylmethyl Glycosides and Their Derivatives. *Angew. Chemie - Int. Ed.* **2009**, *48* (47), 8896–8899. <https://doi.org/10.1002/anie.200904168>.
- (46) Kracker, O.; Góra, J.; Krzciuk-Gula, J.; Marion, A.; Neumann, B.; Stammler, H. G.; Nieß, A.; Antes, I.; Latajka, R.; Sewald, N. 1,5-Disubstituted 1,2,3-Triazole-Containing Peptidotriazolamers: Design Principles for a Class of Versatile Peptidomimetics. *Chem. - A Eur. J.* **2018**, *24* (4), 953–961. <https://doi.org/10.1002/chem.201704583>.
- (47) Said Stålsmeden, A.; Paterson, A. J.; Szigyártó, I. C.; Thunberg, L.; Johansson, J. R.; Beke-Somfai, T.; Kann, N. Chiral 1,5-Disubstituted 1,2,3-Triazoles-Versatile Tools for Foldamers and Peptidomimetic Applications. *Org. Biomol. Chem.* **2020**, *18* (10), 1957–1967. <https://doi.org/10.1039/d0ob00168f>.
- (48) Grob, N. M.; Schibli, R.; Béhé, M.; Valverde, I. E.; Mindt, T. L. 1,5-Disubstituted 1,2,3-Triazoles as Amide Bond Isosteres Yield Novel Tumor-Targeting Minigastrin Analogs. *ACS Med. Chem. Lett.* **2021**, *12* (4), 585–592. <https://doi.org/10.1021/acsmchemlett.0c00636>.
- (49) Vernekar, S. K. V.; Qiu, L.; Zhang, J.; Kankanala, J.; Li, H.; Geraghty, R. J.; Wang, Z. 5'-Silylated 3'-1,2,3-Triazolyl Thymidine Analogues as Inhibitors of West Nile Virus and Dengue Virus. *J. Med. Chem.* **2015**, *58* (9), 4016–4028. <https://doi.org/10.1021/acs.jmedchem.5b00327>.
- (50) Pettersson, M.; Bliman, D.; Jacobsson, J.; Nilsson, J. R.; Min, J.; Iconaru, L.; Guy, R. K.; Kriwacki, R. W.; Andréasson, J.; Grøtli, M. 8-Triazolylpurines: Towards Fluorescent Inhibitors of the MDM2/P53 Interaction. *PLoS One* **2015**, *10* (5), 1–17. <https://doi.org/10.1371/journal.pone.0124423>.
- (51) Hornum, M.; Djukina, A.; Sassnau, A. K.; Nielsen, P. Synthesis of New C-5-Triazolyl-Functionalized Thymidine Analogs and Their Ability to Engage in Aromatic Stacking in DNA:DNA and DNA:RNA Duplexes. *Org. Biomol. Chem.* **2016**, *14* (19), 4436–4447. <https://doi.org/10.1039/c6ob00609d>.
- (52) Kocsis, L.; Szabó, I.; Bosze, S.; Jernei, T.; Hudecz, F.; Csámpai, A. Synthesis, Structure and in Vitro Cytostatic Activity of Ferrocene - Cinchona Hybrids. *Bioorganic Med. Chem. Lett.* **2016**, *26* (3), 946–949. <https://doi.org/10.1016/j.bmcl.2015.12.059>.
- (53) Chen, M.; Li, L.; Nie, H.; Shi, Y.; Mei, J.; Wang, J.; Sun, J. Z.; Qin, A.; Tang, B. Z. N-Type Pyrazine and Triazole-Based Luminogens with Aggregation-Enhanced Emission Characteristics. *Chem. Commun.* **2015**, *51* (53), 10710–10713. <https://doi.org/10.1039/c5cc03181h>.
- (54) Anand, A.; Kulkarni, M. V. Click Chemistry Approach for the Regioselective Synthesis of Iso-Indoline-1,3-Dione Linked 1,4 and 1,5 Coumarinyl 1,2,3-Triazoles and Their Photophysical Properties. *Synth. Commun.* **2017**, *47* (7), 722–733.
- (55) Mekni, N. H. Cu⁺-Catalyzed 1,3-Dipolar Intramolecular Click Opposite Cross Cyclization Reaction of Polyoxyethylene Bis(Azido-Terminal Alkynes): Synthesis of New 1,2,3-Triazolo-Crown Ethers. *J. Heterocycl. Chem.* **2017**, *54* (5), 2664–2669. <https://doi.org/10.1002/jhet.2866>.
- (56) Kumar, N.; Ansari, M. Y.; Kant, R.; Kumar, A. Copper-Catalyzed Decarboxylative Regioselective

- Synthesis of 1,5-Disubstituted 1,2,3-Triazoles. *Chem. Commun.* **2018**, 54 (21), 2627–2630. <https://doi.org/10.1039/c7cc09934g>.
- (57) Kim, W. G.; Kang, M. E.; Lee, J. Bin; Jeon, M. H.; Lee, S.; Lee, J.; Choi, B.; Cal, P. M. S. D.; Kang, S.; Kee, J. M.; Bernardes, G. J. L.; Rohde, J. U.; Choe, W.; Hong, S. Y. Nickel-Catalyzed Azide-Alkyne Cycloaddition to Access 1,5-Disubstituted 1,2,3-Triazoles in Air and Water. *J. Am. Chem. Soc.* **2017**, 139 (35), 12121–12124. <https://doi.org/10.1021/jacs.7b06338>.
- (58) Nanjundaswamy, H. M.; Abrahamse, H. Regioselective Synthesis of 1,5-Disubstituted 1,2,3-Triazoles by Reusable AlCl₃ Immobilized on γ -Al₂O₃. *Synth. Commun.* **2015**, 45 (8), 967–974. <https://doi.org/10.1080/00397911.2014.997366>.
- (59) Mahadari, M. K.; Tague, A. J.; Keller, P. A.; Pyne, S. G. Synthesis of Sterically Congested 1,5-Disubstituted-1,2,3-Triazoles Using Chloromagnesium Acetylides and Hindered 1-Naphthyl Azides. *Tetrahedron* **2021**, 81, 131916. <https://doi.org/10.1016/j.tet.2020.131916>.
- (60) De Nino, A.; Merino, P.; Algieri, V.; Nardi, M.; Di Gioia, M. L.; Russo, B.; Tallarida, M. A.; Maiuolo, L. Synthesis of 1,5-Functionalized 1,2,3-Triazoles Using Ionic Liquid/Iron(III) Chloride as an Efficient and Reusable Homogeneous Catalyst. *Catalysts* **2018**, 8 (9), 1–13. <https://doi.org/10.3390/catal8090364>.
- (61) Maiuolo, L.; Russo, B.; Algieri, V.; Nardi, M.; Di Gioia, M. L.; Tallarida, M. A.; De Nino, A. Regioselective Synthesis of 1,5-Disubstituted 1,2,3-Triazoles by 1,3-Dipolar Cycloaddition: Role of Er(OTf)₃, Ionic Liquid and Water. *Tetrahedron Lett.* **2019**, 60 (9), 672–674. <https://doi.org/10.1016/j.tetlet.2019.01.053>.
- (62) De Nino, A.; Maiuolo, L.; Merino, P.; Nardi, M.; Procopio, A.; Roca-López, D.; Russo, B.; Algieri, V. Efficient Organocatalyst Supported on a Simple Ionic Liquid as a Recoverable System for the Asymmetric Diels-Alder Reaction in the Presence of Water. *ChemCatChem* **2015**, 7 (5), 830–835. <https://doi.org/10.1002/cctc.201402973>.
- (63) Faul, C. F. J. Ionic Self-Assembly for Functional Hierarchical Nanostructured Materials. *Acc. Chem. Res.* **2014**, 47 (12), 3428–3438. <https://doi.org/10.1021/ar500162a>.
- (64) Zhang, D.; Fan, Y.; Yan, Z.; Nie, Y.; Xiong, X.; Gao, L. Reactions of α -Haloacroleins with Azides: Highly Regioselective Synthesis of Formyl Triazoles. *Green Chem.* **2019**, 21 (15), 4211–4216. <https://doi.org/10.1039/c9gc01129c>.
- (65) Kayet, A.; Dey, S.; Pathak, T. A Metal Free Aqueous Route to 1,5-Disubstituted 1,2,3-Triazolylated Monofuranosides and Difuranosides. *Tetrahedron Lett.* **2015**, 56 (41), 5521–5524. <https://doi.org/10.1016/j.tetlet.2015.08.030>.
- (66) Kayet, A.; Datta, D.; Das, A.; Dasgupta, S.; Pathak, T. 1,5-Disubstituted 1,2,3-Triazole Linked Disaccharides: Metal-Free Syntheses and Screening of a New Class of Ribonuclease A Inhibitors. *Bioorganic Med. Chem.* **2018**, 26 (2), 455–462. <https://doi.org/10.1016/j.bmc.2017.12.004>.
- (67) González-Calderón, D.; Mejía-Dionicio, M. G.; Morales-Reza, M. A.; Ramírez-Villalva, A.; Morales-Rodríguez, M.; Jauregui-Rodríguez, B.; Díaz-Torres, E.; González-Romero, C.; Fuentes-Benites, A. Azide-Enolate 1,3-Dipolar Cycloaddition in the Synthesis of Novel Triazole-Based Miconazole Analogues as Promising Antifungal Agents. *Eur. J. Med. Chem.* **2016**, 112, 60–65. <https://doi.org/10.1016/j.ejmech.2016.02.013>.
- (68) Wan, J. P.; Cao, S.; Liu, Y. A Metal- and Azide-Free Multicomponent Assembly toward Regioselective Construction of 1,5-Disubstituted 1,2,3-Triazoles. *J. Org. Chem.* **2015**, 80 (18), 9028–9033. <https://doi.org/10.1021/acs.joc.5b01121>.
- (69) Bai, H. W.; Cai, Z. J.; Wang, S. Y.; Ji, S. J. Aerobic Oxidative Cycloaddition of α -Chlorotosylhydrazones with Arylamines: General Chemoselective Construction of 1,4-Disubstituted and 1,5-Disubstituted 1,2,3-Triazoles under Metal-Free and Azide-Free Conditions. *Org. Lett.* **2015**, 17 (12), 2898–2901. <https://doi.org/10.1021/acs.orglett.5b01000>.
- (70) Thomas, J.; Jana, S.; John, J.; Liekens, S.; Dehaen, W. A General Metal-Free Route towards the Synthesis of 1,2,3-Triazoles from Readily Available Primary Amines and Ketones. *Chem. Commun.* **2016**, 52 (14), 2885–2888. <https://doi.org/10.1039/c5cc08347h>.
- (71) Kayet, A.; Pathak, T. A Metal-Free Route towards 1,5-Disubstituted 1,2,3-Triazolylmethylene Linked Disaccharides: Synthesis in a Biodegradable Hydroxyl-Ammonium-Based Aqueous Ionic Liquid Media. *Tetrahedron Lett.* **2018**, 59 (35), 3341–3344. <https://doi.org/10.1016/j.tetlet.2018.07.052>.
- (72) Silveira-Dorta, G.; Jana, S.; Borkova, L.; Thomas, J.; Dehaen, W. Straightforward Synthesis of Enantiomerically Pure 1,2,3-Triazoles Derived from Amino Esters. *Org. Biomol. Chem.* **2018**, 16 (17), 3168–3176. <https://doi.org/10.1039/c8ob00533h>.
- (73) Zhang, X.; Cui, X.; Wang, W.; Zeng, T.; Wang, Y.; Tan, Y.; Liu, D.; Wang, X.; Li, Y. Base-Promoted Regiospecific Synthesis of Fully Substituted 1,2,3-Triazoles and 1,5-Disubstituted 1,2,3-Triazoles. *Asian J. Org. Chem.* **2020**, 9 (12), 2176–2183. <https://doi.org/10.1002/ajoc.202000479>.

- (74) Kiranmye, T.; Vadivelu, M.; Sampath, S.; Muthu, K.; Karthikeyan, K. Ultrasound-Assisted Catalyst Free Synthesis of 1,4-/1,5-Disubstituted-1,2,3-Triazoles in Aqueous Medium. *Sustain. Chem. Pharm.* **2021**, *19* (August 2020), 100358. <https://doi.org/10.1016/j.scp.2020.100358>.
- (75) Madadi, N. R.; Penthala, N. R.; Howk, K.; Ketkar, A.; Eoff, R. L.; Borrelli, M. J.; Crooks, P. A. Synthesis and Biological Evaluation of Novel 4,5-Disubstituted 2H-1,2,3-Triazoles as Cis-Constrained Analogues of Combretastatin A-4. *Eur. J. Med. Chem.* **2015**, *103*, 123–132. <https://doi.org/10.1016/j.ejmech.2015.08.041>.
- (76) Chai, H.; Guo, R.; Yin, W.; Cheng, L.; Liu, R.; Chu, C. One-Pot, Three-Component Reaction Using Modified Julia Reagents: A Facile Synthesis of 4,5-Disubstituted 1,2,3-(NH)-Triazoles in a Wet Organic Solvent. *ACS Comb. Sci.* **2015**, *17* (3), 147–151. <https://doi.org/10.1021/co5001597>.
- (77) Thomas, J.; Jana, S.; Liekens, S.; Dehaen, W. A Single-Step Acid Catalyzed Reaction for Rapid Assembly of: NH -1,2,3-Triazoles. *Chem. Commun.* **2016**, *52* (59), 9236–9239. <https://doi.org/10.1039/c6cc03744e>.
- (78) Panda, S.; Maity, P.; Manna, D. Transition Metal, Azide, and Oxidant-Free Homo- and Heterocoupling of Ambiphilic Tosylhydrazones to the Regioselective Triazoles and Pyrazoles. *Org. Lett.* **2017**, *19* (7), 1534–1537. <https://doi.org/10.1021/acs.orglett.7b00313>.
- (79) Swarup, H. A.; Kemparajegowda; Mantelingu, K.; Rangappa, K. S. Effective and Transition-Metal-Free Construction of Disubstituted, Trisubstituted 1,2,3-NH-Triazoles and Triazolo Pyridazine via Intermolecular 1,3-Dipolar Cycloaddition Reaction. *ChemistrySelect* **2018**, *3* (2), 703–708. <https://doi.org/10.1002/slct.201702547>.
- (80) Wu, G. L.; Wu, Q. P. Metal-Free Multicomponent Reaction for Synthesis of 4,5-Disubstituted 1,2,3-(NH)-Triazoles. *Adv. Synth. Catal.* **2018**, *360* (10), 1949–1953. <https://doi.org/10.1002/adsc.201701587>.
- (81) Wu, L.; Wang, X.; Chen, Y.; Huang, Q.; Lin, Q.; Wu, M. 4-Aryl- NH -1,2,3-Triazoles via Multicomponent Reaction of Aldehydes, Nitroalkanes, and Sodium Azide. *Synlett* **2016**, *27* (3), 437–441. <https://doi.org/10.1055/s-0035-1560528>.
- (82) Hui, R.; Zhao, M.; Chen, M.; Ren, Z.; Guan, Z. One-Pot Synthesis of 4-Aryl-NH-1,2,3-Triazoles through Three-Component Reaction of Aldehydes, Nitroalkanes and NaN₃. *Chinese J. Chem.* **2017**, *35* (12), 1808–1812. <https://doi.org/10.1002/cjoc.201700367>.
- (83) Jannapu Reddy, R.; Waheed, M.; Karthik, T.; Shankar, A. An Efficient Synthesis of 4,5-Disubstituted-2: H -1,2,3-Triazoles from Nitroallylic Derivatives via a Cycloaddition-Denitration Process. *New J. Chem.* **2018**, *42* (2), 980–987. <https://doi.org/10.1039/c7nj03292g>.
- (84) Shelton, J.; Lu, X.; Hollenbaugh, J. A.; Cho, J. H.; Amblard, F.; Schinazi, R. F. Metabolism, Biochemical Actions, and Chemical Synthesis of Anticancer Nucleosides, Nucleotides, and Base Analogs. *Chem. Rev.* **2016**, *116* (23), 14379–14455. <https://doi.org/10.1021/acs.chemrev.6b00209>.
- (85) Geraghty, R. J.; Aliota, M. T.; Bonnac, L. F. Broad-Spectrum Antiviral Strategies and Nucleoside Analogues. *Viruses* **2021**, *13* (4). <https://doi.org/10.3390/v13040667>.
- (86) Choi, J. S.; Berdis, A. J. Visualizing Nucleic Acid Metabolism Using Non-Natural Nucleosides and Nucleotide Analogs. *Biochim. Biophys. Acta - Proteins Proteomics* **2016**, *1864* (1), 165–176. <https://doi.org/10.1016/j.bbapap.2015.05.010>.
- (87) Xia, Y.; Qu, F.; Peng, L. Triazole Nucleoside Derivatives Bearing Aryl Functionalities on the Nucleobases Show Antiviral and Anticancer Activity. *Mini-Reviews Med. Chem.* **2010**, *10* (9), 806–821. <https://doi.org/10.2174/138955710791608316>.
- (88) Halay, E.; Ay, E.; Şalva, E.; Ay, K.; Karayıldırım, T. Syntheses of 1,2,3-Triazole-Bridged Pyranose Sugars with Purine and Pyrimidine Nucleobases and Evaluation of Their Anticancer Potential. *Nucleosides, Nucleotides and Nucleic Acids* **2017**, *36* (9), 598–619. <https://doi.org/10.1080/15257770.2017.1346258>.
- (89) González-Olvera, R.; Espinoza-Vázquez, A.; Negrón-Silva, G. E.; Palomar-Pardavé, M. E.; Romero-Romo, M. A.; Santillan, R. Multicomponent Click Synthesis of New 1,2,3-Triazole Derivatives of Pyrimidine Nucleobases: Promising Acidic Corrosion Inhibitors for Steel. *Molecules* **2013**, *18* (12), 15064–15079. <https://doi.org/10.3390/molecules181215064>.
- (90) Negrón-Silva, G. E.; González-Olvera, R.; Angeles-Beltrán, D.; Maldonado-Carmona, N.; Espinoza-Vázquez, A.; Palomar-Pardavé, M. E.; Romero-Romo, M. A.; Santillan, R. Synthesis of New 1,2,3-Triazole Derivatives of Uracil and Thymine with Potential Inhibitory Activity against Acidic Corrosion of Steels. *Molecules* **2013**, *18* (4), 4613–4627. <https://doi.org/10.3390/molecules18044613>.
- (91) Elayadi, H.; Smietana, M.; Vasseur, J. J.; Balzarini, J.; Lazrek, H. B. Synthesis of 1,2,3-Triazolyl Nucleoside Analogs as Potential Anti-Influenza A (H3N2 Subtype) Virus Agents. *Arch. Pharm. (Weinheim)*. **2014**, *347* (2), 134–141. <https://doi.org/10.1002/ardp.201300260>.
- (92) De Nino, A.; Algieri, V.; Tallarida, M. A.; Constanzo, P.; Pedrón, M.; Tejero, T.; Merino, P.; Maiuolo, L. Regioselective Synthesis of 1,4,5-Trisubstituted-1,2,3-Triazoles from Aryl Azides and

- Enaminones. *European J. Org. Chem.* **2019**, 2019 (33), 5725–5731. <https://doi.org/10.1002/ejoc.201900889>.
- (93) Kramer, R. A.; Bleicher, K. H.; Wennemers, H. Design and Synthesis of Nucleoprolin Amino Acids for the Straightforward Preparation of Chiral and Conformationally Constrained Nucleopeptides. *Helv. Chim. Acta* **2012**, 95 (12), 2621–2634. <https://doi.org/10.1002/hlca.201200557>.
- (94) Legros, V.; Hamon, F.; Violeau, B.; Turpin, F.; Djedaini-Pilard, F.; Désiré, J.; Len, C. Toward the Supramolecular Cyclodextrin Dimers Using Nucleobase Pairs. *Synthesis (Stuttg.)* **2011**, No. 2, 235–242. <https://doi.org/10.1055/s-0030-1258354>.
- (95) Dalpozzo, R.; De Nino, A.; Maiuolo, L.; Procopio, A.; Romeo, R.; Sindona, G. A Convenient Method for the Synthesis of N-Vinyl Derivatives of Nucleobases. *Synthesis (Stuttg.)* **2002**, No. 2, 172–174. <https://doi.org/10.1055/s-2002-19795>.
- (96) Hunter, D. R.; Haworth, R. A. The Ca²⁺-Induced Membrane Transition in Mitochondria. III. Transitional Ca²⁺ Release. *Arch. Biochem. Biophys.* **1979**, 195 (2), 468–477. [https://doi.org/10.1016/0003-9861\(79\)90373-4](https://doi.org/10.1016/0003-9861(79)90373-4).
- (97) Javadov, S.; Karmazyn, M. Mitochondrial Permeability Transition Pore Opening as an Endpoint to Initiate Cell Death and as a Putative Target for Cardioprotection. *Cell. Physiol. Biochem.* **2007**, 20 (1–4), 1–22. <https://doi.org/10.1159/000103747>.
- (98) Crompton, M.; Costi, A. A Heart Mitochondrial Ca²⁺-Dependent Pore of Possible Relevance to Re-Perfusion-Induced Injury. Evidence That ADP Facilitates Pore Interconversion between the Closed and Open States. *Biochem. J.* **1990**, 266 (1), 33–39. <https://doi.org/10.1042/bj2660033>.
- (99) Veech, R. L.; Valeri, C. R.; Vanitallie, T. B. The Mitochondrial Permeability Transition Pore Provides a Key to the Diagnosis and Treatment of Traumatic Brain Injury. *IUBMB Life* **2012**, 64 (2), 203–207. <https://doi.org/10.1002/iub.590>.
- (100) Halestrap, A. P.; Pasdois, P. The Role of the Mitochondrial Permeability Transition Pore in Heart Disease. *Biochim. Biophys. Acta - Bioenerg.* **2009**, 1787 (11), 1402–1415. <https://doi.org/10.1016/j.bbabi.2008.12.017>.
- (101) Bonora, M.; Pinton, P. The Mitochondrial Permeability Transition Pore and Cancer: Molecular Mechanisms Involved in Cell Death. *Front. Oncol.* **2014**, 4 (NOV), 1–12. <https://doi.org/10.3389/fonc.2014.00302>.
- (102) Šileikytė, J.; Forte, M. Shutting down the Pore: The Search for Small Molecule Inhibitors of the Mitochondrial Permeability Transition. *Biochim. Biophys. Acta - Bioenerg.* **2016**, 1857 (8), 1197–1202. <https://doi.org/10.1016/j.bbabi.2016.02.016>.
- (103) Fancelli, D.; Abate, A.; Amici, R.; Bernardi, P.; Ballarini, M.; Cappa, A.; Carezzi, G.; Colombo, A.; Contursi, C.; Di Lisa, F.; Dondio, G.; Gagliardi, S.; Milanese, E.; Minucci, S.; Pain, G.; Pelicci, P. G.; Saccani, A.; Storto, M.; Thaler, F.; Varasi, M.; Villa, M.; Plyte, S. Cinnamic Anilides as New Mitochondrial Permeability Transition Pore Inhibitors Endowed with Ischemia-Reperfusion Injury Protective Effect in Vivo. *J. Med. Chem.* **2014**, 57 (12), 5333–5347. <https://doi.org/10.1021/jm500547c>.
- (104) Algieri, V.; Algieri, C.; Maiuolo, L.; De Nino, A.; Pagliarani, A.; Tallarida, M. A.; Trombetti, F.; Nesci, S. 1,5-Disubstituted-1,2,3-Triazoles as Inhibitors of the Mitochondrial Ca²⁺-Activated F₁FO₁(Hydrolyase) and the Permeability Transition Pore. *Ann. N. Y. Acad. Sci.* **2021**, 1485 (1), 43–55. <https://doi.org/10.1111/nyas.14474>.
- (105) Neginskaya, M. A.; Solesio, M. E.; Berezhnaya, E. V.; Amodeo, G. F.; Mnatsakanyan, N.; Jonas, E. A.; Pavlov, E. V. ATP Synthase C-Subunit-Deficient Mitochondria Have a Small Cyclosporine A-Sensitive Channel, but Lack the Permeability Transition Pore. *Cell Rep.* **2019**, 26 (1), 11–17.e2. <https://doi.org/10.1016/j.celrep.2018.12.033>.
- (106) Bauer, T. M.; Murphy, E. Role of Mitochondrial Calcium and the Permeability Transition Pore in Regulating Cell Death. *Circ. Res.* **2020**, 280–293. <https://doi.org/10.1161/CIRCRESAHA.119.316306>.
- (107) Izzo, V.; Bravo-San Pedro, J. M.; Sica, V.; Kroemer, G.; Galluzzi, L. Mitochondrial Permeability Transition: New Findings and Persisting Uncertainties. *Trends Cell Biol.* **2016**, 26 (9), 655–667. <https://doi.org/10.1016/j.tcb.2016.04.006>.
- (108) Karch, J.; Bround, M. J.; Khalil, H.; Sargent, M. A.; Latchman, N.; Terada, N.; Peixoto, P. M.; Molkentin, J. D. Inhibition of Mitochondrial Permeability Transition by Deletion of the ANT Family and CypD. *Sci. Adv.* **2019**, 5 (8), 1–8. <https://doi.org/10.1126/sciadv.aaw4597>.
- (109) Urbani, A.; Giorgio, V.; Carrer, A.; Franchin, C.; Arrigoni, G.; Jiko, C.; Abe, K.; Maeda, S.; Shinzawa-Itoh, K.; Bogers, J. F. M.; McMillan, D. G. G.; Gerle, C.; Szabò, I.; Bernardi, P. Purified F₁-ATP Synthase Forms a Ca²⁺-Dependent High-Conductance Channel Matching the Mitochondrial Permeability Transition Pore. *Nat. Commun.* **2019**, 10 (1), 1–11. <https://doi.org/10.1038/s41467-019-12331-1>.
- (110) Mnatsakanyan, N.; Llaguno, M. C.; Yang, Y.; Yan, Y.; Weber, J.; Sigworth, F. J.; Jonas, E. A. A

- Mitochondrial Megachannel Resides in Monomeric F1FO ATP Synthase. *Nat. Commun.* **2019**, *10* (1). <https://doi.org/10.1038/s41467-019-13766-2>.
- (111) Pinke, G.; Zhou, L.; Sazanov, L. A. Cryo-EM Structure of the Entire Mammalian F-Type ATP Synthase. *Nat. Struct. Mol. Biol.* **2020**, *27* (11), 1077–1085. <https://doi.org/10.1038/s41594-020-0503-8>.
- (112) Orriss, G. L.; Leslie, A. G. W.; Braig, K.; Walker, J. E. Bovine F1-ATPase Covalently Inhibited with 4-Chloro-7-Nitrobenzofurazan: The Structure Provides Further Support for a Rotary Catalytic Mechanism. *Structure* **1998**, *6* (7), 831–837. [https://doi.org/10.1016/S0969-2126\(98\)00085-9](https://doi.org/10.1016/S0969-2126(98)00085-9).
- (113) Gledhill, J. R.; Montgomery, M. G.; Leslie, A. G. W.; Walker, J. E. Mechanism of Inhibition of Bovine F1-ATPase by Resveratrol and Related Polyphenols. *Proc. Natl. Acad. Sci. U. S. A.* **2007**, *104* (34), 13632–13637. <https://doi.org/10.1073/pnas.0706290104>.
- (114) Bowler, M. W.; Montgomery, M. G.; Leslie, A. G. W.; Walker, J. E. How Azide Inhibits ATP Hydrolysis by the F-ATPases. *Proc. Natl. Acad. Sci. U. S. A.* **2006**, *103* (23), 8646–8649. <https://doi.org/10.1073/pnas.0602915103>.
- (115) Riordan, J. F.; Sokolovsky, M.; Vallee, B. L. Tetranitromethane. A Reagent for the Nitration of Tyrosine and Tyrosyl Residues of Proteins. *J. Am. Chem. Soc.* **1966**, *88* (17), 4104–4105.
- (116) Rubattu, S.; Di Castro, S.; Schulz, H.; Geurts, A. M.; Cotugno, M.; Bianchi, F.; Maatz, H.; Hummel, O.; Falak, S.; Stanzione, R.; Marchitti, S.; Scarpino, S.; Giusti, B.; Kura, A.; Gensini, G. F.; Peyvandi, F.; Mannucci, P. M.; Rasura, M.; Sciarretta, S.; Dwinell, M. R.; Hubner, N.; Volpe, M. Ndufc2 Gene Inhibition Is Associated with Mitochondrial Dysfunction and Increased Stroke Susceptibility in an Animal Model of Complex Human Disease. *J. Am. Heart Assoc.* **2016**, *5* (2), 1–25. <https://doi.org/10.1161/JAHA.115.002701>.
- (117) Volpe, M.; Iaccarino, G.; Vecchione, C.; Rizzoni, D.; Russo, R.; Rubattu, S.; Condorelli, G.; Ganten, U.; Ganten, D.; Trimarco, B.; Lindpaintner, K. Association and Cosegregation of Stroke with Impaired Endothelium- Dependent Vasorelaxation in Stroke Prone, Spontaneously Hypertensive Rats. *J. Clin. Invest.* **1996**, *98* (2), 256–261. <https://doi.org/10.1172/JCI118787>.
- (118) Berthet, M.; Cheviet, T.; Dujardin, G.; Parrot, I.; Martinez, J. Isoxazolidine: A Privileged Scaffold for Organic and Medicinal Chemistry. *Chem. Rev.* **2016**, *116* (24), 15235–15283. <https://doi.org/10.1021/acs.chemrev.6b00543>.
- (119) Fleisch, H.; Graham, R.; Russel, G.; Francis, M. D. Diphosphonates Inhibit Hydroxyapatite Dissolution in Vitro and Bone Resorption in Tissue Culture and in Vivo. *Science (80-.)*. **1969**, *165* (3899), 1262–1264. <https://doi.org/10.1126/science.165.3899.1264>.
- (120) Coxon, F. P.; Thompson, K.; Roelofs, A. J.; Ebetino, F. H.; Rogers, M. J. Visualizing Mineral Binding and Uptake of Bisphosphonate by Osteoclasts and Non-Resorbing Cells. *Bone* **2008**, *42* (5), 848–860. <https://doi.org/10.1016/j.bone.2007.12.225>.
- (121) Hughes, D. E.; Wright, K. R.; Uy, H. L.; Sasaki, A.; Yoneda, T.; Roodman, D. G.; Mundy, G. R.; Boyce, B. F. Bisphosphonates Promote Apoptosis in Murine Osteoclasts in Vitro and in Vivo. *J. Bone Miner. Res.* **1995**, *10* (10), 1478–1487. <https://doi.org/10.1002/jbmr.5650101008>.
- (122) Rogers, M. J.; Frith, J. C.; Luckman, S. P.; Coxon, F. P.; Benford, H. L.; Mönkkönen, J.; Auriola, S.; Chilton, K. M.; Russell, R. G. G. Molecular Mechanisms of Action of Bisphosphonates. *Bone* **1999**, *24* (5 SUPPL.), 73S-79S. [https://doi.org/10.1016/S8756-3282\(99\)00070-8](https://doi.org/10.1016/S8756-3282(99)00070-8).
- (123) Kavanagh, K. L.; Guo, K.; Dunford, J. E.; Wu, X.; Knapp, S.; Ebetino, F. H.; Rogers, M. J.; Russell, R. G. G.; Oppermann, U. The Molecular Mechanism of Nitrogen-Containing Bisphosphonates as Antiosteoporosis Drugs. *Proc. Natl. Acad. Sci. U. S. A.* **2006**, *103* (20), 7829–7834. <https://doi.org/10.1073/pnas.0601643103>.
- (124) Russell, R. G. G.; Watts, N. B.; Ebetino, F. H.; Rogers, M. J. Mechanisms of Action of Bisphosphonates: Similarities and Differences and Their Potential Influence on Clinical Efficacy. *Osteoporos. Int.* **2008**, *19* (6), 733–759. <https://doi.org/10.1007/s00198-007-0540-8>.
- (125) Juarez, D.; Fruman, D. A. Targeting the Mevalonate Pathway in Cancer. *Trends in Cancer* **2021**, *7* (6), 525–540. <https://doi.org/10.1016/j.trecan.2020.11.008>.
- (126) Roskoski, R. Protein Prenylation: A Pivotal Posttranslational Process. *Biochem. Biophys. Res. Commun.* **2003**, *303* (1), 1–7. [https://doi.org/10.1016/S0006-291X\(03\)00323-1](https://doi.org/10.1016/S0006-291X(03)00323-1).
- (127) Mönkkönen, H.; Auriola, S.; Lehenkari, P.; Kellinsalmi, M.; Hassinen, I. E.; Vepsäläinen, J.; Mönkkönen, J. A New Endogenous ATP Analog (Apppl) Inhibits the Mitochondrial Adenine Nucleotide Translocase (ANT) and Is Responsible for the Apoptosis Induced by Nitrogen-Containing Bisphosphonates. *Br. J. Pharmacol.* **2006**, *147* (4), 437–445. <https://doi.org/10.1038/sj.bjp.0706628>.
- (128) Clézardin, P. Bisphosphonates' Antitumor Activity: An Unravelling Side of a Multifaceted Drug Class. *Bone* **2011**, *48* (1), 71–79. <https://doi.org/10.1016/j.bone.2010.07.016>.
- (129) Gnant, M.; Clézardin, P. Direct and Indirect Anticancer Activity of Bisphosphonates: A Brief Review of Published Literature. *Cancer Treat. Rev.* **2012**, *38* (5), 407–415.

- <https://doi.org/10.1016/j.ctrv.2011.09.003>.
- (130) Agabiti, S. S.; Li, J.; Wiemer, A. J. Geranylgeranyl Diphosphate Synthase Inhibition Induces Apoptosis That Is Dependent upon GGPP Depletion, ERK Phosphorylation and Caspase Activation. *Cell Death Dis.* **2017**, *8* (3), 1–12. <https://doi.org/10.1038/cddis.2017.101>.
- (131) Tkach, V.; Bock, E.; Berezin, V. The Role of RhoA in the Regulation of Cell Morphology and Motility. *Cell Motil. Cytoskeleton* **2005**, *61* (1), 21–33. <https://doi.org/10.1002/cm.20062>.
- (132) Zhang, Y. L.; Wang, R. C.; Cheng, K.; Ring, B. Z.; Su, L. Roles of Rap1 Signaling in Tumor Cell Migration and Invasion. *Cancer Biol. Med.* **2017**, *14* (1), 90–99. <https://doi.org/10.20892/j.issn.2095-3941.2016.0086>.
- (133) Mack, N. A.; Whalley, H. J.; Castillo-Lluva, S.; Malliri, A. The Diverse Roles of Rac Signaling in Tumorigenesis. *Cell Cycle* **2011**, *10* (10), 1571–1581. <https://doi.org/10.4161/cc.10.10.15612>.
- (134) Rondeau, J. M.; Bitsch, F.; Bourcier, E.; Geiser, M.; Hemmig, R.; Kroemer, M.; Lehmann, S.; Ramage, P.; Rieffel, S.; Strauss, A.; Green, J. R.; Jahnke, W. Structural Basis for the Exceptional in Vivo Efficacy of Bisphosphonate Drugs. *ChemMedChem* **2006**, *1* (2), 267–273. <https://doi.org/10.1002/cmdc.200500059>.
- (135) Gabelli, S. B.; McLellan, J. S.; Montalvetti, A.; Oldfield, E.; Docampo, R.; Amzel, L. M. Structure and Mechanism of the Farnesyl Diphosphate Synthase from *Trypanosoma Cruzi*: Implications for Drug Design. *Proteins Struct. Funct. Genet.* **2006**, *62* (1), 80–88. <https://doi.org/10.1002/prot.20754>.
- (136) Hosfield, D. J.; Zhang, Y.; Dougan, D. R.; Broun, A.; Tari, L. W.; Swanson, R. V.; Finn, J. Structural Basis for Bisphosphonate-Mediated Inhibition of Isoprenoid Biosynthesis. *J. Biol. Chem.* **2004**, *279* (10), 8526–8529. <https://doi.org/10.1074/jbc.C300511200>.
- (137) Tarshis, L. C.; Sacchettini, J. C.; Yan, M.; Poulter, C. D. Crystal Structure of Recombinant Farnesyl Diphosphate Synthase at 2.6-Å Resolution. *Biochemistry* **1994**, *33* (36), 10871–10877. <https://doi.org/10.1021/bi00202a004>.
- (138) Poulter, C. D.; Rilling, H. C. Prenyltransferase: The Mechanism of the Reaction. **1980**, *15* (5), 1079–1083.
- (139) Dunford, J. E.; Kwaasi, A. A.; Rogers, M. J.; Barnett, B. L.; Ebetino, F. H.; Russell, R. G. G.; Oppermann, U.; Kavanagh, K. L. Structure-Activity Relationships among the Nitrogen Containing Bisphosphonates in Clinical Use and Other Analogues: Time-Dependent Inhibition of Human Farnesyl Pyrophosphate Synthase. *J. Med. Chem.* **2008**, *51* (7), 2187–2195. <https://doi.org/10.1021/jm7015733>.
- (140) Luckman, S. P.; Coxon, F. P.; Ebetino, F. H.; Russell, R. G. G.; Rogers, M. J. Heterocycle-Containing Bisphosphonates Cause Apoptosis and Inhibit Bone Resorption by Preventing Protein Prenylation: Evidence from Structure- Activity Relationships in J774 Macrophages. *J. Bone Miner. Res.* **1998**, *13* (11), 1668–1678. <https://doi.org/10.1359/jbmr.1998.13.11.1668>.
- (141) Ebetino, F. H.; Hogan, A. M. L.; Sun, S.; Tsoumpra, M. K.; Duan, X.; Triffitt, J. T.; Kwaasi, A. A.; Dunford, J. E.; Barnett, B. L.; Oppermann, U.; Lundy, M. W.; Boyde, A.; Kashemirov, B. A.; McKenna, C. E.; Russell, R. G. G. The Relationship between the Chemistry and Biological Activity of the Bisphosphonates. *Bone* **2011**, *49* (1), 20–33. <https://doi.org/10.1016/j.bone.2011.03.774>.
- (142) Singh, A. P.; Zhang, Y.; No, J. H.; Docampo, R.; Nussenzweig, V.; Oldfield, E. Lipophilic Bisphosphonates Are Potent Inhibitors of Plasmodium Liver-Stage Growth. *Antimicrob. Agents Chemother.* **2010**, *54* (7), 2987–2993. <https://doi.org/10.1128/AAC.00198-10>.
- (143) Zhang, Y.; Cao, R.; Yin, F.; Lin, F. Y.; Wang, H.; Krysiak, K.; No, J. H.; Mukkamala, D.; Houlihan, K.; Li, J.; Morita, C. T.; Oldfield, E. Lipophilic Pyridinium Bisphosphonates: Potent $\gamma\delta$ t Cell Stimulators. *Angew. Chemie - Int. Ed.* **2010**, *49* (6), 1136–1138. <https://doi.org/10.1002/anie.200905933>.
- (144) Malwal, S. R.; Chen, L.; Hicks, H.; Qu, F.; Liu, W.; Shillo, A.; Law, W. X.; Zhang, J.; Chandnani, N.; Han, X.; Zheng, Y.; Chen, C. C.; Guo, R. T.; Abdelkhalik, A.; Seleem, M. N.; Oldfield, E. Discovery of Lipophilic Bisphosphonates That Target Bacterial Cell Wall and Quinone Biosynthesis. *J. Med. Chem.* **2019**, *62* (5), 2564–2581. <https://doi.org/10.1021/acs.jmedchem.8b01878>.
- (145) Sanders, J. M.; Gómez, A. O.; Mao, J.; Meints, G. A.; Van Brussel, E. M.; Burzynska, A.; Kafarski, P.; González-Pacanowska, D.; Oldfield, E. 3-D QSAR Investigations of the Inhibition of Leishmania Major Farnesyl Pyrophosphate Synthase by Bisphosphonates. *J. Med. Chem.* **2003**, *46* (24), 5171–5183. <https://doi.org/10.1021/jm0302344>.
- (146) Shannon, J.; Shannon, J.; Modelevsky, S.; Grippo, A. A. Bisphosphonates and Osteonecrosis of the Jaw. *J. Am. Geriatr. Soc.* **2011**, *59* (12), 2350–2355. <https://doi.org/10.1111/j.1532-5415.2011.03713.x>.
- (147) Molvik, H.; Khan, W. Bisphosphonates and Their Influence on Fracture Healing: A Systematic Review. *Osteoporos. Int.* **2015**, *26* (4), 1251–1260. <https://doi.org/10.1007/s00198-014-3007-8>.

- (148) Eastell, R.; Hannon, R. A. Biomarkers of Bone Health and Osteoporosis Risk. *Proc. Nutr. Soc.* **2008**, *67* (2), 157–162. <https://doi.org/10.1017/S002966510800699X>.
- (149) Russell, L. A. Osteoporosis and Orthopedic Surgery: Effect of Bone Health on Total Joint Arthroplasty Outcome. *Curr. Rheumatol. Rep.* **2013**, *15* (11). <https://doi.org/10.1007/s11926-013-0371-x>.
- (150) Saunders, Y.; Ross, J. R.; Broadley, K. E.; Edmonds, P. M.; Patel, S.; A'Hern, R.; Chinn, R.; Dearnaley, D.; Dowsett, M.; Evans, S.; Feuer, D.; Hardy, J.; Johnston, S.; Normand, C.; Powles, T.; Wonderling, D. Systematic Review of Bisphosphonates for Hypercalcaemia of Malignancy. *Palliat. Med.* **2004**, *18* (5), 418–431. <https://doi.org/10.1191/0269216304pm914ra>.
- (151) Singh, T.; Kaur, V.; Kumar, M.; Kaur, P.; Murthy, R. S. R.; Rawal, R. K. The Critical Role of Bisphosphonates to Target Bone Cancer Metastasis: An Overview. *J. Drug Target.* **2015**, *23* (1), 1–15. <https://doi.org/10.3109/1061186X.2014.950668>.
- (152) Reid, I. R.; Hosking, D. J. Bisphosphonates in Paget's Disease. *Bone* **2011**, *49* (1), 89–94. <https://doi.org/10.1016/j.bone.2010.09.002>.
- (153) Brenner, A. I.; Koshy, J.; Morey, J.; Lin, C.; Dipocce, J. The Bone Scan. *Semin. Nucl. Med.* **2012**, *42* (1), 11–26. <https://doi.org/10.1053/j.semnuclmed.2011.07.005>.
- (154) Seton, M.; Krane, S. M. Use of Zoledronic Acid in the Treatment of Paget's Disease. *Ther. Clin. Risk Manag.* **2007**, *3* (5), 913–918.
- (155) Kieczkowski, G. R.; Jobson, R. B.; Melillo, D. G.; Reinhold, D. F.; Grenda, V. J.; Shinkai, I. Preparation of (4-Amino-1-Hydroxybutylidene)Bisphosphonic Acid Sodium Salt, MK-217 (Alendronate Sodium). An Improved Procedure for the Preparation of 1-Hydroxy-1,1-Bisphosphonic Acids. *J. Org. Chem.* **1995**, *60*, 8310–8312.
- (156) Migianu-Griffoni, E.; Chebbi, I.; Kachbi, S.; Monteil, M.; Sainte-Catherine, O.; Chaubet, F.; Oudar, O.; Lecouvey, M. Synthesis and Biological Evaluation of New Bisphosphonate-Dextran Conjugates Targeting Breast Primary Tumor. *Bioconjug. Chem.* **2014**, *25* (2), 224–230. <https://doi.org/10.1021/bc400317h>.
- (157) Xu, G.; Xie, Y.; Wu, X. A Facile and Direct Synthesis of Alendronate from Pyrrolidone. *Org. Prep. Proced. Int.* **2004**, *36*, 185–187.
- (158) Mustafa, D. A.; Kashemirov, B. A.; McKenna, C. E. Microwave-Assisted Synthesis of Nitrogen-Containing 1-Hydroxymethylbisphosphonate Drugs. *Tetrahedron Lett.* **2011**, *52* (18), 2285–2287. <https://doi.org/10.1016/j.tetlet.2011.02.058>.
- (159) Keglevich, G.; Grün, A.; Garadnay, S.; Greiner, I. Rational Synthesis of Dronic Acid Derivatives. *Phosphorus, Sulfur Silicon Relat. Elem.* **2015**, *190* (12), 2116–2124. <https://doi.org/10.1080/10426507.2015.1072194>.
- (160) Lecouvey, M.; Mallard, I.; Bailly, T.; Burgada, R.; Leroux, Y. A Mild and Efficient One-Pot Synthesis of 1-Hydroxymethylene-1,1-Bisphosphonic Acids. Preparation of New Tripod Ligands. *Tetrahedron Lett.* **2001**, *42* (48), 8475–8478. [https://doi.org/10.1016/S0040-4039\(01\)01844-5](https://doi.org/10.1016/S0040-4039(01)01844-5).
- (161) Mizrahi, D. M.; Waner, T.; Segall, Y. α -Amino Acid Derived Bisphosphonates. Synthesis and Anti-Resorptive Activity. *Phosphorus, Sulfur Silicon Relat. Elem.* **2001**, *173* (November 2012), 1–25.
- (162) Bhushan, K. R.; Tanaka, E.; Frangioni, J. V. Synthesis of Conjugatable Bisphosphonates for Molecular Imaging of Large Animals. *Angew. Chemie - Int. Ed.* **2007**, *46* (42), 7969–7971. <https://doi.org/10.1002/anie.200701216>.
- (163) Vachal, P.; Hale, J. J.; Lu, Z.; Streckfuss, E. C.; Mills, S. G.; MacCoss, M.; Yin, D. H.; Algayer, K.; Manser, K.; Kesiosoglou, F.; Ghosh, S.; Alani, L. L. Synthesis and Study of Alendronate Derivatives as Potential Prodrugs of Alendronate Sodium for the Treatment of Low Bone Density and Osteoporosis. *J. Med. Chem.* **2006**, *49* (11), 3060–3063. <https://doi.org/10.1021/jm060398v>.
- (164) Lolli, M. L.; Rolando, B.; Tosco, P.; Chaurasia, S.; Stilo, A. Di; Lazzarato, L.; Gorassini, E.; Ferracini, R.; Oliaro-Bosso, S.; Fruttero, R.; Gasco, A. Synthesis and Preliminary Pharmacological Characterisation of a New Class of Nitrogen-Containing Bisphosphonates (N-BPs). *Bioorganic Med. Chem.* **2010**, *18* (7), 2428–2438. <https://doi.org/10.1016/j.bmc.2010.02.058>.
- (165) Egorov, M.; Aoun, S.; Padrines, M.; Redini, F.; Heymann, D.; Lebreton, J.; Mathé-Allainmat, M. A One-Pot Synthesis of 1-Hydroxy-1,1-Bis(Phosphonic Acid)s Starting from the Corresponding Carboxylic Acids. *European J. Org. Chem.* **2011**, No. 35, 7148–7154. <https://doi.org/10.1002/ejoc.201101094>.
- (166) Lolli, M. L.; Lazzarato, L.; Di Stilo, A.; Fruttero, R.; Gasco, A. Michael Addition of Grignard Reagents to Tetraethyl Ethenylidenebisphosphonate. *J. Organomet. Chem.* **2002**, *650* (1–2), 77–83. [https://doi.org/10.1016/S0022-328X\(02\)01179-8](https://doi.org/10.1016/S0022-328X(02)01179-8).
- (167) Houghton, T. J.; Tanaka, K. S. E.; Kang, T.; Dietrich, E.; Lafontaine, Y.; Delorme, D.; Ferreira, S. S.; Viens, F.; Arhin, F. F.; Sarmiento, I.; Lehoux, D.; Fadhil, I.; Laquerre, K.; Liu, J.; Ostiguy, V.; Poirier, H.; Moeck, G.; Parr, T. R.; Far, A. R. Linking Bisphosphonates to the Free Amino Groups in

- Fluoroquinolones: Preparation of Osteotropic Prodrugs for the Prevention of Osteomyelitis. *J. Med. Chem.* **2008**, *51* (21), 6955–6969. <https://doi.org/10.1021/jm801007z>.
- (168) Simoni, D.; Gebbia, N.; Invidiata, F. P.; Eleopra, M.; Marchetti, P.; Rondanin, R.; Baruchello, R.; Provera, S.; Marchioro, C.; Tolomeo, M.; Marinelli, L.; Limongelli, V.; Novellino, E.; Kwaasi, A.; Dunford, J.; Buccheri, S.; Caccamo, N.; Dieli, F. Design, Synthesis, and Biological Evaluation of Novel Aminobisphosphonates Possessing an in Vivo Antitumor Activity through a $\Gamma\delta$ -T Lymphocytes-Mediated Activation Mechanism. *J. Med. Chem.* **2008**, *51* (21), 6800–6807. <https://doi.org/10.1021/jm801003y>.
- (169) Valentijn, A. R. P. M.; van den Berg, O.; van der Marel, G. A.; Cohen, L. H.; van Boom, J. H. Synthesis of Pyrophosphonic Acid Analogues of Farnesyl Pyrophosphate. *Tetrahedron* **1995**, *51* (7), 2099–2108. [https://doi.org/10.1016/0040-4020\(94\)01083-C](https://doi.org/10.1016/0040-4020(94)01083-C).
- (170) Beck, J.; Gharbi, S.; Herteg-Fernea, A.; Vercheval, L.; Bebrone, C.; Lassaux, P.; Zervosen, A.; Marchand-Brynaert, J. Aminophosphonic Acids and Aminobis(Phosphonic Acids) as Potential Inhibitors of Penicillin-Binding Proteins. *European J. Org. Chem.* **2009**, No. 1, 85–97. <https://doi.org/10.1002/ejoc.200800812>.
- (171) Giguere, R. J.; Bray, T. L.; Duncan, S. M.; Majetich, G. Application of Commercial Microwave Ovens to Organic Synthesis. *Tetrahedron Lett.* **1986**, *27* (41), 4945–4948.
- (172) Gedye, R.; Smith, R.; Westaway, K.; Ali, H.; Baldisera, L.; Laberge, L.; Rousell, J. The Use of Microwave Ovens for Rapid Organic Synthesis. *Tetrahedron Lett.* **1986**, *27* (3), 279–282. [https://doi.org/10.1016/S0040-4039\(00\)83996-9](https://doi.org/10.1016/S0040-4039(00)83996-9).
- (173) de la Hoz, A.; Díaz-Ortiz, À.; Moreno, A. Microwaves in Organic Synthesis. Thermal and Non-Thermal Microwave Effects. *Chem. Soc. Rev.* **2005**, *34* (2), 164–178. <https://doi.org/10.1039/b411438h>.
- (174) Martina, K.; Cravotto, G.; Varma, R. S. Impact of Microwaves on Organic Synthesis and Strategies toward Flow Processes and Scaling Up. *J. Org. Chem.* **2021**, *86* (20), 13857–13872. <https://doi.org/10.1021/acs.joc.1c00865>.
- (175) Sweygens, N.; Alewaters, N.; Dewil, R.; Appels, L. Microwave Effects in the Dilute Acid Hydrolysis of Cellulose to 5-Hydroxymethylfurfural. *Sci. Rep.* **2018**, *8* (1), 1–11. <https://doi.org/10.1038/s41598-018-26107-y>.
- (176) Haque, E.; Khan, N. A.; Park, H. J.; Jhung, S. H. Synthesis of a Metal-Organic Framework Material, Iron Terephthalate, by Ultrasound, Microwave, and Conventional Electric Heating: A Kinetic Study. *Chem. - A Eur. J.* **2010**, *16* (3), 1046–1052. <https://doi.org/10.1002/chem.200902382>.
- (177) Bougrin, K.; Loupy, A.; Soufiaoui, M. Microwave-Assisted Solvent-Free Heterocyclic Synthesis. *J. Photochem. Photobiol. C Photochem. Rev.* **2005**, *6* (2–3), 139–167. <https://doi.org/10.1016/j.jphotochemrev.2005.07.001>.
- (178) Rai, K. M. L. Heterocycles via Oxime Cycloadditions. In *Synthesis of Heterocycles via Cycloadditions II. Topics in Heterocyclic Chemistry, vol 13*; Springer: Berlin, Heidelberg, 2008; pp 1–69. https://doi.org/10.1007/7081_2008_112.
- (179) Namboothiri, I. N. N.; Rastogi, N. Isoxazolines from Nitro Compounds: Synthesis and Applications. In *Isoxazolines from Nitro Compounds: Synthesis and Applications. In: Hassner, A. (eds) Synthesis of Heterocycles via Cycloadditions I. Topics in Heterocyclic Chemistry, vol 12*; Springer: Berlin, Heidelberg, 2008; pp 1–44. https://doi.org/10.1007/7081_2007_101.
- (180) Andrade, M. M.; Barros, M. T.; Pinto, R. C. Exploiting Microwave-Assisted Neat Procedures: Synthesis of N-Aryl and N-Alkyl nitrones and Their Cycloaddition En Route for Isoxazolidines. *Tetrahedron* **2008**, *64* (46), 10521–10530. <https://doi.org/10.1016/j.tet.2008.08.101>.
- (181) Dugovič, B.; Fišera, L.; Hametner, C.; Prónayová, N. Diastereoselectivity of Nitron 1,3-Dipolar Cycloaddition to Baylis-Hillman Adducts. *Arkivoc* **2003**, *2003* (14), 162–169. <https://doi.org/10.3998/ark.5550190.0004.e15>.
- (182) Blanáriková, I.; Dugovic, B.; Fišera, L.; Hametner, C.; Prónayová, N. 1,3-Dipolar Cycloadditions of D-Erythrose- and D-Threose-Derived Nitrones to Maleimides. *Arkivoc* **2001**, *2001* (2), 109–121. <https://doi.org/10.3998/ark.5550190.0002.213>.
- (183) Ondruš, V.; Orság, M.; Fišera, L.; Prónayová, N. Stereoselectivity of N-Benzyl-C-Ethoxycarbonyl Nitron Cycloaddition to (S)-5-Hydroxymethyl-2(5H)-Furanone and Its Derivatives. *Tetrahedron* **1999**, *55* (34), 10425–10436. [https://doi.org/10.1016/S0040-4020\(99\)00568-2](https://doi.org/10.1016/S0040-4020(99)00568-2).
- (184) Maiuolo, L.; Merino, P.; Algieri, V.; Nardi, M.; Di Gioia, M. L.; Russo, B.; Delso, I.; Tallarida, M. A.; De Nino, A. Nitrones and Nucleobase-Containing Spiro-Isoxazolidines Derived from Isatin and Indanone: Solvent-Free Microwave-Assisted Stereoselective Synthesis and Theoretical Calculations. *RSC Adv.* **2017**, *7* (77), 48980–48988. <https://doi.org/10.1039/c7ra09995a>.
- (185) Maiuolo, L.; Algieri, V.; Russo, B.; Tallarida, M. A.; Nardi, M.; Gioia, M. L. Di; Merchant, Z.; Merino, P.; Delso, I.; Nino, A. De. Synthesis, Biological and in Silico Evaluation of Pure Nucleobase-Containing Spiro (Indane-Isoxazolidine) Derivatives as Potential Inhibitors of MDM2-P53

- Interaction. *Molecules* **2019**, *24* (16), 1–14. <https://doi.org/10.3390/molecules24162909>.
- (186) Chiacchio, U.; Corsaro, A.; Iannazzo, D.; Piperno, A.; Romeo, G.; Romeo, R.; Saita, M. G.; Rescifina, A. Synthesis of Methyleneisoxazolidine Nucleoside Analogues by Microwave-Assisted Nitronene Cycloaddition. *European J. Org. Chem.* **2007**, No. 28, 4758–4764. <https://doi.org/10.1002/ejoc.200700171>.
- (187) Gotkowska, J.; Balzarini, J.; Piotrowska, D. G. Synthesis of Novel Isoxazolidine Analogues of Homonucleosides. *Tetrahedron Lett.* **2012**, *53* (52), 7097–7100. <https://doi.org/10.1016/j.tetlet.2012.10.074>.
- (188) Kim, J. N.; Lee, H. J.; Lee, C. K.; Kim, H. S. Synthesis and Structure Identification of Some 5-(Alkoxyiminomethyl)Uracil Derivatives. *Korean J. Med. Chem.* **1997**, *7* (1), 55–62. <https://doi.org/10.1021/ol8022193>.
- (189) Bortolini, O.; Nino, A. De; Eliseo, T.; Gavioli, R.; Maiuolo, L.; Russo, B.; Sforza, F. Synthesis and Biological Evaluation of Diastereoisomerically Pure N,O-Nucleosides. *Bioorganic Med. Chem.* **2010**, *18* (19), 6970–6976. <https://doi.org/10.1016/j.bmc.2010.08.024>.
- (190) Malhotra, S.; Balwani, S.; Dhawan, A.; Raunak, Kumar, Y.; Singh, B. K.; Olsen, C. E.; Prasad, A. K.; Parmar, V. S.; Ghosh, B. Design, Synthesis and Biological Activity Evaluation of Regioisomeric Spiro-(Indoline-Isoxazolidines) in the Inhibition of TNF- α -Induced ICAM-1 Expression on Human Endothelial Cells. *Medchemcomm* **2012**, *3* (12), 1536–1547. <https://doi.org/10.1039/c2md20216f>.
- (191) Chakraborty, B.; Sharma, P. K.; Rai, N.; Sharma, C. D. Solvent-Free One-Pot 1,3-Dipolar Cycloaddition Reactions of Dihydropyran Derived Nitronene. *J. Chem. Sci.* **2012**, *124* (3), 679–685. <https://doi.org/10.1007/s12039-011-0207-z>.
- (192) Richard, M.; Chapleur, Y.; Pellegrini-Moïse, N. Spiro Sugar-Isoxazolidine Scaffold as Useful Polyfunctional Building Block for Peptidomimetics Design. *Carbohydr. Res.* **2016**, *422*, 24–33. <https://doi.org/10.1016/j.carres.2016.01.005>.
- (193) Chiacchio, U.; Rescifina, A.; Saita, M. G.; Iannazzo, D.; Romeo, G.; Mates, J. A.; Tejero, T.; Merino, P. Zinc(II) Triflate-Controlled 1,3-Dipolar Cycloadditions of C-(2-Thiazolyl)Nitronenes: Application to the Synthesis of a Novel Isoxazolidinyl Analogue of Tiazofurin. *J. Org. Chem.* **2005**, *70* (22), 8991–9001. <https://doi.org/10.1021/jo051572a>.
- (194) Bortolini, O.; D'Agostino, M.; De Nino, A.; Maiuolo, L.; Nardi, M.; Sindona, G. Solvent-Free, Microwave Assisted 1,3-Cycloaddition of Nitronenes with Vinyl Nucleobases for the Synthesis of N,O-Nucleosides. *Tetrahedron* **2008**, *64* (35), 8078–8081. <https://doi.org/10.1016/j.tet.2008.06.074>.
- (195) Chiacchio, M. A.; Borrello, L.; Di Pasquale, G.; Pollicino, A.; Bottino, F. A.; Rescifina, A. Synthesis of Functionalized Polyhedral Oligomeric Silsesquioxane (POSS) Macromers by Microwave Assisted 1,3-Dipolar Cycloaddition. *Tetrahedron* **2005**, *61* (33), 7986–7993. <https://doi.org/10.1016/j.tet.2005.06.006>.
- (196) Taillefumier, C.; Enderlin, G.; Chapleur, Y. Cycloaddition of Nitronenes and Nitrile Oxides to Activated Exo-Glycols. *Lett. Org. Chem.* **2005**, *2* (3), 226–230.
- (197) Cheng, Q.; Zhang, W.; Tagami, Y.; Oritani, T. Microwave-Induced 1,3-Dipolar Intramolecular Cycloadditions of N-Substituted Oximes, Nitronenes, and Azomethine Ylides for the Chiral Synthesis of Functionalized Nitrogen Heterocycles. *J. Chem. Soc. Perkin 1* **2001**, No. 4, 452–456. <https://doi.org/10.1039/b006000n>.
- (198) Singh, S.; Ishar, M. P. S.; Singh, G.; Singh, R. Efficient, Microwave-Assisted Intramolecular 1,3-Dipolar Cycloadditions of Oximes and N-Methylnitronenes Derived from o-Alkenylmethoxy-Acetophenones. *Can. J. Chem.* **2005**, *83* (3), 260–265. <https://doi.org/10.1139/v05-049>.
- (199) Zanolini, A.; Brandi, A.; De Meijere, A. A New Three-Component Cascade Reaction to Yield 3-Spirocyclopropanated β -Lactams. *European J. Org. Chem.* **2006**, No. 5, 1251–1255. <https://doi.org/10.1002/ejoc.200500838>.
- (200) Dhameliya, T. M.; Chudasma, S. J.; Patel, T. M.; Dave, B. P. A Review on Synthetic Account of 1,2,4-Oxadiazoles as Anti-Infective Agents. *Mol. Divers.* **2022**, No. 0123456789. <https://doi.org/10.1007/s11030-021-10375-4>.
- (201) Bokach, N. A.; Kukushkin, V. Y. 1,3-Dipolar Cycloaddition of Nitronenes to Free and Coordinated Nitriles: Routes to Control the Synthesis of 2,3-Dihydro-1,2,4-Oxadiazoles. *Russ. Chem. Bull.* **2006**, *55* (11), 1869–1882. <https://doi.org/10.1007/s11172-006-0528-0>.
- (202) Charmier, M. A. J.; Kukushkin, V. Y.; Pombeiro, A. J. L. Microwave-Assisted [2 + 3] Cycloaddition of Nitronenes to Platinum-(II) and -(IV) Bound Organonitriles. *Dalt. Trans.* **2003**, No. 12, 2540–2543. <https://doi.org/10.1039/b301892j>.
- (203) Desai, B.; Danks, T. N.; Wagner, G. Cycloaddition of Nitronenes to Free and Coordinated (E)-Cinnamonitrile: Effect of Metal Coordination and Microwave Irradiation on the Selectivity of the Reaction. *Dalt. Trans.* **2003**, *2* (12), 2544–2549. <https://doi.org/10.1039/b302086j>.

- (204) Sharma, V.; Kalia, R.; Raj, T.; Gupta, V. K.; Suri, N.; Saxena, A. K.; Sharma, D.; Bhella, S. S.; Singh, G.; Ishar, M. P. S. Synthesis and Cytotoxic Evaluation of Substituted 3-(3'-Indolyl-/3'-Pyridyl)-Isoxazolidines and Bis-Indoles. *Acta Pharm. Sin. B* **2012**, *2* (1), 32–41. <https://doi.org/10.1016/j.apsb.2011.12.009>.
- (205) Bortolini, O.; Mulani, I.; De Nino, A.; Maiuolo, L.; Nardi, M.; Russo, B.; Avnet, S. Efficient Synthesis of Isoxazolidine-Substituted Bisphosphonates by 1,3-Dipolar Cycloaddition Reactions. *Tetrahedron* **2011**, *67* (31), 5635–5641. <https://doi.org/10.1016/j.tet.2011.05.098>.
- (206) Bortolini, O.; Mulani, I.; De Nino, A.; Maiuolo, L.; Melicchio, A.; Russo, B.; Granchi, D. Synthesis of a Novel Class of Gem-Phosphonate-Phosphates by Reductive Cleavage of the Isoxazolidine Ring. *Curr. Org. Synth.* **2014**, *11* (3), 461–465. <https://doi.org/10.2174/15701794113109990061>.
- (207) Piperno, A.; Giofrè, S. V.; Iannazzo, D.; Romeo, R.; Romeo, G.; Chiacchio, U.; Rescifina, A.; Piotrowska, D. G. Synthesis of C-4' Truncated Phosphonated Carbocyclic 2'-Oxa-3'-Azanucleosides as Antiviral Agents. *J. Org. Chem.* **2010**, *75* (9), 2798–2805.
- (208) Shimizu, T.; Ishizaki, M.; Nitada, N. The Effects of Lewis Acid on the 1,3-Dipolar Cycloaddition Reaction of C-Arylaldonitrone with Alkenes. *Chem. Pharm. Bull* **2002**, *50* (7), 908–921.
- (209) Kröhnke, F. Über Enol-Betaine (I. Mitteil.). *Berichte der Dtsch. Chem. Gesellschaft (A B Ser.)* **1935**, *68* (6), 1177–1195. <https://doi.org/10.1002/cber.19350680637>.
- (210) Kakehi, A. Reactions of Pyridinium N-Ylides and Their Related Pyridinium Salts. *Heterocycles* **2012**, *85* (7), 1529–1577. <https://doi.org/10.3987/REV-12-735>.
- (211) Sowmiah, S.; Esperança, J. M. S. S.; Rebelo, L. P. N.; Afonso, C. A. M. Pyridinium Salts: From Synthesis to Reactivity and Applications. *Org. Chem. Front.* **2018**, *5* (3), 453–493. <https://doi.org/10.1039/c7qo00836h>.
- (212) Tomashenko, O. A.; Khlebnikov, A. F.; Mosiagin, I. P.; Novikov, M. S.; Grachova, E. V.; Shakirova, J. R.; Tunik, S. P. A New Heterocyclic Skeleton with Highly Tunable Absorption/Emission Wavelength via H-Bonding. *RSC Adv.* **2015**, *5* (115), 94551–94561. <https://doi.org/10.1039/c5ra17755c>.
- (213) Galenko, E. E.; Tomashenko, O. A.; Khlebnikov, A. F.; Novikov, M. S. Metal/Organo Relay Catalysis in a One-Pot Synthesis of Methyl 4-Aminopyrrole-2-Carboxylates from 5-Methoxyisoxazoles and Pyridinium Ylides. *Org. Biomol. Chem.* **2015**, *13* (38), 9825–9833. <https://doi.org/10.1039/c5ob01537e>.
- (214) Funt, L. D.; Novikov, M. S.; Starova, G. L.; Khlebnikov, A. F. Synthesis and Properties of New Heterocyclic Betaines: 4-Aryl-5-(Methoxycarbonyl)-2-Oxo-3-(Pyridin-1-ylm-1-yl)-2,3-Dihydro-1H-Pyrrol-3-Ides. *Tetrahedron* **2018**, *74* (20), 2466–2474. <https://doi.org/10.1016/j.tet.2018.03.071>.
- (215) Funt, L. D.; Tomashenko, O. A.; Novikov, M. S.; Khlebnikov, A. F. An Azirine Strategy for the Synthesis of Alkyl 4-Amino-5-(Trifluoromethyl)-1 H -Pyrrole-2-Carboxylates. *Synth.* **2018**, *50* (24), 4809–4822. <https://doi.org/10.1055/s-0037-1610840>.
- (216) Funt, L. D.; Tomashenko, O. A.; Khlebnikov, A. F.; Novikov, M. S.; Ivanov, A. Y. Synthesis, Transformations of Pyrrole- and 1,2,4-Triazole-Containing Ensembles, and Generation of Pyrrole-Substituted Triazole NHC. *J. Org. Chem.* **2016**, *81* (22), 11210–11221. <https://doi.org/10.1021/acs.joc.6b02200>.
- (217) Funt, L. D.; Tomashenko, O. A.; Mosiagin, I. P.; Novikov, M. S.; Khlebnikov, A. F. Synthesis of Pyrrolotriazoloisoquinoline Frameworks by Intramolecular Cu-Mediated or Free Radical Arylation of Triazoles. *J. Org. Chem.* **2017**, *82* (14), 7583–7594. <https://doi.org/10.1021/acs.joc.7b01341>.
- (218) Kucukdisli, M.; Opatz, T. A Modular Synthesis of Polysubstituted Indolizines. *European J. Org. Chem.* **2012**, No. 24, 4555–4564. <https://doi.org/10.1002/ejoc.201200424>.
- (219) Belguedj, R.; Bouraiou, A.; Bouacida, S.; Merazig, H.; Chibani, A. Pyridinium Ylides in the One-Pot Synthesis of a New Quinoline/Indolizine Hybrid. *Zeitschrift fur Naturforsch. - Sect. B J. Chem. Sci.* **2015**, *70* (12), 885–887. <https://doi.org/10.1515/znb-2015-0118>.
- (220) Gao, T.; Chen, X.; Jiang, L.; Wu, M.; Guo, H.; Wang, J.; Sun, S.; Oiler, J.; Xing, Y. General and Direct Synthesis of Indolizine-1-Carbaldehydes by 1,3-Dipolar Cycloaddition of Phenylpropionaldehyde with Pyridinium Ylides. *European J. Org. Chem.* **2016**, *2016* (29), 4957–4960. <https://doi.org/10.1002/ejoc.201600945>.
- (221) Georgescu, E.; Dumitriascu, F.; Georgescu, F.; Draghici, C.; Barbu, L. A Novel Approach for the Synthesis of 5-Pyridylindolizine Derivatives via 2-(2-Pyridyl)Pyridinium Ylides. *J. Heterocycl. Chem.* **2013**, *50*, 78–82. <https://doi.org/10.1002/jhet>.
- (222) Liu, J.; Yan, P.; Li, Y.; Zhou, Z.; Ye, W.; Yao, J.; Wang, C. Iodine-Promoted Synthesis of Acylindolizine Derivatives from Acetylenecarboxylates and Pyridinium, Isoquinolinium, or Quinolinium Ylides. *Monatshfte fur Chemie* **2014**, *145* (4), 617–625. <https://doi.org/10.1007/s00706-013-1120-6>.
- (223) Yavari, I.; Ghafouri, K.; Naeimabadi, M.; Halvagar, M. R. A Synthesis of Functionalized 2-Indolizin-

- 3-Yl-1,3-Benzothiazoles from 1-(1,3-Benzothiazol-2-Ylmethyl)Pyridinium Iodide and Acetylenic Esters. *Synlett* **2018**, 29 (2), 243–245. <https://doi.org/10.1055/s-0036-1590910>.
- (224) Douglas, T.; Pordea, A.; Dowden, J. Iron-Catalyzed Indolizine Synthesis from Pyridines, Diazo Compounds, and Alkynes. *Org. Lett.* **2017**, 19 (23), 6396–6399. <https://doi.org/10.1021/acs.orglett.7b03252>.
- (225) Briocche, J.; Meyer, C.; Cossy, J. Synthesis of 2-Aminoindolizines by 1,3-Dipolar Cycloaddition of Pyridinium Ylides with Electron-Deficient Ynamides. *Org. Lett.* **2015**, 17 (11), 2800–2803. <https://doi.org/10.1021/acs.orglett.5b01205>.
- (226) Berger, R.; Wagner, M.; Feng, X.; Müllen, K. Polycyclic Aromatic Azomethine Ylides: A Unique Entry to Extended Polycyclic Heteroaromatics. *Chem. Sci.* **2015**, 6 (1), 436–441. <https://doi.org/10.1039/c4sc02793k>.
- (227) Motornov, V. A.; Tabolin, A. A.; Nelyubina, Y. V.; Nenajdenko, V. G.; Ioffe, S. L. Copper-Mediated Oxidative [3 + 2]-Annulation of Nitroalkenes and Pyridinium Ylides: General Access to Functionalized Indolizines and Efficient Synthesis of 1-Fluoroindolizines. *Org. Biomol. Chem.* **2019**, 17 (6), 1442–1454. <https://doi.org/10.1039/C8OB03126F>.
- (228) Luo, N.; Li, M.; Wang, T.; Li, Y.; Wang, C. Highly Efficient Synthesis of 1-Nitroindolizine Derivatives via the DBU/Acetic Acid System. *ChemistrySelect* **2019**, 4 (37), 11121–11124. <https://doi.org/10.1002/slct.201902621>.
- (229) Allgäuer, D. S.; Mayr, H. One-Pot Two-Step Synthesis of 1-(Ethoxycarbonyl)Indolizines via Pyridinium Ylides. *European J. Org. Chem.* **2013**, No. 28, 6379–6388. <https://doi.org/10.1002/ejoc.201300784>.
- (230) Abaszadeh, M.; Seifi, M. Ultrasound-Assisted 1,3-Dipolar Cycloaddition and Cyclopropanation Reactions for the Synthesis of Bis-Indolizine and Bis-Cyclopropane Derivatives. *Org. Biomol. Chem.* **2014**, 12 (39), 7859–7863. <https://doi.org/10.1039/c4ob01305k>.
- (231) Hu, H.; Feng, J.; Zhu, Y.; Gu, N.; Kan, Y. Copper Acetate Monohydrate: A Cheap but Efficient Oxidant for Synthesizing Multi-Substituted Indolizines from Pyridinium Ylides and Electron Deficient Alkenes. *RSC Adv.* **2012**, 2 (23), 8637–8644. <https://doi.org/10.1039/c2ra21213g>.
- (232) Dontsova, N. E.; Nesterov, V. N.; Shestopalov, A. M. Effect of Solvent Nature on the Regioselectivity of the Reactions of Pyridinium Ylides with E-1,2-Di(Alkylsulfonyl)-1,2-Dichloroethene. from the Reaction of 1,3-Dipolar Cycloaddition to the Reaction of Nucleophilic Addition-Elimination (AdN-E1,5). *Tetrahedron* **2013**, 69 (24), 5016–5021. <https://doi.org/10.1016/j.tet.2013.03.098>.
- (233) Ramesh, V.; Devi, N. S.; Velusamy, M.; Shanmugam, S. Catalyst Free Synthesis of Highly Functionalized Indolizines from In Situ Generated Pyridinium Ylides via One-Pot Multicomponent Reaction. *ChemistrySelect* **2019**, 4 (13), 3717–3721. <https://doi.org/10.1002/slct.201900665>.
- (234) An, J.; Yang, Q. Q.; Wang, Q.; Xiao, W. J. Direct Synthesis of Pyrrolo[2,1-a]Isoquinolines by 1,3-Dipolar Cycloaddition of Stabilized Isoquinolinium N-Ylides with Vinyl Sulfonium Salts. *Tetrahedron Lett.* **2013**, 54 (29), 3834–3837. <https://doi.org/10.1016/j.tetlet.2013.05.053>.
- (235) Zhang, Q.; Wang, B.; Ma, H.; Ablajan, K. Transition-Metal-Free Catalyzed [3+2] Cycloadditions/Oxidative Aromatization Reactions for the Synthesis of Annulated Indolizines. *New J. Chem.* **2019**, 43 (43), 17000–17003. <https://doi.org/10.1039/c9nj03076j>.
- (236) Liu, R.; Wang, X.; Sun, J.; Yan, C. G. A Facile Synthesis of Tricyclic Skeleton of Alkaloid 261C by Double [3+2] Cycloaddition of Pyridinium Ylide. *Tetrahedron Lett.* **2015**, 56 (48), 6711–6714. <https://doi.org/10.1016/j.tetlet.2015.10.049>.
- (237) Day, J.; McKeever-Abbas, B.; Dowden, J. Stereoselective Synthesis of Tetrahydroindolizines through the Catalytic Formation of Pyridinium Ylides from Diazo Compounds. *Angew. Chemie - Int. Ed.* **2016**, 55 (19), 5809–5813. <https://doi.org/10.1002/anie.201511047>.
- (238) Dawood, K. M.; Elamin, M. B.; Farag, A. M. Microwave-Assisted Synthesis of Arylated Pyrrolo[2,1-a]Isoquinoline Derivatives via Sequential [3 + 2] Cycloadditions and Suzuki-Miyaura Cross-Couplings in Aqueous Medium. *J. Heterocycl. Chem.* **2015**, 53 (6), 1928–1934. <https://doi.org/10.1002/jhet.2508>.
- (239) Liu, Y.; Hu, H.; Zhou, J.; Wang, W.; He, Y.; Wang, C. Application of Primary Halogenated Hydrocarbons for the Synthesis of 3-Aryl and 3-Alkyl Indolizines. *Org. Biomol. Chem.* **2017**, 15 (23), 5016–5024. <https://doi.org/10.1039/c7ob00980a>.
- (240) Shi, F.; Zhang, Y.; Lu, Z.; Zhu, X.; Kan, W.; Wang, X.; Hu, H. Transition-Metal-Free Synthesis of Indolizines from Electron-Deficient Alkenes via One-Pot Reaction Using TEMPO as an Oxidant. *Synth.* **2016**, 48 (3), 413–420. <https://doi.org/10.1055/s-0035-1560973>.
- (241) Tan, C.; Yan, P.; Ye, W.; Yao, J.; Wu, W.; Wang, C. Iodine-Promoted Synthesis of 1-Alkyl-3-Aroylindolizines from N-(Aroylmethyl)Pyridinium Salts and Aliphatic Aldehydes. *Heteroat. Chem.* **2013**, 25 (1), 72–81. <https://doi.org/10.1002/hc.21137>.
- (242) Krishnan, J.; Vedhanarayanan, B.; Sasidhar, B. S.; Varughese, S.; Nair, V. NHC-Mediated Synthesis

- of Pyrrolo[2,1-a]Isoquinolines and Their Photophysical Investigations. *Chem. - An Asian J.* **2017**, *12* (6), 623–627. <https://doi.org/10.1002/asia.201601683>.
- (243) Shu, W. M.; He, J. X.; Zhang, X. F.; Wang, S.; Wu, A. X. TFA-Mediated DMSO-Participant Sequential Oxidation/1,3-Dipolar Cycloaddition Cascade of Pyridinium Ylides for the Assembly of Indolizines. *J. Org. Chem.* **2019**, *84* (5), 2962–2968. <https://doi.org/10.1021/acs.joc.8b02755>.
- (244) Tokimaru, Y.; Ito, S.; Nozaki, K. Synthesis of Pyrrole-Fused Corannulenes: 1,3-Dipolar Cycloaddition of Azomethine Ylides to Corannulene. *Angew. Chemie - Int. Ed.* **2017**, *56* (49), 15560–15564. <https://doi.org/10.1002/anie.201707087>.
- (245) Sun, J.; Wang, F.; Hu, H.; Wang, X.; Wu, H.; Liu, Y. Copper(II)-Catalyzed Carbon-Carbon Triple Bond Cleavage of Internal Alkynes for the Synthesis of Annulated Indolizines. *J. Org. Chem.* **2014**, *79* (9), 3992–3998. <https://doi.org/10.1021/jo500456d>.
- (246) Wang, F.; Shen, Y.; Hu, H.; Wang, X.; Wu, H.; Liu, Y. Copper(II)-Catalyzed Indolizines Formation Followed by Dehydrogenative Functionalization Cascade to Synthesize 1-Bromoindolizines. *J. Org. Chem.* **2014**, *79* (20), 9556–9566. <https://doi.org/10.1021/jo501626b>.
- (247) Xu, J.; Hu, H.; Liu, Y.; Wang, X.; Kan, Y.; Wang, C. Four-Component Reaction for the Synthesis of Indolizines by Copper-Catalyzed Aerobic Oxidative Dehydrogenative Aromatization. *European J. Org. Chem.* **2017**, *2017* (2), 257–261. <https://doi.org/10.1002/ejoc.201601272>.
- (248) Wang, W.; Han, J.; Sun, J.; Liu, Y. CuBr-Catalyzed Aerobic Decarboxylative Cycloaddition for the Synthesis of Indolizines under Solvent-Free Conditions. *J. Org. Chem.* **2017**, *82* (6), 2835–2842. <https://doi.org/10.1021/acs.joc.6b02455>.
- (249) Yavari, I.; Naeimabadi, M.; Halvagar, M. R. FeCl₃-Catalyzed Formation of Indolizine Derivatives via the 1,3-Dipolar Cycloaddition Reaction between Azomethine Ylides and Chalcones or Dibenzylideneacetones. *Tetrahedron Lett.* **2016**, *57* (33), 3718–3721. <https://doi.org/10.1016/j.tetlet.2016.07.004>.
- (250) Singh, G. S.; Mmatli, E. E. Recent Progress in Synthesis and Bioactivity Studies of Indolizines. *Eur. J. Med. Chem.* **2011**, *46* (11), 5237–5257. <https://doi.org/10.1016/j.ejmech.2011.08.042>.
- (251) Sharma, V.; Kumar, V. Indolizine: A Biologically Active Moiety. *Med. Chem. Res.* **2014**, *23* (8), 3593–3606. <https://doi.org/10.1007/s00044-014-0940-1>.
- (252) Dawood, K. M.; Abbas, A. A. Inhibitory Activities of Indolizine Derivatives: A Patent Review. *Expert Opin. Ther. Pat.* **2020**, *0* (0). <https://doi.org/10.1080/13543776.2020.1798402>.
- (253) Shrivastava, S. K.; Srivastava, P.; Bandresh, R.; Tripathi, P. N.; Tripathi, A. Design, Synthesis, and Biological Evaluation of Some Novel Indolizine Derivatives as Dual Cyclooxygenase and Lipoxygenase Inhibitor for Anti-Inflammatory Activity. *Bioorganic Med. Chem.* **2017**, *25* (16), 4424–4432. <https://doi.org/10.1016/j.bmc.2017.06.027>.
- (254) Darwish, E. S. Facile Synthesis of Heterocycles via 2-Picolinium Bromide and Antimicrobial Activities of the Products. *Molecules* **2008**, *13* (5), 1066–1078. <https://doi.org/10.3390/molecules13051066>.
- (255) Lepesheva, G. I.; Waterman, M. R. Sterol 14 α -Demethylase Cytochrome P450 (CYP51), a P450 in All Biological Kingdoms. *Biochim. Biophys. Acta - Gen. Subj.* **2007**, *1770* (3), 467–477. <https://doi.org/10.1016/j.bbagen.2006.07.018>.
- (256) Nasir, A. I.; Gundersen, L. L.; Rise, F.; Antonsen, Ø.; Kristensen, T.; Langhelle, B.; Bast, A.; Custers, I.; Haenen, G. R. M. M.; Wikström, H. Inhibition of Lipid Peroxidation Mediated by Indolizines. *Bioorganic Med. Chem. Lett.* **1998**, *8* (14), 1829–1832. [https://doi.org/10.1016/S0960-894X\(98\)00313-8](https://doi.org/10.1016/S0960-894X(98)00313-8).
- (257) Weide, T.; Arve, L.; Prinz, H.; Waldmann, H.; Kessler, H. 3-Substituted Indolizine-1-Carbonitrile Derivatives as Phosphatase Inhibitors. *Bioorganic Med. Chem. Lett.* **2006**, *16* (1), 59–63. <https://doi.org/10.1016/j.bmcl.2005.09.051>.
- (258) Huang, W.; Zuo, T.; Luo, X.; Jin, H.; Liu, Z.; Yang, Z.; Yu, X.; Zhang, L.; Zhang, L. Indolizine Derivatives as HIV-1 VIF-ElonginC Interaction Inhibitors. *Chem. Biol. Drug Des.* **2013**, *81* (6), 730–741. <https://doi.org/10.1111/cbdd.12119>.
- (259) Maartens, G.; Celum, C.; Lewin, S. R. HIV Infection: Epidemiology, Pathogenesis, Treatment, and Prevention. *Lancet* **2014**, *384* (9939), 258–271. [https://doi.org/10.1016/S0140-6736\(14\)60164-1](https://doi.org/10.1016/S0140-6736(14)60164-1).
- (260) Zhou, H.; Danger, D. P.; Dock, S. T.; Hawley, L.; Roller, S. G.; Smith, C. D.; Handlon, A. L. Synthesis and SAR of Benzisothiazole- and Indolizine- β -D-Glucopyranoside Inhibitors of SGLT2. *ACS Med. Chem. Lett.* **2010**, *1* (1), 19–23. <https://doi.org/10.1021/ml900010b>.
- (261) Kim, N. D.; Park, E. S.; Kim, Y. H.; Moon, S. K.; Lee, S. S.; Ahn, S. K.; Yu, D. Y.; No, K. T.; Kim, K. H. Structure-Based Virtual Screening of Novel Tubulin Inhibitors and Their Characterization as Anti-Mitotic Agents. *Bioorganic Med. Chem.* **2010**, *18* (19), 7092–7100. <https://doi.org/10.1016/j.bmc.2010.07.072>.
- (262) Moon, S. H.; Jung, Y.; Kim, S. H.; Kim, I. Synthesis, Characterization and Biological Evaluation of

- Anti-Cancer Indolizine Derivatives via Inhibiting β -Catenin Activity and Activating P53. *Bioorganic Med. Chem. Lett.* **2016**, *26* (1), 110–113. <https://doi.org/10.1016/j.bmcl.2015.11.021>.
- (263) O’Conor, C. J.; Chen, T.; González, I.; Cao, D.; Peng, Y. Cancer Stem Cells in Triple-Negative Breast Cancer: A Potential Target and Prognostic Marker. *Biomark. Med.* **2018**, *12* (7), 813–820. <https://doi.org/10.2217/bmm-2017-0398>.
- (264) Wang, B.; Zhang, X.; Li, J.; Jiang, X.; Hu, Y.; Hua, H. Preparation of Indolizine-3-Carboxamides and Indolizine-3-Carbonitriles by 1, 3-Dipolar Cycloaddition of 7V-(Cyanomethyl)Pyridinium Ylides to Alkenes in the Presence of Tetrakispyridinecobalt(n) Dichromate or Manganese(IV) Oxide. *J. Chem. Soc. - Perkin Trans. 1* **1999**, No. 11, 1571–1579. <https://doi.org/10.1039/a809581g>.
- (265) Dawood, K. M.; Ragab, E. A.; Khedr, N. A. Facile Access to Benzothiazole-Containing Pyrrolo[1,2-a]Quinolines and Pyrrolo[2,1-a]Isoquinolines via Nitrogen Ylides. *J. Chinese Chem. Soc.* **2009**, *56* (6), 1180–1185. <https://doi.org/10.1002/jccs.200900170>.
- (266) Joshi, D. R.; Kim, I. Regioselective Synthesis of 1-Cyano-3-Arylindolizines: Construction of Pyrroles via DDQ-Mediated Ring Closure of Cyclopropyl Pyridines. *Adv. Synth. Catal.* **2022**, 3016–3022. <https://doi.org/10.1002/adsc.202200590>.
- (267) Chandrasekhar, S.; Sumithra, G.; Yadav, J. S. Deprotection of Mono and Dimethoxy Phenyl Methyl Ethers Using Catalytic Amounts of DDQ. *Tetrahedron Lett.* **1996**, *37* (10), 1645–1646. [https://doi.org/10.1016/0040-4039\(96\)00081-0](https://doi.org/10.1016/0040-4039(96)00081-0).
- (268) Liu, L.; Floreancig, P. E. 2,3-Dichloro-5,6-Dicyano-1,4-Benzoquinone-Catalyzed Reactions Employing MnO₂ as a Stoichiometric Oxidant. *Org. Lett.* **2010**, *12* (20), 4686–4689. <https://doi.org/10.1021/ol102078v>.
- (269) Yi, H.; Liu, Q.; Liu, J.; Zeng, Z.; Yang, Y.; Lei, A. DDQ-Catalyzed Oxidative C–O Coupling of Sp³ C–H Bonds with Carboxylic Acids. *ChemSusChem* **2012**, *5* (11), 2143–2146. <https://doi.org/10.1002/cssc.201200458>.
- (270) Baek, J.; Je, E. K.; Kim, J.; Qi, A.; Ahn, K. H.; Kim, Y. Experimental and Theoretical Studies on the Mechanism of DDQ-Mediated Oxidative Cyclization of N-Aroylhydrazones. *J. Org. Chem.* **2020**, *85* (15), 9727–9736. <https://doi.org/10.1021/acs.joc.0c00937>.
- (271) Talele, T. T. The “Cyclopropyl Fragment” Is a Versatile Player That Frequently Appears in Preclinical/Clinical Drug Molecules. *J. Med. Chem.* **2016**, *59* (19), 8712–8756. <https://doi.org/10.1021/acs.jmedchem.6b00472>.
- (272) Lovering, F.; Bikker, J.; Humblet, C. Escape from Flatland: Increasing Saturation as an Approach to Improving Clinical Success. *J. Med. Chem.* **2009**, *52* (21), 6752–6756. <https://doi.org/10.1021/jm901241e>.
- (273) Hiesinger, K.; Dar’In, D.; Proschak, E.; Krasavin, M. Spirocyclic Scaffolds in Medicinal Chemistry. *J. Med. Chem.* **2021**, *64* (1), 150–183. <https://doi.org/10.1021/acs.jmedchem.0c01473>.
- (274) Khetmalis, Y. M.; Shivani, M.; Murugesan, S.; Chandra Sekhar, K. V. G. Oxindole and Its Derivatives: A Review on Recent Progress in Biological Activities. *Biomed. Pharmacother.* **2021**, *141* (June), 111842. <https://doi.org/10.1016/j.biopha.2021.111842>.
- (275) Cao, Z. Y.; Zhou, J. Catalytic Asymmetric Synthesis of Polysubstituted Spirocyclopropyl Oxindoles: Organocatalysis versus Transition Metal Catalysis. *Org. Chem. Front.* **2015**, *2* (7), 849–858. <https://doi.org/10.1039/c5qo00092k>.
- (276) Moldvai, I.; Gács-Baitz, E.; Balázs, M.; Incze, M.; Szántay, C. Synthesis of Spiro[Cyclopropane-1,3’[3H]Indol]-2’(1’H)-Ones with Antihypoxic Effects. *Arch. Pharm. (Weinheim)*. **1996**, *329* (12), 541–549. <https://doi.org/10.1002/ardp.19963291206>.
- (277) Wang, L.; Cao, W.; Mei, H.; Hu, L.; Feng, X. Catalytic Asymmetric Synthesis of Chiral Spiro-Cyclopropyl Oxindoles from 3-Alkenyl-Oxindoles and Sulfoxonium Ylides. *Adv. Synth. Catal.* **2018**, *360* (21), 4089–4093. <https://doi.org/10.1002/adsc.201800937>.
- (278) Mei, H.; Pan, G.; Zhang, X.; Lin, L.; Liu, X.; Feng, X. Catalytic Asymmetric Ring-Opening/Cyclopropanation of Cyclic Sulfur Ylides: Construction of Sulfur-Containing Spirocyclopropyloxindoles with Three Vicinal Stereocenters. *Org. Lett.* **2018**, *20* (24), 7794–7797. <https://doi.org/10.1021/acs.orglett.8b03187>.
- (279) Kang, J. W.; Li, X.; Chen, F. Y.; Luo, Y.; Zhang, S. C.; Kang, B.; Peng, C.; Tian, X.; Han, B. Protecting Group-Directed Annulations of Tetra-Substituted Oxindole Olefins and Sulfur Ylides: Regio- and Chemoselective Synthesis of Cyclopropane- and Dihydrofuran-Fused Spirooxindoles. *RSC Adv.* **2019**, *9* (22), 12255–12264. <https://doi.org/10.1039/c9ra02192b>.
- (280) You, Y.; Quan, B. X.; Wang, Z. H.; Zhao, J. Q.; Yuan, W. C. Divergent Synthesis of Oxindole Derivatives: Via Controllable Reactions of Isatin-Derived Para-Quinone Methides with Sulfur Ylides. *Org. Biomol. Chem.* **2020**, *18* (24), 4560–4565. <https://doi.org/10.1039/d0ob00979b>.
- (281) Warghude, P. K.; Dharpure, P. D.; Bhat, R. G. Cycloaddition of Isatin-Derived MBH Carbonates and 3-Methyleneoxindoles to Construct Diastereoselective Cyclopentenyl Bis-Spirooxindoles and

- Cyclopropyl Spirooxindoles: Catalyst Controlled [3 + 2] and [2 + 1] Annulations. *Tetrahedron Lett.* **2018**, 59 (46), 4076–4079. <https://doi.org/10.1016/j.tetlet.2018.10.004>.
- (282) Kapure, J. S.; Reddy, C. N.; Adiyala, P. R.; Nayak, R.; Nayak, V. L.; Nanubolu, J. B.; Singarapu, K. K.; Maurya, R. A. Diastereoselective Synthesis of Spiro[Cyclopropane-1,3'-Indolin]-2'-Ones through Metal-Free Cyclopropanation Using Tosylhydrazone Salts. *RSC Adv.* **2014**, 4 (72), 38425–38432. <https://doi.org/10.1039/c4ra05755d>.
- (283) Li, T.; Duan, S.; Ding, W.; Liu, Y.; Chen, J.; Lu, L.; Xiao, W. Synthesis of CF₃-Containing 3,3'-Cyclopropyl Spirooxindoles by Sequential [3 + 2] Cycloaddition/Ring Contraction of Ylideneoxindoles with 2,2,2-Trifluorodiazoethane. *J. Org. Chem.* **2014**, 79, 2296–2302.
- (284) Pesciaoli, F.; Righi, P.; Mazzanti, A.; Bartoli, G.; Bencivenni, G. Organocatalytic Michael-Alkylation Cascade: The Enantioselective Nitrocyclopropanation of Oxindoles. *Chem. - A Eur. J.* **2011**, 17 (10), 2842–2845. <https://doi.org/10.1002/chem.201003423>.
- (285) Robertson, D. W.; Krushinski, J. H.; Pollock, G. D.; Wilson, H.; Kauffman, R. F.; Hayes, J. S. Dihydropyridazinone Cardiotonics: Synthesis and Inotropic Activity of 5'-(1,4,5,6-Tetrahydro-6-Oxo-3-Pyridazinyl)Spiro[Cycloalkane-1,3'-[3H]Indol]-2'(1'T)-Ones. *J. Med. Chem.* **1987**, 30 (5), 824–829. <https://doi.org/10.1021/jm00388a014>.
- (286) Palomba, M.; Rossi, L.; Sancineto, L.; Tramontano, E.; Corona, A.; Bagnoli, L.; Santi, C.; Pannecouque, C.; Tabarrini, O.; Marini, F. A New Vinyl Selenone-Based Domino Approach to Spirocyclopropyl Oxindoles Endowed with Anti-HIV RT Activity. *Org. Biomol. Chem.* **2016**, 14 (6), 2015–2024. <https://doi.org/10.1039/c5ob02451j>.
- (287) Zhou, M.; En, K.; Hu, Y.; Xu, Y.; Shen, H. C.; Qian, X. Zinc Triflate-Mediated Cyclopropanation of Oxindoles with Vinyl Diphenyl Sulfonium Triflate: A Mild Reaction with Broad Functional Group Compatibility. *RSC Adv.* **2017**, 7 (7), 3741–3745. <https://doi.org/10.1039/C6RA24985J>.
- (288) Qin, H.; Miao, Y.; Zhang, K.; Xu, J.; Sun, H.; Liu, W.; Feng, F.; Qu, W. A Convenient Cyclopropanation Process of Oxindoles via Bromoethylsulfonium Salt. *Tetrahedron* **2018**, 74 (47), 6809–6814. <https://doi.org/10.1016/j.tet.2018.09.042>.
- (289) Dou, X.; Lu, Y. Diastereodivergent Synthesis of 3-Spirocyclopropyl-2-Oxindoles through Direct Enantioselective Cyclopropanation of Oxindoles. *Chem. - A Eur. J.* **2012**, 18 (27), 8315–8319. <https://doi.org/10.1002/chem.201200655>.
- (290) Dou, X.; Yao, W.; Zhou, B.; Lu, Y. Asymmetric Synthesis of 3-Spirocyclopropyl-2-Oxindoles via Intramolecular Trapping of Chiral Aza-Ortho-Xylylene. *Chem. Commun.* **2013**, 49 (80), 9224–9226. <https://doi.org/10.1039/c3cc45369c>.
- (291) Ošek, M.; Noole, A.; Žari, S.; Öeren, M.; Järving, I.; Lopp, M.; Kanger, T. Asymmetric Diastereoselective Synthesis of Spirocyclopropane Derivatives of Oxindole. *European J. Org. Chem.* **2014**, 2014 (17), 3599–3606. <https://doi.org/10.1002/ejoc.201402061>.
- (292) Noole, A.; Ošek, M.; Pehk, T.; Öeren, M.; Järving, I.; Elsegood, M. R. J.; Malkov, A. V.; Lopp, M.; Kanger, T. 3-Chlorooxindoles: Versatile Starting Materials for Asymmetric Organocatalytic Synthesis of Spirooxindoles. *Adv. Synth. Catal.* **2013**, 355 (5), 829–835. <https://doi.org/10.1002/adsc.201300019>.
- (293) Zhang, J. R.; Jin, H. S.; Sun, J.; Wang, J.; Zhao, L. M. Time-Economical Synthesis of Bis-Spiro Cyclopropanes via Cascade 1,6-Conjugate Addition/Dearomatization Reaction of Para-Quinone Methides with 3-Chlorooxindoles. *European J. Org. Chem.* **2020**, 2020 (31), 4988–4994. <https://doi.org/10.1002/ejoc.202000830>.
- (294) Ding, R.; Wolf, C. Organocatalytic Asymmetric Synthesis of α -Oxetanyl and α -Azetidyl Tertiary Alkyl Fluorides and Chlorides. *Org. Lett.* **2018**, 20 (3), 892–895. <https://doi.org/10.1021/acs.orglett.8b00039>.
- (295) Chen, L.; He, J. DABCO-Catalyzed Michael/Alkylation Cascade Reactions Involving α -Substituted Ammonium Ylides for the Construction of Spirocyclopropyl Oxindoles: Access to the Powerful Chemical Leads against HIV-1. *J. Org. Chem.* **2020**, 85 (8), 5203–5219. <https://doi.org/10.1021/acs.joc.9b03164>.
- (296) Cao, Z. Y.; Zhou, F.; Yu, Y. H.; Zhou, J. A Highly Diastereo- and Enantioselective Hg(II)-Catalyzed Cyclopropanation of Diazoindoles and Alkenes. *Org. Lett.* **2013**, 15 (1), 42–45. <https://doi.org/10.1021/ol302998m>.
- (297) Cao, Z. Y.; Wang, X.; Tan, C.; Zhao, X. L.; Zhou, J.; Ding, K. Highly Stereoselective Olefin Cyclopropanation of Diazoindoles Catalyzed by a C₂-Symmetric Spiroketal Bisphosphine/Au(I) Complex. *J. Am. Chem. Soc.* **2013**, 135 (22), 8197–8200. <https://doi.org/10.1021/ja4040895>.
- (298) Tone, M.; Nakagawa, Y.; Chanthamath, S.; Fujisawa, I.; Nakayama, N.; Goto, H.; Shibatomi, K.; Iwasa, S. Highly Stereoselective Spirocyclopropanation of Various Diazoindoles with Olefins Catalyzed Using Ru(II)-Complex. *RSC Adv.* **2018**, 8 (70), 39865–39869. <https://doi.org/10.1039/C8RA09212E>.

- (299) Karthik, G.; Rajasekaran, T.; Sridhar, B.; Reddy, B. V. S. Catalyst and Solvent-Free Cyclopropanation of Electron-Deficient Olefins with Cyclic Diazoamides for the Synthesis of Spiro[Cyclopropane-1,3'-Indolin]-2'-One Derivatives. *Tetrahedron Lett.* **2014**, *55* (51), 7064–7067. <https://doi.org/10.1016/j.tetlet.2014.10.137>.
- (300) Jiang, T.; Kuhen, K. L.; Wolff, K.; Yin, H.; Bieza, K.; Caldwell, J.; Bursulaya, B.; Tuntland, T.; Zhang, K.; Karanewsky, D.; He, Y. Design, Synthesis, and Biological Evaluations of Novel Oxindoles as HIV-1 Non-Nucleoside Reverse Transcriptase Inhibitors. Part I. *Bioorganic Med. Chem. Lett.* **2006**, *16* (8), 2105–2108. <https://doi.org/10.1016/j.bmcl.2006.01.066>.
- (301) Jiang, T.; Kuhen, K. L.; Wolff, K.; Yin, H.; Bieza, K.; Caldwell, J.; Bursulaya, B.; Wu, T. Y. H.; He, Y. Design, Synthesis, and Biological Evaluations of Novel Oxindoles as HIV-1 Non-Nucleoside Reverse Transcriptase Inhibitors. Part 2. *Bioorganic Med. Chem. Lett.* **2006**, *16* (8), 2109–2112. <https://doi.org/10.1016/j.bmcl.2006.01.073>.
- (302) Sampson, P. B.; Liu, Y.; Forrest, B.; Cumming, G.; Li, S.; Patel, N. K.; Edwards, L.; Laufer, R.; Feher, M.; Ban, F.; Awrey, D. E.; Mao, G.; Plotnikova, O.; Hodgson, R.; Beletskaya, I.; Mason, J. M.; Luo, X.; Nadeem, V.; Wei, X.; Kiarash, R.; Madeira, B.; Huang, P.; Mak, T. W.; Pan, G.; Pauls, H. W. The Discovery of Polo-Like Kinase 4 Inhibitors: Identification of (1R,2S)-2-(3-((E)-4-(((Cis)-2,6-Dimethylmorpholino)Methyl)Styryl)-1H-indazol-6-yl)-5'-Methoxyspiro[Cyclopropane-1,3'-Indolin]-2'-One (CFI-400945) as a Potent, Orally Active Antitumor Agent. *J. Med. Chem.* **2015**, *58* (1), 147–169. <https://doi.org/10.1021/jm5005336>.
- (303) Eberle, M. K.; Kahle, G. G.; Shapiro, M. J. Preparation of Spiro[Cyclopropane-1,3'-[3H]Indol]Ones from Isatin in a Novel One-Step Process. A Study of Long-Range Chiral Recognition. *J. Org. Chem.* **1982**, *47*, 2210–2212.
- (304) Qi, W. J.; Han, Y.; Yan, C. G. Diastereoselective Synthesis of Functionalized Spiro[Cyclopropane-1,3'-Indolines] and Spiro[Indoline-3,1'-Cyclopropane-2',3''-Indolines]. *Tetrahedron* **2016**, *72* (33), 5057–5063. <https://doi.org/10.1016/j.tet.2016.06.020>.
- (305) Peng, C.; Zhai, J.; Xue, M.; Xu, F. Lanthanide Amide-Catalyzed One-Pot Functionalization of Isatins: Synthesis of Spiro[Cyclopropan-1,3'-Oxindoles] and 2-Oxoindolin-3-yl Phosphates. *Org. Biomol. Chem.* **2017**, *15* (18), 3968–3974. <https://doi.org/10.1039/c7ob00640c>.
- (306) Hajra, S.; Roy, S.; Saleh, S. K. A. Domino Corey-Chaykovsky Reaction for One-Pot Access to Spirocyclopropyl Oxindoles. *Org. Lett.* **2018**, *20* (15), 4540–4544. <https://doi.org/10.1021/acs.orglett.8b01840>.
- (307) Hirano, S.; Suzuki, K. T. Exposure, Metabolism, and Toxicity of Rare Earths and Related Compounds. *Environ. Health Perspect.* **1996**, *104* (SUPPL. 1), 85–95. <https://doi.org/10.1289/ehp.96104s185>.
- (308) Nardi, M.; Di Gioia, M. L.; Costanzo, P.; De Nino, A.; Maiuolo, L.; Oliverio, M.; Olivito, F.; Procopio, A. Selective Acetylation of Small Biomolecules and Their Derivatives Catalyzed by Er(OTf)₃. *Catalysts* **2017**, *7* (9). <https://doi.org/10.3390/catal7090269>.
- (309) Maiuolo, L.; Russo, B.; Algieri, V.; Nardi, M.; Di Gioia, M. L.; Tallarida, M. A.; De Nino, A. Regioselective Synthesis of 1,5-Disubstituted 1,2,3-Triazoles by 1,3-Dipolar Cycloaddition: Role of Er(OTf)₃, Ionic Liquid and Water. *Tetrahedron Lett.* **2019**, *60* (9), 672–674. <https://doi.org/10.1016/j.tetlet.2019.01.053>.
- (310) Wedal, J. C.; Evans, W. J. A Rare-Earth Metal Retrospective to Stimulate All Fields. *J. Am. Chem. Soc.* **2021**, *143* (44), 18354–18367. <https://doi.org/10.1021/jacs.1c08288>.
- (311) Kepp, K. P. A Quantitative Scale of Oxophilicity and Thiophilicity. *Inorg. Chem.* **2016**, *55* (18), 9461–9470. <https://doi.org/10.1021/acs.inorgchem.6b01702>.
- (312) Di Bernardo, P.; Choppin, G.; Portanova, R.; Zanonato, P. L. Lanthanide(III) Trifluoromethanesulfonate Complexes in Anhydrous Acetonitrile. *Inorganica Chim. Acta* **1997**, *207* (1), 89–91. [https://doi.org/10.1016/S0020-1693\(00\)91459-2](https://doi.org/10.1016/S0020-1693(00)91459-2).
- (313) Bayer, U.; Anwander, R. Carbonyl Group and Carbon Dioxide Activation by Rare-Earth-Metal Complexes. *Dalt. Trans.* **2020**, *49* (48), 17472–17493. <https://doi.org/10.1039/d0dt03578e>.
- (314) Ryu, H.; Seo, J.; Ko, H. M. Synthesis of Spiro[Oxindole-3,2'-Pyrrolidine] Derivatives from Benzynes and Azomethine Ylides through 1,3-Dipolar Cycloaddition Reactions. *J. Org. Chem.* **2018**, *83* (22), 14102–14109. <https://doi.org/10.1021/acs.joc.8b02117>.
- (315) Boyle, T. J.; Cramer, R. E.; Fasulo, F. A.; Padilla, N. Solvation Coordination Compounds of Scandium Chloride from the Dehydration of Scandium Chloride Hexahydrate. *Polyhedron* **2021**, *208*, 115437. <https://doi.org/10.1016/j.poly.2021.115437>.
- (316) Heravi, M. M.; Zadsirjan, V. Prescribed Drugs Containing Nitrogen Heterocycles: An Overview. *RSC Adv.* **2020**, *10* (72), 44247–44311. <https://doi.org/10.1039/d0ra09198g>.
- (317) Shaikh, A. R.; Farooqui, M.; Satpute, R. H.; Abed, S. Overview on Nitrogen Containing Compounds and Their Assessment Based on 'International Regulatory Standards.' *J. Drug Deliv. Ther.* **2018**, *8* (6-s), 424–428. <https://doi.org/10.22270/jddt.v8i6-s.2156>.

- (318) Vitaku, E.; Smith, D. T.; Njardarson, J. T. Analysis of the Structural Diversity, Substitution Patterns, and Frequency of Nitrogen Heterocycles among U.S. FDA Approved Pharmaceuticals. *J. Med. Chem.* **2014**, *57* (24), 10257–10274. <https://doi.org/10.1021/jm501100b>.
- (319) Zard, S. Z. Recent Progress in the Generation and Use of Nitrogen-Centred Radicals. *Chem. Soc. Rev.* **2008**, *37* (8), 1603–1618. <https://doi.org/10.1039/b613443m>.
- (320) Minozzi, M.; Nanni, D.; Spagnolo, P. From Azides to Nitrogen-Centered Radicals: Applications of Azide Radical Chemistry to Organic Synthesis. *Chem. - A Eur. J.* **2009**, *15* (32), 7830–7840. <https://doi.org/10.1002/chem.200802710>.
- (321) Kim, S.; Joe, G. H.; Do, J. Y. Highly Efficient Intramolecular Addition of Aminyl Radicals to Carbonyl Groups: A New Ring Expansion Reaction Leading to Lactams. *J. Am. Chem. Soc.* **1993**, *115* (8), 3328–3329.
- (322) Moreno-Vargas, A. J.; Vogel, P. Regioselective Rearrangement of 7-Azabicyclo[2.2.1]Hept-2-Aminyl Radicals: First Synthesis of 2,8-Diazabicyclo[3.2.1]Oct-2-Enes and Their Conversion into 5-(2-Aminoethyl)-2,3,4-Trihydroxypyrrolidines, New Inhibitors of α -Mannosidases. *Tetrahedron Lett.* **2003**, *44* (27), 5069–5073. [https://doi.org/10.1016/S0040-4039\(03\)01141-9](https://doi.org/10.1016/S0040-4039(03)01141-9).
- (323) Kim, S.; Yeon, K. M.; Yoon, K. S. 1,5-Hydrogen Transfers from Carbon to N-Tributyltin Substituted Nitrogen. *Tetrahedron Lett.* **1997**, *38* (22), 3919–3922. [https://doi.org/10.1016/S0040-4039\(97\)00779-X](https://doi.org/10.1016/S0040-4039(97)00779-X).
- (324) Samano, M. C.; Robins, M. J. Efficient Reduction of Azides to Amines with Tributylstannane. High-Yield Syntheses of Amino and Diamino Deoxynucleosides. *Tetrahedron Lett.* **1991**, *32* (44), 6293–6296. [https://doi.org/10.1016/0040-4039\(91\)80150-5](https://doi.org/10.1016/0040-4039(91)80150-5).
- (325) Newman, S. G.; Bryan, C. S.; Perez, D.; Lautens, M. The Use of Bromotrichloromethane in Chlorination Reactions. *Synthesis (Stuttg.)*. **2011**, No. 2, 342–346. <https://doi.org/10.1055/s-0030-1258368>.
- (326) Benati, L.; Leardini, R.; Minozzi, M.; Nanni, D.; Spagnolo, P.; Strazzari, S.; Zanardi, G.; Calestani, G. Radical Chain Reactions of α -Azido Ketones with Tributyltin Hydride: Reduction vs Nitrogen Insertion and 1,2-Hydrogen Shift in the Intermediate N-Stannylaminyl Radicals. *Tetrahedron* **2002**, *58* (18), 3485–3492. [https://doi.org/10.1016/S0040-4020\(02\)00302-2](https://doi.org/10.1016/S0040-4020(02)00302-2).
- (327) Flores, M.; Díez, D. 2,8-Diheterobicyclo[32.1]Octane Ring Systems: Natural Occurrence, Synthesis and Properties. *Synlett* **2014**, *25* (12), 1643–1666. <https://doi.org/10.1055/s-0033-1339132>.
- (328) Moreno-Vargas, A. J.; Schütz, C.; Scopelliti, R.; Vogel, P. Synthesis of Enantiomerically Pure 1,2-Diamine Derivatives of 7-Azabicyclo[2.2.1]Heptane. New Leads as Glycosidase Inhibitors and Rigid Scaffolds for the Preparation of Peptide Analogues. *J. Org. Chem.* **2003**, *68* (14), 5632–5640. <https://doi.org/10.1021/jo0301088>.
- (329) Moreno-Vargas, A. J.; Robina, I.; Petricci, E.; Vogel, P. Synthesis of D- and l-2,3-Trans-3,4-Cis-4,5-Trans-3,4-Dihydroxy-5-Hydroxymethylproline and Tripeptides Containing Them. *J. Org. Chem.* **2004**, *69*, 4487–4491.
- (330) Moreno-Clavijo, E.; Moreno-Vargas, A. J.; Carmona, A. T.; Robina, I. Strain-Promoted Retro-Dieckmann-Type Condensation on [2.2.2]- and [2.2.1]Bicyclic Systems: A Fragmentation Reaction for the Preparation of Functionalized Heterocycles and Carbocycles. *Org. Biomol. Chem.* **2013**, *11* (40), 7016–7025. <https://doi.org/10.1039/c3ob41160e>.
- (331) Huisgen, R.; Ooms, P. H.; Mingin, M.; Allinger, N. L. Exceptional Reactivity of the Bicyclo[2.2.1]Heptene Double Bond. *J. Am. Chem. Soc.* **1980**, *102* (11), 3951–3953.
- (332) Trastoy, B.; Eugenia Pérez-Ojeda, M.; Sastre, R.; Chiara, J. L. Octakis(3-Azidopropyl)Octasilsesquioxane: A Versatile Nanobuilding Block for the Efficient Preparation of Highly Functionalized Cube-Octameric Polyhedral Oligosilsesquioxane Frameworks through Click Assembly. *Chem. - A Eur. J.* **2010**, *16* (12), 3833–3841. <https://doi.org/10.1002/chem.200902422>.
- (333) Zipse, H. Radical Stability: A Theoretical Perspective. *Top. Curr. Chem.* **2006**, *263*, 183–189. <https://doi.org/10.1002/chin.200650275>.
- (334) Benati, L.; Bencivenni, G.; Leardini, R.; Minozzi, M.; Nanni, D.; Scialpi, R.; Spagnolo, P.; Zanardi, G. Thermal Reactions of Tributyltin Hydride with α -Asido Esters: Unexpected Intervention of Tin Triazene Adducts under Both Nonradical and Radical Conditions. *J. Org. Chem.* **2005**, *70* (8), 3046–3053. <https://doi.org/10.1021/jo0478095>.
- (335) Pettersen, E. F.; Goddard, T. D.; Huang, C. C.; Couch, G. S.; Greenblatt, D. M.; Meng, E. C.; Ferrin, T. E. UCSF Chimera - A Visualization System for Exploratory Research and Analysis. *J. Comput. Chem.* **2004**, *25* (13), 1605–1612. <https://doi.org/10.1002/jcc.20084>.
- (336) Frisch, M. J. ; Trucks, G. W. ; Schlegel, H. B. ; Scuseria, G. E. ; Robb, M. A. ; Cheeseman, J. R. ; Scalmani, G. ; Barone, V. ; Petersson, G. A. ; Nakatsuji, H. ; Li, X. ; Caricato, M. ; Marenich, A. V. ; Bloino, J. ; Janesko, B. G. ; Gomperts, R. ; Mennucci, B. ; Hratchian, H. P. ; Ortiz, J. V. ; Izmaylov,

- A. F.; Sonnenberg, J. L. ; Williams-Young, D. ; Ding, F. ; Lipparini, F. ; Egidi, F. ; Goings, J. ; Peng, B. ; Petrone, A. ; Henderson, T. ; Ranasinghe, D.; Zakrzewski, V. G. ; Gao, J. ; Rega, N. ; Zheng, G. ; Liang, W. ; Hada, M. ; Ehara, M. ; Toyota, K. ; Fukuda, R. ; Hasegawa, J. ; Ishida, M. ; Nakajima, T. ; Honda, Y. ; Kitao, O. ; Nakai, H. ; Vreven, T. ; Throssell, K. ; Montgomery, J. A. , J. ; Peralta, J. E. ; Ogliaro, F. ; Bearpark, M. J. ; Heyd, J. J. ; Brothers, E. N. ; Kudin, K. N. ; Staroverov, V. N. ; Keith, T. A. ; Kobayashi, R. ; Normand, J. ; Raghavachari, K. ; Rendell, A. P. ; Burant, J. C. ; Iyengar, S. S. ; Tomasi, J. ; Cossi, M. ; Millam, J. M. ; Klene, M. ; Adamo, C. ; Cammi, R. ; Ochterski, J. W. ; Martin, R. L. ; Morokuma, K. ; Farkas, O. ; Foresman, J. B. ; Fox, D. J. Gaussian 16, Revision C.01. Wallingford CT 2016.
- (337) Zhao, Y.; Truhlar, D. G. The M06 Suite of Density Functionals for Main Group Thermochemistry, Thermochemical Kinetics, Noncovalent Interactions, Excited States, and Transition Elements: Two New Functionals and Systematic Testing of Four M06-Class Functionals and 12 Other Function. *Theor. Chem. Acc.* **2008**, *120* (1–3), 215–241. <https://doi.org/10.1007/s00214-007-0310-x>.
- (338) Scalmani, G.; Frisch, M. J. Continuous Surface Charge Polarizable Continuum Models of Solvation. I. General Formalism. *J. Chem. Phys.* **2010**, *132* (11). <https://doi.org/10.1063/1.3359469>.
- (339) Bortolini, O.; De Nino, A.; Garofalo, A.; Maiuolo, L.; Procopio, A.; Russo, B. Erbium Triflate in Ionic Liquids: A Recyclable System of Improving Selectivity in Diels-Alder Reactions. *Appl. Catal. A Gen.* **2010**, *372* (2), 124–129. <https://doi.org/10.1016/j.apcata.2009.10.020>.
- (340) Bortolini, O.; Nino, A. De; Garofalo, A.; Maiuolo, L.; Russo, B. Mild Oxidative Conversion of Nitroalkanes into Carbonyl Compounds in Ionic Liquids. *Synth. Commun.* **2010**, *40* (16), 2483–2487. <https://doi.org/10.1080/00397910903267921>.
- (341) Ilangovan, A.; Satish, G. Direct Amidation of 2'-Aminoacetophenones Using I2-TBHP: A Unimolecular Domino Approach toward Isatin and Iodoisatin. *J. Org. Chem.* **2014**, *79* (11), 4984–4991. <https://doi.org/10.1021/jo500550d>.
- (342) Mamuye, A. D.; Monticelli, S.; Castoldi, L.; Holzer, W.; Pace, V. Eco-Friendly Chemoselective N-Functionalization of Isatins Mediated by Supported KF in 2-MeTHF. *Green Chem.* **2015**, *17* (8), 4194–4197. <https://doi.org/10.1039/c5gc01002k>.
- (343) Buxton, C. S.; Blakemore, D. C.; Bower, J. F. Reductive Coupling of Acrylates with Ketones and Ketimines by a Nickel-Catalyzed Transfer-Hydrogenative Strategy. *Angew. Chemie - Int. Ed.* **2017**, *56* (44), 13824–13828. <https://doi.org/10.1002/anie.201707531>.
- (344) Sun, Z.; Xiang, K.; Tao, H.; Guo, L.; Li, Y. Synthesis of 2-Substituted 3-Chlorobenzofurans via TMSCl-Mediated Nucleophilic Annulation of Isatin-Derived Propargylic Alcohols. *Org. Biomol. Chem.* **2018**, *16* (33), 6133–6139. <https://doi.org/10.1039/c8ob01731j>.
- (345) Zhang, Y.; Luo, L.; Ge, J.; Yan, S. Q.; Peng, Y. X.; Liu, Y. R.; Liu, J. X.; Liu, C.; Ma, T.; Luo, H. Q. “on Water” Direct Organocatalytic Cyanoarylmethylation of Isatins for the Diastereoselective Synthesis of 3-Hydroxy-3-Cyanomethyl Oxindoles. *J. Org. Chem.* **2019**, *84* (7), 4000–4008. <https://doi.org/10.1021/acs.joc.8b03194>.
- (346) Bojack, G.; Baltz, R.; Dittgen, J.; Fischer, C.; Freigang, J.; Getachew, R.; Grill, E.; Helmke, H.; Hohmann, S.; Lange, G.; Lehr, S.; Porée, F.; Schmidt, J.; Schmutzler, D.; Yang, Z.; Frackenhohl, J. Synthesis and Exploration of Abscisic Acid Receptor Agonists Against Drought Stress by Adding Constraint to a Tetrahydroquinoline-Based Lead Structure. *European J. Org. Chem.* **2021**, *2021* (23), 3442–3457. <https://doi.org/10.1002/ejoc.202100415>.
- (347) Chai, J. Da; Head-Gordon, M. Long-Range Corrected Hybrid Density Functionals with Damped Atom-Atom Dispersion Corrections. *Phys. Chem. Chem. Phys.* **2008**, *10* (44), 6615–6620. <https://doi.org/10.1039/b810189b>.
- (348) Hay, P. J.; Wadt, W. R. Ab Initio Effective Core Potentials for Molecular Calculations. Potentials for K to Au Including the Outermost Core Orbitals. *J. Chem. Phys.* **1985**, *82* (1), 299–310. <https://doi.org/10.1063/1.448975>.
- (349) Ribeiro, R. F.; Marenich, A. V.; Cramer, C. J.; Truhlar, D. G. Use of Solution-Phase Vibrational Frequencies in Continuum Models for the Free Energy of Solvation. *J. Phys. Chem. B* **2011**, *115* (49), 14556–14562. <https://doi.org/10.1021/jp205508z>.
- (350) Li, Y. P.; Gomes, J.; Sharada, S. M.; Bell, A. T.; Head-Gordon, M. Improved Force-Field Parameters for QM/MM Simulations of the Energies of Adsorption for Molecules in Zeolites and a Free Rotor Correction to the Rigid Rotor Harmonic Oscillator Model for Adsorption Enthalpies. *J. Phys. Chem. C* **2015**, *119* (4), 1840–1850. <https://doi.org/10.1021/jp509921r>.
- (351) Hratchian, H. P.; Schlegel, H. B. Following Reaction Pathways Using a Damped Classical Trajectory Algorithm. *J. Phys. Chem. A* **2002**, *106* (1), 165–169. <https://doi.org/10.1021/jp012125b>.
- (352) Chen, Z.; Trudell, M. L. A Simplified Method for the Preparation of Ethynyl P-Tolyl Sulfone and Ethynyl Phenyl Sulfone. *Synth. Commun.* **1994**, *21*, 3149–3155. <https://doi.org/10.1080/00397919308020392>.

- (353) Eisch, J. J.; Shafii, B.; Odom, J. D.; Rheingold, A. L. Aromatic Stabilization of the Triarylborirene Ring System by Tricoordinate Boron and Facile Ring Opening with Tetracoordinate Boron1. *J. Am. Chem. Soc.* **1990**, *112* (5), 1847–1853. <https://doi.org/10.1021/ja00161a031>.
- (354) Kobayashi, T.; Uchiyama, Y. Neighboring Effect of Pyrazole Rings: Regio- and Stereoselective Wagner-Meerwein Rearrangement in Electrophilic Addition Reactions of Norbornadiene-Fused Pyrazoles. *J. Chem. Soc. Perkin Trans. 1* **2000**, No. 16, 2731–2739. <https://doi.org/10.1039/b002454f>.
- (355) Kaiser, H. P.; Muchowski, J. M. Catalytic Hydrogenation of Pyrroles at Atmospheric Pressure. *J. Org. Chem.* **1984**, *49* (22), 4203–4209. <https://doi.org/10.1021/jo00196a020>.
- (356) Gerenkamp, M.; Grimme, S. Spin-Component Scaled Second-Order Møller-Plesset Perturbation Theory for the Calculation of Molecular Geometries and Harmonic Vibrational Frequencies. *Chem. Phys. Lett.* **2004**, *392* (1–3), 229–235. <https://doi.org/10.1016/j.cplett.2004.05.063>.
- (357) Kendall, R. A.; Dunning, T. H.; Harrison, R. J. Electron Affinities of the First-Row Atoms Revisited. Systematic Basis Sets and Wave Functions. *J. Chem. Phys.* **1992**, *96* (9), 6796–6806. <https://doi.org/10.1063/1.462569>.

Experimental Section

Chapter 1: 1,2,3-triazoles: synthesis, biological activity, and docking studies

Research line 1a - Pyrimidine nucleobase-containing 1,5-disubstituted 1,2,3-triazoles: synthesis and molecular docking studies

Materials and Methods

Commercial starting materials were purchased from Merck (Milan, Italy) or Alfa Aesar (Karlsruhe, Germany) and were used without further purification. Reactions were monitored by TLC using silica plates 60-F264, commercially available from Merck (Milano, Italy). ¹H and ¹³C NMR spectra and two-dimensional NMR spectra were recorded at 300 and 500 MHz and 125.7 MHz, respectively, in DMSO-*d*₆ using tetramethylsilane (TMS) as internal standard (Bruker Avance 500 MHz with a 5 mm TBO probe, Rheinstetten, Germany). Chemical shifts are given in parts per million and coupling constants in Hertz. The purity and the regiochemistry were established by NMR spectra (¹H NMR experiments). High-resolution mass spectra (HRMS) were recorded with a Bruker Compact QTOF instrument (Bruker, Billerica, MA, USA). HRMS spectra were acquired in positive ion mode, with a mass resolution of 30000. Mass calibration was performed with a solution of sodium formate clusters and processed in HPC mode. Spectra acquisition was performed in flow injection, with a full scan mode in the range of 50 to 500 *m/z*. N₂ was the source of dry gas (*V* = 4 L/min, *T* = 180 °C). The ion formula of each compound was calculated with the Smart Formula tool of the Bruker software platform, analyzing the isotopic pattern ratio with 4 mDa mass confidence.

General procedure for nucleobases propargylation

In a three-necked round-bottomed flask, equipped with a bubble condenser and magnetic stir bar, the opportune nucleobase **189a-c** (39.6 mmol, 1 eq) in dry hexamethyldisilazane (HMDS, 139 mmol, 3.5 eq) was suspended under nitrogen atmosphere. Subsequently, trimethylsilyl chloride (8.71 mmol, 0.22 eq) and (NH₄)₂SO₄ (1.98 mmol, 0.05 eq) were added and the mixture was stirred at 145 °C for 2 h. After completion, the solution was cooled to room temperature and the HMDS was evaporated under vacuum. Then, the obtained silylated nucleobase **190a-c** was dissolved in dry acetonitrile (150 mL) without any further purification. Propargyl bromide **191** (39.6 mmol, 1 eq) was added dropwise at 80 °C for 30 min and the reaction was stirred under reflux for 12 h. After cooling to room temperature, acetonitrile was removed under vacuum and the crude was purified by silica flash chromatography (eluent mixture CHCl₃/CH₃OH 8:2) to give a solid product **192-194**.

1-propargylthymine (192). White solid, yield 92%. (CHCl₃/acetone/CH₃OH 8:1:1); ¹H NMR (300 MHz, DMSO-*d*₆): δ (ppm) = 1.76 (d, *J*=1.23 Hz, 3H; CH₃), 3.39 (t, *J*=2.50 Hz, 1H; C≡CH), 4.46 (d, *J*= 2.50 Hz, 2H; CH₂), 7.56 (d, *J*=1.23 Hz, 1H; CH), 11.38 (s, 1H; NH). ¹³C APT NMR (75 MHz, DMSO-*d*₆): δ (ppm) = 12.37, 36.77, 76.09, 79.12, 109.86, 140.57, 150.82, 164.59. HRMS (ESI): *m/z* calcd for C₈H₉N₂O₂: 165.0659 [M+H]⁺, found 165.0653; *m/z* calcd for C₈H₈N₂O₂Na: 187.0483 [M+Na]⁺, found 187.0473.

1-propargyluracil (193). White solid, yield 90%. (CHCl₃/acetone/CH₃OH 8:1:1); ¹H NMR (300 MHz, DMSO-*d*₆): δ (ppm) = 3.43 (t, *J*=2.50 Hz, 1H; C≡CH), 4.50 (d, *J*= 2.50 Hz, 2H; CH₂), 5.62 (d, *J*= 7.89 Hz, 1H; CH), 7.70 (d, *J*=7.89 Hz, 1H; CH), 11.40 (s, 1H; NH). ¹³C APT NMR (75 MHz, DMSO-*d*₆): δ (ppm) = 37.08, 76.29, 78.92, 102.16, 144.24, 150.85, 164.01. HRMS (ESI): *m/z* calcd for C₇H₆N₂O₂Na: 173.0321 [M+Na]⁺, found 173.0318.

5-fluoro-1-propargyluracil (194). White solid, yield 87%. (CHCl₃/acetone/CH₃OH 8:1:1); ¹H NMR (300 MHz, DMSO-*d*₆): δ (ppm) = 3.45 (t, *J*=2.50 Hz, 1H; C≡CH), 4.45 (d, *J*= 2.50 Hz, 2H; CH₂), 8.13 (d, *J*=6.67 Hz, 1H; CH), 11.93 (bd, *J*=4.39 Hz, 1H; NH). ¹³C APT NMR (75 MHz, DMSO-*d*₆): δ (ppm) = 37.46, 76.58, 78.58, 129.38 (d), 140.27 (d), 149.51, 157.80 (d). HRMS (ESI): *m/z* calcd for C₇H₅FN₂O₂Na: 191.0227 [M+Na]⁺, found 191.0223.

General procedure for 1,5-disubstituted 1,2,3-triazoles 198-209.

In a 50 mL two-necked round-bottomed flask, equipped with a bubble condenser and magnetic stir bar, propargyl nucleobase **192-194** (1.52 mmol, 1 eq) was dissolved in DMF (8 mL). Subsequently, FeCl₃ (0.304 mmol, 0.2 eq) and opportune azide **18, 195-197** (3.05 mmol, 2 eq) were added and the mixture was stirred at 120 °C for 8 h. DMF was removed under vacuum by generating an azeotrope with toluene, and the obtained crude solid was purified on a flash silica gel column (eluent mixture: CHCl₃/acetone/CH₃OH 8:1:1 v/v/v) to obtain the desired solid product **198-209**. The configuration of regioisomers was attributed from spectroscopic data.

1-[1-phenyl-1,2,3-triazol-5-yl-methyl]-thymine (198). White solid, yield 88%. (CHCl₃/acetone/CH₃OH 8:1:1); ¹H NMR (300 MHz, DMSO-*d*₆): δ (ppm) = 1.77 (s, 3H; CH₃), 5.00 (s, 2H; CH₂), 7.43-7.53 (m, 1H; Ar), 7.58 (t, *J*=7.83 Hz, 2H; Ar), 7.67 (s, 1H; CH), 7.89 (d, *J*=7.83 Hz, 2H; Ar), 8.79 (s, 1H, CH), 11.37 (s, 1H; NH). ¹³C APT NMR (75 MHz, DMSO-*d*₆): δ (ppm) = 12.16, 42.35, 109.21, 120.23, 121.87, 128.89, 130.04, 136.70, 141.28, 144.03, 150.96, 164.51. HRMS (ESI): *m/z* calcd for C₁₄H₁₄N₅O₂: 284.1142 [M+H]⁺, found 284.1142; *m/z* calcd for C₁₄H₁₃N₅O₂Na: 306.0967 [M+Na]⁺, found 306.0960; *m/z* calcd for C₁₄H₁₃N₅O₂K: 322.0706 [M+K]⁺, found 322.0699.

1-[1-phenyl-1,2,3-triazol-5-yl-methyl]-uracil (199). White solid, yield 90%. (CHCl₃/acetone/CH₃OH 8:1:1); ¹H NMR (300 MHz, DMSO-*d*₆): δ (ppm)= 5.04 (s, 2H; CH₂), 5.62 (d, *J*=7.80 Hz, 1H; CH), 7.43-7.54 (m, 1H; Ar), 7.54-7.67 (m, 2H; Ar), 7.80 (d, *J*=7.80 Hz, 1H; CH), 7.85-7.96 (m, 2H; Ar), 8.80 (s, 1H; CH), 11.36 (s, 1H; NH). ¹³C APT NMR (75 MHz, DMSO-*d*₆): δ (ppm)= 42.54, 101.59, 120.24, 121.88, 128.90, 130.04, 136.68, 143.85, 145.63, 150.96, 163.90. HRMS (ESI): *m/z* calcd for C₁₃H₁₂N₅O₂: 270.0986 [M+H]⁺, found 270.0986; *m/z* calcd for C₁₃H₁₁N₅O₂Na: 292.0810 [M+Na]⁺, found 292.0805; *m/z* calcd for C₁₃H₁₁N₅O₂K: 308.0550 [M+K]⁺, found 308.0544.

5-fluoro-1-[1-phenyl-1,2,3-triazol-5-yl-methyl]-uracil (200). White solid, yield 88%. (CHCl₃/acetone/CH₃OH 8:1:1); ¹H NMR (300 MHz, DMSO-*d*₆): δ (ppm) = 5.01 (s, 2H; CH₂), 7.43-7.54 (m, 1H; Ar), 7.59 (t, *J*=7.97 Hz, 2H; Ar), 7.89 (d, *J*=7.97 Hz, 2H; Ar), 8.24 (d, *J*=6.70 Hz, 1H; CH), 8.80 (s, 1H; CH), 11.91 (s, 1H; NH). ¹³C APT NMR (75 MHz, DMSO-*d*₆): δ (ppm)= 43.24, 120.51, 122.17, 129.22, 130.35, 130.36 (d, *J*=33.70 Hz), 136.99, 140.31 (d, *J*=229.50 Hz), 144.05, 149.94, 158.02 (d, *J*=25.84 Hz). HRMS (ESI): *m/z* calcd for C₁₃H₁₁FN₅O₂: 288.0891 [M+H]⁺, found 288.0888; *m/z* calcd for

$C_{13}H_{10}FN_5O_2Na$: 310.0716 $[M+Na]^+$, found 310.0706; m/z calcd for $C_{13}H_{10}FN_5O_2K$: 326.0456 $[M+K]^+$, found 326.0445.

1-[1-benzyl-1,2,3-triazol-5-yl-methyl]-thymine (201). White solid, yield 85%. ($CHCl_3$ /acetone/ CH_3OH 8:1:1); 1H NMR (300 MHz, $DMSO-d_6$): δ (ppm)= 1.75 (s, 3H; CH_3), 4.89 (s, 2H; CH_2), 5.57 (s, 2H; CH_2), 7.24-7.44 (m, 5H; Ar), 7.63 (s, 1H; CH), 8.14 (s, 1H; CH), 11.33 (s, 1H; NH). ^{13}C APT NMR (75 MHz, $DMSO-d_6$): δ (ppm)= 17.01, 47.39, 57.94, 113.96, 128.71, 133.10, 133.26, 133.85, 141.02, 146.27, 147.93, 155.81, 169.36. HRMS (ESI): m/z calcd for $C_{15}H_{16}N_5O_2$: 298.1299 $[M+H]^+$, found 298.1291.

1-[1-benzyl-1,2,3-triazol-5-yl-methyl]-uracil (202). White solid, yield 87%. ($CHCl_3$ /acetone/ CH_3OH 8:1:1); 1H NMR (300 MHz, $DMSO-d_6$): δ (ppm)= 4.92 (s, 2H; CH_2), 5.58 (d, 1H, $J=7.5$ Hz; CH), 7.27-7.40 (m, 5H; Ar), 7.75 (d, $J=7.5$ Hz, 1H; CH), 8.14 (s, 1H; CH), 11.33 (s, 1H; NH). ^{13}C APT NMR (75 MHz, $DMSO-d_6$): δ (ppm)= 42.90, 53.28, 101.70, 124.10, 128.46, 128.62, 129.21, 136.38, 143.14, 145.96, 151.19, 164.13. HRMS (ESI): m/z calcd for $C_{14}H_{14}N_5O_2$: 284.1142 $[M+H]^+$, found 284.1138; m/z calcd for $C_{14}H_{13}N_5O_2Na$: 306.0967 $[M+Na]^+$, found 306.0957.

5-fluoro-1-[1-benzyl-1,2,3-triazol-5-yl-methyl]-uracil (203). White solid, yield 84%. ($CHCl_3$ /acetone/ CH_3OH 8:1:1); 1H NMR (300 MHz, $DMSO-d_6$): δ (ppm)= 4.90 (s, 2H; CH_2), 5.58 (s, 2H; CH_2), 7.29-7.34 (m, 3H; Ar), 7.34-7.39 (m, 2H; Ar), 8.16 (s, 1H; CH), 8.18 (d, $J=6.75$ Hz, 1H; CH), 11.63 (s, 1H; NH). ^{13}C NMR (75 MHz, $DMSO-d_6$): δ (ppm)= 43.30, 53.35, 124.16, 128.49, 128.64, 129.23, 136.37, 139.24, 141.06, 142.96, 149.87, 157.93. HRMS (ESI): m/z calcd for $C_{14}H_{13}FN_5O_2$: 302.1048 $[M+H]^+$, found 302.1038; m/z calcd for $C_{14}H_{12}FN_5O_2Na$: 324.0873 $[M+Na]^+$, found 324.0856.

1-[1-(4-nitrophenyl)-1,2,3-triazol-5-yl-methyl]-thymine (204). Pale-yellow solid, yield 83%. ($CHCl_3$ /acetone/ CH_3OH 8:1:1); 1H NMR (300 MHz, $DMSO-d_6$): δ (ppm)= 1.77 (s, 3H; CH_3), 5.03 (s, 2H; CH_2), 7.68 (s, 1H; CH), 8.22 (d, $J=9.01$ Hz, 2H; Ar), 8.44 (d, 2H, $J=9.01$ Hz; Ar), 9.00 (s, 1H; CH), 11.39 (s, 1H; NH). ^{13}C NMR (125 MHz, $DMSO-d_6$): δ (ppm)= 12.55, 42.77, 109.74, 121.25, 122.75, 126.12, 141.68, 141.72, 145.11, 147.35, 151.37, 164.98. HRMS (ESI): m/z calcd for $C_{14}H_{12}N_6O_4Na$: 351.0812 $[M+Na]^+$, found 351.0812.

1-[1-(4-nitrophenyl)-1,2,3-triazol-5-yl-methyl]-uracil (205). Pale-yellow solid, yield 86%. ($CHCl_3$ /acetone/ CH_3OH 8:1:1); 1H NMR (300 MHz, $DMSO-d_6$): δ (ppm)= 5.09 (s, 2H; CH_2), 5.66 (d, 1H, $J=7.84$ Hz, CH), 7.83 (d, 1H, $J=7.84$ Hz, CH), 8.24 (d, 2H, $J=8.78$

Hz, Ar), 8.45 (d, 2H, $J=8.78$ Hz, Ar), 9.02 (s, 1H, CH), 11.39 (s, 1H, NH). ^{13}C NMR (125 MHz, DMSO- d_6): δ (ppm)= 42.94, 102.04, 121.17, 122.72, 126.06, 141.25, 144.92, 146.01, 147.29, 151.34, 164.34. HRMS (ESI): m/z calcd for $\text{C}_{13}\text{H}_{10}\text{N}_6\text{O}_4\text{Na}$: 337.0656 $[\text{M}+\text{Na}]^+$, found 337.0653.

5-fluoro-1-[1-(4-nitrophenyl)-1,2,3-triazol-5-yl-methyl]-uracil (206). Pale-yellow solid, yield 82%. ($\text{CHCl}_3/\text{acetone}/\text{CH}_3\text{OH}$ 8:1:1); ^1H NMR (300 MHz, DMSO- d_6): δ (ppm)= 5.07 (s, 2H; CH_2), 7.98 (m, 2H; Ar), 8.06 (d, $J=6.75$ Hz, 1H; CH), 8.47 (m, 2H; Ar), 9.02 (s, 1H; CH), 11.90 (s, 1H; NH). ^{13}C NMR (125 MHz, DMSO- d_6): δ (ppm)= 43.36, 121.24, 126.92, 135.31, 141.07, 141.31, 144.85, 147.39, 148.38, 150.03, 158.20. HRMS (ESI): m/z calcd for $\text{C}_{13}\text{H}_{10}\text{FN}_6\text{O}_4$: 333.0742 $[\text{M}+\text{H}]^+$, found 333.0733; m/z calcd for $\text{C}_{13}\text{H}_9\text{FN}_6\text{O}_4\text{Na}$: 355.0567 $[\text{M}+\text{Na}]^+$, found 355.0554; m/z $[\text{M}+\text{K}]^+$ calcd for $\text{C}_{13}\text{H}_9\text{FN}_6\text{O}_4\text{K}$: 371.0306 $[\text{M}+\text{K}]^+$, found 371.0293.

1-[1-(4-methoxyphenyl)-1,2,3-triazol-5-yl-methyl]-thymine (207). White solid, yield 89%. ($\text{CHCl}_3/\text{acetone}/\text{CH}_3\text{OH}$ 8:1:1); ^1H NMR (300 MHz, DMSO- d_6): δ (ppm)= 1.77 (s, 3H; CH_3), 3.82 (s, 3H; CH_3), 4.98 (s, 2H; CH_2), 7.12 (d, 2H, $J=9.05$ Hz; Ar), 7.66 (s, 1H; CH), 7.79 (d, 2H, $J=9.05$ Hz; Ar), 8.67 (s, 1H; CH), 11.35 (s, 1H; NH). ^{13}C NMR (125 MHz, DMSO- d_6): δ (ppm)= 12.45, 42.63, 56.04, 109.47, 115.32, 122.12, 122.21, 130.43, 141.58, 144.04, 151.24, 159.77, 164.80. HRMS (ESI): m/z calcd for $\text{C}_{15}\text{H}_{16}\text{N}_5\text{O}_3$: 314.1248 $[\text{M}+\text{H}]^+$, found 314.1245; m/z calcd for $\text{C}_{15}\text{H}_{15}\text{N}_5\text{O}_3\text{Na}$: 336.1073 $[\text{M}+\text{Na}]^+$, found 336.1062; m/z calcd for $\text{C}_{15}\text{H}_{15}\text{N}_5\text{O}_3\text{K}$: 352.0812 $[\text{M}+\text{K}]^+$, found 352.0805.

1-[1-(4-methoxyphenyl)-1,2,3-triazol-5-yl-methyl]-uracil (208). White solid, yield 90%. ($\text{CHCl}_3/\text{acetone}/\text{CH}_3\text{OH}$ 8:1:1); ^1H NMR (300 MHz, DMSO- d_6): δ (ppm)= 3.82 (s, 3H; CH_3), 5.02 (s, 2H; CH_2), 5.62 (d, 1H, $J=7.89$ Hz; CH), 7.12 (m, 2H; Ar), 7.79 (m, 3H; Ar and CH), 8.69 (s, 1H; CH), 11.37 (s, 1H; NH). ^{13}C NMR (125 MHz, DMSO- d_6): δ (ppm)= 42.83, 56.02, 101.86, 115.31, 122.07, 122.20, 130.41, 143.87, 145.93, 151.26, 159.77, 164.21. HRMS (ESI): m/z calcd for $\text{C}_{14}\text{H}_{14}\text{N}_5\text{O}_3$: 300.1091 $[\text{M}+\text{H}]^+$, found 300.1086; m/z calcd for $\text{C}_{14}\text{H}_{13}\text{N}_5\text{O}_3\text{Na}$: 322.0916 $[\text{M}+\text{Na}]^+$, found 322.0903; calcd for $\text{C}_{14}\text{H}_{13}\text{N}_5\text{O}_3\text{K}$: 338.0655 m/z $[\text{M}+\text{K}]^+$, found 338.0642.

5-fluoro-1-[1-(4-methoxyphenyl)-1,2,3-triazol-5-yl-methyl]-uracil (209). White solid, yield 88%. ($\text{CHCl}_3/\text{acetone}/\text{CH}_3\text{OH}$ 8:1:1); ^1H NMR (300 MHz, DMSO- d_6): δ (ppm)= 3.82 (s, 3H; CH_3), 4.99 (s, 2H; CH_2), 7.12 (m, 2H; Ar), 7.79 (m, 2H; Ar), 8.24 (d, $J=6.70$ Hz, 1H; CH), 8.70 (s, 1H; CH), 11.91 (d, $J=6.67$ Hz, 1H; NH). ^{13}C NMR (125 MHz,

DMSO-*d*₆): δ (ppm)= 43.24, 56.04, 115.33, 122.17, 130.38, 130.43, 139.38, 141.21, 143.77, 149.94, 158.03, 159.79. HRMS (ESI): *m/z* calcd for C₁₄H₁₂FN₅O₃Na: 340.0816[M+Na]⁺, found 340.0809.

Docking studies

For each receptor, the docking cavity was centered on the binding site of the crystallographic ligand and allowed to extend in a spherical surrounding volume with a radius of 15 Å radius. In cases where a metal ion was present at the binding site, the docking cavity was centered on it and metal parameters were set to maintain the same coordination number as in the crystallographic structure. In absence of metals, the XYZ coordinates that defined the center of the cavity were obtained from the position of the cocrystallized ligand, choosing an atom that was reasonably at the center of the ligand. The number of genetic algorithm runs was set to 20 for each analyzed ligand. Protein structures were prepared using UCSF Chimera,¹ by reverting selenomethionine to methionine, eliminating alternate locations of side chains, adding hydrogen atoms, assigning appropriate protein atom types, and removing the co-crystallized ligand and solvent molecules. Crystallographic ligands were docked after adding hydrogen atoms with UCSF Chimera and without optimizing their geometries. Conversely, the geometries of the screened ligands **198-209** were optimized quantum mechanically. Geometry optimizations and frequency calculations for stationary point characterization were carried out with Gaussian16² using the M06-2X hybrid functional,³ the 6-31G(d,p) basis set, and ultrafine integration grids. Bulk solvent effects in water were considered implicitly through the IEF-PCM polarizable continuum model.⁴ As for the potential receptors, 26 targets were initially selected from the Protein Data Bank (**Figure A1**). The main selection criterion was the presence of a triazole (i.e. 1,2,3- and 1,2,4-triazoles) scaffold or structurally similar heterocycles (i.e. imidazoles, thiazoles) in the crystallographic structure of the ligand-receptor complex. Docking simulations were performed and keeping the coordinates of the protein fixed while allowing flexibilization of the ligands around their rotatable bonds.

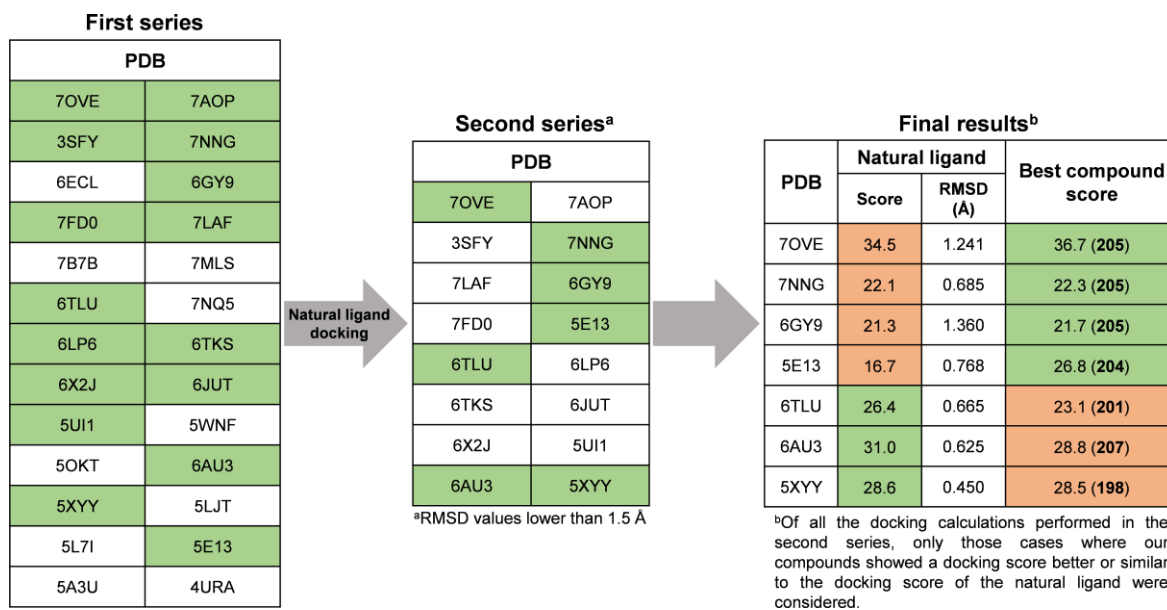


Figure A1. Workflow describing the approach used to validate the docking protocol and select the target receptors (first series) and to evaluate the binding capacity of compounds **198-209** to them.

Research line 1b - 1,5-DTs as mitochondrial Ca²⁺-activated F₁F₀-ATP(hydrol)ase: synthesis and *in vitro* studies

Materials and Methods

All reagents and commercial ionic liquids were purchased from Sigma-Aldrich (St. Gallen, Switzerland) or Alfa Aesar (Karlsruhe, Germany) and used without purification. Reactions were monitored by TLC using silica plates 60-F264 commercially available from Merck (Darmstadt, Germany). ¹H and ¹³C NMR spectra were recorded at 300 and 75 MHz, respectively, in CDCl₃ using tetramethylsilane (TMS) as the internal standard (Bruker (Billerica, MA, USA) ACP 300 MHz). Chemical shifts are given in parts per million and coupling constants in Hertz. LC-MS analyses were carried out using an Agilent 6540 UHD Accurate–Mass Q-TOF LC-MS (Agilent, Santa Clara, CA, USA) fitted with an electrospray ionization source (Dual AJS ESI) operating in positive ion mode. Chromatographic separation was achieved using a C18 RP analytical column (Poroshell 120, SB-C18, 50 x 2.1 mm, 2.7 mm) at 30 °C with an elution gradient from 5% to 95% of B over 13 min, A being H₂O (0.1% FA) and B CH₃CN (0.1% FA). Flow rate was 0.4 mL min⁻¹.

Synthesis of 1-Methyl pyridinium trifluoromethanesulfonate

1-methyl pyridinium trifluoromethanesulfonate ([mpy]OTf) was prepared by halide-free direct synthesis as reported in the literature.⁵⁻⁷

General Procedure for Synthesis of 1,5-Disubstituted-1,2,3-Triazoles 212 and 213

In a two-necked round bottom flask, equipped with a bubble condenser and magnetic stir bar, ionic liquid (5 mL), FeCl₃ (20 mol %), (*E*)-nitrostyrene **210-211** (1 eq.), and phenyl azide **18** (2 eq.) were placed. The reaction was conducted at 100 °C for the appropriate time. The crude was extracted with dichloromethane (3x5 mL) and the combined organic layer was evaporated under vacuum. The crude product was purified on a flash silica gel column by using hexane/ethyl acetate (9:1 v/v) to obtain the desired product (**213** and **213**).

1,5-Diphenyl-1,2,3-triazole (212). ¹H NMR (CDCl₃, 300 MHz): δ (ppm) 7.22-7.31 (m, 2H, Ar), 7.36-7.44 (m, 5H, Ar), 7.44-7.50 (m, 3H, Ar), 7.90 (s, 1H, CH); ¹³C NMR (CDCl₃, 75 MHz): δ (ppm) 125.23, 126.79, 128.61, 128.87, 129.24, 129.37, 133.41, 136.64, 137.75. ESI(+)-MS: *m/z* [M+H]⁺ calcd for C₁₄H₁₂N₃ 222.1026, found: 222.0591.

5-(2-Nitrophenyl)-1-phenyl-1,2,3-triazole (213). ¹H NMR (CDCl₃, 300 MHz): δ (ppm) 7.28-7.31 (m, 1H, Ar), 7.33-7.42 (m, 3H, Ar), 7.46 (dd, 1H, *J*=7.42 Hz, 1.70 Hz, Ar), 7.60-7.75 (m, 3H, Ar), 7.84 (s, 1H, CH), 8.04 (dd, 1H, *J*=7.90 Hz, 1.60 Hz, Ar); ¹³C NMR (CDCl₃, 75 MHz): δ (ppm) 122.56, 124.53, 125.17, 129.38, 129.46, 130.92, 132.78, 133.45, 133.75, 135.94, 148.34. ESI(+)-MS: *m/z* [M+H]⁺ calcd for C₁₄H₁₁N₄O₂ 267.0877, found: 267.1267.

References

- (1) Pettersen, E. F.; Goddard, T. D.; Huang, C. C.; Couch, G. S.; Greenblatt, D. M.; Meng, E. C.; Ferrin, T. E. UCSF Chimera - A Visualization System for Exploratory Research and Analysis. *J. Comput. Chem.* **2004**, *25* (13), 1605–1612. <https://doi.org/10.1002/jcc.20084>.
- (2) Frisch, M. J. ; Trucks, G. W. ; Schlegel, H. B. ; Scuseria, G. E. ; Robb, M. A. ; Cheeseman, J. R. ; Scalmani, G. ; Barone, V. ; Petersson, G. A. ; Nakatsuji, H. ; Li, X. ; Caricato, M. ; Marenich, A. V. ; Bloino, J. ; Janesko, B. G. ; Gomperts, R. ; Mennucci, B. ; Hratchian, H. P. ; Ortiz, J. V. ; Izmaylov, A. F.; Sonnenberg, J. L. ; Williams-Young, D. ; Ding, F. ; Lipparini, F. ; Egidi, F. ; Goings, J. ; Peng, B. ; Petrone, A. ; Henderson, T. ; Ranasinghe, D.; Zakrzewski, V. G. ; Gao, J. ; Rega, N. ; Zheng, G. ; Liang, W. ; Hada, M. ; Ehara, M. ; Toyota, K. ; Fukuda, R. ; Hasegawa, J. ; Ishida, M. ; Nakajima, T. ; Honda, Y. ; Kitao, O. ; Nakai, H. ; Vreven, T. ; Throssell, K. ; Montgomery, J. A., Jr. ; Peralta, J. E. ; Ogliaro, F. ; Bearpark, M. J. ; Heyd, J. J. ; Brothers, E. N. ; Kudin, K. N. ; Staroverov, V. N. ; Keith, T. A. ; Kobayashi, R. ; Normand, J. ; Raghavachari, K. ; Rendell, A. P. ; Burant, J. C. ; Iyengar, S. S. ; Tomasi, J. ; Cossi, M. ; Millam, J. M. ; Klene, M. ; Adamo, C. ; Cammi, R. ; Ochterski, J. W. ; Martin, R. L. ; Morokuma, K. ; Farkas, O. ; Foresman, J. B. ; Fox, D. J. Gaussian 16, Revision C.01. Wallingford CT 2016.
- (3) Zhao, Y.; Truhlar, D. G. The M06 Suite of Density Functionals for Main Group Thermochemistry, Thermochemical Kinetics, Noncovalent Interactions, Excited States, and Transition Elements: Two New Functionals and Systematic Testing of Four M06-Class Functionals and 12 Other Function. *Theor. Chem. Acc.* **2008**, *120* (1–3), 215–241. <https://doi.org/10.1007/s00214-007-0310-x>.
- (4) Scalmani, G.; Frisch, M. J. Continuous Surface Charge Polarizable Continuum Models of Solvation. I. General Formalism. *J. Chem. Phys.* **2010**, *132* (11). <https://doi.org/10.1063/1.3359469>.
- (5) Bortolini, O.; De Nino, A.; Garofalo, A.; Maiuolo, L.; Procopio, A.; Russo, B. Erbium Triflate in Ionic

- Liquids: A Recyclable System of Improving Selectivity in Diels-Alder Reactions. *Appl. Catal. A Gen.* **2010**, 372 (2), 124–129. <https://doi.org/10.1016/j.apcata.2009.10.020>.
- (6) Bortolini, O.; Nino, A. De; Garofalo, A.; Maiuolo, L.; Russo, B. Mild Oxidative Conversion of Nitroalkanes into Carbonyl Compounds in Ionic Liquids. *Synth. Commun.* **2010**, 40 (16), 2483–2487. <https://doi.org/10.1080/00397910903267921>.
- (7) De Nino, A.; Maiuolo, L.; Merino, P.; Nardi, M.; Procopio, A.; Roca-López, D.; Russo, B.; Algieri, V. Efficient Organocatalyst Supported on a Simple Ionic Liquid as a Recoverable System for the Asymmetric Diels-Alder Reaction in the Presence of Water. *ChemCatChem* **2015**, 7 (5), 830–835. <https://doi.org/10.1002/cctc.201402973>.

Chapter 2: Isoxazolidine bisphosphonates as potential farnesyl pyrophosphate synthase inhibitors

Research line 2 - New class of isoxazolidine bisphosphonates as potential human farnesyl pyrophosphate synthase (*hFPPS*) inhibitors

Materials and Methods

Commercial starting materials were used without further purification. Solvents were distilled before use. ^1H and ^{13}C NMR spectra were recorded at 300 and 500 MHz and 75.5 and 125.7 MHz, respectively, in CDCl_3 , $\text{DMSO-}d_6$, and D_2O using tetramethylsilane (TMS) as internal standard (Bruker ACP 300 MHz and 500 MHz), whereas for ^1H -decoupled and ^{31}P NMR (202.4 MHz) an external standard was used. Chemical shifts are given in parts per million and coupling constants in Hertz. Chemical shifts are given in ppm and coupling constants in Hz. The regio- and diastereoisomers ratios were established by ^1H NMR spectroscopy. The reactions of esters were achieved on a Microwave instrument Synthos 3000 from Anton Paar, equipped with a 4 x 24MG5 rotor and an IR probe as external control of the temperature. 0.3–3 mL glass vials sealed with a dedicated PEEK screw-cup together with a reliable PTFE seal were used for all reactions.

General procedure for the synthesis of the esters 166a-h, 166'a-h and 167a-h, 167'a-h Nitron (**165a-h** (1 mol) and vinyl ester **164** (2 mol) were introduced in apposite vessel that is arranged in a microwave oven under irradiation at 750 W. The reaction is conducted until the complete transformation of reactants. The crude, obtained by any pretreatment, was purified by flash chromatography collecting the mixture of regioisomers and diastereoisomers **166-166'** and **167-167'** (Hexane/Ethyl acetate 8:2 v/v). The mixture was purified by preparative HPLC only for the esters **166c** and **167c**, **166h** and **167h** to do a complete characterization and a configuration assignment of all stereoisomers.

Characterization of isolated esters 166 and 167

(trans) 2-methyl-4-(ethoxycarbonyl)-3-(4-nitrophenyl)isoxazolidine (166c) ^1H NMR (CDCl_3 , 500 MHz): δ (ppm) 1.19 (t, $J = 7.15$ Hz, 3H, CH_3), 2.59 (s, 3H, CH_3), 3.30 (td, $J = 7.71$ Hz; $J = 5.90$ Hz, 1H, CH), 3.91 (d, $J = 7.71$ Hz, 1H, CH), 4.13 (qd, $J = 7.15$ Hz; $J = 0.60$ Hz, 2H, CH_2), 4.20 (dd, $J = 5.90$ Hz, $J = 2.40$ Hz, 2H, CH_2), 7.57 (m, 2H, Ar), 8.15

(m, 2H, Ar). ^{13}C APT NMR (CDCl_3 , 125 MHz): δ (ppm) 14.14, 43.08, 57.54, 61.56, 68.37, 74.44, 123.96, 128.58, 146.27, 171.50. ESI(+)-MS: m/z $[\text{M}+\text{Na}]^+$ calcd for $\text{C}_{13}\text{H}_{16}\text{N}_2\text{O}_5\text{Na}$, 303.0957, found 303.0946.

(cis) 2-methyl-4-(ethoxycarbonyl)-3-(4-nitrophenyl)isoxazolidine (166'c) ^1H NMR (CDCl_3 , 500 MHz): δ (ppm) 0.77 (t, $J = 7.15$ Hz, 3H, CH_3), 2.59 (s, 3H, CH_3), 3.47-3.61 (m, 1H, CH_2), 3.61-3.74 (m, 1H, CH_2), 3.79 (tb, $J = 8.50$, 1H, CH), 3.98 (db, $J = 9.35$ Hz, 2H, CH_2), 4.20 (t, $J = 8.50$ Hz, 1H, CH_2), 4.36 (t, $J = 8.17$ Hz, 1H, CH_2), 7.48 (d, $J = 8.80$ Hz, 2H, Ar), 8.11 (d, $J = 8.80$ Hz, 2H, Ar). ^{13}C APT NMR (CDCl_3 , 125 MHz): δ (ppm) 13.68, 43.43, 53.71, 60.91, 67.95, 73.62, 123.34, 129.37, 144.06, 147.69, 169.74. ESI(+)-MS: m/z $[\text{M}+\text{Na}]^+$ calcd for $\text{C}_{13}\text{H}_{16}\text{N}_2\text{O}_5\text{Na}$, 303.0957, found 303.0946.

(trans) 2-methyl-5-(ethoxycarbonyl)-3-(4-nitrophenyl)isoxazolidine (167c) ^1H NMR (CDCl_3 , 500 MHz): δ (ppm) 1.25 (t, $J = 7.14$ Hz, 3H, CH_3), 2.49-2.62 (m, 1H, CH_2), 2.67 (s, 3H, CH_3), 2.74-2.87 (m, 1H, CH_2), 3.85 (t, $J = 7.82$ Hz, 1H, CH), 4.20 (q, $J = 7.14$ Hz, 2H, CH_2), 4.61 (dd, $J = 9.14$ Hz, $J = 5.35$ Hz, 1H, CH), 7.51 (d, $J = 8.70$ Hz, 2H, Ar), 8.14 (d, $J = 8.70$ Hz, 2H, Ar). ^{13}C APT NMR (CDCl_3 , 125 MHz): δ (ppm) 14.15, 42.84, 43.88, 61.63, 70.69, 75.39, 123.98, 128.35, 146.04, 147.73, 170.97. ESI(+)-MS: m/z $[\text{M}+\text{Na}]^+$ calcd for $\text{C}_{13}\text{H}_{16}\text{N}_2\text{O}_5\text{Na}$, 303.0957, found 303.0946.

(cis) 2-methyl-4-(ethoxycarbonyl)-3-(4-nitrophenyl)isoxazolidine (167'c) ^1H NMR (CDCl_3 , 500 MHz): δ (ppm) 1.24 (t, $J = 7.15$ Hz, 3H, CH_3), 2.48-2.57 (m, 1H, CH_2), 2.58 (s, 3H, CH_3), 2.90-3.05 (m, 1H, CH_2), 3.63 (sb, 1H, CH), 4.20 (qd, $J = 7.15$ Hz, $J = 1.55$ Hz, 2H, CH_2), 4.62 (dd, $J = 9.08$ Hz, $J = 5.15$ Hz, 1H, CH), 7.50 (d, $J = 8.80$ Hz, 2H, Ar), 8.13 (d, $J = 8.80$ Hz, 2H, Ar). ^{13}C APT NMR (CDCl_3 , 125 MHz): δ (ppm) 14.20, 42.48, 43.24, 61.59, 71.85, 74.68, 123.96, 128.66, 146.30, 147.78, 171.76. ESI(+)-MS: m/z $[\text{M}+\text{Na}]^+$ calcd for $\text{C}_{13}\text{H}_{16}\text{N}_2\text{O}_5\text{Na}$, 303.0957, found 303.0946.

(trans) 2-methyl-4-(ethoxycarbonyl)-3-(4-chlorophenyl)isoxazolidine (166h) ^1H NMR (CDCl_3 , 500 MHz): δ (ppm) 1.17 (t, $J = 7.15$ Hz, 3H, CH_3), 2.55 (s, 3H, CH_3), 3.29 (m, 1H, CH), 3.72 (m, 1H, CH), 4.95 (qd, $J = 7.15$, $J = 2.58$ Hz, 2H, CH_2), 4.14-4.23 (m, 2H, CH_2), 7.22-7.34 (m, 4H, Ar). ^{13}C APT NMR (CDCl_3 , 125 MHz): δ (ppm) 14.15, 42.82, 57.29, 61.31, 68.45, 75.02, 128.97, 129.19, 134.03, 136.63, 171.86. ESI(+)-MS: m/z $[\text{M}+\text{Na}]^+$ calcd for $\text{C}_{13}\text{H}_{16}\text{ClNO}_3\text{Na}$, 292.0716, found 292.0710.

(cis) 2-methyl-4-(ethoxycarbonyl)-3-(4-chlorophenyl)isoxazolidine (166'h) ^1H NMR (CDCl_3 , 500 MHz): δ (ppm) 1.24 (t, $J = 7.17$ Hz, 3H, CH_3), 2.45-2.52 (m, 1H, CH_2), 2.54 (s, 3H, CH_3), 2.83-2.96 (m, 1H, CH_2), 3.34-3.52 (m, 1H, CH), 4.20 (qd, $J = 7.17$ Hz, $J = 3.65$ Hz, 2H, CH_2), 4.50-4.63 (m, 1H, CH), 7.21-7.27 (m, 4H, Ar). ^{13}C APT NMR (CDCl_3 , 125 MHz): δ (ppm) 14.13, 42.48, 42.90, 61.24, 72.08, 74.55, 128.84, 129.13, 133.88, 136.79, 171.83. ESI(+)-MS: m/z $[\text{M}+\text{Na}]^+$ calcd for $\text{C}_{13}\text{H}_{16}\text{ClNO}_3\text{Na}$, 292.0716, found 292.0710.

(trans) 2-methyl-5-(ethoxycarbonyl)-3-(4-chlorophenyl)isoxazolidine (167h) ^1H NMR (CDCl_3 , 500 MHz): δ (ppm) 1.23 (t, $J = 7.15$ Hz, 3H, CH_3), 2.46-2.55 (m, 1H, CH_2), 2.53 (s, 3H, CH_3), 2.81-2.92 (m, 1H, CH_2), 3.37-3.57 (m, 1H, CH), 4.19 (qd, $J = 7.15$ Hz, $J = 2.62$ Hz, 2H, CH_2), 4.54 (dd, $J = 9.12$ Hz, $J = 5.54$ Hz, 1H, CH), 7.19-7.44 (m, 4H, Ar). ^{13}C APT NMR (CDCl_3 , 125 MHz): δ (ppm) 14.13, 42.48, 42.89, 61.24, 72.07, 74.55, 128.84, 129.13, 133.88, 136.78, 171.82. ESI(+)-MS: m/z $[\text{M}+\text{Na}]^+$ calcd for $\text{C}_{13}\text{H}_{16}\text{ClNO}_3\text{Na}$, 292.0716, found 292.0710.

(cis) 2-methyl-5-(ethoxycarbonyl)-3-(4-chlorophenyl)isoxazolidine (167'h) ^1H NMR (CDCl_3 , 500 MHz): δ (ppm) 1.23 (t, $J = 7.15$ Hz, 3H, CH_3), 2.48-2.59 (m, 1H, CH_2), 2.61 (s, 3H, CH_3), 2.64-2.74 (m, 1H, CH_2), 3.55-3.73 (m, 1H, CH), 4.18 (q, $J = 7.15$ Hz, 2H, CH_2), 4.60 (dd, $J = 9.29$ Hz, $J = 5.12$ Hz, 1H, CH), 7.21-7.29 (m, 4H, Ar). ^{13}C APT NMR (CDCl_3 , 125 MHz): δ (ppm) 14.15, 43.04, 43.53, 61.46, 70.95, 75.14, 128.92, 133.84, 136.64, 171.20. ESI(+)-MS: m/z $[\text{M}+\text{Na}]^+$ calcd for $\text{C}_{13}\text{H}_{16}\text{ClNO}_3\text{Na}$, 292.0716, found 292.0710.

General procedure for the synthesis of the bisphosphonate acids 162 and 163.

To a solution of ester (**166** and **167**) ($6.13 \cdot 10^{-4}$ mol) in ethanol (15 mL) a 3 M aqueous solution of NaOH (12 mL) was added. The reaction mixture was stirred at room temperature for 12 h. Then, the solvents were removed in vacuo, 5 mL of water was added and the pH was adjusted to 4 with an aqueous solution of HCl (9:1 v:v). The mixture was extracted with ethyl acetate (3 x 15 mL), dried over Na_2SO_4 , filtered, and concentrated to give the crude carboxylic acid **168** and **169**. The residue was placed in 15 mL of *dry* CH_2Cl_2 , in an N_2 atmosphere. Oxalyl chloride ($7.35 \cdot 10^{-4}$ mol) was added and stirring was maintained for 3 h, then, the solvent was removed under reduced pressure. A solution of the crude and tris-trimethylsilyl phosphite ($1.23 \cdot 10^{-3}$ mol) in 15 mL of *dry* THF was stirred for 12 h at room temperature. The crude was concentrated

in vacuo and 15 mL of methanol was added to the residue, stirring the solution for 3 h at room temperature. Finally, after concentration of the solvent until 2 mL, the residue was purified by coprecipitation with diethyl ether. The isomers of **162c-163c** and **162h-163h** were resynthesized starting from isolated ester isomers **166c** and **167c**, **166h** and **167h** for a fully characterization and stereochemistry assignment.

Characterization of isolated isoxazolidine bisphosphonates

(trans) 2-methyl-3-(4-nitrophenyl)-isoxazolidinyl-4,4-bisphosphonic acid (162c) ¹H NMR (D₂O, 500 MHz): δ (ppm) 3.10 (s, 3H, CH₃), 3.64-3.81 (m, 1H, CH), 4.55-4.65 (m, 1H, CH₂), 4.70-4.81 (m, 1H, CH₂), 5.26 (d, J = 6.90 Hz, 1H, CH), 7.38-7.49 (m, 4H, Ar). ¹³C APT NMR (D₂O, 125 MHz): δ (ppm) 35.71, 40.61, 73.29, 84.46, 124.46, 128.20, 129.61, 130.45, 136.11. ³¹P NMR (D₂O, 162 MHz): δ (ppm) 15.27 (m, 1P), 16.34 (m, 1P). ESI(-)-MS: m/z [M-H]⁻ calcd for C₁₁H₁₅N₂O₁₀P₂, 397.0207, found 397.0210.

(cis) 2-methyl-3-(4-nitrophenyl)-isoxazolidinyl-4,4-bisphosphonic acid (162'c) ¹H NMR (D₂O, 500 MHz): δ (ppm) 2.92 (s, 3H, CH₃), 2.93-3.01 (m, 1H, CH₂), 3.10-3.19 (m, 1H, CH₂), 5.07-5.19 (m, 1H, CH), 7.42 (d, J = 8.60 Hz, 2H, Ar), 7.50 (d, J = 8.60 Hz, 2H, Ar). ¹³C APT NMR (D₂O, 125 MHz): δ (ppm) 35.71, 40.61, 73.29, 84.46, 124.46, 128.20, 129.61, 130.45, 136.11. ³¹P NMR (D₂O, 162 MHz): δ (ppm) 14.28 (m, 1P), 16.16 (m, 1P). ESI(-)-MS: m/z [M-H]⁻ calcd for C₁₁H₁₅N₂O₁₀P₂, 397.0207, found 397.0210.

(trans) 2-methyl-3-(4-nitrophenyl)-isoxazolidinyl-5,5-bisphosphonic acid (163c) ¹H NMR (D₂O, 500 MHz): δ (ppm) 2.92 (s, 3H, CH₃), 2.93-3.02 (m, 1H, CH₂), 3.09-3.21 (m, 1H, CH₂), 5.08-5.20 (m, 1H, CH), 7.42 (d, J = 8.62 Hz, 2H, Ar), 7.50 (d, J = 8.62 Hz, 2H, Ar). ¹³C APT NMR (D₂O, 125 MHz): δ (ppm) 35.71, 40.61, 73.29, 84.46, 124.46, 128.20, 129.61, 130.45, 136.11. ³¹P NMR (D₂O, 162 MHz): δ (ppm) 14.71 (m, 1P), 16.26 (m, 1P). ESI(-)-MS: m/z [M-H]⁻ calcd for C₁₁H₁₅N₂O₁₀P₂, 397.0207, found 397.0210.

(cis) 2-methyl-3-(4-nitrophenyl)-isoxazolidinyl-5,5-bisphosphonic acid (163'c) ¹H NMR (DMSO-d₆, 500 MHz): δ (ppm) 2.58 (s, 3H, CH₃), 2.71-2.89 (m, 2H, CH₂), 4.73-4.87 (m, 1H, CH), 7.74 (d, J = 8.70 Hz, 2H, Ar), 8.23 (d, J = 8.70 Hz, 2H, Ar). ¹³C APT NMR (D₂O, 125 MHz): δ (ppm) 34.58, 40.88, 73.40, 85.39, 127.75, 128.84, 129.73, 130.32, 136.38. ³¹P NMR (D₂O, 162 MHz): δ (ppm) 13.96 (m, 1P), 16.07 (m, 1P). ESI(-)-MS: m/z [M-H]⁻ calcd for C₁₁H₁₅N₂O₁₀P₂, 397.0207, found 397.0210.

(trans) 2-methyl-3-(4-chlorophenyl)-isoxazolidinyl-4,4-bisphosphonic acid (162h) ¹H NMR (D₂O, 500 MHz): δ (ppm) 2.92 (s, 3H, CH₃), 2.93-3.02 (m, 1H, CH₂), 3.10-3.19 (m, 1H, CH₂), 5.06-5.20 (m, 1H, CH), 5.86-5.95 (m, 1H, CH), 7.39-7.45 (m, 2H, Ar), 7.46-7.53 (m, 2H, Ar). ¹³C APT NMR (DMSO-d₆, 125 MHz): δ (ppm) 35.71, 40.61, 73.29, 84.46, 124.46, 128.20, 129.61, 130.45, 136.11. ³¹P NMR (D₂O, 162 MHz): δ (ppm) 10.90 (m, 1P), 11.21 (m, 1P). ESI(-)-MS: m/z [M-H]⁻ calcd for C₁₁H₁₅ClNO₈P₂, 385.9967, found 385.9977.

(cis) 2-methyl-3-(4-chlorophenyl)-isoxazolidinyl-4,4-bisphosphonic acid (162'h) ¹H NMR (D₂O, 500 MHz): δ (ppm) 2.78-2.98 (m, 1H, CH₂), 3.07 (s, 3H, CH₃), 3.32-3.49 (m, 1H, CH₂), 4.73-4.82 (m, 1H, CH), 5.17-5.31 (m, 1H, CH), 7.37-7.51 (m, 4H, Ar). ¹³C APT NMR (DMSO-d₆, 125 MHz): δ (ppm) 34.65, 40.88, 73.40, 85.39, 127.75, 128.84, 129.73, 130.32, 136.38. ³¹P NMR (D₂O, 162 MHz): δ (ppm) 13.06 (s, 1P), 14.93 (s, 1P). ESI(-)-MS: m/z [M-H]⁻ calcd for C₁₁H₁₅ClNO₈P₂, 385.9967, found 385.9977.

(trans) 2-methyl-3-(4-chlorophenyl)-isoxazolidinyl-5,5-bisphosphonic acid (163h) ¹H NMR (D₂O, 500 MHz): δ (ppm) 2.76-2.94 (m, 1H, CH₂), 3.03 (s, 3H, CH₃), 3.29-3.45 (m, 1H, CH₂), 4.69-4.78 (m, 1H, CH), 5.14-5.26 (m, 1H, CH), 7.34-7.40 (m, 2H, Ar), 7.40-7.46 (m, 2H, Ar). ¹³C APT NMR (DMSO-d₆, 125 MHz): δ (ppm) 34.58, 40.88, 73.40, 85.39, 127.75, 129.73, 130.32, 136.20, 136.38. ³¹P NMR (D₂O, 162 MHz): δ (ppm) 13.06 (s, 1P), 14.93 (s, 1P). ESI(-)-MS: m/z [M-H]⁻ calcd for C₁₁H₁₅ClNO₈P₂, 385.9967, found 385.9977.

(cis) 2-methyl-3-(4-chlorophenyl)-isoxazolidinyl-5,5-bisphosphonic acid (163'h) ¹H NMR (D₂O, 500 MHz): δ (ppm) 2.93 (s, 3H, CH₃), 2.94-3.01 (m, 1H, CH₂), 3.09-3.20 (m, 1H, CH₂), 5.07-5.20 (m, 1H, CH), 5.87-5.96 (m, 1H, CH), 7.38-7.46 (m, 2H, Ar), 7.47-7.54 (m, 2H, Ar). ¹³C APT NMR (DMSO-d₆, 125 MHz): δ (ppm) 35.71, 40.61, 73.29, 84.46, 124.46, 128.20, 129.61, 130.45, 136.11. ³¹P NMR (D₂O, 162 MHz): δ (ppm) 10.92 (m, 1P), 11.33 (m, 1P). ESI(-)-MS: m/z [M-H]⁻ calcd for C₁₁H₁₅ClNO₈P₂, 385.9967, found 385.9977.

Chapter 3: Pyridinium ylide: useful tools in multicomponent synthesis

Research line 3a - DDQ-mediated multicomponent access to polysubstituted indolizines

Materials and Methods

Commercial reagents and solvents were used as received from Merck or Thermo Fischer. Reactions were monitored by TLC using silica plates 60-F264 commercially available from Merck (Darmstadt, Germany). Flash chromatography separations were carried out with silica gel columns. ^1H , ^{13}C , and NOESY nuclear magnetic resonance (NMR) spectra were obtained on a Bruker NMR spectrometer AVANCE 500 MHz Wide Bore (operating at 500 and 126 MHz, respectively), a Bruker NMR spectrometer 400 MHz (operating at 400 and 101 MHz, respectively) or a Bruker ACP 300 Mhz (operating at 300 and 75 MHz, respectively) in CDCl_3 ($^1\text{H} = \delta$ 7.26 ppm, $^{13}\text{C} = \delta$ 77.16 ppm) or $\text{DMSO}-d_6$ ($^1\text{H} = \delta$ 2.50 ppm, $^{13}\text{C} = \delta$ 39.50 ppm). The chemical shifts (δ) reported are given in parts per million (ppm). The signal splitting patterns were described as s = singlet, d = doublet, t = triplet, q = quartet, p = pentuplet, dd = doublet of doublet, dt = doublet of triplet, td = triplet of doublet, tt = triplet of triplet, ddd = doublet of doublet of doublet, and m = multiplet, with coupling constants (J) in hertz (Hz). HR-MS spectra were acquired with a Bruker Compact Q-TOF instrument (Bruker, Billerica, MA, USA). The spectra were acquired in positive ion mode, with a mass resolution of 30000. Mass calibration was performed with a solution of sodium formate clusters and processed in HPC mode. Spectra acquisition was performed in flow injection, with a full scan mode in the range of 50 to 500 m/z . N_2 was the source of dry gas ($V = 4\text{L}/\text{min}$, $T = 180\text{ }^\circ\text{C}$). The ion formula of each compound was calculated with the Smart Formula tool of the Bruker software platform, analyzing the isotopic pattern ratio with 4 mDa mass confidence. All samples were dissolved in MeOH. Known compounds are referenced.

General procedure for the synthesis of the indolizines 167a-j

2-Bromoacetophenone **164** (1.5 mmol), methyl acrylate **166** (1.5 mmol), K_2CO_3 (7.5 mmol), FeCl_3 (4.5 mmol), DDQ (0.15 mmol), pyridine **165** (3.0 mmol), and 15 mL of *dry* DMF were added to a flamed system consisting of a 2-neck flask equipped with a condenser. The system was stirred at 100 $^\circ\text{C}$ for 8 h. At the end of the reaction, the solvent was removed by a rotary evaporator, subsequently removing the remaining traces of the same by azeotrope mixture with toluene (3x5 mL) and ethanol (3x5 mL).

Finally, the crude was dried by a vacuum pump, and the product was purified by flash chromatography (Ex:AcOEt 9.5:0.5).

methyl 3-benzoylindolizine-1-carboxylate (167a) Yellow solid, yield 98%. ¹H NMR (500 MHz, CDCl₃) δ 10.03 (dt, $J_1 = 6.84$ Hz, $J_2 = 1.11$ Hz, 1H), 8.46 (dt, $J_1 = 8.67$ Hz, $J_2 = 1.14$ Hz, 1H), 7.86 (d, $J = 6.87$ Hz, 3H), 7.48-7.73 (m, 4H), 7.16 (td, $J_1 = 6.95$ Hz, $J_2 = 1.29$ Hz, 1H), 3.95 (s, 3H). ¹³C NMR (125 MHz, CDCl₃) δ 190.25, 166.87, 139.80, 131.48, 129.18, 129.03, 128.92, 128.53, 128.37, 127.80, 119.41, 116.89, 115.35, 105.84, 51.28. MS: m/z (%) = 279 (100) [M⁺], 248 (67), 220 (20), 202 (24), 105 (34), 77 (28). HRMS (ESI-QTOF) m/z : [M+H]⁺ Calcd for C₁₇H₁₄NO₃: 280.0968; Found: 280.0964.

ethyl 3-benzoylindolizine-1-carboxylate (167b) Yellow solid, yield 96%. ¹H NMR (500 MHz, CDCl₃) δ 9.97 (d, $J = 7.05$ Hz, 1H), 8.39 (d, $J = 8.95$ Hz, 1H), 7.82 (d, $J = 6.35$ Hz, 3H), 7.59 (tt, $J_1 = 7.45$ Hz, $J_2 = 1.30$ Hz, 1H), 7.52 (t, $J = 7.1$ Hz, 1H), 7.44-7.48 (m, 1H), 7.10 (td, $J_1 = 6.95$ Hz, $J_2 = 1.30$ Hz, 1H), 4.38 (q, $J = 7.15$ Hz, 2H), 1.40 (t, $J = 7.10$ Hz, 3H). ¹³C NMR (125 MHz, CDCl₃) δ 185.57, 164.06, 139.85, 131.45, 129.21, 129.05, 129.01, 128.94, 128.37, 127.70, 122.46, 119.47, 115.28, 106.23, 60.10, 14.52. MS: m/z (%) = 293 (100) [M⁺], 265 (16), 248 (73), 221 (24), 188 (24), 105 (42), 77 (36). HRMS (ESI-QTOF) m/z : [M+H]⁺ Calcd for C₁₈H₁₆NO₃: 294.1125; Found: 294.1119.

3-benzoyl-2-methylindolizine-1-carbaldehyde (167c) Brown solid, yield 44%. ¹H NMR (500 MHz, CDCl₃) δ 9.54 (d, $J = 7.0$ Hz, 1H), 8.45 (d, $J = 8.8$ Hz, 1H), 7.69 (dd, $J_1 = 5.0$ Hz, $J_2 = 1.35$ Hz, 2H), 7.59 (tt, $J_1 = 7.0$ Hz, $J_2 = 1.45$ Hz, 1H), 7.50 (d, $J = 5.0$ Hz, 2H), 7.07 (td, $J_1 = 10.0$ Hz, $J_2 = 1.40$ Hz, 1H), 2.20 (s, 3H). ¹³C NMR (125 MHz, CDCl₃) δ 187.70, 184.22, 140.68, 139.20, 137.77, 132.05, 129.14, 128.68, 128.62, 128.50, 122.75, 118.56, 115.74, 113.57, 12.34. MS: m/z (%) = 262 (100) [M⁺], 234 (30), 204 (13), 186 (9), 105 (13), 77 (32). HRMS (ESI-QTOF) m/z : [M+H]⁺ Calcd for C₁₇H₁₄NO₂: 264.1019; Found: 264.1019.

methyl 3-benzoyl-2-pentylindolizine-1-carboxylate (167d) Yellow solid, yield 72%. ¹H NMR (500 MHz, CDCl₃) δ 9.36 (dt, $J_1 = 7.05$ Hz, $J_2 = 1.10$ Hz, 1H), 8.33 (dt, $J_1 = 10.0$ Hz, $J_2 = 1.25$ Hz, 1H), 7.67-7.69 (m, 2H), 7.56 (tt, $J_1 = 7.45$ Hz, $J_2 = 1.90$ Hz, 1H), 7.47 (tt, $J_1 = 7.45$ Hz, $J_2 = 1.55$ Hz, 2H), 7.31-7.34 (m, 1H), 6.92 (td, $J_1 = 5.0$ Hz, $J_2 = 1.40$ Hz, 1H), 3.91 (s, 3H), 2.64 (t, $J = 8.0$ Hz, 2H), 1.37 (quint, $J = 10.0$ Hz, 2H), 1.07 (sext, $J = 7.3$ Hz, 2H), 0.94 (quint, $J = 10.0$ Hz, 2H), 0.75 (t, $J = 10.0$ Hz, 3H). ¹³C NMR (125 MHz, CDCl₃) δ 188.29, 165.12, 142.93, 140.98, 139.61, 131.71, 128.47, 128.44, 128.05, 126.83,

122.43, 119.48, 114.21, 104.04, 50.90, 31.84, 31.46, 26.45, 22.11, 13.94. MS: m/z (%) = 349 (59) [M^+], 293 (65), 265 (41), 244 (21), 233 (28), 204 (26), 188 (32), 105 (100), 77 (37). HRMS (ESI-QTOF) m/z : [$M+H$]⁺ Calcd for $C_{22}H_{24}NO_3$: 350.1751; Found: 350.1752.

(1-nitro-2-phenylindolizin-3-yl)(phenyl)methanone (167e) Yellow solid, yield 82%. 1H NMR (500 MHz, $CDCl_3$) δ 6.91 (td, $J_1 = 10.0$ Hz, $J_2 = 1.45$ Hz, 1H), 7.00-7.03 (m, 5H), 7.08-7.10 (m, 2H), 7.13-7.20 (m, 2H), 7.41-7.43 (m, 2H), 7.56 (dt, $J_1 = 10.0$ Hz, $J_2 = 1.25$ Hz, 1H), 9.81 (dq, $J_1 = 7.17$ Hz, $J_2 = 0.80$ Hz, 1H). ^{13}C NMR (125 MHz, $CDCl_3$) δ 188.41, 138.12, 134.59, 133.94, 131.97, 130.99, 130.81, 130.33, 129.21, 128.14, 128.04, 127.67, 127.41, 124.28, 121.38, 119.40, 116.41. MS: m/z (%) = 342 (100) [M^+], 325 (10), 312 (32), 295 (16), 267 (32), 248 (20), 237 (24), 105 (76), 77 (72). HRMS (ESI-QTOF) m/z : [$M+H$]⁺ Calcd for $C_{21}H_{15}N_2O_3$: 343.1077; Found: 343.1095.

(1-nitro-2-(thiophen-2-yl)indolizin-3-yl)(phenyl)methanone (167f) Yellow solid, yield 59%. 1H NMR (500 MHz, $CDCl_3$) δ 6.65 (dd, $J_1 = 5.05$ Hz, $J_2 = 3.6$ Hz, 1H), 6.87 (dd, $J_1 = 3.60$ Hz, $J_2 = 1.25$ Hz, 1H), 7.16-7.21 (m, 5H), 7.33 (tt, $J_1 = 7.45$ Hz, $J_2 = 1.30$ Hz, 1H), 7.52-7.54 (m, 1H), 7.64 (dd, $J_1 = 9.2$ Hz, $J_2 = 1.10$ Hz, 1H), 9.34 (dt, $J_1 = 7.05$ Hz, $J_2 = 1.1$ Hz, 1H). ^{13}C NMR (125 MHz, $CDCl_3$) δ 188.30, 138.07, 134.52, 132.25, 130.91, 130.41, 130.26, 129.27, 128.90, 128.40, 127.87, 127.51, 127.00, 126.36, 119.42, 116.47. MS: m/z (%) = 348 (100) [M^+], 302 (20), 273 (14), 105 (90), 77 (85). HRMS (ESI-QTOF) m/z : [$M+H$]⁺ Calcd for $C_{19}H_{13}N_2O_3S$: 349.0646; Found: 349.0663.

(2-(furan-2-yl)-1-nitroindolizin-3-yl)(phenyl)methanone (167g) Brown solid, yield 14%. 1H NMR (500 MHz, $CDCl_3$) δ 6.16 (q, $J = 1.8$ Hz, 1H), 6.68 (dd, $J_1 = 3.43$ Hz, $J_2 = 0.75$ Hz, 1H), 7.07 (q, $J = 0.8$ Hz, 1H), 7.17 (td, $J_1 = 10.0$ Hz, $J_2 = 1.35$ Hz, 1H), 7.23-7.26 (m, 2H), 7.37 (tt, $J_1 = 7.4$ Hz, $J_2 = 1.30$ Hz, 1H), 7.56 (dd, $J_1 = 8.35$ Hz, $J_2 = 1.30$ Hz, 2H), 7.63 (dd, $J_1 = 6.9$ Hz, $J_2 = 1.10$ Hz, 1H), 8.65 (dt, $J_1 = 9.05$ Hz, $J_2 = 1.15$ Hz, 1H), 9.37 (dt, $J_1 = 7.05$ Hz, $J_2 = 1.10$ Hz, 1H). ^{13}C NMR (125 MHz, $CDCl_3$) δ 188.00, 143.49, 142.43, 138.55, 134.38, 132.19, 130.20, 128.92, 128.34, 128.05, 127.62, 127.53, 122.13, 119.46, 116.58, 115.54, 11.66. MS: m/z (%) = 332 (73), 303 (93), 287 (58), 258 (17), 105 (87), 77 (100) [M^+]. HRMS (ESI-QTOF) m/z : [$M+H$]⁺ Calcd for $C_{22}H_{14}F_3N_2O_3$: 411.0951; Found: 411.0966.

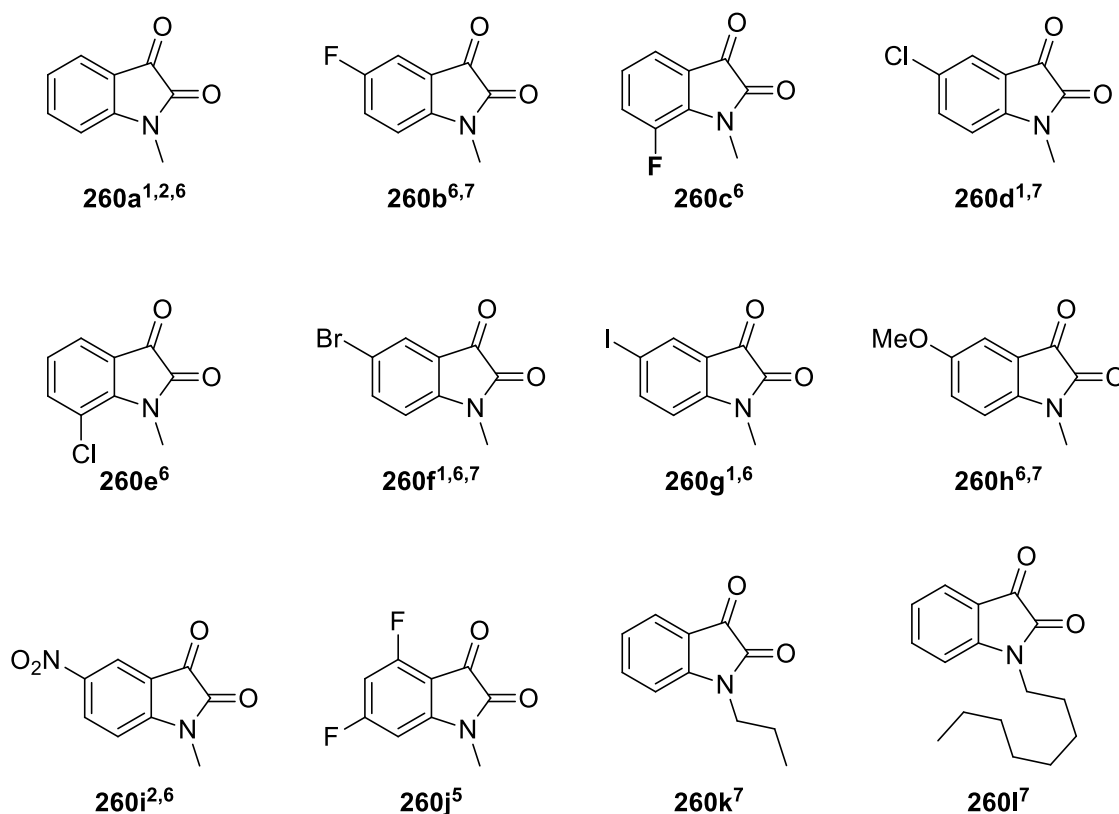
(1-nitro-2-(2-(trifluoromethyl)phenyl)indolizin-3-yl)(phenyl)methanone (167h) Yellow solid, yield 7%. 1H NMR (500 MHz, $CDCl_3$) δ 7.08-7.15 (m, 4H), 7.20-7.26

(m, 5H), 7.16-7.21 (m, 5H), 7.43 (dd, $J_1 = 10.0$ Hz, $J_2 = 1.80$ Hz, 1H), 7.68 (dd, $J_1 = 9.35$ Hz, $J_2 = 1.11$ Hz, 1H), 8.66 (dt, $J_1 = 10.0$ Hz, $J_2 = 1.15$ Hz, 1H), 9.50 (dt, $J_1 = 10.0$ Hz, $J_2 = 1.0$ Hz, 1H). ^{13}C NMR (125 MHz, CDCl_3) δ 188.24, 138.64, 134.22, 132.44, 131.71, 130.91, 130.72, 130.67, 129.81, 128.63, 128.54, 128.43, 127.80, 126.17 ($J = 4.6$ Hz), 124.94, 122.76, 121.83, 119.30, 116.70. MS: m/z (%) = 410 (93) [M^+], 341 (100), 295 (13), 105 (56), 77 (60). HRMS (ESI-QTOF) m/z : [$\text{M}+\text{H}$] $^+$ Calcd for $\text{C}_{19}\text{H}_{13}\text{N}_2\text{O}_4$: 333.0870; Found: 333.0879.

Research line 3b - Highly diastereoselective multicomponent synthesis of spirocyclopropyl oxindoles enabled by rare-earth metal salts

N-alkyl isatin derivatives

Isatin derivatives **260a**-**260k** are known compounds and were synthesized according to the literature procedure.¹⁻⁷ Compound **260l** has been synthesized using the same procedure as compound **260k**.



General procedure for the synthesis of spirocyclopropyl oxindoles

In a 10 mL three-necked round-bottomed flask, equipped with a bubble condenser and magnetic stir bar, a mixture composed of *dry* pyridine (5 mL), **260a-l** (1 eq.), triethyl phosphonoacetate **2** (1 eq.), 2-bromoacetophenone **3** (2.5 eq.), $\text{Sc}(\text{OTf})_3$ (20 mol%),

and K₂CO₃ (6 eq.) was placed. The reaction was warmed at 70 °C for 6 h. The crude was evaporated under a vacuum through an azeotrope made up of adding toluene to the reaction mixture (3x5 mL). The residues of toluene were evaporated in the same fashion, using an azeotrope made up of adding ethanol to the mixture (3x5 mL). The crude was then extracted through a liquid/liquid separation, using ethyl acetate (EtOAc), water, and brine, and purified on a flash silica gel column by using EtOAc/hexane (1:4 v/v) to obtain the desired product (**264a-l**).

(1R,2S,3S)-ethyl-3-benzoyl-1'-methyl-2'-oxospiro[cyclopropane-1,3'-indoline]-2-carboxylate 264a (major isomer): obtained using *N*-methylisatin **1a**, triethyl phosphonoacetate **2**, and 2-bromoacetophenone **3**. Purified by normal phase chromatography (EtOAc:Hexane, 1:4) to yield **5a** as major isomer (33 mg, 95%, **5a:5b**: 91:9 *dr*), as red solid. ¹H NMR (400 MHz, CDCl₃) δ 7.95 – 7.93 (m, 2H), 7.60 – 7.51 (m, 1H), 7.43 (t, *J* = 7.7 Hz, 2H), 7.25 (dd, *J* = 7.7, 1.2 Hz, 1H), 7.19 (dd, *J* = 7.6, 0.7 Hz, 1H), 6.99 (td, *J* = 7.6, 1.0 Hz, 1H), 6.87 (d, *J* = 7.8 Hz, 1H), 4.35 – 4.24 (m, 2H), 4.23 (d, *J* = 7.7 Hz, 1H), 3.63 (d, *J* = 7.7 Hz, 1H), 3.32 (s, 3H), 1.31 (t, *J* = 7.1 Hz, 3H). ¹³C NMR (126 MHz, CDCl₃) δ 191.70, 171.75, 166.23, 144.12, 136.63, 133.82, 128.74, 128.56, 128.35, 124.23, 122.60, 122.48, 108.24, 61.72, 39.59, 38.93, 35.00, 26.80, 14.16. HRMS (MALDI-TOF) *m/z*: [M+H]⁺ Calcd for C₂₁H₂₀NO₄: 350.1387; Found: 350.282.

(1R,2R,3R)-ethyl-3-benzoyl-1'-methyl-2'-oxospiro[cyclopropane-1,3'-indoline]-2-carboxylate 264a' (minor isomer): ¹H NMR (400 MHz, CDCl₃) δ 7.79 (dd, *J* = 8.4, 1.3 Hz, 2H), 7.62 – 7.48 (m, 2H), 7.45 – 7.34 (m, 3H), 7.15 (td, *J* = 7.7, 1.1 Hz, 1H), 6.94 (d, *J* = 7.8 Hz, 1H), 4.37 – 4.08 (m, 2H), 3.85 (d, *J* = 7.8 Hz, 1H), 3.51 (d, *J* = 7.8 Hz, 1H), 3.16 (s, 3H), 1.26 (t, *J* = 7.1 Hz, 3H). ¹³C NMR (126 MHz, CDCl₃) δ 189.95, 171.04, 167.71, 144.58, 136.05, 133.55, 128.74, 128.69, 128.39, 124.10, 122.71, 122.64, 108.34, 61.73, 39.63, 39.01, 35.20, 26.64, 14.13. HRMS (MALDI-TOF) *m/z*: [M+H]⁺ Calcd for C₂₁H₂₀NO₄: 350.1387; Found: 350.279.

(1R,2S,3S)-ethyl-3-benzoyl-5'-fluoro-1'-methyl-2'-oxospiro[cyclopropane-1,3'-indoline]-2-carboxylate 264b (major isomer): obtained using 5-fluoro-*N*-methylisatin **1b**, triethyl phosphonoacetate **2**, and 2-bromoacetophenone **3**. Purified by normal phase chromatography (EtOAc:Hexane, 1:4) to yield **6a** as major isomer (35 mg, 95%, **6a:6b**: 90:10 *dr*), as brown oil. ¹H NMR (400 MHz, CDCl₃) δ 7.96 (dd, *J* = 8.5, 1.3 Hz, 2H), 7.73 – 7.51 (m, 1H), 7.53 – 7.39 (m, 2H), 7.07 – 6.89 (m, 2H), 6.78 (dd, *J* =

8.5, 4.2 Hz, 1H), 4.40 – 4.15 (m, 3H), 3.60 (d, $J = 7.8$ Hz, 1H), 3.31 (s, 3H), 1.31 (t, $J = 7.1$ Hz, 3H). ^{13}C NMR (126 MHz, CDCl_3) δ 191.46, 171.52, 165.94, 159.99, 158.08, 140.14, 136.50, 133.99, 128.72 (d, $J = 23.2$ Hz), 125.77 (d, $J = 9.4$ Hz), 114.65 (d, $J = 23.9$ Hz), 111.04 (d, $J = 26.6$ Hz), 108.61 (d, $J = 8.5$ Hz), 61.84, 38.88, 35.39, 29.29, 26.94, 14.15. HRMS (MALDI-TOF) m/z : $[\text{M}+\text{Na}]^+$ Calcd for $\text{C}_{21}\text{H}_{18}\text{FNNaO}_4$: 390.1112; Found: 390.269.

(1R,2S,3S)-ethyl-3-benzoyl-7'-fluoro-1'-methyl-2'-oxospiro[cyclopropane-1,3'-indoline]-2-carboxylate 264c (major isomer): obtained using 7-fluoro-*N*-methylisatin **1c**, triethyl phosphonoacetate **2**, and 2-bromoacetophenone **3**. Purified by normal phase chromatography (EtOAc:Hexane, 1:4) to yield **7a** as major isomer (33 mg, 90%, **7a:7b**: 91:9 *dr*), as brown oil. ^1H NMR (400 MHz, CDCl_3) δ 8.16 – 7.73 (m, 2H), 7.67 – 7.51 (m, 1H), 7.52 – 7.39 (m, 3H), 7.09 – 6.81 (m, 3H), 4.28 (qt, $J = 7.1, 3.5$ Hz, 2H), 4.22 (d, $J = 7.8$ Hz, 1H), 3.61 (d, $J = 7.8$ Hz, 1H), 3.54 (d, $J = 2.8$ Hz, 3H), 1.32 (t, $J = 7.1$ Hz, 3H). ^{13}C NMR (126 MHz, CDCl_3) δ 191.37, 171.46, 165.93, 148.76, 146.83, 136.50, 133.97, 128.82, 128.57, 126.98 (d, $J = 3.5$ Hz), 123.10 (d, $J = 6.5$ Hz), 118.28 (d, $J = 3.3$ Hz), 116.38 (d, $J = 19.0$ Hz), 61.84, 39.44, 35.43, 29.42, 29.37, 14.15. HRMS (MALDI-TOF) m/z : $[\text{M}+\text{H}]^+$ Calcd for $\text{C}_{21}\text{H}_{19}\text{FNO}_4$: 368.1293; Found: 368.291.

(1R,2S,3S)-ethyl-3-benzoyl-5'-chloro-1'-methyl-2'-oxospiro[cyclopropane-1,3'-indoline]-2-carboxylate 264d (major isomer): obtained using 5-chloro-*N*-methylisatin **1d**, triethyl phosphonoacetate **2**, and 2-bromoacetophenone **3**. Purified by normal phase chromatography (EtOAc:Hexane, 1:4) to yield **8a** as major isomer (36 mg, 93%, **8a:8b**: 90:10 *dr*), as brown oil. ^1H NMR (400 MHz, CDCl_3) δ 8.07 – 7.84 (m, 2H), 7.67 – 7.52 (m, 1H), 7.51 – 7.41 (m, 2H), 7.27 – 7.20 (m, 1H), 6.79 (dd, $J = 8.1, 0.6$ Hz, 2H), 4.36 – 4.14 (m, 3H), 3.61 (d, $J = 7.8$ Hz, 1H), 3.30 (s, 3H), 1.31 (t, $J = 7.1$ Hz, 3H). ^{13}C NMR (101 MHz, CDCl_3) δ 191.40, 171.37, 165.88, 142.69, 136.48, 134.02, 128.82, 128.65, 128.33, 128.15, 125.85, 123.14, 109.10, 61.87, 39.35, 38.95, 35.42, 26.93, 14.15. HRMS (MALDI-TOF) m/z : $[\text{M}+\text{H}]^+$ Calcd for $\text{C}_{21}\text{H}_{19}\text{ClNO}_4$: 384.0997; Found: 384.260.

(1R,2S,3S)-ethyl-3-benzoyl-7'-chloro-1'-methyl-2'-oxospiro[cyclopropane-1,3'-indoline]-2-carboxylate 264e (major isomer): obtained using 7-chloro-*N*-methylisatin **1e**, triethyl phosphonoacetate **2**, and 2-bromoacetophenone **3**. Purified by normal phase chromatography (EtOAc:Hexane, 1:4) to yield **9a** as major isomer (34 mg, 90%, **9a:9b**: 91:9 *dr*), as brown oil. ^1H NMR (400 MHz, CDCl_3) δ 7.92 (dd, $J = 8.5,$

1.3 Hz, 2H), 7.68 – 7.51 (m, 1H), 7.48 – 7.40 (m, 2H), 7.17 (dd, $J = 8.2, 1.2$ Hz, 1H), 7.05 (dd, $J = 7.6, 1.2$ Hz, 1H), 6.88 (dd, $J = 8.2, 7.6$ Hz, 1H), 4.27 (qd, $J = 7.1, 3.1$ Hz, 2H), 4.22 (d, $J = 7.9$ Hz, 1H), 3.69 (s, 3H), 3.60 (d, $J = 7.9$ Hz, 1H), 1.31 (t, $J = 7.1$ Hz, 3H). ^{13}C NMR (101 MHz, CDCl_3) δ 191.28, 172.12, 165.91, 139.90, 136.44, 134.02, 130.72, 128.83, 128.57, 126.87, 123.30, 120.80, 115.79, 77.36, 77.04, 76.73, 61.87, 39.72, 39.13, 35.43, 30.32, 14.15. HRMS (MALDI-TOF) m/z : $[\text{M}+\text{H}]^+$ Calcd for $\text{C}_{21}\text{H}_{19}\text{ClNO}_4$: 384.0997; Found: 384.239.

(1R,2S,3S)-ethyl-3-benzoyl-5'-bromo-1'-methyl-2'-oxospiro[cyclopropane-1,3'-indoline]-2-carboxylate 264f (major isomer): obtained using 5-bromo-*N*-methylisatin **1f**, triethyl phosphonoacetate **2**, and 2-bromoacetophenone **3**. Purified by normal phase chromatography (EtOAc:Hexane, 1:4) to yield **10a** as major isomer (38 mg, 92%, **10a:10b**: 90:10 *dr*), as brown oil. ^1H NMR (400 MHz, CDCl_3) δ 7.98 – 7.94 (m, 2H), 7.62 – 7.55 (m, 1H), 7.51 – 7.43 (m, 2H), 7.40 (dd, $J = 8.3, 2.0$ Hz, 1H), 7.36 (d, $J = 2.0$ Hz, 1H), 6.74 (d, $J = 8.3$ Hz, 1H), 4.33 – 4.21 (m, 3H), 3.61 (d, $J = 7.7$ Hz, 1H), 3.30 (s, 3H), 1.31 (t, $J = 7.2$ Hz, 3H). ^{13}C NMR (126 MHz, CDCl_3) δ 191.39, 171.26, 165.86, 143.18, 136.51, 134.00, 131.25, 128.82, 128.65, 126.22, 125.85, 115.41, 109.58, 61.86, 39.00, 35.47, 29.29, 26.89, 14.14. HRMS (MALDI-TOF) m/z : $[\text{M}+\text{H}]^+$ Calcd for $\text{C}_{21}\text{H}_{19}\text{BrNO}_4$: 428.0492; Found: 428.203.

(1R,2S,3S)-ethyl-3-benzoyl-5'-iodo-1'-methyl-2'-oxospiro[cyclopropane-1,3'-indoline]-2-carboxylate 264g (major isomer): obtained using 5-iodo-*N*-methylisatin **1g**, triethyl phosphonoacetate **2**, and 2-bromoacetophenone **3**. Purified by normal phase chromatography (EtOAc:Hexane, 1:4) to yield **11a** as major isomer (43 mg, 90%, **11a:11b**: 90:10 *dr*), as brown oil. ^1H NMR (400 MHz, CDCl_3) δ 8.00 – 7.90 (m, 2H), 7.58 (ddd, $J = 7.2, 6.1, 1.5$ Hz, 2H), 7.51 (d, $J = 1.7$ Hz, 1H), 7.46 (t, $J = 7.7$ Hz, 2H), 6.64 (d, $J = 8.2$ Hz, 1H), 4.35 – 4.15 (m, 3H), 3.59 (d, $J = 7.8$ Hz, 1H), 3.29 (s, 3H), 1.31 (t, $J = 7.1$ Hz, 3H). ^{13}C NMR (126 MHz, CDCl_3) δ 191.36, 171.07, 165.85, 143.84, 137.24, 136.52, 133.98, 131.33, 128.80, 128.63, 126.52, 110.17, 85.19, 61.85, 39.03, 35.44, 29.70, 26.83, 14.14. HRMS (MALDI-TOF) m/z : $[\text{M}+\text{H}]^+$ Calcd for $\text{C}_{21}\text{H}_{19}\text{INO}_4$: 476.0353; Found: 476.209.

(1R,2S,3S)-ethyl-3-benzoyl-5'-methoxy-1'-methyl-2'-oxospiro[cyclopropane-1,3'-indoline]-2-carboxylate 264h (major isomer): obtained using 5-methoxy-*N*-methylisatin **1h**, triethyl phosphonoacetate **2**, and 2-bromoacetophenone **3**. Purified

by normal phase chromatography (EtOAc:Hexane, 1:4) to yield **12a** as major isomer (36 mg, 95%, **12a:12b**: 94:6 *dr*), as brown oil. ^1H NMR (400 MHz, CDCl_3) δ 7.95 (dd, $J = 8.5$, 1.3 Hz, 2H), 7.62 – 7.51 (m, 1H), 7.47 – 7.40 (m, 3H), 6.86 – 6.71 (m, 2H), 4.38 – 4.24 (m, 2H), 4.22 (d, $J = 7.7$ Hz, 1H), 3.76 (s, 3H), 3.59 (d, $J = 7.8$ Hz, 1H), 3.29 (s, 3H), 1.31 (t, $J = 7.2$ Hz, 3H). ^{13}C NMR (126 MHz, CDCl_3) δ 191.66, 171.49, 166.22, 155.91, 137.67, 136.66, 133.82, 128.74, 128.60, 125.41, 113.41, 109.50, 108.58, 61.72, 55.86, 39.84, 38.90, 35.11, 26.87, 14.16. HRMS (MALDI-TOF) m/z : $[\text{M}+\text{H}]^+$ Calcd for $\text{C}_{22}\text{H}_{22}\text{NO}_5$: 380.1492; Found: 380.306.

(1R,2S,3S)-ethyl-3-benzoyl-1'-methyl-5'-nitro-2'-oxospiro[cyclopropane-1,3'-indoline]-2-carboxylate 264i (major isomer): obtained using 5-nitro-*N*-methylisatin **1i**, triethyl phosphonoacetate **2**, and 2-bromoacetophenone **3**. Purified by normal phase chromatography (EtOAc:Hexane, 1:4) to yield **13a** as major isomer (18 mg, 45%, **13a:13b**: 90:10 *dr*), as pale yellow solid. ^1H NMR (500 MHz, CDCl_3) δ 8.50 (d, $J = 2.3$ Hz, 1H), 8.37 (dd, $J = 8.7$, 2.3 Hz, 1H), 7.83 – 7.73 (m, 2H), 7.60 – 7.51 (m, 1H), 7.43 – 7.35 (m, 2H), 7.02 (d, $J = 8.7$ Hz, 1H), 4.33 – 4.16 (m, 2H), 3.99 (d, $J = 8.0$ Hz, 1H), 3.55 (d, $J = 8.0$ Hz, 1H), 3.23 (s, 3H), 1.29 (t, $J = 7.1$ Hz, 3H). ^{13}C NMR (126 MHz, CDCl_3) δ 188.80, 171.15, 167.00, 149.77, 143.44, 135.62, 133.90, 128.85, 128.29, 125.68, 124.87, 118.91, 107.94, 62.22, 40.11, 38.24, 35.96, 27.06, 14.06. HRMS (ESI-QTOF) m/z : $[\text{M}+\text{H}]^+$ Calcd for $\text{C}_{21}\text{H}_{18}\text{N}_2\text{O}_6$: 395.1238; Found: 395.1251.

(1R,2S,3S)-ethyl-3-benzoyl-2'-oxo-1'-propylspiro[cyclopropane-1,3'-indoline]-2-carboxylate 264k (major isomer): obtained using *N*-propylisatin **1k**, triethyl phosphonoacetate **2**, and 2-bromoacetophenone **3**. Purified by normal phase chromatography (EtOAc:Hexane, 1:4) to yield **15a** (35 mg, 93%, **15a:15b**: 91:9 *dr*), as red solid. ^1H NMR (500 MHz, CDCl_3) δ 7.90 (dd, $J = 8.5$, 1.3 Hz, 2H), 7.55 – 7.46 (m, 1H), 7.42 – 7.35 (m, 2H), 7.21 (td, $J = 7.7$, 1.2 Hz, 1H), 7.16 – 7.12 (m, 1H), 6.93 (td, $J = 7.7$, 1.0 Hz, 1H), 6.86 (d, $J = 7.9$ Hz, 1H), 4.24 (qd, $J = 7.2$, 1.7 Hz, 2H), 4.19 (d, $J = 7.7$ Hz, 1H), 3.78 (dd, $J = 7.6$, 6.6 Hz, 2H), 3.61 (d, $J = 7.7$ Hz, 1H), 1.74 (h, $J = 7.3$ Hz, 2H), 1.27 (t, $J = 7.1$ Hz, 3H), 0.96 (t, $J = 7.4$ Hz, 3H). ^{13}C NMR (126 MHz, CDCl_3) δ 190.65, 170.76, 165.23, 142.46, 135.56, 132.77, 127.68, 127.46, 127.22, 123.29, 121.43, 121.30, 107.53, 60.64, 40.97, 38.36, 37.99, 33.87, 19.75, 13.11, 10.20. HRMS (ESI-QTOF) m/z : $[\text{M}+\text{H}]^+$ Calcd for $\text{C}_{23}\text{H}_{24}\text{NO}_4$: 378.1700; Found: 378.1708.

(1R,2S,3S)-ethyl-3-benzoyl-1'-octyl-2'-oxospiro[cyclopropane-1,3'-indoline]-2-carboxylate 264l (major isomer): obtained using *N*-octylisatin **1**, triethyl phosphonoacetate **2**, and 2-bromoacetophenone **3**. Purified by normal phase chromatography (EtOAc:Hexane, 1:4) to yield **16a** (41 mg, 91%, **16a:16b**: 90:10 *dr*), as red solid. ¹H NMR (500 MHz, CDCl₃) δ 7.91 (dd, *J* = 8.5, 1.2 Hz, 2H), 7.56 – 7.50 (m, 1H), 7.43 – 7.37 (m, 1H), 7.23 (td, *J* = 7.7, 1.2 Hz, 1H), 7.17 – 7.14 (m, 1H), 6.95 (td, *J* = 7.6, 1.0 Hz, 1H), 6.87 (d, *J* = 7.7 Hz, 1H), 4.30 – 4.22 (m, 2H), 4.20 (d, *J* = 7.7 Hz, 1H), 3.87 – 3.74 (m, 2H), 3.62 (d, *J* = 7.7 Hz, 1H), 1.71 (p, *J* = 7.3 Hz, 2H), 1.45 – 1.18 (m, 15H), 0.97 – 0.82 (m, 3H). ¹³C NMR (126 MHz, CDCl₃) δ 190.66, 170.64, 165.22, 142.46, 135.59, 132.76, 127.68, 127.47, 127.22, 123.32, 121.46, 121.29, 107.50, 60.64, 39.50, 38.41, 38.01, 33.83, 30.75, 28.21, 28.18, 26.45, 25.81, 21.60, 13.14, 13.05. HRMS (ESI-QTOF) *m/z*: [M+H]⁺ Calcd for C₂₈H₃₄NO₄: 448.2482; Found: 448.2505.

Computational studies

Full geometry optimizations and transition structure (TS) searches were carried out with Gaussian 16⁸ using the ωB97X-D hybrid functional,⁹ 6-31G(d,p) basis set for C, N, O, and H, and LANL2DZ¹⁰ effective core potential for Sc and Br atoms with ultrafine integration grids. Bulk solvent effects in pyridine were considered implicitly through the IEF-PCM polarizable continuum model.¹¹ The possibility of different conformations was considered for all structures. All stationary points were characterized by a frequency analysis performed at the same level used in the geometry optimizations from which thermal corrections were obtained at 343.15 K. The quasiharmonic approximation reported by Truhlar *et al.*¹² and Head-Gordon *et al.*¹³ was used to replace the harmonic oscillator approximation for the calculation of the vibrational contribution to entropy and enthalpy, respectively. Scaled frequencies were not considered. Mass-weighted intrinsic reaction coordinate (IRC) calculations were carried out by using the Hratchian and Schlegel scheme¹⁴ to ensure that the TSs indeed connected the appropriate reactants and products. Gibbs free energies (ΔG) were used for the discussion on the relative stabilities of the considered structures. The lowest energy conformer for each calculated stationary point (**Figure C1**) was considered in the discussion; all the computed structures can be obtained from authors upon request. Electronic energies, entropies, enthalpies, Gibbs free energies, and the lowest frequencies of the calculated structures are summarized in **Table C1**.

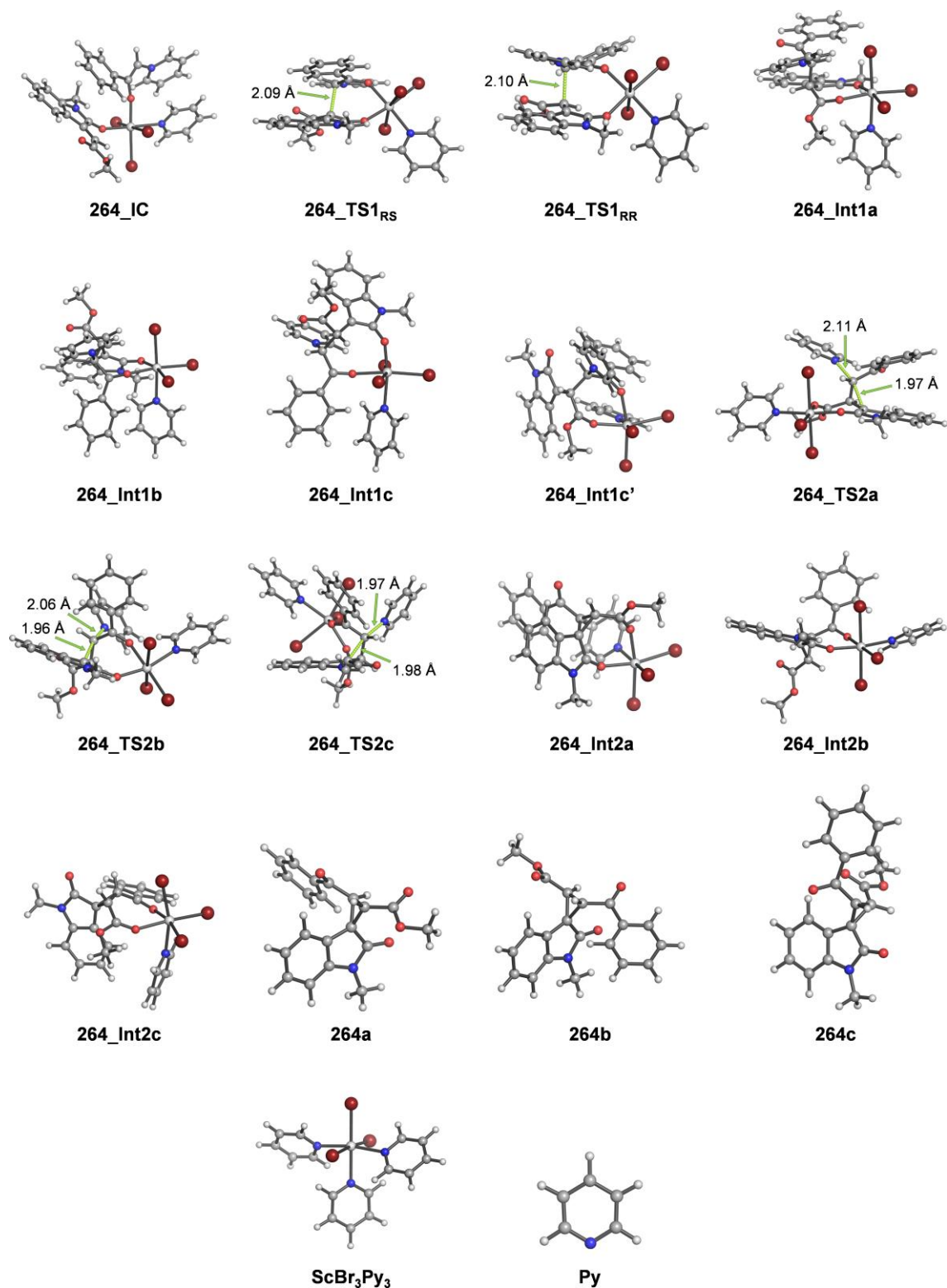


Figure C1. Lowest energy geometries for the reactants, transition states, intermediates and products for the reaction pathways calculated with PCM(pyridine)/ ω B97X-D/6-31G(d,p)+LANL2DZ(Sc,Br).

Table C1. Energies, entropies, and lowest frequencies of the lowest energy calculated structures.^a

Structure	E _{elec} (Hartree)	E _{elec} + ZPE (Hartree)	H (Hartree)	S (cal mol ⁻¹ K ⁻¹)	G (Hartree)	Lowest freq. (cm ⁻¹)	# imag. freq.
264_IC	-1710.481414	0.523066	-1709.915627	278.8	-1710.054398	11.7	0
264_TS1RS	-1710.446428	0.523312	-1709.881123	273.9	-1710.016854	-522.1	1
264_TS1RR	-1710.456122	0.523733	-1709.890398	268.9	-1710.025620	-478.0	1
264_Int1a	-1710.493585	0.526045	-1709.925608	271.9	-1710.061497	14.5	0
264_Int1b	-1710.487575	0.526188	-1709.919452	272.5	-1710.055204	14.9	0
264_Int1c	-1710.485007	0.525749	-1709.917496	275.1	-1710.053392	8.8	0
264_Int1c'	-1710.440462	0.526314	-1709.872002	265.5	-1710.006671	24.8	0
264_TS2a	-1710.442804	0.522058	-1709.878656	277.5	-1710.015566	-522.0	1
264_TS2b	-1710.441536	0.521387	-1709.878339	282.6	-1710.016284	-554.2	1
264_TS2c	-1710.411052	0.522524	-1709.846268	269.9	-1709.982475	-451.7	1
264_Int2a	-1462.260401	0.431409	-1461.792033	248.3	-1461.915361	13.8	0
264_Int2b	-1462.256426	0.431223	-1461.788476	251.8	-1461.912294	11.1	0
264_Int2c	-1462.250759	0.431232	-1461.782668	246.2	-1461.905864	19.7	0
5a	-1127.708759	0.333948	-1127.350081	172.0	-1127.437990	14.7	0
5b	-1127.710687	0.334278	-1127.351582	170.2	-1127.439120	22.0	0
5c	-1127.706756	0.334286	-1127.347652	170.0	-1127.435187	18.8	0
Py	-248.207338	0.089931	-248.110851	71.2	-248.149811	391.4	0
ScBr ₃ Py ₃	-830.986690	0.279524	-830.682479	185.7	-830.777670	31.6	0

^aEnergy values calculated at the PCM(pyridine)/ ω B97X-D/6-31G(d,p) level. 1 Hartree = 627.51 kcal mol⁻¹. Thermal corrections at 343.15 K.

References

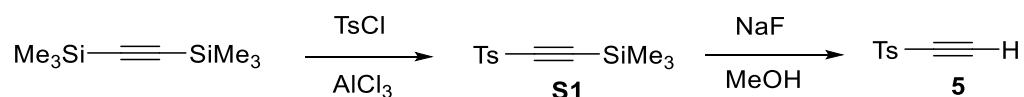
- (1) Ilangoan, A.; Satish, G. Direct Amidation of 2'-Aminoacetophenones Using I₂-TBHP: A Unimolecular Domino Approach toward Isatin and Iodoisatin. *J. Org. Chem.* **2014**, *79* (11), 4984–4991. <https://doi.org/10.1021/jo500550d>.
- (2) Mamuye, A. D.; Monticelli, S.; Castoldi, L.; Holzer, W.; Pace, V. Eco-Friendly Chemoselective N-Functionalization of Isatins Mediated by Supported KF in 2-MeTHF. *Green Chem.* **2015**, *17* (8), 4194–4197. <https://doi.org/10.1039/c5gc01002k>.
- (3) Buxton, C. S.; Blakemore, D. C.; Bower, J. F. Reductive Coupling of Acrylates with Ketones and Ketimines by a Nickel-Catalyzed Transfer-Hydrogenative Strategy. *Angew. Chemie - Int. Ed.* **2017**, *56* (44), 13824–13828. <https://doi.org/10.1002/anie.201707531>.
- (4) Sun, Z.; Xiang, K.; Tao, H.; Guo, L.; Li, Y. Synthesis of 2-Substituted 3-Chlorobenzofurans via TMSCl-Mediated Nucleophilic Annulation of Isatin-Derived Propargylic Alcohols. *Org. Biomol. Chem.* **2018**, *16* (33), 6133–6139. <https://doi.org/10.1039/c8ob01731j>.
- (5) Ryu, H.; Seo, J.; Ko, H. M. Synthesis of Spiro[Oxindole-3,2'-Pyrrolidine] Derivatives from Benzynes and Azomethine Ylides through 1,3-Dipolar Cycloaddition Reactions. *J. Org. Chem.* **2018**, *83* (22), 14102–14109. <https://doi.org/10.1021/acs.joc.8b02117>.
- (6) Zhang, Y.; Luo, L.; Ge, J.; Yan, S. Q.; Peng, Y. X.; Liu, Y. R.; Liu, J. X.; Liu, C.; Ma, T.; Luo, H. Q. “on Water” Direct Organocatalytic Cyanoarylmethylation of Isatins for the Diastereoselective Synthesis of 3-Hydroxy-3-Cyanomethyl Oxindoles. *J. Org. Chem.* **2019**, *84* (7), 4000–4008. <https://doi.org/10.1021/acs.joc.8b03194>.
- (7) Bojack, G.; Baltz, R.; Dittgen, J.; Fischer, C.; Freigang, J.; Getachew, R.; Grill, E.; Helmke, H.; Hohmann, S.; Lange, G.; Lehr, S.; Porée, F.; Schmidt, J.; Schmutzler, D.; Yang, Z.; Frackenpohl, J. Synthesis and Exploration of Abscisic Acid Receptor Agonists Against Drought Stress by Adding Constraint to a Tetrahydroquinoline-Based Lead Structure. *European J. Org. Chem.* **2021**, *2021* (23), 3442–3457. <https://doi.org/10.1002/ejoc.202100415>.
- (8) Frisch, M. J. ; Trucks, G. W. ; Schlegel, H. B. ; Scuseria, G. E. ; Robb, M. A. ; Cheeseman, J. R. ;

- Scalmani, G. ; Barone, V. ; Petersson, G. A. ; Nakatsuji, H. ; Li, X. ; Caricato, M. ; Marenich, A. V. ; Bloino, J. ; Janesko, B. G. ; Gomperts, R. ; Mennucci, B. ; Hratchian, H. P. ; Ortiz, J. V. ; Izmaylov, A. F. ; Sonnenberg, J. L. ; Williams-Young, D. ; Ding, F. ; Lipparini, F. ; Egidi, F. ; Goings, J. ; Peng, B. ; Petrone, A. ; Henderson, T. ; Ranasinghe, D. ; Zakrzewski, V. G. ; Gao, J. ; Rega, N. ; Zheng, G. ; Liang, W. ; Hada, M. ; Ehara, M. ; Toyota, K. ; Fukuda, R. ; Hasegawa, J. ; Ishida, M. ; Nakajima, T. ; Honda, Y. ; Kitao, O. ; Nakai, H. ; Vreven, T. ; Throssell, K. ; Montgomery, J. A., J. ; Peralta, J. E. ; Ogliaro, F. ; Bearpark, M. J. ; Heyd, J. J. ; Brothers, E. N. ; Kudin, K. N. ; Staroverov, V. N. ; Keith, T. A. ; Kobayashi, R. ; Normand, J. ; Raghavachari, K. ; Rendell, A. P. ; Burant, J. C. ; Iyengar, S. S. ; Tomasi, J. ; Cossi, M. ; Millam, J. M. ; Klene, M. ; Adamo, C. ; Cammi, R. ; Ochterski, J. W. ; Martin, R. L. ; Morokuma, K. ; Farkas, O. ; Foresman, J. B. ; Fox, D. J. Gaussian 16, Revision C.01. Wallingford CT 2016.
- (9) Chai, J. Da; Head-Gordon, M. Long-Range Corrected Hybrid Density Functionals with Damped Atom-Atom Dispersion Corrections. *Phys. Chem. Chem. Phys.* **2008**, *10* (44), 6615–6620. <https://doi.org/10.1039/b810189b>.
- (10) Hay, P. J.; Wadt, W. R. Ab Initio Effective Core Potentials for Molecular Calculations. Potentials for K to Au Including the Outermost Core Orbitals. *J. Chem. Phys.* **1985**, *82* (1), 299–310. <https://doi.org/10.1063/1.448975>.
- (11) Scalmani, G.; Frisch, M. J. Continuous Surface Charge Polarizable Continuum Models of Solvation. I. General Formalism. *J. Chem. Phys.* **2010**, *132* (11). <https://doi.org/10.1063/1.3359469>.
- (12) Ribeiro, R. F.; Marenich, A. V.; Cramer, C. J.; Truhlar, D. G. Use of Solution-Phase Vibrational Frequencies in Continuum Models for the Free Energy of Solvation. *J. Phys. Chem. B* **2011**, *115* (49), 14556–14562. <https://doi.org/10.1021/jp205508z>.
- (13) Li, Y. P.; Gomes, J.; Sharada, S. M.; Bell, A. T.; Head-Gordon, M. Improved Force-Field Parameters for QM/MM Simulations of the Energies of Adsorption for Molecules in Zeolites and a Free Rotor Correction to the Rigid Rotor Harmonic Oscillator Model for Adsorption Enthalpies. *J. Phys. Chem. C* **2015**, *119* (4), 1840–1850. <https://doi.org/10.1021/jp509921r>.
- (14) Hratchian, H. P.; Schlegel, H. B. Following Reaction Pathways Using a Damped Classical Trajectory Algorithm. *J. Phys. Chem. A* **2002**, *106* (1), 165–169. <https://doi.org/10.1021/jp012125b>.

Chapter 4: Quantum mechanical studies on expansion reactions of norbornane derivatives

Research line 4a - Studies on the regioselective rearrangement of azanorbornanic aminyl radicals into 2,8-diazabicyclo[3.2.1]oct-2-ene systems

Synthesis of alkyne 5 and cyclic pyrrole 6c



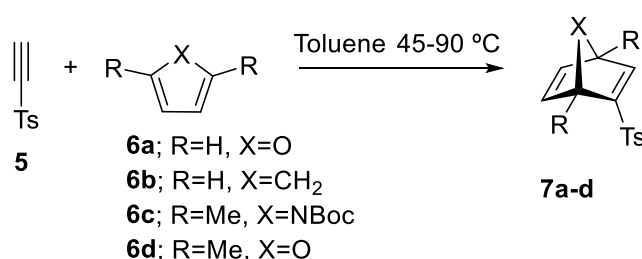
***p*-Tolyl [(2-trimethylsilyl)ethynyl] sulfone (S1)**¹ A mixture of AlCl₃ (14.7 g, 110 mmol) and tosyl chloride (21.9 g, 114 mmol) was dissolved in dry DCM (100 mL) and stirred under an argon atmosphere for 20 min at r.t. After this time, the crude was filtered through celite and the resultant liquid was added dropwise to a solution of commercial bis(trimethylsilyl) acetylene (23 mL, 102 mmol) in dry DCM (100 mL) at 0 °C for 1 h. After the addition, the reaction was allowed to warm at r.t. overnight. Once the reaction has finished, the mixture was poured into a solution of HCl in cold water (20%). The organic layer was washed with an aqueous solution of HCl (1M), with brine, and dried over anhydrous Na₂SO₄. The solvent was removed under reduced pressure and the resultant solid was recrystallized from Cy affording the desired product S1 as a grey powder (14.1 g, 55%). ¹H NMR (300 MHz, CDCl₃, 298K, δ ppm, J Hz) δ 7.90-7.87 (m, 2H, ArH), 7.39-7.36 (m, 2H, ArH), 2.47, (s, 3H, CH₃), 0.12 (s, 9H, Si(CH₃)₃).

Ethynyl *p*-tolyl sulfone (5)² To a solution of *p*-tolyl [(2-trimethylsilyl)ethynyl] sulfone S1 (2.0 g, 8.1 mmol) in methanol (16 mL), a solution of NaF (504 mg, 12.0 mmol) in water (8 mL) was added dropwise at 0 °C, and the reaction was stirred at this temperature for 30 min. Then, the reaction was diluted with diethyl ether and washed with an aqueous saturated solution of NaHCO₃. The organic layer was separated, and dried over anhydrous Na₂SO₄ and the solvent was removed under reduced pressure, affording the desired pure product 5 as a white powder (1.4 g, 94%) without the need for a further purification step. ¹H NMR (300 MHz, CDCl₃, 298 K, δ ppm, J Hz) δ 7.92-7.89 (m, 2H, ArH), 7.41-7.38 (m, 2H, ArH), 3.45 (s, 1H, C≡C-H), 2.47 (s, 3H, CH₃ of Ts).

***N*-Boc-2,5-dimethylpyrrole (6c)** The synthesis of this compound was performed by a different procedure than the previously reported one.³ To a stirred solution of commercial 2,5-dimethylpyrrole (1.9 mL, 21 mmol) in acetonitrile (20 mL), 4-

dimethylaminopyridine (260 mg, 2.1 mmol) and Boc2O (4.82 g, 22 mmol) were added. After 24 h at r.t., all the starting material was consumed (TLC) and the mixture was diluted with Et₂O and washed with a 1M aqueous solution of NaHSO₄, water, and a 1M solution of NaHCO₃. The organic layer was dried over anhydrous Na₂SO₄ and filtered. The solvent was removed under reduced pressure. The compound was purified by silica gel column chromatography (AcOEt/Cy 1:40) affording the desired product **6c** (3.0 g, 73%) as a brown oil. ¹H NMR (300 MHz, CDCl₃, 298 K, δ ppm, *J* Hz) δ 5.79 (s, 2H, ArH), 2.38 (s, 6H, CH₃), 1.60 (s, 9H, C(CH₃)₃).

Synthesis of (7-hetero)norbornadienes 7a-d



(rac)-2-Tosyl-7-oxabicyclo[2.2.1]hepta-2,5-diene (7a).⁴ To a solution of ethynyl *p*-tolyl sulfone **5** (1.7 g, 9.6 mmol) in dry toluene (13 mL) under an argon atmosphere, commercial furan **6a** (7.0 mL, 96 mmol) was added. The mixture was heated at 70 °C for 4 h. Then, the solvent was removed and the reaction mixture was purified by silica gel column chromatography (DCM→ DCM/Acetone 40:1), affording **7a** as a brown powder (1.1 g, 46%). IR ($\bar{\nu}$, cm⁻¹) 1593, 1314, 1305, 1291, 1270, 1148, 1120, 1108, 1085, 1041, 1018, 1003, 874, 864, 813, 798, 753, 704, 664, 652. ¹H NMR (300 MHz, CDCl₃, 298 K, δ ppm, *J* Hz) δ 7.76-7.73 (m, 2H, ArH), 7.60 (d, 1H, *J* = 1.9, H3), 7.37-7.34 (m, 2H, ArH), 7.05 (dd, 1H, *J* = 5.3, *J* = 1.9, H5 or H6), 6.97 (dd, 1H, *J* = 5.3, *J* = 1.9, H5 or H6), 5.63-5.62 (m, 1H, H1 or H4), 5.37 (m, 1H, H1 or H4), 2.44 (s, 3H, CH₃ of Ts). ¹³C NMR (75.4 MHz, CDCl₃, 298 K, δ ppm) δ 160.0, 152.2 (C5 or C6), 145.1 (C2 or C3), 143.9 (CHAr), 142.3 (CHAr), 135.8 (C2 or C3), 130.2 (CAr), 128.1 (CAr), 84.3 (C1 or C4), 82.6 (C1 or C4), 21.8 (CH₃ of Ts). ESI-HRMS *m/z* calcd. for C₁₃H₁₂O₃SNa (M+Na)⁺: 271.0396, found: 271.0399.

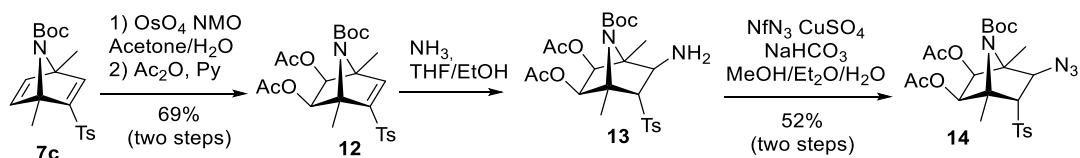
(rac)-2-Tosylbicyclo[2.2.1]hepta-2,5-diene (7b). Commercially available dicyclopentadiene **6b** (3.9 g, 29.5 mmol) was cracked at 200 °C and condensed over a solution of ethynyl *p*-tolyl sulfone **5** (0.4 g, 2.3 mmol) in dry toluene (3 mL) under argon atmosphere. Once all the dicyclopentadiene was cracked, the toluene was removed and

the reaction mixture was purified by column chromatography on silica gel (Et₂O/Cy 1:2) affording **7b** as a white powder (0.5 g, 95%). ¹H NMR (300 MHz, CDCl₃, 298 K δ ppm, *J* Hz) δ 7.70-7.68 (m, 2H, ArH), 7.46-7.45 (m, 1H, H3), 7.32-7.29 (m, 2H, ArH), 6.61 (m, 2H, H5, H6), 3.80-3.77 (m, 1H, H4), 3.68 (m, 1H, H1), 2.40 (s, 3H, CH₃ of Ts), 2.19-2.06 (m, 2H, H7a, H7b).

(rac)-N-Boc-1,4-dimethyl-2-tosyl-7-azabicyclo[2.2.1]hepta-2,5-diene (7c). To a solution of *N*-Boc-2,5-dimethylpyrrole **6c** (3.0 g, 15 mmol) in dry toluene under Ar atmosphere, ethynyl *p*-tolyl sulfone **5** (570 mg, 3.1 mmol) was added. The mixture was heated at 90 °C overnight. Then, toluene was removed under reduced pressure and the reaction mixture was purified by silica gel column chromatography (AcOEt/Cy 1:5) to afford **7c** as a yellowish powder (970 mg, 85%). IR ($\bar{\nu}$ cm⁻¹) 3082, 2978, 1695, 1603, 1556, 1456, 1307, 1143, 822, 790. ¹H NMR (300 MHz, CDCl₃, 298 K, δ ppm, *J* Hz) δ 7.49 (s, 1H, H3), 7.33, 7.75 (2 m, 2H each, ArH), 6.72 (d, 1H, *J* = 5.2, H5 or H6), 6.59 (d, 1H, H5 or H6), 2.44 (s, 3H, CH₃ of Ts), 1.97 (s, 3H, CH₃), 1.83 (s, 3H, CH₃), 1.32 (s, 9H, C(CH₃)₃). ¹³C NMR (75.4 MHz, CDCl₃, 298 K, δ ppm) δ 160.5 (C=O), 159.7 (C3), 154.7 (C2), 149.3, 146.9 (C5, C6), 144.8, 136.6 (CAr), 129.9, 128.3 (CHAR), 81.4 (C(CH₃)₃), 77.7, 76.6 (C1, C4), 28.3 (C(CH₃)₃), 21.8 (CH₃ of Ts), 17.4, 16.3 (CH₃). ESI-HRMS *m/z* calcd. for C₂₀H₂₅NO₄SNa (M+Na)⁺: 398.1402; found: 398.1391.

(rac)-1,4-Dimethyl-2-tosyl-7-oxabicyclo[2.2.1]hepta-2,5-diene (7d). To a solution of ethynyl *p*-tolyl sulfone **5** (1.2 g, 6.4 mmol) in dry toluene (20 mL) under argon atmosphere, commercial 2,5-dimethylfuran **6d** (3.4 mL, 32 mmol) was added. The mixture was heated at 50 °C overnight. Then, the solvent was removed and the reaction mixture was purified by silica gel column chromatography (Et₂O/Cy 1:6), affording **7d** as a brown solid (1.4 g, 79%). IR ($\bar{\nu}$, cm⁻¹) 1596, 1446, 1384, 1301, 1224, 1145, 1086, 982, 815, 749. ¹H NMR (300 MHz, CDCl₃, 298 K, δ ppm, *J* Hz) δ 7.71 (d, 2H, *J* = 8.3, ArH), 7.41 (s, 1H, H3), 7.41 (d, 2H, *J* = 8.3, ArH), 6.82 (d, 1H, *J* = 5.1, H5 or H6), 6.73 (d, 1H, *J* = 5.1, H5 or H6), 2.44 (s, 3H, CH₃ of Ts), 1.76 (s, 3H, CH₃), 1.62 (s, 3H, CH₃). ¹³C NMR (75.4 MHz, CDCl₃, 298 K, δ ppm) δ 161.1 (C2), 157.6 (C3), 148.6, 146.2 (C5, C6), 144.8, 136.2 (CAr), 130.0, 128.2 (CHAR), 91.9, 91.3 (C1, C4), 21.8 (CH₃ of Ts), 16.5, 15.6 (CH₃). ESI-HRMS *m/z* calcd. for C₁₅H₁₆O₃SNa (M+Na)⁺: 299.0718, found: 299.0713.

Synthesis of azanorbornadienic β-azido sulfone 14 and intermediate compounds

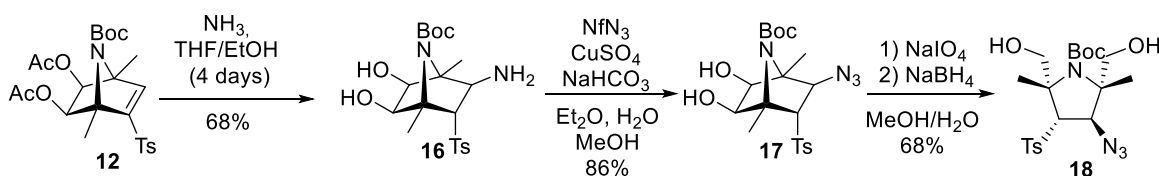


(rac)-N-Boc-5,6-exo-di-O-acetyl-1,4-dimethyl-2-tosyl-7-azabicyclo[2.2.1]hept-2-ene (12). To a solution of **7c** in acetone (33 mL) and water (4 mL), NMO (324.0 mg, 2.4 mmol), and OsO₄ (4 wt. % in H₂O, 0.8 mL, 0.13 mmol) were added. The mixture was stirred for 1 h at r.t. Then, the solution was cooled at 0 °C and a saturated aqueous solution of NaHSO₃ was added. The reaction mixture was extracted with AcOEt and the organic layer was washed with brine and dried over Na₂SO₄. The solvent was removed under reduced pressure and the reaction mixture was purified by chromatography column on silica gel (AcOEt/Cy 1:3 → 1:2) affording **12** (450 mg, 69%) as a white powder. IR ($\bar{\nu}$ cm⁻¹) 3083, 2981, 2941, 1738 (C=O), 1710 (C=O), 1596, 1369, 1331, 1245, 1222, 1156, 1090, 959, 943, 820, 700, 665, 604. ¹H NMR (300 MHz, CDCl₃, 298 K, δ ppm, *J* Hz) δ 7.76-7.74 (m, 2H, ArH), 7.38-7.35 (m, 2H, ArH), 6.81 (bs, 1H, H3), 4.91 (d, *J* = 6.1, 1H, H5 or H6), 4.80 (d, 1H, H5 or H6), 2.45 (bs, 3H, CH₃ of Ts), 2.09 (bs, 3H, COOCH₃), 2.08 (bs, 3H, COOCH₃), 1.71, 1.70 (2bs, 3H each, CH₃), 1.35 (bs, 9H, C(CH₃)₃). ¹³C NMR (75.4 MHz, CDCl₃, 298 K, δ ppm) δ 169.89, 169.86 (COOCH₃), 155.0 (C=O Boc), 152.5 (C2), 149.7 (C3), 145.5, 136.2 (CAr), 130.2, 128.4 (CHAR), 81.5 (C(CH₃)₃), 72.81, 72.80 (C1, C4), 72.3, 70.8 (C5, C6), 28.2 (C(CH₃)₃), 21.8 (CH₃ of Ts), 20.62, 20.58 (COOCH₃), 15.5, 14.1 (CH₃). ESI-HRMS *m/z* calcd. for C₂₄H₃₁NO₈SNa (M+Na)⁺: 516.1663; found: 516.1661.

(rac)-N-Boc-3-exo-azido-exo-di-O-acetyl-1,4-dimethyl-2-endo-tosyl-7-azabicyclo[2.2.1]heptane (14). Compound **12** (358 mg, 0.8 mmol) was dissolved in EtOH (20 mL) and THF (20 mL) at 0 °C. Then, NH₃ gas was bubbled for 2 min and the reaction was allowed to warm to r.t. for 10 min. Then, the solvent was removed under reduced pressure to give bicyclic amine **13** that was used without purification in the next step. To a solution of **13** in MeOH (3 mL) and water (1 mL), NaHCO₃ (497 mg, 5.9 mmol), a solution of NfN₃ (540 mg, 1.7 mmol) in Et₂O (2.3 mL) and CuSO₄·5H₂O (50 mg, 0.2 mmol) were added and the mixture was stirred at r.t. for 24 h. The organic solvents were removed under reduced pressure and the resultant aqueous mixture was extracted with DCM and washed with an aqueous saturated solution of NaHCO₃. The organic layer was dried over Na₂SO₄ and filtered, the solvent was removed under

reduced pressure. The crude product was purified by column chromatography on silica gel (AcOEt/ Cy 1:4 → 1:2) affording **14** as a white powder (231.7 mg, 50%). IR ($\bar{\nu}$ cm⁻¹) 2979, 2936, 2107 (N₃), 1751 (C=O), 1703 (C=O), 1596, 1457, 1366, 1342, 1291, 1238, 1146, 1083, 848, 812, 707, 653. ¹H NMR (300 MHz, CDCl₃, 298 K, δ ppm, *J* Hz) δ 7.87-7.84 (m, 2H, ArH), 7.43-7.40 (m, 2H, ArH), 5.78 (d, 1H, *J*_{5,6} = 6.6, H5 or H6), 5.13 (d, 1H, H5 or H6), 4.05 (d, 1H, *J*_{3,2} = 4.0, H2 or H3), 3.44 (d, 1 H, H2 or H3), 2.46 (s, 3H, CH₃ of Ts), 2.10, 2.09 (2s, 3H each, COOCH₃), 1.59 (s, 3H, CH₃), 1.53 (s, 3H, CH₃), 1.43 (s, 9H, C(CH₃)₃). ¹³C NMR (75.5 MHz, CDCl₃, δ ppm) δ 169.7, 169.5 (COOCH₃), 155.3 (C=O), 146.2, 136.0 (CAr), 130.5, 128.7 (CHAr), 81.7 (C(CH₃)₃), 74.6 (C2 or C3), 73.7 (C5 or C6), 72.7 (C1 or C4), 72.3 (C5 or C6), 70.1 (C1 or C4), 68.5 (C2 or C3), 28.3 (C(CH₃)₃), 21.9 (CH₃ of Ts), 20.6, 20.5 (COOCH₃) 17.3, 14.2 (CH₃). ESI-HRMS *m/z* calcd. for C₂₄H₃₂N₄O₈SNa (M+Na)⁺: 559.1833; found: 515.1823.

Synthesis of pyrrolidinic β -azido sulfone **18** and intermediate compounds



(rac)-N-Boc-1,4-dimethyl-2-endo-tosyl-3-exo-amino-7-azabicyclo[2.2.1]heptane-exo-5,6-diol (16**)**. To a solution of **12** (225.2 mg, 0.5 mmol) in THF (20 mL) and EtOH (20 mL), NH₃ was bubbled at 0 °C for 5 min. Then the solution was allowed to warm to r.t. After 4 days, the solvent was removed and the reaction mixture was purified by a chromatography column on silica gel (DCM/MeOH 50:1) affording **16** (147 mg, 68%) as a white foam. IR ($\bar{\nu}$ cm⁻¹) 3403, 2971, 2359, 1687 (C=O), 1596, 1456, 1364, 1138, 1085, 1058, 1024, 984, 953, 917, 807, 707, 661. ¹H NMR (300 MHz, DMSO-*d*₆, 353 K, δ ppm, *J* Hz) δ 7.82-7.79 (m, 2H, ArH), 7.47-7.45 (m, 2H, ArH), 5.09 (d, 1H, *J* = 6.2, OH), 4.63 (d, 1H, *J* = 6.7, OH), 4.26 (t, 1H, *J* = 6.2, H5 or H6), 3.45 (t, 1H, *J* = 6.5, H5 or H6), 3.09-3.05 (m, 2H, H2, H3), 2.42 (bs, 3H, CH₃ of Ts), 1.60 (s, 3H, CH₃), 1.33 (bs, 12 H, C(CH₃)₃, CH₃). ¹³C NMR (75.4 MHz, DMSO-*d*₆, 353 K, δ ppm) δ 155.5 (C=O), 144.6, 137.3 (CAr), 129.9, 128.1 (CHAr), 78.8 (C(CH₃)₃), 76.2 (C2 or C3), 73.0 (C5 or C6), 70.4 (C5 or C6), 69.9 (C1, C4), 59.2 (C2 or C3), 28.0 (C(CH₃)₃), 21.1 (CH₃ of Ts), 17.8, 13.8 (CH₃). ESI-HRMS *m/z* calcd. for C₂₀H₃₁N₂O₆S (M+H)⁺: 427.1897; found: 427.1888.

(rac)-N-Boc-3-exo-azido-1,4-dimethyl-2-endo-tosyl-7-azabicyclo[2.2.1]heptane-5,6-exo-diol (17). To a solution of **16** (131.1 mg, 0.31 mmol) in MeOH (3.5 mL) and water (0.5 mL), NaHCO₃ (104.2 mg, 1.2 mmol), CuSO₄·5H₂O (20.0 mg, 0.1 mmol) and a solution of NfN₃ (201.6 mg, 0.6 mmol) in Et₂O (2.1 mL) were added. The reaction was stirred at r.t. for 3.5 h. Then, the reaction was diluted with DCM, washed with water, and a saturated solution of NaHCO₃. The organic layer was dried over Na₂SO₄ and filtered, and the solvent was removed under reduced pressure. The crude product was purified by column chromatography on silica gel (AcOEt/Cy 1:3→1:2), affording **17** (113.3 mg, 87%) as a white powder. IR ($\bar{\nu}$ cm⁻¹) 3388, 2979, 2930, 2103 (N₃), 1699 (C=O), 1597, 1455, 1366, 1289, 1255, 1143, 1083, 951, 910, 814, 706, 683, 659. ¹H NMR (300 MHz, CDCl₃, 298 K, δ ppm, *J* Hz) δ 7.81-7.79 (m, 2H, ArH), 7.43-7.40 (m, 2H, ArH), 4.64 (d, 1H, *J* = 6.1, H5 or H6), 3.84 (d, 1H, *J* = 6.1, H5 or H6), 3.75 (d, 1H, *J* = 3.9, H3), 3.34 (d, 1H, *J* = 3.9, H2), 2.47 (CH₃ of Ts), 1.82, 1.60 (2s, 3H each, CH₃), 1.42 (s, 9H, C(CH₃)₃). ¹³C NMR (75.4 MHz, CDCl₃, 298 K, δ ppm) δ 157.3 (CO), 146.1, 136.5 (CAr), 130.6, 128.4 (CHAr), 81.8 (C(CH₃)₃), 74.7 (C2), 74.4 (C1 or C4), 74.3 (C5 or C6), 71.8 (C1 or C4), 71.6 (C5 or C6), 68.0 (C3), 28.3 (C(CH₃)₃), 21.9 (CH₃ of Ts), 17.4, 14.2 (CH₃). ESI-HRMS *m/z* calcd. for C₂₀H₂₈N₄O₆SNa (M+Na)⁺: 475.1622; found: 475.1614.

(2S,3R,4S,5S)- and (2R,3S,4R,5R)-(rac)-N-Boc-3-azido-2,5-bis(hydroxymethyl)-2,5-dimethyl-4-tosyl-pyrrolidine (18). To a solution of **17** (96.0 mg, 0.2 mmol) in MeOH (2 mL) and water (0.6 mL) at 0 °C, NaIO₄ (98.4 mg, 0.5 mmol) was added. After stirring the reaction at r.t. for 1 h, the reaction mixture was filtered over celite. Then, NaBH₄ (17.4 mg, 0.5 mmol) was added to the filtrate and the reaction was stirred at r.t. for 15 min. Next, a saturated aq. solution of citric acid was added, and the mixture was diluted with AcOEt and washed with water. The organic layer was dried over Na₂SO₄, filtered and the solvent was removed under reduced pressure. The product was purified through column chromatography on silica gel (AcOEt/Cy 1:3→1:2) affording **18** (71.5 mg, 68%) as a white foam. IR ($\bar{\nu}$ cm⁻¹) 3484, 2974, 2928, 2114 (N₃), 1687 (C=O), 1598, 1473, 1390 1353, 1294, 1254, 1138, 1083, 1056, 1000, 870, 817, 770, 678, 663. ¹H NMR (300 MHz, DMSO-*d*₆, 353K, δ ppm, *J* Hz) δ 7.85-7.82 (m, 2H, ArH), 7.50-7.47 (m, 2H, ArH), 4.73 (d, 1H, *J* = 11.9, H3), 4.07-3.92 (m, 2H, CH₂OH), 3.84 (d, 1H, *J* = 10.5, CHHOH), 3.67 (d, 1H, *J* = 11.9, H4), 3.66 (d, 1H, *J* = 10.5, CHHOH), 2.44 (s, 3H, CH₃ of Ts), 1.61 (s, 3H, CH₃), 1.43 (s, 9H, C(CH₃)₃), 1.12 (s, 3H, CH₃). ¹³C NMR (75.5 MHz, DMSO-*d*₆, 353K, δ ppm) δ 151.5 (C=O), 144.2 (CAr), 138.3 (CAr), 129.3 (CHAr), 127.2 (CHAr),

79.4 ($C(CH_3)_3$), 70.7 (C4), 66.6 (C2 or C5), 64.9 (CH_2OH), 64.5 (C2 or C5), 63.6 (C3), 61.9 (CH_2OH), 27.8 ($C(CH_3)_3$), 23.6 (CH_3), 20.6 (CH_3 of Ts), 17.4 (CH_3). ESI-HRMS m/z calcd. for $C_{20}H_{30}N_4O_6SNa$ ($M+Na$)⁺: 477.1778; found: 477.1773.

Quantum mechanical calculations

Full geometry optimizations and transition structure (TS) searches were carried out with Gaussian 16⁵ using the M06-2X hybrid functional,⁶ 6-31G(d,p) basis set for C, N, O, S, and H, and LANL2DZ effective core potential⁷ for the tin atoms with ultrafine integration grids. Bulk solvent effects in toluene were considered implicitly through the IEF-PCM polarizable continuum model.⁸ The possibility of different conformations was considered for all structures. All stationary points were characterized by a frequency analysis performed at the same level used in the geometry optimizations from which thermal corrections were obtained at 383.75 K. The quasiharmonic approximation reported by Truhlar *et al.* was used to replace the harmonic oscillator approximation for the calculation of the vibrational contribution to enthalpy and entropy.⁹ Scaled frequencies were not considered. Mass-weighted intrinsic reaction coordinate (IRC) calculations were carried out by using the Hratchian and Schlegel scheme¹⁰ to ensure that the TSs indeed connected the appropriate reactants and products. For the calculation of bond dissociation energies (BDEs),¹¹ single-point energy calculations using the correlated ab initio SCS-MP2 methods, in combination with the cc-pVTZ basis set,¹² were performed on the M06-2X/6-31G(d) optimized geometries. BDEs were defined as the difference in zero-point energies between the neutral species and the sum of the isolated radicals generated upon homolytic C–H cleavage (**Table D2**). Gibbs free energies (ΔG) were used for the discussion on the relative stabilities of the considered structures. The lowest energy conformer for each calculated stationary point (**Figure D6**) was considered in the discussion; all the computed structures can be obtained from authors upon request. Electronic energies, entropies, enthalpies, Gibbs free energies, and the lowest frequencies of the calculated structures are summarized in **Table D1**. Cartesian coordinates of the lowest energy structures calculated with PCM(toluene)/M06-2X/6-31G(d,p) are shown in **Table D3**.

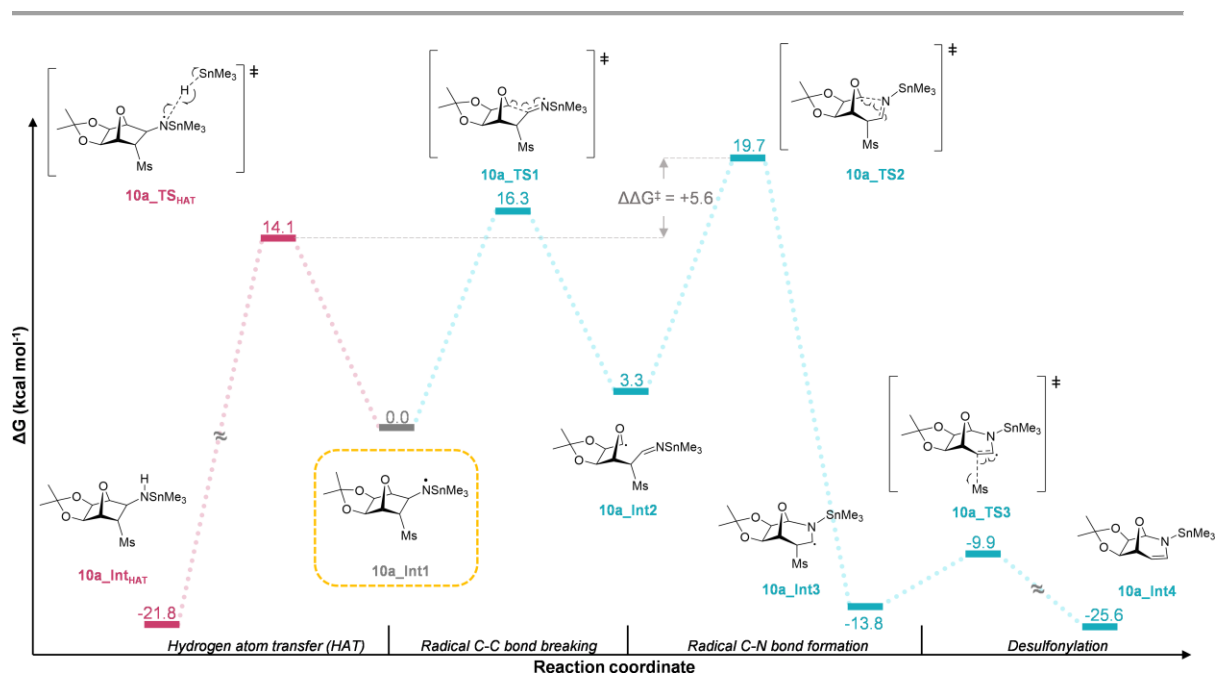


Figure D1. Minimum energy reaction pathway for the model of oxonorbornane derivative **10a** calculated with PCM(toluene)/M06-2X/6-31G(d,p).

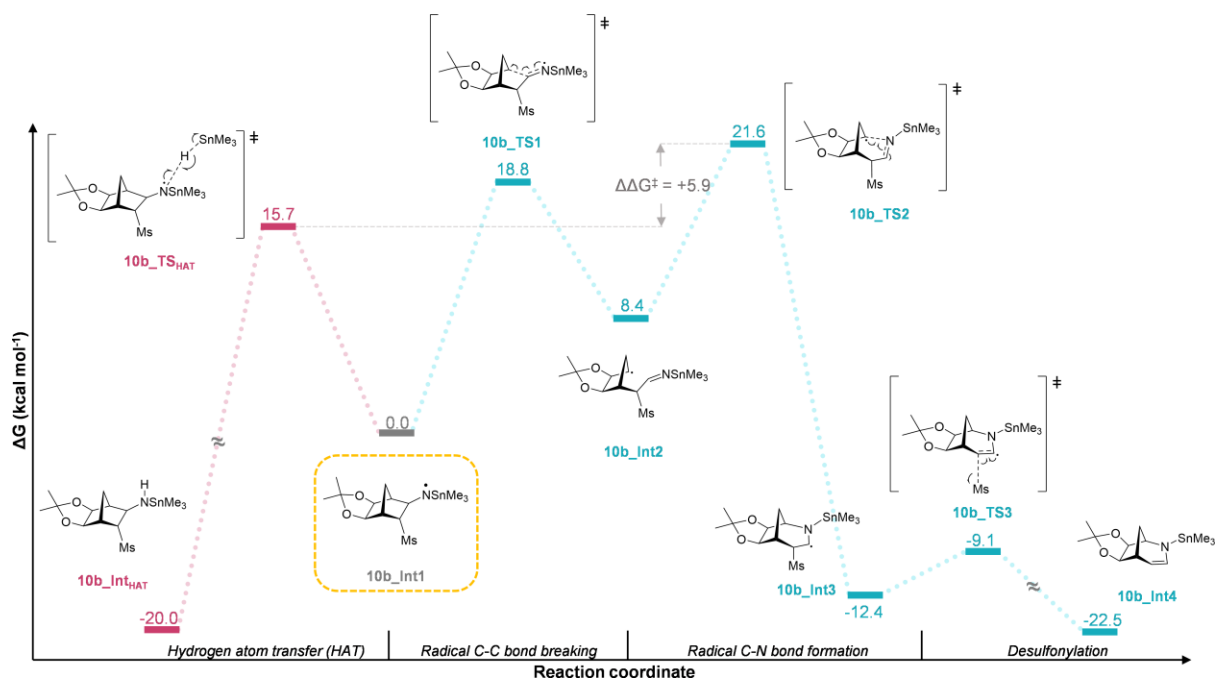


Figure D2. Minimum energy reaction pathway for the model of norbornane derivative **10b** calculated with PCM(toluene)/M06-2X/6-31G(d,p).

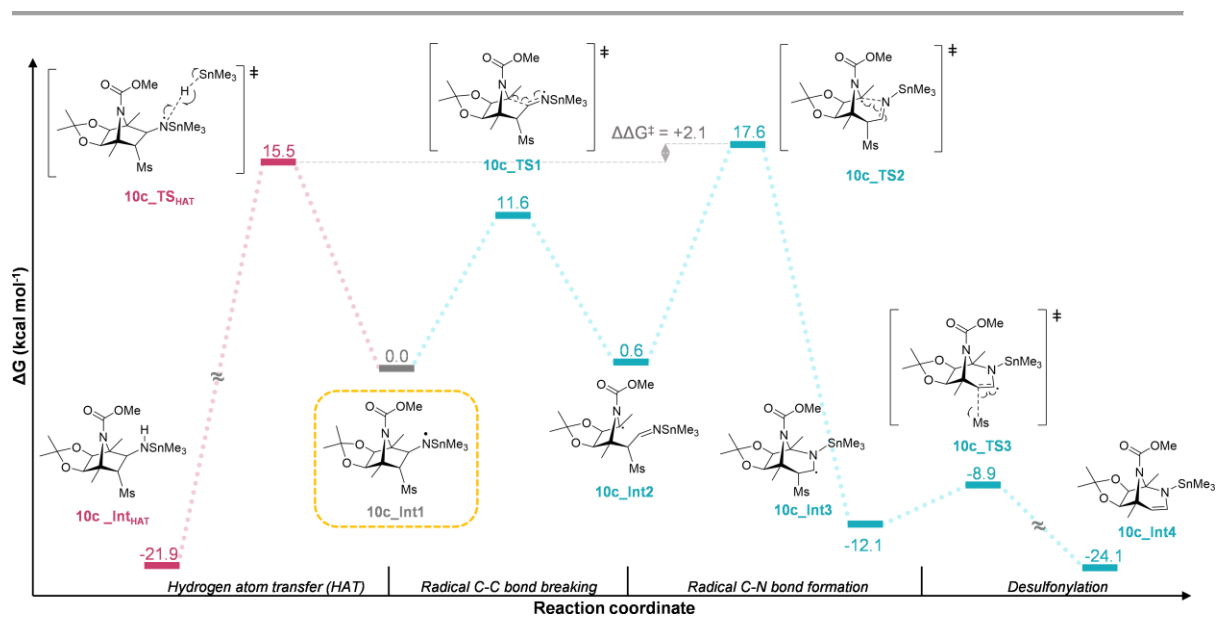


Figure D3. Minimum energy reaction pathway for the model of 1,4-dimethylazanorbornane derivative **10c** calculated with PCM(toluene)/M06-2X/6-31G(d,p).

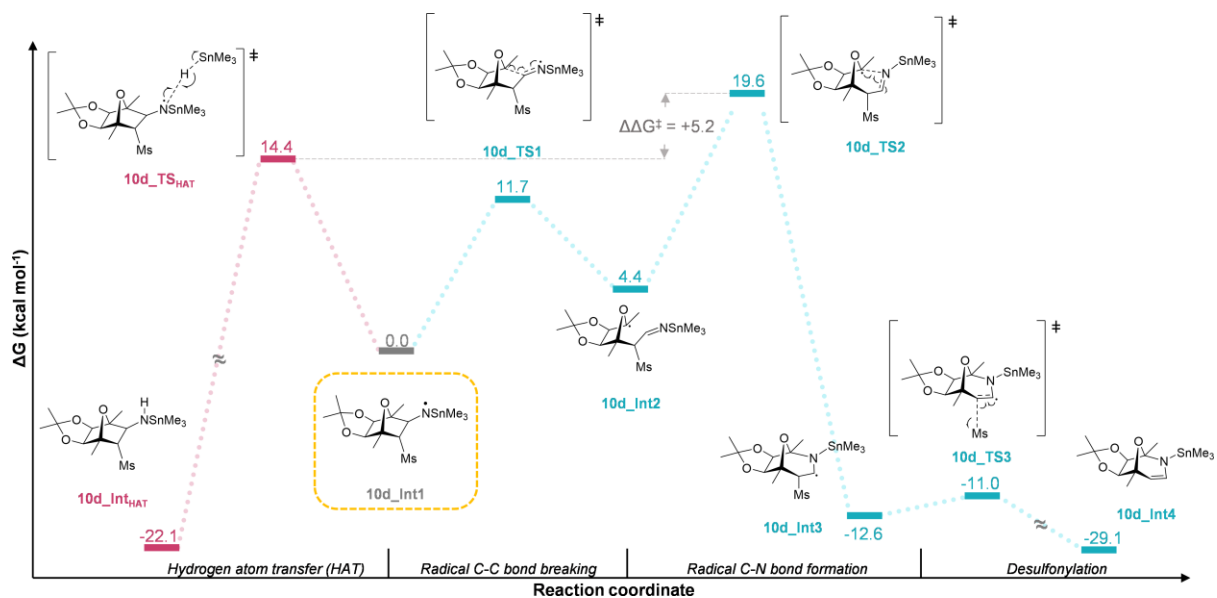


Figure D4. Minimum energy reaction pathway for the model of 1,4-dimethyloxonorbornane derivative **10d** calculated with PCM(toluene)/M06-2X/6-31G(d,p).

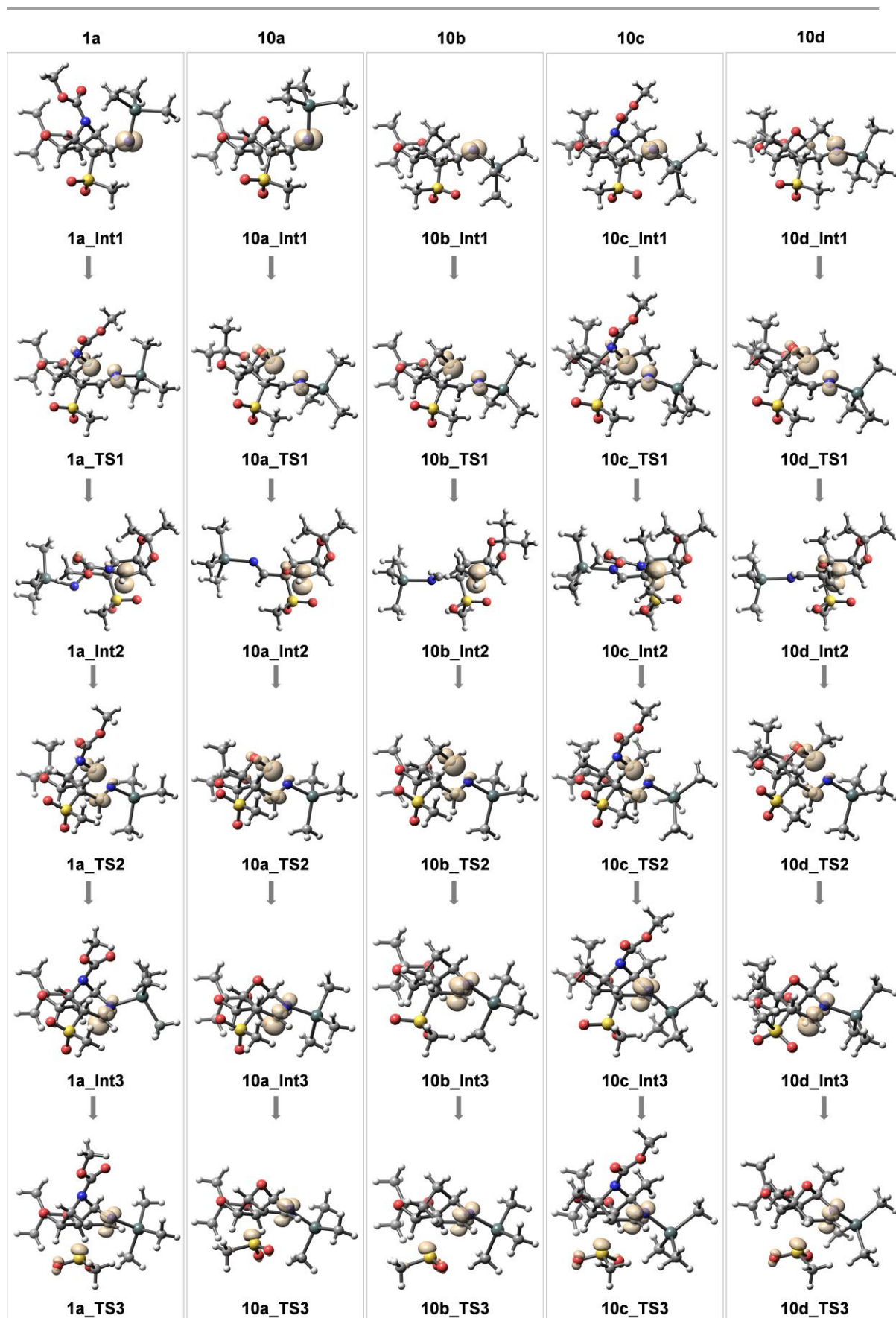
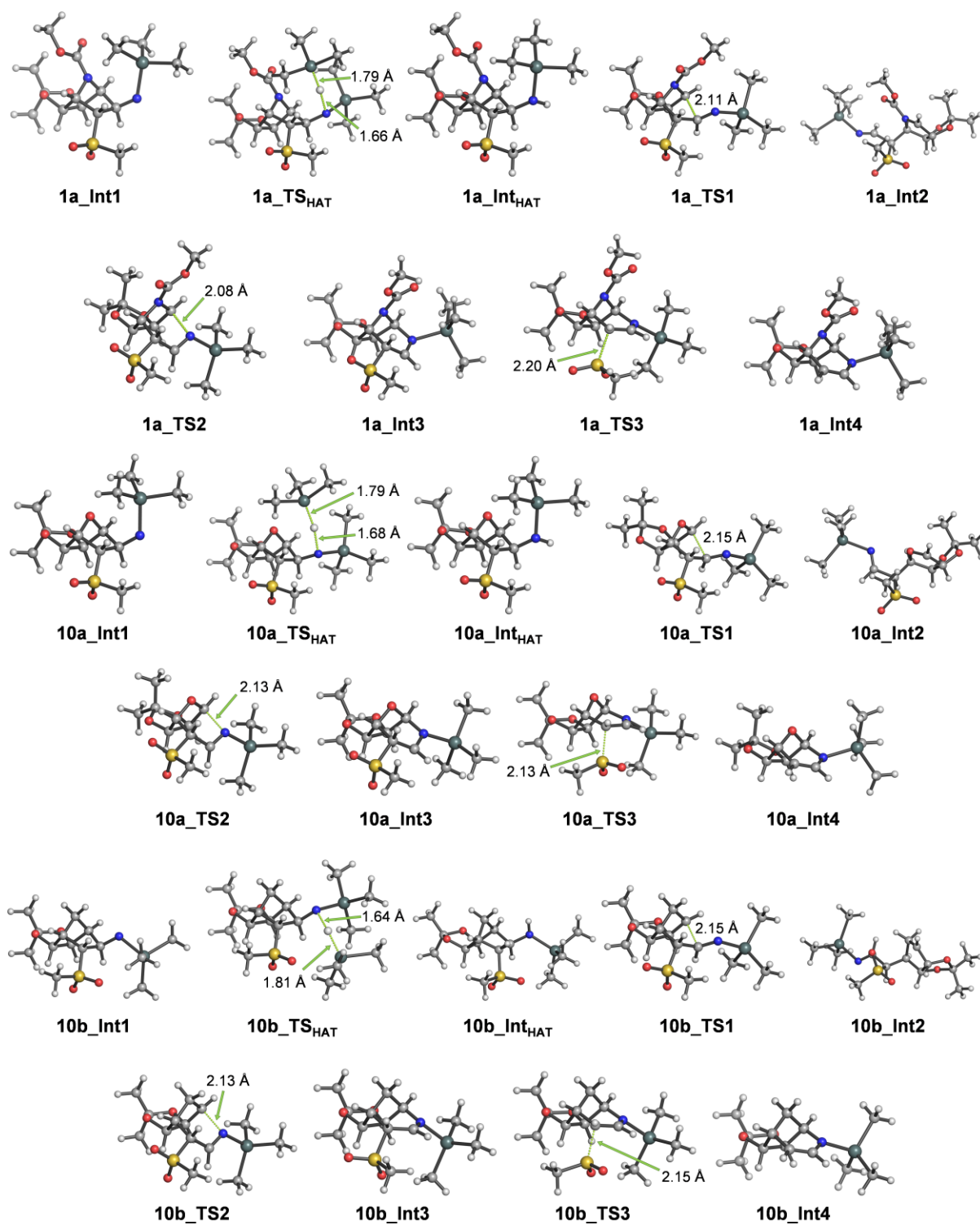


Figure D5. DFT-computed spin density of the radical intermediates and transition structures for the ring expansion reaction.



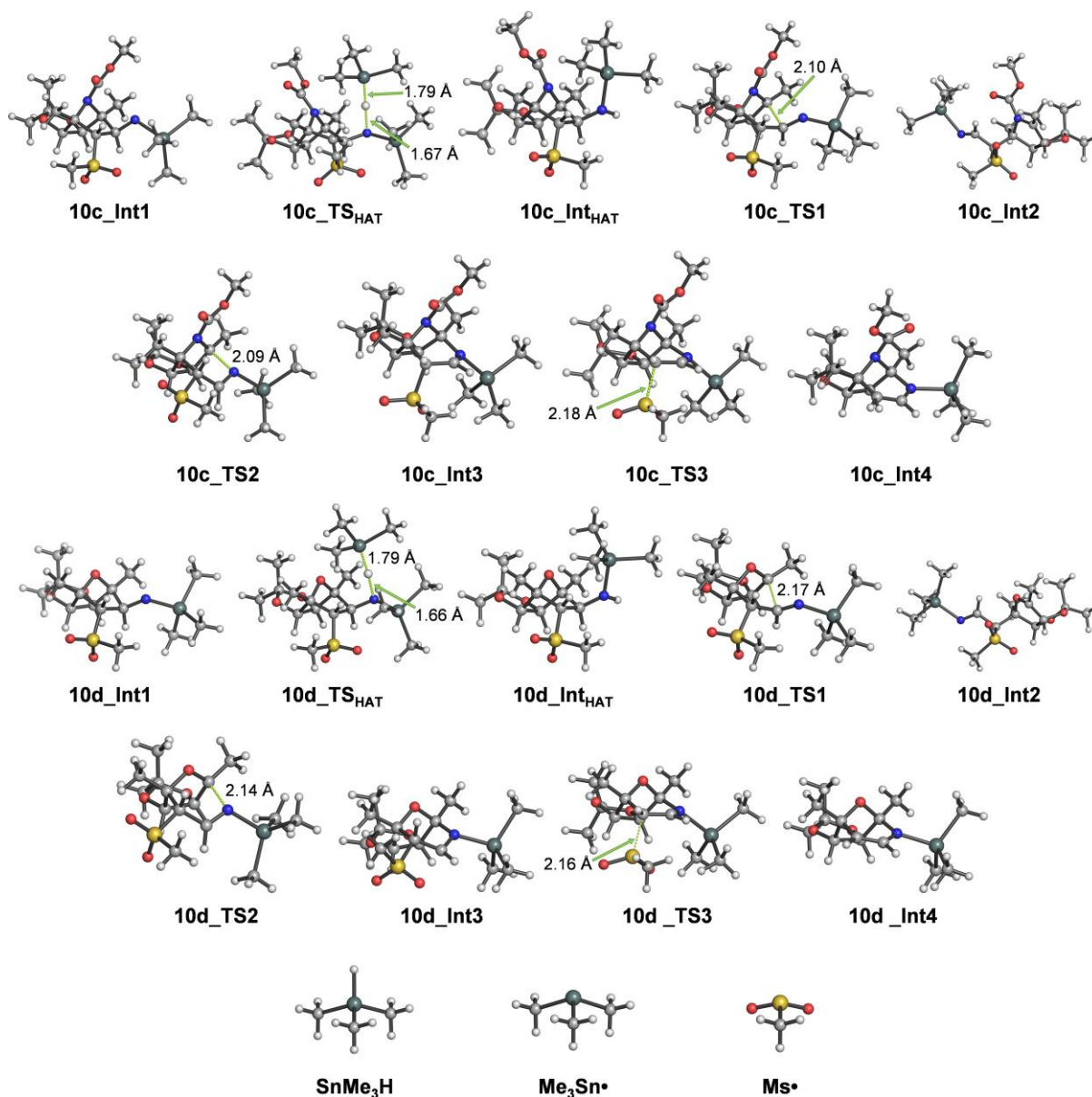


Figure D6. Geometries for the reactants, transition states, intermediates and products for the computed reaction pathway calculated with PCM(toluene)/M06-2X/6-31G(d,p)+LANL2DZ(Sn).

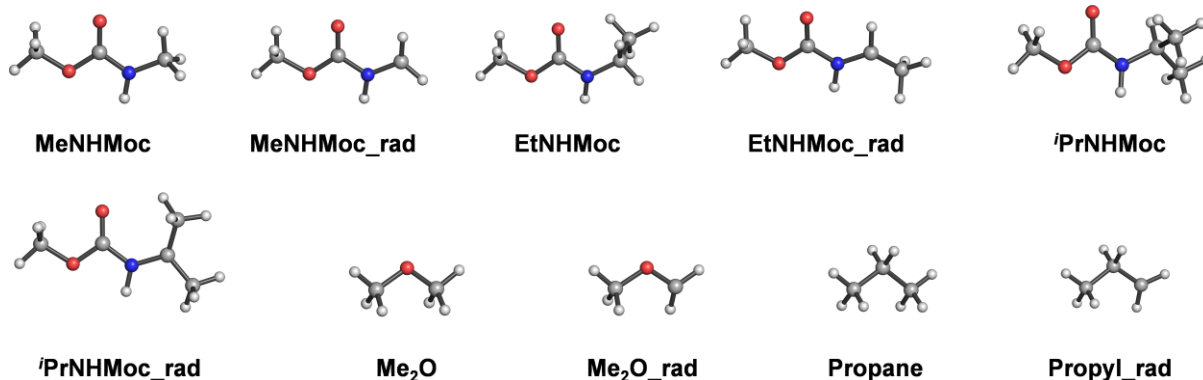


Figure D7. Geometries for neutral and radical species calculated with M06-2X/6-31G(d,p) for the estimation of the BDE.

Table D1. Energies, entropies, and lowest frequencies of the lowest energy calculated structures.^a

Structure ^b	E _{elec} (Hartree)	E _{elec} +ZPE (Hartree)	H (Hartree)	S (cal mol ⁻¹ K ⁻¹)	G (Hartree)	Lowest freq. (cm ⁻¹)	# imag. freq.
1a_Int1	-1549.665235	0.425211	-1549.193085	213.6	-1549.323691	14.2	0
1a_Int2	-1549.660593	0.422000	-1549.189979	219.3	-1549.324111	17.5	0
1a_Int3	-1549.688642	0.424827	-1549.216532	214.9	-1549.347936	30.8	0
1a_Int4	-961.340678	0.376207	-960.925484	185.6	-961.039004	37.4	0
1a_Int _{HAT}	-1550.337062	0.438529	-1549.851563	211.8	-1549.981061	37.7	0
1a_TS1	-1549.637764	0.421875	-1549.168611	215.2	-1549.300200	-448.9	1
1a_TS2	-1549.634191	0.421312	-1549.165418	215.3	-1549.297056	-584.2	1
1a_TS3	-1549.678970	0.423846	-1549.208159	213.8	-1549.338901	-150.3	1
1a_TS _{HAT}	-1673.286532	0.540273	-1672.685099	262.5	-1672.845620	-626.2	1
10a_Int1	-1341.718822	0.369116	-1341.309759	189.4	-1341.425584	36.9	0
10a_Int2	-1341.706778	0.365373	-1341.299334	197.9	-1341.420372	19.4	0
10a_Int3	-1341.739484	0.368570	-1341.330401	191.7	-1341.447614	23.3	0
10a_Int4	-753.389231	0.319497	-753.037213	163.6	-753.137244	16.6	0
10a_Int _{HAT}	-1342.389823	0.381953	-1341.967615	188.8	-1342.083060	34.8	0
10a_TS1	-1341.687784	0.365426	-1341.281693	192.9	-1341.399650	-438.1	1
10a_TS2	-1341.682700	0.365043	-1341.277178	191.3	-1341.394180	-572.1	1
10a_TS3	-1341.733335	0.367807	-1341.325684	189.2	-1341.441371	-168.4	1
10a_TS _{HAT}	-1465.339379	0.483564	-1464.801189	241.2	-1464.948677	-539.0	1
10b_Int1	-1305.831647	0.393125	-1305.397905	191.8	-1305.515217	25.9	0
10b_Int2	-1305.810856	0.388739	-1305.379319	200.4	-1305.501870	22.8	0
10b_Int3	-1305.851066	0.392526	-1305.417580	191.9	-1305.534928	24.7	0
10b_Int4	-717.498259	0.343737	-717.121670	163.9	-717.221926	20.0	0
10b_Int _{HAT}	-1306.499764	0.405942	-1306.052891	191.2	-1306.169797	28.6	0
10b_TS1	-1305.797327	0.389263	-1305.366946	193.5	-1305.485310	-536.1	1

10b_TS2	-1305.792846	0.388720	-1305.363043	192.7	-1305.480860	-548.1	1
10b_TS3	-1305.845832	0.392189	-1305.413377	190.1	-1305.529643	-154.6	1
10b_TS_{HAT}	-1429.451578	0.508242	-1428.888502	240.8	-1429.035740	-713.6	1
10c_Int1	-1628.262098	0.480625	-1627.729561	228.5	-1627.869286	16.4	0
10c_Int2	-1628.256592	0.478130	-1627.725146	234.1	-1627.868283	15.7	0
10c_Int3	-1628.283262	0.480923	-1627.750788	225.2	-1627.888520	30.2	0
10c_Int4	-1039.933542	0.432333	-1039.457797	197.5	-1039.578561	32.2	0
10c_Int_{HAT}	-1628.936853	0.495149	-1628.390444	223.1	-1628.526856	39.7	0
10c_TS1	-1628.240670	0.478006	-1627.710578	229.3	-1627.850827	-387.3	1
10c_TS2	-1628.231837	0.477936	-1627.702149	227.4	-1627.841214	-544.4	1
10c_TS3	-1628.277982	0.480248	-1627.746728	223.7	-1627.883509	-156.0	1
10c_TS_{HAT}	-1751.885233	0.596759	-1751.223245	273.0	-1751.390189	-552.8	1
10d_Int1	-1420.323581	0.423948	-1419.854466	205.9	-1419.980410	27.3	0
10d_Int2	-1420.311562	0.421667	-1419.843153	212.9	-1419.973364	18.1	0
10d_Int3	-1420.346288	0.425094	-1419.876763	202.3	-1420.000451	32.6	0
10d_Int4	-831.996617	0.375448	-831.584354	175.5	-831.691665	19.6	0
10d_Int_{HAT}	-1420.996920	0.437670	-1420.514188	203.0	-1420.638337	35.2	0
10d_TS1	-1420.301989	0.421469	-1419.835191	206.9	-1419.961726	-351.6	1
10d_TS2	-1420.289812	0.421020	-1419.823667	205.2	-1419.949182	-521.7	1
10d_TS3	-1420.342798	0.423613	-1419.874905	201.1	-1419.997865	-176.2	1
10d_TS_{HAT}	-1543.946665	0.539337	-1543.348125	253.3	-1543.503035	-601.9	1
Ms[*]	-588.340007	-588.294052	-588.285989	75.5	-588.332135	200.9	0
SnMe₃H	-123.618016	-123.501958	-123.487836	99.3	-123.548586	90.6	0
SnMe₃[*]	-122.986716	-122.878633	-122.864881	99.8	-122.925916	76.5	0

^aEnergy values calculated at the PCM(toluene)/M06-2X/6-31G(d,p) level. 1 Hartree = 627.51 kcal mol⁻¹. Thermal corrections at 383.75 K. ^bExcept for **Int_{HAT}**, **Int4** and **SnMe₃H**, all species correspond to doublet spin states; all species are neutral

Table D2. Energies, enthalpies, free energies, and entropies of the QM structures calculated for the estimation of the BDE of various C–H bonds.^a

Structure^b	E_{elec}^c (Hartree)	ZPE correction^d (Hartree)	H correction^d (Hartree)	S^d (cal mol⁻¹ K⁻¹)	G correction^d (Hartree)	Lowest freq.^d (cm⁻¹)
H	-0.499810	0.000000	0.002360	27.4	-0.010654	
MeNHMoc	-323.158690	0.109158	0.117459	84.2	0.077940	60.2
MeNHMoc_{rad}	-322.495210	0.094992	0.103067	82.7	0.063771	112.0
Me₂O	-154.727123	0.080930	0.086135	64.3	0.055602	216.8
Me₂O_{rad}	-154.061022	0.066901	0.072193	65.6	0.041011	180.6
Propane	-118.862186	0.104601	0.110048	65.4	0.078968	220.5
Propyl_{rad}	-118.187676	0.089235	0.095061	68.2	0.062670	142.4
EtNHMoc	-362.384877	0.138138	0.147454	89.4	0.105500	74.3

EtNHMoc_rad	-361.721858	0.123662	0.133234	91.5	0.090006	78.2
ⁱ PrNHMoc	-401.611532	0.166206	0.176867	95.9	0.132107	61.2
ⁱ PrNHMoc_rad	-400.946475	0.152248	0.163285	100.2	0.116874	31.1

^a1 Hartree = 627.51 kcal mol⁻¹. ^bExcept for **MeNHMoc**, **Me₂O**, **Propane**, **EtNHMoc**, and **ⁱPrNHMoc**, all species correspond to doublet spin states; all species are neutral. ^cEnergy obtained from single-point calculations with SCS-MP2/cc-pVTZ. ^dVibrational, thermal and entropic corrections obtained from frequency calculations on geometries optimized at the M06-2X/6-31G(d,p) level. Thermal corrections at 383.75 K.

References

- (1) Chen, Z.; Trudell, M. L. A Simplified Method for the Preparation of Ethynyl P-Tolyl Sulfone and Ethynyl Phenyl Sulfone. *Synth. Commun.* **1994**, *21*, 3149–3155. <https://doi.org/10.1080/00397919308020392>.
- (2) Eisch, J. J.; Shafii, B.; Odom, J. D.; Rheingold, A. L. Aromatic Stabilization of the Triarylborirene Ring System by Tricoordinate Boron and Facile Ring Opening with Tetracoordinate Boron. *J. Am. Chem. Soc.* **1990**, *112* (5), 1847–1853. <https://doi.org/10.1021/ja00161a031>.
- (3) Kobayashi, T.; Uchiyama, Y. Neighboring Effect of Pyrazole Rings: Regio- and Stereoselective Wagner-Meerwein Rearrangement in Electrophilic Addition Reactions of Norbornadiene-Fused Pyrazoles. *J. Chem. Soc. Perkin Trans. 1* **2000**, No. 16, 2731–2739. <https://doi.org/10.1039/b002454f>.
- (4) Kaiser, H. P.; Muchowski, J. M. Catalytic Hydrogenation of Pyrroles at Atmospheric Pressure. *J. Org. Chem.* **1984**, *49* (22), 4203–4209. <https://doi.org/10.1021/jo00196a020>.
- (5) Frisch, M. J.; Trucks, G. W.; Schlegel, H. B.; Scuseria, G. E.; Robb, M. A.; Cheeseman, J. R.; Scalmani, G.; Barone, V.; Petersson, G. A.; Nakatsuji, H.; Li, X.; Caricato, M.; Marenich, A. V.; Bloino, J.; Janesko, B. G.; Gomperts, R.; Mennucci, B.; Hratchian, H. P.; Ortiz, J. V.; Izmaylov, A. F.; Sonnenberg, J. L.; Williams-Young, D.; Ding, F.; Lipparini, F.; Egidi, F.; Goings, J.; Peng, B.; Petrone, A.; Henderson, T.; Ranasinghe, D.; Zakrzewski, V. G.; Gao, J.; Rega, N.; Zheng, G.; Liang, W.; Hada, M.; Ehara, M.; Toyota, K.; Fukuda, R.; Hasegawa, J.; Ishida, M.; Nakajima, T.; Honda, Y.; Kitao, O.; Nakai, H.; Vreven, T.; Throssell, K.; Montgomery, J. A., Jr.; Peralta, J. E.; Ogliaro, F.; Bearpark, M. J.; Heyd, J. J.; Brothers, E. N.; Kudin, K. N.; Staroverov, V. N.; Keith, T. A.; Kobayashi, R.; Normand, J.; Raghavachari, K.; Rendell, A. P.; Burant, J. C.; Iyengar, S. S.; Tomasi, J.; Cossi, M.; Millam, J. M.; Klene, M.; Adamo, C.; Cammi, R.; Ochterski, J. W.; Martin, R. L.; Morokuma, K.; Farkas, O.; Foresman, J. B.; Fox, D. J. Gaussian 16, Revision C.01. Wallingford CT 2016.
- (6) Zhao, Y.; Truhlar, D. G. The M06 Suite of Density Functionals for Main Group Thermochemistry, Thermochemical Kinetics, Noncovalent Interactions, Excited States, and Transition Elements: Two New Functionals and Systematic Testing of Four M06-Class Functionals and 12 Other Function. *Theor. Chem. Acc.* **2008**, *120* (1–3), 215–241. <https://doi.org/10.1007/s00214-007-0310-x>.
- (7) Hay, P. J.; Wadt, W. R. Ab Initio Effective Core Potentials for Molecular Calculations. Potentials for K to Au Including the Outermost Core Orbitals. *J. Chem. Phys.* **1985**, *82* (1), 299–310. <https://doi.org/10.1063/1.448975>.
- (8) Scalmani, G.; Frisch, M. J. Continuous Surface Charge Polarizable Continuum Models of Solvation. I. General Formalism. *J. Chem. Phys.* **2010**, *132* (11). <https://doi.org/10.1063/1.3359469>.
- (9) Ribeiro, R. F.; Marenich, A. V.; Cramer, C. J.; Truhlar, D. G. Use of Solution-Phase Vibrational Frequencies in Continuum Models for the Free Energy of Solvation. *J. Phys. Chem. B* **2011**, *115* (49), 14556–14562. <https://doi.org/10.1021/jp205508z>.
- (10) Hratchian, H. P.; Schlegel, H. B. Following Reaction Pathways Using a Damped Classical Trajectory Algorithm. *J. Phys. Chem. A* **2002**, *106* (1), 165–169. <https://doi.org/10.1021/jp012125b>.
- (11) Gerenkamp, M.; Grimme, S. Spin-Component Scaled Second-Order Møller-Plesset Perturbation Theory for the Calculation of Molecular Geometries and Harmonic Vibrational Frequencies. *Chem. Phys. Lett.* **2004**, *392* (1–3), 229–235. <https://doi.org/10.1016/j.cplett.2004.05.063>.
- (12) Kendall, R. A.; Dunning, T. H.; Harrison, R. J. Electron Affinities of the First-Row Atoms Revisited. Systematic Basis Sets and Wave Functions. *J. Chem. Phys.* **1992**, *96* (9), 6796–6806. <https://doi.org/10.1063/1.462569>.

Annex I

Poster contributions to national and international events

First name contributions

M. A. Tallarida, F. Olivito, C. D. Navo, V. Algieri, A. Jiritano, P. Costanzo, A. De Nino, G. Jiménez-Osés, L. Maiuolo, “Highly Diastereoselective Multicomponent Access to Spirocyclopropyl Oxindoles Enabled by Non-Chiral Rare Earth Metal Salts”, 13th Spanish-Italian Symposium on Organic Chemistry (SISOC-XIII), **2022**, Tarragona (Spain).

M. A. Tallarida, F. Olivito, C. D. Navo, V. Algieri, A. Jiritano, P. Costanzo, A. De Nino, G. Jiménez-Osés, L. Maiuolo, “Non-Chiral Rare Earth Metal Salts-Enabled Highly Diastereoselective Multicomponent Synthesis of Spirocyclopropyl Oxindoles”, XL National Congress of Italian Chemical Society, Division of Organic Chemistry (CDCO), **2022**, Palermo (Italy).

M. A. Tallarida, F. Olivito, C. D. Navo, V. Algieri, A. Jiritano, C. Bartucca, P. Costanzo, A. De Nino, G. Jiménez-Osés, L. Maiuolo, “Highly Diastereoselective Multicomponent Access to Spirocyclopropyl Oxindoles Enabled by Rare Earth Metal Triflates”, 19th Ischia Advanced School of Organic Chemistry (IASOC), **2022**, Ischia (Italy).

M. A. Tallarida, V. Algieri, F. Olivito, A. Jiritano, P. Costanzo, L. Maiuolo, A. De Nino, “Er(OTf)₃-Catalyzed Multicomponent Synthesis of Spirocyclopropyl Oxindoles as Potential MDM2 Protein Inhibitors”, XXVII National Congress of Italian Chemical Society (SCI), **2021**, virtual.

Other contributions

C. Algieri, F. Trombetti, V. Algieri, M. A. Tallarida, F. Olivito, A. Jiritano, L. Maiuolo, P. Costanzo, A. De Nino, S. Nesci, “SAR studies around the pyrazole core scaffold highlight the role of the F₁F₀-ATPase on mitochondrial permeability transition pore formation”, Proteine, **2022**, Pisa (Italy).

V. Algieri, F. Olivito, M. A. Tallarida, A. Jiritano, L. Maiuolo, P. Costanzo, C. Algieri, S. Nesci, A. De Nino, “Regioselective Synthesis of 1,3,4,5-Tetrasubstituted Pyrazoles by Eliminative Enaminone-Nitrilimine 1,3-Dipolar Cycloaddition”, XXVII National Congress of Italian Chemical Society (SCI), **2021**, virtual.

P. Costanzo, F. Olivito, A. Jiritano, V. Algieri, M. A. Tallarida, L. Maiuolo, A. De Nino, “Highly oleophilic and reusable polyurethane composites for the removal of oils from fresh water and seawater”, XXVII National Congress of Italian Chemical Society (SCI), **2021**, virtual.

L. Maiuolo, V. Algieri, F. Olivito, A. Jiritano, M. A. Tallarida, P. Costanzo, C. Algieri, F. Trombetti, S. Nesci, A. De Nino, “Polysubstituted 1,2,3-Triazoles: synthesis and biological application”, XXVII National Congress of Italian Chemical Society (SCI), **2021**, virtual.

A. Jiritano, F. Olivito, V. Algieri, M. A. Tallarida, P. Costanzo, L. Maiuolo, A. De Nino, "Synthesis of cellulose citrate and its application for the removal of cationic dyes from contaminated water", XXVII National Congress of Italian Chemical Society (SCI), **2021**, virtual.

F. Olivito, V. Algieri, M. A. Tallarida, A. Jiritano, A. Tursi, P. Costanzo, E. Sicilia, L. Maiuolo, A. De Nino, "New approaches for polyurethanes production: from catalysis to renewable synthesis", XXVII National Congress of Italian Chemical Society (SCI), **2021**, virtual.

V. Algieri, F. Olivito, C. Algieri, A. Jiritano, M. A. Tallarida, L. Maiuolo, P. Costanzo, S. Nesci, A. De Nino, "Eliminative 1,3-dipolar cycloaddition for the regioselective synthesis of 1,3,4,5-tetrasubstituted pyrazoles", Merck Young Chemists' Symposium (MYCS), **2021**, Rimini (Italy).

F. Olivito, V. Algieri, P. Costanzo, A. Jiritano, M. A. Tallarida, L. Maiuolo, A. De Nino, "Renewable polymers: conversion, synthesis, applications", Merck Young Chemists' Symposium (MYCS), **2021**, Rimini (Italy).

C. Algieri, V. Algieri, D. La Mantia, C. Bernardini, L. Maiuolo, F. Trombetti, M. A. Tallarida, A. De Nino, M. Forni, A. Pagliarani, M. Fabbri, S. Nesci, "New generation molecules as modulators of the mitochondrial permeability transition and potential therapeutic agents", 45th FEBS Congress, **2021**, virtual.

Additional courses

Ph.D. 3.0 - "The third mission of university within the third level of formation: *valorization of research and enterprise creation*", 2 ECTS. Organizer: University of Calabria, November - December **2020**. Virtual.

Ph.D. 3.0 - "The third mission of university within the third level of formation: *euromanaging, intellectual property, and copyright*". Organizer: University of Calabria, November **2021** - February **2022**. Virtual.

Seminars

Prof. F. Himo, "*Modeling reactions in self-assembled capsules*", University of Calabria, Dept. of Chemistry and Chemical Technologies. February **2020**.

"*Precision Medicine and SLA: State-of-art and Future Perspectives*", University of Calabria, University Club. February **2020**.

Dr. E. Vannini, "*Halting Glioma Growth and Sparing Neuronal Function via Rho GTPase Activation*", Dept. of Pharmacy, Health and Nutritional Sciences. December **2019**.

BSc and MSc thesis co-supervising activity

"Erbium-catalyzed multicomponent synthesis of spirocyclopropyl oxindoles as potential inhibitors of the complex p53-MDM2/MDMX", Vincenzo Spinoso, BSc in Chemistry, July **2021**.

"Nanocellulose: a versatile material for various applications", Concetta Bartucca, BSc in Chemistry. July **2020**.

"Multicomponent synthesis of polysubstituted indolizines *via* 1,3-dipolar cycloadditions with potential pharmacological activity", Veronica Cozzolino, MSc in Chemistry and Pharmaceutical Technologies. April **2021**.

"Synthesis of 1,2,3-indolizine derivatives with potential biological activity *via* 1,3-dipolar cycloadditions: a multicomponent approach", Carmelina Bartucca, MSc in Chemistry and Pharmaceutical Technologies. April **2021**.

Other activities

Member of the organizing committee of the event "*Global Women's Breakfast: Building Bonds to Create Future Leaders*". University of Calabria, Congress Center "B. Andreatta". February **2020**.

College counselor for the Dept. of Chemistry and Chemical Technologies of University of Calabria. Event: *Unical Risponde*, **2021**.

College counselor for the Dept. of Chemistry and Chemical Technologies of University of Calabria. Event: *Open Days*, **2020**.

Annex II

List of co-authored papers published or submitted during the Ph.D. program

**Corresponding author*

Within the thesis

De Nino, A.;* Maiuolo, L.;* Costanzo, P.;* Algieri, V.; Jiritano, A.; Olivito, F.; Tallarida, M. A. Recent Progress in Catalytic Synthesis of 1,2,3-Triazoles. *Catalysts* **2021**, 11 (9), 1-48. <https://doi.org/10.3390/catal11091120>.

Algieri, V.; Algieri, C.; Maiuolo, L.;* De Nino, A.;* Pagliarani, A.; Tallarida, M. A.; Trombetti, F.; Nesci, S.* 1,5-Disubstituted-1,2,3-Triazoles as Inhibitors of the Mitochondrial Ca²⁺-Activated F₁F₀-ATP(Hydrolyase) and the Permeability Transition Pore. *Ann. N. Y. Acad. Sci.* **2021**, 1485 (1), 43-55. <https://doi.org/10.1111/nyas.14474>.

Gil de Montes, E.; Tallarida, M. A.; Carmona, A. T.; Navo, C. D.; Robina, I.; Elías-Rodríguez, P.; Jiménez-Osés, G.;* Moreno-Vargas, A. J.* Studies on the Regioselective Rearrangement of Azanorbornanic Aminyl Radicals into 2,8-Diazabicyclo[3.2.1]Oct-2-Ene Systems. *J. Org. Chem.*, **2022**, 87, 24, 16483-16491.

Algieri, V.;* Costanzo, P.;* Tallarida, M. A.; Olivito, F.; Jiritano, A.; Fiorani, G.; Peccati, F.; Jiménez-Osés, G.; Maiuolo, L.; De Nino, A. Regioselective Synthesis and Molecular Docking Studies of Nucleobases. *Molecules*, **2022**, 27 (23), 8467.

Algieri, C.; Bernardini, C.; Marchi, S.; Forte, M.; Tallarida, M. A.; Bianchi, F.; La Mantia, D.; Stanzione, R.; Cotugno, M.; Costanzo, P.; Trombetti, F.; Maiuolo, L.; Forni, M.; De Nino, A.; Di Nonno, F.; Sciarretta, S.; Volpe, M.; Rubattu, S.; Nesci, S.* 1,5-Disubstituted-1,2,3-Triazoles Counteract Mitochondrial Dysfunction Acting on F₁F₀-ATPase in Models of Cardiovascular Diseases. *Pharmacol. Res.*, 187, 106561, **2023**.

Tallarida, M. A.;* Olivito, F.; Navo, C. D.; Algieri, V.; Jiritano, A.; Costanzo, P.; Poveda, A.; Moure, M. J.; Jiménez-Barbero, J.; Maiuolo, L.; Jiménez-Osés, G.;* De Nino, A.* Highly Diastereoselective Multicomponent Synthesis of Spirocyclopropyl Oxindoles Enabled by Rare-Earth Metal Salts. *Org. Lett.*, **Submitted**.

Outside the thesis

De Nino, A.; Tallarida, M. A.;* Algieri, V.;* Olivito, F.; Costanzo, P.; De Filpo, G.; Maiuolo, L. Sulfonated Cellulose-Based Magnetic Composite as Useful Media for Water Remediation from Amine Pollutants. *Appl. Sci.* **2020**, 10 (22), 1-15. <https://doi.org/10.3390/app10228155>.

Maiuolo, L.; Algieri, V.;* Olivito, F.;* Tallarida, M. A.;* Costanzo, P.; Jiritano, A.; De Nino, A. Chronicle of Nanocelluloses (NCs) for Catalytic Applications: Key Advances. *Catalysts* **2021**, 11 (1), 96.

Maiuolo, L.;* Olivito, F.;* Ponte, F.;* Algieri, V.; Tallarida, M. A.; Tursi, A.; Chidichimo, G.; Sicilia, E.; De Nino, A. A Novel Catalytic Two-Step Process for the Preparation of Rigid Polyurethane

Foams: Synthesis, Mechanism and Computational Studies. *React. Chem. Eng.* **2021**, 6 (7), 1238-1245. <https://doi.org/10.1039/d1re00102g>.

De Nino, A.;* Olivito, F.;* Algieri, V.; Costanzo, P.; Jiritano, A.; Tallarida, M. A.; Maiuolo, L. Efficient and Fast Removal of Oils from Water Surfaces *via* Highly Oleophilic Polyurethane Composites. *Toxics* **2021**, 9 (8). <https://doi.org/10.3390/toxics9080186>.

Maiuolo, L.;* Olivito, F.;* Algieri, V.; Costanzo, P.; Jiritano, A.; Tallarida, M. A.; Tursi, A.; Sposato, C.; Feo, A.; De Nino, A.* Synthesis, Characterization and Mechanical Properties of Novel Bio-Based Polyurethane Foams Using Cellulose-Derived Polyol for Chain Extension and Cellulose Citrate as a Thickener Additive. *Polymers (Basel)*. **2021**, 13, 2802.

Olivito, F.;* Algieri, V.;* Jiritano, A.; Tallarida, M. A.; Tursi, A.; Costanzo, P.; Maiuolo, L.; De Nino, A.* Cellulose Citrate: A Convenient and Reusable Bio-Adsorbent for Effective Removal of Methylene Blue Dye from Artificially Contaminated Water. *RSC Adv.* **2021**, 11 (54), 34309-34318. <https://doi.org/10.1039/d1ra05464c>.

Olivito, F.;* Algieri, V.; Tallarida, M. A.; Jiritano, A.; Costanzo, P.; Maiuolo, L.; De Nino, A.* Eco-Friendly High Yield Synthesis of HMF from Glucose and Fructose by Selective Catalysis with Water-Tolerant Rare Earth Metal Triflates Assisted by Choline Chloride. *Green Chem.*, **2023**, 00, 00, DOI: 10.1039/D2GC04046H

V. Algieri,* C. Algieri, P. Costanzo, G. Fiorani, A. Jiritano, F. Olivito, Tallarida M. A., F. Trombetti, S. Nesci, A. De Nino,* L. Maiuolo, "Novel regioselective synthesis of 1,3,4,5-tetrasubstituted pyrazoles and biochemical valuation on F1FO-ATPase and mitochondrial permeability transition pore formation", *Pharmaceutics* **2023**, 15 (2), 498.